ORNL-3314
UC-10 – Chemical Separations Processes
for Plutonium and Uranium
TID-4500 (17th ed., Rev.)

CHEMICAL TECHNOLOGY DIVISION

ANNUAL PROGRESS REPORT

FOR PERIOD ENDING JUNE 30, 1962

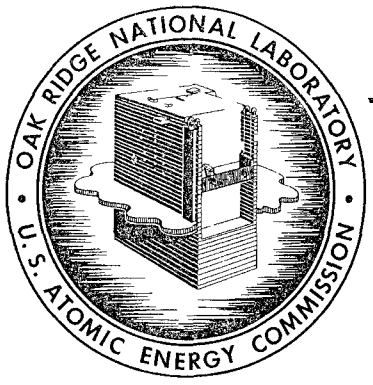

OAK RIDGE NATIONAL LABORATORY
operated by
UNION CARBIDE CORPORATION
for the
U.S. ATOMIC ENERGY COMMISSION

Printed in USA. Price $3.50 . Available from the

Office of Technical Services
U. S Department of Commerce
Washington 25, D C

LEGAL NOTICE

This report was prepared as an account of Government sponsored work Neither the United States nor the Commission nor any person acting on behalf of the Commission

A Makes any warranty or representation express or implied, with respect to the accuracy completeness or usefulness of the information contained in this report, or that the use of any information apparatus method, or process disclosed in this report may not infringe privately owned rights, or

B Assumes any liabilities with respect to the use of or for damages resulting from the use of any information apparatus, method, or process disclosed in this report

As used in the above, "person acting on behalf of the Commission" includes any employee or contractor of the Commission to the extent that such employee or contractor prepares handles or distributes or provides access to, any information pursuant to his employment or contract with the Commission.

DISCLAIMER

This report was prepared as an account of work sponsored by an agency of the United States Government. Neither the United States Government nor any agency Thereof, nor any of their employees, makes any warranty, express or implied, or assumes any legal liability or responsibility for the accuracy, completeness, or usefulness of any information, apparatus, product, or process disclosed, or represents that its use would not infringe privately owned rights. Reference herein to any specific commercial product, process, or service by trade name, trademark, manufacturer, or otherwise does not necessarily constitute or imply its endorsement, recommendation, or favoring by the United States Government or any agency thereof. The views and opinions of authors expressed herein do not necessarily state or reflect those of the United States Government or any agency thereof.

DISCLAIMER

Portions of this document may be illegible in electronic image products. Images are produced from the best available original document.

ORNL-3314

Contract No. W-7405-eng-26

CHEMICAL TECHNOLOGY DIVISION

ANNUAL PROGRESS REPORT

for Period Ending June 30, 1962

F. L. Culler – Division Director
D. E. Ferguson – Chemical Development Section A Chief
R. E. Blanco – Chemical Development Section B Chief
K. B. Brown – Chemical Development Section C Chief
M. E. Whatley – Unit Operations Section Chief
H. E. Goeller – Process Design Section Chief
J. C. Bresee – Pilot Plant Section Chief

DATE ISSUED

SEP [illegible] 1962

OAK RIDGE NATIONAL LABORATORY
Oak Ridge, Tennessee
operated by
UNION CARBIDE CORPORATION
for the
U. S. ATOMIC ENERGY COMMISSION

Summary

1. POWER REACTOR FUEL PROCESSING

Processes for Graphite-Base Fuels

Cold laboratory and engineering development of four processes for uranium- and/or thorium-bearing graphite-base fuels is in progress. These include mechanical grinding and leaching with 13–15 *M* HNO_3, combustion-ash dissolution, 90%-HNO_3 disintegration-leaching, and chloride volatilization. Studies were made with both coated- and uncoated-particle fuels, but the only aqueous-based process that is applicable to all graphite-base fuels appears to be the grind-leach.

Mechanical grinding followed by leaching with nitric acid or fluoride-catalyzed nitric acid generally resulted in recovery of >99% of the uranium and thorium. Coated-particle fuels had to be ground fine enough (– 200 mesh) to ensure rupture of the pyrolytic graphite or Al_2O_3 particle coatings. Combustion followed by dissolution of the ash in an acid reagent resulted in nearly quantitative recovery of the uranium and thorium except from fuels that contain Al_2O_3-coated fuel particles, where the inertness of the sintered alumina precludes its dissolution in an aqueous reagent. The ignition temperature of graphite was lowered from about 700 to 300–400°C by presoaking the fuel in lead acetate, $KMnO_4$, or copper nitrate solutions. Simultaneous disintegration and leaching with 90% HNO_3 recovered >99% of the uranium and thorium from fuels that did not contain coated particles. Both pyrolytic carbon and Al_2O_3 coatings were impervious to boiling 90% HNO_3, but boiling 90% HNO_3, slowly oxidized graphite. Most of the carbon that was oxidized was converted to carbon oxides, but about 10% was converted to water-soluble organic acids, 60–80% of which was mellitic acid.

Processes for Uranium and Thorium Carbide Fuels

Uranium monocarbide reacted at temperatures between 25 and 100°C with water, 6 *N* HCl, or 20 *N* NaOH to yield principally methane, some hydrogen, and small quantities of saturated C_2- to C_8-hydrocarbons. The major products of the reaction of UC with 4 or 16 *M* HNO_3 were carbon oxides and water-soluble polycarboxylic acids, including mellitic and oxalic. Water hydrolysis of thorium monocarbide, as of UC, yielded principally methane. Hydrolysis studies with mixtures of the higher uranium carbides (U_2C_3 and UC_2), indicated that saturated C_2- to C_8-hydrocarbons were a primary product of the sesquicarbide reaction, while the dicarbide yielded mostly nonvolatile hydrocarbons and some free hydrogen. The hydrolysis studies indicated that the net result of heat-treating $UC_{1.5}$ at 1600°C was disproportionation of UC to uranium metal plus the sesquicarbide, although stoichiometric UC was stable under the same heat-treatment conditions.

Processes for UO_2-BeO Fuels

Uranium can be recovered from GCRE-type reactor fuels, which are 70% UO_2–30% BeO pellets clad in Hastelloy-X, either by chopping and dissolving the pellets in 8 *M* HNO_3–2 *M* H_2SO_4 or 8 *M* HNO_3–0.5 *M* HF, or by dissolving the cladding in 2–4 *M* HNO_3 containing 3–5 *M* HCl and leaching the UO_2 from the pellets with the resulting decladding solution. In simulated chop-leach experiments, Gas-Cooled Reactor Experiment fuel pellets dissolved completely in about 8 hr in boiling 8 *M* HNO_3–0.5 *M* HF; the Hastelloy-X cladding was simultaneously attacked at a rate of

only 0.3 mg min^{-1} cm^{-2}. Dissolution of the 30-mil cladding in 2–3 *M* HNO_3 containing 3–4 *M* HCl required about 3 hr; leaching of the pellets with the resulting solution, which contained about 40 g of Hastelloy per liter, for an additional 6–7 hr recovered 99.6–99.8% of the uranium. Fuels containing >90% BeO are best dissolved in boiling H_2SO_4 or HF-NH_4F solutions. The initial rates of dissolution in 3 to 16 *M* H_2SO_4 can be represented by

$$\log R \text{ (where } R = \text{rate expressed as mg min}^{-1}\text{ cm}^{-2}) = 0.223 \times \text{molarity of } H_2SO_4 - 2.81 .$$

In HF solutions, the initial dissolution rate increased from 0 to 1.5 mg min^{-1} cm^{-2} as the HF concentration increased from 0 to 20 *M*.

Processes for Zirconium- and Stainless Steel-Containing Fuels

The Neuflex head-end treatment, a nitrate-free process for dissolving uranium-zirconium-tin alloy fuels containing up to 10% uranium, was developed in cold, small-engineering-scale tests. The dissolvent is NH_4F-H_2O_2, and the product is UO_2F_2 solution, which is not amenable to TBP solvent extraction but which can be satisfactorily solvent-extracted to recover uranium by the Dapex process, which uses D2HPA and DAAP. Ammonium carbonate stripping yields a uranyl tricarbonate product. Dissolution rates were 2–20 mg min^{-1} cm^{-2} at terminal free-fluoride-to-uranium ratios of 50 to 100. The dissolution off-gas consists of 2 moles of H_2, 4 moles of NH_3, and traces of O_2 per mole of zirconium dissolved. The dissolver solution is diluted with water prior to solvent extraction. In laboratory-scale batch cascade extractions uranium recovery was good and separation from zirconium was by a factor of 10^4.

The Zirflex decladding process at full-activity level was demonstrated in 22 laboratory-scale hot-cell tests with PWR blanket, Zircaloy-clad UO_2, fuel samples irradiated from 182 to 17,700 Mwd/ton. The cladding dissolved in 6 *M* NH_4F–1 *M* NH_4NO_3 in 2.5 hr and the pellets in 4 *M* HNO_3–0.1 *M* $Al(NO_3)_3$ in 5 hr. Little fracturing of high-density (96% of theoretical) pellets was noted. Uranium and plutonium average losses to the cladding solution were 0.01 and 0.09%, respectively. Little difference in losses and rates was noted between cold and hot tests.

In laboratory studies on development of a process for zirconium-base fuels compatible with titanium equipment, an instantaneous zirconium dissolution rate of 10 mg min^{-1} cm^{-2} and a titanium corrosion rate of <0.1 mil/month in refluxing 3 *M* HNO_3–1.2 *M* HF–0.4 *M* HBF_4–0.6 *M* Cr(III)–0.4 *M* Cr(VI)–0.46 *M* Zr were obtained.

Two methods for removing chloride from nitrate solutions were evaluated. The addition of 150% of the stoichiometric amount of hydrogen peroxide to zirconium–11 *M* chloride solutions decreased the chloride content to 0.07 *M*. At chloride concentrations below 3 *M*, hydrogen peroxide was <10% efficient, and complete removal of chloride was not possible. Development effort on chloride stripping from Darex solutions with NO_2 sparging was discontinued when chloride concentrations <0.01 *M* (350 ppm) were not achieved routinely with reasonable excesses of NO_2 even in a 20-ft-high packed column. Initial tests with NO met with some success, 0.01 to 0.02 *M* chloride being achieved with 450% of theoretical NO required.

Addition of HBF_4 or molybdic acid to the Darex dissolvent did not solubilize silica in fuels containing >0.5% silicon. However, treatment of a solution of APPR fuel, containing 2% silicon, produced a silica precipitate that did not plug lines and equipment as did that formed with untreated APPR fuel solutions. With HBF_4, 17% of the fluoride was volatilized; addition of 0.01 *M* zirconium decreased the fluoride volatility to 2%.

A preliminary phase study of the constant-boiling system H_2O-HCl-Zr showed a series of hydrated compounds with melting points of 68–110°C and boiling points of 100–112°C between 0.5 and 4.2 *M* Zr. Removal of zirconium tetrachloride from off-gas streams by hydrolysis during passage over boiling, near azeotropic, HCl-Zr solutions appeared feasible.

Corrosion Studies

Haynes 25 and 21 were superior to titanium in resisting corrosion in boiling Darex dissolvent containing 0.1 *M* HBF_4. Maximum rates were 0.36, 2.4, and 60 mils/month, respectively. Unwelded Corronel 230, a new alloy, developed for HF-oxidant service, was corroded at maximum rates of 2.83, 59.9, and 0.71 mils/month in 10 *M* HNO_3–0.5 *M* HF at 60°C and at boiling without and with the addition of 0.75 *M* Al^{3+}, respectively. Titanium was corroded at a rate of 0.07 mil/month

in the latter solution. Rates of Corronel 230 in 1 *M* HNO_3–3 *M* HF, at 60°C and at boiling were 4.97 and >2700 mils/month, respectively. In boiling 1 *M* HF with and without the addition of 0.06 *M* H_2O_2, rates were 12.7 and 43.7 mils/month, respectively.

In refluxing 20 to 23 *M* HNO_3, maximum corrosion rates of titanium and Corronel 230 were 0.07 and 7.27 mils/month. In boiling 20 *M* HNO_3–50 g/liter uranium solution containing free graphite, the corrosion rates for titanium, mild steel, and type 1100 aluminum were 0.03, 688, and 127 mils/month, respectively. In boiling 23 *M* HNO_3–1 *M* HF, types 6061 aluminum and 309SNb stainless steel were corroded at rates of 0.01 and 0.6 mil/month, respectively. In 90% HNO_3–10% H_2SO_4, Nichrome V, Carpenter 20SNb, types 304 and 347 stainless steel, INOR-8, LCNA, and CD4MCu were corroded at maximum rates of 0.20, 2.6, 4.1, 3.1, 0.17, 0.52, and 1.74 mils/month, respectively.

In flowing modified Zirflex dissolver solution at the boiling point, welded type 347 stainless steel and rolled, unwelded Haynes 21 were corroded at maximum rates of 6.45 and 0.68 mils/month, respectively. In modified Zirflex solvent-extraction feed solutions at 50°C, LCNA, Carpenter 20SNb, and types 304L and 347 stainless steel were corroded at maximum rates of 0.04 to 0.25, 0.08 to 0.46, 0.38 to 0.49, and 0.10 to 0.19 mil/month, respectively. In spent Zirflex core dissolvent (35°C) containing 0 to 0.09 *M* uncomplexed fluoride, titanium and Hastelloy-F were corroded at maximum rates varying from 0 to 8.5 and from 0.08 to 0.69 mils/month, respectively. Type 347 stainless steel was corroded at a maximum rate of 0.02 mil/month in 1 *M* HNO_3–2 *M* acetic acid–45 g of $UO_2(NO_3)_2 \cdot 6H_2O$/liter under heat transfer conditions.

In chloride volatilization processing tests, INOR-8, Nichrome V, and Haynes 25 were corroded at average rates of 0.7, 2, and 6 and 100, 800, and 800 mils/month at 500 and 700°C, respectively, in dry chlorine gas. Rates in CCl_4-N_2 were about the same as those in chlorine. Rates in oxygen at 725°C and in anhydrous HCl at 600°C were 0.02, 0.01, 0.01, 0 and 5.30, 5.63, 16.4, and 1.2 mils/month for Haynes 25, Nichrome V, INOR-8, and Pyroceram 9608, respectively.

Solvent Extraction Studies

The UO_2 dissolver solutions prepared in the Zirflex hot-cell tests were evaluated through one cycle of 30% TBP solvent extraction. Uranium and plutonium recoveries were nearly quantitative, and gamma decontamination factors were 2×10^4 and 7×10^3, respectively. In solvent recycle tests with these feeds, solvent degradation was much less when *n*-dodecane was the diluent than when Amsco 125-82 was used.

The acid Thorex process was satisfactorily modified to provide for simultaneous recovery of uranium and thorium from Consolidated Edison Darex cladding and Thorex core solutions. Only 1% of the fission product activity was removed from irradiated ThO_2 slurry by 6 hr of leaching with 1 to 5 *M* HNO_3. When a solution containing 116 g of thorium per liter, 6.2 *M* HNO_3, and 3.76×10^6 counts min^{-1} ml^{-1} of Pa^{233} was passed through a column of unfired Vycor glass, about 97% of the protactinium and <0.01% of the thorium was adsorbed. The protactinium was eluted with oxalic acid. In solvent extraction with 30% TBP, about 98% of the tracer concentrations of protactinium and 99.9% of the thorium and uranium were extracted. Decontamination factors were 70 and 10^5, respectively, from ruthenium and rare-earth elements, the principal neutron poisons. Laboratory experiments with synthetic solutions indicated that thorium may be removed from U^{233} product solutions by either ion exchange or solvent extraction processes.

Modifications in the uranium-aluminum and uranium-zirconium alloy fuel solvent extraction flowsheets were developed which provide increased plant capacity and decreased waste volumes. No difficulties were encountered in solvent extraction of solutions made by the 90% HNO_3 leaching of Pebble Bed Reactor graphite-base fuel containing tracer amounts of fission products, but about half the zirconium and niobium were adsorbed on the graphite during leaching, and 1% of the ruthenium volatilized during the evaporation of the excess acid. In studies on the distribution of Nb^{95} between 30% TBP in *n*-dodecane and aqueous nitric acid, the amount of niobium in the extractable form decreased from ~30% in 4 *M* HNO_3 to ≦5% in 0.1 *N* acid-deficient solution, and the distribution coefficient of the extractable portion decreased from 0.05 to ~0.008. The presence of chemical degradation products of TBP and Amsco 125-82 increased the amount of extractable niobium, the distribution coefficient of the extractable form, and the amount of niobium retained by the organic phase. Plutonium was

strongly adsorbed from 0.5 *M* HNO_3 on zirconia-silica-phosphate. Flow capacities and stage efficiencies were determined for a variety of flowsheet conditions. Tests of a dilute Purex flowsheet, designed to eliminate intercycle evaporation, in the 2-in.-diam pulsed columns showed considerably lower flow and uranium production capacity than expected. Electrostatic treatment of solvent extraction streams improved de-entrainment 20- to 50-fold.

Mechanical Processing

The mechanical dejacketing of the Core 1 fuel assemblies from the Sodium Reactor Experiment, which were irradiated to 675 Mwd/ton and decayed for 2 years, was successfully completed, and the declad fuel was shipped to the Savannah River Plant. The irradiated fuel cladding was highly hardened and much more difficult to handle than the ductile unirradiated assemblies. The cladding on about 7% of the fuel had to be chipped off with remotely operated hand tools. The slugs were satisfactorily steam-cleaned and recanned, and 18 liters of NaK was destroyed with steam. Two NaK explosions occurred, but damage to equipment was minor and no injuries or spread of activity occurred.

Installation of the cold shear-leach facility in building 4505 was completed and engineering demonstration of this process on unirradiated prototype power reactor fuels started. The shear and leacher were completely tested hydraulically and mechanically. The shear blade showed little wear after 3000 cuts on stainless-steel-clad porcelain mock fuel. Particle-size determinations indicated that small-size fines were predominantly porcelain and large pieces mostly metal. Less than 0.1% of all particles were <0.25 μ. It was determined that fuel could not be sheared to lengths <0.5 in. without closing the tubing. An assembly can be sheared down to 1.5 in. terminal length. Sulfuric acid dissolution of cladding scrap from Yankee fuel samples irradiated to 8130 Mwd/ton showed only 0.02% of the uranium and plutonium in the clad after leaching and washing.

Engineering Studies

Designs of pilot plants for the Darex and Shear-Leach processes were begun as a joint ORNL-ICPP (Idaho Chemical Processing Plant) effort. The pilot plants were to be installed at the ICPP, but both projects were cancelled by the AEC in April 1962. Full criteria were prepared for the Darex pilot plant and transmitted to the ICPP, along with the half-completed Darex design formerly planned for cell 3, building 3019. ORNL and the ICPP then jointly prepared engineering flowsheets, and design of process equipment was started. Criteria had been started for the Shear-Leach installation and location studies begun by an architect-engineer when it was cancelled. Assistance was provided the ICPP on their plans for a plutonium solvent extraction and isolation facility. Criteria were prepared by ORNL for a trilaurylamine (TLA) extraction system that would permit the ICPP to compare this with existing anion exchange methods.

2. FLUORIDE VOLATILITY PROCESSING

Processing of Uranium-Zirconium Alloy Fuel

Modifications to the Fluoride Volatility Pilot Plant required to scrub the dissolver off-gas with liquid HF were completed, and the system performed excellently in all tests. The last five of a series of flowsheet demonstration runs (TU-8 to TU-12) with nonirradiated fully enriched zirconium-uranium alloy fuel elements were successfully completed, and 5.2- to 6.5-yr-decayed uranium-zirconium alloy fuel was successfully processed in six runs. Automatic data logging and digital computer techniques were routinely used for processing data.

Application to Stainless-Steel-Containing Fuels

Stainless steel dissolution rates and component solubilities were determined in 29-36-35 mole % LiF-NaF-BeF_2, as were dissolution rates in 40-49-11 and 36-44-20 mole % LiF-NaF-BeF_2. Simulated EBR meltdown fuel containing trapped NaK was dissolved in molten NaF-LiF-ZrF_4 with HF with no difficulty.

Application to Short-Decayed UO_2 Fuel and Other Oxides

Uranium was successfully recovered from unirradiated Zircaloy-clad UO_2 pins which had decayed only 15–30 days. Overall process decon-

tamination factors varied from the order of 10^2 for Mo γ activity to 10^8 for Sr β activity. Radioactivity from I^{131} γ, Te β, Mo β, Nb γ, and Ru γ tended to disappear in the dissolution step. Scouting tests made with irradiated BeO-UO_2 and ThO_2-UO_2 fuels indicated the feasibility of using the fused salt volatility process but also showed that more work is needed in developing the chemistry and the optimum salt system for each case. Parallel slabs of zirconium oxide were hydrofluorinated in 26-43-31 mole % NaF-LiF-ZrF_4 for rate comparisons with previous Zircaloy-2 dissolutions.

General Process Development

Comparison of the resistance of INOR-8 vs Alloy 79-4 in NaF-LiF with ZrF_4 and BeF_2 indicated the potential usefulness of the latter as a hydrofluorination construction material. However, corrosion was high at the salt-vapor interface when dissolving Zircaloy-2 in 50.5-37.0-12.5 mole % NaF-LiF-BeF_2 with HF at 650°C. Alloy 79-4 was more resistant than either L-nickel or INOR-8 in a NaF-LiF-ZrF_4 melt with and without BeF_2 under fluorination conditions. Generally, the BeF_2-containing melt was the more corrosive. INOR-8 corrosion data accumulated during prototype hydrofluorination rate studies were correlated with the kinematic viscosity of molten salt. Results were favorable when UF_6 was volatilized from 29-36-35 mole % LiF-NaF-BeF_2 fused salt (~350°C liquidus); such a low-melting-point salt might be valuable in minimizing fluorinator corrosion. Nickel vessels were corroded rapidly with 40-49-11 mole % LiF-NaF-BeF_2 at 600°C. Prototype equipment was revised for study of salt recycle in Zircaloy-2 processing (for cost reduction) and to provide for inclusion of beryllium compounds in the study. The sodium fluoride-UF_6 reaction kinetics study resulted in a mathematical model in agreement with experimental observations.

3. WASTE TREATMENT AND DISPOSAL

High-Activity Waste Treatment

The design of a pilot plant for the demonstration of the pot calcination process for converting high-activity wastes to solids at the Idaho Chemical Processing Plant was carried through the preparation of engineering flowsheets in cooperation with personnel of Phillips Petroleum Company. This pilot-plant study will be moved from Idaho to Hanford as a result of a recent AEC decision.

Engineering-scale studies with simulated Purex, TBP-25, and Darex wastes demonstrated the operability of both continuous and batch evaporators in feeding 8-in.-diam by 90-in.-high pot calciners at rates of 10 to 25 liters/hr. The volume of noncondensable off-gas from the process ranged from 15 to 50 ft^3/hr. Solids, deposited radially in the pots during calcination, contained an average of a few tenths percent nitrate and had bulk densities of about 1.2 g/cc in the case of Purex and Darex and 0.7 g/cc in the case of TBP-25 waste. Volatilization of sulfate from the calciner to the evaporator was limited to <1% by the addition of calcium nitrate solution. Mercury was completely volatilized, together with up to 50% of the ruthenium. Ruthenium volatility can be decreased by adding reducing agents such as NO or phosphite.

Design and procurement of mechanical equipment for remotely positioning and connecting the calciner to process equipment in the pilot plant were completed. The equipment was assembled and is being tested at Georgia Nuclear Laboratories, Dawsonville, Georgia.

Simulated highly radioactive wastes from the TBP-25, Purex, and Darex processes were incorporated in glassy or microcrystalline solids by adding phosphite or hypophosphite and other fluxing agents and calcining. Volume reductions varied from about 7 to 9.3 for TBP-25 and from about 2.9 to 6.6 for Darex. Corresponding densities varied from about 2.35 to 2.84 g/cc and from about 2.2 to 3.8 g/cc, respectively, and softening points from 850 to 1000°C and from 850 to 900°C. The addition of phosphite or hypophosphite to 1.5 to 2.5 *M* not only provided a fluxing agent but also decreased the ruthenium volatility to <0.1% in batch and in small semicontinuous experiments. Semiengineering-scale fixation of TBP-25 waste in a true glass incorporating 26 wt % simulated waste oxides was accompanied by volatilization of 12.5% of the ruthenium, with physical entrainment of 0.02% or less. The thermal conductivity of this glass varied from 1.05 to 1.60 $Btu\,hr^{-1}\,ft^{-1}\,(°F)^{-1}$ between 300 and 1050°F (softening point, ~1100°F).

Vapor-liquid equilibrium data and solution densities were determined for TBP-25, Darex, and Purex wastes for concentrations from 0.5 to 1.5

to 2 times those of the expected waste solutions and at acid concentrations as high as 7 *M* when such solutions were stable.

In nitrate solutions, the logarithm of the ruthenium distillation factor was a linear function of the logarithm of the nitric acid molarity in the distillate. Dissolved salts increased the relative volatility. Addition of 0.1 *M* H_3PO_3 decreased the relative volatility by factors varying from 38.8 for simulated Darex waste to 447 for 12 *M* HNO_3. Addition of 1.5 to 2.5 *M* phosphite or hypophosphite to simulated TBP-25 waste solution lowered the ruthenium volatility to 0.1% or less during calcination up to 900°C.

Stainless steel appears to be a satisfactory construction material for both the calciner pot and the waste storage tanks. Type 304L stainless steel was corroded with average penetrations of 0.14, 1.11, and 4.5 mils when exposed to TBP-25, TBP-25 + glass additives, and Purex + glass additives, respectively, for 19 to 24 hr, including the evaporation-fixation cycle and final heating to 900°C. Intergranular corrosion occurred in the Purex environment. Corrosion was maximum in all environments during the relatively short time at high temperature when the last water and acid were being expelled. Little further internal corrosion is expected during storage. Type 304L stainless steel can be used for the calcination pot if sulfate volatility from Purex waste is properly controlled and if maximum fixation temperatures are kept below 900°C. Atmospheric corrosion in dry air at 900°C was <16.8 mils/yr.

Stainless steels exposed in simulated Darex waste solution for 6082 hr at 80°C showed overall rates of about 0.9 mil/month and grain-boundary attack but no intergranular attack. The addition of organic inhibitors and lowering the temperatures 40 to 50°C decreased the rate to a few hundredths of a mil per month. These stainless steel tanks are probably satisfactory for the storage of acid nitrate wastes.

Low-Activity Waste Treatment

A scavenging–ion exchange process for removing trace amounts of fission products from process waste water was demonstrated with ORNL waste in a 600-gal/hr pilot plant. When the feed is adjusted to a pH of 11.6 with caustic in a flash mixer, a precipitate is formed which scavenges the colloidal solids and part of the radioactivity. After flocculation, the solids are separated with a sludge-blanket clarifier and polishing filter and are further concentrated for disposal by a sludge filter. The clarified liquid is passed through a bed of Duolite CS-100 phenolic resin for sorption of most of the remaining activity. After passage of 2000 bed volumes through the ion exchange column, the plant effluent contained <3% of the maximum permissible concentration of Sr^{90} and Cs^{137} in drinking water for continuous occupational exposure. The Sr^{90} decontamination factors ranged from 2,047 to 12,160, representing >99.9% removal; Cs^{137} decontamination factors ranged from 77 to 3444 for the same operating time. Other tests in the pilot plant showed a 50% breakthrough point for Cs^{137} at 2800 resin-column volumes, demonstrated the feasibility of the split-elution method with 0.5 *M* HNO_3, and showed no effect from the variation of the length-to-diameter ratio of the resin bed.

Laboratory studies with tap water showed (1) that calcium hardness remaining in the clarifier effluent can be decreased from 70 ppm to <10 ppm by the addition of 25 ppm of lime at 25°C but that it was ineffective with ORNL waste containing complexing agents, (2) that vermiculite is not suitable for use with the high-caustic head-end treatment of ORNL waste and, (3) that the treatment of 20,000 bed volumes in a complete demineralization flowsheet should be possible before regeneration of the resin is required.

A conceptual design and cost estimate for a 750,000-gal/day plant for treating the total ORNL process waste stream indicated a capital cost of $511,000 and an estimated operating cost of 54 cents per 1000 gal.

Engineering, Economics, and Hazards Evaluations

A study undertaken to evaluate the economics and hazards associated with alternative methods of waste management in a nuclear power industry showed that costs for converting acid and reacidified Purex and Thorex wastes to solids by pot calcination and for producing glass from acid Thorex wastes ranged from 0.87×10^{-2} mill/kwh_e for processing acid Purex and Thorex wastes in 24-in.-diam vessels to 5.0×10^{-2} mill/kwh_e for processing reacidified Purex and Thorex wastes in 6-in.-diam vessels.

A preliminary conceptual design and cost estimate for a solids disposal facility in salt indicated costs of 6×10^{-3} to 30×10^{-3} mill/kwh$_e$. Of the total costs, 60 to 85% was attributable to salt removal, indicating that the best possible estimates of this item will be required for the more detailed final study.

Heat-transfer calculations of shipping containers for pot-calcined wastes of various ages showed that as many as thirty-six 6-in.-diam pots of calcined acid Purex waste can be shipped in a single-finned carrier after 2.4 years' decay without mechanical cooling en route. Four 24-in.-diam pots of acid Purex waste can be shipped, per carrier, after 11 yr of decay.

4. SOLVENT EXTRACTION TECHNOLOGY

Final Cycle Plutonium Recovery by Amine Extraction

Chemical and physical performance of the chemical flowsheet developed for final-cycle plutonium purification by tertiary amine extraction was demonstrated in countercurrent runs with simulated feeds and with Purex plant solutions. Plutonium distributions confirmed the previous equilibrium measurements, with satisfactory recoveries and concentration factors. Decontamination factors from the simulated solutions with tracer zirconium-niobium were near or above analytical limits, but those from Purex solutions were only 100–500, much lower than expected and than required for an acceptable plutonium product. In cold engineering tests in a 2-in.-diam pulsed column and in mixer-settlers, flow capacities and stage efficiencies were determined for a variety of flowsheet conditions.

Extraction of Rare Earths by Tertiary Amines from Chloride Solutions

Detailed examination of the behavior of lanthanides, yttrium, and scandium in the amine chloride extraction method for separating transplutoniums from lanthanides showed yttrium less extractable than any lanthanide under all conditions tested. Scandium extraction was higher than that of yttrium but varied greatly with extractant composition. The order of extractability of the lanthanides varied with extractant and aqueous composition, with maximum extraction near the middle of the series from 11 *N* LiCl–0.01 *N* HCl but, with most extractants tested, at the high-weight end from 8 *N* LiCl–2 *N* $AlCl_3$.

Metal Nitrate Extraction by Amines

Continued studies on amine extraction of fission-product metal nitrates showed marked variation in the extraction of nitrosyl ruthenium with age and contact time. Extraction of nitrato complexes (tetra- and penta- most extractable) passed through maxima at ~3 *M* HNO_3 in the absence of nitrate salts but continued to rise with decreasing acidity in the presence of sodium nitrate (~6 *M* NO_3^-) down to <0.5 *M* HNO_3; E_a^0(Ru) was up to ~0.6 with ~0.25 *M* amine. Extractions of nitro complexes were in a similar range but rose with decreasing acidity both with and without nitrate salt present.

Metal Chloride Extraction by Amines

Extraction of iron(III) from chloride solutions by several amines varied in the order quaternary > tertiary > secondary >> primary, and (with secondary amine) aromatic diluent > (aliphatic + alcohol) diluent. It increased throughout with increasing chloride concentration (acid or salt) up to 10 *M*, except for slight decreases at >8 *M* HCl with the quaternary and tertiary.

Acid Recovery by Amine Extraction

A useful balance between acid extraction power by amines and amenability to water stripping of the extracted acid was obtained by proper choice of the degree of steric hindrance from alkyl branching close to the nitrogen. N-Benzyldi(2-ethylhexyl)amine, in particular, was found capable of extracting >90% of the sulfuric acid from Sulfex decladding process waste and releasing it to a stripping solution which can reach a concentration of ~1 *M* H_2SO_4.

Extraction Performance and Cleanup of Degraded Process Extractants

Continued tests of diluent nitration showed it to be more severe in the presence of TBP. The degradation as measured by tracer zirconium-niobium

extraction, by nitroparaffin determination, or by total organic nitrogen determination, was essentially the same from heating and from irradiation, for example, 10 hr reflux with 2 *M* HNO_3 was equivalent to ~100 whr/liter of Co^{60} gamma irradiation. Amsco 125-82 was less susceptible to nitration after being scrubbed with concentrated H_2SO_4.

Of many scrubbing agents tested, ethanolamine proved most effective in removing zirconium-niobium–extracting impurities from degraded solvent. However, the economic value appears marginal because of appreciable loss of both TBP and ethanolamine and the relatively high price of the latter.

Continued search for diluents more stable to nitration showed large variations in stability with structure of alkylbenzenes. Di- and cycloalkylbenzenes were less stable than simple monoalkylbenzenes, with indication that triethylbenzene was even more stable and monoalkylbenzenes more stable when iso-branched than when either more branched or normal. These comparisons apply only to side-chain nitration, nitration of the benzene ring does not produce zirconium-niobium extractants, although it must still be considered in respect to physical properties and safety.

Suppression of Zirconium-Niobium and Ruthenium Extraction by TBP-Amsco from Aqueous Feeds Pretreated with Oximinoketones and Oxalic Acid

Significant suppression of zirconium-niobium and ruthenium extraction was demonstrated on treating aqueous feeds with certain oximinoketones, a class of compounds previously proposed as intermediary in similar suppressions by treatment with acetone plus nitrite. Further study of oximinoketones showed that a part of their effect was due to oxalic acid, present as either a synthesis by-product or a decomposition product of the oximinoketone. Direct batch tests showed oxalic acid more effective than oximinoketones in suppressing zirconium-niobium and ruthenium extraction but indicated some limitations through impaired extractions or precipitation of plutonium, uranium, and thorium. In spite of such limitations, the use of oxalic acid feed treatment, in processing actual irradiated-fuel solutions, improved the decontamination of uranium from gross beta and gamma activity by a factor of 20–30, without any impairment of overall uranium or plutonium recovery.

New Extractants

In continuing examination of new potential extractants supplied by manufacturers, a commercial supply of di-*sec*-butyl phenylphosphonate (DSBPP) compared well with the previous research preparation, and a number of new or modified amines compared well with previously available amines in assay and performance. Secondary amine contamination was removed from tertiary amines by column cation exchange in an isopropanol medium.

Gel-Liquid Extraction

Preliminary evaluations of the gel-liquid extraction technique, which uses the tertiary amine Alamine-336 absorbed in polystyrene-divinylbenzene beads, showed high separations but slow equilibration in the transplutonium–lanthanide–lithium chloride system. While this technique does not appear competitive with conventional solvent extraction for separations in that system, the results indicate possible advantages in systems offering only small separation factors and with extractants limited by poor miscibility with common diluents.

Solvent Extraction Equilibria and Kinetics

Continued studies of alkaline earth extraction by di(2-ethylhexyl)phosphate ($[HX]_2 + NaX$) in benzene showed $E_a^0(Sr) \propto [H^+]^{-1.7}$ (average) at pH <4, passing through maxima near pH 4.5–5.5, and independent of pH at >7. The maxima occurred at lower pH with higher reagent concentration (0.015 to 0.5 *M* X^-), in each case close to the pH where the mole ratio $NaX/\Sigma X \approx 0.25$. The extraction maxima disappeared when all sodium nitrate was replaced with strontium nitrate, $E_a^0(Sr) \propto [X^-]$ at all levels of $NaX/\Sigma X$, suggesting extraction into micelles of the reagent.

The relative affinities of the alkali ions for di(2-ethylhexyl)phosphate in extraction from nitrate-hydroxide solutions was Cs ≈ Rb < K < Na << Li << H. Results were similar with 0.5, 0.1, and 0.05 *M* X^-. The relative affinity of lithium in particular increased considerably with a decrease of aqueous pH and organic $MX/\Sigma X$.

Water extraction and the concomitant volume increase on conversion of $[HX]_2$ to NaX was measured in detail in the system D2EHPA-benzene–

Page xi is missing from hardcopy

Page xii is missing from hardcopy

of magnetite concrete and a 54-in.-thick compound window of oil and lead glass will provide sufficient shielding. The interior walls of the cells are expected to read <1 r/hr from neutron activation ten days after credible exposure to spontaneous fission neutrons.

Tentative maximum permissible environmental concentrations of the actinides were calculated. A hazard analysis based on these values indicates that the TRU facility design meets current containment criteria.

7. PLUTONIUM-ALUMINUM ALLOY FUEL PROCESSING

Plutonium was recovered from 24 highly irradiated plutonium-aluminum alloy rods. Objectives of the program included recovery of plutonium rich in the higher isotopes, generation of feed material for future transuranic flowsheet demonstrations, and the demonstration of a flowsheet for recovery of highly burned plutonium by anion exchange methods. A total of 675 g of plutonium meeting specifications was recovered, with average decontamination factors from fission products of 1×10^6. Overall losses averaged 1%, the bulk (80%) of which occurred in the first cycle during the scrubbing step. The Permutit SK resin used was severely degraded after receiving a dose of 4×10^8 rad.

8. PRODUCTION OF URANIUM-232

A total of 32.9 mg of U^{232} for nuclear cross-section measurements was prepared by neutron irradiation of Pa^{231} and chemical isolation of the uranium. The principal product solution contained 21.58 mg of U^{232} with an isotopic composition 98.90% U^{232}, 0.0127% U^{233}, 0.0095% U^{235}, and 1.075% U^{238}. The remainder of the U^{232} product contains about 0.03% U^{233} and 0.003% U^{235}. Uranium-235 and U^{238} contamination resulted from ~7 ppm of natural uranium in the Pa_2O_5 from which the U^{232} was produced and from traces of uranium in process reagents.

Six Al-Pa_2O_5 cermet targets containing a total of 48.1 g Pa^{231} were fabricated. Two irradiations were made. In the first irradiation, one target containing 7.35 g of Pa^{231} was irradiated to 4.7×10^{18} *nvt* and processed for uranium recovery after 43-hr decay and again after 91-hr decay. In the second irradiation, five targets containing a total of 40.6 g of Pa^{231} were irradiated to 4.1×10^{18} *nvt* and processed for uranium recovery after 43-hr decay and again after 77-hr decay. The irradiated slugs were processed by dissolution in HCl and HCl-HF and anion exchange. The uranium was further purified by a second anion exchange cycle and a TBP extraction.

Another 1 g of U^{232} containing about 1% U^{233} is being prepared by a longer reirradiation of the Pa^{231}.

9. URANIUM PROCESSING

Uranium mill waste streams normally contain Ra^{226} at a concentration too high to permit direct discharge to the environment. The radium was removed to below specification limits (10×10^{-12} curie/liter) from simulated plant waste solution by adsorption on natural and synthetic zeolites.

UO_2 particles (<10 μ) were enclosed in BeO by drying and igniting a suspension prepared in a syrupy solution of basic beryllium formate or oxalate. The refractory BeO was obtained as a slightly porous glassy mass, or (by a dispersion technique) as small spherical beads, which, however, were more porous and would require subsequent densification.

10. PROTACTINIUM CHEMISTRY

Present chemical processing methods are not adequate for large quantities of Pa^{233} in thorium fuels. To obtain basic protactinium chemical information for future process development the chemistry of protactinium in sulfuric acid solutions is being investigated by solvent extraction, solubility, and spectrophotometric methods. The solubility is 0.12–0.20 mg/ml in 27–33 *N* sulfuric acid, but increases below 20 *N* acid to as much as 6 mg/ml. Protactinium hydrolysis occurs at concentrations below 10 *N*. Organic amines will extract protactinium from sulfuric acid solutions, the order of extraction being tertiary < secondary < primary. The extractability increased approximately linearly with amine concentration, and increased quite rapidly with decreasing sulfuric acid concentration. A single absorption peak occurs at 2250 A in sulfuric acid concentrations above 15 *N*, but the peak is displaced to <1950 A, the limit of measurement, in concentrations below 7.5 *N*.

11. THORIUM OXIDE IRRADIATIONS

Code P-82 thorium oxide pellets (1650°C fired) showed little damage after being irradiated three months in the LITR under D_2O at 250°C and dry in aluminum capsules under a helium atmosphere. Average weight loss as a result of the wet-irradiation was 0.4% and of the dry, <0.05%. Irradiation markedly enhanced the wear resistance of the pellet surfaces, but, once the surface layers were removed during the first one or two hours of a standard spouting bed test, the wear rates of the irradiated materials were comparable to those of the unirradiated pellets. Irradiation in water also produced a small increase in void volume and a large number of small pores probably associated with individual fission events. Metallographs of the unirradiated and wet-irradiated pellets showed essentially no differences.

Two series of thorium oxide powders fired at 650, 800, 900, 1100, and 1500°C were irradiated dry in aluminum capsules for 16 and 22 months in the Low Intensity Test Reactor. The 650, 800, and 900°C-fired oxides became red and sintered into hard, glossy fragments. The 1100°C-fired materials formed off-white, chalky plugs, and the 1500°C fired oxides were blue powders. The specific surface areas of oxide fired at $\leqq$1100°C were markedly decreased by the irradiation although the estimated maximum temperatures of the powders during irradiation were <1000°C. Little or no sintering and only slight particle damage occurred in the 1500°C-fired powders. The sintering probably resulted from recrystallization processes induced by fission fragment irradiation.

12. GAS RECOMBINATION STUDIES

A palladium-on-thoria catalyst was developed for use in aqueous reactor slurries to recombine radiolytic deuterium and oxygen. At low deuterium partial pressures and under oxygen in excess of the stoichiometric ratio the specific catalytic activity was more than sufficient to recombine the radiolytic gases rapidly with very small concentrations of palladium. Under these conditions the reaction was first order with respect to the deuterium partial pressure and 0.5 order with respect to the oxygen partial pressures respectively. The apparent activation energy for recombination in the temperature range 250–280°C was 19–26 kcal/mole. Most simulated fission product accumulations did not affect catalytic activity.

Definitive correlations between catalytic activities observed in laboratory autoclave experiments and those obtained in pump loop experiments or observed in in-pile autoclave experiments have not been obtained. However, the specific activity based on the palladium concentration of a slurry of solids irradiated in an in-pile pump loop experiment was as high as those obtained with other slurry-palladium catalyst systems which had not been irradiated, indicating that simultaneous reactor irradiation and pumping under O_2 did not decrease catalytic activity.

13. THORIUM FUEL CYCLE DEVELOPMENT

The sol-gel process developed for preparing 3–10 wt % mixed uranium-thorium oxide for use in fuel element fabrication by vibratory compaction. The process was simplified to a four-step operation and demonstrated on a scale of 7 kg of oxide per batch. The steam denitration step was demonstrated to be capable of close product control on batches of ThO_2 up to 22.5 kg. Thoria spheroids of high attrition resistance were also prepared. Fifteen fuel irradiation capsules containing vibratorily compacted sol-gel oxide have given satisfactory performance under irradiation at heat fluxes up to 600,000 Btu hr^{-1} ft^{-2} for irradiations of up to 17,000 Mwd per ton of thorium. Two instrumented pins were irradiated at center line temperatures of 3600 and 2800°F and cladding temperatures of 1300 and 1000°F for 3 months without significant change. The effective thermal conductivity compares favorably with pelleted fuels.

Design of the Kilorod facility for fabricating metal-clad oxide reactor tubes for the BNL critical experiment by the sol-gel-vibratory compaction method was completed, and fabrication and installation are now in progress.

14. THORIUM RECOVERY FROM ROCKS

An extensive survey with a portable gamma-ray spectrometer of over 300 sq miles of surface outcrops of the Conway granite in New Hampshire indicate an average thorium content of 56 $\pm$ 6 ppm. If this concentration persists with depth, and this

will be determined by drilling during the next year, the thorium reserves in the Conway formation will amount to tens of millions of tons. The granite contains smaller but significant concentrations of uranium. Based on studies of 13 different samples, estimated recovery costs of thorium plus uranium have ranged from $23 to $83 per pound. Several samples of less extensive granite formations from the New England states contain thorium at concentrations equivalent to the Conway. Volcanic rock samples from Italy and Nevada contain 12–50 ppm thorium but resist acid leaching. Sublateritic soil samples from the southeastern United States contain only 5–16 ppm thorium.

15. RADIATION EFFECTS ON CATALYSTS

Conversion of Cyclohexanol to Cyclohexene with $MgSO_4$ and $MgSO_4$-Na_2SO_4 Catalyst

Contrary to published data, radioactive $MgSO_4$ and $MgSO_4$-Na_2SO_4 were less effective in the conversion of cyclohexanol to cyclohexene than were the corresponding nonradioactive catalysts. Both radioactive and nonradioactive catalysts lost catalytic activity on aging.

16. HIGH-TEMPERATURE CHEMISTRY

Detailed drawings were completed for the spectrophotometer system designed for operation at temperatures up to 330°C and pressures up to 3000 psi. A miniature loop system was designed and constructed for use at 150°C and 200 psi. A method based on graphical summation of photon contributions from electron energy distributions was developed for calculating Cerenkov radiation intensity from beta- and/or gamma-emitting sources.

17. MECHANISMS OF SEPARATIONS PROCESSES

The distribution of nitric acid between aqueous and TBP–Amsco 125-82 solutions, for all diluent/TBP ratios and up to ~5 *M* HNO_3 in the aqueous phase, were described mathematically by an equation that can be interpreted in terms of the mean activity coefficients of TBP + TBP·H_2O and TBP·HNO_3 + TBP·HNO_3·H_2O in the organic phase. The same description applies to many literature data. Preliminary transpirational measurements of the vapor pressure of TBP over nearly dry and over water-saturated TBP were obtained to help determine the thermodynamic equilibrium constant for the distribution of nitric acid between aqueous and TBP–Amsco 125-82 solutions. Partial pressures of nitric acid over aqueous solutions of 2–16 *M* HNO_3 were determined by the transpirational technique and used to obtain activity coefficients and the thermodynamic constant for dissociation of this acid into the ions H^+ and NO_3^-.

Fundamental and applied studies of the foam separation process were continued. Surface tensions of solutions of sodium dodecylbenzene sulfonate containing added H^+, Na^+, Ca^{2+}, or Ce^{3+} ions gave essentially the same value of α ($\alpha = 1.4 \times 10^6$ cm^3/mole), which is a measure of the tendency of a surfactant to concentrate at the solution surface. This is interpreted to mean that the surfactant-cation complexes of all these ions have the same degree of surface activity when expressed in terms of the concentration of the undissociated complex in solution. Screening tests, now essentially complete, showed eight surfactants out of 107 commercial products that warrant detailed study. Each of these could be used over a range of acidities but shows decreasing separation of strontium from solution as the calcium concentration exceeds ~10^{-4} *M*. Studies of some of the parameters of countercurrent foam columns showed, with dodecylbenzene sulfonate surfactant and ORNL tap water, that the height of a theoretical transfer unit for strontium removal is 1–2 cm of foam, thereby requiring only ~1 ft of foam height for good decontamination. Volumetric solution throughputs up to 1.65 gal min^{-1} per ft^3 of foam were achieved. A head-end precipitator to remove calcium and magnesium, prior to foam decontamination of low-activity-level waste, also gave a strontium decontamination factor of ~10^2 and a cesium decontamination factor of 10–40 when grundite clay was added to the waste to a level of ~0.5 lb per 1000 gal.

18. EQUIPMENT DECONTAMINATION

Samples of gas loop piping were spray decontaminated with oxalate-peroxide. Cesium-137 and iodine-131 were deposited on metals from high-temperature helium and decontaminated by various reagents. The behavior of hydrogen peroxide as a corrosion accelerator or inhibitor in many types of

decontamination solutions was studied. Noncorrosive mixtures effective for at least 12 hr at 95°C in the presence of carbon steel were developed. Other noncorrosive peroxide decontamination solutions effective at lower temperatures were found. The decontamination effectiveness of acidic fluorides, with corrosion inhibited by peroxide, was demonstrated with plutonium and americium activity on stainless steel samples.

19. RADIATION DAMAGE TO ION EXCHANGE RESIN

After (0.75–0.77) $\times$ 10^9 r (2.0–2.1 whr per g of dry resin) irradiation, 10–20% (dry basis) of the cation-exchange resin Dowex 50W was decomposed and dissolved in a flowing stream of water. The specific wet resin volume increased 10–15%, but there was no evidence of fissuring or fragmentation. The moisture content increased 10–15%. The resin lost 40–50% of its original strong acid capacity but gained ~5% weak acid capacity. The sulfur loss was 1.0–1.2 atoms/100 ev, and only 75–80% of the sulfur remaining on the polymer was present as the active sulfonate group. Analyses of the collected effluents indicated that degradation products included sulfate, sulfonate, and oxalate in the acid form.

Eighty percent of a sample of Dowex 50W X-8 resin dissolved in the water stream, and 95% of its total capacity was lost, after an exposure of 3.9 $\times$ 10^9 r (13.8 whr per g of dry resin). Amberlite 200, a highly cross-linked, porous resin, lost 15% of its weight by an irradiation of 0.97 $\times$ 10^9 r (2.6 whr per g of dry resin), and increased 20% in surface area and 25% in median pore diameter. The total capacity loss was 44%.

20. FUEL SHIPPING STUDIES

Prototype fuel shipping casks, weighing 1.5 to 6 tons each, were dropped from heights of from 6 in. to 20 ft onto a drop pad. The casks were instrumented with strain gages, accelerometers, compressometers, and inertia switches to measure strain, deceleration, and deformation. Data obtained in the tests are being correlated for scaleup to full sized casks.

The experimental program on dissipation of fission product heat from fuel shipping casks was completed. Mathematical methods developed for predicting maximum temperatures up to 300°C gave results to within 20°C of experimentally determined values

21. GAS-COOLED REACTOR COOLANT PURIFICATION

In a kinetic study of the catalytic oxidation of small amounts of hydrogen, carbon monoxide, and methane with oxygen in a bulk helium stream, three empirical equations were developed which correlate the data and are suitable for design purposes. A more fundamental study on the oxidation of these contaminants with copper oxide pellets experimentally verified mathematical models based on diffusion through the pellet pores for hydrogen and carbon monoxide and a surface-dependent reaction for methane. The differential equations from the models were solved numerically with a high-speed computer.

The product water and carbon dioxide could be easily sorbed on a fixed bed of molecular sieves. The combination of oxidation and sorption is an excellent method for purifying gas coolants of gas-cooled reactors.

22. CHEMICAL ENGINEERING RESEARCH

A folded 50-ft-long thermal diffusion column with a cellophane membrane, and with controlled countercurrent flow, was successfully used to separate cobalt and cupric ions in aqueous sulfate solution. Observed HTU's with a 1-ft-long column were less than those calculated from a slug-flow model. A modification of the stacked-clone high-speed contactor incorporating cylindrical sections achieved 40–75% stage efficiencies at throughputs of 1200 to 2000 cc/min with the uranyl nitrate–1 *M* $NaNO_3$(aq)–18.3% TBP-Amsco system.

23. CANE PROGRAM

The sequenced gas samples functioned as designed in the Gnome test. Preliminary work on the hypervelocity jetting of uranium cones indicated that recovery of irradiated uranium targets from an underground detonation may be possible. Chemical studies of isotopic exchange of hydrogen isotopes in the hydrogen-water system, with either materials

from natural salt formations as catalysts or with high thermal energy from a plasma jet at 10,000–12,000°K, indicated that tritium produced by a detonation in salt will be lost to environmental water. Studies of the oxidation of hydrogen to water by the sulfates in natural salt show that this mechanism also leads to mixing of tritium with environmental water.

24. ASSISTANCE PROGRAMS

AHBR and MSCR Processing Plant Studies

Conceptual fuel processing and reconstitution plant studies were made for the conceptual AHBR (Aqueous Homogeneous Breeder Reactor) power station, based on a Thorex-sol-gel process, for capacities of 266 and 1117 kg of thorium per day. A similar study was made for the conceptual MSCR (Molten Salt Converter Reactor) power station, based on a fluoride volatilization process, for daily capacities of 1.2 and 12 ft^3 of fused-salt fuel containing 35 and 350 kg of thorium and 2.83 and 28.3 kg of uranium, respectively. Process flowsheets, equipment lists, building layouts, and estimated capital costs, were made for each of the four cases.

High-Radiation-Level Analytical Laboratory

Design of the facility was completed and submitted for bids, and, after review of the bids, the project budget was increased from $2,000,000 to $2,500,000. The contractor will be selected in the near future and construction is scheduled to begin about August 1962.

Plant Waste Improvements

Criteria were completed and detailed design of the facilities by UCNC-ORNL and Paducah Engineering Departments was started. Consultation and design review services were provided for an intermediate-activity-level waste evaporator and two high-activity-level waste storage tanks. The scope of the program was changed to substitute a Melton Valley waste collection and transfer system for the low-activity-level waste treatment facility previously proposed.

Thorium Fuel Cycle Development Facility

The scope of this project, formerly called the U^{233} Metallurgical Development Laboratory, was increased to include facilities for fuel processing as well as reconstitution and refabrication. Two new cells were added to the three formerly described, and shielding for the entire facility was increased to 5.5 ft of normal concrete to accommodate low-decontamination process demonstration. A new preliminary study based on the revised criteria is being made by an architect-engineer.

Metal Recovery Canal Cleanout

Twenty-five tons of spent Brookhaven Reactor fuel that had been stored in the Metal Recovery Building Canal for 1–2 years was removed, canned, and shipped. Radiation exposures of personnel conducting the operation averaged about 6 mrem per man-hr of work. The principal contaminant in the activity burden (0.2–0.3 $\mu c/ml$) of the canal water was Cs^{137}, which accounted for >95% of the total. Visibility in the canal was improved and maintained by recirculating the water through a 40-μ-pore filter.

Safety and Containment

Assistance work on plant safety and containment included (1) completion of the containment changes and additions to buildings 4507 and 3508, (2) installation of an improved off-gas ventilation system for the HRLAF cells, (3) design and cost estimation of a contaminated off-gas filter carrier for general plant use; (4) completion of a new alpha laboratory in room 211 of building 3019; (5) completion of the relocated U^{233} solution storage facility in cell 3 of building 3019, (6) an independent hazards evaluation of the HRLEL, (7) a 16-hr course on radiochemical facility hazards evaluation prepared for and presented to the Office of Radiation Safety and Control.

Criticality Studies

Assistance efforts on criticality problems included (1) neutron multiplication measurements on the U^{233} storage tank in building 3019, (2) an

exhaustive study on the feasibility and safety of using soluble nuclear poisons as a primary criticality control; (3) design and installation of a stainless-steel-clad borax-filled poison network for the Fluoride Volatility Pilot Plant caustic filter; (4) drop-testing of the Pyrex-filled HRT fuel solution carrier.

Carriers and Chargers

A very thorough containment and safety review of the IWW carrier, for shipment of ~100,000 curies of waste solution from Hanford to ORNL, was made. This review was requested by Hanford and the AEC and was made under the proposed AEC shipping standard, CFR Title 10, Part 72.

Eurochemic Assistance

ORNL continued to coordinate the Eurochemic program and to review and exchange pertinent technical information. Preproject study (scope) for the Eurochemic facilities has been completed and detailed design is in progress. The overall project is about 40% designed and 10% constructed.. Current official costs are $24,000,000 for construction, with $30,700,000 total investment. Final plutonium purification will be by 10% TLA extraction followed by direct precipitation from the organic product. The final preproject study has been prepared for modifications and additional facilities needed for enriched uranium processing. A preliminary cost estimate indicates that $1,500,000 additional capital investment will be required.

Contents

1. Power Reactor Fuel Processing

Laboratory- and engineering-scale development of processes for recovering fissionable and fertile material from irradiated power reactor fuels is continuing. Work included cold chemical development of new head-end processes for stainless-steel- and Zircaloy-clad fuels and the more advanced graphite and ceramic fuels. Process development for the Darex, Sulfex, and Zirflex processes was completed, and work on head-end processes for graphite-base, uranium and thorium carbide, and UO_2-BeO fuels intensified.

The extensive corrosion-test program on candidate materials of construction for the new head-end processes was continued.

Cold and tracer-level solvent extraction compatibility studies were conducted on many of the fuel solutions prepared in the head-end development program.

The building 4507 hot cells were put back in operation after the completion of the extensive containment modifications, and verification tests of both the Zirflex head-end and modified Purex solvent extraction flowsheets for the Zircaloy-clad UO_2 PWR blanket were completed with fuel samples irradiated to 16,000 Mwd/ton.

The Sodium Reactor Experiment fuel-decladding program was successfully concluded, and the 250-ton fuel shear, the rotary feeder, and rotary leacher complex were installed and completely checked out.

In design, liaison with the Idaho Chemical Processing Plant design of the Darex Pilot Plant was well advanced, and criteria for the Chop-Leach Pilot Plant were nearly completed when these pilot plants were canceled in April 1962.

1.1 PROCESSES FOR GRAPHITE-BASE FUELS

Two classes of graphite fuels are being developed: those in which uncoated uranium and/or thorium oxide or carbide particles are dispersed homogeneously throughout the matrix, and the coated-particle fuels in which carbon-coated carbide or Al_2O_3-coated oxide fuel particles are dispersed throughout the matrix. Processes being developed for recovering uranium and thorium from these fuels are: (1) grinding followed by acid leaching of the uranium and/or thorium from the resultant powder, (2) combustion followed by dissolution of the oxide ash, (3) simultaneous disintegration and leaching in 90% HNO_3, and (4) chloride volatility methods.

Grind-Leach Process

Grinding followed by leaching is applicable to all types of graphite-base fuels and involves mechanical grinding of the fuel, followed by leaching of the resultant powder with a nitric acid solution. The uranium recovery from fuels containing uncoated particles increases with increasing uranium content of the fuel and with increasing nitric acid concentration in the leachant.[1,2] Recoveries are also enhanced by finer grinding (with fuel containing 2% uranium, recoveries increased from 96 to 99% on grinding from 4 to 325 mesh).[1] With fuels containing both uranium and thorium, the nitric acid leachant must contain about 0.05 *M* fluoride ion to ensure dissolution of the thorium.[3] Leaching of −200-mesh ungraphitized fuels (1 to 2% uranium, 8 to 20% thorium) twice – 4 hr for each leach, with boiling 13 *M* HNO_3–0.04 *M* NaF–0.1 *M* $Al(NO_3)_3$ – recovered at least 99.6% of the

[1]M. J. Bradley and L. M. Ferris, *Nucl. Sci. Eng.* 8, 432 (1960).

[2]M. J. Bradley and L. M. Ferris, *Recovery of Uranium and Thorium from Graphite Fuels. I. Laboratory Development of a Grind-Leach Process*, ORNL-2761 (Mar. 17, 1960).

[3]L. M. Ferris, A. H. Kibbey, and M. J. Bradley, *Processes for Recovery of Uranium and Thorium from Graphite-Base Fuel Elements. Part II*, ORNL-3186 (Nov. 16, 1961).

uranium and thorium.[3] However, when the same techniques were applied to −200-mesh graphitized specimens containing 1.5% uranium and 7.2% thorium, recoveries were only about 90% (Table 1.1). This behavior is unexplained at present.

Coated-particle fuels must be ground fine enough to ensure rupture of the particle coatings if adequate uranium and/or thorium recoveries are to be achieved. In preliminary laboratory tests with specimens containing 100- to 200-μ particles, uranium and thorium recoveries were greater than 99% when the specimens were ground to 200 mesh prior to leaching (Table 1.2).

Combustion-Dissolution Process

This process is applicable to all types of graphite fuels except, possibly, those containing Al_2O_3-coated particles.

The ignition temperature of most graphite fuels in oxygen is about 700°C, the actual combustion temperature being much higher. Carbon monoxide is the primary product formed unless there is an excess of oxygen. Selection of a suitable grate for the carbon burner is difficult, and the oxide ash produced is sintered. These conditions can be partially mitigated by burning at temperatures below 500°C. Preliminary experiments showed that the ignition temperature can be lowered several hundred degrees by use of a catalyst such as manganese, copper, or lead compounds. For example, as received, the United Carbon Products spectroscopic grade graphite does not ignite below 720°C in oxygen. The ignition temperature, however, can be lowered to about 345°C by presoaking the graphite in 0.07 *M* lead acetate solution. The catalytic effect is noticeable below the ignition temperature for each catalyst tested. Untreated

Table 1.1. Recovery of Uranium and Thorium by Leaching of Ground Graphitized Fuels Containing UO_2 and ThO_2

Specimens contained 1.5% uranium, 7.2% thorium, fuel particles uncoated; each leach, 4 hr

Particle Size (mesh)	Leaching Agent	Recoveries (%)					
		First Leach and 3 Washes		Second Leach and 1 Wash		Graphite Residue	
		U	Th	U	Th	U	Th
−4 +8	15.8 *M* HNO_3	86.7	84.0	2.6	5.7	10.8	10.3
−16 +30	15.8 *M* HNO_3	84.0	82.8	6.1	4.1	9.9	14.2
−200	15.8 *M* HNO_3–0.04 *M* NaF–0.04 *M* $Al(NO_3)_3$	91.4	88.0	0.95	1.6	7.6	10.4
−200	13 *M* HNO_3–0.04 *M* NaF–0.1 *M* $Al(NO_3)_3$	86.4	84.3	1.3	3.0	12	13
−200	15.8 *M* HNO_3	92.8	88.7	0.6	1.4	6.8	9.9

Table 1.2. Recoveries by Acid Leaching of −200-Mesh Coated-Particle Fuels

Fuel	Fuel Composition (%)		Leachant	Leaching Conditions	Recoveries (%)	
	U	Th			U	Th
Al_2O_3-coated UO_2	8.0		15.8 *M* HNO_3	One 6-hr leach	99	
C-coated UC_2-ThC_2	9.7	33.8	15.8 *M* HNO_3	Two 4-hr leaches	98.8	99.9
C-coated UC_2-ThC_2	9.6	33.5	13 *M* HNO_3–0.04 *M* NaF–0.1 *M* $Al(NO_3)_3$	Two 4-hr leaches	99.4	99.9

graphite showed at most a 0.4% weight loss when exposed for 3 hr in a stream of oxygen at 460°C, but a piece of graphite that had been soaked 3 min in 0.25 *M* $KMnO_4$ solution lost 34% of its weight under the same conditions (Table 1.3). Further work on such catalysts is now in progress.

The ash from fuel containing only uranium and carbon is readily dissolved in boiling nitric acid; the dissolvent for thorium-bearing fuel must contain fluoride ion.[3] Impurities or fuel element coatings such as iron or SiC produce ashes from which leaching of the uranium is not quantitative,[3,4] but the addition of other reagents such as HF or HCl to the nitric acid alleviates this problem.

The ash from fuels containing carbon-coated particles is readily dissolved in nitric acid or fluoride-catalyzed nitric acid, while that from fuels containing BeO-coated particles can probably be dissolved by one of the processes developed for sintered BeO.[5] Processing of fuels containing Al_2O_3-coated particles by the combustion-dissolution technique does not appear feasible owing to the inertness of sintered alumina to aqueous reagents.

[4] *Chem. Technol. Div. Ann. Progr. Rept., Aug. 31, 1961*, ORNL-3153.

[5] K. S. Warren, L. M. Ferris, and A. H. Kibbey, *Dissolution of BeO- and Al_2O_3-Base Reactor Fuel Elements. Part I*, ORNL-3220 (Jan. 30, 1962).

90%-HNO_3 Process

This process is applicable only to graphite fuels that do not contain coated fuel particles.[3,6] Uncoated fuel specimens containing 0.7 to 13% UO_2 disintegrated in 10 hr in boiling 21.5 *M* HNO_3 to powders having mean particle sizes of 100 to 170 μ (Fig. 1.1). Unfueled graphite was disintegrated only slightly, to a mean particle size of about 9000 μ, in the same time. Fuel elements coated with pyrolytic carbon (or SiC) will therefore require at least rough crushing prior to the 90%-HNO_3 treatment.

Uranium recoveries from both graphitized and ungraphitized fuels which did not contain coated fuel particles were generally greater than 99% after two 4-hr leaches with boiling 90% HNO_3 (Table 1.4). Thorium recoveries, however, were only about 95% in two leaches, but increased to greater than 99% when the fuel was leached a third time. The presence of 0.05 *M* HF in the leachant did not increase thorium recovery. Leaching temperature was important. With HTGR-2 fuel samples, uranium and thorium losses to the graphite residue were decreased from about 10 to 0.2% when the leaching temperature was increased from 25°C to the boiling point, about 93°C. The two types of

[6] M. J. Bradley and L. M. Ferris, *Ind. Eng. Chem.* 53, 279 (1961).

Table 1.3. Catalysis of Combustion of United Carbon Products Graphite[a]

Reaction time 3 hr

Catalyst[b]	Ignition Temperature (°C)	Combustion Temperature (°C)	Weight Loss (%)
None	720	311	0.00
		334	0.00
		459	0.37
		459	0.05
		471	0.23
0.07 *M* Lead acetate	345	311	3.2
		334	6.0
0.25 *M* $KMnO_4$	482	448	33.6
		459	34.4
3.15 *M* $Cu(NO_3)_2$	482	459	13.5
		471	11.9

[a] United Carbon Products Co. Ultra Purity Spectroscopic graphite, lot No. 5387, density 1.55 g/cc.

[b] Each specimen soaked 3 min in indicated solution.

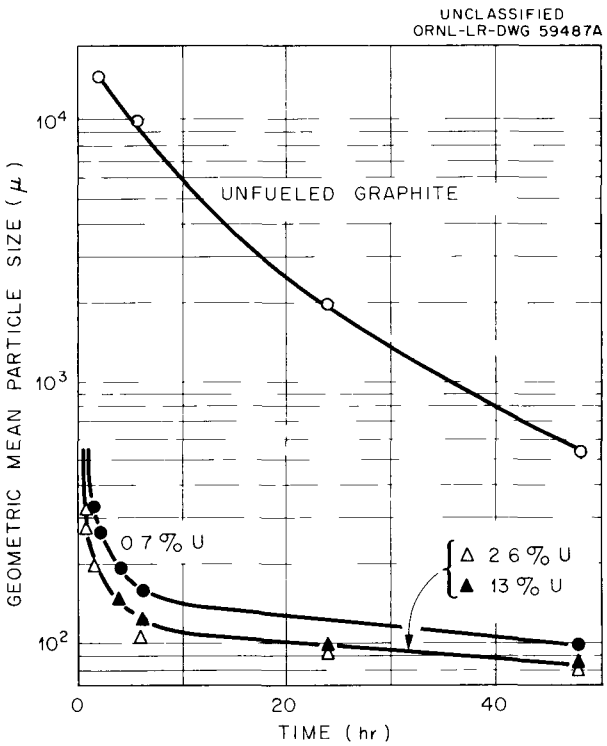

Fig. 1.1. Effect of Time and Uranium Content on the Mean Particle Size of the Residue from the Disintegration of Graphite-UO_2 Fuel Specimens with Boiling 90% HNO_3.

fuel samples used in these studies were: (1) HTGR-1 (High-Temperature Graphite Reactor), which contained about 1.5% uranium and 7.2% thorium as oxide particles dispersed homogeneously throughout an ungraphitized matrix; and (2) HTGR-2, which contained about 1.2% uranium and 15% thorium as 150-μ dicarbide particles dispersed in a graphitized matrix.

Neither the 90%-HNO_3 method nor electrolytic disintegration appears applicable to the processing of fuels containing pyrolytic-carbon- or Al_2O_3-coated particles. Although the graphite matrixes disintegrated readily in boiling 90% HNO_3, less than 7% of the uranium and thorium were recovered in two 4-hr leaches (Table 1.5). In one experiment a fuel specimen containing carbon-coated UC_2-ThC_2 particles was anodically disintegrated, but uranium and thorium recoveries were only 6.3 and 2.1% respectively. Similar results were obtained at Battelle Memorial Institute (BMI) with fuel containing Al_2O_3-coated oxide particles.[7]

Since the coated particles were not markedly affected by boiling 90% HNO_3, this method is being considered as a destructive test for determining

[7] R. A. Ewing, T. S. Elleman, and R. B. Price, *Trans. Am. Nucl. Soc.* 4(1), 152 (1961).

Table 1.4. Recovery of Uranium and Thorium from Uncoated Graphite Fuels by 90% HNO_3

Each leach 4 hr

Content (%)		Temperature (°C)	Recoveries (%)							
			First Leach and Washes		Second Leach and Washes		Third Leach and Washes		Residue	
U	Th		U	Th	U	Th	U	Th	U	Th
1.5	7.2	93	96.4	85.5	2.6	7.7			1.1	6.8
1.45	6.95	93	98.6	86.2	1.37	11.8			0.24	1.93
1.47[a]	7.14	93	97.6	87.2	2.37	7.98			0.16	4.81
1.50	7.21	93	97.7	85.5	2.31	13.0	0.10	1.17	0.06	0.25
1.18	14.3	25	80.7	83.7	8.0	5.8			11.4	10.4
1.28	15.0	93	95.3	99.0	4.58	0.88			0.10	0.16

[a] Leachant contained 0.05 *M* HF.

the effect of the fabrication method, itself, on the integrity of the particles. The amount of uranium (and/or thorium) dissolved during the acid treatment is related to the number of defective particle coatings. In testing of two types of carbon-coated UC_2 particles, only about 2% of the uranium was dissolved from batch 1 in two 6-hr leaches, indicating that the particle coatings were quite impervious to nitric acid (Table 1.6). However, with batch 2, about 48% of the uranium was solubilized in two leaches. Since the corresponding weight loss was about that expected assuming that no carbon was oxidized, it was concluded that the coatings on these particles were defective. Further evaluation of this testing technique is in progress.

In the processing of graphite-base fuel elements by the 90%-HNO_3 process (or the grind-leach process), the extent of graphite oxidation and the nature of the products formed are of interest. Preliminary experiments indicated that the graphite was attacked slightly or not at all when the nitric acid concentration is less than about 16 *N*. However, in boiling 90% HNO_3, graphite is slowly oxidized, yielding mainly volatile carbon oxides but also small amounts of water-soluble organic acids. With powdered samples of type GBF graphite, less than 3% was oxidized in reaction times up to 100 hr; even after 200 to 500 hr of digestion, only 60 to 70% of the graphite had been oxidized (Table 1.7). The color of the acid solution changed

Table 1.5. Uranium and Thorium Recovery from Coated-Particle Fuels by 90%-HNO_3 and Electrolytic Disintegration Methods

Each specimen leached twice, 4 hr each, with boiling nitric acid

Disintegration Method	Fuel	HNO_3 Conc (*M*)	Fuel Composition (%)		Recoveries (%)	
			U	Th	U	Th
90%-HNO_3	Pyrolytic-carbon-coated UC_2	21.5	4.0		1.5	
90%-HNO_3	Pyrolytic-carbon-coated UC_2	21.5	8.0		5.9	
90%-HNO_3	Pyrolytic-carbon-coated UC_2-ThC_2	21.5	9.7	33.5	6.5	4.6
90%-HNO_3	Al_2O_3-coated UO_2	21.5	8.0		0.8	
Electrolytic[a]	Pyrolytic-carbon-coated UC_2-ThC_2	15.8	9.9	33.1	6.3	2.1

[a]Specimen anodically disintegrated at 93°C; current density about 1 amp/cm^2.

Table 1.6. Evaluation of Carbon-Coated UC_2 Particles by 90%-HNO_3 Method

Each sample leached twice, 6 hr each, with boiling 90% nitric acid

Batch No.	Uranium Content of Sample (%)	Uranium Solubilized (%)		Weight Loss (%)	
		First Leach	Second Leach	Calcd	Experimental
1	69.24	0.34	2.5	1.9	0
1	68.58	0.33	1.0	0.9	0
2	44.00	11.8	35.8	21	16.9
2	43.86	11.5	36.4	21	17.2

Table 1.7. Reaction of Type GBF Graphite with Boiling 90% HNO_3

Run No.	Reaction Time (hr)	Total Carbon Oxidized (%)	Amount of Carbon Solubilized (%)	Neut. Eq. of Organic Acid Product (g/eq)	Amount of Mellitic Acid in Product (%)
1	50	1.6	~0.1	89	
2	100	2.3	~0.2	87.6	
3	212	69	5.8	62.7	60
4	350				57
5	475	56	3.0	59.2	77

from wine-red to yellow as the reaction time increased from 100 to 500 hr. Of the carbon oxidized, only about 10% was converted to organic acids. From 60 to 80% of the total acids was mellitic acid (benzene hexacarboxylic acid). The neutralization equivalent of the acids decreased from about 89 to 59 g/eq as the reaction time increased from 50 to 475 hr, suggesting that the precursors to mellitic acid were high-molecular-weight polynuclear acids. As expected, infrared analysis of the acids showed only C=O, O−H, and C−H bonding; there was no evidence of organo-nitro compounds.

Since graphite is only slightly attacked by nitric acid in normal processing times, most of the carbon found in solution on leaching fuels that contain carbides will result from the carbide-nitric acid reaction (see Sec 1.2).

1.2 PROCESSES FOR URANIUM AND THORIUM CARBIDE FUELS

Processing developments with these fuels included studies on the hydrolysis of various uranium and thorium carbides with water, acids, and caustic.

Hydrolysis of Uranium Monocarbide in Water, NaOH, HCl, and HNO_3

Near stoichiometric uranium monocarbide reacted with water at temperatures between 25 and 100°C to produce a greenish-brown uranium(IV) precipitate and 93 ml (STP) of gas per gram of carbide hydrolyzed, consisting chiefly of methane (86 vol %) and hydrogen (11 vol %),[8] with small quantities of saturated C_2- to C_8-hydrocarbons. The gaseous products contained all the carbon originally present in the carbide. Hydrolysis at 80°C of uranium monocarbide containing 17% dispersed uranium metal yielded the expected gaseous products and an additional 2 moles of hydrogen per mole of uranium metal.

Scouting studies indicated that hydrolysis of UC at 80°C with 6 *N* HCl or 20 *N* NaOH yielded the same hydrocarbon products as water did, although the reaction rates were much lower; complete reaction of a 4-g specimen required 3 hr in water, 5 hr in 6 *N* HCl, and 2 days in 20 *N* NaOH. When 20 *N* NaOH was used, only 70% of the uranium in the product solution was tetravalent, and the H/U atom ratio in the products was 4.32, compared with 4.01 for water or 6 *N* HCl.

When high-purity uranium monocarbide was reacted with boiling 4 and 16 *N* HNO_3, 32 and 21%, respectively, of the carbon was converted to a mixture of water-soluble polycarboxylic acids. The solutions produced were deep wine-red in color. These acid mixtures were isolated by extraction of the uranium from the dissolution product solution with tributyl phosphate and evaporation of the resulting uranium-free solution. Each mixture had a neutralization value of about 70 g per equivalent and was soluble only in polar solvents. X-ray diffractometry indicated that both mixtures contained mellitic acid (benzene hexacarboxylic acid) and oxalic acid. The mixture obtained by dissolving UC in 16 *N* HNO_3 contained about 50% mellitic acid. Further characterization of these mixtures of organic acids is in progress.

[8] M. J. Bradley and L. M. Ferris, "Hydrolysis of Uranium Carbides Between 25 and 100°C. I. Uranium Monocarbide," to appear in *Inorganic Chemistry*, Aug. 1962.

Preparation and Hydrolysis of Uranium Sesquicarbide and Dicarbide

All attempts to prepare pure U_2C_3 and UC_2 have been unsuccessful. Arc melting of $UC_{1.5}$ followed by heating at 1600°C for 60 hr yielded a material with the x-ray structure reported by Battelle for U_2C_3, but microscopy showed that the specimen actually contained large amounts of three impurity phases. The best synthesis of UC_2 by the ORNL Metals and Ceramics Division was a specimen with a combined-C/U ratio of 1.73 and a nominal composition of $UC_{1.93}$; however, after arc melting 12 times, much of the carbon was still present as graphite. Increasing the nominal C/U ratio above 1.93 actually decreased the combined-C/U ratio; that is, the nominal $UC_{2.00}$ specimen had a combined-C/U ratio of 1.68, while the nominal $UC_{2.20}$ mixture had a combined-C/U ratio of only 1.55. Attempts to increase the amount of combined carbon in $UC_{2.00}$ by increasing the number of arc melts from 12 to 24, increasing the time each was held molten from 2 to 4 min, and heating at 2000°C for 6 hr were all unsuccessful.

Since pure specimens of U_2C_3 and UC_2 were not available, the hydrolysis of several uranium carbide mixtures was investigated in hopes that some indication of the chemistry of the pure compounds would be obtained. For as-cast specimens, which should be mixtures of UC and UC_2, according to the phase diagram,[9] the volume of gas evolved and the methane concentration decreased as the combined-C/U ratio increased from 0.96 to 1.73, while the quantity of free hydrogen, saturated C_2- to C_8-hydrocarbons, unsaturated hydrocarbons, and nonvolatile hydrocarbons, including waxes, increased (Table 1.8, rows 2, 4, 5, and 6). The $UC_{1.5}$ specimen which had been heat-treated at 1600°C to form the sesquicarbide yielded considerably more saturated C_2- to C_8-hydrocarbons than the as-cast specimens, and virtually no methane (Table 1 8, last row). The uranium in the solid product was always tetravalent; therefore each uranium atom should yield four hydrogen atoms upon hydrolysis. The experimental H/C atom ratio for the saturated C_2- to C_8-hydrocarbons was 2.73 in all cases, which is close to the 2.67 shown by Eq. (3) below. Finally, the "missing" hydrogen (assuming 4H per U) to "missing" C (combined C minus gaseous C) ratio was always 1.6. Therefore, the primary reactions that occur in the hydrolysis of a uranium carbide mixture are:

$$U + 2H_2O \rightarrow UO_2 + 2H_2 , \quad (1)$$

$$UC + 2H_2O \rightarrow UO_2 + CH_4 , \quad (2)$$

$$U_2C_3 + 4H_2O \rightarrow 2UO_2 + 3CH_{2.67} \text{ (volatile, saturated hydrocarbons)} , \quad (3)$$

$$UC_2 + 2H_2O \rightarrow UO_2 + 2CH_{1.6} \text{ (mostly nonvolatile)} + 0.4H_2 , \quad (4)$$

For simplicity, the water of hydration was eliminated from the above equations. The nonvolatile products from the UC_2 hydrolysis have not been characterized. The estimated compositions of the fuel specimens, based on the above equations, are shown in Table 1.9.

While the extent of side reactions cannot be established until pure specimens of U_2C_3 and UC_2 are available, the estimated compositions based on these idealized equations should be useful, qualitatively, for studying carbide mixtures. These estimated compositions seem to indicate that heating of arc-melted $UC_{1.5}$ at 1600°C for 60 hr results in the disproportionation of the uranium monocarbide,

$$3UC \rightarrow U + U_2C_3 ,$$

while the uranium dicarbide is virtually unchanged. Thus, as-cast specimen 4B appeared to be about 2% U, 33% UC, 29% U_2C_3, and 36% UC_2, whereas, after being heated, specimen U_2C_3-1A seemed to be 13% U, 1% UC, 48% U_2C_3, and 37% UC_2 (Tables 1.8 and 1.9). Metallographically, the heated specimen was a four-phase mixture. Stoichiometric UC was stable to 60 hr of heating at 1600°C; therefore, the solid state reactions involved in the heating of $UC_{1.5}$ are more complex than those in the simple disproportionation of UC.

Hydrolysis of Thorium Monocarbide

The hydrolysis of thorium monocarbide was similar to that of uranium monocarbide, yielding 93 ml (STP) of gas per gram of sample, consisting principally of methane and hydrogen (Table 1.8, rows 2 and 3). The thorium monocarbide gave slightly

[9] *Proceedings of the Uranium Carbide Meeting Held at ORNL, Oak Ridge, Tenn., Dec. 1–2, 1960*, TID-7603, p 17.

Table 1.8. Reaction of Uranium and Thorium Carbides with Water at 80°C

Material Reacted	Specimen No.	Carbide Composition (mg atoms/g)			Hydrolysis Products							
					Volume of Gas Evolved (ml/g)	Gas Composition (mg atoms/g)					Nonvolatile Carbon Compounds[d] (mg atoms C/g)	
		Metal	Total C	Free C		Free H_2	C					
							CH_4	Saturated C_2-C_8 Hydrocarbons[b]	Unsaturated Hydrocarbons[c]	Total Gaseous Carbon	Total	Wax[e]
As-cast[a]												
$UC_{0.83}$	6B	4.03	3.33		105.8	3.43	2.83	0.48		3.31		
$UC_{0.96}$	2A, B, C	4.01	3.87		93.2	0.92	3.58	0.31		3.89		
$ThC_{0.98}$	ThC-1A	4.10	4.01		93.1	1.28	3.32	0.41	0.02	3.75	0.26	
$UC_{1.48}$	4B	3.91	5.83	0.04	63.9	1.75	1.29	1.69	0.28	3.26	2.53	0.60
$UC_{1.64}$	5B	3.87	6.69	0.34	49.6	1.33	0.70	2.03	0.39	3.12	3.23	1.33
$UC_{1.73}$	UC_2-1A	3.83	7.39	0.77	41.8	1.50	0.25	1.99	0.43	2.67	3.95	1.63
Heated 60 hr at at 1600°C												
$UC_{1.47}$	U_2C_3-1A	3.91	5.77	0.03	57.3	2.94	0.05	2.72	0.19	2.96	2.78	Present

[a] Ratio of combined carbon to uranium.

[b] All known isomers from C_2H_6 through C_6H_{14}.

[c] Ethylene, butene-1, *cis*- and *trans*-butene-2.

[d] By difference: combined carbon minus gaseous carbon.

[e] After dissolution of uranium residue in 6 *N* HCl.

Table 1.9. Estimated Composition of Uranium Carbide Mixtures

See text for assumptions

Specimen No.	Ratio of Combined C to U	Amount (wt %)					
		U	UC	U_2C_3	UC_2	Free Carbon	Total
6B	0.83	21.3	70.8	8.0		0.05	100
2A, 2B, 2C	0.96	5.8	89	5.3		0.05	100
4B	1.48	2	33	29	36	0.05	100
UC_2-4A	1.86		6.6	35	64	0.30	106
U_2C_3-1A	1.47	13	1.2	48.5	37	0.04	100

less methane, more hydrogen, and more higher hydrocarbons. This was expected because the microstructure showed greater carbide impurity (and therefore more free metal) in the ThC than in the UC.

1.3 PROCESSES FOR UO_2-BeO FUELS

Fuels with High UO_2 Content

Two methods for processing Gas-Cooled Reactor Experiment (GCRE) fuel elements, 70% UO_2–30% BeO pellets clad in Hastelloy-X (46% Ni, 22% Cr, 17% Fe, and 10% Mo), are being developed on a laboratory scale. In the first method, the fuel elements are chopped to expose the mixed oxide core, which is then dissolved in boiling 8 *M* HNO_3–2 *M* H_2SO_4 or 8 *M* HNO_3–0.5 *M* HF.[10] In the second method, a modified Darex process, the Hastelloy-X cladding is dissolved in boiling 2 to 4 *M* HNO_3 containing 3 to 5 *M* HCl, which also leaches the uranium and a small amount of the BeO from the core pellets, leaving the bulk of the BeO as an insoluble residue.

To demonstrate the feasibility of the chop-leach method, GCRE fuel pellets were dissolved in boiling 8 *M* HNO_3–2 *M* H_2SO_4 in the presence of a piece of Hastelloy-X. The pellets dissolved completely in 20 hr, but the Hastelloy dissolved at an average rate of only 2.8×10^{-3} mg min^{-1} cm^{-2}. The final solution contained about 4 g of uranium per liter. In a similar experiment, GCRE fuel pellets dissolved in boiling 8 *M* HNO_3–0.5 *M* NaF in 8 hr, while the Hastelloy dissolved at a rate of about 0.3 mg min^{-1} cm^{-2}. In the absence of fuel pellets, the dissolution rate of Hastelloy-X in the latter dissolvent was about 0.2 mg min^{-1} cm^{-2}.

In modified-Darex-process studies with simulated GCRE fuel elements (13 g of 66.5% UO_2–33.5% BeO pellets clad in 23.8 g of Hastelloy-X tubing), about 3 hr was required to penetrate the 30-mil cladding with 400 ml of boiling 3 *M* HNO_3–3 *M* HCl. At this point, rapid leaching of the UO_2 began. Leaching for 6 hr after decladding dissolved 99.8% of the uranium but only 20% of the beryllium oxide. Once dissolution of the uranium started, little further attack of the Hastelloy occurred. About 20% of the original cladding remained as a residue, mainly as solid end-caps. In boiling 2 *M* HNO_3–4 *M* HCl, a simulated fuel element was declad in about 3 hr, but in an additional 7 hr in the resulting solution the uranium recovery from the pellets was 99.6%, with only 28% of the BeO matrix dissolved. The product solutions from each experiment were essentially the same: about 40 g of Hastelloy, 20 g of uranium, and 0.5 to 1 g of beryllium per liter.

Fuels Containing < 10% UO_2

Sintered UO_2-BeO fuels containing more than 90% BeO are extremely difficult to dissolve in aqueous reagents.[10] The best solvents found were (1) concentrated sulfuric acid and (2) hydrofluoric acid containing ammonium fluoride. Sintered

[10] K. S. Warren, L. M. Ferris, and A. H. Kibbey, *Dissolution of BeO- and Al_2O_3-Base Reactor Fuel Elements. Part I*, ORNL-3220 (Jan. 30, 1962).

beryllia (density 2.87 g/cc, about 95% of theoretical) and BeO–5% UO_2 dissolved at about the same rates in boiling sulfuric acid solutions, the initial rates increasing from about 0.01 to 3.5 mg min^{-1} cm^{-2} as the acid concentration was increased from 4 to 16 *M* (Fig. 1.2). Approximate values for the initial rates can be calculated from the equation: log *R* (where *R* = rate expressed as mg min^{-1} cm^{-2}) = 0.223 × molarity of H_2SO_4 – 2.81.

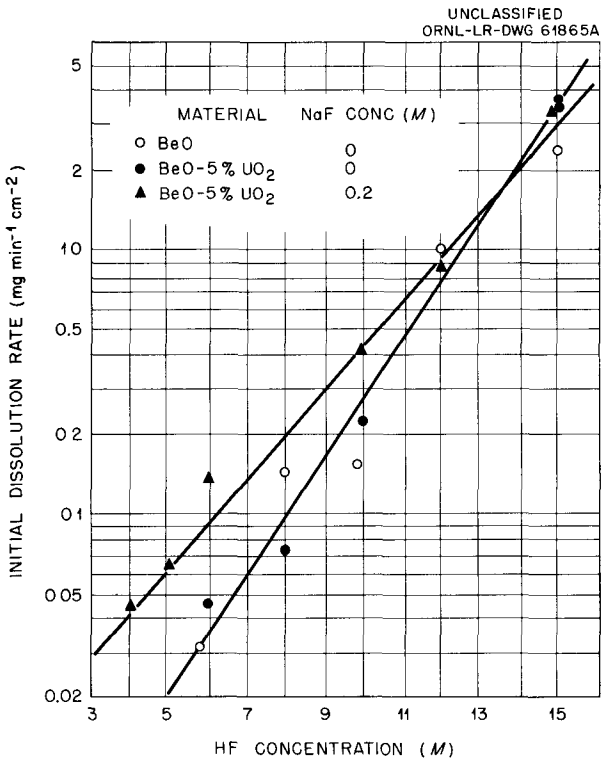

Fig. 1.2. Initial Dissolution Rates of BeO and BeO–5% UO_2 in Boiling Sulfuric Acid and H_2SO_4–0.2 *M* NaF Solutions.

In boiling HF solutions the initial rate of dissolution increased from 0 to about 1.5 mg min^{-1} cm^{-2} as the HF concentration increased from 0 to 20 *M* (Fig. 1.3). Addition of NH_4F to the solutions had only a slight beneficial effect on the dissolution rate when the HF concentration was <5 *M*; however, in 10 to 20 *M* HF solutions the rate was nearly doubled when NH_4F was present in concentrations of 3 to 5 *M*.

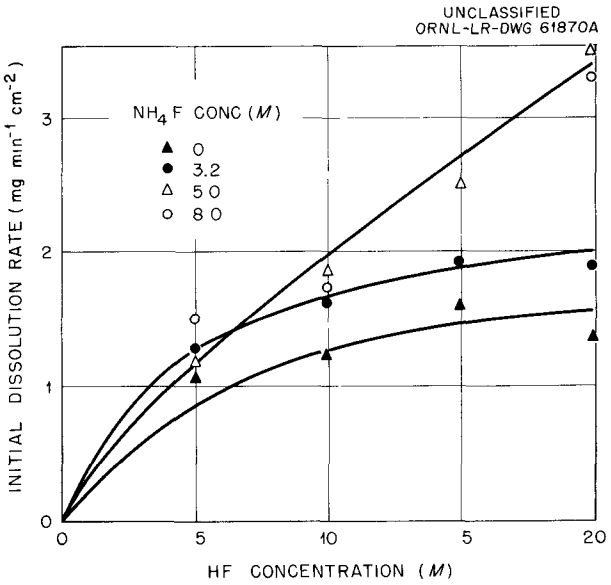

Fig. 1.3. Effect of Ammonium Fluoride Concentration on the Initial Dissolution Rates of BeO–5% UO_2 in Boiling Mixtures with Hydrofluoric Acid.

1.4 PROCESSES FOR ZIRCONIUM- AND STAINLESS-STEEL-CONTAINING FUELS

Neuflex Process

The Neuflex process (Fig. 1.4*a*) for recovering fissile and fertile material from zirconium-containing power reactor fuels was developed as an alternative to the Zirflex[11] and Modified Zirflex[12] methods (Table 1.10). The Neuflex process eliminates NH_4NO_3, which is used in the Zirflex dissolvent, and uses water rather than HNO_3-$Al(NO_3)_3$ to dilute the dissolution product to a more stable neutral-fluoride solvent extraction feed. The zirconium loading attainable is determined by the relation between the free fluoride and zirconium solubility and not by the degree of aluminum complexing. Higher terminal free-fluoride concentrations can be used than in the Zirflex process,

[11] J. L. Swanson, "The Zirflex Process," *Proc. U.N. Intern. Conf. Peaceful Uses At. Energy, 2nd, Geneva, 1958* 17, 155 (1959).

[12] T. A. Gens, *Modified Zirflex Process for Dissolution of 1–10% U-Zr Alloy Fuels in Aqueous NH_4F-NH_4NO_3-H_2O_2: Laboratory Development*, ORNL-2905 (Mar. 4, 1960).

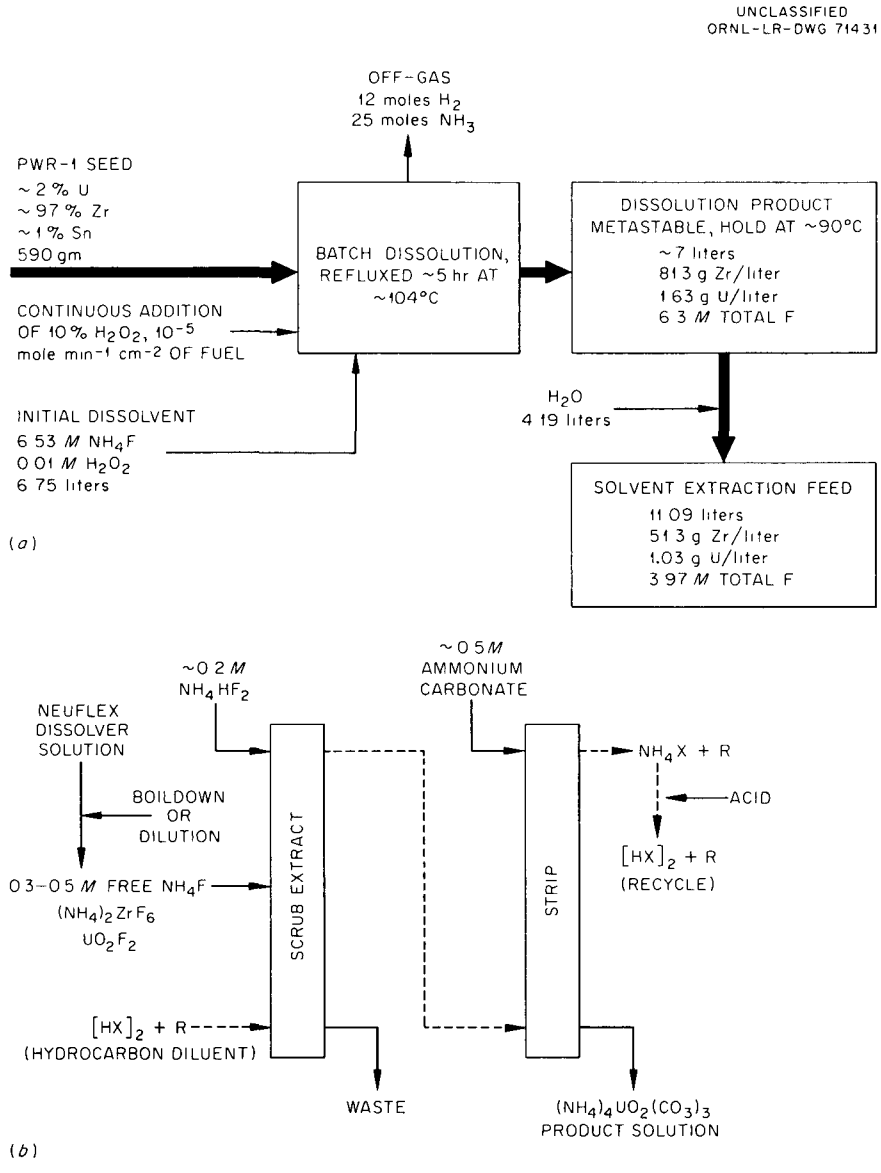

Fig. 1.4. Neuflex Process. (*a*) Dissolution of PWR-1 seed, (*b*) tentative extraction flowsheet. HX = di(2-ethylhexyl)phosphoric acid; R = trioctylphosphine oxide or diamyl amylphosphonate.

which results in shorter dissolution times. Uranium cannot be extracted by the conventional TBP method, but the Dapex[13] process reagents, di(2-ethylhexyl)phosphoric acid (D2EHPA) and diamyl amylphosphonate (DAAP), may be used.

Four batch dissolutions in small engineering-scale equipment (6-in. diam) demonstrated the feasibility of the Neuflex process for the dissolution of uranium-zirconium-tin fuels having uranium contents as high as 8% (Table 1.11). The dissolvent was 6.5 *M* NH_4F, and H_2O_2 was added continuously to oxidize U(IV) to the more soluble U(VI) immediately, thus preventing U(IV) precipitation from fuels containing more than 2% uranium. Instantaneous dissolution rates, which varied from 2 to 20 mg min^{-1} cm^{-2}, were similar to those obtained in the modified Zirflex process. Since oxidized zirconium dissolves by penetration of the oxide film and subsequent undercutting,

[13] *Chem. Technol. Div. Chem. Dev. Sect. C Progr. Rept. April–July 1961*, ORNL CF-61-7-76, p 6.

Table 1.10. Comparison of Three Related Processes for Dissolution of Zirconium Alloys

	Decladding (Removing Zircaloy Cladding from UO_2 Core Pellets)[a]		Integral Dissolution (Simultaneous Dissolution of Zircaloy Cladding and U-Zr Core Alloy)	
	Zirflex	Neuflex	Neuflex	Modified Zirflex
Uranium solubilized	Small amount, U(IV), lost	Small amount, U(VI); recovered by solvent extraction	All present, U(VI); recovered by solvent extraction	All present, U(VI); recovered by solvent extraction
Extractant	None[b]	Dapex	Dapex	TBP
Dissolvent	NH_4F-NH_4NO_3	NH_4F-H_2O_2	NH_4F-H_2O_2	NH_4F-NH_4NO_3-H_2O_2
Stabilizer	H_2O	H_2O	H_2O	HNO_3-$Al(NO_3)_3$
Gaseous products per mole of Zr dissolved	5 moles NH_3, traces H_2 and O_2	4 moles NH_3, 2 moles H_2	4 moles NH_3, 2 moles H_2	5 moles NH_3, traces $H_2 + O_2$
Scrubbed off-gas	Small volume of flammable mixture of $H_2 + O_2$	Large volume of $H_2 + O_2$; H_2 concentration above flammable range	Large volume of $H_2 + O_2$; H_2 concentration above flammable range	Small volume of flammable mixture of $H_2 + O_2$
Waste solution	Neutral fluoride	Neutral fluoride	Neutral fluoride	Acid aluminum fluoride

[a] After decladding by either process, the UO_2 pellets are dissolved in HNO_3 and the uranium is extracted with TBP.

[b] If only TBP extraction were available it is felt that the small amount of uranium lost (0.0 to 0.5%) to the decladding solution would not be recovered since relatively large volumes of acid waste would be generated.

Table 1.11. Summary of Neuflex Dissolutions in 6-in.-diam Batch Dissolver

Run No.	Dissolvent (*M*)		Fuel		F/Zr Ratio	H_2O_2 Addition Rate (moles min^{-1} cm^{-2})	Dissolution Time (hr)	Amount Dissolved (%)	Solvent Extraction Feed		
	NH_4F	NH_4NO_3	Type	Plate Thickness (in.)					Zr (g/liter)	U (g/liter)	F^-/U
5	6.53	0.00	8% U-Zr	0.122	8	0.5	2	100	31.9	2.8	51
7	6.53	0.53	8% U-Zr	0.122	8	1.2	3	99	33.3	2.9	82
8	6.53	0.15	8% U-Zr	0.122	8.8	2.0	2.3	100	32.3	2.65	82
9	6.53	0.00	~2% U-Zr (PWR seed)	0.081	7	1.1	4.7	>99	51.3	1.03	115

the surface condition of the material was an important determinant of the time required for complete dissolution.

The F^-/Zr ratio in the solution decreases steadily as dissolution proceeds, since each mole of zirconium in solution complexes 6 moles of fluoride. To minimize dissolution time and ensure solution stability, a terminal free-fluoride-to-uranium ratio of 50 to 100 must be maintained. For each value of the terminal ratio selected, a corresponding minimum dilution with water is required to keep the zirconium in solution.

The dissolution off-gas consisted of 4 moles of NH_3 and 2 moles of H_2, with traces of O_2 per mole of zirconium dissolved. The NH_3 was removed quantitatively by scrubbing with dilute nitric acid, which was recirculated through a packed tower. The remaining mixture of H_2 and O_2 was H_2-rich and generally above the limit of flammability for H_2-O_2 mixtures. Hydrogen evolution provided a convenient method of monitoring the dissolution progress. The addition rate of H_2O_2 was not critical so long as the concentration was sufficient to oxidize all uranium to yellow U(VI); excess H_2O_2 only diluted the product and contributed oxygen to the off-gas (Fig. 1.5). It should be possible to maintain the oxygen concentration in the off-gas at (3.5 ± 1.5)% by increasing the H_2O_2 addition rate during the period of rapid dissolution and decreasing it as dissolution approaches completion.

The tentative extraction flowsheet (Fig. 1.4*b*) uses di(2-ethylhexyl)phosphoric acid (D2EHPA, HX) in synergistic combination with a phosphonate ester or a phosphine oxide to extract the uranium. The nearly neutral dissolver solution is essentially a mixture of ammonium fluozirconate and free ammonium fluoride, with a low concentration of uranyl fluoride, pH about 6 (Table 1.12). D2EHPA presumably extracts the simple uranyl ion, in direct competition with its complexing by fluoride. Hence the extraction coefficients are strongly dependent on the free-fluoride concentration (Fig. 1.6*a*, negative slope ~3.5) and somewhat on pH in the range 5 to 7 (Fig. 1.6*b*, negative slope <1). The permissible fluoride concentration varies with both the D2EHPA concentration and the synergistic combination chosen, but <0.5 *M* appears satisfactory for ~0.1 *M* D2EHPA + 0.05 *M* TOPO (trioctylphosphine oxide) or ~0.3 *M* D2EHPA + 0.15 *M* DAAP (diamyl amylphosphonate).

Table 1.12. Composition of Neuflex Dissolver Solutions from Unirradiated Prototype Fuel Samples

Dissolver Solution No.	Solution Concentration (*M*)					pH
	U	Zr	F	NH_4	Free NH_4	
Z1	0.004	0.34	2.7	1.5	0.7	~6
C-Zr-9	0.006	0.55	3.4	1.6	0.5	6.0–6.4

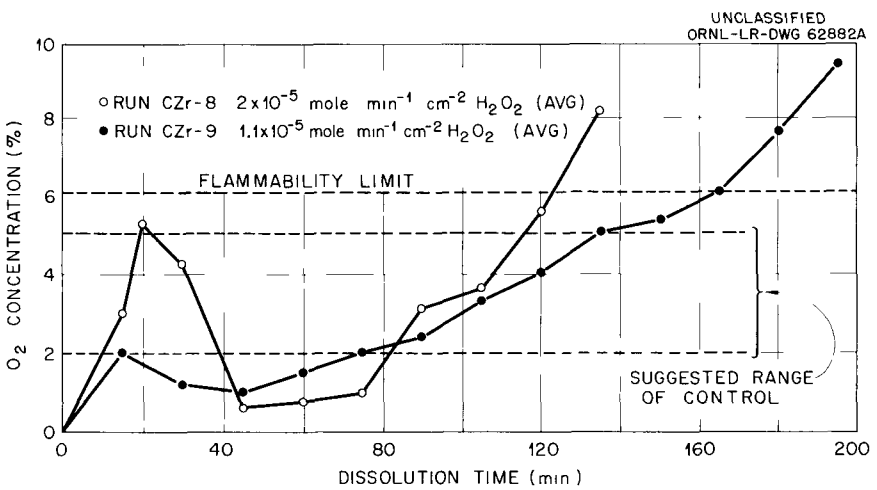

Fig. 1.5. Oxygen Concentration in Scrubbed Off-Gas from Neuflex Process as a Function of Dissolution Time.

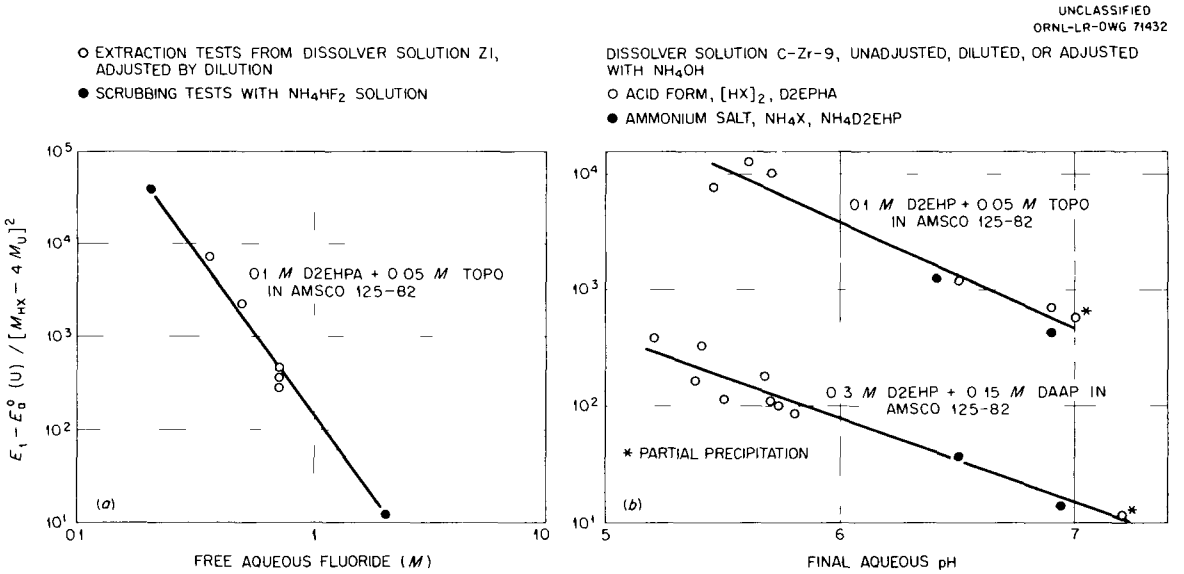

Fig. 1.6. Neuflex Extraction. Variation of uranium extraction with (*a*) aqueous free fluoride concentration and (*b*) pH.

The extraction coefficients are expected to vary with the square of the free D2EHPA concentration in extractions from complexing or noncomplexing solutions.[14] This is confirmed for the present system by the agreement of extraction isotherm data (Fig. 1.7) with the predicted form of the extraction equation, $E_a^o(U) = E_1(M_{HX} - 4M_U)^2$, where E_1 is the value of the intrinsic extraction coefficient extrapolated to 1 *M* free HX.

The flowsheet has not been tested in countercurrent operation, but the extraction, scrubbing, and stripping steps have been tested together in batch cascade (cross current) tests. In a typical test (Fig. 1.7), 99% of the extracted uranium was stripped in one stage and >99.8% in three stages at A/O = ½, and the overall decontamination factor of uranium from zirconium was ~10^4. The use of dilute ammonium bifluoride solution in the scrubbing section had almost no effect on the extraction section operation.

The ammonium carbonate stripping step has been studied in detail[15,16] with either a dilute

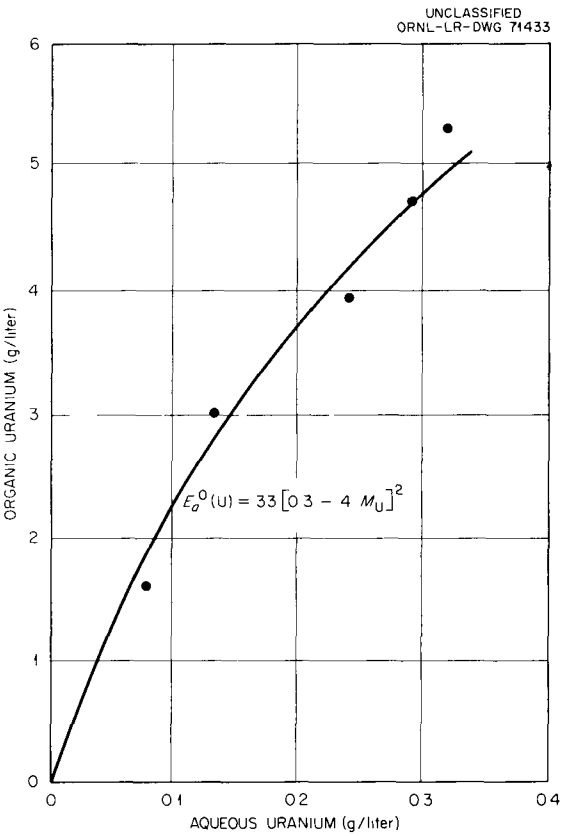

Fig. 1.7. Neuflex Extraction: Uranium Extraction Isotherm. From cascade test with 0.3 *M* D2EHPA + 0.15 *M* DAAP, dissolver solution Z1 diluted 1:1 with water.

[14] C. F. Baes *et al.*, "The Extraction of Uranium(VI) from Acid Perchlorate Solutions by Di(2-ethylhexyl)phosphoric Acid in *n*-Hexane," *J. Phys. Chem.* 62, 129–36 (1958).

[15] C. A. Blake *et al.*, *Progress Report, Further Studies of the Dialkylphosphoric Acid Extraction (Dapex) Process for Uranium*, ORNL-2172 (Dec. 18, 1956), p 41.

[16] F. J. Hurst and D. J. Crouse, *Recovery of Uranium from Di(2-ethylhexyl)phosphoric Acid (Dapex) Extractant with Ammonium Carbonate*, ORNL-2952 (June 30, 1960).

solution to produce an ammonium uranyl tricarbonate solution or with a more concentrated recycling solution to precipitate ammonium uranyl tricarbonate crystals. The extractant leaves the stripping section as the ammonium salt. Depending on the concentrations and volume ratios used, it may be expedient either to recycle the ammonium salt or to reacidify part or all of the extractant before recycle.

Zirflex Process Demonstration at Full Activity Level[17-19]

In 22 tests of the Zirflex decladding process for Zircaloy-2-clad UO_2 fuel, PWR blanket pins irradiated to levels between 182 and 17,700 Mwd/ton were successfully declad with boiling 6 *M* NH_4F–1 *M* NH_4NO_3. Cladding dissolution was complete, except for the end plugs, in 2.5 hr, in close agreement with results obtained with unirradiated specimens. Although some fuel-pellet fracture was observed, specially prepared high-density (96% of theoretical) UO_2 pellets were largely intact after decladding, while the regular PWR pellets of lower density (93 to 95% of theoretical) were extensively shattered into $\frac{1}{16}$- to $\frac{1}{4}$-in.-diam fragments (Table 1.13, Fig. 1.8). In the latter case 0.5 to 1% of the total UO_2 was reduced to fines smaller than 10 mesh. Soluble uranium and plutonium losses to the decladding waste solution, 0.01 to 0.09%, were virtually

[17] J. H. Goode and M. G. Baillie, *Hot-Cell Demonstration of the Zirflex and Sulfex Processes. Report No. 1*, ORNL TM-111 (Jan. 11, 1962).

[18] *Ibid., Report No. 2*, ORNL TM-130 (Jan. 26, 1962).

[19] *Ibid., Report No. 3*, ORNL TM-187 (in press).

Table 1.13. Uranium and Plutonium Losses During Decladding of Irradiated Zircaloy-clad UO_2 in 6 *M* NH_4F–1 *M* NH_4NO_3

Irradiation Level (Mwd/ton)	Theoretical UO_2 Density (%)	Pellet Condition[a]	Soluble U Loss (%)	Soluble Pu Loss (%)	Decladding Time (hr)	Dissolver Purge Gas
182	93–95	S	0.01	0.01	1.5	None
216		S	0.04	0.02	2.1	None
262		S	0.01	0.03	2.5	None
6,150		S	0.04	0.08	2.5	None
7,100		S	0.05	0.03	2.5	None
8,950		S	0.04	0.01	3.0	None
13,100		S		0.08	2.5	None
13,700		S	0.11	0.08	3.3	None
14,600	96	IF	0.04	0.06	3.5	None
14,600		IF	0.09	0.08	2.5	None
16,800		IF	0.08	0.01	2.0	None
16,800		IF	0.03	0.02	10.0	None
16,800		IF	0.07	0.02	8.0	None
16,800		IF	0.04		6.0	None
17,400		IF	0.07	0.05	3.5	Air
17,400		IF	0.09	0.01	4.1	Air
17,400		IF	0.08	0.01	3.0	Air
17,700		IF	0.05	0.04	4.0	None
17,700		IF	0.06	0.02	3.0	None
17,700		IF	0.04	0.01	3.0	N_2
17,700		IF	0.04	0.03	3.0	N_2

[a] S = Shattered; IF = intact or fractured.

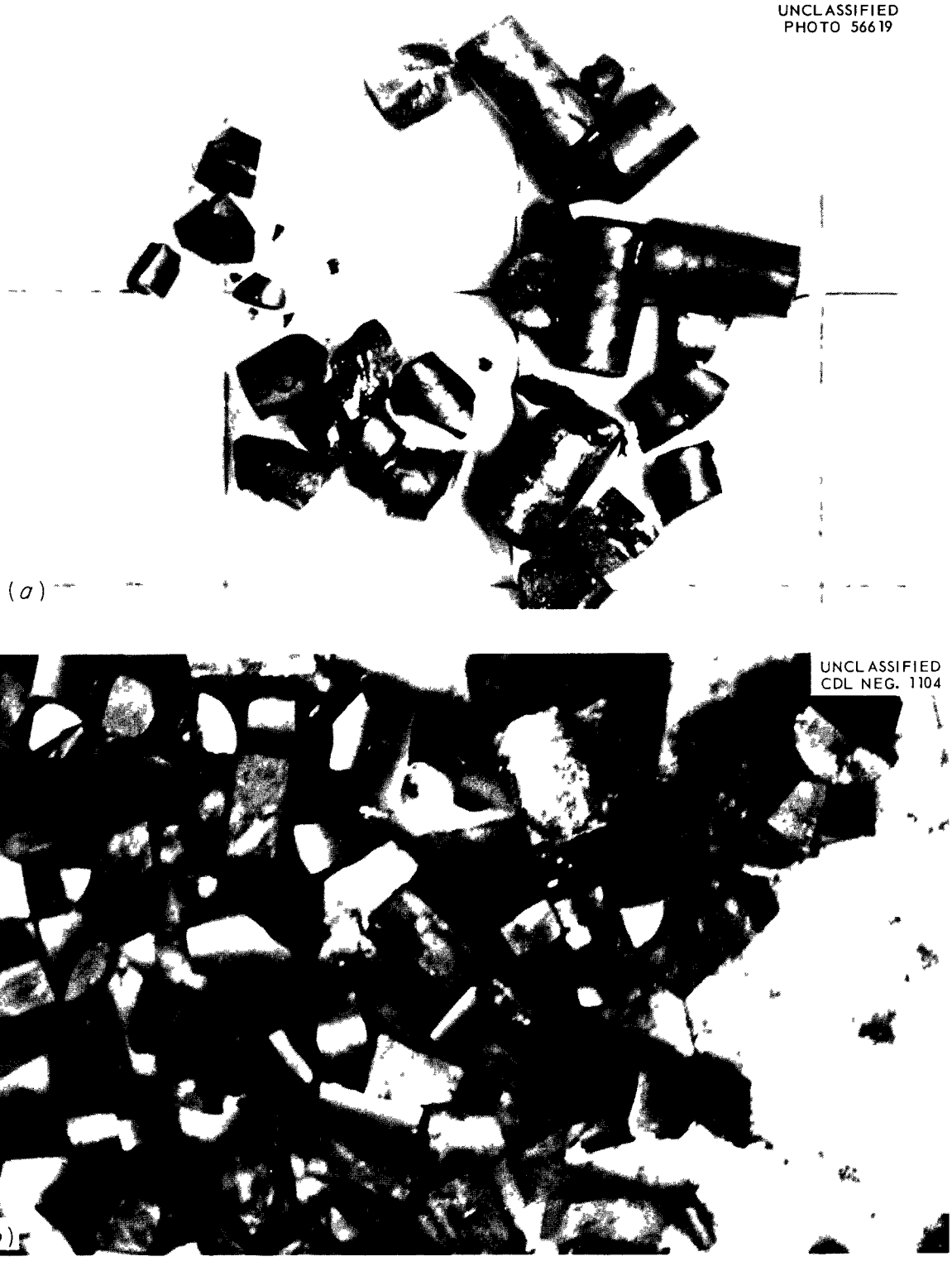

Fig. 1.8. UO_2 Pellets Declad by the Zirflex Process. (*a*) High-density pellets, 96% of theoretical, irradiated to 16,800 Mwd/ton; (*b*) low-density pellets, 93–95% of theoretical, irradiated to 6150 Mwd/ton. Photos taken on 1-in. grids.

unaffected by variables such as the time of pellet exposure to the decladding solution and the presence or absence of an oxidizing atmosphere (air). The uranium loss appears to be determined solely by the solubility of U(IV) in boiling 6 *M* NH_4F–1 *M* NH_4NO_3.

About 99.5% of both high- and low-density fuel pellets subsequently dissolved in 4 *M* HNO_3–0.1 *M* $Al(NO_3)_3$ in 5 hr, which was slightly faster than the rate for unirradiated pellets. Subsequent solvent extraction experiments with these solutions are described in Sec 1.6.

Zirconium Dissolution in Titanium Equipment

A flowsheet[20,21] for continuous dissolution of Zircaloy-2 in a titanium dissolver was developed in which refluxing 3 *M* HNO_3–1.2 *M* HF–0.4 *M* HBF_4–0.6 *M* Cr(III)–0.4 *M* Cr(VI)–0.46 *M* Zr is the dissolvent (Fig. 1.9). An instantaneous dissolution rate of 10 mg min^{-1} cm^{-2} and a titanium vessel corrosion rate of <0.1 mil/month are predicted from batch laboratory experiments. Tests in a small-scale continuous titanium dissolver are now proposed.

The dissolvent concentration is held constant by monitoring the product stream in order to adjust the rate of addition of dissolvent makeup, which is 5.5 *M* HNO_3–0.4 *M* HBF_4–0.5 *M* $(NH_4)_2Cr_2O_7$–1.2 *M* HF. The low titanium corrosion rate is achieved by pre-exposing the titanium to air and dissolvent in order to produce a protective surface film. The dissolver solution is stable at all temperatures from 20°C to the boiling point. Adjustment of the solution to 0.7 *M* Al^{3+} to complex fluoride ion before solvent extraction produces a 30% volume increase and yields a solution that is stable at room temperature but in which hydrolysis and precipitation occur on warming.

Another reagent investigated for use in continuous dissolution is 16 *M* HNO_3–2.6 *M* F^-–0.025 *M* HBF_4–1.4 *M* Zr. Short-term titanium corrosion rates were 0.1 mil/month, and Zircaloy-2 dissolution rates were 3 mg min^{-1} cm^{-2}.

[20] T. A. Gens, *Dissolution of Zirconium Reactor Fuels in Titanium Equipment*, ORNL TM-22 (Oct. 1961).

[21] W. E. Clark and T. A. Gens, *A Study of Dissolution of Reactor Fuels Containing Zirconium in a Titanium Vessel*, ORNL-3118 (Oct. 1961).

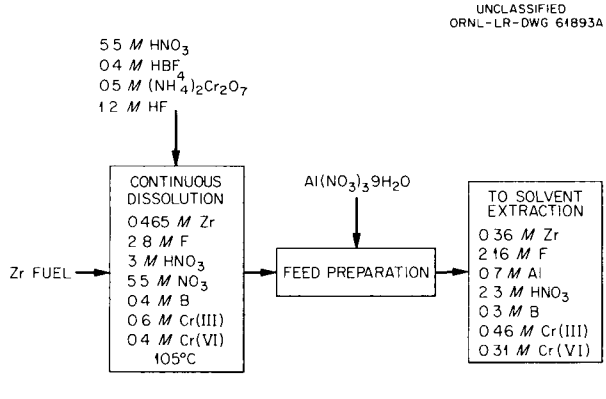

Fig. 1.9. Process for Dissolution of Zirconium-Containing Reactor Fuels in Titanium Equipment.

Removal of Chloride from Darex and Zircex Dissolver Solution

As alternatives to chloride distillation, NO and NO_2 stripping of Darex[22] dissolver solutions made 8 to 13 *M* in nitric acid, and H_2O_2 oxidation of Zircex[23] chloride solutions were studied.

With NO gas at 25°C as the stripping medium for Darex dissolver product in a 20-ft-high column and with NO (gas) to Cl^- (liquid) mole ratios of 4.5 and 7.5, chloride in the liquid effluent was decreased to 0.01 to 0.02 *M*. In small engineering-scale tests with NO_2 at 50°C, in 3-, 6-, and 20-ft-high packed columns, chloride removal was improved by greater column length, lower stainless steel concentrations, lower liquid rates, and higher vapor velocities. However, even with NO_2 in amounts greater than 400% of stoichiometric in the 20-ft-high column, the chloride concentration in the effluent was not decreased to the specified <350 ppm (0.01 *M*). Oxidation with hydrogen peroxide was not feasible for Darex solutions, since dissolved stainless steel catalyzes the decomposition of hydrogen peroxide and prevents its reaction with chloride, and chloride was only partially removed from chloride-zirconium systems. On addition of 50% of the stoichiometric amount of hydrogen peroxide to zirconium–11 *M* chloride

[22] W. E. Clark, J. R. Flanary, and F. G. Kitts, *The Darex Process: The Treatment of Stainless Steel Reactor Fuels with Dilute Aqua Regia*, ORNL-2712 (in press).

[23] T. A. Gens and R. L. Jolley, *New Laboratory Developments in the Zircex Process*, ORNL-2992 (Apr. 1961).

solutions at 98°C, the reaction $2HCl + H_2O_2 \rightarrow Cl_2$ (gas) + $2H_2O$ was 160% efficient (Fig. 1.10). However, the final chloride concentration was still 2.6 *M*. Increasing the amount of hydrogen peroxide to 150% of the stoichiometric amount decreased the chloride concentration to 0.07 *M*, but the overall efficiency for hydrogen peroxide usage decreased to 66%. At chloride concentrations below 3 *M*, hydrogen peroxide was less than 10% efficient. The presence of zirconium ions in 11 *M* chloride solution increased the efficiency by 33% over that for 11 *M* HCl alone.

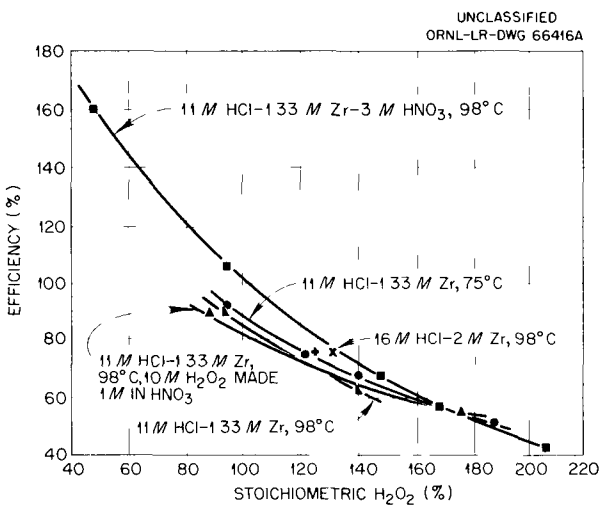

Fig. 1.10. Removal of Chloride from Zircex Waste Solutions by the Reaction $2HCl + H_2O_2 \rightarrow Cl_2(g) + 2H_2O$. Added H_2O_2 as 10 *M*.

Solids Removal from Darex Solutions

The presence of ~2 wt % of silicon in stainless steel–uranium dioxide cermet APPR fuel makes processing difficult in a continuous Darex system. As the fuel is dissolved in boiling 5 *M* HNO_3–2 *M* HCl, 50 g (dry weight) of hydrous, gelatinous $SiO_2 \cdot 3H_2O$ is precipitated per kilogram of fuel dissolved and then is deposited on the titanium equipment. The silica is removed from the solution by vacuum filtration at an average filtration rate in laboratory equipment of only 0.04 ml min^{-1} cm^{-2}. However, with the high-silicon-content APPR fuel and the presence of as little as 0.005 *M* HBF_4 during dissolution, a fluoride-stabilized silica precipitate formed which was (1) readily removed by vacuum filtration at an average rate of 0.5 ml min^{-1} cm^{-2} or (2) passed through the chloride stripping column without filtration. About 87% of the solids passed through the column, and those solids that were held up were easily washed through with hot nitric acid or water. During chloride stripping, 17% of the fluoride was volatilized and appeared in the nitric-hydrochloric acid condensate. The presence of 0.01 *M* zirconium decreased fluoride volatilization to 2% during chloride stripping.

The addition of fluoboric acid or molybdic acid to the nitric-hydrochloric acid dissolvent prevented the precipitation of silica by forming a soluble complex. Solubility was limited, however, and this approach would be practical only for stainless steel–uranium dioxide fuels containing $\leq$0.3 wt % silicon.

Zirconium Tetrachloride Desublimation

In the chloride volatility (Zircex) process in which zirconium-base fuel is reacted with HCl gas at ~500°C to produce nonvolatile UCl_3 and volatile $ZrCl_4$,[23] the collection of the sublimed zirconium tetrachloride has been a serious problem because of difficulties in the remote operation of a solids condenser and plugging at the point at which the off-gas is cooled below the zirconium tetrachloride sublimation temperature, about 300°C. The conventional dry-condensation method used in zirconium plants[24] is unsuitable for use in remotely operated radiochemical plants.

Laboratory-scale studies indicated the feasibility of removing zirconium tetrachloride from the Zircex process off-gas by hydrolysis during passage over boiling, near-azeotropic hydrochloric acid–zirconium solutions. A preliminary phase study of this system showed a series of hydrated compounds whose melting points increased from about 68 to 110°C as the zirconium concentration increased from 0.5 to 4.2 *M*. The boiling points of the solutions ranged between 100 and 112°C. Distillation removed hydrogen chloride and water but no zirconium.

---

[24] W. A. Du Praw, "Problems in the Processing of Zirconium and Its Compounds," from *First Conference, Analytical Chemistry in Nuclear Reactor Technology, November 4–6, 1957*, TID-7555 (August 1958), p 138.

Tests are planned on zirconium chloride removal from off-gas over product solutions as concentrated as 4 *M* zirconium, followed by rectification of the wet hydrogen chloride product gas and recycle of dry hydrogen chloride.

1.5 CORROSION STUDIES[25]

Corrosion studies included evaluation of materials of construction for the Darex, modified Zirflex, HNO_3-HF, and chloride-volatility fuel-processing methods. The containment of fuming nitric acid for the disintegration and leaching of graphite-base fuels, and of fuming nitric–sulfuric acid mixtures for dissolving beryllia was investigated. Other studies included the exposure of various materials in nitric acid vapor for possible fuel-processing and waste-disposal applications.

Darex Process

Equipment made of high-cobalt alloys may possibly be used for the processing of both stainless-steel-base fuels by the Darex process and zirconium-base fuels by the Zirflex or modified Zirflex processes. Welded specimens of Haynes alloys 6B, 25, and 21 all suffered intergranular attack in initial Darex solution. Overall maximum corrosion rates for the as-welded alloys were 3.64 (192 hr), 0.36 (408 hr), and 17.6 mils/month (192 hr), respectively. Heat-treatment of Haynes 21 lowered the rate to 3.27 mils/month, but the very low rates reported by Battelle Memorial Institute[26] for unwelded, cold-rolled specimens were not approached. Lowering the carbon content of the alloy and/or adding a carbide stabilizer should eliminate or decrease the tendency toward intergranular attack.

A proposed change in the Darex flowsheet may require the addition of up to 0.1 *M* HBF_4 in order to prevent plugging of the chloride stripping column by silica. Titanium was corroded at a maximum rate of 12.5 mils/month in a 120-hr exposure to spent Darex solution containing 0.1 *M* HBF_4. The rate in the proposed initial dissolver solution (5 *M* HNO_3–2 *M* HCl–0.1 *M* HBF_4–0.025 *M* $Na_2B_4O_7$) at 85°C was 60 mils/month.

Modified Zirflex Process

In modified Zirflex dissolution tests, welded type 347 stainless steel and unwelded Haynes 21 were corroded at maximum rates of 6.45 (500 hr) and 0.68 mil/month (689 hr), respectively, in flowing 5.4 *M* NH_4F–0.33 *M* NH_4NO_3–0.001 *M* H_2O_2 at the boiling point. The stainless steel suffered extensive edge corrosion and pitting attack. The Haynes 21 alloy was free from any visible localized attack.

Both LCNA[27] and type 347 stainless steel appear satisfactory for modified Zirflex solvent-extraction equipment. LCNA, Carpenter 20SNb, and types 304L and 347 stainless steel were exposed at 50°C in a number of possible modified Zirflex feed solutions with compositions varying from 0.75 to 1.5 *M* HNO_3, 0.6 to 1.0 *M* Al^{3+}, 0.36 to 0.49 *M* Zr^{4+}, and 2.44 to 3.33 *M* F^-. Overall maximum rates for all alloys varied from 0.04 to 0.25, from 0.08 to 0.46, from 0.38 to 0.49, and from 0.10 to 0.19 mil/month for exposures of 336, 336, 700, and 700 hr, respectively. In general, rates were higher in the higher acid solutions. Aluminum additions (~0.8 *M*) did not improve corrosion resistance appreciably. Both the 304L and Carpenter 20SNb showed intergranular attack; the type 347 stainless steel showed a light pickling, while the LCNA showed some local etching.

Multipurpose Centrifuge Tests

Tests designed to select a material of construction for a multipurpose centrifuge for clarification of dissolver solutions at 35°C from the Darex, Sulfex, and Zirflex processes[28] were completed. In tests with UO_2 core dissolver solution from the Zirflex decladding process, the maximum corrosion rates of titanium and Hastelloy F varied

---

[25] Work done by members of the Reactor Chemistry Division.

[26] P. D. Miller *et al.*, "Evaluation of Container Materials for Zircex and Darex Nuclear Fuel Recovery Processes," BMI-1242, Dec. 11, 1957; cf. *Ind. Eng. Chem.* 51, 32 (1959).

[27] A low-carbon nickel alloy similar to Ni-o-nel but with 0.005% carbon.

[28] *Chem. Technol. Div. Ann. Progr. Rept. May 31, 1961*, ORNL-3153.

from 0 to 8.5 and from 0.08 to 0.69 mils/month, respectively, depending on the concentration of uncomplexed fluoride, which varied from 0 to 0.09 *M*. Hastelloy F is superior to titanium for this service unless the fluoride is complexed.

Stainless Steel in Nitric-Acetic Acids

In tests in nitric-acetic acid mixtures which result from the stripping of plutonium from trilaurylamine, type 347 stainless steel showed excellent corrosion resistance under heat transfer conditions. The maximum rate was 0.02 mil/month for a 96-hr exposure in 1 *M* HNO_3–2 *M* acetic acid–45 g/liter $UO_2(NO_3)_2 \cdot 6H_2O$.[29] The specimen was exposed as a steam tube through which heat was supplied to the solution at about 5000 Btu hr^{-1} ft^{-2}. The solution temperature was about 103°C.

Corronel 230 in Nitric-Hydrofluoric Acids

Acid mixtures of fluoride and an oxidant are among the most versatile of aqueous dissolvents. A container material other than expensive gold or the platinum metals would be of great value to the nuclear fuel processing program.

Corronel 230, an alloy reputedly developed for nitrate-fluoride service,[30] permits some extension of the use of uncomplexed fluoride solutions. Unwelded Corronel was corroded at maximum rates of 59.9 and 2.83 mils/month (96 hr) in refluxing 10 *M* HNO_3–0.5 *M* HF at ~116 and 60°C, respectively. Low-carbon Hastelloy F,[31] type 309SNb stainless steel, and Haynes experimental alloys EB4358 and EB5459 all showed rates >200 mils/month under the same conditions, accompanied by aggressive localized attack. The Corronel suffered a severe but uniform acid etch in the boiling solution. When the fluoride was complexed by the addition of 0.75 *M* $Al(NO_3)_3$, the Corronel rate (408 hr) was lowered to 0.71 mil/month, compared with 0.28 mil/month for titanium. Corronel dissolved at rates $\geq$ 2700 mils/month in tests of 4 hr duration in boiling 1 *M* HNO_3–3 *M* HF; at 60°C the maximum rate was 4.97 mils/month and occurred in the vapor phase. In boiling 1 *M* HF, Corronel was corroded in the solution phase at a maximum rate of 43.7 mils/month for a 48-hr exposure; in boiling 1 *M* HF–0.06 *M* H_2O_2 the maximum rate was 12.7 mils/month and occurred in the vapor phase.

Nitric Acid Corrosion

Titanium has been found to be the most resistant of the conventional materials of construction to boiling nitric acid in both solution and vapor phases. Tests in connection with the UO_2 core dissolution steps that follow the Darex, Sulfex, and Zirflex decladding and the chloride-volatility processing schemes indicate that stainless steel and nickel alloys are susceptible to intergranular attack in the vapor phase. The maximum corrosion rate observed for titanium in a nitrate system was about 0.75 mil/month for a 1000-hr exposure.[32]

Ni-o-nel suffered aggressive intergranular attack in the vapor above boiling nitric acid. Maximum overall rates were 1.3 (1344 hr), 1.9, 3.4, 7.2, 20.5, and >36 mils/month (648 hr) in 4, 6, 8, 10, 12, and 15.8 *M* HNO_3, respectively; overall rates increased with exposure time. LCNA[27] and Hastelloy F suffered intergranular attack above boiling 6 *M* HNO_3; overall rates were 1.89 and 2.35 mils/month, respectively, in a 672-hr exposure. Previously reported tests in which type 347 stainless steel was compared with these two alloys in and above boiling Purex waste solution[28] indicated its resistance value falls between them. Maximum rates for titanium, on the other hand, were 0.03 mil/month above refluxing initial Purex waste solution (1000 hr) and 0.33 mil/month above refluxing 15 *M* HNO_3–1.0 *M* H_2SO_4 (1145 hr). There was some localized attack in the heat-affected zone near weldments in the latter solution.

In boiling 4 *M* HNO_3, Nichrome V and INOR-8 were corroded at maximum rates of 0.21 (672 hr) and >295 (115 hr) mils/month, respectively. The

---

[29] Uranium was used as a stand-in for plutonium in the tests.

[30] D. M. Donaldson *et al.*, *Reprocessing Fast Reactor Fuels at Dounreay*, presented at the AIME Annual Meeting, Oct. 25, 1961.

[31] A special vacuum-melted heat obtained from R. F. Maness at Hanford.

[32] *Chem. Technol. Div. Ann. Progr. Rept. Aug. 31, 1960*, ORNL-2993.

INOR-8 specimen in the solution disintegrated, and the Nichrome V vapor-phase specimen showed incipient grain boundary attack, although none was observed on the solution or interface specimens. Corronel 230 suffered intergranular attack in refluxing 20 to 23 *M* HNO_3; the maximum rate for 384 hr of exposure was 7.27 mils/month. The rate for titanium in the same solution was 0.07 mil/month for 168 hr. In a boiling mixture (50 g of uranium per liter, free graphite, and 20 *M* in HNO_3), titanium, mild steel, and type 1100 aluminum were corroded at rates of 0.03 (164 hr), 688 (24 hr), and 127 (24 hr) mils/month, respectively. The addition of 300 ppm of fluoride did not passivate the aluminum, but in boiling 23 *M* HNO_3–1 *M* HF, type 6061 aluminum was corroded at a maximum rate of only 0.01 mil/month vs 0.6 mil/month for type 304SNb stainless steel in 144 hr of exposure. In 90% (21 *N*) HNO_3–10% (36 *N*) H_2SO_4, Nichrome V, Carpenter-20SNb, types 347 and 304L stainless steel, INOR-8, LCNA, and CD4MCu were corroded at maximum rates of 0.20, 2.6, 4.1, 3.1, 0.17, 0.52, and 1.74 mils/month in exposures of 24, 24, 96, 96, 672, and 672 hr, respectively.

Chloride Volatility Process

Materials of construction are available for a chloride volatility process, but the approximate conditions and cycle times must be known in order to make more definitive corrosion tests. Specimens of Haynes 25, Nichrome V, and INOR-8 exposed 24 hr to flowing chlorine at temperatures between 490 and 730°C showed average rates of 6, 2, 0.7, and 800, 800, 100 mils/month at 500 and 700°C, respectively. There was considerable scatter in the data, probably because of small variations in temperature and gas-flow rates. Rates for Nichrome V and Haynes 25 in CCl_4-N_2, required for decomposing ZrO_2, were identical with those for chlorine within the probable experimental error. Rates for 188-hr exposures in oxygen at 725°C were 0.02, 0.01, 0.01, and 0 mil/month for Haynes 25, Nichrome V, INOR-8, and Pyroceram 9608, respectively. Rates for 34-hr exposures of these same materials in dry HCl at 600°C were 5.30, 5.63, 16.4, and 1.2 mils/month, respectively, but possibly would be lower with adequate temperature control.

1.6 SOLVENT EXTRACTION STUDIES

Zirflex Process Evaluation at Full Activity Level

First-Cycle Solvent Extraction Tests. – Solvent extraction runs were conducted in miniature mixer-settlers with highly irradiated (16,000 Mwd/ton) pellet solutions obtained from the Zirflex head-end experiments (Sec 1.4). A modified Purex process was used to test the compatibility of uranium and plutonium recovery from the highly irradiated fuel solution by extraction with 30% tri-*n*-butyl phosphate in Amsco 125-82. In one cycle, uranium and plutonium were recovered nearly quantitatively and decontaminated from gross fission product gamma activities by factors of 2×10^4 and 7×10^3, respectively. No deleterious effects on decontamination or recovery of uranium and plutonium were observed as a result of the increased level of irradiation over that encountered in the standard Purex process. However, some solvent degradation was noted during recycle of the TBP diluted with Amsco 125-82.

Solvent Degradation. – In an auxiliary experiment to the Zirflex solvent extraction tests described above, the same solvent was recycled six times through a solvent extraction system to determine the solvent degradation effects of multiple contacting. Batch equilibrations were made in order to simulate operation of the process in the mini-mixer settlers through the six cycles of extraction, scrubbing, and stripping, followed by two sodium carbonate washes and one nitric acid wash for solvent cleanup prior to recycle. The feed-solution uranium concentration was about 100 g/liter. Activities were 10^8 gross alpha counts min^{-1} ml^{-1}, 10^7 plutonium alpha counts min^{-1} ml^{-1}, 10^{10} gross gamma counts min^{-1} ml^{-1}, and 10^{10} gross beta counts min^{-1} ml^{-1}, which exposed the solvent to energies of about 0.6 whr/liter per cycle. The first tests made with purified TBP diluted with Amsco 125-82, a branched-chain hydrocarbon containing about 7% unsaturates formed by the polymerization of butenes and pentenes, showed radiation degradation, with the formation of uranium-retaining agents that could not be removed from the organic phase by the carbonate and acid washes. After six cycles, the cleaned solvent retained between 0.5 and 1.8 g of uranium per liter. In a second test, TBP diluted with *n*-dodecane or its commercial equivalent Adakane-12 did not show the

same degradation, and after six cycles retained only 0.09 g of uranium per liter. Plutonium retention and decontamination from fission products did not appear to be affected by either diluent at these radiation levels.

Development of Flowsheets for Thorium-Uranium Fuel

The acid Thorex process for use with stainless-steel-clad UO_2-ThO_2 Consolidated Edison fuel was further modified, and nitric acid leaching of ThO_2 slurry fuel as a means of removing fission products was evaluated. Other work included (1) the development of an adsorption process with powdered unfired Vycor glass as the adsorbent and a solvent extraction process with 30% TBP as the extractant for Pa^{233} recovery, (2) ion exchange and solvent extraction studies on cleanup of stored U^{233}, and (3) diluent studies for the acid Thorex process.

Darex-Thorex Process. – Additional experiments were made with the acid Thorex process,[33–35] designed for thorium-uranium fuels decayed for six months or thereabouts in order to avoid the necessity of Pa^{233} recovery. Results showed that the 2 to 3% uranium and thorium loss may be recovered from the solution (Darex-process-dissolved stainless steel cladding) by adding chloride-free cladding solution to the lower section of the acid Thorex extraction column.[36] Uranium and thorium losses were 0.001 and 0.4%, and decontamination factors for ruthenium, zirconium-niobium, and rare earths were 560, 9000, and 2.5×10^5, respectively. These results are not substantially different from the values obtained with the usual acid Thorex process where 13 *M* HNO_3 is added below the extraction feed plate.

ThO_2 Slurry Fuel. – In laboratory experiments with prepumped ThO_2 slurry from the Reactor Chemistry Division in-pile loop, < 1% of the fission product activity was removed by boiling in 1 *M* or 5 *M* HNO_3 for 6 hr. In similar experiments reported in the literature,[37] with ThO_2 to which Ce^{144} had been added to simulate irradiated material, > 70% of the activity was removed.

Recovery of Pa^{233}. – In processing of short-decayed thorium-uranium fuel by present flowsheets, the protactinium is relegated to waste which is reprocessed several months later, after the Pa^{233} has decayed to U^{233}, in order to recover the uranium. Two new methods were developed, using tracer quantities of Pa^{233}, for the separation and recovery of the protactinium during the initial processing.

In the first method, protactinium was removed from aqueous nitrate and hydrochloric acid solutions by adsorption on unfired Vycor glass powder. In the early experiments the protactinium-containing solutions were batch-mixed with the Vycor, but in later experiments the solutions were run through small Vycor-packed glass columns. The adsorption coefficients were computed as follows:

$$\frac{\text{counts/min of } Pa^{233} \text{ per gram of Vycor}}{\text{counts/min of } Pa^{233} \text{ per milliliter of feed solution}} .$$

In 15-min batch contacts of nitric acid solutions of Pa^{233} (6×10^5 counts min^{-1} ml^{-1}) with 10 g of 100- to 200-mesh Vycor per liter of solution, under nonequilibrium conditions, the coefficients increased from ~400 in 1 *M* HNO_3 to a maximum of 1500 in 6 to 8 *M* HNO_3. No adsorption was observed from a 0.1 *N* acid-deficient solution (Table 1.14). Although the adsorption capacity has not been measured, preliminary experiments with 6 *M* HNO_3 showed that > 6 μg of Pa^{233} (120 mc) may be adsorbed on 1 g of 100- to 200-mesh Vycor, with no decrease in the adsorption coefficient.

The adsorption of protactinium from nitrate solutions was directly dependent on the contact time, the nitrate salt concentration of the solution, and the particle size of the Vycor. Adsorption was essentially at equilibrium after 1 hr of contact. An adsorption coefficient of 3×10^3 was obtained on a 60-min contacting of a 6 *M* HNO_3 solution containing 5×10^5 counts min^{-1} ml^{-1} Pa^{233} with 10 g of Vycor (100 to 200 mesh) per liter (Table 1.14). Coefficients were lower for solutions that

[33] *Chem. Technol. Div. Ann. Progr. Rept. May 31, 1961*, ORNL-3153.

[34] R. H. Rainey and J. Moore, *Nucl. Sci. Eng.* 10(4), 367–71 (1961).

[35] ORNL-3155 (in press).

[36] *Chem. Div. Sec. B Quart. Progr. Rept. Apr.–June 1961*, ORNL TM-1.

[37] D. G. Gardner, *Nucl. Sci. Eng.* 10, 228–34 (1961).

Table 1.14. Adsorption of Protactinium on 100–200 Mesh Unfired Vycor

Contact Time (min)	Adsorption Coefficient						
	0.1 *M* Acid Deficient	0.1 *M* HNO_3	1 *M* HNO_3	4 *M* HNO_3	6 *M* HNO_3	8 *M* HNO_3	10 *M* HNO_3
15	0	470	420	1100	1500	1600	1400
60	0.2	750	760	2150	3100	2900	2200
240	0	1400	880	2400	3200	2900	2800

were 0.1 *N* in HNO_3 and 6 *N* in various nitrates [e.g., 2300, 1000, 1000, 820, 210, and 20 in the presence of 6 *N* $Al(NO_3)_3$, $NaNO_3$, NH_4NO_3, $Ca(NO_3)_2$, $LiNO_3$, and $Th(NO_3)_4$, respectively]. The effectiveness of the thorium in decreasing the adsorption of Pa^{233} from nitric acid solutions varied inversely with the nitric acid concentration. About 1.5 times as much thorium was required in 2 *M* HNO_3 as in 0.1 *M* HNO_3 in order to decrease the coefficient by a factor of 10.

In a column experiment, 97% of the Pa^{233} was adsorbed along with less than 0.01% of the thorium. The solution was 6.2 *M* in HNO_3, had a thorium concentration of 116 g/liter, and a Pa^{233} concentration of 3.76×10^6 counts min^{-1} ml^{-1}; 250 ml was used. The column was 27 cm long, 8 mm in diameter, and contained 80- to 100-mesh Vycor. The average flow rate was 2.2 ml min^{-1} cm^{-2}. Eighty percent of the adsorbed activity was removed by passing 25 ml of 0.5 *M* oxalic acid through the inverted column at a flow rate of 1.0 ml min^{-1} cm^{-2}. The product solution contained less than 0.05 mg/ml Th and 2.9×10^7 counts min^{-1} ml^{-1} Pa^{233}, or 7.6 times the protactinium concentration of the feed. Subsequent eluate contained a lower concentration of protactinium, but the concentration could be increased by increasing the contact time of the glass with the eluant.

In hydrochloric acid solutions Pa^{233} adsorption maxima occurred at 0.1 and 4 *M* HCl, and a minimum occurred at 1 *M*. The coefficients were 430, 300, and 180, respectively, and decreased to 71 as the acid concentration was further increased to 10 *M* HCl. The protactinium tracer was added to the HCl solutions as irradiated $Th(NO_3)_4$, which contributed 0.06 *M* nitrate to the solutions.

The second method developed for the recovery of Pa^{233} is a low-decontamination solvent extraction process, in which protactinium, thorium, and uranium are separated from neutron poisons by coextraction with TBP. High decontamination from low-cross-section fission products such as zirconium and niobium is not necessary because the product must be remotely handled in subsequent operations. Flowsheet conditions were:

Feed	Th, 40 g/liter; U, 2.5 g/liter; 5 *M* in HNO_3; 1 *M* in $Al(NO_3)_3$; 0.04 *M* in F; 1 vol
Scrub	5 *M* in HNO_3; 1 *M* in $Al(NO_3)_3$; 0.4 vol
Extractant	30% TBP in Amsco
Stages	5 extraction, 4 scrub

About 98% of the protactinium and >99.9% of the uranium and thorium were separated from ruthenium and rare earths by factors of 70 and 10^5, respectively. Most of the zirconium and niobium were extracted with the fuel. Protactinium material balances were unsatisfactory, ranging from 90 to 170%.

The quantity of protactinium in fully irradiated Consolidated Edison Thorium Reactor fuel will equal about 0.1% of the weight of thorium at the time of discharge. This would result in a protactinium concentration of about 20 ppm in the solvent extraction feed if processed 30 days after discharge. Since the solubility of protactinium[38,39] in this system is largely unknown, a complete study of its solubility in nitrate systems was started.

[38] Thompson, AECD-2488, AECD-1897.

[39] H. F. McDuffie, *HRP Quart. Progr. Rept.*, ORNL-3061 and ORNL-3167.

Removal of Thorium from U^{233} Product. – In order to minimize the shielding requirements for the handling of U^{233} in fuel fabrication,[40] the uranium is generally reprocessed just before use in order to remove the decay daughters of the contaminant U^{232}, principally Th^{228}. This problem is pertinent because of the forthcoming Brookhaven National Laboratory (BNL) Kilorod commitment. Both ion exchange and solvent extraction processes removed >99% of the thorium from the uranium in laboratory experiments with synthetic solutions.

In the ion exchange experiments a solution containing 25 g of uranium and 0.25 g of thorium per liter and 0.25 *N* in HNO_3 was passed through a 50- to 100-mesh Dowex 50-8X ion exchange column at about 0.7 ml min^{-1} cm^{-2}. After 8 g of uranium per milliliter of resin had been passed through the column, the resin contained 99% of the thorium and 1% of the uranium. More than 99% of the uranium and 3% of the thorium adsorbed on the resin were eluted by 20 vol of 0.5 *M* HNO_3 fed at a rate of 1 ml min^{-1} cm^{-2}. The remaining thorium, which contained about 0.01% of the original uranium, was eluted with about 20 vol of a mixture that was 3 *M* in ammonium acetate and 1.5 *M* in acetic acid. The flow rate was 1 ml min^{-1} cm^{-2}.

Several processes were developed for use in the Thorex Pilot Plant solvent extraction processing equipment for cleaning up stored U^{233} for the BNL Kilorod program. A decontamination factor from thorium of 100 is adequate. The addition of 0.03 *M* NaF to the 0.1 *M* $Al(NO_3)_3$ scrub in a Purex-type flowsheet increased decontamination from thorium by a factor of about 4 over the value obtained with 0.1 *M* $Al(NO_3)_3$ alone. With a scrub 0.03 *M* in NaF and 0.3 *M* in NH_4NO_3, thorium in the product was below analytical detection. Processes using 2.5% TBP or 2.5% di-*sec*-butyl phenyl phosphonate as extractant, aluminum nitrate or thorium nitrate as salting agent, and either static or countercurrent scrub were all satisfactory.

The most satisfactory flowsheet, with 2.5% di-*sec*-butyl phenyl phosphonate extractant, decontaminated the product from thorium by a factor of about 10^6. Flowsheet conditions were:

Feed	U, 5 g/liter; 1.5 *M* $Th(NO_3)_4$; 0.8 *M* $Al(NO_3)_3$, 0.075 *N* acid deficient; 1 vol
Scrub	0.6 *M* $Al(NO_3)_3$, 0.075 *N* acid deficient; 0.4 vol
Extractant	2.5% di-*sec*-butyl phenyl phosphonate in diethyl benzene, 2.0 vol
Stages	6 extraction, 3 scrub

Diluent for Acid Thorex Process. – The use of *sec*-butyl benzene as a diluent for TBP in the acid Thorex process resulted in a fivefold increase in decontamination over Amsco 125-82 or Solvesso-100. However, when the solvents were degraded by 1 hr of refluxing in 6 *M* HNO_3, the decontamination factor with Amsco 125-82 was twice as large as for the other diluents. Treatment of the degraded solvents with carbonate did not improve the decontamination. The distribution coefficient of thorium at the feed plate was 0.45 with Amsco 125-82, compared with 0.40 for the other diluents.

Uranium Recovery from Uranium-Zirconium and Uranium-Aluminum Alloy Fuels

Laboratory countercurrent batch extraction experiments with unirradiated U-Zr alloy fuel solutions to which fission product tracers were added showed no variation in decontamination or uranium recovery between feeds prepared by the modified Zirflex or the HF dissolution process. Decontamination factors from ruthenium and zirconium-niobium were 2.6×10^3 and 2×10^5, respectively, and the uranium loss was about 0.01%. Flowsheet conditions were:

Feed	U, 3.3 g/liter; Zr, 40 g/liter; 1 *M* NH_4^+, 0.78 *M* Al^{3+}, 0.78 *M* H^+, 3.3 *M* F^-; 1 vol
Scrub	1 *M* HNO_3, 0.2 vol
Solvent	5% TBP in Amsco 125-82, 1 vol
Stages	7 extraction, 6 scrub

In tests with synthetic U-Al alloy fuel solution, decontamination factors for ruthenium and zirconium-niobium were increased by about 2 by using

[40] A. T. Gresky and E. D. Arnold, *Products Produced in Continuous Neutron Irradiation of Thorium*, ORNL-1817 (Feb. 6, 1956).

an acid-deficient instead of an acid feed and a nitric acid–water scrub instead of an aluminum nitrate scrub. This small improvement in decontamination would probably not justify the modifications of the Idaho Chemical Processing Plant (ICPP) equipment that would be required in order to incorporate the proposed flowsheet changes. When the present U-Al fuel-solution feed was maintained but a nitric acid–water scrub was used, there was no increase in decontamination, but the volume of the concentrated aqueous waste was decreased 20%.

Laboratory solubility experiments indicated that U-Al and U-Zr fuel solutions may be mixed to give a single solvent-extraction feed of the approximate composition of the present ICPP U-Zr type of feed. Processing of this mixed feed would result in essentially doubling the capacity of the ICPP solvent extraction plant. Solutions of unirradiated U-Al and U-Zr fuel mixed at 80°C in the ratio of 2.5 to 3.0 vols of U-Al fuel solution to one vol of U-Zr fuel solution contained a large amount of precipitate after 24 hr. Mixtures with volume ratios of 0.75, 1.0, 1.5, 2.0, and 3.5 contained only a slight hazy precipitate after six weeks.

Uranium Recovery from Graphite Fuels

In solvent extraction tests on spiked low-activity-level (10^8 counts min^{-1} ml^{-1}) fuel solutions prepared from unirradiated Pebble Bed Reactor fuel by the 90%-HNO_3 disintegration-leach process,[41] no difficulties were encountered in the extraction of the uranium from the adjusted feed with 7% TBP in Amsco.[42] Solvent extraction decontamination factors were 1700, 500, and 10^5 from ruthenium, zirconium-niobium, and rare earths, respectively. During leaching, the graphite had adsorbed 1, 30, 50, and 5% of those elements, respectively. In evaporation of the dissolver solution to 3 *M* HNO_3 for solvent extraction, 1% of the ruthenium volatilized.

Solvent Extraction of Niobium

Laboratory studies according to the Martin procedure[43] for determining distribution coefficients of Nb^{95} between 30% TBP in *n*-dodecane and aqueous nitric acid showed that the amount of niobium present in an extractable form decreased from ~30% in 4 *M* HNO_3 to $\leq$5% in 0.1 *N* acid-deficient solution. The distribution coefficient of the extractable portion decreased from 0.05 to ~0.008 as the aqueous acidity decreased over the same range. The presence of 3% of chemically degraded TBP increased the distribution coefficient of the extractable niobium ten times or more and the amount of extractable niobium to greater than 80%. Distribution coefficients were minimum with 2.0 *M* HNO_3. For solvents containing 3% of chemically degraded TBP and 7% of degraded Amsco, the amount of extractable niobium was $\geq$95%, and the amount of the extracted niobium retained by the organic phase increased from 6 to 50% as the aqueous acidity decreased from 4 to 0.1 *M* HNO_3. The maximum distribution coefficient for Nb^{95} between acid-deficient solutions and solvent containing degradation products was 0.008. The aqueous solubility of the niobium extracted in the degraded reagents varied inversely with the acidity of the aqueous phase.

Purex Process Studies

Dilute Purex Flowsheet. – A modified Purex flowsheet designed to use first-cycle uranium product as feed for the second cycle without intercycle evaporation was evaluated on an engineering scale in 2-in.-diam pulsed columns. The flowsheet differs from the standard Purex process in that the uranium concentration in the feed is 65 rather than 320 g/liter, and a higher feed-to-organic flow ratio is required to maintain the same uranium loading in the organic.

In nozzle-plate pulsed columns operated with the organic phase continuous, the total flow capacity was lower and the uranium production capacity only 30 to 40% of that obtained with the standard Purex flowsheet. The probable reasons for the poor performance are the higher ratio of

[41] M. J. Bradley, *Ind. Eng. Chem.* 53, 279 (1961).

[42] J. G. Moore and R. H. Rainey, *Extraction of Niobium-95 from Nitric Acid Solutions with Tri-n-butyl Phosphate*, ORNL-3285 (in press).

[43] F. S. Martin and G. M. Gillies, *The Chemistry of Ruthenium, Part I. The Formation and Examination of an Extractable Ruthenium Nitrate in Macroscopic Amounts*, AERE-C/R-816 (1951).

dispersed-to-continuous flow in the dilute flowsheet (a/o of 1.5 vs 0.45) and the lower density of the aqueous phase at the feed point. The cartridges in the extraction column had 0.125-in.-diam holes, and with 10% free area the capacity was 350 gal hr^{-1} ft^{-2} at a pulse frequency of 50 cpm and 560 gal hr^{-1} ft^{-2} at 35 cpm; with 23% free area, the capacity was 680 at 50 cpm and 880 at 35 cpm.

Plutonium Adsorption. – Preliminary batch equilibration experiments showed that 99% of the plutonium was removed from 50 ml of solution that contained approximately 1.8 g of uranium per liter, 0.5 *M* HNO_3, 0.1 *M* $NaNO_2$, and 2.7×10^4 counts min^{-1} ml^{-1} of plutonium on contacting the solution with 0.5 mg of a zirconium-silicon-phosphate exchanger. In a similar solution containing 4 *M* HNO_3, only 12% of the plutonium was removed. The exchanger was prepared with a $ZrO_2 : SiO_2 : P_2O_5$ ratio of 1.0 : 4.8 : 0.7. The contact time was 17 hr.

Attempts to adsorb plutonium from nitric acid solutions on unfired Vycor glass were unsuccessful.

Bottom Interface Control for Pulsed Column

In engineering-scale tests in 2-in.-diam pulsed columns, the column was operated without an interface as an alternative to controlling the interface at the bottom of the column. A mixture containing all the heavy aqueous phase plus some light phase was let down through a standard pressure pot to an external phase separator where the interface was controlled simply by using a jackleg for the aqueous outlet. The solvent was recycled to the bottom of the column with an airlift. Automatic control was demonstrated by operating the airlift with a constant air flow rate and using the solvent level in a small surge tank to control the pressure on the pressure pot, thereby regulating the flow rate of dispersion from the column to the phase separator.

The main difficulty with this arrangement was a tendency for the flow rate of the dispersion to cycle as the ratio of aqueous to solvent changed. The frequency and amplitude of the cycle were minimized to less than 0.1 in./min in the column by using a solvent recycle rate sufficient to maintain the aqueous content of the dispersion at less than 40% and by using relatively sluggish gain and reset settings on the controller. The response during transients caused by startup and step changes of the controller was fast enough to maintain control without flooding or loss of interface in the phase separator.

Electrostatic De-entrainment of Solvent Extraction Streams

In small-scale cold tests with a Petrolite Company electrostatic unit, entrained aqueous phase was decreased to typical values of 0.001 to 0.002% for a Purex 1AP Immi mixer-settler stream and to less than 0.001% for a 6% TBP 1AP stream. Aqueous entrainment in the organic effluent from the unit with and without electric power was 0.02% and 0.0095%, respectively, representing removal factors of 10 to 20 due to the electrostatic-precipitation effect alone. Hot-cell testing of the effect of the precipitator on solvent extraction decontamination was not possible because of cell-scheduling difficulties.

1.7 MECHANICAL PROCESSING

The irradiated SRE-fuel-decladding program was satisfactorily completed, the facility in Cell A of Building 3026 was decontaminated, and the equipment was dismantled. The declad uranium metal fuel slugs were shipped to the Savannah River Plant (SRP) for chemical processing. The 250-ton fuel shear was received from the manufacturer (the Birdsboro Corporation), installed on the third floor of Building 4505, and completely shaken down. The rotary feeder and leacher and their auxiliary equipment were installed in cells 1A and 1B of Building 4505 and checked out mechanically and hydraulically. A shearing and leaching demonstration on unirradiated prototype stainless-steel-clad UO_2 fuel was begun. In hot-cell tests, Yankee Atomic (stainless steel-clad UO_2) fuel samples irradiated to 8130 Mwd/ton were sheared and then leached with nitric acid, and the metal residue was rinsed with nitric and dissolved in sulfuric acid to evaluate uranium and plutonium loss and fission-product retention on the nitric acid-leached cladding. The SRE fuel decladding

operation and the 250-ton shear operation were both documented in color moving pictures.[44,45]

Dejacketing of the Sodium Reactor Experiment (SRE) Core 1

Twenty-six seven-rod spent fuel clusters from the SRE Core I, which was irradiated to ~675 Mwd/ton and decayed for two years, were successfully declad, steam cleaned, recanned, and placed in temporary storage. After about six months' storage, the canned fuel was shipped to SRP for chemical recovery of uranium and plutonium. The decladding equipment was decontaminated, encased in plastic, and stored in Building 3505.

The fuel element is a cluster of seven 92-in.-long, $\frac{3}{4}$-in.-diam rods, each containing 12 NaK (22% Na, 78% K) bonded, 2.7%-enriched, 6-in.-long uranium metal slugs clad in a 10-mil-wall type 304 stainless steel tube. A helium-filled space, ~18 in. long, at the top end of each rod allows for expansion of the NaK bond (~100 cc) and the collection of fission gases. Each outer rod is wrapped with an external spiral spacer wire.

The operations involved in decladding an SRE fuel assembly included (1) transfer of the assembly from the shipping cask to the cell; (2) removal of the assembly end hardware and the tube spacer wires by abrasive disk sawing; (3) removal of the fuel slugs and NaK from the fuel tube (see below); (4) steam cleaning of NaK and oil from the fuel slugs and subsequent recanning of the 12 slugs per rod in an aluminum can for storage; and (5) the waste-handling operations of flattening and rolling of the empty fuel tube into a spiral and destruction of the NaK with steam for disposal to intermediate-level waste. A photograph of the assembled equipment in cell A of Building 3026 is shown in Fig. 1.11, and a flowsheet and time cycle of the various steps in the operation are given in Fig. 1.12.

The three mechanical decladding methods evaluated were: (1) dejacketing of the fuel rods by hydraulic expansion of the jacket and hydraulic expulsion of NaK and fuel slugs under oil; (2) fuel dislodgement and expulsion by a long mechanical screw that passed through the full length of the fuel tube; and (3) transverse roll cutting of the clad near slug junctures into twelve 6-in. lengths, each about one slug long, and longitudinal roll cutting in an oil-filled auxiliary decladder, after which the slit claddings were pried or cut from the slug with a special chisel.

The second method was used only when the first was unsuccessful and the third only when the first two failed. With unirradiated fuel rods, the first method was almost always successful; however, with the irradiated fuel the first method was successful with only 16% of the 175 rods processed. The second method was required for 77% of the rods, and the third procedure, which was very time-consuming, had to be used with 7% of the rods.

Based on total operational time, including maintenance, the dejacketing production rate was 2.0 kg of uranium an hour. Near the end of the program, when ideal operating conditions prevailed, a rate of 9.2 kg/hr was reached. Of the 830 hr of operation logged, 30% went for processing and the rest for repairs and maintenance. About half the downtime resulted from repairs to the NaK disposal system, which was damaged twice by explosions and fires when water accidentally contacted the NaK through leaky valves.

In general, the mechanical components of the decladding complex performed as planned. Abrasive-saw removal of both the inert adapters and the fuel rod spacer wires worked well. The hardened fuel jackets put unexpectedly high stresses on some portions of the complex. The inability of the main hydraulic decladder to expand the claddings was disappointing because ductile fuel prototypes had been easily expanded and processed. The fuel-slug ejection screw was generally satisfactory. Roll cutting of claddings was more difficult than expected. Roll cutters with a 60° included angle, V-edge, made from Carpenter, Vega-KW tool steel hardened to Rockwell C-60 to 65 and ground under oil, dulled and chipped when cutting on the irradiated uranium rods.

The two explosions that occurred during destruction of the NaK showed that a simpler, more foolproof method is required. Tests are planned to evaluate the deliberate formation of a NaK-oil emulsion and its destruction by spraying it through

---

[44] "Mechanical Dejacketing of SRE Core 1 Fuel," 16 mm, color and sound, 12 min, ORNL Public Relations Department.

[45] "Shearing of Reactor Fuels," 16 mm color, silent, 4 min, ORNL Public Relations Department.

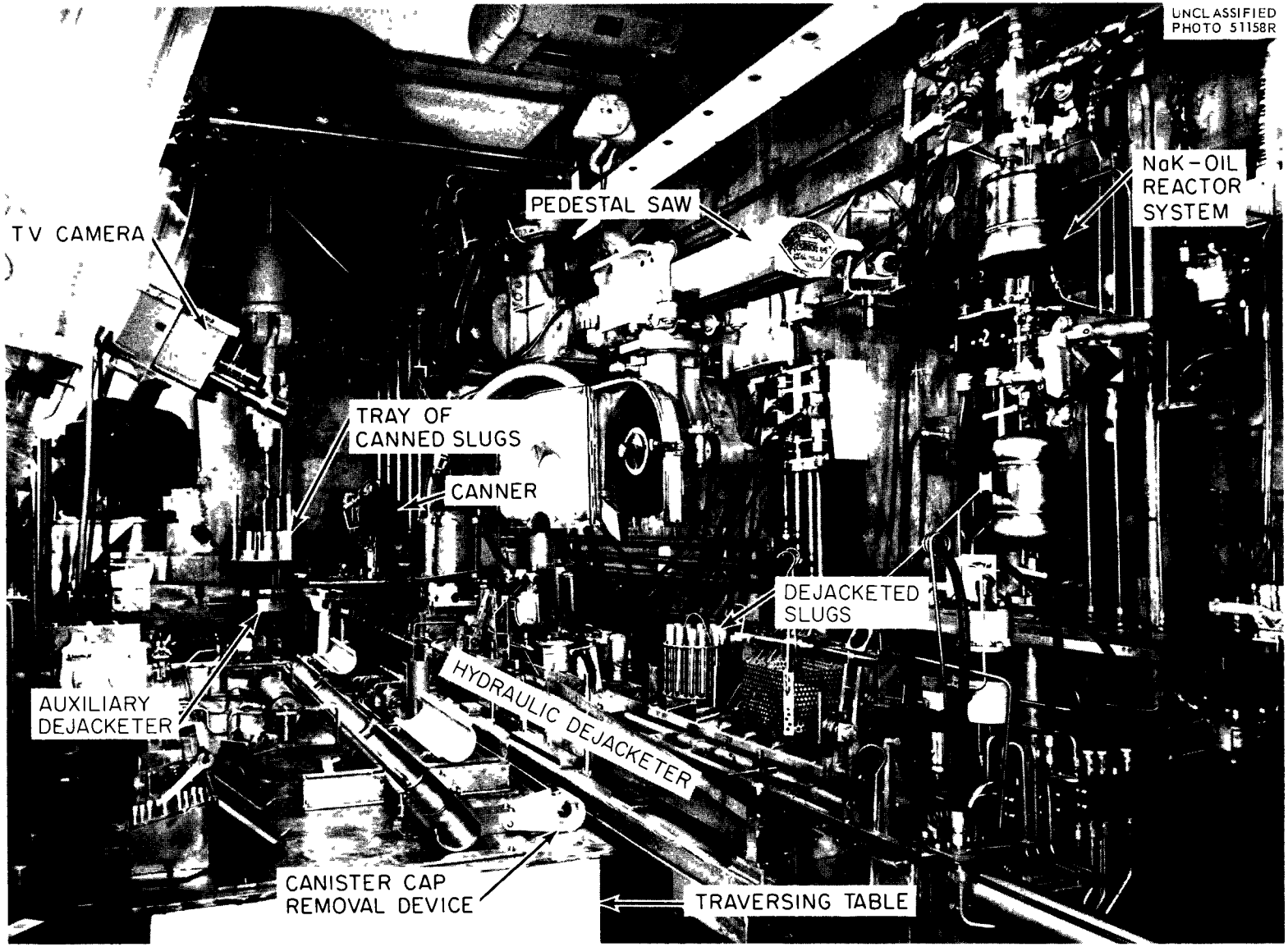

Fig. 1.11. Mechanical Processing Equipment for Decladding the SRE Core I Fuel. Interior view, cell A, ORNL Segmenting Facility.

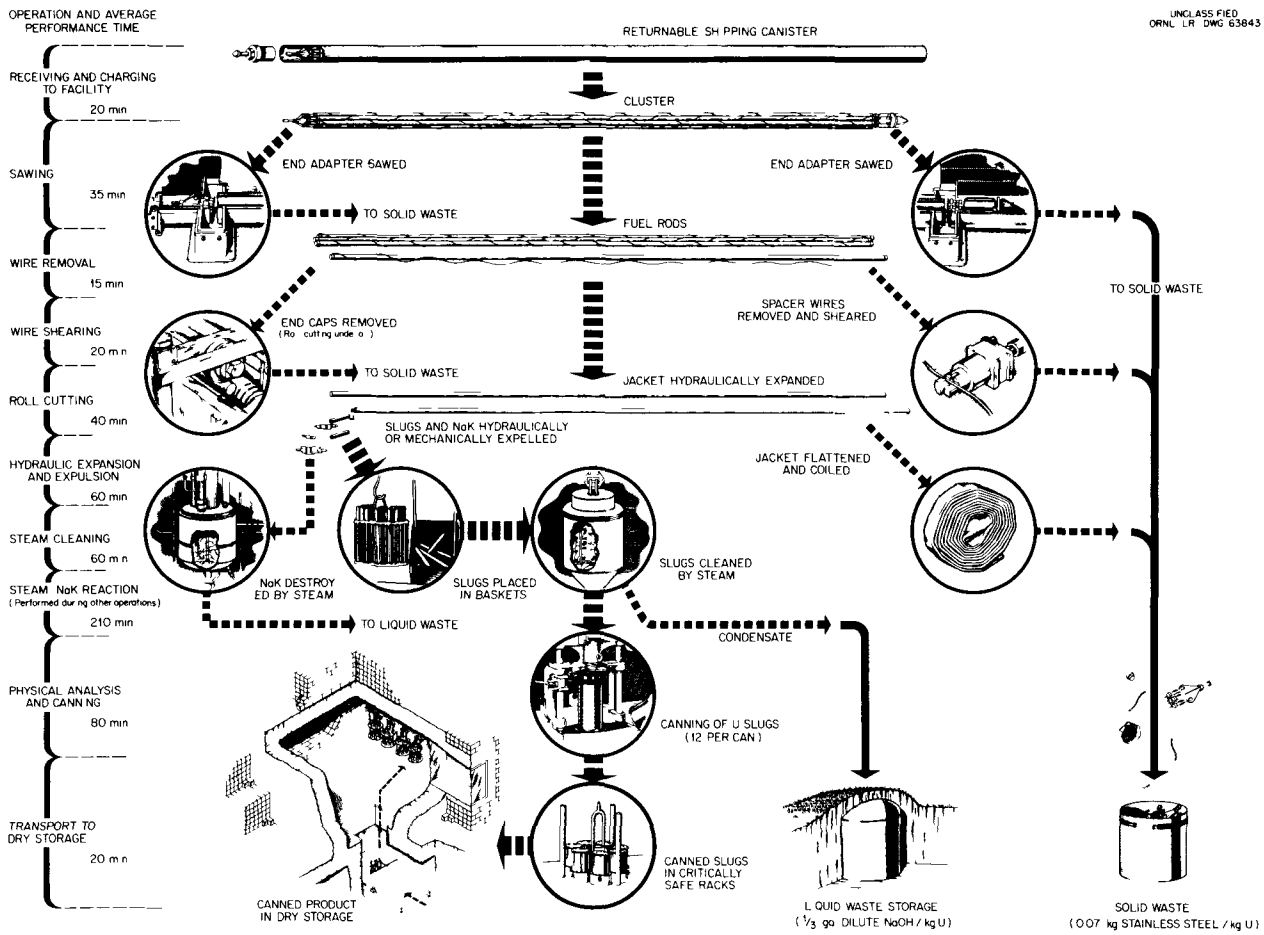

Fig. 1.12. Mechanical Decladding Flowsheet – SRE Core I Fuel.

a nozzle into water. Handling of liquid-NaK-bonded fuel under an oil blanket in a shielded cell with an air atmosphere appears to be quite practical when the amount of NaK handled at any time is strictly limited.

Water-soluble polyvinyl acetate paint mixed with white billboard paint and sprayed onto stainless steel cell walls decreased glare, increased lighting, and expedited cleaning and decontamination of walls by built-in water sprays or portable steam lances.

The cell discharge-air absolute filters and the cloth filters in the portable vacuum cleaner used for collecting fines from abrasive-disk sawing became the most radioactive areas in the cell, giving readings of 200 and 10 r/hr at contact, respectively. The activity on the cell air filters is believed to have resulted from the NaK explosions and water spray from cell washdown. Contamination of the cell was controlled easily, permitting entry by appropriately dressed personnel. The activity level increased threefold after the NaK explosions.

Electrical motors on an overhead heavy-duty manipulator were a prime source of heavy-equipment failure. In one incident a drive gear was sheared on the 3-ton crane. Several minor repairs were required on the model-8 manipulators, such as replacement of torn boots and broken tapes.

The average uranium loss during the program, as determined by dissolving entire clads in 3 *M* HCl–4 *M* HNO_3, was 0.02%; the maximum for any fuel cluster was 0.2%. The average and maximum plutonium losses were 2×10^{-4} to 2×10^{-3}%, respectively (Table 1.15). Such losses apparently result from the formation of stainless steel–uranium reaction products or adherence of particles dislodged from the slugs, or both.

The primary method of decladding failed because the irradiated claddings were much harder than expected, and hydraulic oil pressures, which in tests on unirradiated rods had produced up to 380 mils expansion before bursting the tubes, expanded the irradiated tubes only 0 to 5 mils.

Metallurgical examination of randomly selected samples of portions of the type 304 stainless steel claddings taken from the central rod and an outer rod of several fuel clusters showed intergranular attack of the cladding external surfaces (Fig. 1.13) from about the midpoint of a fuel rod

Table 1.15. Typical Analysis of Dissolved SRE Core I Fuel Claddings

Type 304 stainless steel cladding, 10-mil wall
Collapsed coils, 280 g per batch
3 *M* HCl–4 *M* HNO_3 decladding reagent, 6 liters

Element	Concentration	Element	Concentration (counts min^{-1} ml^{-1})
U	0.0018 g/liter	Co 58-60	6.3×10^7
Pu	292 counts min^{-1} ml^{-1}	Sr 89, 90	6.0×10^4
Cr	17%	Cs 137	1.7×10^4
C	0.04%	Ru 106	2.4×10^4
Gross gamma	7.2×10^{-7}%	Zr 95	$< 1 \times 10^3$

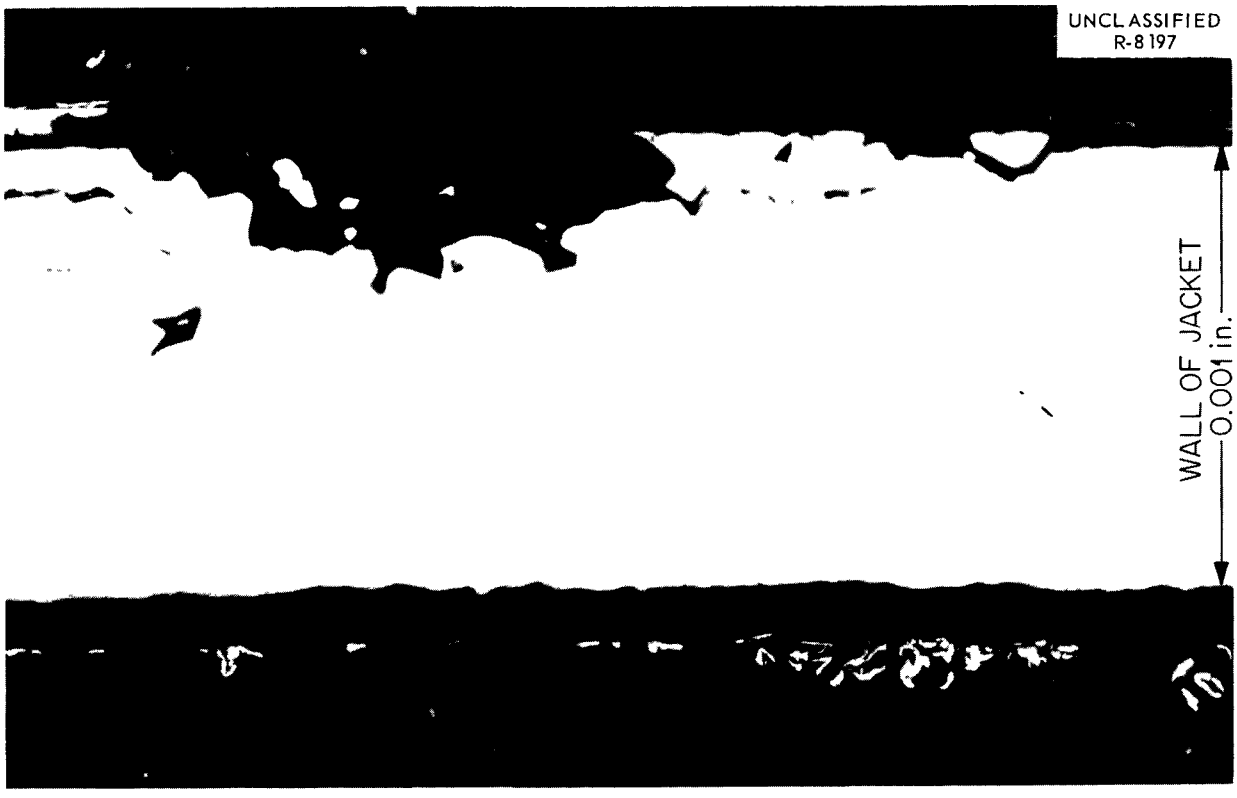

Fig. 1.13. Top Portion of Type 304 SS Fuel Cladding (10 Mils Thick), Showing Intergranular Attack.

up to the top. Specimens were easily broken (Fig. 1.14) when bent. An unidentified metallic layer was found on external cladding surfaces on the lower portions of the fuel rods, but specimens from these areas did not break on bending. Stainless steel–uranium reaction products (Figs. 1.15, 1.16) were confined to extremely small areas but were distributed fairly uniformly over internal cladding surfaces.

The microhardness of the 10-mil-thick wall of one clad varied from 240 to 400 DPH (diamond pyramid hardness, 0.5-kg load). The hardness of unirradiated fuel cladding was about 180 DPH. The uranium slugs were pitted and were bent as much as 7 to 20 mils, elongated 1 to 6%, and swollen 1 to 5%. Hardness measurements on a single slug specimen ranged from 200 to 300 DPH for a 1-kg load.

The 18 liters of NaK handled during the program contained about 1 curie of Cs^{137} and traces of other fission products, uranium, and plutonium (Table 1.16). The NaK was collected and destroyed in 100-ml increments by reaction with steam in the NaK disposal system.

Metallic and aqueous liquid waste resulting from the disassembly and decladding, steam cleaning of slugs, and the destruction of NaK amounted to about 0.07 kg and 1.15 liters per kilogram of uranium processed, respectively. For each fuel cluster processed, the inert metallic

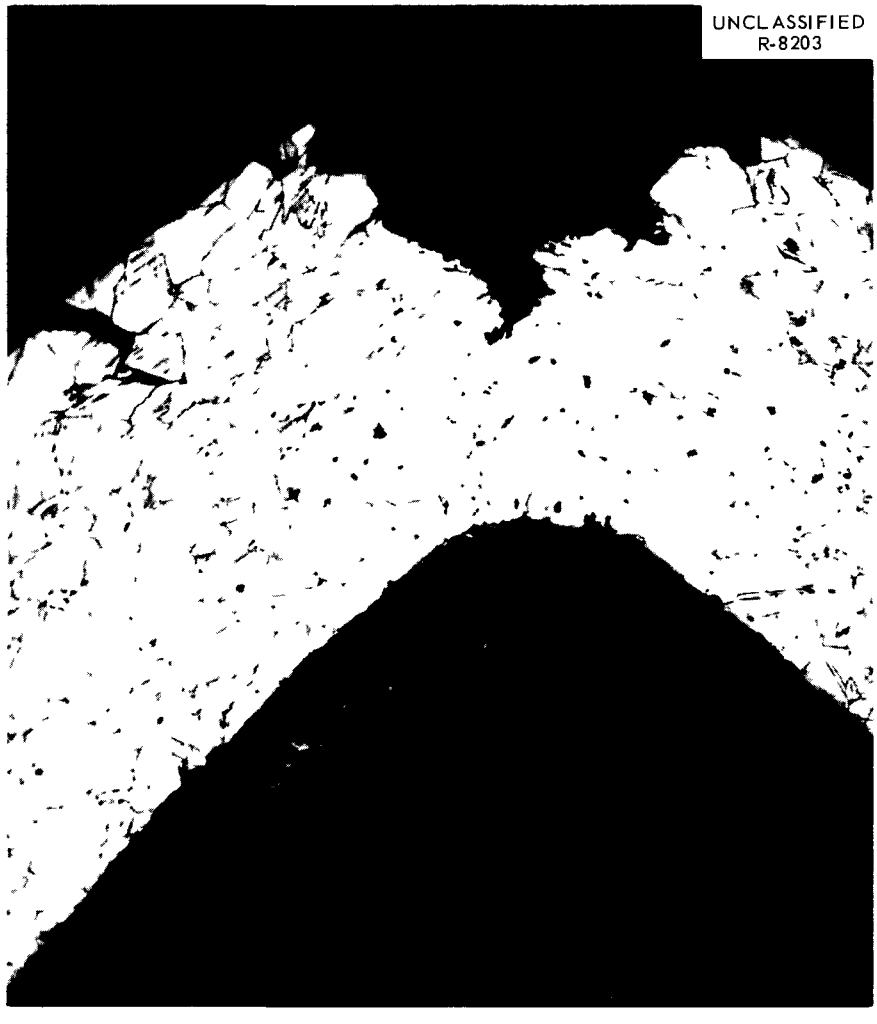

Fig. 1.14. Bend Specimen from Type 304 SS Fuel Cladding Taken from Area Showing Sensitization, Intergranular Attack, Cold Working, and Hardening.

Fig. 1.15. Stainless Steel–Uranium Reaction Products on Interior Surface of 304 SS Cladding.

portions, loosely packed, occupied about 3 gal. The total liquid waste amounted to 22 gal per fuel cluster.

The mechanical decladding program was completed successfully, but at production rates lower by a factor of about 2 to 3 than predicted from the processing of unirradiated prototype fuel. The stainless steel–uranium reaction products on the interior surfaces of the claddings is a potential source of a high uranium loss and probably defeats those mechanical processing methods which physically separate the fuel and cladding before chemical processing.

The three mechanical methods evaluated in this program could not adequately cope with hardened and/or embrittled claddings, bent and swollen slugs adhering to the jacket, or badly damaged fuel. The custom decladding method required for badly damaged fuel, and used when the two main methods failed, is much too time-consuming for practical use.

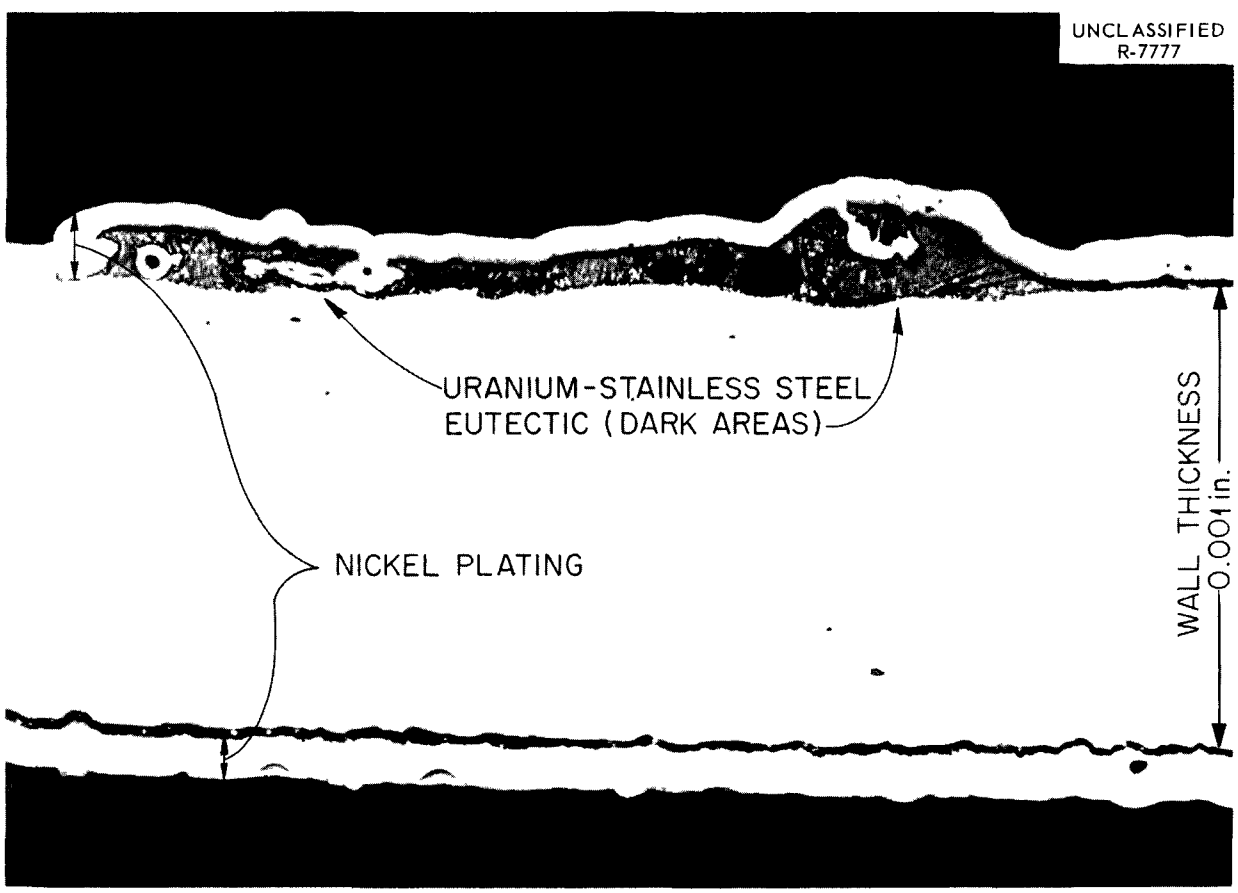

Fig. 1.16. Cross Section of Cladding (10 Mils Thick), Showing Uranium–Stainless Steel Reaction Product.

Table 1.16. Typical Analysis of NaK from Irradiated SRE Core I Fuel Rod

Element	Concentration (counts min^{-1} g^{-1})	Element	Concentration
Gross gamma	3.9×10^7	U	$< 1 \times 10^{-4}$ mg/g
Gross beta	9×10^6	N	0.36 ppm
Gross alpha	< 100	C	148 ppm
TRE, beta	2.5×10^5	K	78%
Cs 137	8.6×10^6	Na	22%

Shear and Leach Development

The shearing and leaching program to determine the feasibility of (1) semicontinuously shearing stainless-steel- and Zircaloy-clad fuel assemblies and (2) leaching the exposed UO_2 or UO_2-ThO_2 core material from the 0.25- to 1.5-in.-long sheared sections with nitric acid was continued. The hardware comprising the mechanical shear-leach complex was field tested, altered as required, provided with an electrical interlock system, and installed on the third floor and in cells 1-A and 1-B of Building 4505. The chemical processing equipment will be operated at rates of about 10 kg of uranium per hour. A mathematical model was developed from laboratory bench-scale leaching tests to predict the operation of the full-scale leacher but has not yet been verified in engineering-scale tests. Wear testing of the gibs and stepped blade of the shear with porcelain-filled ORNL Mark I fuel was satisfactorily completed, and the particle-size distributions of various sheared lengths were determined.

The mechanical shearing and leaching complex (Fig. 1.17), consists of a stainless steel 250- to 320-ton shear with a horizontal-acting stepped blade and feeding system (Fig. 1.18), a spiral inclined rotary conveyer-feeder, a spiral inclined rotary leacher with valving that will pass sheared solids but seal against nitric acid fumes when closed, and auxiliary tanks, piping, and instrumentation.

In operations now in progress, a fuel assembly is picked up with a crane and inserted into the fuel-element envelope of the shear by means of a loading arm. A pusher arm is then moved into position and pushes the fuel assembly into the shear against a stop beyond the shear blade to position the fuel properly during each cut. A step-shaped blade shears the assembly into sections 0.25 to 1.5 in. long. The stop and the stepped blades are mounted on a movable ram. The fuel assembly is constrained during shearing by an inner and outer gag and the fixed blade. After the complete stroke of the shear, the gags are released and the fuel assembly is advanced for the next cut. The sheared sections are stored as discrete batches in the conveyer-feeder, which provides a surge storage capacity of up to 14 hr. The feed is delivered to the leacher as required. The leacher, a combination dissolver and wash vessel, contains four countercurrent leaching flights, two discharge flights, and four countercurrent wash flights in which the empty jackets may be washed with water or nitric acid. The entire complex is sealed to contain all particulate matter.

Fifty-one Kanigen- and Nicrobraz-50-brazed ORNL Mark I porcelain-filled prototype fuel assemblies, each containing a 6- by 6-square array of thirty-six 0.5-in. stainless steel tubes, were sheared for particle-size-distribution measurements and blade-wear studies. The shortest practical length for shearing the prototype fuel was 0.5 in. Shearing to shorter lengths is easily accomplished, but severe flattening of the tubular jacket occurs, trapping significant amounts of ceramic fuel (Fig. 1.19).

The sheared material (Fig. 1.20) was segregated by length, and each group was analyzed for size distribution of both ceramic and metallic particles (Table 1.17). Particles > 2000 μ contained 70 to 90% of the stainless steel, whereas porcelain comprised 85 to 99.6% of particles < 2000 μ. Braze

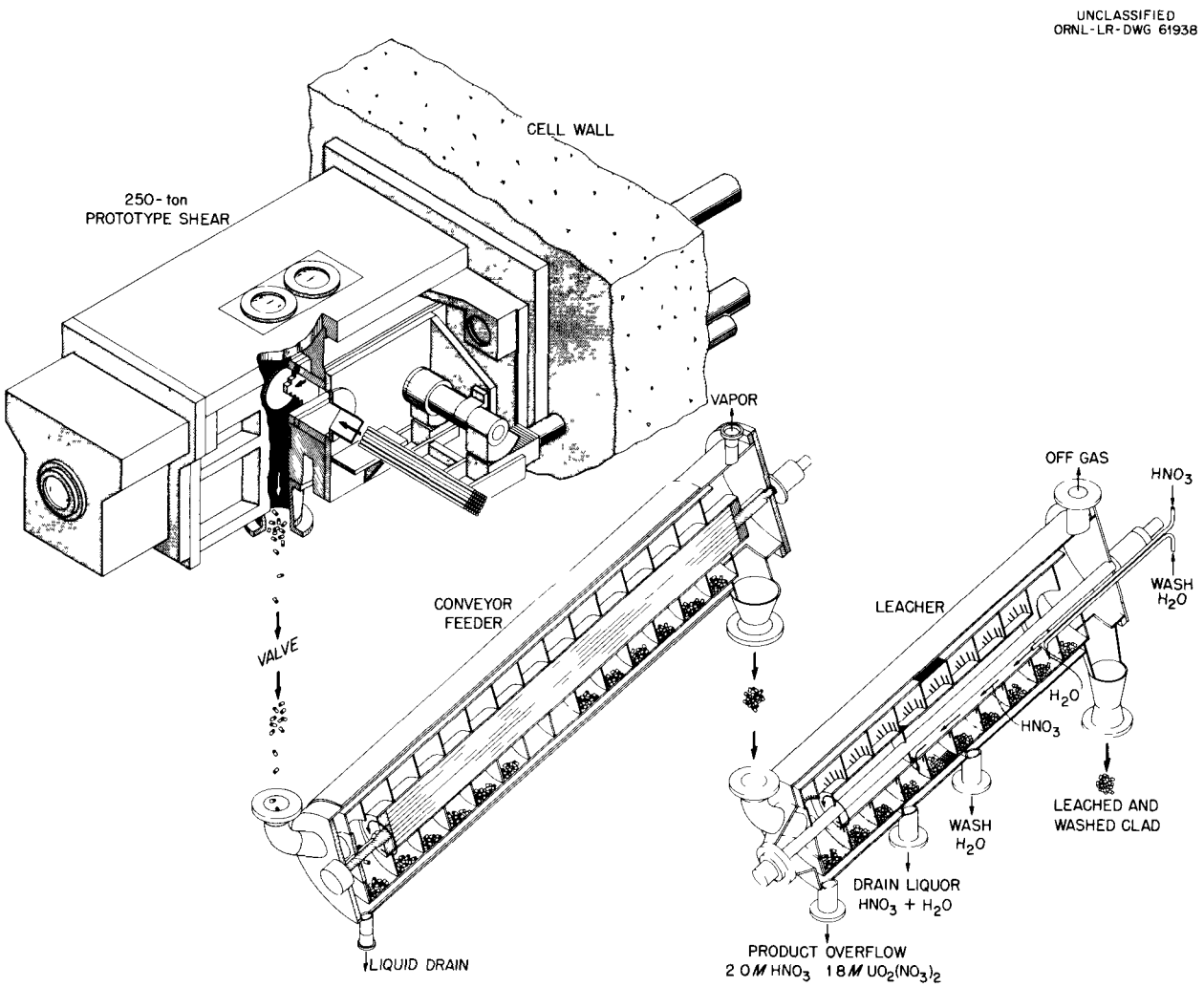

Fig. 1.17. Shear and Leach Complex, Indicating Relative Position of Major Equipment Components and Flow of Materials.

metal was present in the amount of 0.1 to 1.0% in all particle sizes measured, 9520 to <44 μ. No appreciable difference in particle-size distributions from Nicrobraz-50- or Kanigen-brazed elements was noted. For 1-, 0.75-, 0.5-, and 0.25-in.-long cuts, the fractions of material <9520 μ were 11, 16, 33, and 69%, respectively; for the portion <44 μ, the fractions were 1.5, 2.4, 4.3, and 5.2%. The smallest particle measured was 0.25 μ, constituting 0.035 to 0.08% of the particles.

Both ductile and carburized-hardened ORNL Mark I fuel prototypes were sheared without difficulty. Ductile fuel containing tube sheets at each end of an assembly was sheared equally as well but produced undesirable chunks of tubing at the tube sheets, rather than discrete pieces. When a highly embrittled, carburized (1.7 to 2.7% carbon), porcelain-filled Mark I prototype fuel assembly was sheared, the stainless steel tubing shattered badly, exposing more of the core material than when the ductile tubing was sheared.

The terminal portion of a fuel assembly can be held during shearing by a combination of two independently acting inner and outer gags. The shortest practical terminal length appears to be 1.5 in., including end caps.

Component equipment testing of the conveyer feeder and leacher with 1-in.-long sheared sections

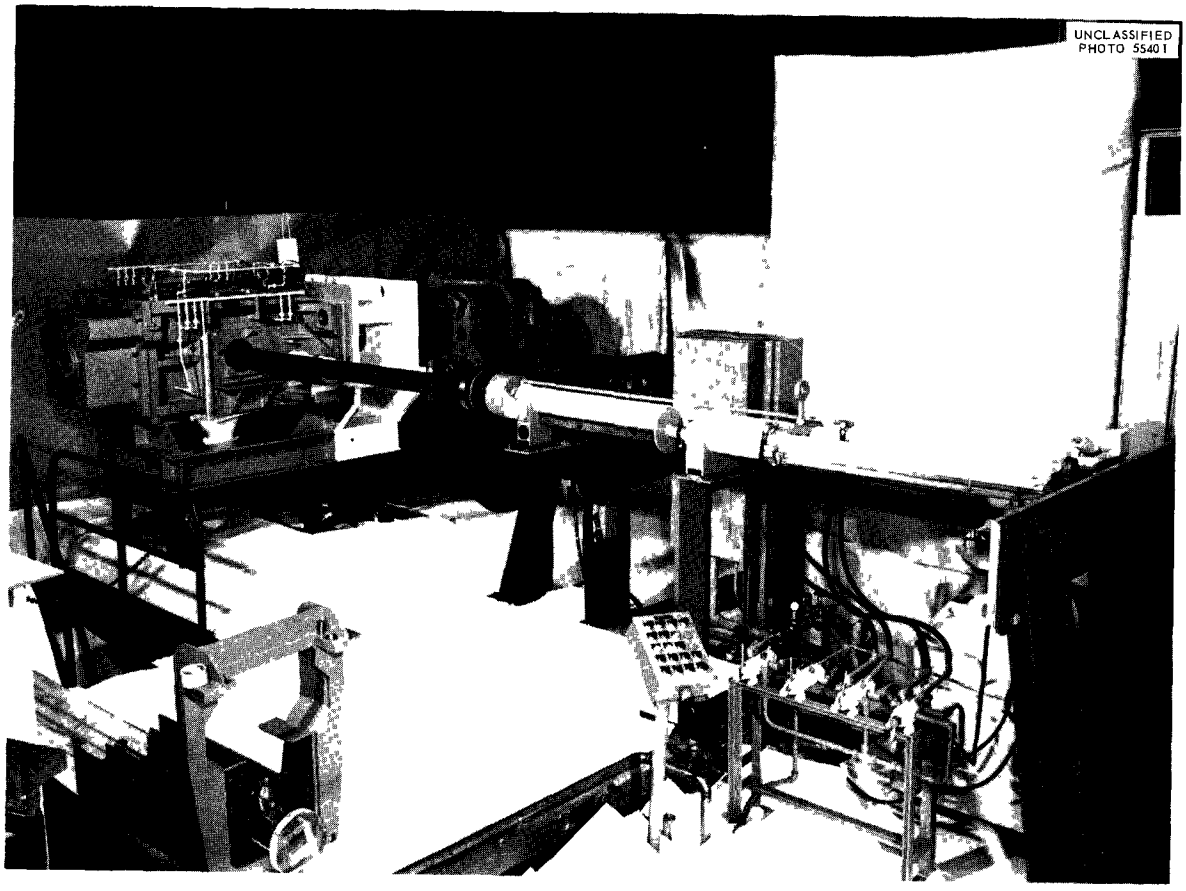

Fig. 1.18. 250-ton Prototype Shear and Feed Mechanism.

Fig. 1.19. Comparison of Product from Shearing ORNL Mark I Fuel into 0.25-, 0.50-, and 1-in. Lengths.

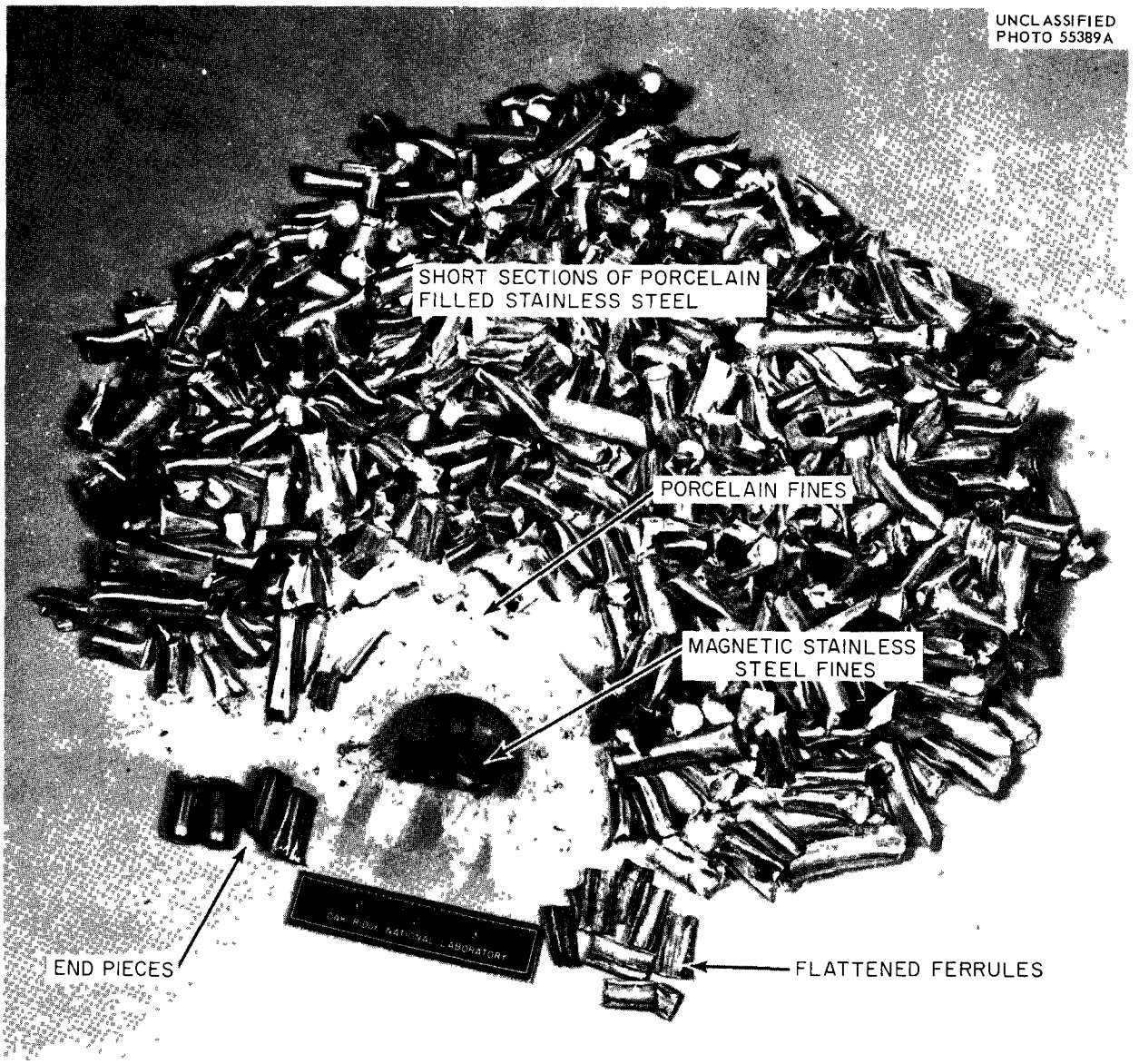

Fig. 1.20. Composite Material Obtained from Shearing of a Porcelain-Filled Mark I Prototype Fuel Assembly.

of porcelain-filled, stainless-steel-clad ORNL Mark I fuel show that the largest batch of stainless-steel-clad UO_2 fuel that can be submerged in the counterflowing acid of the leacher is 6.5 kg of UO_2 or about 2.25 liters per flight. The slip angle of this 2.25-liter fuel batch for the conveyer feeder and leacher is 28 to 32° and is independent of length of cut (0.25, 0.5, 0.75, 1 in.) or elevation of the unit (5, 10, 15, 20°). The slip angle is defined as the angle measured from the vertical axis of the leacher or conveyer-feeder bisecting a batch of fuel at rest to the center of the batch of fuel at the moment slippage first occurs. For proper submergence of the fuel in acid, the leacher is rotated 388° and reversed 28° each time fuel is advanced against counterflowing acid.

In hot-cell laboratory tests,[46] residues of sectioned prototype type 304L stainless-steel-clad UO_2 Yankee Atomic reactor fuel specimens were

[46] J. H. Goode and M. G. Baillie, *Leaching and Washing of Sectioned, Irradiated WCAP Fuel Specimens*, ORNL CF-62-3-77 (Mar. 28, 1962).

Table 1.17. Porcelain, Stainless Steel, and Braze Metal Percentage Distribution at Various Particle Diameters Produced by the Shearing of ORNL Mark I Fuel into 1-, 0.75-, 0.50-, and 0.25-in. Lengths

Horizontally actuated ORNL 250-ton shear with a stepped blade, operated at 1.22 in./sec and ~4.2 cuts per minute

Fuel: $3\frac{5}{8}$-in.-square bundle of 36 type 304 stainless steel tubes, $\frac{1}{2}$ in. OD by 72 in. long, with spacer ferrules (0.25 × 1 in.) brazed on at ~12-in. intervals. The tubes are filled with ~1600 g of porcelain sections, 0.42 in. OD by 3 in. long

Particle Diameter (μ)	Amount (%)													
	1-in. Cut			Carburized Assembly[a] 1-in. Cut		0.75-in. Cut			0.50-in. Cut			0.25-in. Cut		
	Porcelain	Stainless Steel	Braze	Porcelain	Stainless Steel	Porcelain	Stainless Steel	Braze	Porcelain	Stainless Steel	Braze	Porcelain	Stainless Steel	Braze
9519–4760	31.0	68.0	1.0	48.6	51.4	9.0	90.75	0.25	59.0	40.7	0.3	9.2	90.6	0.2
4759–2000	49.6	49.8	0.6	43.6	56.4	60.0	39.5	0.5	68.0	31.4	0.6	29.8	69.7	0.5
1999–1190	85.0	14.6	0.4	62.2	37.8	97.1	2.7	0.2	95.0	4.8	0.2	90.2	9.7	0.1
1189–590	98.2	1.3	0.5	74.1	25.9	99.0	0.9	0.1	98.0	1.9	0.1	97.7	2.1	0.2
589–297	99.1	0.4	0.5	87.0	13.0	99.4	0.4	0.2	99.2	0.6	0.2	98.9	0.8	0.3
296–149	99.3	0.3	0.4	89.7	10.3	99.4	0.3	0.3	99.4	0.4	0.2	98.8	0.7	0.5
148–74	99.2	0.3	0.5	93.0	7.0	99.3	0.3	0.4	99.5	0.3	0.2	98.6	0.6	0.8
73–44	99.2	0.4	0.4	92.4	7.6	99.4	0.2	0.4	99.5	0.3	0.2	98.5	0.5	1.0
<44	98.6	1.0	0.4	95.2	4.8	99.0	0.7	0.3	99.6	0.2	0.2	98.2	0.8	1.0

[a]Distribution of single cut of carburized (1.7 to 2.7% C) ORNL Mark I assembly.

leached and washed in nitric acid, and the cladding was subsequently dissolved in sulfuric acid to simulate the extent of fission product, uranium, and plutonium residue on the scrap stainless steel shells from the chop-leach process. The sectioned fuel specimens, irradiated up to 8130 Mwd/ton and decayed for three years, were leached 5 hr with 4 *M* HNO_3 to produce a modified Purex feed solution containing 100 g of uranium per liter and 3 *M* HNO_3. After removal of this solution, the shells were washed three times with 4 *M* HNO_3, which removed the uranium, plutonium, and fission products, and then completely dissolved in 4 *M* H_2SO_4. Analysis of the dissolved stainless steel showed that $<0.02\%$ of the uranium and plutonium remained with the clad. Fission-product activity retained by the clad was negligible and was completely masked by the cobalt-60 and other activated stainless steel constituents. Typical decladding solution analyses were: 2.44 *M* H_2SO_4, 55 g of stainless steel per liter, 6.77×10^9 Co^{60} gamma counts min^{-1} ml^{-1}, 0.003 mg of uranium per milliliter, and 10^3 plutonium alpha counts min^{-1} ml^{-1}.

1.8 ENGINEERING STUDIES

The cooperative ORNL-ICPP pilot plant effort begun last year was extended to include (1) design of a Darex Pilot Plant and of a Chop Leach Facility for installation at the ICPP and (2) consultation on the modification of ICPP solvent extraction facilities and installation there of a plutonium solvent extraction and isolation facility to permit the processing of low-enrichment uranium-plutonium fuels. The Darex and Chop Leach programs were canceled by the AEC in April 1962.

Darex Pilot Plant

The objective of this design was to develop a high-throughput process suitable for future commercial application. Flowsheet studies were made to determine the feasibility of designing a Darex Pilot Plant that could demonstrate either batch or continuous processing. For it, the basic design previously planned for installation in cell 3 of Building 3019 was rearranged, extra vessels in the aqua regia preparation system were removed, and continuous chloride-removal equipment was added. The latter consists of an airlift feed system taking dissolver product from the feed adjustment tank to a chloride stripper tower, where the chloride is removed by 15.8 *M* HNO_3 vapor stripping. Stripper column bottoms are continuously evaporated to remove excess nitric acid and then diluted in a geometrically safe tank to the appropriate solvent extraction feed concentration prior to transfer to ordinary process equipment for sampling and possibly a solids removal step. The system as originally planned included provisions for low-temperature continuous stripping of chloride with NO_2, but this feature was eliminated when further experiments indicated that this method of chloride removal was not feasible.

Material balance flowsheets were prepared for the batch Darex processing of APPR and Consolidated Edison fuels and the continuous Darex processing of APPR and Yankee Atomic fuel and used as the basis for a preliminary process flowsheet prepared jointly by ORNL and ICPP. The flowsheet incorporated the integral chloride-stripping-tower for the reboiler-feed evaporator system developed by ORNL during an analysis of control system dynamics and liquid-vapor equilibrium data for nitric acid in the presence of stainless steel salts. Preliminary results of cold engineering studies at ICPP of this chloride stripping system were favorable.

The storage of dilute, chloride-bearing radioactive waste such as might originate from off-gas scrubbers or system cleanout was to be eliminated by providing a chloride-proof vessel off-gas disposal system discharging directly to the plant stack. Excess chlorine compounds in the pilot plant system would be discarded by distillation and/or decomposition into this off-gas system.

Tests to define the aqua regia composition necessary to prevent cyclic passivation of fuel

in the continuous dissolver in the presence of a large fuel charge indicated that 4 *M* HNO_3–3 *M* HCl would be required rather than the previously considered 5 *M*–2 *M* dissolvent.

Preparation of equipment specification design sheets and of detailed engineering flowsheets were under way when the project was terminated.

Shear-Leach Pilot Plant

Joint meetings of ORNL and ICPP Shear-Leach Groups were held in order to disseminate information useful in the design and installation of the chop-leach complex at ICPP for hot pilot-plant testing with spent power-reactor fuels. A brochure was prepared to provide ICPP with all data accumulated to date, and the ICPP had engaged an architect-engineer to study the suitability of the several possible locations in existing facilities when the project was canceled.

Plutonium Isolation Facility

The ORNL-ICPP cooperative pilot plant program envisioned the providing of plutonium tail-end facilities at the ICPP so that fuels containing plutonium could be processed. Engineering information on pulsed-column and mixer-settler performance and the design of plutonium load-out facilities was forwarded to ICPP in order to permit evaluation of the trilaurylamine extraction flowsheet for the proposed installation. Flowsheet tests with HAPO Purex IBP solution in mini-mixer-settlers in a hot cell showed satisfactory plutonium recovery but much less fission product decontamination than expected from results shown with tracer levels of activity. The reason for this will be investigated, and it was recommended that the ICPP group should defer consideration of the TLA extraction flowsheet for plutonium until the fission product decontamination deficiency had been resolved.

2. Fluoride Volatility Processing

2.1 PROCESSING OF URANIUM-ZIRCONIUM ALLOY FUEL

Modifications[1] to the Volatility Pilot Plant required to scrub the dissolver off-gas with liquid HF were completed. The off-gas solids were removed from the gas stream by impingement in a flash cooler (FV-1001, Fig. 2.1) followed by scrubbing with liquid HF. The HF was distilled (FV-1005) for recycle, off-gas condensables were completely condensed (FV-2001), and the collected solids were flushed from FV-1003 to FV-1009 and then to the drain.

[1] *Chem. Technol. Div. Ann. Progr. Rept. May 31, 1961*, ORNL-3153, p 30.

Eight dissolution runs were completed with non-irradiated simulated Zircaloy-2 and with zirconium-uranium alloy. In the flowsheet used, the fuel elements were dissolved in equimolar molten NaF-LiF containing 25 to 45 mole % ZrF_4 at 650–500°C, by means of HF, which converted the zirconium-uranium alloy to ZrF_4 and UF_4, both soluble in the fluoride salt. Submicron-size solids generated during the dissolution were scrubbed from the off-gas by HF.[1] The UF_4 was converted to volatile UF_6 by fluorination at 500°C with elemental fluorine, and the UF_6 was further decontaminated from fission products by absorption on and desorption from a NaF bed at 100°C and 400°C, respectively. The product UF_6 was collected in cold traps.

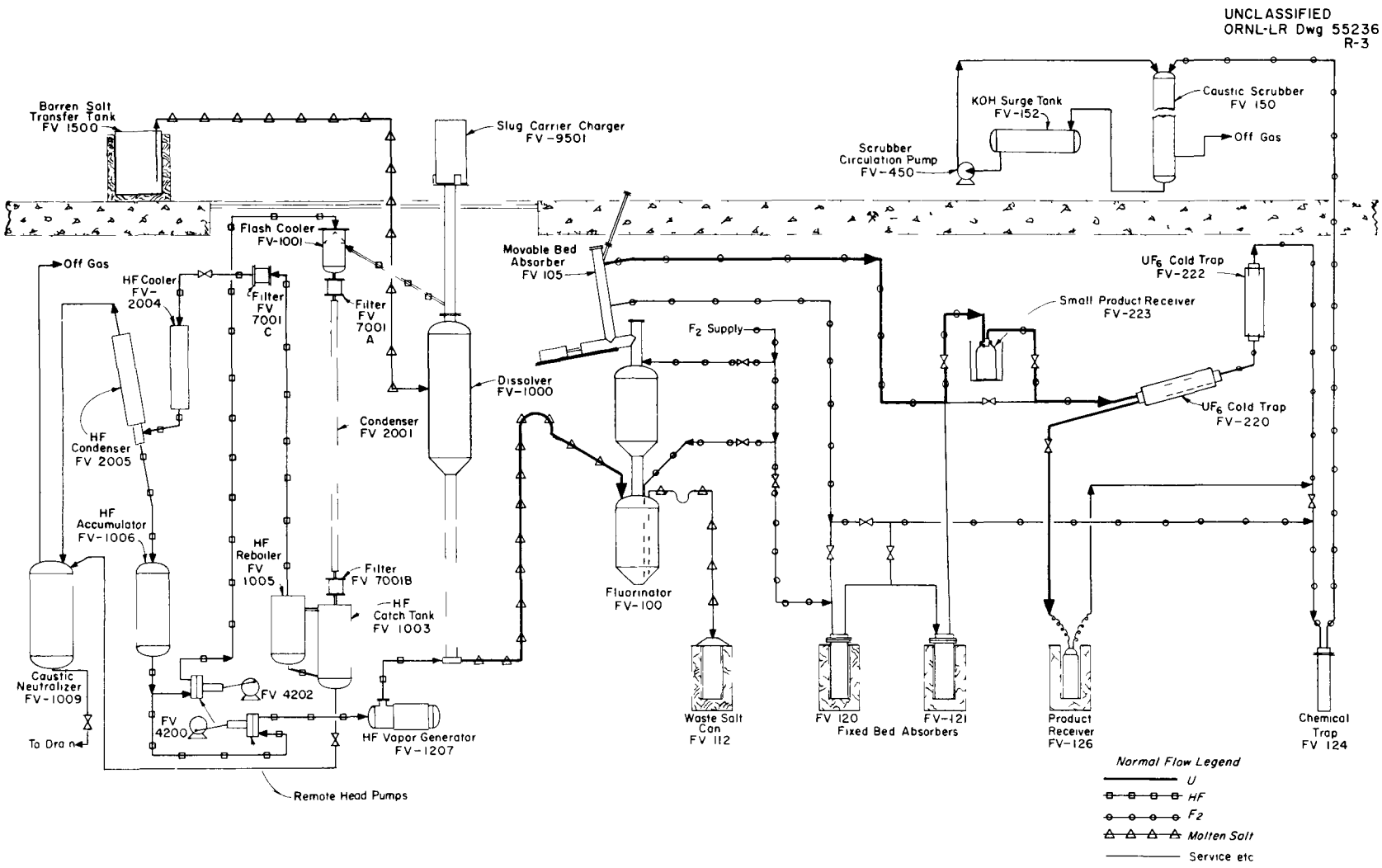

Fig. 2.1. Schematic Diagram of Fluoride Volatility Pilot Plant.

Of the eight nonirradiated fuel dissolution runs, three (T-8 through T-10, Table 2.1) were made with simulated fuel, Zircaloy-2, to evaluate the new dissolver off-gas scrubbing system. Solids removal efficiency averaged >99% per run. Solids accumulated on the filter (FV-7001C, Fig. 2.1) as an oily film on the inlet face of the Yorkmesh cartridge rather than as loose particulate material. Dissolution rates for two of the three runs (T-9 and T-10) were equal to the rate in run T-7 (2.8 kg/hr), the only other run in which two simulated fuel elements were used per dissolution. Run T-8 was terminated at 70% completion because of accidental charging of high ZrF_4 content (42 mole %) salt to the dissolver. The T-8 fuel heel and associated metallic sludge (vessel corrosion products in reduced state[2]) caused salt transfer difficulties during run T-9. The high dissolution rate in TU-8 was attributed, in part, to an abnormal fuel element submergence, which occurred when the fuel lodged at the top of the dissolver 5-in.-ID lower section and was initially only ~95% submerged in salt.

In the other five runs, with nonirradiated uranium-zirconium alloy, average dissolution rates were 3.12 kg/hr for 90% completion (Table 2.1).

Correlation of the dissolution-rate data from 22 nonirradiated fuel pilot plant runs with salt kinematic viscosity and HF mass velocity was generally poor (Fig. 2.2). A least-squares line was evaluated and the standard error of estimate and standard deviation were calculated for evaluation of the linear regression correlation coefficient. The best empirical correlation obtained (correlation coefficient 0.57) for the range of the HF flow was:

$$r = 0.068 + 0.0001\ \nu^{-1/3}\ W\ ,$$

[2]G. I. Cathers, R. L. Jolley, and E. C. Moncrief, *Laboratory-Scale Demostration of the Fused Salt Volatility Process*, ORNL TM-80, p 7, (Dec. 1961).

Table 2.1. Summary of Dissolution Runs

Runs T-8 through T-10: Zircaloy-2, ~30 kg per element, two elements per run
Runs TU-8 through TU-12: nonirradiated fully enriched zirconium-uranium alloy fuel, ~1% U, ~40 kg of fuel per run
Runs R-1 through R-6: 5.2 and 6.5 yr decayed enriched zirconium-uranium alloy fuel, ~25 kg per element
Initial molten salt: 28 to 39–30 to 42–23 to 42 mole % NaF-LiF-ZrF_4

Run No.	Salt Temp. (°C)		Avg. Dissolution Rate[a] (kg/hr)	Time[a] (hr)	Avg. HF Flow Rate (g/min)	Avg. HF Utilization[a] (%)
	Max.	Min.				
T-8	640	500	1.60[b]	23.2[b]	150	15.9[b]
T-9	560	510	2.90	11.0	190	22.3
T-10	640	490	2.75	17.5	162	25.8
TU-8	652	495	4.80	7.4	122	52.0
TU-9	665	480	2.70	14.1	180	20.6
TU-10	650	495	2.50	14.5	150	24.5
TU-11	665	495	2.30	16.0	150	23.5
TU-12	640	505	3.30	11.2	150	32.0
R-1	650	500	1.80	26.4	150	17.1
R-2	650	495	3.10	14.0	150	29.8
R-3	645	490	3.18	12.3	75–150	31.2
R-4	655	550	5.34	8.0	75–150	54.6
R-5	660	500	2.86	14.0	75–150	30.3
R-6	650	495	2.48	17.4	75–150	27.6

[a]Based on 90% completion of dissolution.
[b]Run terminated at 70% completion.

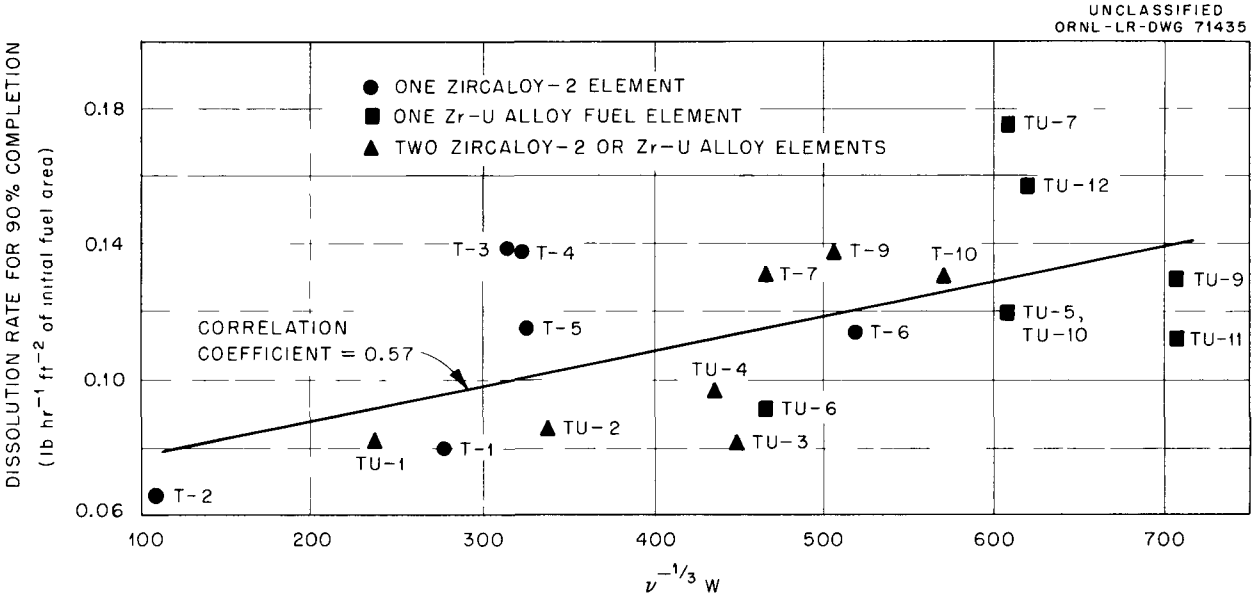

Fig. 2.2. Correlation of Volatility Pilot Plant Dissolution Data.

where

r = dissolution rate, lb hr^{-1} ft^{-2},

ν = salt kinematic viscosity, ft^2/hr,

W = HF mass velocity, lb hr^{-1} ft^{-2}.

The correlation coefficient decreased from 0.57 to 0.35 when the HF mass velocity was modified by inclusion of a geometric constant, W_0.[3] The low coefficient was attributed primarily to two uncontrolled dissolution factors: (1) the variable relation between the vessel and the fuel which existed during progressive dissolution of the matrix fuel, and (2) the effect on the dissolution rate of the metallic sludge from vessel corrosion.

Average fluorine utilization was 5.7% and fluorination time 106 min (to obtain 10 ppm of uranium in the salt) in runs TU-8 through TU-12 (Table 2.2). These values are below the overall TU series averages of 6.3% and 91 min; the range of the TU series fluorinations was from 11.7% and 55 min to 4.7% and 119 min. The spread in the fluorination results was attributed to the low uranium concentrations in the salt.

The uranium product cation impurity levels during runs TU-8 to TU-11 fluctuated greatly (Table 2.3). The run TU-9 product, with <49 ppm total cations, was the cleanest; increases were significant in run TU-10 for all impurities except molybdenum. The high copper content is unexplained. The fluorination reaction products appear to have been channeled through the NaF bed of the temperature-zoned absorber in run TU-10. The increase in the sodium content from 10 to 440 ppm indicates NaF dust entrainment. The molybdenum content of 23 ppm was that after HF removal by flashing, and the initial value was probably a factor of 5–10 greater.

Decontamination of uranium from fission products was demonstrated in six runs with 5.2 and 6.5-yr-decayed (>15% burnup) zirconium-uranium alloy fuel (analytical results for several runs are incomplete). The average fuel element dissolution rate (3.39 kg/hr) for runs R-2 to R-6 (Table 2.1) was greater than the TU-series average (2.90 kg/hr). During the R-1 dissolution, ~50% longer was required for complete dissolution for unexplained reasons. The low R-series average fluorine utilization (3.5% excluding run R-3) was attributed to the low initial uranium levels in the salt. The average product cation impurity level (636 ppm) for runs R-1 to R-3 (Table 2.3) was

[3] *Chem. Technol. Div. Ann. Progr. Rept. May 31, 1961*, ORNL-3153.

Table 2.2. Summary of Fluorination Studies

Initial molten salt: 28 to 37–26 to 32–38 to 40 mole % NaF-LiF-ZrF_4, containing UF_4 as below
Fluorination temperature: 495–515°C

Run No.	Salt U Conc. (ppm)		F_2 Flow (standard liters per min)	Fluorination Time (min)	F_2 Utilization[a] (%)	Mole Ratio of F_2 Used[a] to Original U	Fluorination Time to Obtain 10 ppm U in Salt (min)	Total Nonrecoverable U Losses	
	Initial	Final						(g)	(wt %)
TU-8	2430	2.0	6 16	100 20	5.2	19.3	111	0.415	0.08
TU-9	2455	5.0	6	100	7.8	12.8	89	1.360	0.20
TU-10	2250	6.3	6 14	100 23	4.7	21.5	119	0.887	0.28
TU-11	3000	2.2	6 14	100 20	4.7	21.5	106	0.245	0.07
TU-12	2560	4.0	6 14	100 20	6.3	16.0	103	1.270	0.16
R-1	1473	12.5	6 10 14	101 9 15	~2.7			7.020[b]	2.20
R-2	2252	0.8	6 14	101 19	4.9	20.5	81	0.143	0.03
R-3	1564	7.3	6 14	202 58	1.5	69.0	240[c]	1.438	0.45
R-4	938	3.0	6 14	101 19	3.6	27.9	94	0.681	0.32
R-5	1116	4.0	6 13.4	101 19	3.4	29.2	100	0.773	0.36
R-6	1400	0.8	6 13	101 49	2.2	46.2	134	0.134	0.06

[a] Based on time required to obtain 10 ppm U in waste salt.
[b] Loss due to excessive NaF discharge from temperature-zoned absorber.
[c] Attributed to lower than normal fluorinator salt interface temperatures.

lower than the TU-series average (732 ppm), but higher than six individual runs of the TU-series.

Fission-product decontamination factors for the uranium recovery system (fluorination and sorption-desorption steps) were 10^8–10^{10} for Cs^{137}, Sr^{90}, and rare earths, and 10^4–10^8 for Ru^{106}, Sb^{125}, and Nb^{95} (Table 2.4). All specific fission product activities were below the analytical limits of detection in the products. Contamination of the product with Pu, Np, and Tc was less than in laboratory studies,[4] averaging <1 ppb, <86 ppm, and <72 ppm, respectively, for the first four runs. Uranium and fission product entrainment during dissolution is also presented in Table 2.5 based on burnup calculations assuming no specific fission product decay prior to reactor shutdown.

Collection of pilot plant data by a data logger and processing by a digital computer (the Oracle)

[4] G. I. Cathers, R. L. Jolley, and E. C. Moncrief, *Laboratory-Scale Demonstration of the Fused Salt Volatility Process*, ORNL TM-80, p 16 (December 1961).

Table 2.3. Cation Impurities of UF_6 Product of Volatility Process

Run No. 3	Amount (ppm of UF_6)[a]												
	Cr	Cu	Fe	Li	Mo	Na	Ni	Sn	Zr	Np	Tc	Pu	Total
TU-8	<1	<1	<1	<1	100	12	15	<1	<1				<133
TU-9	<1	<1	<1	<1	19	10	14	<1	<1				<49
TU-10	188	1005	180	<5	23	440	910	460	24				<3235
TU-11	<1	1	<1	<1	47	420	3	<1	<1				<476
R-1	130	83	24	<1	32	155	52	<1	<1	157	<1	$<10^{-3}$	<637
R-2	12	12	40	<1	350	180	15	<5	<3	177	69	$<10^{-3}$	<864
R-3	<80	17	6	<1	130	96	1	<4	<4	8	59	$<10^{-3}$	<406
R-4	<1	27	13		560		<5	<10	<5	3	159		

[a]Run TU-12 product was collected without sampling; complete R-series analytical results not available.

Table 2.4. Uranium Recovery System Approximate Decontamination Factors

Fuel: 5.2 to 6.5-yr-decayed enriched zirconium-uranium alloy fuel

Run No.	Decontamination Factors[a]								
	Gross β	Gross γ	TRE β	Cs^{137}	Ru^{106}	Zr^{95}	Nb^{95}	Sr^{90}	Sb^{125}
R-1	5×10^6	10^7	10^8	$\sim5\times10^9$	$\sim5\times10^5$	$\sim5\times10^6$	$\sim10^5$	$\sim10^9$	$\sim10^7$
R-2	5×10^6	10^8	10^{10}	$\sim10^9$	$\sim10^6$	$\sim5\times10^5$	$\sim10^6$	$\sim5\times10^9$	$\sim10^7$
R-3	10^6	5×10^7	$\sim10^8$	$\sim10^9$	$\sim10^8$	$\sim10^4$	$\sim10^5$		$\sim10^4$
R-4	10^6	10^8	$\sim10^9$		$\sim10^5$				$\sim10^6$

[a]Complete R-series analytical results not available.

Table 2.5. Activity Entrainment to Dissolver Off-gas System

Fuel: 5.2 to 6.5-yr-decayed enriched zirconium-uranium alloy fuel
Feed salt: 28 to 39–30 to 42–23 to 42 mole % NaF-LiF-ZrF_4

Run No.	Amount (% of total in Dissolver Salt[a])						
	Gross β	Gross γ	U	Ru^{106}	Nb^{95}	Sb^{125}	Cs^{137}
R-1	~0.09	~0.2	<0.02	~2.6	<0.6	~5.4	
R-2	~0.09	~0.2	<0.02	~0.3	<5.0	~12.0	<0.6
R-3	~0.005	~0.2	<0.02	~0.03	<0.1	~14.5	
R-4	~0.05	~0.4	<0.03	~0.2	<0.02	~30	

[a]Complete R-series analytical results not available.

was demonstrated successfully, and 8500 data logs were processed and permanently stored on magnetic tape during the first twelve months. Photographic curves were the most practical and efficient vehicle for data dissemination.[5]

The value of automatic data logging and curve plotting of the Volatility Pilot Plant conditions is graphically illustrated in a typical curve made during autoresistance heating of a process pipe line (Fig. 2.3*a*). Since this process temperature was not continuously recorded at the panel board, the temperature excursion at 9–10 hr was completely missed with manual logging. An example of a multiple-variable curve showing three process temperatures of the dissolver off-gas scrubbing system in run T-8 is given in Fig. 2.3*b*.

2.2 APPLICATION TO STAINLESS-STEEL-CONTAINING FUELS

Dissolution of fuels containing type 347 stainless steel in molten LiF-NaF-ZrF_4 appears feasible[6] and is the basis of one flowsheet for processing the EBR-1 Core 2 fuel (88-10-2 wt % U–347 SS–Zr). The maximum solubility of stainless steel fluorides in this system appears to be in the composition region which includes the 26-37-37 % eutectic. Approximately eutectic LiF-NaF-BeF_2 (ref 7) and eutectic (46-12-42 mole %) LiF-NaF-KF also have an appreciable solubility for stainless steel fluorides. If such systems should be used, a compromise would have to be made between optimum hydrofluorination rate and maximum stainless steel solubility.

Tests with 29-36-35 mole % LiF-NaF-BeF_2 (liquidus temperature ~350°C) showed FeF_2 solubilities of 6.1, 6.1, and 2.2 wt % at 600, 500, and 400°C, respectively, with corresponding NiF_2 solubilities of 2.6, 1.3, and 0.22 wt %, and CrF_2 solubilities of 0.90, 0.82, and 0.43 wt %. Hydrofluorination dissolution rates for type 347 stainless

[5]E. C. Moncrief and M. C. Hill, *Digital Computer Processing of Pilot Plant Data*, ORNL TM-95, (Dec. 1961).

[6]*Chem. Technol. Div. Ann. Progr. Rept. May 31, 1961*, ORNL-3153, p 34.

[7]R. E. Thoma (Ed.) *Phase Diagrams of Nuclear Reactor Materials*, ORNL-2548, p 43.

UNCLASSIFIED
ORNL-LR-DWG 64637A

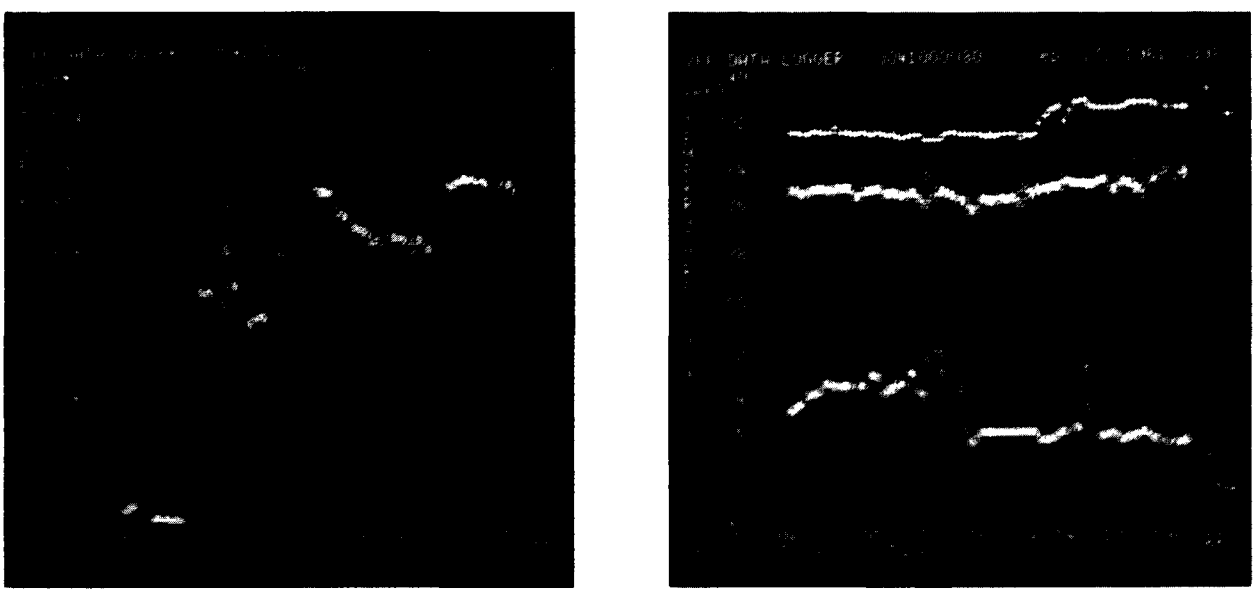

(*a*) (*b*)

Fig. 2.3. Oracle Curve Plots of Volatility Pilot Plant Operations. (*a*) Plot of molten-salt autoresistance-heated line showing temperature excursion at 10 hr. (*b*) Plot of off-gas system temperatures during a typical run.

steel in 29-36-35 mole % LiF-NaF-BeF_2 fused salt were 0.012, 0.43, and 0.13 mg min^{-1} cm^{-2}, respectively, at 400, 500, and 600°C in 5-hr tests. Rates in 40-49-11 and 36-44-20 mole % LiF-NaF-BeF_2 at 600°C were 2.5 and 1.9 mg min^{-1} cm^{-2}, respectively.

Dissolution of EBR meltdown fuel containing trapped NaK coolant would probably cause no difficulties. Simulated fuel, a 10-mil-wall type 304 stainless steel tube containing 8 cc of NaK, was immersed in molten NaF-LiF-ZrF_4 and HF was admitted at 0.25 lb/hr. The temperature was held at 500°C for 4 hr and raised to 600°C. The tube wall was penetrated at the end of 5 hr as evidenced by a salt splash in the reactor, at an average penetration rate of 2 mil/hr. The NaK reaction did not cause any noticeable change other than the salt splash, which was probably due to a sudden release of hydrogen and/or NaK vapor.

2.3 APPLICATION TO SHORT-DECAYED UO_2 FUEL AND OTHER OXIDES

Process Tests with Irradiated UO_2 Decayed 15–30 Days

In six laboratory tests, the fused salt-fluoride volatility process (Fig. 2.4) was successfully used with Zircaloy-clad UO_2 pins that had decayed 15 to 30 days, indicating that the process is potentially as useful with short-decayed fuel as with fuel that has decayed >100 days usually used in aqueous processing. Radioactive iodine and tellurium, which form volatile fluorides, were separated from UF_6 product in the NaF absorption

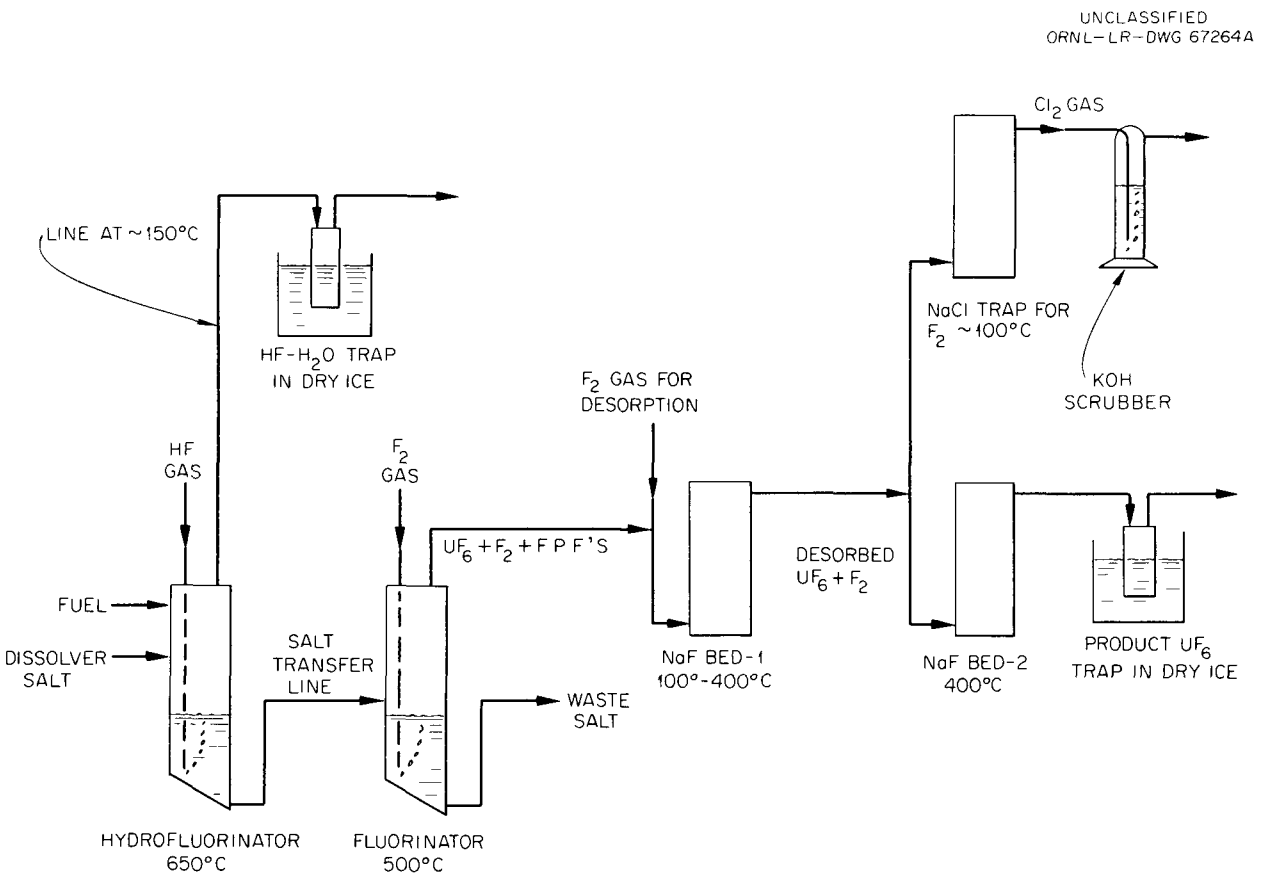

Fig. 2.4. Schematic of Flowsheet Used in Processing Short-Decayed Uranium Fuel.

step operated at 100°C. Radioactive niobium, ruthenium, and zirconium behaved in accordance with previous work, resulting also in good decontamination of the UF_6 product from their respective fluorides.[8]

The behavior in the NaF step of $Mo^{99}F_6$ (half life of 6.7 hr) was in agreement with work which determined that the decomposition temperature of the MoF_6-NaF complex is 230°C at 760 mm Hg pressure compared to 360°C for the more stable UF_6-NaF complex system. The disappearance of radioactive iodine, tellurium, niobium, ruthenium, and molybdenum in the fused salt dissolution step indicated precipitation or volatilization and condensation at the top of the dissolution reactor, with not much of any of these fluorides being carried out of the vessel with the excess HF. Dissolution rates for the irradiated UO_2 fuel were approximately the same as those with unirradiated material.

The tests (Table 2.6) were made with slightly enriched, short-decayed, UO_2 fuel with a gross burnup of 0.05 to 0.10%. Approximately 31.5 g of UO_2 and 15.4 g of Zircaloy-2 cladding were dissolved by hydrofluorination at 650°C in 1 kg of 31-24-45 mole % LiF-NaF-ZrF_4, resulting in a final composition of approximately 30-23-45-1.1 mole % LiF-NaF-ZrF_4-UF_4. Uranium was recovered by volatilization of the UF_6 formed by fluorination at 600°C. The dissolution rate of UO_2 was 11.5 mg min^{-1} cm^{-2} in cold tests; rates with the irradiated fuel varied from 8.2 to 16.5 mg min^{-1} cm^{-2}, due to experimental difficulties in manipulation of the hot-cell equipment.

Fission-product activities in the UF_6 product varied less than that of natural uranium for Sr β to 50-fold that of natural uranium for Mo γ (Table 2.7). Overall process decontamination factors varied from the order of 10^2 for Mo γ to 10^8 for Sr β (Table 2.8). Overall decontamination factors were high for Ru γ, Nb γ, I γ, and Te β activities, which are of more concern than Mo^{99} with its short half-life of 6.7 hr. Decontamination was particularly high from Zr γ, Sr β, Ba β, and Cs γ as expected from the low volatility of their fluorides.

The chief difference between processing of long- and short-decayed fuel is the presence of I^{131} activity in the latter. More than 99% of the I^{131} γ activity disappeared in the dissolution step (Fig. 2.5), as did also the Te β, Mo β, Nb γ, and

[8] *Chem. Technol. Div. Ann. Progr. Rept. May 31, 1961*, ORNL-3153.

Table 2.6. Conditions and Results in Processing of Short-decayed UO_2

Run No.	Dissolution at 650°C					UF_6 Volatilization,[b] (%)	UF_6 Recovery,[c] (%)
	Time (hr)	HF Flow Rate, STP (ml/min)	HF Utilization Efficiency (%)	HF Reaction,[a] (%)	UO_2 Dissolution Rate (mils/hr)		
1	7	750	5.0	59	8.2	98.8	98.8
2	6.5	1000	7.7	90	14.3	99.0	99.1
3	9	1000	4.4	118		99.7	99.7
4	7	1000	5.1	78	12.0	99.7	96.3
5	8	1000	4.3	98	16.5	90.0	89.3
6	7	1000	3.9	82	12.9	64.9	74.3

[a] Based on uranium concentration in salt.

[b] Based on initial and final uranium concentrations in salt; fluorination at 500°C for 3 hr, 300 ml of F_2 per minute, and absorption on first NaF bed.

[c] Based on recovered UF_6 and waste salt loss, loss in NaF beds being negligible. Desorption from first NaF bed through second NaF bed to UF_6 trap with 100 ml of F_2 per min for 1 hr.

Table 2.7. Activities in Product UF_6 from Fluoride Volatility Tests with Short-Decayed Fuel

Corrected to basis of time of final process desorption step

Run No.	Ratio of Activity Found to That of Natural U[a]												
	Zr γ	Sr β	Ba β	Cs γ	Ru γ	Nb γ	I γ	Te β	Mo β	U^{237} β	U^{237} γ	Calc. F.P.	
												Gross β	Gross γ
1		0.45		<0.1	22	13	12	$<10^{-2}$	56	2.5×10^{3}	1.6×10^{3}	56	47
2	1.3	9.0×10^{-2}	$<10^{-2}$	1.9	<0.1	3.4	3.8	$<10^{-2}$	48	1.2×10^{3}	7.8×10^{2}	48	10
3	28		$<10^{-2}$		<0.1	23	1.3	4.1×10^{-2}	3.2	4.1×10^{3}	2.9×10^{3}	3.2	52
4	8.0	2.1×10^{-3}	$<10^{-2}$		<0.1	2.2	21	5.9×10^{-3}	70	3.0×10^{3}	2.1×10^{3}	70	31
5	0.55	$<10^{-2}$	2.4×10^{-3}		0.26	2.6	120	1.9×10^{-3}	12	1.6×10^{3}	9.8×10^{2}	12	124
6	1.5	5.5×10^{-3}	$<10^{-2}$	1.1	2.6	19	16	7.5×10^{-2}	9.2	9.0×10^{2}	6.4×10^{2}	9.2	40

[a]Natural uranium activity taken as 80 β cpm and 8 γ cpm per mg U.

Table 2.8. Decontamination Factors in Fused Salt-Fluoride Volatility Process Laboratory Runs on Short-Decayed Fuel

Run No.	Overall Process Decontamination Factors								
	Zr γ	Sr β	Ba β	Cs γ	Ru γ	Nb γ	I γ	Te β	Mo β
1		9.0×10^5		4.2×10^7	3.2×10^5	8.3×10^5	4.3×10^5	8.3×10^6	3.1×10^2
2	1.1×10^7	4.5×10^6	4.3×10^7	8.4×10^5	6.2×10^7	3.3×10^6	7.0×10^5	4.8×10^6	77
3	5.3×10^5		1.2×10^8		9.1×10^7	5.3×10^5	5.9×10^6	3.2×10^6	1.5×10^4
4	2.0×10^6	2.3×10^8	6.2×10^7		7.7×10^7	6.3×10^6	2.0×10^5	1.2×10^7	1.2×10^2
5	5.3×10^7	9.1×10^7	2.7×10^8		4.8×10^7	1.2×10^7	1.9×10^4	4.8×10^7	40
6	1.5×10^7	1.3×10^8	5.6×10^7	3.2×10^5	4.0×10^6	1.2×10^6	1.9×10^5	9.1×10^5	3.2×10^2

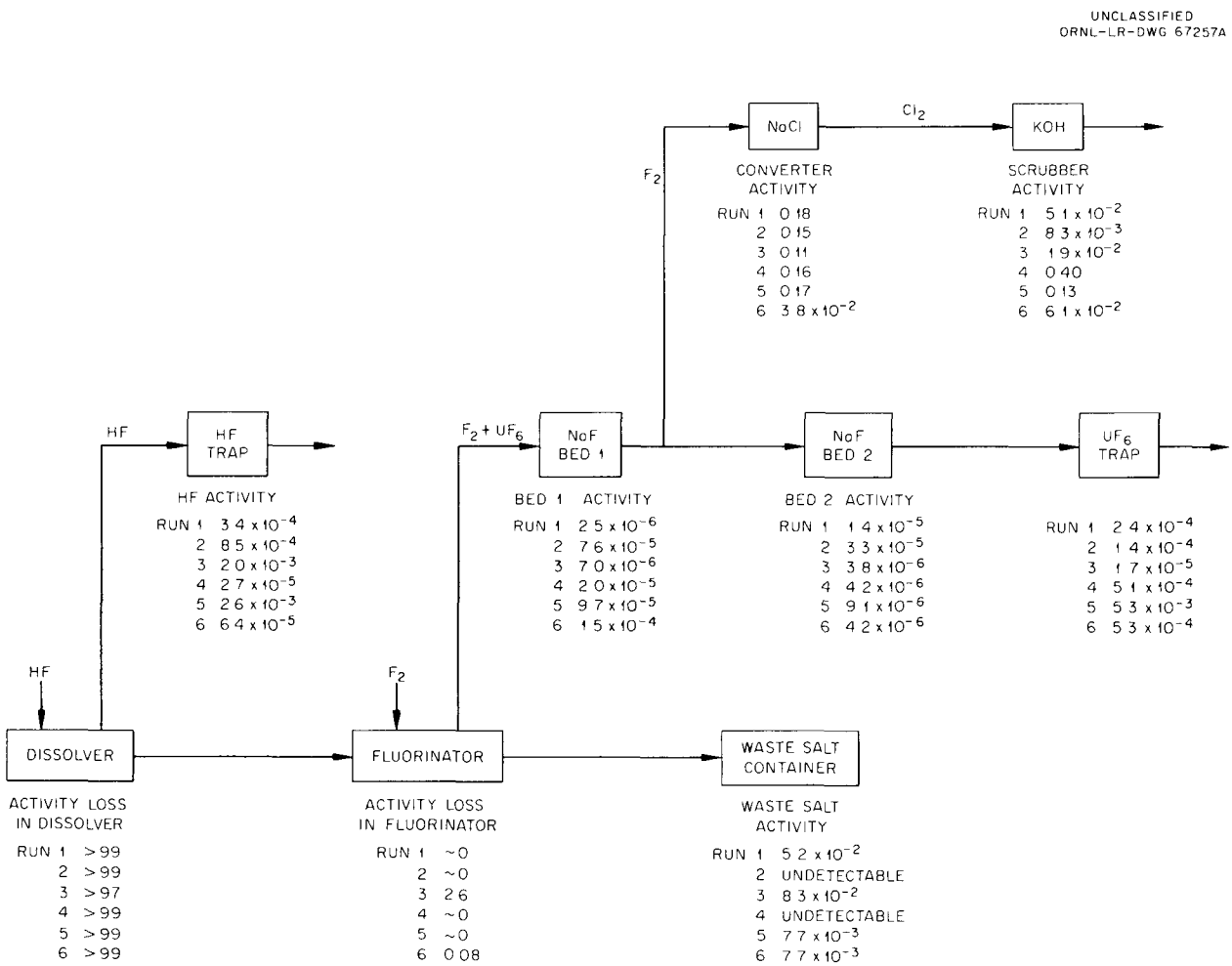

Fig. 2.5. Iodine Gamma Activity Distribution in Fused Salt–Fluoride Volatility Process Laboratory Runs on Short-Decayed Highly Irradiated UO_2 Fuel. Values are given as percentages of feed activities.

Ru γ. The I γ that remained, presumably volatilized with the UF_6 as IF_7, was separated from the UF_6 in the NaF absorption system. The molybdenum and ruthenium disappearance in the dissolution step is attributed to a reduction mechanism which resulted in plating out of these substances on the walls of the nickel dissolution vessel. From 1 to 10% of the Nb γ activity accompanied the excess HF, the remainder being either condensed on the walls in the upper vapor space or precipitated in the salt. The absence of Mo β and I γ activities in the waste HF indicates that these substances did not volatilize to any extent from the salt. The anomalous fission product behavior would perhaps be significant in operation of a molten-salt reactor or in processing of its fuel. The high Cs γ activity found (Table 2.9) was due to prior use of the equipment in processing very high burnup fuel with a long decay period.

Process Tests with Irradiated $BeO-UO_2$ and ThO_2-UO_2 Fuels

The results of tests with irradiated $BeO-UO_2$ and ThO_2-UO_2 fuels generally indicated the feasibility of this approach for such fuels, but more work is needed in developing the chemistry and the optimum salt system in each case.

Irradiated $BeO-UO_2$ fuel containing Y_2O_3 was hydrofluorinated at 650°C in 40-49-11 mole % LiF-NaF-BeF_2 in two runs and in 36-32-32 mole % LiF-NaF-ZrF_4 in one run. Fluorination of the products at 500°C volatilized only 60 to 95% of the total uranium, probably because of incomplete dissolution. Analyses of the hydrofluorinated salts indicated that only 8 and 29% of the BeO had dissolved in the first two runs, in contrast to 79% in the third run. Presumably, in dissolution some preferential leaching of the UO_2 occurred. The high result of

Table 2.9. Activities in Feed UO_2 and Dissolution Salt in Fluoride Volatility Laboratory Runs on Short-Decayed Fuel[a]

Run No.	Zr γ	Sr β	Ba β	Cs γ	Ru γ	Nb γ	I γ	Te β	Mo β
				Calculated in Feed (cpm/mg U)					
1	1.1×10^8	3.6×10^7	4.9×10^7	8.8×10^5	5.6×10^7	8.8×10^7	4.0×10^7	6.5×10^6	1.4×10^6
2	1.1×10^8	3.3×10^7	3.5×10^7	9.8×10^5	5.0×10^7	9.0×10^7	2.2×10^7	3.9×10^6	3.0×10^5
3	1.2×10^8	4.2×10^7	9.7×10^7	1.1×10^6	7.0×10^7	9.8×10^7	6.0×10^7	1.1×10^7	3.8×10^6
4	1.3×10^8	3.8×10^7	5.0×10^7	1.0×10^6	6.2×10^7	1.1×10^8	3.3×10^7	5.7×10^6	6.5×10^5
5	2.3×10^8	7.3×10^7	5.2×10^7	2.4×10^6	1.0×10^8	2.5×10^8	1.8×10^7	7.1×10^6	3.9×10^4
6	1.8×10^8	5.7×10^7	4.4×10^7	1.6×10^6	8.2×10^7	1.9×10^8	2.4×10^7	5.7×10^6	2.4×10^5
				Found in Dissolution Salt (% of that in feed)					
1	76	77	94	3800	1.6	28	0.20	1.6	<<1
2	83	94	130	1300	3.6	27			<<1
3	140	96	71	330	8.2	57	1.7	4.3	
4	90	101	87	190	4.2	56			<<1
5	96	250	107	570	11	52		11	<<1
6	110	107	83	175	12	67		8.2	<<1

[a]Procedure of ORNL-2127, Part I, Vol. I; activities corrected to time of desorption and obtaining of UF_6 product; conversion of dis/min to cpm based on recommended geometry and counting efficiencies for different radioisotopes. Radionuclides used: 63-d Zr^{95}; 54-d Sr^{89}, 28-y Sr^{90}; 12.8-d Ba^{140}; 2.0-y Cs^{134}, 13-d Cs^{136}, 26.6-y Cs^{137}; 41-d Ru^{103}, 1.0-y Ru^{106}; 35-d Nb^{95}; 8.0-d I^{131}; 90-d Te^{127m}, 33-d Te^{129m}, 77-d Te^{132}; 67-h Mo^{99}.

the last run possibly means that ZrF_4 promotes the hydrofluorination of BeO, perhaps through metathesis. Decontamination of the recovered UF_6 in each run was high. Irradiated ThO_2-UO_2, in two runs, was hydrofluorinated at 650°C in 36-24-40 mole % LiF-NaF-ZrF_4, and the product was fluorinated at 600°C. As in the BeO-UO_2 runs, both dissolution and UF_6 volatilization were incomplete. The most notable feature of this work was observance of the behavior of Pa^{233}. In the second run 10.6% of the protactinium was volatilized (probably as PaF_5) with the excess HF over a 19-hr period at 650°C; in the first run, which was probably not carried as near completion, <0.01% volatilized. In both tests, PaF_5 volatilization was negligible (0.01 to 0.03%) in the 3-hr fluorination period at 600°C. The contrast between the 600 and 650°C volatilization behavior is striking, although the results agree with the observation that PaF_5 has low volatility, with a sublimation or boiling point as high as 500 to 600°C.[9]

ZrO_2 Hydrofluorination

Zirconium oxide in an array of 2 by 4 by ¼ in. parallel slabs reacted with HF in molten 26-43-31 mole % NaF-LiF-ZrF_4 in an INOR-8 reactor (Table 2.10, Fig. 2.6) at about twice the rate of Zircaloy-2 simulated fuel elements. In a copper-lined dissolver, where metallic particles resulting from vessel corrosion are not present, the rate curve for Zircaloy-2 dissolution is smooth. These conditions are nearer those for zirconium oxide dissolution than to the dissolution of Zircaloy-2 in an INOR-8 vessel.

Partial dissolution of the Zircaloy-2 left a deposit of metallic particles on the element because of zirconium metal reduction of nickel fluoride formed by vessel corrosion. Immersion of the partially dissolved Zircaloy-2 elements from runs DO-4 and DO-8 in boiling ammonium oxalate solution removed metallic particles before the final weighing. No ammonium oxalate treatment was used in run DO-1, which may partially account for its low apparent dissolution rate. The low dissolution rate in run DO-8 is due to the low specific HF feed rate. The rate for Zircaloy-2, after being cleaned in Run DO-4, was identical to that in a copper-lined vessel with very similar HF flow and temperature conditions.

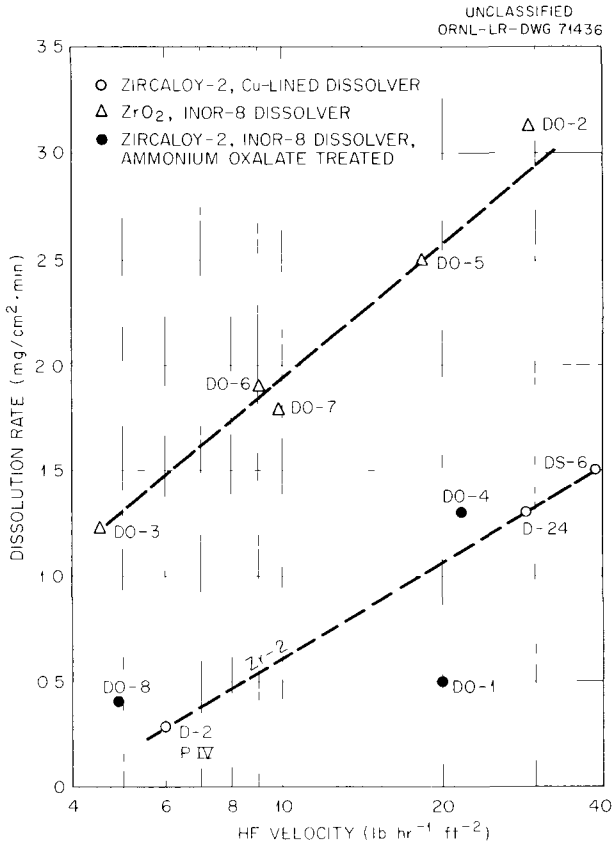

Fig. 2.6. Comparison of Dissolution Rates of Zircaloy-2 and ZrO_2.

Corrosion

Preliminary results of corrosion studies[10] indicated that with BeO at 570°C corrosion should not be a problem under the conditions studied. Further work (Table 2.11), in which ZrO_2 was dissolved in 43-57 mole % NaF-LiF at 700°C for comparison with results of an earlier study[10] on corrosion in melt alone and in the presence of dissolving Zircaloy-2 indicated that in dissolution of ZrO_2 corrosion should be similar to that with melt alone.

[9] F. T. Miles *et al.*, "A Continuously Separating Breeder Blanket Using ThF_4," *Nucleonics*, pp 26–29, July 1954.

[10] *Chem. Technol. Ann. Progr. Rept. May 31, 1961*, ORNL-3153, p 35.

Table 2.10. Dissolution Ratio of Zircaloy-2 and ZrO_2 in Different Dissolvers

Run No.	Dissolution Specimen	Dissolver	Cross Sectional Area (ft^2)		HF Feed Rate		Temp (°C)	Salt Comp. (mole %)			Dissolution Rate (mg min^{-1} cm^{-2})
			Dissolver	Element	lb/hr	lb hr^{-1} ft^{-2}		NaF	LiF	ZrF_4	
D-2	Zircaloy-2	Cu lined	0.179	0.0274	1.06	7	650	55		45	0.27
D-24		Cu lined	0.0935	0.0256	2.0	29	600	68		32	1.3
DS-6		Cu lined, with draft tube	0.0451	0.0152	1.0	39	600	24	42	34	1.5
DO-4		INOR-8, 3.5-in. diam, 24-in. high	0.0666	0.0152	1.12	21.8	615	26	43	31	1.3
DO-1		INOR-8, 3.5-in. diam, 13.5-in.high	0.0666	0.0152	1.06	2.0	600	26	43	31	0.5
DO-8			0.0666	0.0152	0.25	4.9	615	26	43	31	0.4
DO-5	ZrO_2		0.0666	0.0053	1.12	18.3	615	26	43	31	2.5
DO-6			0.0666	0.0053	0.56	9.1	615	26	43	31	1.9
DO-7			0.0666	0.0053	0.60	9.8	615	26	43	31	1.8
DO-2			0.0666	0.0053	1.51	29	700	26	43	31	3.13
DO-3			0.0666	0.0053	0.23	4.5	600	26	43	31	1.24

Table 2.11. Corrosion of INOR-8 in Molten Fluoride During Hydrofluorination of Fuel Components

HF flow rate: 10 g/hr

Sample Location	Maximum Penetration Rate, mils/month			
	53-47 mole % $NaF-ZrF_4$, 570°C, 300 hr, BeO Dissolved	43-57 mole % NaF-LiF, 700°C		
		200 hr, ZrO_2 Dissolved	214 hr, Zircaloy-2 Dissolved	93 hr, Salt Alone
Vapor	1	44	Slight	~43
Interface	5	97	31	~60
Liquid	0.1–1.6	34	Slight	~43

2.4 GENERAL PROCESS DEVELOPMENT

Hydrofluorination Corrosion

Further laboratory-scale studies[11] (Table 2.12) showed the potential usefulness of Alloy 79-4 (79% nickel, 4% molybdenum, plus iron and trace elements) as a hydrofluorinator construction material and indicated the high corrosion rate to be expected at the interface when dissolving Zircaloy-2 in 50.5-37.0-12.5 mole % $NaF-LiF-BeF_2$ with HF at 650°C. The latter melt was developed in an attempt to provide a cheaper initial mixture for a nonrecycle dissolution scheme than the equimolar NaF-LiF–25 mole % ZrF_4 now being used in the Fluoride Volatility Pilot Plant. Intergranular corrosion was noted on Alloy 79-4 exposed to $NaF-LiF-ZrF_4$, which would have to be balanced against the slightly less favorable results obtained with INOR-8 under fluorination conditions (see below) for a vessel to be used for both hydrofluorination and fluorination.

Correlation of corrosion data accumulated during prototype hydrofluorination rate studies with the kinematic viscosity of molten salt showed the relation $R = k\nu^{-2.5}$ In HF rate, where R is the corrosion rate of INOR-8 in HF-sparged sodium-lithium-zirconium fluoride, k is a constant, and ν is the kinematic viscosity (Fig. 2.7). At an HF rate of 40 lb/hr per square foot of reactor cross section, the corrosion rate was 5.2 mils/month at a kinematic viscosity of 0.0950 ft^2/hr (23 mole % ZrF_4, 650°C) and was less than a measurable amount after 40-hr exposure at a kinematic viscosity of 0.1860 ft^2/hr (33 mole % ZrF_4, 550°C).

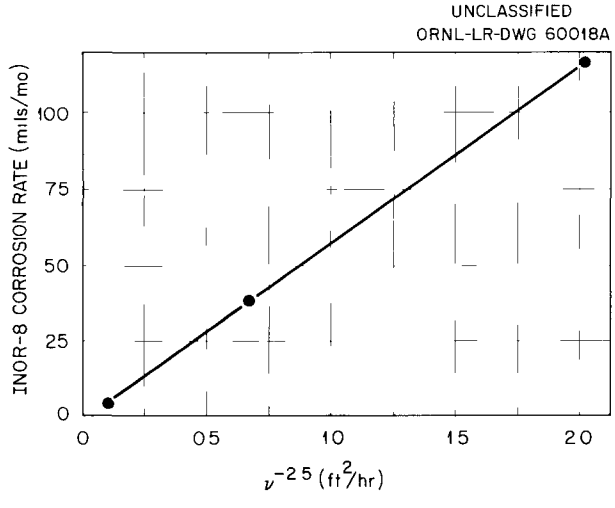

Fig. 2.7. Correlation of INOR-8 Corrosion Rate with ν, Kinematic Viscosity, at HF Rate of 4.0 lb/hr.

Fluorination Corrosion

The superiority of Alloy 79-4 as a fluorinator construction material over INOR-8 and L-nickel in $NaF-LiF-ZrF_4$ melts alone and with BeF_2 was also shown[12] (Table 2.13). However, the higher

[11] Made at Battelle Memorial Institute under subcontract.

[12] P. D. Miller *et al.*, *Construction Materials for the Hydrofluorinator of the Fluoride Volatility Process*, BMI-1348, (June 3, 1959).

Table 2.12. Corrosion of INOR-8 and Alloy 79-4 in Molten Fluoride During Hydrofluorination

Zircaloy-2 added periodically to simulate continuous dissolution conditions

Run Time: 200 hr

Temperature: 650°C

Metal	Penetration Rate, mils/month							
	(37.5-37.5-25 Mole %) $NaF-LiF-ZrF_4$				(50.5-37.5-12.5 Mole %) $NaF-LiF-BeF_2$			
	23 g/hr HF				9.6 g/hr HF			
	Basis	V[a]	I	L	Basis	V	I	L
INOR-8	Max i.g.[b]	0			[c]	7	110[d]	7[c]
	Max wt loss	0.1	0.3	Gain	wt	0.6		Gain
Alloy 79-4	Max i.g.[b]	0.9	5.5	2.7	[c]	3	88[d]	3[d]
	Max wt loss	0.5	0.3	0.6	wt	0.5		

[a] V = vapor; I = interface; L = liquid.

[b] Intergranular.

[c] Microscopic measurement of metal remaining. Losses too low for measurement with micrometer.

[d] Maximum of micrometer and microscopic measurements.

Table 2.13. Corrosion of INOR-8 Alloy 79-4, and L-Nickel in Molten Fluoride During Fluorination

UF_4 added periodically as source of UF_6

Temperature: 500°C

Metal	Maximum Penetration Rate, mils/month					
	27.5-27.5-45 mole % $NaF-LiF-ZrF_4$, 148 hr F_2			27.8-20.4-6.8-45 mole % $NaF-LiF-BeF_2-ZrF_4$, 162 hr F_2		
	V[a]	I	L	V	I	L
INOR-8	3	11	11	9	38	6
Alloy 79-4[b]	1	4	2	7	13	5
L-Nickel	8	25	28	11	31	22

[a] V = vapor; I = interface; L = liquid.

[b] Ni, 79%; Mo, 4%; Fe, balance.

corrosion of the BeF_2-containing melt is evident. More detailed data presented elsewhere[13] show that the L-nickel corrosion under fluorination conditions is almost entirely intergranular attack.

Since Alloy 79-4 contains no chromium, it would be expected to have rather poor resistance to air oxidation at elevated temperatures. Total corrosion rates attributable to high-temperature oxidation of as-received Alloy 79-4, L-nickel, and INOR-8 were 1.1, 1.6, and 1.6 mils/month, respectively, compared to rates of 2.2 and 0.0 mils/month for aluminum-coated and chromium-coated Alloy 79-4. Thus, uncoated Alloy 79-4 is probably usable, but chromium treatment gives essentially complete protection.[14]

In exploratory studies in the Fluoride Volatility Pilot Plant fluorinator, in which test rods were exposed to actual operating conditions during all nonradioactive runs, no significant improvements were noted from a fluorine preconditioning treatment of L-nickel or from the use of high-purity vacuum-melted nickel. Neither were essential differences noted from the exposure of binaries of nickel and the following alloys: 2% Mn; 5, 10, and 20% Fe; 5 and 10% Co; 1 and 3% Al; and 0.05, 0.1, and 1% Mg.

[13] F. W. Fink *et al.*, BMI, "Corrosion Investigation of 'L' Nickel Under Fluorination Conditions," letter to R. P. Milford, ORNL, Sept. 15, 1961.

[14] P. D. Miller *et al.*, *Corrosion Investigation of HyMu 80, INOR-8, and 'L' Nickel Under Fluorination Conditions and Under Air Oxidation Conditions*, BMI-X-192, (Feb. 26, 1962).

Volatilization of UF_6 from BeF_2 Salt Compositions at Low Temperatures

Laboratory-scale work with 29-36-35 mole % LiF-NaF-BeF_2 fused salt (~350°C liquidus) gave favorable UF_6 volatilization results, indicating the possibility of using this or similar low melting salt systems at low temperatures to minimize fluorination corrosion. In separate tests at 400, 450, and 500°C with salt containing ~1 wt % UF_4, the corresponding residual concentrations after a 1-hr fluorination were 0.67, 0.19, and 0.04 wt %; after a 2-hr period the concentrations were 0.19, 0.03, and 0.04; and after a 3-hr period they were 0.04, 0.05, and 0.03. All the concentrations eventually decreased only to the 0.03–0.05% range, apparently as the result of insufficient care being taken in cross-contamination in sampling, but further work is needed in this area.

Fluorination of UF_6 from melts with a high alkali fluoride content has resulted in the past in severe corrosion (e.g., in the eutectic sodium-potassium-lithium fluoride system). This seemed also the case in fluorination tests with 40-49-11 mole % LiF-NaF-BeF_2 salt at 600°C, where the nickel corrosion rate was >10 mils/hr. However, cursory corrosion results with 20 and 35 mole % BeF_2 indicated insignificant attack.

Recycle and One-Vessel Process Testing

A program of recycle testing in prototype equipment with provisions for dilution and purification by chemical reaction and settling has been established (Fig. 2.8). The most costly component of the NaF-LiF-ZrF_4 solvent salt used for dissolution of fuel containing Zircaloy-2 is the ZrF_4. Since large quantities of this material are formed in the dissolution reaction, recycled waste salt can be diluted with NaF-LiF to provide starting salt at a considerably lower cost. The recycle process will concentrate all soluble or suspended impurities in the waste salt, and this concentration might interfere with subsequent dissolutions. A number of recycle methods are possible if the use of both a one-vessel and two-vessel (hydrofluorinator and fluorinator) process is considered. The simplest systems (cases I and IV, Fig. 2.9) require new fuel elements to be charged to a vessel containing molten salt. Since this is considered an undesired complexity, the equipment setup shown in Fig. 2.8 is designed to suit case V, which is a single vessel modification of case III.

UF_6 Absorption

The temperature and concentration dependence of the rate of absorption of UF_6 on NaF was established from studies with single layers of NaF pellets in a fixed bed. With increased temperature, the initial absorption rate increased, with absorption confined more nearly to the periphery of the pellet. However, due to the physical blockage of the pores in the NaF, this effective capacity was lower than at lower temperatures. With an increase in the UF_6 concentration in the flowing stream, there was a straight-forward increase in the absorption rate. The density of the complex $UF_6 \cdot 3NaF$ was measured as 3.88 g/cm^3 at 26°C.

A mathematical model predicting the experimentally observed characteristics of the absorption process was devised. The associated partial differential equations were coded for solution with a digital computer, and preliminary agreement between calculated and experimental results was observed. Future work will include calculations for a multilayer bed of NaF with provision for removal of fluorides other than UF_6, for example, MoF_6 and NbF_5.

F_2 Disposal

Two methods of destroying waste fluorine were investigated experimentally. In one case fluorine was reacted with picnic grade charcoal at rates up to 2.25 standard liters/min in a 4-in.-diam bed. The effluent gas contained less than 100 ppm of fluorine, and was composed largely of CF_4 and other fluorocarbons. Significant amounts of HF and water were formed, apparently from compounds present in the charcoal, and a small amount of resinous solid (probably polymerized fluorocarbons) condense in the off-gas line. The second method was reaction of sulfur dioxide and fluorine to form sulfuryl fluoride (SO_2F_2). The entering gases were preheated to ~200°C and reacted in a 3-in.-diam pipe. At 1.7 standard liters/min of fluorine the reaction zone temperature was 270° C without cooling. In future tests the off-gas composition will be evaluated for completeness of reaction at various flow rates.

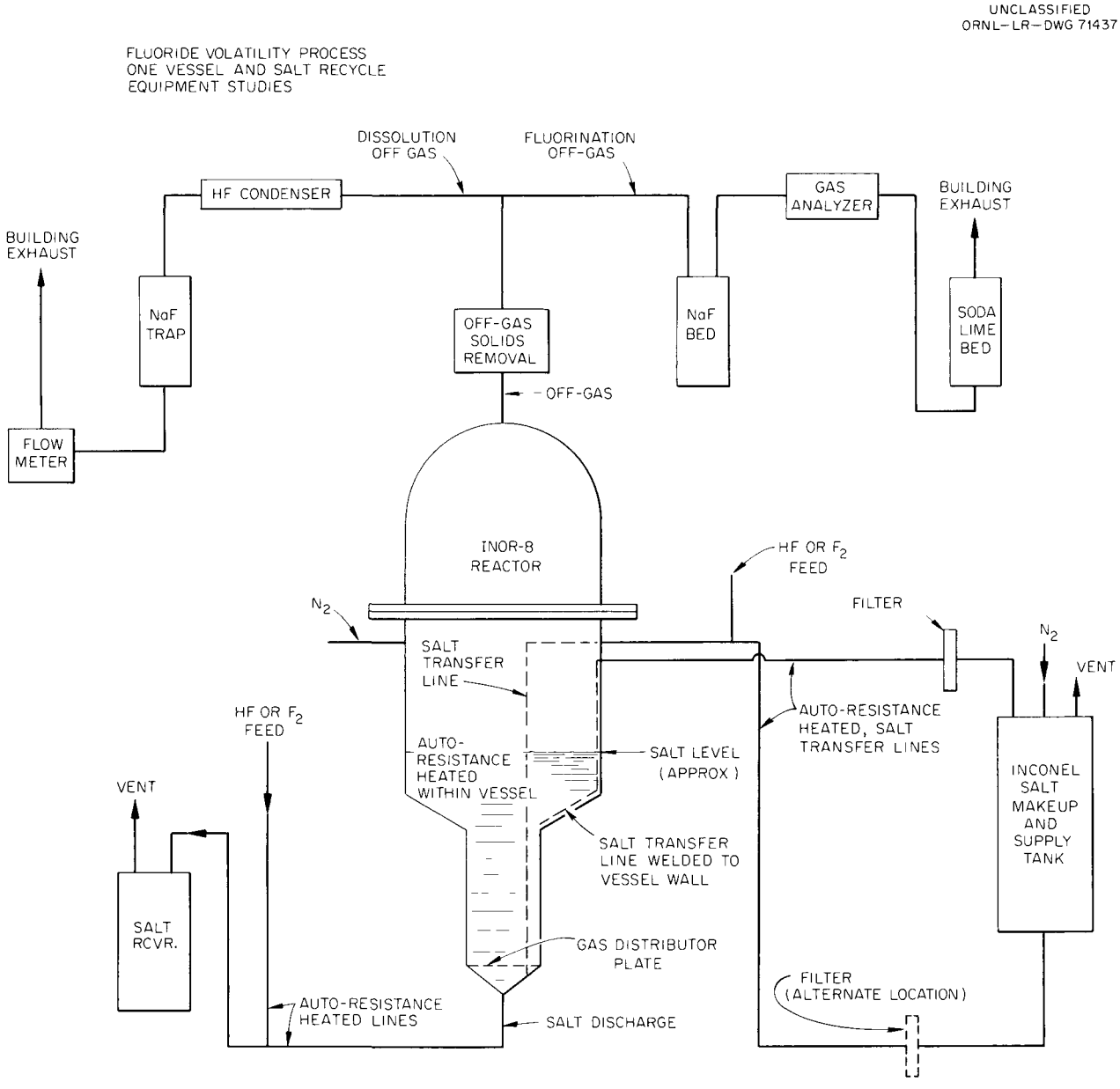

Fig. 2.8. Single-Vessel Process with Recycle.

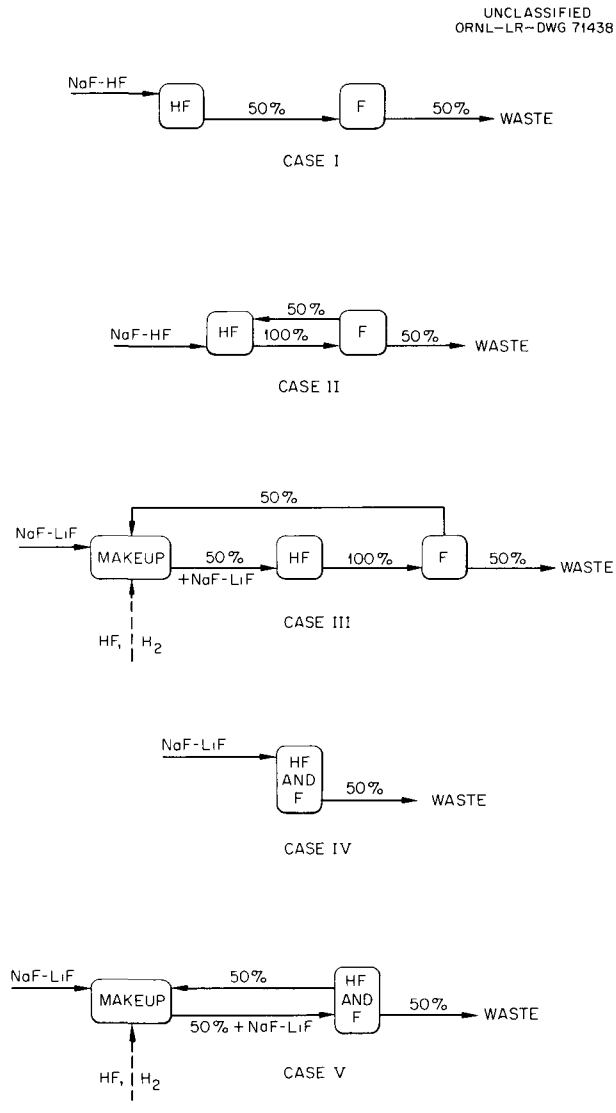

Fig. 2.9. Salt Recycle Flow Diagrams. For all cases percentages refer to the volume of a batch.

Molten-Salt Atomizer

The use of a molten-salt atomizer as a means of fluorination or as a means of producing particles suitable for a fluid or fixed bed process was investigated. A heated nozzle discharging about 0.3 ft^3/hr of $NaF-LiF-ZrF_4$ salt was surrounded by a concentric vapor phase nozzle delivering ~5000 ft^3/hr of air. Spherical particles ranging from 25 to 100 μ in diam were produced (Fig. 2.10). The particle diameter was varied by changing the volumetric ratio of the liquid and gas phases. A relatively low pressure drop (~10 psig) across the molten-salt nozzle was required.

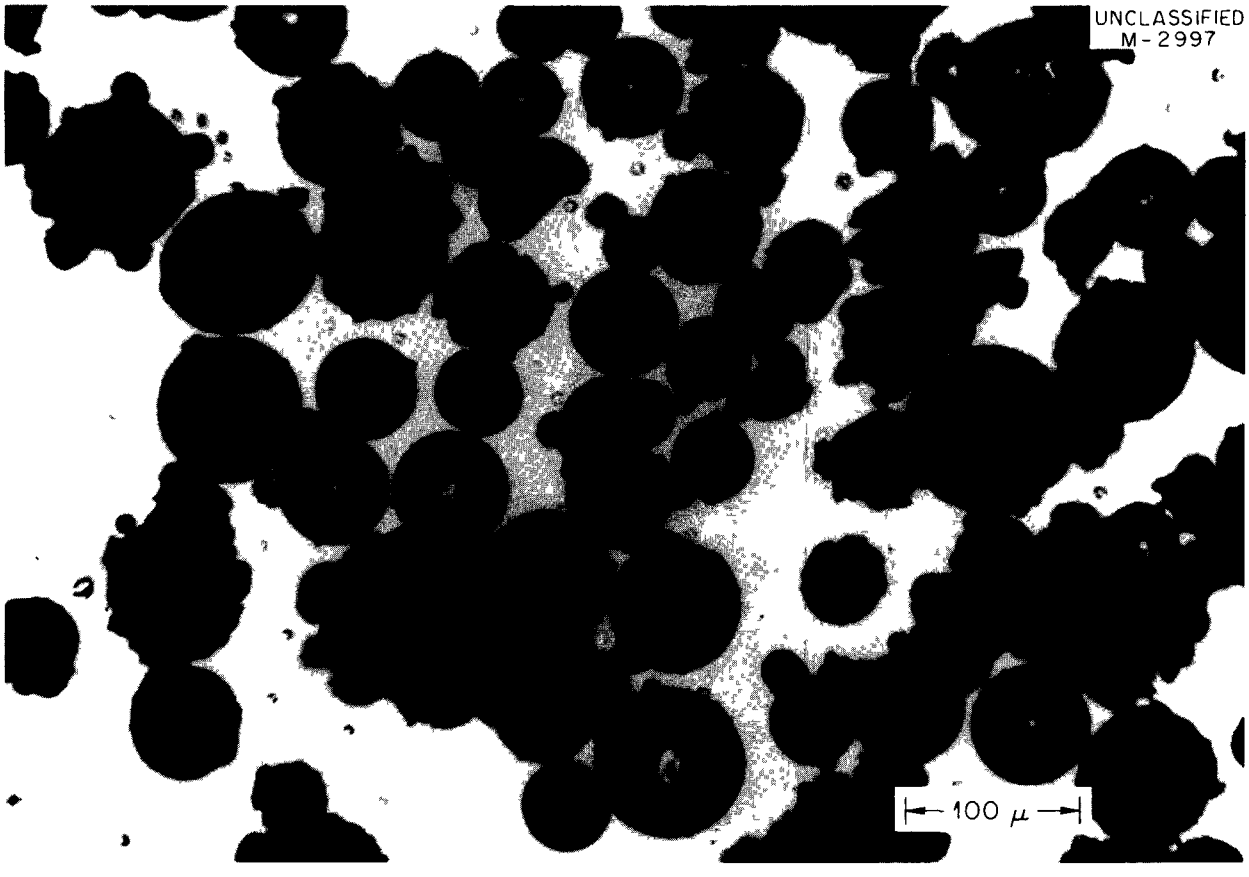

Fig. 2.10. Atomized Salt.

3. Waste Treatment and Disposal

This program is concerned with the development and demonstration on a pilot-plant scale of processes for the treatment and final disposal of radioactive wastes resulting from reactor operations and reactor fuel processing in the forthcoming nuclear power industry. In addition to the normal desire for improvement in present methods of waste management, a major incentive for pursuing this work arises from the different types of wastes to be expected from a nuclear power industry, compared with those now being produced. Waste management will grow more complex both because of a greater variety of reactors and fuel types and because of more stringent health and safety requirements demanded by an expanding population.

Principal emphasis has been on high- and low-activity liquid wastes. A process has been advanced through the laboratory and nonradioactive engineering stage for converting high-activity wastes to solids by high-temperature pot calcination. The wastes are evaporated to dryness, and the residual solids are calcined in a cylindrical stainless steel pot which, when sealed, also serves as the final storage container. The process is not

only suitable for handling a variety of waste types, but also offers the possibility of fixing the fission products in glassy materials of very low solubility. A pilot plant was designed, in cooperation with Phillips Petroleum Company, to demonstrate the process with actual wastes at the Idaho Chemical Processing Plant (ICPP). At the end of FY 1962, the Division of Reactor Development, Washington, decided to move this program to Hanford; design studies are now being initiated for this change.

A combination process (scavenging plus ion exchange) for decontaminating very dilute salt solutions such as cooling water and canal water has been developed and demonstrated with ORNL process waste in a 600-gal/hr pilot plant. Based on the performance of this pilot plant, design criteria can be specified for a 750,000-gal/day plant to decontaminate the total process-waste stream to <3% of the maximum permissible concentration of radionuclides in drinking water $(MPC)_w$, for continuous occupational exposure.

An economic and hazards evaluation of alternative methods for the treatment and disposal of highly radioactive liquid and solid wastes was undertaken jointly with the Health Physics Division. Following a cost study of interim liquid storage in tanks, the economics of pot calcination were investigated and preliminary costs for solid-waste shipment and disposal in salt formations estimated.

3.1 HIGH-ACTIVITY WASTE TREATMENT

In the pot-calcination process, radioactive waste is evaporated as much as possible without precipitation of solids and is then pumped to an externally heated vessel in which it is thermally decomposed to metal oxides and sulfates at temperatures up to 900°C (Fig. 3.1). After the calcination is complete, the vessel is disconnected from the system, sealed, and transported to a permanent storage site. The gaseous nitrogen

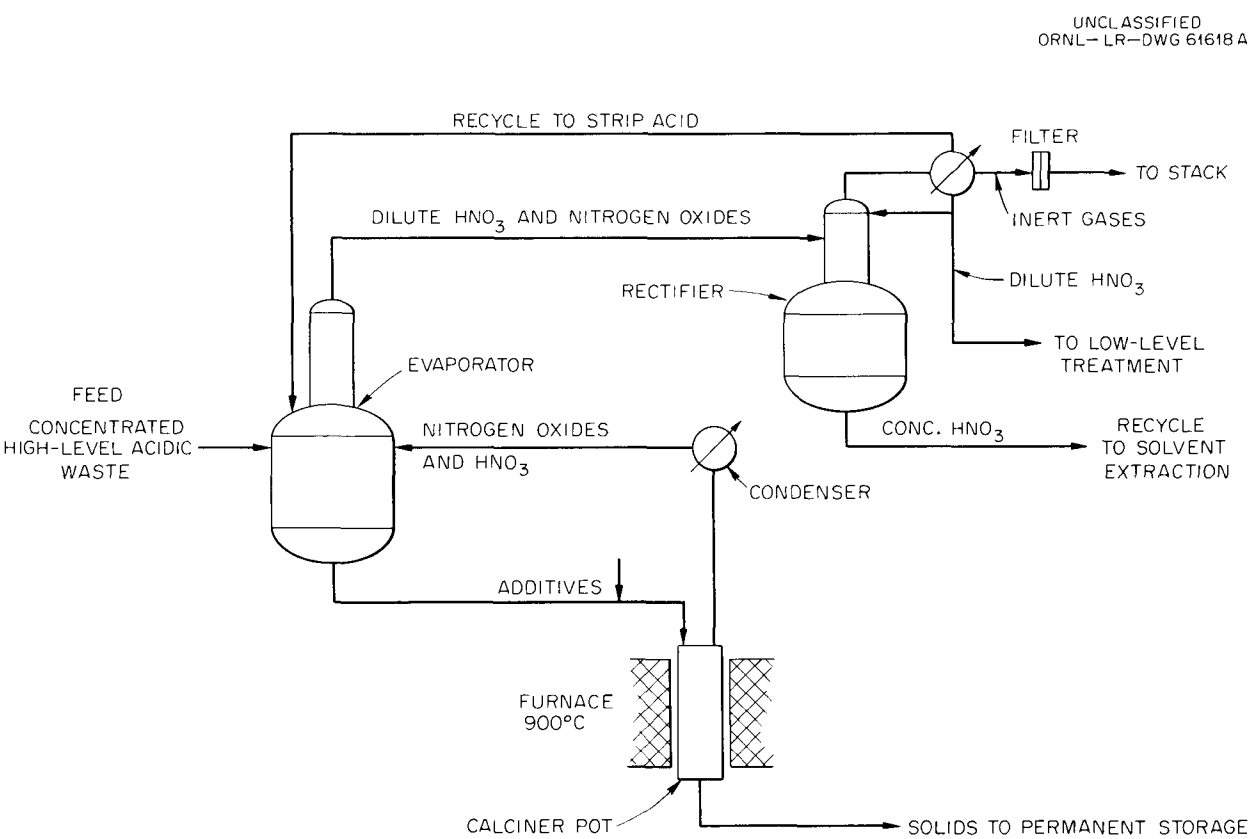

Fig. 3.1. Flowsheet for Converting High-Level Wastes to Solids.

oxides produced by the high-temperature decomposition of nitrates are recycled to the evaporator and then to a rectifier. During passage through the evaporator and rectifier, in which there is excess oxygen, the nitrous and nitric oxides are reabsorbed to form nitric acid. A small volume of noncondensable gas is passed through a York-mesh or impingement plate de-entrainer to remove fission products and then is vented through filters to a stack. The nitric acid thus decontaminated is concentrated by distillation, and the concentrated acid is recycled to the fuel processing plant. The distillate, part of which is recycled to the evaporator to strip nitric acid, is subsequently handled as low-activity waste. The volume of off-gas discharged is small, being only that from instrument bubblers and system leakage. The system can be made essentially continuous, with one evaporator feeding a number of calcining pots operating in sequence.

The diameter of the pot is determined by the heat-generation rate in the calcined radioactive solids, the maximum allowable wall temperature of the pot, and the thermal conductivity of the deposited solids. Further, it is necessary that the temperature of the waste solids remain below the calcination temperature during long-term storage. Otherwise, residual nitrate or sulfate may be decomposed during transportation and storage, causing pressurization of the pot and possibly accelerated corrosion. The pots will vary in size from 6 to 24 in. in diam and from 8 to 15 ft in height, the diameter being limited by the ability to lose decay heat under storage conditions and the length by the size and weight of shipping cask.

The design of a pilot plant for the demonstration of the pot-calcination process has progressed through the process- and engineering-flowsheet stages, and remotely operated mechanical equipment has been designed and built. Work on both engineering and laboratory scales with synthetic Purex, TBP-25, and Darex wastes (Table 3.1) was performed in support of the pilot plant design. Engineering studies were concerned with the operability of both continuous and batch evaporators in series with the pot and with obtaining information required to construct chemical and material-balance flowsheets. Laboratory work was devoted to studies of vapor-liquid equilibria, ruthenium volatility, preparation of glasses for fixation of the fission products and measurement of their thermal conductivities, and corrosion under process conditions.

Table 3.1. Compositions of Simulated High-Activity Wastes

Component	Concentration (moles/liter)		
	Purex	TBP-25	Darex
Al^{3+}	0.1	1.72	
Fe^{3+}	0.5	0.003	1.2
Cr^{3+}	0.01		0.4
Ni^{2+}	0.01		0.2
Na^{+}	0.6	0.1	
H^{+}	5.6	1.26	2.0
Hg^{2+}		0.02	
NH_4^{+}		0.05	
Mn^{2+}			0.04
NO_3^{-}	6.1	6.6	7.2
SO_4^{2-}	1.0	0.026	
Cl^{-}			0.001

Pilot Plant Design

Chemical flowsheets for batch and continuous processing of TBP-25 and Purex wastes and for the continuous processing of Darex waste were completed, and, in conjunction with Phillips personnel, cell layouts and process and engineering flowsheets were prepared. A subsequent decision by the AEC changed the intended location of the pilot plant from ICPP to Hanford, with the expectation that as much as possible of the original design be retained.

A simplified process flowsheet with equipment capacities based on maximum flow rates is given in Fig. 3.2. The rates will be maximum when feeding 12-in.-diam pots, but provisions were made for the plant to accommodate also 6- or 8-in.-diam pots when processing wastes with high fission-product heat evolution. The plant will use either continuous or batch evaporation, and the calciner will be fed either by gravity from the concentrated feed tank or by pump.

The equipment will be made of type 304L stainless steel, except for the evaporator, calciner condenser, and fractionator, which will be of titanium. Titanium was selected for these vessels because of its resistance to chloride and Cr(VI) attack from Darex wastes, resistance to boiling,

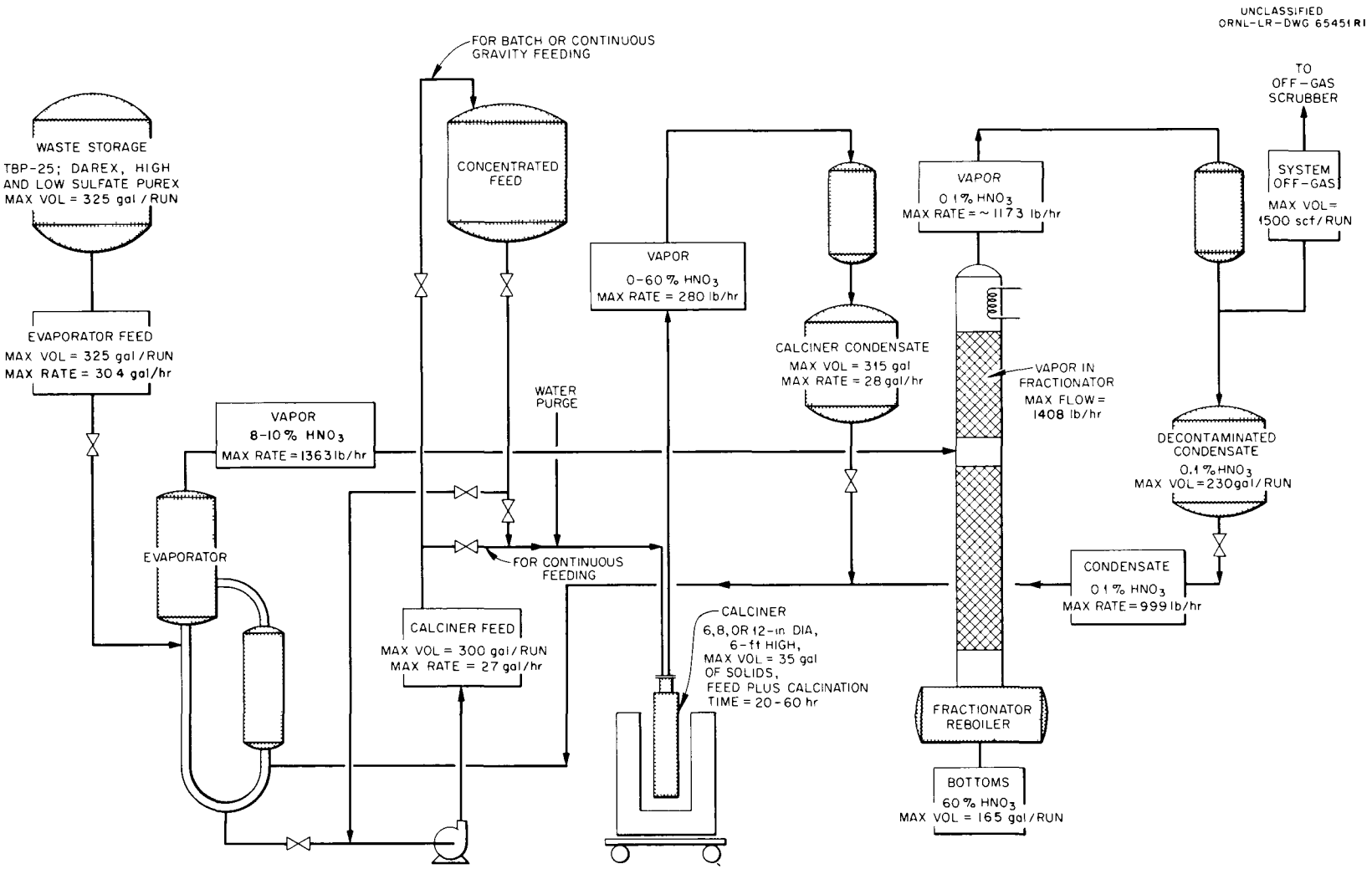

Fig. 3.2. ICPP Pot Calcination Pilot Plant. Maximum flow rates and liquid volumes based on use of a 12-in.-diam pot.

concentrated HNO_3 solutions, and the absence of grain boundary corrosion, which is observed when Purex solutions are contacted with stainless steel.

Engineering-Scale Studies

Engineering-scale studies were made on the evaporation and calcination steps of the pot-calcination flowsheet. The studies were performed with a continuous evaporator and a batch evaporator in series with an 8-in.-diam by 90-in.-long stainless steel calciner pot. Both units have distinct advantages. The continuous evaporator combines the advantages of small size and low holdup and permits a somewhat more compact and efficient process. The batch evaporator, with a simpler control system, allows more precise control of calciner feed composition and density and, because of its long holdup time, affords an opportunity for the decomposition of any organic-solvent degradation products that might be present before they are fed to the calciner.

The continuous evaporator is a thermosyphon type, equipped with a 22-ft external heat exchanger that uses 100-psi steam for heating (Fig. 3.3). The evaporator has a boilup rate of 4 to 6 liters/min and operates normally with 25 to 30 liters of holdup. A bottom drawoff from the evaporator connects to a pump loop that flows past the calciner pot and returns to the evaporator. To decrease chances of plugging and to maintain a constant feed to the calciner, a 10-gpm flow is maintained in this loop by a canned-rotor pump. The pipe for the small sidestream of liquid drawn off through a control valve into the calciner pot is kept as short as possible, 2 ft, and the control valve is placed as near the operating loop as possible. A water purge bled into the feed stream downstream of the control valve at 1 liter/hr decreases the frequency of plugging.

The calciner vapor is condensed in a 15-ft^2 downdraft heat exchanger and returned directly to the evaporator. The liquid is supercooled to recover 85–95% of the nitrogen oxides and decrease the gas volume for better decontamination. Recycled water and feed are added to the evaporator through their individual control valves from head tanks. The evaporator vapor passes through a de-entraining section consisting of 24 in. of Yorkmesh packing and then to a 34-ft^2 heat exchanger that operates downdraft. The condensable fraction of the vapor goes to a condensate receiver, where it is measured and discharged through a pressure seal. The noncondensable vapor goes to the off-gas system, where it is filtered, and the volume is measured in a wet test meter.

The batch evaporator system (Fig. 3.3) consists of a submerged-coil evaporator and feed holdup tank capable of processing a 150-gal batch of waste solution. The 22-ft^2 steam coil is designed to operate at a boilup rate of 3 liters/min with a 200% freeboard. A feed batch is concentrated in the evaporator at the same time that a previously evaporated batch is fed to the calciner from the feed holdup tank; either a canned-rotor pump or a submerged centrifugal pump (Nagle type CWO-CS) is used. Condensate from the calciner is recycled continuously to the evaporator, where it is combined with the new batch of material being prepared for the subsequent run. After passing through an impingement baffle for de-entrainment of particulates, the evaporator overheads are condensed, measured, and discharged similarly to the overheads from the continuous unit.

The impingement entrainment separator (Fig. 3.4) designed for the batch evaporator was based on the work of Schlea and Walsh.[1] Of the two impingement plates provided, the first removes the bulk of the entrained liquid at impingement velocities up to 33 fps. The second plate is designed to remove particles in the 3- to 10-μ range at impingement velocities up to 90 fps. At higher velocities, re-entrainment will occur. Pressure differences across this device of as much as 5 in. H_2O have been observed during operation.

The calciner pots (Fig. 3.5) were made of 8-in.-diam sched-5 stainless steel pipe with an overall height of about 90 in. and with an internal baffle about 6 in. from the top. A 3-in. flange on Grayloc coupling at the top of the pot permitted connection of the feed and off-gas lines in a single operation. The pots were suspended in a 54-kw electric resistance furnace which was divided into six sections, each about 13 in. high. Twenty-four

[1] C. S. Schlea and J. D. Walsh, "De-entrainment in Evaporators," paper presented at AIChE, 42d National Meeting, Feb. 21–24, 1960.

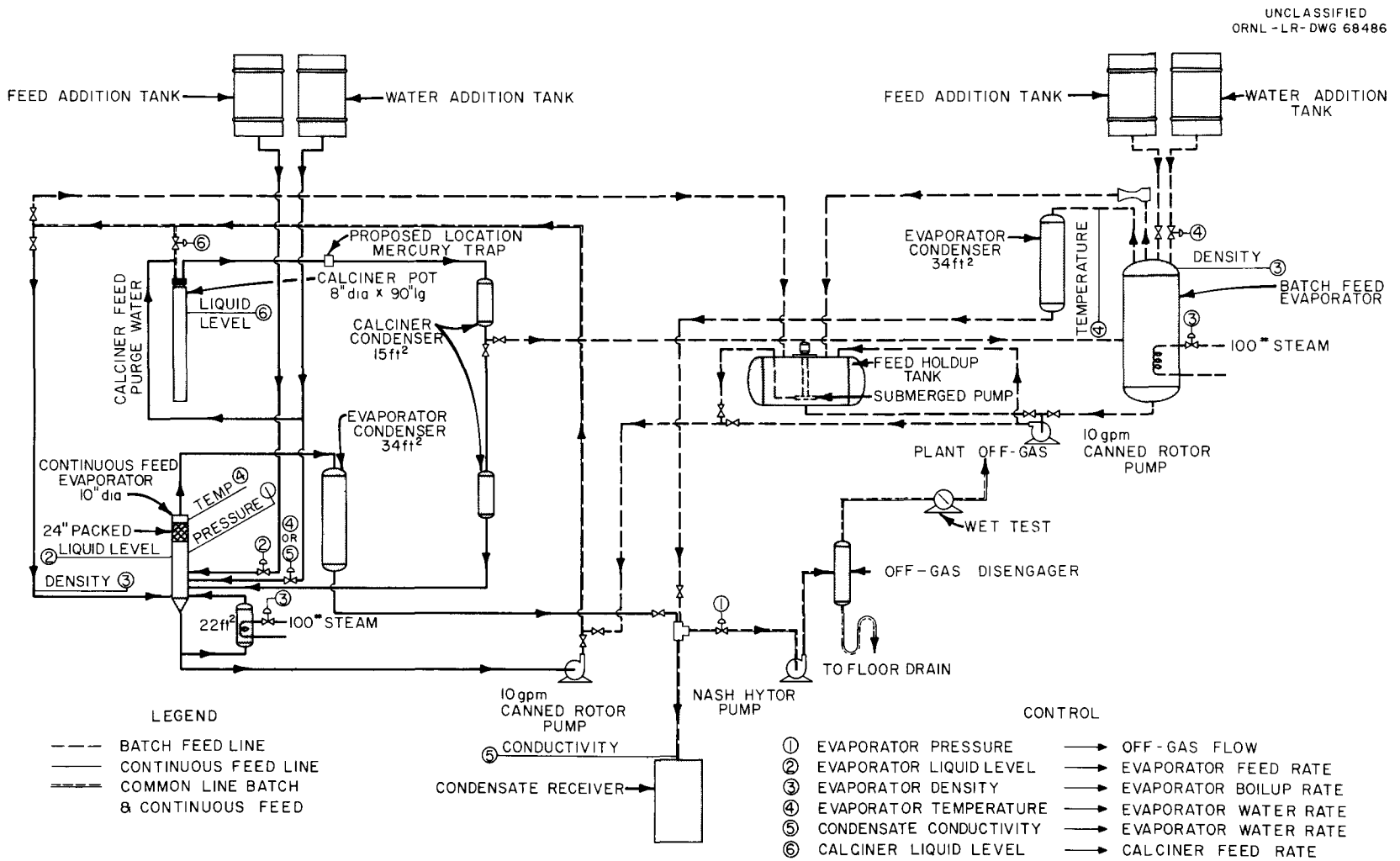

Fig. 3.3. Process Flowsheet for Engineering Development of Pot Calcination.

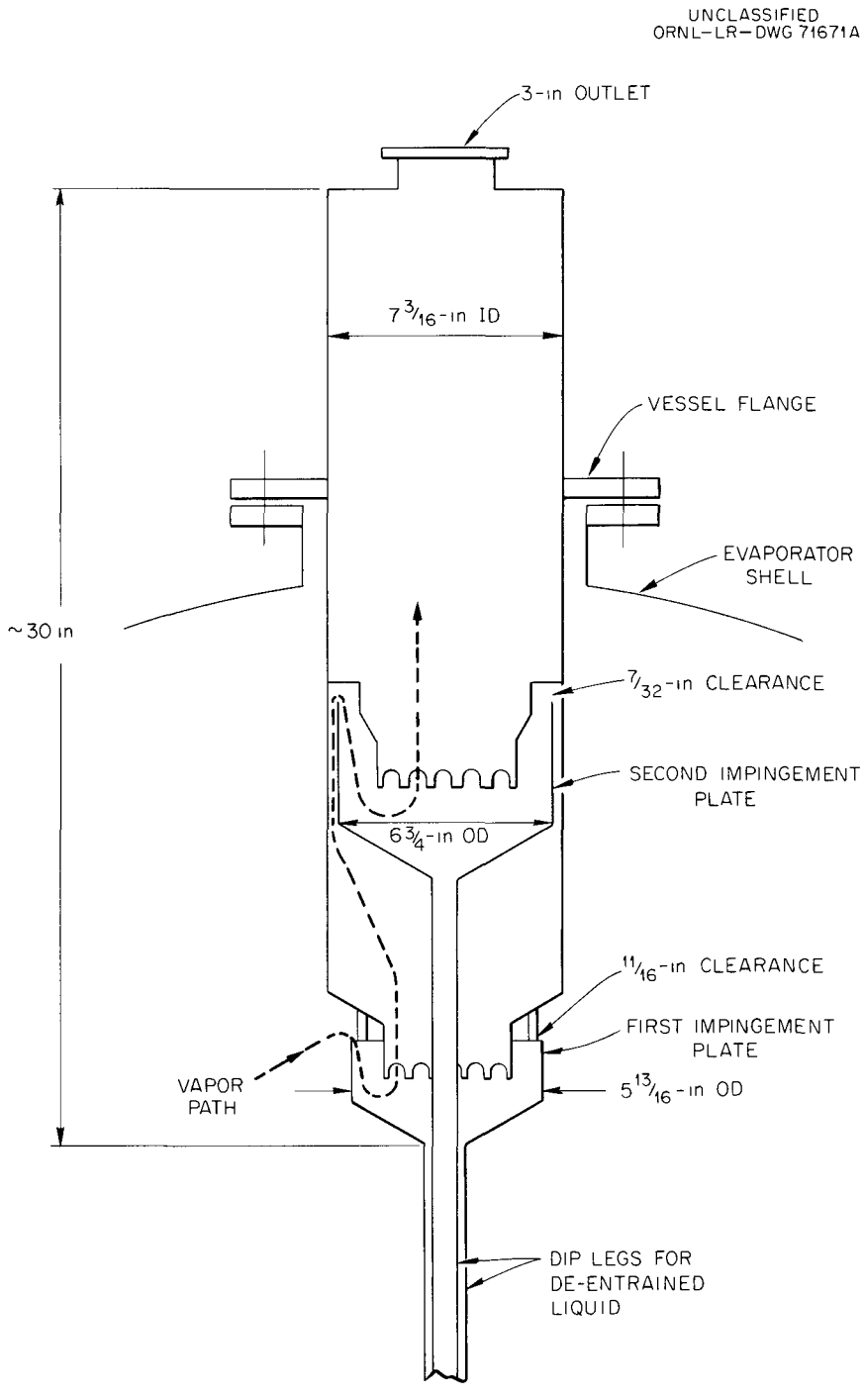

Fig. 3.4. Impingement Deentrainer for Batch Evaporator.

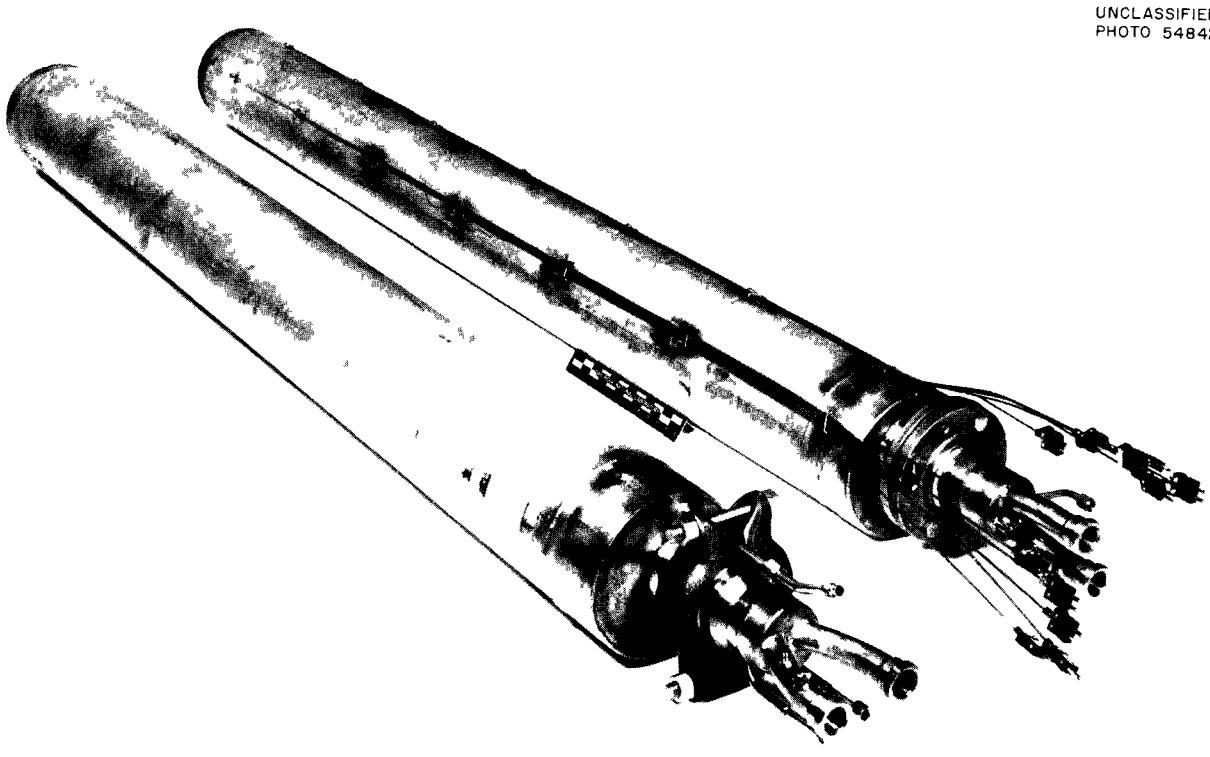

Fig. 3.5. Waste-Calciner Vessels.

thermocouples were used for experimental purposes. These thermocouples were in six sets, each set including one attached to the exterior of the pot, one inside the pot 1 in. from the wall, one inside the pot at the center line, and one in each furnace section. In addition, there was one thermocouple for a differential liquid-level control system.

The calciner pot had a nominal water boilup rate of 1 liter/min at the full 54-kw heat input. As the solids were radially deposited on the walls of the vessel, the heat transfer to the pot decreased. The external wall of the calciner was held at a maximum of 900°C by the furnace, which was divided into six sections, each about 13 in. high. The furnace temperature could go to 1050°C before there was danger of burnout.

The variables that must be controlled in the process are listed below.

1. Acidity in the evaporator. The evaporator is operated with an acidity of 6 *M* or less to decrease ruthenium volatility. This concentration is maintained by adding water to the evaporator, the amount being controlled by the nitric acid concentration of the liquid when metal ions are present in varying concentrations. The vapor temperature and liquid density are related, and the preferred operating range is between 0.5 and 0.7 *M* iron and between 4 and 6 *M* hydrogen ion for Purex waste. Increasing the rate of water addition increased the vapor volume and therefore the required capacity of the evaporator.
2. Metal ion concentration in the evaporator. The metal ion concentration in the evaporator is kept at a maximum, limited by solution stability, by controlling the liquid density, which is done by controlling the amount of steam used to vaporize the liquid.
3. Liquid level in the evaporator. The liquid level in the evaporator is controlled by the amount of evaporator feed added to the system.
4. Pressure in the evaporator. The pressure in the evaporator is kept below atmospheric, to prevent outleakage of radioactive off-gas, by regulating the off-gas vacuum pump.

5. Calciner-pot liquid level. A satisfactory differential temperature device consisted of a rod down the center of the calciner pot extending 9 to 12 in. below the liquid level (Fig. 3.6). When the liquid level was above the top center thermocouple in the pot but not at the control rod itself, the rod was heated by radiation from the walls of the pot. When liquid reached the end of the rod, the rod began to transfer its heat to the liquid. The temperature at the thermocouple point is a function of the height of liquid on the thermocouple rod, and, by maintaining a temperature difference of 100°C between the two thermocouples, it is possible to maintain a liquid level 4 in. lower than the thermocouple in the rod. A differential pressure bubbler was unsatisfactory because it gave a high-liquid signal when, toward the end of a test, the bubbler tubes plugged.

Experimental Results. – Twenty-eight tests were made with synthetic Purex, TBP-25, and Darex wastes (Table 3.1). Of these, seven were made with the batch evaporator, and in four runs, 1 ml each of monobutyl phosphate (MBP) and dibutyl phosphate (DBP) was added to the feed to simulate solvent-degradation products possibly present in some high-activity wastes. The best average results from Purex tests are shown in a material balance flowsheet (Fig. 3.7).

Calcium nitrate, calcium hydroxide, and magnesium nitrate were added to the calciner feed and directly to the calciner to suppress sulfate volatility. The direct addition of calcium nitrate to the calciner was most satisfactory. When a stoichiometric excess of calcium or magnesium plus sodium (with respect to sulfate) was maintained, less than 1% of the sulfate was detected in the calciner. Analysis of the cake indicated a poor sulfate material balance (Table 3.2). Calcium is preferable to magnesium because of its higher thermal stability.[2]

Feed rates ranged from 60 to 5 liters/hr and averaged 25 liters/hr for Purex, 15–20 liters/hr for TBP-25, and 10–15 liters/hr for Darex waste. Feeding was generally terminated when the feed rate dropped below 5–10 liters/hr. Organic compounds in the feed resulted in severe foaming in the pot, decreased the flow rates 30–300%, and decreased the bulk densities of calcined solids 25–50%. The volume of water required to strip

[2] *Chem. Technol. Div. Ann. Progr. Rept. May 31, 1961*, ORNL-3153.

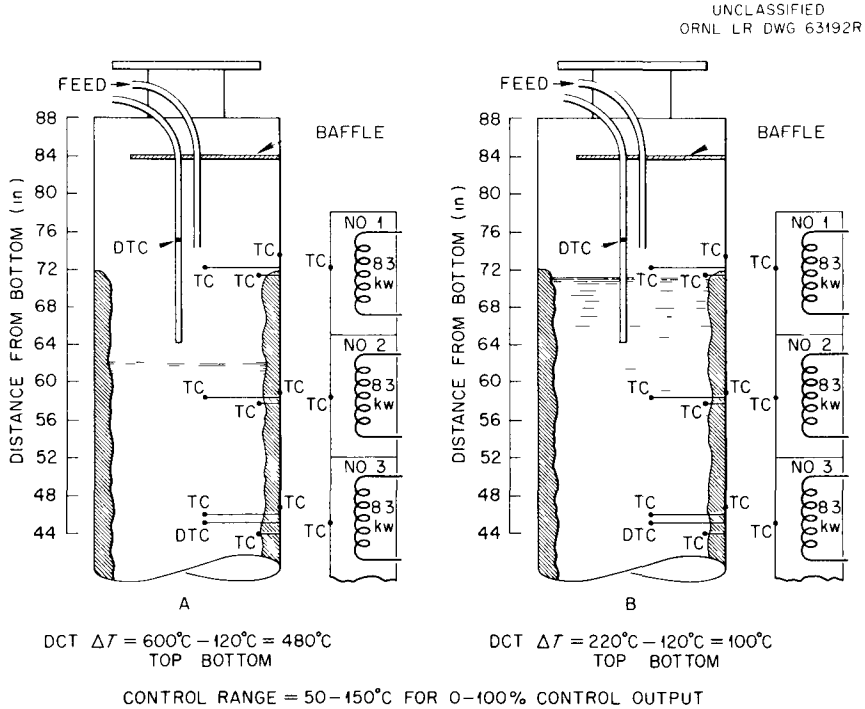

Fig. 3.6. Dual-Thermocouple Temperature Control System.

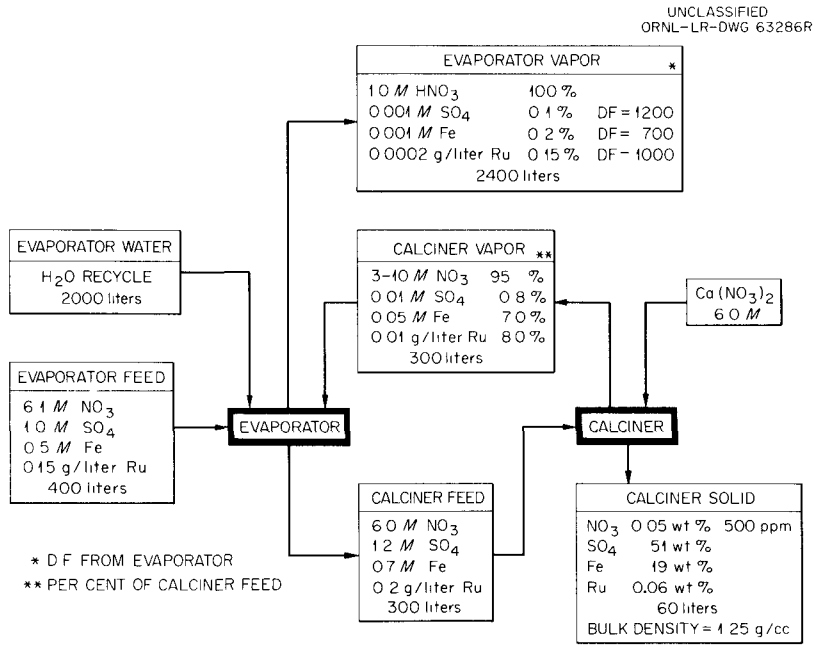

Fig. 3.7. Purex Waste Material Distribution Flowsheet.

nitric acid from the evaporator solution varied from factors of 2 to almost 8 times the volume of the feed, and the concentration of the major nonvolatile salts in the wastes was maintained within acceptable ranges. The noncondensable off-gas, including air leakage to the system and instrument purge air, ranged from about 1 to 3.5 ft^3 per liter of feed, or 15 to 50 ft^3/hr. Residual nitrate in the calcined solids ranged from a few hundreths to several percent by weight, the higher values representing samples taken near the top of the pot, where temperatures of 900°C had not been attained. Bulk densities of the solids averaged 1.3 g/cc for Purex, 0.7 g/cc for TBP-25, and 1.2 g/cc for Darex waste.

The radial deposition of solids during calcination resulted in the formation of a liquid core down the center of the pot, which produced a final longitudinal void space representing about 10% of the pot capacity (Figs. 3.8–3.10).

An indication of the efficiency of the entrainment separator in the batch evaporator was obtained from the concentration of nonvolatile Fe^{3+} in the overhead condensate (Table 3.3). Runs 46 and 51 indicated an increase in entrainment (presumably due to re-entrainment) at boilup rates above 400 lb/hr (velocity above 90 fps). This effect was not apparent in run 60.

Decontamination factors across the Yorkmesh de-entrainer in the continuous evaporator were about 1000. Since this evaporator was not optimized for de-entrainment, a larger factor could be expected in a specially designed unit with larger freeboard.

While decontamination of the calciner off-gas is of less importance because it is recycled to the evaporator, ruthenium and mercury pose potential problems because of their volatility under process conditions. In runs containing nonradioactive ruthenium in concentrations expected with actual wastes (0.15 g/liter), 2 to 3% of the ruthenium was volatilized from the evaporator and 2–50% volatilized from the pot to the evaporator (Table 3.4). These results are in general agreement with laboratory results, which showed that 50 to 70% of the ruthenium volatilized in the absence of reducing agents. Mercury decomposed and volatilized in the calcination pot and concentrated in the evaporator (Table 3.4). More mercury than was expected remained with the calcined solids in some cases, probably because of incomplete calcination. Complete volatilization of mercury

Table 3.2. Summary of Engineering-Scale Tests

Batch evaporator used in runs marked with asterisk, others continuous

Run No.	Type of Feed	Av System Feed Rate (liters/hr)	Feed Volume (liters)	Water-to-Feed Volume Ratio	Evaporator Fe or Al Conc[a] (g/liter)	Sulfate in Solids (% of feed)	Off-Gas Volume/Feed Ratio[b] (ft^3/liter)	NO_3^- in Solids[c] (wt %)	Solids Density[d] (g/cc)
36	Purex[e]	20.5	456	2.5	32–22		0.18	0.3–0.1	1.29
37	Purex[f]	21.0	404	2.4	35–22	92	0.97	0.15–0.03	1.15
38	TBP-25	27.6	442	3.3	58–14		0.25	0.5–0.1	0.56
39	TBP-25	30.6	489	7.4	78–30		0.27	0.2–0.05	0.56
40	Purex[f]	26.6	373	5.6	36–21	102	0.55	0.15–0.03	1.17
41	Purex[g]	65.2	391	3.7	58–20	66		4.1–0.8	1.33
42	Purex[g]	49.0	495	4.4	56–33	92		2.3–0.02	1.50
43	Purex[e]	System leak	594.5		61–36	79		0.9–0.008	
44	Purex[g]	40.9	409	7.8	106–36	91	2.02	0.14–0.06	1.14
45*	Purex[g]	25.2	328	3.9	37–27	93	2.2	4.7–0.01	1.17
46*	Purex[g]	25.8	325	4.1	35–27	140	3.5	3.7–0.01	1.55
47	TBP-25	30.6	429	3.4	103–54		1.9	6.0–0.36	0.57
48	TBP-25	15.0	468	2.8	72–42		3.5	6.0–0.10	0.77
49	TBP-25	17.6	478	2.6	56–36		1.9	6.0–0.36	0.83
50	TBP-25[b]	11.5	346	2.4	66–35		2.4	4.1–0.08	0.52
51*	TBP-25[b]	7.0	308	2.5	62–53		3.2	6.0–0.08	0.59
52*	TBP-25[b]	9.8	440	2.3	65–49		2.4	0.18–0.06	0.44
54	TBP-25	17.2	428	2.7	52–36		1.8	0.85–0.1	0.65
55	TBP-25	19.4	469	3.5	80–35		1.4	0.56–0.1	0.60
56	Darex	13.6	383	4.1	82–47		1.4	0.09–0.02	0.86
57	Darex	8.9	641	3.2	99–53		2.2	0.53–0.01	1.4
58	Darex	16.5	576	3.0	120–98		0.84		1.42
59*	TBP-25[b]	12.4	397				1.3	1.0–0.07	0.61
60*	Darex	8.6	336	5.5	128–76		1.8		1.29
61*	Darex	10.6	307	3.8	112–93			2–0.1	1.13
62	TBP-25	16.8	446	4.5	70–36		1.0		0.63
63	TBP-25	16.3	421	2.3	55–39		0.9	2.0–0.2	0.61
64	TBP-25	11.6	560	2.0	54–31		1.19	0.2–0.002	0.80

[a] Range of concentration during calciner feeding.

[b] Includes 10 to 20 ft^3/hr system leakage.

[c] Nitrate range from top to bottom of pot.

[d] Density based on full pot volume of 60 liters.

[e] No additive for sulfate.

[f] Magnesium added to feed such that $Na^+ + Mg^{2+}$ was 10% excess above SO_4^{2-}.

[g] Calcium nitrate solution added directly to calciner in excess of free SO_4^{2-}.

[h] One milliliter of MBP and DBP added to each liter of feed before processing.

UNCLASSIFIED
PHOTO 56043

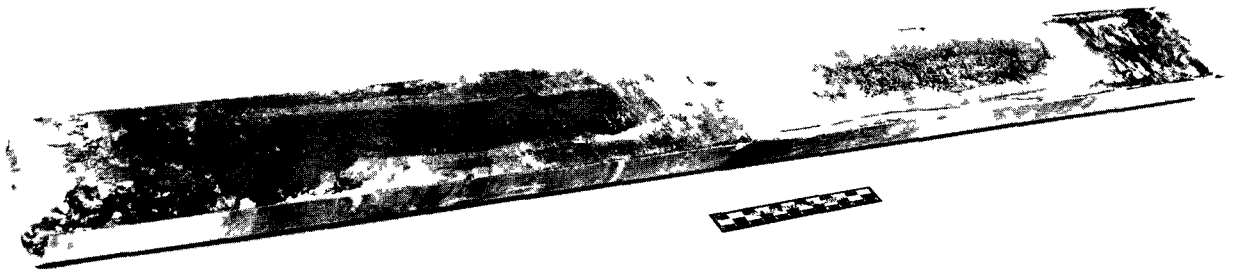

Fig 38. Purex Calcined Waste with Calcium

UNCLASSIFIED
PHOTO 55670

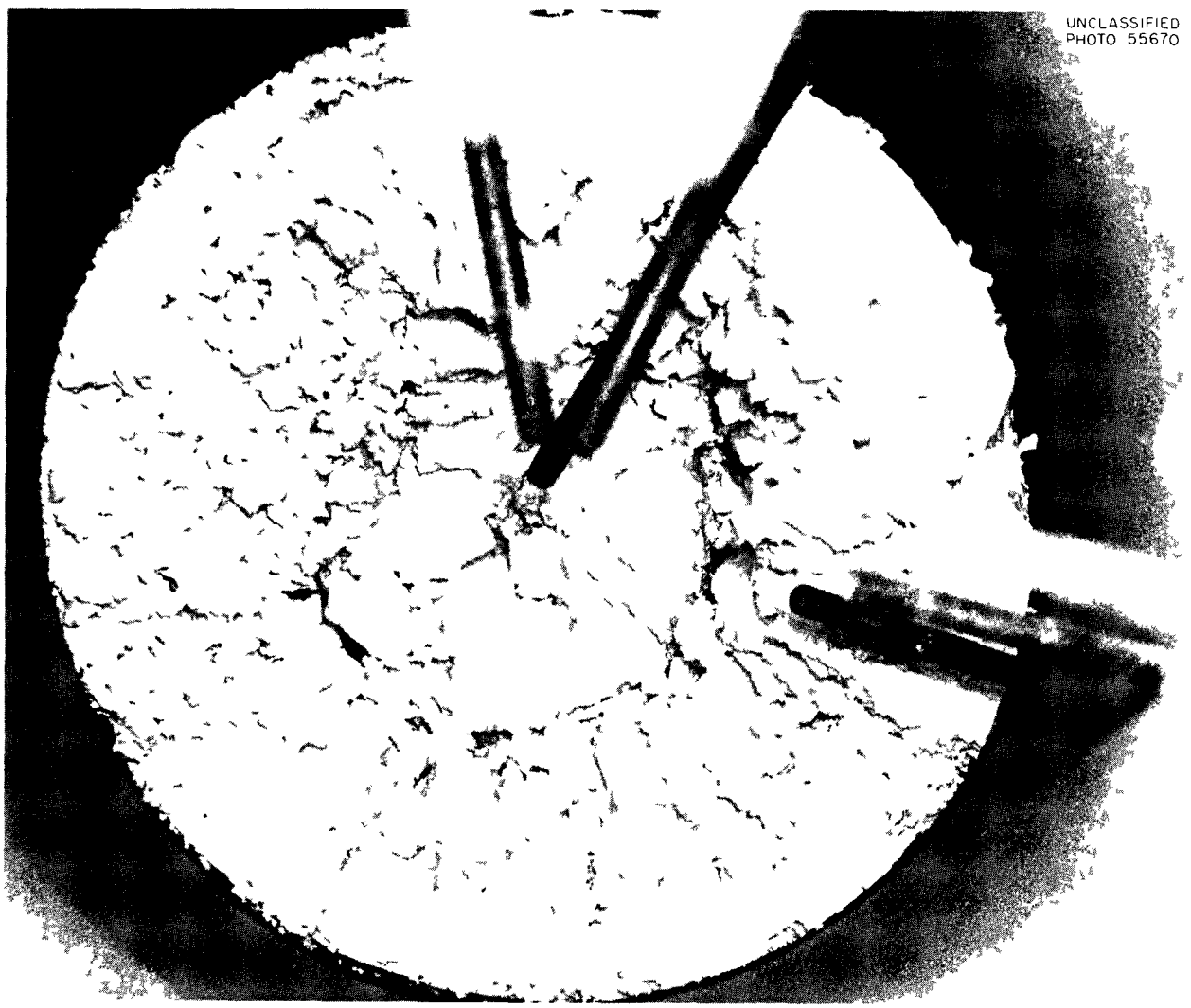

Fig 39 TBP-25 Calcined Waste.

UNCLASSIFIED
PHOTO 56239

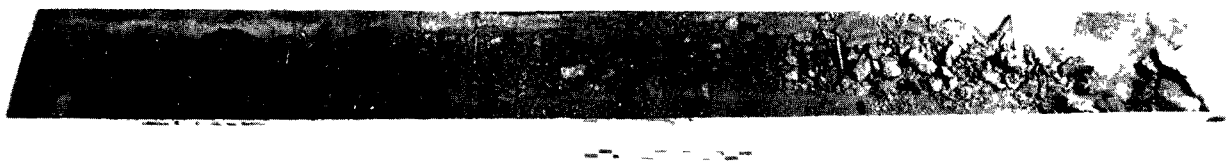

Fig. 3.10. Darex Calcined Waste.

Table 3.3. Efficiency of Impingement Entrainment Separator in the Batch Evaporator

Run No.	Waste	Fe^{3+} Concentrations		Boilup Rates (lb/hr)
		Evaporator (g/liter)	Evaporator Overhead (ppm)	
46	Purex	32–38	1–3	0–360
		28–33	5–7	440–500
51	TBP-25	0.19–0.36	Up to 1	0–390
		0.22–0.26	2	504–570
52	TBP-25	0.23–0.44	Up to 1	0–430
60	Darex	96–131	Up to 1	0–500
61	Darex	0.90–2.4[a]	Up to 2	

[a]Evaporation of only the calciner condensate during run.

is expected at 900°C. A trap for removing mercury compounds by condensation near 300°C was designed and built for testing with this equipment. Nozzles are provided in the trap for spraying the deposited solids with nitric acid after each run in order to dissolve them for disposal to waste tanks. The final mercury and ruthenium concentrations in the pot (listed in Table 3.4), and the amount of ruthenium volatilized (Fig. 3.7), may be low because in the experimental equipment it was possible to raise the top of the pot to only 700°C rather than to the desired 900.

Mechanical Development

The mechanical development program is being carried out in three phases at the Lockheed Nuclear Products facility at Georgia Nuclear Laboratory, and it includes: (1) Heliarc welding and mechanical closure tests to develop a permanent seal for the pots, (2) remote mechanical equipment tests to demonstrate the positioning of the pot and the connecting of it to its feed and off-gas lines, and (3) demonstration of a remote welding machine should the welded seal developed in the first phase (see below) appear promising.

Phase 1. – Seal welding of a series of five permanent pot closures was completed, and the closures are being leak-tested under simulated pot-storage conditions, involving cycling the temperature between 25 and 300°C at 150-psi internal pressure. To date, leak rates on three of the specimens have been less than 0.2 standard cc of helium gas per year, determined by a helium mass-spectrometer leak detector. The specified maximum permissible leak rate is 32 cc/year.

The initial leak test on a Grayloc mechanical seal was unsuccessful because of a visible nick in the ring which limited the maximum obtainable vacuum to 40 μ. Replacement of the seal ring permitted a vacuum of 10 μ to be obtained. Leak rates will be determined as above.

Phase 2. – A cell mockup will be used to demonstrate the positioning of a pot calciner plus connecting it to and disconnecting it from the process lines. The pot will be lowered into the furnace mounted on a dolly (Fig. 3.11), positioned beneath its filling cap, lifted along with the furnace by jacks mounted on the dolly, and clamped to the process lines by a screw clamp

Table 3.4. Final Inventory and Material Balance for Ruthenium and Mercury

Test No.	Input to System (g)	Inventory in Evaporator (g)	Output via Condensate (g)	In Calcined Solid (g)	Balance (%)
		Ruthenium (Feed: 0.15 g Inactive Ruthenium per Liter)			
42	79.28	5.9		38.7	56.24
43	74.84	2.55		31.36	45.41
44	50.31	7.73	8.72	22.77	78
50	83.04	6.675	1.58	41.85	60.34
51	64.68	55.8	2.87	60.18	183.74
52	114.4	37.5		58.08	83.55
54	81.32	5.05	1.51	68.25	92.1
55	89.1	6.73	1.79	45.6	60.76
59	79.4	6.65			8.38
61	81.355	1.628	1.53	44.35	58.38
		Mercury (Feed: 0.01 M Hg)			
47	1857	192	197	356	40.0
48	2049	270	164	756	58
49	2772	162	56	310	19
50	1591	206	60	2154	150.7
51	1232	1889.6	83.65	531	203.1
52	3190	951		211.2	36.4
54	1510.8	522.5	41.9	278.85	55.83
55	2875	442.5	81.87	95	21.55
59	1627.7	1273		720.4	122.47
62	1908.8	440	39.14	1086	82.05
63	1957	127	46.9	693.7	44.3
64	2565	211.25	142.89	276.48	24.47

operated remotely or by a shaft extending through the cell wall. A gasketed connector (Fig. 3.12) will seal the vapor, feed, and probe lines from each other and the environment. It incorporates the weld design tested in phase 1 for permanent sealing of the pots. The Grayloc connector will also be demonstrated.

After the pot has been filled, the clamp will be opened and the pot and furnace lowered slightly. During this operation, air from exhaust ports in the connector assembly will sweep across the seal face to prevent cell contamination. A temporary metal plate cap will then be dropped on top of the pot connector by means of the slide mechanism. The pot and furnace will be lowered to the mobile position and moved to the sealing station, where a permanent seal will be attached. After being sealed in the radioactive pilot plant, the pots will be removed from the furnace and stored for observation of pressure and temperature buildup. A vent on the caps will permit relief of any excess pressure that may build up.

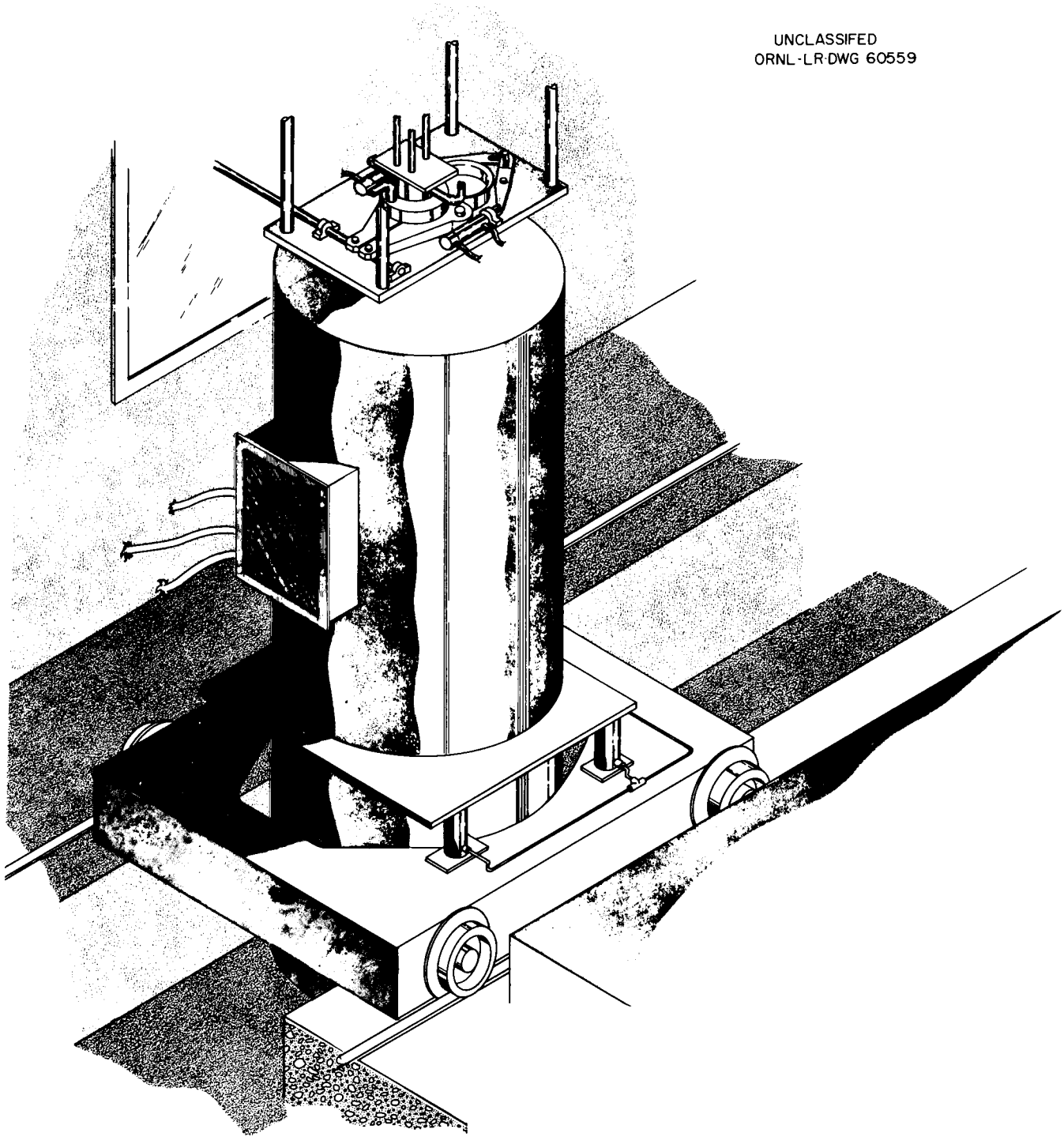

Fig. 3.11. Radioactive Pilot-Plant Pot-Calciner Arrangement.

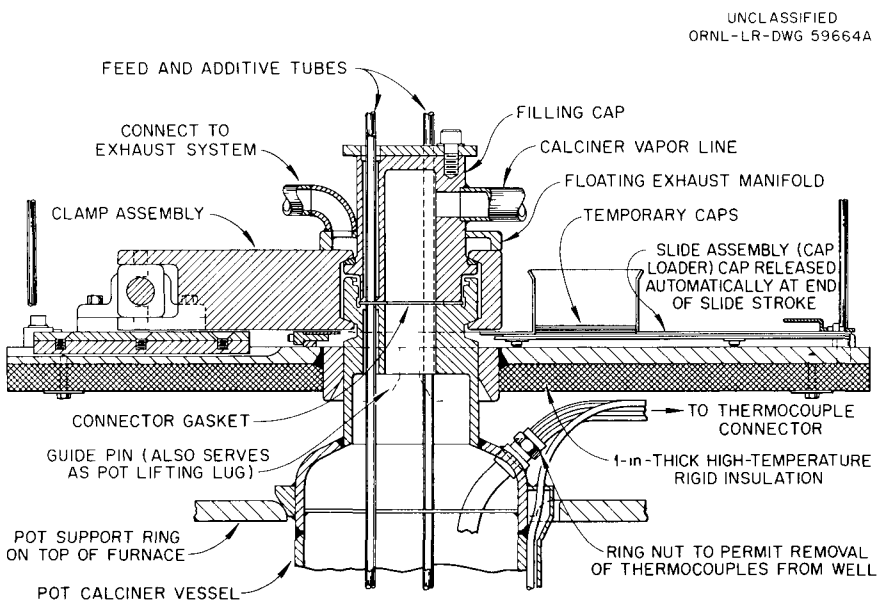

Fig. 3.12. Gasketed Connector Assembly for Calciner Pots.

The furnace mockup and dolly were made and delivered to Georgia Nuclear Laboratory. The filling station and calcination-pot design was completed at ORNL and sent out for bids. Completion of the program is scheduled for Nov. 1, 1962.

Laboratory-Scale Studies

Fixation in Glassy Solids. – Simulated TBP-25, Purex, and Darex waste oxides were incorporated into glassy solids by fluxing with phosphite plus one or more other fluxing agents (borax, silica, sodium hydroxide, aluminum phosphate, and the oxides of lead, calcium, and magnesium).

The products formed from TBP-25 waste appeared to be true glasses over a fairly wide range of compositions[3,4] (Table 3.5). Initial softening points varied from about 825 to 1000°C. After initial melting, softening points were as much as 200 to 300°C lower than their initial values. The waste oxides in the glass varied from about 26 to 35 wt %. Densities ranged from 2.4 to 3.8 g/cc, and volume reduction factors (from the concentrated waste solution) varied from 7.2 to 9.3. The leach rate for a typical glass (nominal composition 26% waste oxides, 40.5% P_2O_5, 15.9% PbO, 18.1% Na_2O) spiked with Cs^{317} decreased from 2.1×10^{-6} after one week to 2.5×10^{-7} g cm^{-2} day^{-1} at the end of the fifth week when leached in a stream of distilled water. When the glass was produced on a semiengineering scale (in a pot 24 in. long and 4 in. in diam, semicontinuous operation), the density and volume reduction were the same as for the small sample. X-ray analyses showed amorphous patterns. Thermal conductivity varied from 1.05 Btu hr^{-1} ft^{-1} $°F^{-1}$ at 300°C to 1.60 at 1050°F, factors of about 10 greater than that of the calcined product without fluxing agents[5] (see below).

The glassy solids from the fixation of Purex-waste oxides were often microcrystalline, particularly when prepared in a large batch that cooled slowly. Satisfactory products incorporated 36–45 wt % waste oxides, had densities of 2.6–2.8 g/cc, volumes representing 4.8–6.9 gal of glass per ton of uranium, and initial softening

[3] R. E. Blanco and E. G. Struxness, *Waste Treatment and Disposal, Progr. Rept. June–July 1961*, ORNL-TM-15.

[4] *Ibid., Aug.–Sept. 1961*, ORNL-TM-49.

[5] H. W. Godbee and J. T. Roberts, *Laboratory Development of a Pot Calcination Process for Converting Liquid Wastes to Solids*, ORNL-2986 (Aug. 30, 1961).

Table 3.5. Compositions of Glasses Incorporating Waste Oxides

	Purex Waste (High Sulfate)	Darex Waste (Stainless Steel Nitrates–HNO_3)	TBP-25 Waste [$Al(NO_3)_3$-HNO_3]
Compound (wt %)			
Fe_2O_3	8.6–11.9	9.2–20.0	0.06–0.09
Al_2O_3	1.1–1.6	0–23.5	25.0–33.8
NiO	~0.2	1.2–3.0	
Cr_2O_3	~0.2	2.7–6.4	
Na_2O	15.5–34.4	17.2–21.7	18.6–25.5
P_2O_5	25.9–32.5	21.1–45.9	38.9–48.1
SO_3	17.3–23.9		
PbO		0–33.1	0–15.9
MnO_2		0.3–0.8	
MgO	0–13.3		0–0.2
B_2O_3	0–15.6	0–20.8	0–11.6
SiO_2			0–9.5
CaO	0–12.0		
RuO_2	~0.1	0.003–0.01	~0.01
Waste oxides	31.4–44.5	13–32	27.1–35.2
Density, g/cc	2.67–2.78	2.7–3.8	2.41–2.84
Volume reduction	6.5–8.3	2.9–6.6	7.2–9.3
Approximate initial softening point, °C	830–950	850–900	850–1000

points of 840–975°C[6,7] (Table 3.5). The addition of the extra acid anions necessary for glass formation necessitated careful control of temperature during the calcination-fixation process in order to avoid loss of SO_3 by volatilization. Thermogravimetric analysis of a typical Purex "glass" (with a nominal composition of 41.6% waste oxides, 30.9% P_2O_5, 3.4% B_2O_3, 9.2% MgO, 14.9% added Na_2O, and an initial softening point of about 850°C) indicated that SO_3 was volatilized slowly, if at all, below 900°C and rapidly above 1000°C. It appears feasible to operate at temperatures high enough to produce glassy products and yet low enough to avoid substantial loss of SO_3.

Glassy products containing 13 to 32% of Darex waste solids were prepared. Densities varied from 2.7 to 3.8 g/cc, volume reductions from 2.9 to 6.6, and initial softening points from 850 to 900°C (Table 3.5). The production of true glasses incorporating >20% Darex-waste oxides is difficult owing to the exceptionally high content of iron, nickel, and chromium, which do not form glasses.

The thermal conductivity k of a glass incorporating 26% TBP-25 waste oxides, measured *in situ* in the original 24-in.-high by 4-in.-diam stainless steel pot, increased from 1.05 at 300°F to 1.60 Btu hr^{-1} ft^{-1} $°F^{-1}$ at 1050°F (Fig. 3.13).

[6]R. E. Blanco and E. G. Struxness, *Waste Treatment and Disposal, Progr. Rept. Apr.–May 1961*, ORNL CF-61-7-3.

[7]Although the initial softening point of the glass as formed by evaporation, calcination, and melting is about 950°C, the softening point of the glass after being formed is about 600°C.

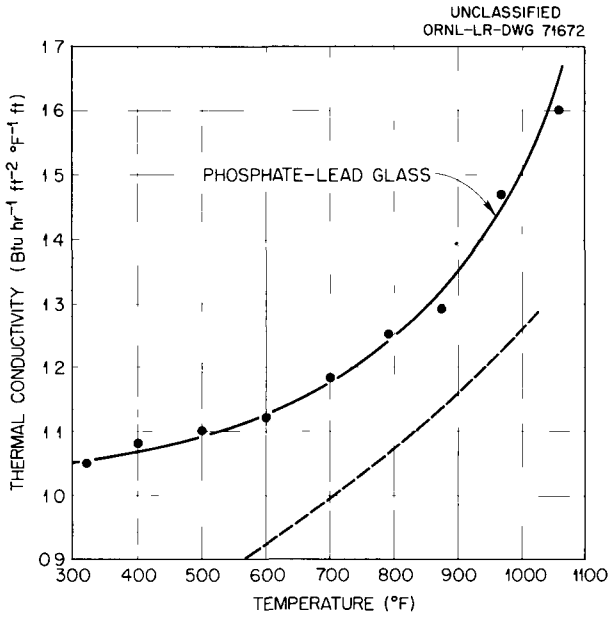

Fig. 3.13. Thermal Conductivity of a Phosphate-Lead Glass Incorporating 26% TBP-25 Waste Oxides. Soda-lime-silica glass curve shown for comparison.

Sodium hypophosphite and lead oxide had been added to the waste to prevent ruthenium volatility and to serve as glass formers and modifiers. The positive, nonlinear, temperature coefficient of thermal conductivity for the phosphate-lead glass is characteristic of amorphous solids. Since the liquid state represents a more disordered state, the thermal conductivity of the glass should be slightly less after softening begins at about 1100°F (~600°C).[7] Measured values were 1.51 at 1145°F and 1.40 at 1150°F. Since the conductivity apparatus was not constructed for measurements on fluids, no values were determined at higher temperatures.

Ruthenium Volatility. – The separation of nitric acid from fission product ruthenium by distillation is favored by (1) low acid concentration, (2) distillation under reduced pressure, and (3) the presence of phosphite in the still pot.

The volatilization of ruthenium from nitric acid depends largely on the past history of the solution. To provide a basis for studies of comparative ruthenium volatility from various acid nitrate solutions, solutions were spiked with radioactive ruthenium (Ru^{106}) chloride and then distilled in a Gillespie equilibrium still. Under these conditions the volatility of ruthenium from otherwise pure nitric acid ($\leqq 10$ *M*) was reproducible and could be expressed by the empirical equation:

$$\log \frac{M_{Ru(vapor)}}{M_{Ru(liquid)}} = 1.04 \log M_{HNO_3(vapor)} - 2.23$$

(Fig. 3.14).[8] The presence of 1.7 *M* $Al(NO_3)_3$ at a given nitric acid concentration in the still pot appreciably increased the relative volatility of

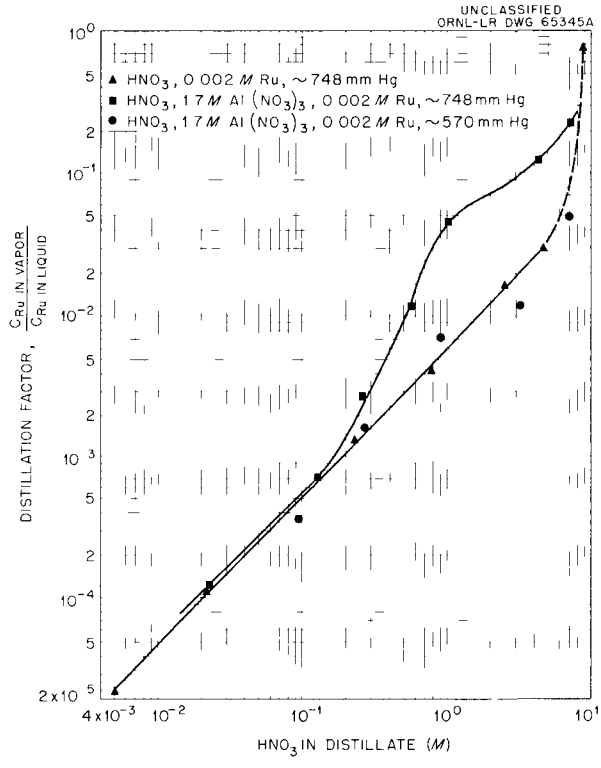

Fig. 3.14. Volatilization of Ruthenium from Acid Nitrate Solutions.

the ruthenium, lowering the distillation pressure to ~570 mm Hg, thereby reducing the relative volatility of the ruthenium to approximately the same value as for the corresponding nitric acid solution without aluminum (Fig. 3.14). Lowering the distillation pressure of pure HNO_3-$RuCl_3$ solutions had a negligible effect on the relative volatilities of ruthenium and HNO_3.

[8] R. E. Blanco and E. G. Struxness, *Waste Treatment and Disposal, Progr. Rept. Oct.–Nov. 1962*, ORNL-TM-133.

The separation factor

$$\frac{C_{HNO_3(vapor)}/C_{HNO_3(solution)}}{C_{Ru(vapor)}/C_{Ru(solution)}}$$

for nitric acid from ruthenium by distillation was varied from about 10 to 100 for the HNO_3-$RuCl_3$ solution and from about 5.5 to about 100 for the $AlCl_3$ solution over the acid concentration range 1 to 10 *M* (Fig. 3.15). The addition of 0.1 *M*

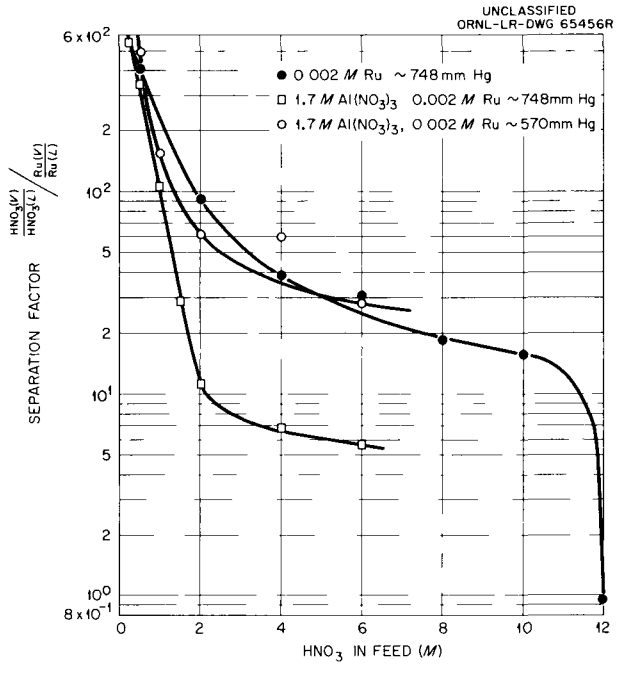

Fig. 3.15. Separation Factor for HNO_3 from Ruthenium by Distillation.

H_3PO_3 to various nitrate solutions of interest lowered the volatility of ruthenium by factors which varied from 420 for 12 *M* HNO_3 to 38.4 for simulated Darex waste. Separation factors for HNO_3 from ruthenium were proportionately increased (Table 3.6).

About 2 to 2.5 *M* phosphite was required to lower ruthenium volatility to 0.1% in small-scale batch experiments with TBP-25 (aluminum) waste carried to 900°C (Fig. 3.16) vs 1.5 *M* when carried to 500°C.[6] About 3 to 12% was volatilized in semi-engineering-scale fixation experiments with pots 4 in. in diam and 24 in. high, in which glass-making additives were used as well as phosphite. These high volatilities are tentatively attributed to a combination of air leakage into the equipment and to local overheating in the larger-scale experiments.[9]

Corrosion. – Stainless steel appears to be a satisfactory material of construction for the calcination-fixation pot and for the interim waste storage tanks. Stainless steel undergoes intergranular attack during long exposures in refluxing nitric acid; titanium is therefore preferred for the condenser, rectifier, and other overhead equipment that will be exposed to hot HNO_3 from the evaporation and fixation processes.

Stainless steel exposed in simulated waste solutions subjected to a single batch evaporation-fixation cycle was corroded aggressively for a brief period during the expulsion of the last amounts of acid, water, and nitrate from the system at temperatures higher than 900°C. With further exposure at the maximum temperature, the corrosion rate continued to decrease, and long-term internal corrosion rates should be negligible. External atmospheric corrosion after fixation (maximum estimated temperature 300°C) should also be negligible; corrosion of type 304L stainless steel in air at 815°C is listed as less than 5 mils/yr.[10] Type 304L stainless steel was corroded at overall rates of 5.10 and 1.59 mils/month when exposed to a single TBP evaporation-calcination cycle followed by a "soaking period" at ~900°C for total exposure times of 24 and 168 hr, respectively (Table 3.7). Corresponding rates for previously reported Purex tests without additives were 6.7–7.9 mils/month.[2] The addition of glass-forming fluxes increased the container corrosion to 42.2 and 120–145 mils/month for TBP-25 and Purex wastes, respectively, for a single evaporation-fixation cycle. Stainless steel should be a satisfactory container for both waste types provided that the additives are selected so as to minimize or eliminate the volatilization of sulfate and if the maximum fixation temperature does not exceed 950°C.

Tanks of types 304L and 347 stainless steel can be used for the interim storage of simulated Darex-Purex waste solutions. Exposure in simulated Darex waste solution (5 *M* HNO_3, 1.82 *M* dissolved stainless steel, 100 ppm Cl^-) at 80°C

---

[9] D. T. Gillespie, *Ind. Eng. Chem., Anal. Ed.* 18, 575–77 (1946).

[10] H. H. Uhlig, pp 730–40 in *Corrosion Handbook*, Wiley, New York, 1955.

Table 3.6. Effect of 0.1 *M* H_3PO_3 on Ruthenium Volatility During Distillation of Nitrate Solutions

Solution	Activity of Ru in Distillate (counts min^{-1} ml^{-1})		Reduction Factor	Separation Factor,[a] HNO_3 from Ru	
	No H_3PO_3	0.1 *M* H_3PO_3		No H_3PO_3	0.1 *M* H_3PO_3
12 *M* HNO_3	2.78×10^5	662	420	0.956	378
6 *M* HNO_3[b]	3.76×10^5	145	2593	0.126	364
1.7 *M* $Al(NO_3)_3$–2 *M* HNO_3	1.77×10^4	85	208	11.1	2055
TBP-25	9.08×10^3	40	227	13.8	4920
Purex	3.17×10^4	650	48.8	2.22	117
Darex	9.64×10^4	2.51×10^3	38.4	1.50	57.5

[a] Defined as $\dfrac{C_{HNO_3(vapor)}/C_{HNO_3(solution)}}{C_{Ru(vapor)}/C_{Ru(solution)}}$.

[b] Ru added as the nitrosyl hydroxide.

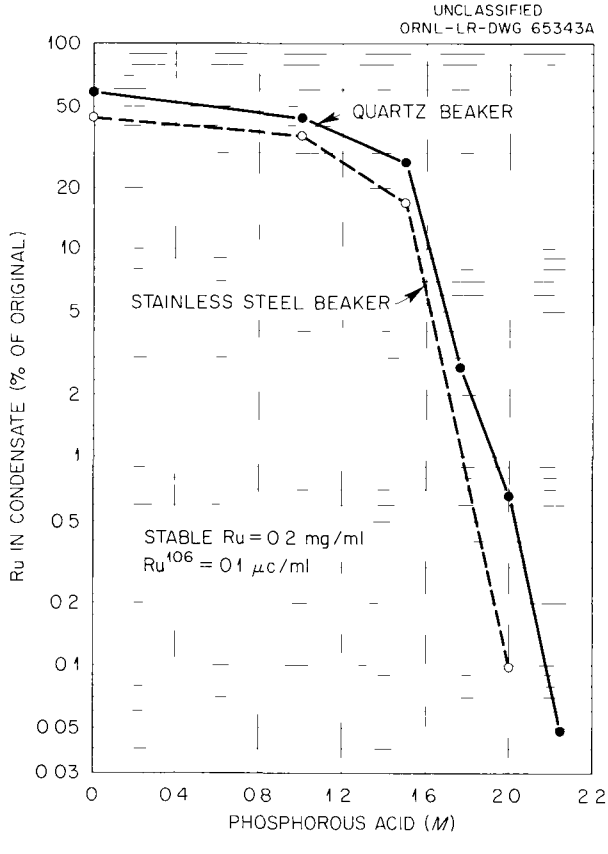

Fig. 3.16. Effect of Phosphorous Acid on Ruthenium Volatility from TBP-25 Waste on Batch Calcination to 1000°C.

resulted in maximum overall rates of 0.80 and 0.89 mil/month, respectively. Grain-boundary attack did not develop into intergranular attack. Small amounts of certain organics (e.g., glycerol and plasticizers leached from polyethylene) decreased this rate to a few hundredths of a mil per month. Lowering the acid concentration to 2 *M* and the temperature to 50°C also reduced the corrosion rate.

Vapor-Liquid Equilibrium. – Vapor-liquid equilibria were measured for simulated TBP-25, Purex, and Darex wastes over concentration ranges varying from half to twice those of normal waste. Acid concentrations were varied from 0.5 to 5.0 *M* for TBP-25 and from 2.0 to 7.0 *M* for Purex and Darex wastes. Some concentrated TBP-25 and Darex solutions could not be prepared because of solubility limitations. Distillations were carried out in Gillespie stills[9] at atmospheric pressure (740–750 mm Hg) and at about 565 mm Hg. Still-bottom densities, measured at 25, 50, 75, and 100°C for each stable solution studied, are given elsewhere.[11]

Design of Radioactive-Cell Equipment. – Equipment is being designed and constructed for a small-scale pot-calcination experiment to be run with batches of actual waste solution from ICPP

[11] *Bimonthly Rept. Aug.–Sept. 1961*, ORNL-TM-49, pp 15–16, 18–23.

Table 3.7. Corrosion Data for Stainless Steel Containers Used in the Evaporation-Fixation Step

Type of Stainless Steel	Environment	Approximate Maximum Temperature (°C)	Exposure Time (hr)	Overall Corrosion Rate (mils/month)	Average Total Penetration (mils)
304L	Purex plus additives[a]	900	24	120–145[b,c]	4.0–4.8
304L	Purex plus additives[a]	110	~2	0	0
	(exposure interrupted and	850	1	0	0
	corrosion determined as	950	2	1330[c]	4.0
	indicated)	950	75	19	2.0
	Overall		~80	57	6.0
304L	Purex plus additives[a]	900	78	80[c]	8.68
304L	TBP-25	900	24	5.10	0.17
		900	168	1.59	0.37
304L	TBP-25 plus additives[a]	920	19	42.2	1.11
		910	345	5.4	2.59
347	TBP-25	900	24	10.5	0.35
		900	168	1.93	0.45

[a]Additives: to Purex, 49.4 g/liter of $Na_2B_4O_7 \cdot 10H_2O$, 105 g/liter of $NaH_2PO_4 \cdot H_2O$, 167.3 g/liter of 30% H_3PO_3, 8.72 g/liter of NaOH, 80.1 g/liter of $Ca(OH)_2$; to TBP-25, 112.1 g/liter of $NaH_2PO_2 \cdot H_2O$, 11.6 g/liter of PbO.

[b]Duplicate specimens exposed.

[c]Intergranular corrosion noted.

and Hanford and with batches of "spiked" synthetic waste solution. Information to be obtained from this experiment will include the volatility of fission products during evaporation and calcination, the pressure buildup in the calciner pot after calcination is completed, and the extent to which the segregation of nonvolatile fission products occurs.

In this experiment (Fig. 3.17) waste solution will be charged from the carrier on the roof of the cell and be moved from the transfer tank to the feed tank to the calciner pot by air lifts. The vapor from the calciner pot will travel through a jacketed section of line to the condenser and to a scrubber and will be recycled through a gas pump to the calciner pot. Calcined wastes will be removed into the carrier on the roof.

3.2 LOW-ACTIVITY WASTE TREATMENT

The development of a scavenging–ion exchange process (Fig. 3.18) for the routine removal of trace amounts of fission products from large volumes of process water has progressed through the laboratory, design, and pilot-plant phases. In a series of runs in a 600-gal/hr pilot plant (Figs. 3.19 and 3.20) the economic, chemical, and equipment factors of the process were measured. In this process the contamination is removed in two basic steps: (1) scavenging of a portion of the activity with sodium hydroxide and an iron coagulant, followed by solution clarification and filtration, and (2) sorbing of Cs^{137} and Sr^{90} on carboxylic-phenolic resin.

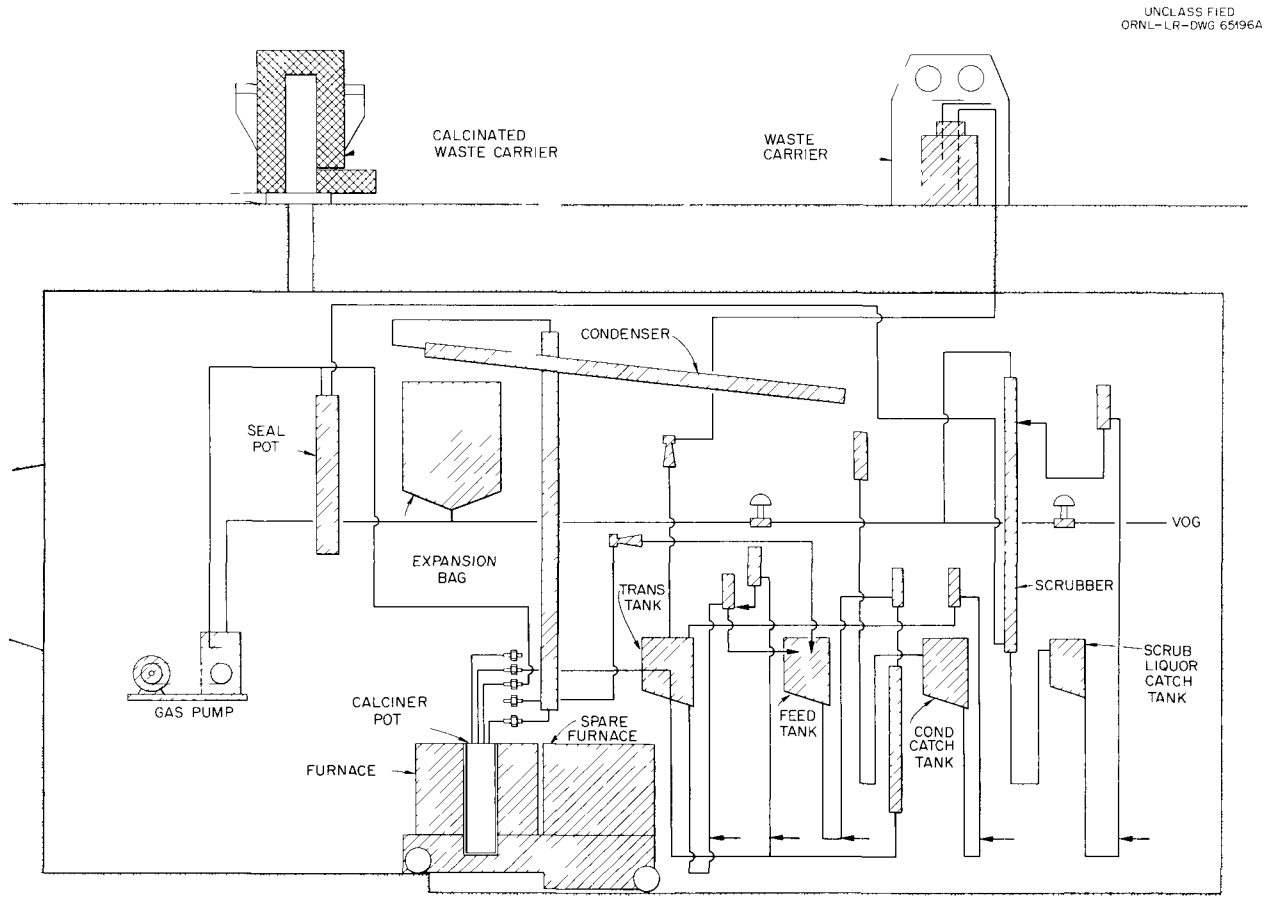

Fig. 3.17. Hot-Cell Pot Calcination Experiment.

Pilot-Plant Process Description

Slightly radioactive waste water from the million-gallon ORNL equalization basin is pumped into the plant at 10 gal/min, where it is adjusted to 0.01 *M* NaOH in a flash mixer with an 18-sec holdup. Ferrous sulfate is added to the mixer as a coagulant in amount sufficient to make the solution 5 ppm with respect to iron. The solution then flows by gravity to a lightly agitated 270-gal flocculator where the light floc of insoluble carbonates, algae, foreign sediment, and ferric hydroxide agglomerates into large particles, which carry a significant fraction of the fission products. The solution and floc flow, again by gravity, to a 1980-gal clarifier, where the solutions pass up through a 4- to 5-ft sludge blanket. The sludge, containing 60% of the Sr^{90}, is continuously withdrawn, filtered, and packaged for disposal. The clarifier effluent is transferred to a surge drum and then pumped through a sand or anthracite polishing filter for additional hardness and turbidity removal. The filtered solution is pumped through one of two resin columns filled with 28 gal of Duolite

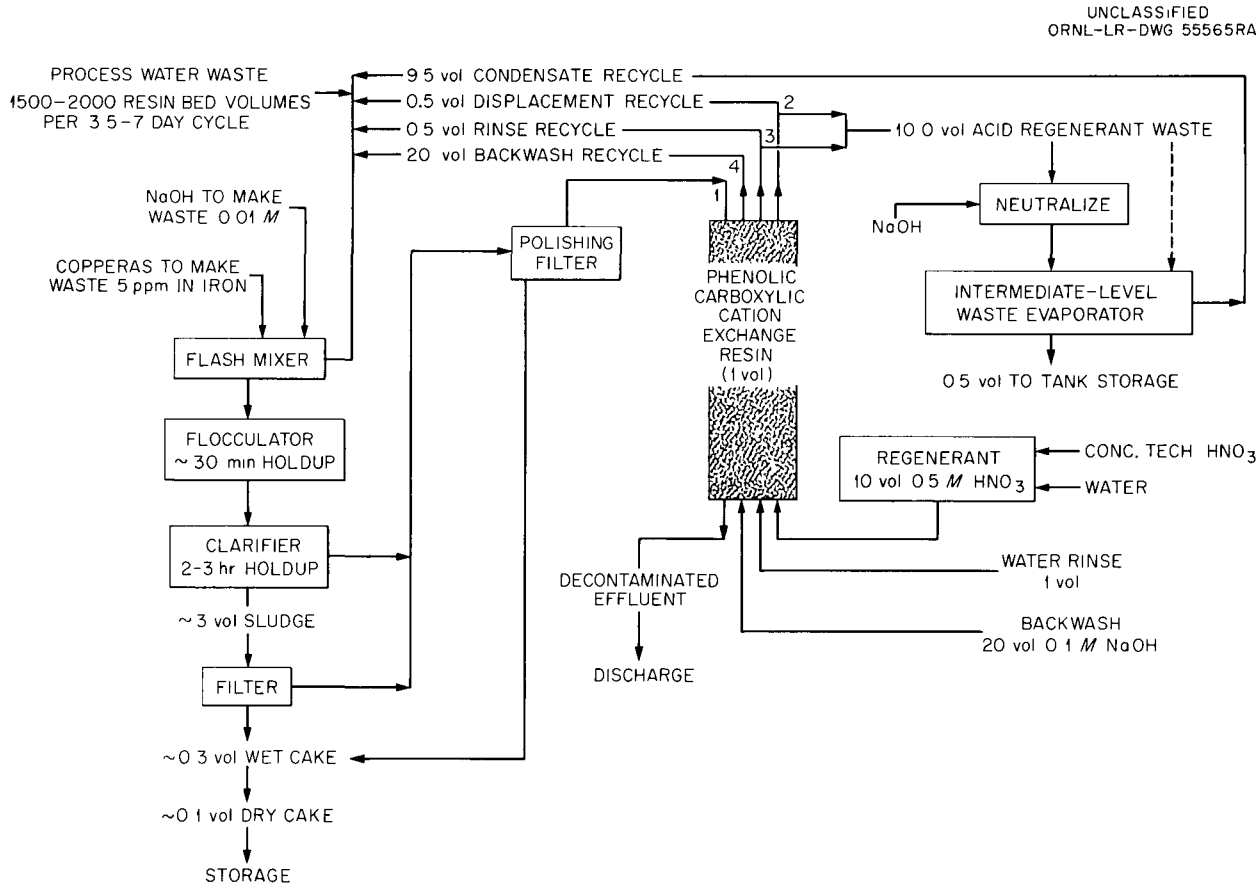

Fig. 3.18. Process-Water Decontamination with Carboxylic-Phenolic Ion Exchange Resin.

CS-100 cation exchange resin for removal of the remaining hazardous fission products, principally Cs^{137} and Sr^{90}.

When 2000 resin-bed volumes, or 56,000 gal of waste water, have been passed through the bed, the feed flow is stopped, the fission products are eluted with 10 vol of 0.5 *M* HNO_3, and the resin is washed with water and regenerated with 0.1 *M* NaOH.

Pilot-Plant Operation

Nine demonstration runs were completed. Volumes of 50,000 to 90,000 gal of ORNL process waste water were treated per run, representing 1800 to 3000 resin bed volumes; run durations varied from 71 to 146 hr of continuous operation. At the 2000-bed-volume level, the plant effluent contained <3% of current $(MPC)_w$ values for Sr^{90} and Cs^{137} for continuous occupational exposure,[12] and overall decontamination factors were at least three times greater than those obtained in the laboratory and semi-pilot plant. Decontamination factors from Sr^{90} (Table 3.8) ranged from 2047 to 12,160, representing more than a 99.9% removal in up to 2000 bed volumes, and those from Cs^{137} ranged from 77 to 3444 for the same operating period.

The sixth run in the series (HR-6)[13] was made in order to ascertain the resin-column breakthrough point. Cesium was the first to break through at the 50% level after 2800 bed volumes. At 2916

[12] NBS Handbook 69, *Maximum Permissible Body Burdens and Maximum Permissible Concentrations in Air and in Water for Occupational Exposure*, June 5, 1959.

[13] R. E. Brooksbank, *Low Level Waste Treatment Pilot Plant — Run HR-6 Summary* (in preparation).

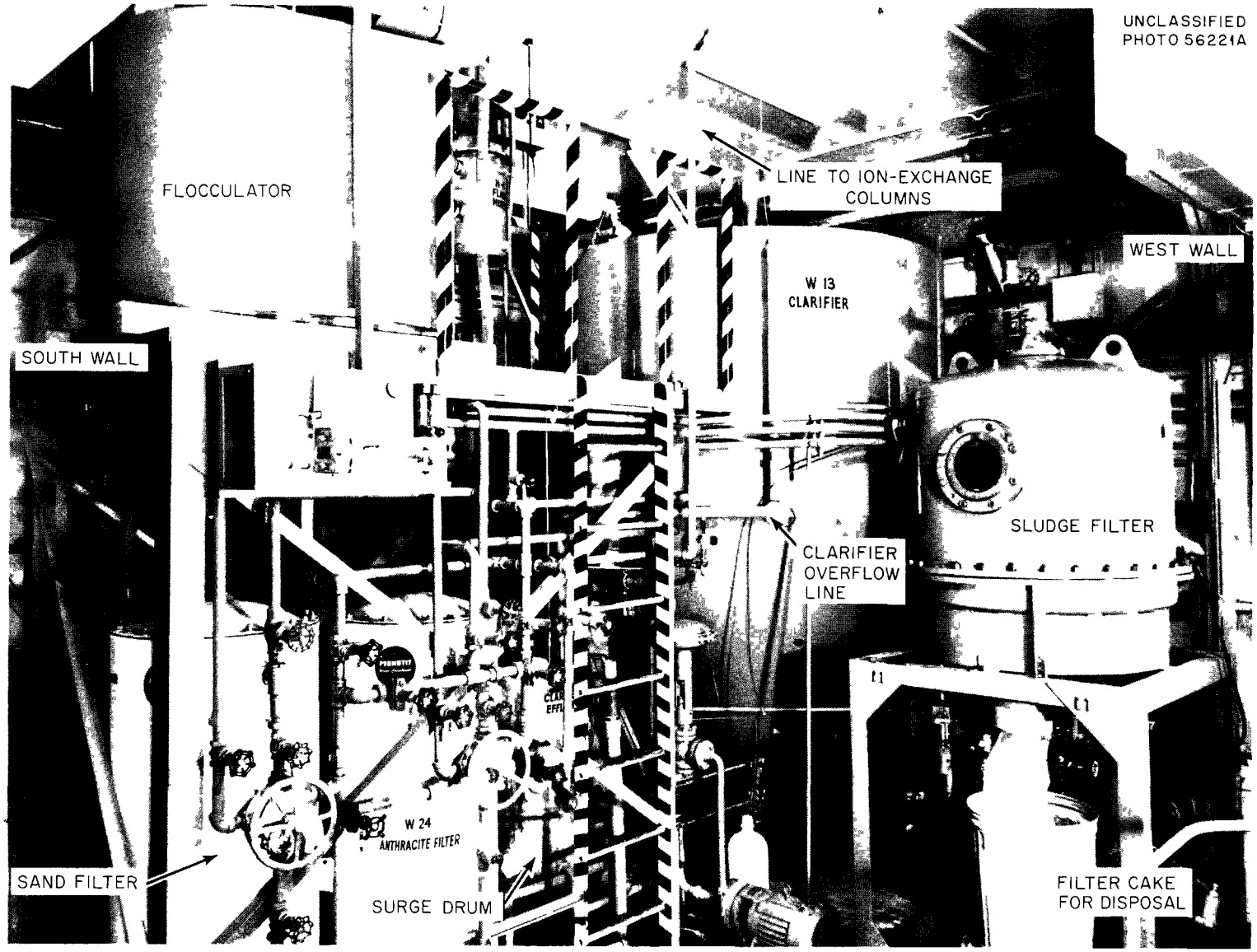

Fig. 3.19. Low-Activity Waste Treatment Pilot Plant – Pretreatment Equipment.

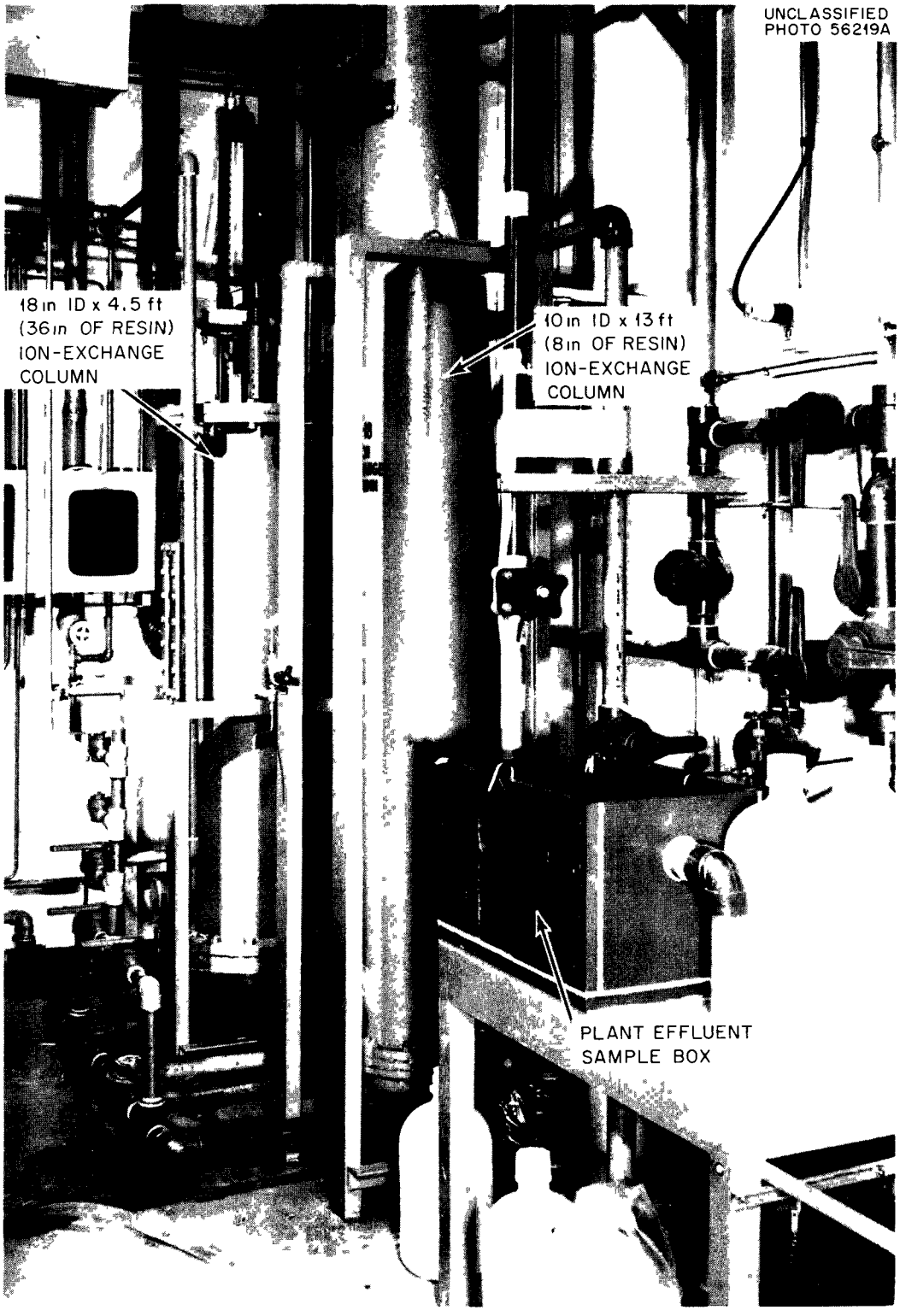

Fig. 3.20. Low-Activity Waste Treatment Pilot Plant – Ion Exchange Columns.

Table 3.8. Overall Removal of Activity from ORNL Waste

Run No.	Bed Volumes	Gross β		Gross γ		Sr^{90}		Cs^{137}		Co^{60}		TRE	
		DF	Percent Removed	DF	Percent Removed	DF	Percent Removed	DF	Percent Removed	DF	Percent Removed	DF	Percent Removed
HR-1	2000	30	96.70	44	97.70	2,956	>99.99	288	99.7	16	93.9	4	71.6
HR-2	2086	46	97.80	25	96.10	2,047	>99.9	246	99.6	11	91.3	28	96.5
HR-3	1959	42	97.6	10	89.90	4,982	>99.9	429	99.8	6	82.8	22	95.6
HR-4	1789	37	97.30	16	93.80	5,588	>99.9	2520	>99.9	4	74.3	31	96.8
HR-5	2046					2,316	99.96	543	99.82				
HR-6[a]	3118	12	91.96	5	77.92	20	95.11	6	82.30	5	80.91	21	95.33
HR-7	2086	34	97.04	19	94.71	12,160	99.99	451	99.78	121	91.80	24	95.77
HR-8[b]	2000	4	71.43	3	65.21	4,200	99.98	3444	99.90	3	63.33	21	95.22
HR-9	2131	26	95.40	14	93.10	>8,196[c]	99.99	~77	98.70	12	91.20	56	98.20

[a] Breakthrough run.
[b] High-activity run.
[c] None of this isotope found in plant effluent.

bed volumes, Sr^{90} in the plant effluent was 11.5 dis min^{-1} ml^{-1}, representing 520% of $(MPC)_w$ or 17% of the Sr^{90} level in the feed. Removal factors[14] for Sr^{90} and Cs^{137} from the saturated resin were 3.1×10^3 and 1.8×10^3, respectively.

Ion Exchange Column Performance. – The use of the "split-elution" procedure to decrease the volume of waste was adequately demonstrated. In this procedure, five volumes of 0.5 *M* HNO_3 eluent from the tail end of the previous elution is used as the initial removal solution. The second five volumes, containing almost no fission product contamination, is held for the subsequent elution cycle.

Two ion exchange columns (10 in. in diam by 8 ft high, and 18 in. in diam by 32 in. high) were tested to provide scaleup data for a full-scale plant. A full-scale plant would use a 4-ft-diam by 8-ft-high column. The 10-in.-diam column was scaled down at constant liquid velocity from the proposed plant bed. The 18-in.-diam by 32-in.-high bed has the same height-to-diameter ratio as that in the proposed plant and was designed to determine whether the data obtained from the 8-ft-high bed would require correction for a lower ratio when scaling up to full plant size. Two demonstration runs were made with the short bed and the rest with the 8-ft bed, with no differences in performance. A total of 403,000 gal of process waste was put through the same inventory of resin in the 8-ft resin column without noticeable decrease in resin performance.

Clarifier Operation. – Supersaturation of the clarifier effluent with calcium and other alkali-metal carbonates resulted in postprecipitation and formation of a scale on piping and equipment. The average total hardness of this stream varied between 60 and 70 ppm (as $CaCO_3$), and its decrease would substantially increase the on-stream life of the polishing filters and resin.

Minor changes were made in the precipitation equipment and reagents in order to induce complete precipitation. The addition of 25 ppm of slaked lime to the flash mixer decreased the effluent hardness from 70 to 56 ppm, but the flocculated precipitate was less dense, making control of the sludge-blanket level difficult. Recycling of sludge from the bottom of the clarifier, at various rates, to the flocculator in order to provide additional nuclei to aid in precipitation did not decrease the hardness but produced a denser sludge with better filtering characteristics. Recent laboratory development work (see below) indicated that supersaturation can be decreased by increasing the feed temperature from 18 to 24°C, along with the addition of lime, and that addition of the coagulant ($FeSO_4 \cdot 7H_2O$) to the flocculator rather than to the flash mixer should precipitate more of the carbonates.

Sludge Filtration. – Filtering the sludge from the bottom of the clarifier is difficult because the de-watered sludge is slick and slimy, due to the presence of algae, organic contaminants, and detergents that are dumped into the retention basin during decontamination operations. Pressurized sludge filtration was demonstrated with a single-frame Eimco-Burwell plate-and-frame pressure filter. The filtered sludge cake was enclosed in a canvas filter bag completely contained within the cavity formed by the frame and the two end plates in order to eliminate the necessity of installing elaborate containment around the filter, the pressure drop now being across the filter bag and not across the rubber seal gaskets between the frame and end plates. Pressure filters using this enclosed-bag method are not available commercially; additional design and development work will be necessary if this approach is used.

An Oliver rotary-drum vacuum filter was not suitable for processing the sludge. A small portion of the sludge penetrated the precoated surface of diatomaceous earth, forming an impervious layer through which the available pressure drop (25–28 in. Hg) across the drum was insufficient to force water at an acceptable rate.

Pressure filtration has advantages over vacuum filtration: better volume reduction, more compact cake; less auxiliary equipment (vacuum pump, vacuum condensate receiver, condensate draw-off pump, and a variable-speed drive mechanism); less maintenance and less attention from operating personnel; absence of any effect from erratic sludge composition and feed rate; shorter precoating time; and less waste of precoating material. The disadvantages are the additional containment required, the longer air-drying time necessary to ensure a firm, compact filter cake, and somewhat more difficult cleanup after cake removal.

[14] Removal factor = (peak activity of isotope during elution cycle)/(activity of isotope after 10 bed volumes of eluant).

Polishing-Filter Operation. – The clarifier effluent is pumped through an anthracite or sand filter for polishing prior to entering the ion exchange columns. This polishing filter not only removes colloidal calcium carbonate but also assists in the precipitation of carbonates from the supersaturated stream, thereby decreasing the hardness from 70 to 10 ppm. In all runs the filtrate was sparkling clear, with a turbidity of 1–2 ppm.

There are two filters in parallel, each with a 33-in.-deep bed and a cross-sectional area of 3.14 ft^2, which results in a flow rate of 3.2 gal min^{-1} ft^{-2} at the design feed rate of 10 gal/min. One filter contains quartz sand (28–30 mesh) and the other anthracite coal of an effective size of 0.89 mm and a uniformity coefficient of 1.58.

Although sand gave an average filtrate hardness of 5–6 ppm, compared with 8–14 for anthracite, it was more difficult to backwash, and accumulated carbonates could not be removed by slowly backwashing with 0.5 *M* HNO_3. The anthracite, after the same on-stream service as the sand, was clean and evenly distributed after being backflushed with water, although there was evidence of a $CaCO_3$ layer after 12 runs. The on-stream life of the anthracite filter ranged from 80 to 98 hr, which is greater than the equivalent of 2000 resin-bed volumes, and it is regarded as a satisfactory filter for this process. The two filters cost about the same.

Process Improvement

Prior to construction and operation of the 600-gal/hr pilot-plant unit, a 60-liters/hr semi-pilot model was operated through eight flowsheet[15] cycles to demonstrate the process with ORNL waste under continuous operating conditions and to verify design data required in process scaleup. Decontamination factors of at least 1000 from strontium and 100 from cesium, overall effluent radioactivities of $<10\%$ $(MPC)_w$, and overall volume reductions of about 3000 were consistently obtained, verifying results obtained in batch laboratory studies.

[15]R. R. Holcomb and J. T. Roberts, *Low-Level Waste Treatment by Ion Exchange. II. Use of a Weak Acid, Carboxylic-Phenolic, Ion-Exchange Resin*, ORNL-TM-5 (Sept. 25, 1961).

Laboratory Pilot-Plant Support

The laboratory development program provided support for the pilot-plant operation by prescribing simple control analysis and routine makeup procedures. A continuous-stream turbidimeter with a 0–5 or 0–25 ppm range on the clarifier overflow stream gave turbidity values within ±1 ppm of those obtained by two other laboratory methods. A continuous total-hardness analyzer with 0–10 ppm range, used to determine hardness in the ion exchange column effluents, could not be corrected to yield quantitative results because of the high pH of the effluent stream; however, a hardness breakthrough of >5 ppm could be detected. Since calcium breaks through before strontium, the detection of calcium will be useful in determining when to terminate a cycle prior to strontium breakthrough.

The head-end or scavenging precipitation steps were studied extensively in standard jar tests with ORNL tap water. Various treatments such as lime, caustic, lime-caustic in various ratios, and each of these with various amounts of iron as coagulant, were compared for the effects of flash mixing time, flocculation time, and temperature. The optimum procedure called for a combination of 0.01 *M* caustic and 25 ppm lime at 24–26°C, producing a residual hardness of about 15 ppm without clarification (Table 3.9). Trial of this method in a continuous laboratory clarifier, including the substitution of 5% sludge recirculation for the lime addition and adding 5 ppm of iron for floc formation, decreased the residual hardness to less than 10 ppm with less than 1 min of flash mixing and ~1 min of flocculation. Jar tests indicated that a flash-mixing time of 15–30 min will at least halve this residual hardness. Although this method was effective with tap water it was not as successful on ORNL low-activity waste that contained trace amounts of complexing agents.

The laboratory sludge-blanket settler with an inner cone was operated successfully at 250 ml/min with a 10-min holdup in the inner-cone sludge blanket. This represents an equipment-size reduction of 10 to 20 over the present pilot plant clarifier equipment and would decrease the capital cost of a full-scale plant correspondingly.

Other Laboratory Studies. – BO-4 vermiculite was not promising as a substitute exchanger in the scavenging–ion exchange process. Tests were

made in columns ($\frac{7}{8}$ in. in inner diam and 6 in. high) at flow rates of 1, 5, 15, and 50 ml/min. The fine-mesh vermiculite was preceded by a 5-μ filter since it was subject to plugging, which resulted in high pressure drops and even complete stoppage. Cesium and strontium breakthrough or leakage occurred at or prior to 1500 bed volumes in all cases except at a flow rate of 0.25 ml min^{-1} cm^{-2}. After 1500 bed volumes had passed through the vermiculite at this low flow rate, an indicated strontium decontamination factor of 1000 was retained. The very low flow rates with treated vermiculite make it unusable for low-activity waste treatment.

Table 3.9. Comparison of Various Methods for Decreasing Hardness of ORNL Tap Water[a]

Treatment	Residual Total Hardness	
	With Fe^{3+}	Without Fe^{3+}
Jar Tests Without Clarification at Room Temperature		
100 ppm $Ca(OH)_2$	75–80	95–100
0.01 *M* NaOH	60–65	50–55
0.01 *M* NaOH and 50 ppm $Ca(OH)_2$	35–40	20–25
0.01 *M* NaOH and 25 ppm $Ca(OH)_2$	30–35	13–15
0.01 *M* NaOH and 25 ppm $CaCO_3$		35–40
Continuous Laboratory Clarifier		
0.01 *M* NaOH and sludge recirculation	8–13	

[a]Total hardness in the tap water varied from an extreme high of 110 ppm to an extreme low of about 75 ppm. The usual value was between 95 and 105 ppm.

A study to determine the feasibility of complete demineralization and recycle of ORNL process waste was initiated. A strong-acid cation resin (TCD-1) reduced the concentration of calcium in ORNL tap water by a factor of 1000 at 750 bed volumes throughput. A weak-acid cation resin (IRC-50) reduced the calcium concentration initially by a factor of 1000, but of only 3 at 1000 bed volumes. A combination of weak- and strong-acid resin in series gave a concentration reduction of >1000 for calcium up to ~2000 bed volumes. Assuming that demineralized water could be recirculated through a plant and that it would regain only 10% of the initial hardness during reuse, a mixture of weak- and strong-acid cation exchangers could operate for 20,000 bed volumes before requiring regeneration.

Comparative Design Study of Low-Activity Waste Treatment Processes

Several processes for treating ORNL process waste water were reviewed to determine the optimum technique for a plant to treat the full 750,000 gal/day produced. Criteria adopted for establishing a satisfactory process are listed below.

1. Effluent from the treatment process should contain no greater than the "environmental" $(MPC)_w$ of radionuclides; the controlling concentration for average ORNL low-activity waste is, for Sr^{90}, 10^{-7} μc per cc of water.
2. The process must be sufficiently flexible to handle a wide range of chemical compositions in the waste fed to it and must not be seriously affected by complexing and chelating agents commonly found in the waste.
3. Capital and operating costs of the treatment plant must be the lowest for achieving the desired decontamination. Processes reviewed included expansion and process improvement of the existing lime-soda treatment plant, addition of a second stage (vermiculite adsorption columns) to the lime-soda plant, evaporation, soil adsorption, and the scavenging–cation exchange process with either nitric acid or HCl for resin regeneration. The other processes were less efficient than the scavenging–ion exchange process, either because of high costs (evaporation) or inadequate decontamination and operating problems (improved lime-soda or vermiculite). Soil adsorption seems impractical because of the very large area required for the volumes of water to be treated.

The scavenging–cation exchange procedure offers the advantages of (1) volume reduction factors of 1500 to 2000 (raw waste feed to radioactive exit streams); (2) decontamination factors from strontium of >2000 and from cesium of 300, both demonstrated repeatedly on actual waste; (3) relatively low capital investment required (about $500,000) and low operating costs (about 54 cents

per 1000 gal); (4) high probability of automatic operation. The main disadvantage is that rather precise chemical adjustments are required at several points, imposing more than ordinary care in operation.

Design Projection of Scavenging–Ion Exchange Process to Full-Scale Plant

A design proposal for a 750,000-gal/day treatment plant was projected from early laboratory-scale experiments with a 5 *M* HCl-regeneration scavenging–ion exchange flowsheet (Fig. 3.21), and estimates of capital investment and operating costs were based on this projection. A later cost study to determine any major difference between the HCl and HNO_3 flowsheets (Fig. 3.22) indicated that capital and operating costs for the two procedures are within a few percent of each other. For treating ORNL low-activity waste, the HNO_3 flowsheet offers the attraction of requiring standard reagents and materials of construction (stainless steels) that are compatible with existing equipment-decontamination methods. Also, this flowsheet might allow significant savings by eliminating the regenerant-acid evaporator if the intermediate-activity waste evaporator currently being designed for ORNL can be partly assigned to handle this stream. The decision to eliminate the smaller evaporator would be an administrative rather than a technical one, as it must depend on the scheduling of operations and allocation of costs for the intermediate-activity evaporator.

The full-scale plant would be similar to the pilot plant described in Sec 3.2 (Pilot Plant Process Description), except that all flows would be about 50 times greater. The 750,000 gal/day of process waste water would be fed from the present equalization basin to a flash mixer where 394 gal/day of 50% NaOH would be added by a metering pump controlled by a pH meter to raise the pH to about 12 (approximately 0.01 *M* NaOH). The flocculator could probably be eliminated, in which case the effluent from the flash mixer would go to a sludge-blanket clarifier. The 4700 gal/day of sludge separated from the waste water in the clarifier would be pumped to an Eimco moving-belt filter, which would yield 176 gal/day of dewatered sludge cake for disposal by burial, tank storage, or calcining. An enclosed pressure filter might be substituted for the moving-belt sludge filter.

Effluent from the clarifier would be pumped through a polishing filter (U.S. Filter Co. "Auto-Jet" or similar pressure leaf filter) to remove the last traces of solids, giving high decontamination factors and preventing the plugging of the ion exchange resin columns. Success with sand and anthracite filters in the pilot plant may indicate substitution of these for the proposed precoated leaf filter. The polishing-filter effluent passes downward through an ion-exchange column 4.5 ft in diameter, 16 ft high, containing 117 ft^3 (bed height, 7.6 ft) of phenolic resin (Duolite C-3 for the HCl flowsheet or CS-100 for the HNO_3 flowsheet). Two columns are proposed in order to provide for a 3.5-day cycle (3 days loading and half a day for regenerating). Each loading can handle 1,313,000 gal of waste water or 300 gal/min based on a 1500 bed-volume capacity for the resin. The >2000 bed-volume resin capacity demonstrated in the pilot plant illustrates the conservative basis of the design projection and indicates that better volume reduction (smaller volumes of radioactive effluents and solids) can be expected than are shown on the flowsheets. The pressure drop through each column is expected to be 37 psig. The unusually deep bed is used to achieve uniform flow distribution and high activity removal. Cation radioactivity is removed from the waste by the resin, and the softened water from the column discharged to the creek.

Regeneration of the resin by the split-elution method proceeds as follows (as numbered in sequence in Fig. 3.22):

1*a*. Waste water remaining in the resin is displaced to the equalization basin by passing 0.5 bed volume (438 gal) of 0.5 *N* HNO_3 from a recycle-acid storage tank upward through the column.

1*b*. The first elution of contaminated salts and acid is forced to a regenerant-acid evaporator feed tank by passing 4.5 bed volumes of 0.5 *N* HNO_3 upward through the column.

2*a*. One-half bed volume of fresh 0.5 *N* HNO_3 is passed through the resin to displace contaminated acid to the evaporator feed tank.

2*b*. Then, 4.5 volumes of fresh 0.5 *N* HNO_3 is passed through the column to the recycle-acid storage tank to complete the elution.

3*a*. The acid remaining in the resin is displaced to the recycle storage tank by passing 0.5 vol of demineralized water through the bed.

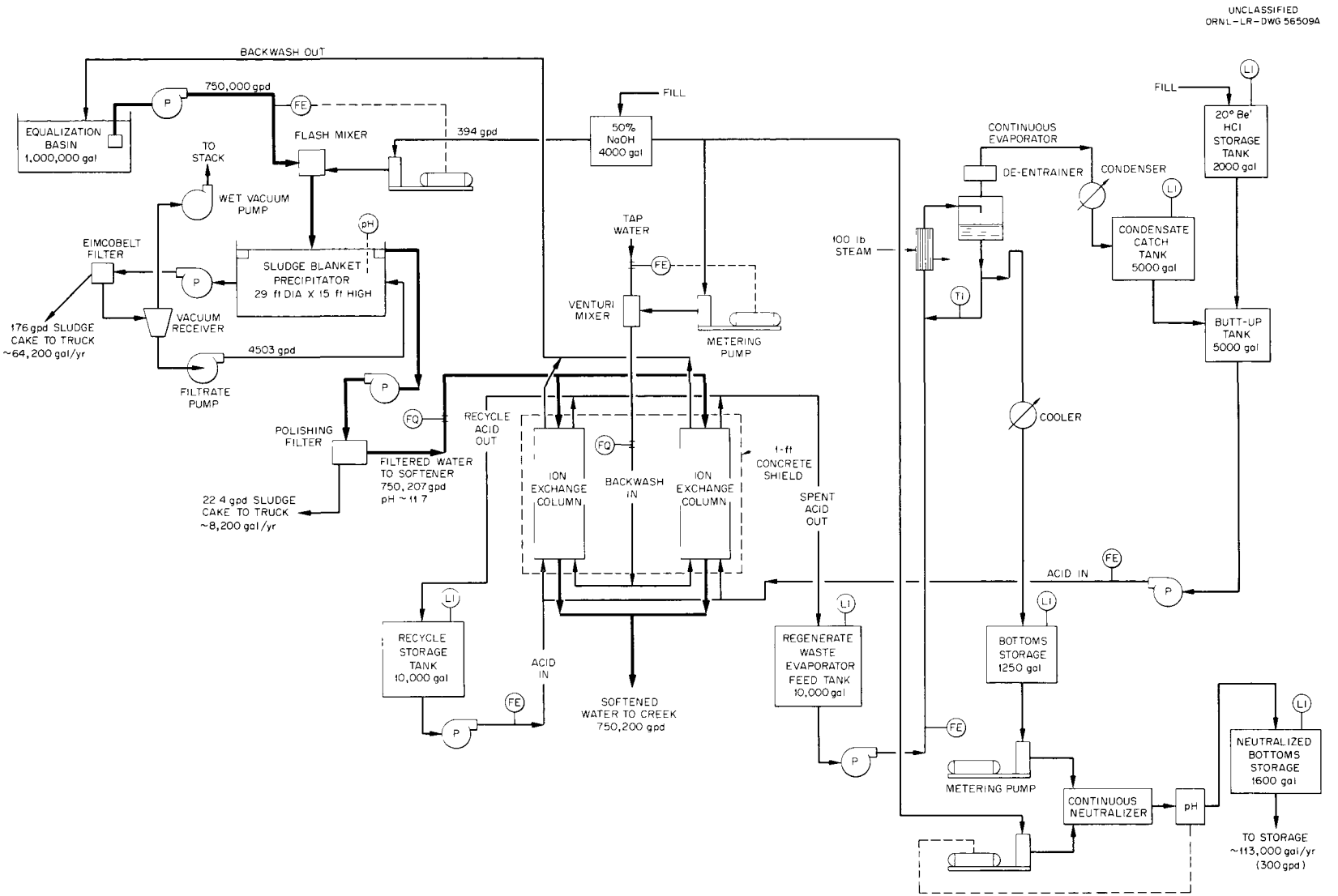

Fig. 3.21. HCl Flowsheet. Scavenging–ion exchange process for low-activity waste treatment.

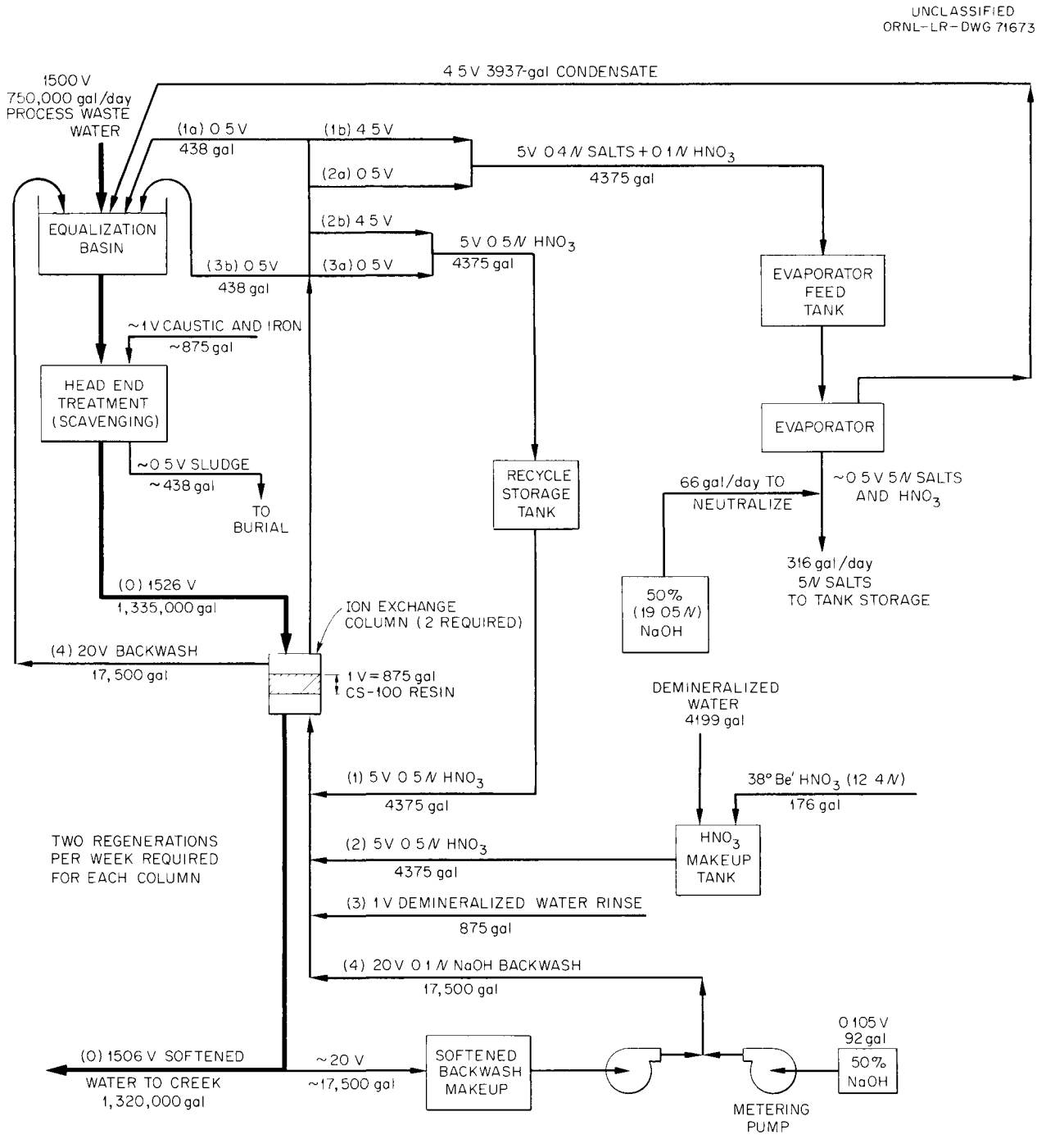

Fig. 3.22. Split-Elution HNO_3 Flowsheet. Scavenging–ion exchange process for treating low-level waste.

3*b*. The resin is rinsed with 0.5 vol of demineralized water, which is sent to the equalization basin.

4. The resin is finally backwashed and restored to the sodium form by 20 bed volumes of 0.1 *N* NaOH, which is sent to the equalization basin.

In the HNO_3 flowsheet the regenerant acid is too dilute to make recovery for reuse worthwhile, and the condensate from the evaporation is sent to the equalization basin. The flowsheet lists only a 10-to-1 volume reduction in the evaporation, but laboratory tests indicate that the volume reduction may be 20 or 30 to 1 if the evaporation is made before the contaminated acid is neutralized for storage in the existing ORNL concrete tanks. In the HCl flowsheet the 5 *N* regenerant acid is too concentrated to discard; it is estimated that 90% of the HCl from the first elution step can be recovered by evaporation. The remaining 10%, containing the radioactive salts removed from the waste plus inert solids in the solution, must be drained from the evaporator as bottoms and neutralized for storage in the concrete tanks.

Cost Estimates for 750,000-gal/day Scavenging–Ion Exchange Treatment Plant

Capital and operating costs were estimated for a full-scale treatment plant for ORNL low-activity waste, based on the flowsheet projected by an engineering study from laboratory-scale experiments before pilot-plant data were available. The estimated capital costs, including all equipment installed, piping, instruments, electrical wiring, and a building to house all equipment except the sludge blanket precipitator (clarifier), were about $393,000 (Table 3.10). Engineering costs at 10% of this total and contingencies at 20% bring the estimate of capital costs to about $511,000. There appears to be no significant cost difference between the HNO_3 and the HCl flowsheets unless the regenerant-acid evaporator can be eliminated from the HNO_3 flowsheet by use of the proposed stainless steel 600-gal/hr ORNL intermediate-activity waste evaporator. The HCl flowsheet requires a separate regenerant-acid evaporator because of different materials of construction. Elimination of the 150-gal/hr evaporator, its condensate catch tank, bottoms storage tank, continuous neutralizer, and neutralized bottoms storage tank would reduce the capital cost of the low-activity waste-treatment plant to approximately $400,000, but some fraction of the capital cost of the intermediate-activity evaporator should be charged against the low-activity plant if the large evaporator processes regenerant acid. This charge could be a disadvantage to the low-activity waste treatment costs, as heavier shielding and other factors in the intermediate-activity-level evaporator design may impose a much higher capital cost per gallon of capacity than the small evaporator requires.

Operating costs for a full-scale scavenging–ion exchange treatment plant (Table 3.11) were estimated to be about 54 cents per 1000 gal, exclusive of amortization charges. Amortization of the $511,000 investment over 20 years adds 9 cents per 1000 gal to the operating cost. The utilities cost of 4 cents per 1000 gal could be decreased to 2 cents if the regenerant-acid evaporator is eliminated. The labor and supervision charge is based on 1.5 men per shift (part time for one man, with one supervisor operating the whole ORNL waste system) and includes plant overhead charge. The solid-waste removal cost is based on packaging the filter sludge in plastic-lined fiber drums and burying them in the ORNL waste-disposal area. The cost of disposal of the concentrated acid to evaporator bottoms or to waste tanks or burial has not been estimated.

3.3 ENGINEERING, ECONOMICS, AND HAZARDS EVALUATIONS

A study was undertaken in cooperation with the ORNL Health Physics Division to evaluate the economics and hazards associated with alternative methods for the ultimate disposal of highly radioactive liquid and solid wastes. All steps between fuel processing and ultimate storage will be considered, and the study should define an optimal combination of operations for each disposal method and indicate the most promising methods for experimental study.

A 6-tonne/day fuel processing plant is assumed, processing 1500 tonnes/year of uranium converter fuel at a burnup of 10,000 Mwd/tonne, and 270 tonnes/year of thorium converter fuel at a burnup of 20,000 Mwd/tonne. This hypothetical plant would process all the fuel from a 15,000-Mw_e nuclear economy, which may be in existence by 1975. The preliminary operations to be evaluated are interim liquid storage, conversion to solids by pot calcination, interim storage of solids in pots, and shipment of calcined solids. The ultimate disposal methods to be evaluated include the storing of calcined solids in salt deposits,

Table 3.10. Estimated Capital Costs for 750,000-gal/day Scavenging–Ion Exchange Low-Activity Waste Treatment Plant

Item	Cost of Equipment	Cost of Installation	Total Cost
Sludge-blanket precipitator (29-ft diam, 15-ft height) and water meter	$25,000		
Automatic chemical feeders and blowdown	2,500	$ 9,200	
Concrete pad		1,200	$ 37,900
Flash mixer	500	200	700
Polishing filter, 250 ft^2 (U.S. Filter Co.)	17,000	1,000	18,000
Eimcobelt vacuum filter	7,000		
Vacuum receiver, wet vacuum pump, filtrate pump	1,200	2,500	10,700
4000-gal carbon steel storage tank for 50% NaOH, 9 ft high, 9 ft in diam	3,300	700	4,000
2 ion exchange columns, 16 ft high, 4.5 ft in diam, Saran lined	9,600		36,000
234 ft^3 of Duolite C-3 resin for columns at $22 per ft^3	5,150	500	5,650
IX automatic controls and valves	3,600 (installed)		3,600
10,000-gal recycle storage tank, 12 ft high, 12 ft in diam, Saran lined	11,000	1,500	12,500
10,000-gal evaporator feed tank, 12 ft high, 12 ft in diam, Saran lined	11,000	1,500	12,500
Continuous evaporator, package unit, 150 gal/hr rating	50,000	20,000	70,000
5000-gal condensate catch tank, 10.5 ft high, 9 ft in diam, Saran lined	7,500	1,000	8,500
5000-gal butt-up tank, 10.5 ft high, 9 ft in diam, Saran lined	7,500	1,000	8,500
2000-gal HCl storage tank, 7 ft high, 7 ft in diam, Saran lined	5,000	600	5,600
1600-gal neutralized-bottoms storage tank, 6.5 ft high, 6.5 ft in diam, Saran lined	4,000	600	4,600
1250-gal bottoms-storage tank, 6 ft high, 6 ft in diam, Saran lined	3,700	500	4,200
Continuous neutralizer	4,000	1,000	5,000
Piping			20,000
Instrumentation			5,000
Electrical wiring			10,000
Building, 52 ft long, 44 ft wide, 24 ft high (55,000 ft^3), at $2 per cubic foot			110,000
Total	$78,600	$39,300	$392,950

Table 3.11. Scavenging–Ion Exchange Process: Operating Costs for 750,000-gal/day Treatment Plant

	Cost per 1000 gal of Feed (cents)
Chemicals, filter aid and resin	20
Utilities (steam, electric power, and water)	4
Labor and supervision	17
Solid waste removal and burial	4
Maintenance (5% per yr of initial capital cost)	9
Total	54

in vaults, and in vertical shafts, and liquids in salt deposits, in porous geologic formations by deep-well injection, in impermeable formations by hydrofracture, and in tanks.

A cost study of interim liquid storage was completed for the storage of acid Purex (50 gal/tonne of uranium processed), neutralized Purex (60 gal/tonne), acid conventional Thorex (400 gal/tonne), and neutralized Thorex (640 gal/tonne) wastes. For storage times of 0.5 to 30 years, costs ranged from 2.0×10^{-3} to 9.3×10^{-3} mill/kwh$_e$ for storage of acid wastes and from 1.5×10^{-3} to 4.7×10^{-3} mill/kwh$_e$ for alkaline wastes. Details are given elsewhere.[16]

A cost study on the conversion of high-activity solutions to solids by pot calcination was completed. Costs were calculated for processing Purex and Thorex wastes in acid and reacidified (after alkaline storage) forms and for producing Thorex glass from acid wastes. Calcination-vessel designs provided for right circular cylinders similar to those used in the engineering development studies. The vessels studied were 6, 12, and 24 in. in diameter, made of sched-40 type 347 stainless steel pipe, 10 ft high. Vessel costs, based on estimates from private industry, were $500, $855, and $2515. Costs were calculated for wastes decayed 120 days and 1, 3, 10, and 30 years after reactor discharge prior to calcination. Aging had negligible effect on costs for processing in a given vessel size because vessel and operating costs were much higher than capital costs in all cases. Aging permits larger vessels to be used, however, and costs for processing in 6-in.-diam vessels were 2 to 3 times as high as for processing in 24-in.-diam vessels.

The lowest cost was 0.87×10^{-2} mill/kwh$_e$ for processing acid Purex and Thorex wastes in 24-in.-diam vessels, and the highest was 5.0×10^{-2} mill/kwh$_e$ for processing reacidified Purex and Thorex wastes in 6-in.-diam vessels (Table 3.12). About 7 years of interim liquid storage would be required before acid Purex waste could be processed in 24-in.-diam vessels. Details of this study are given elsewhere.[17]

Shipping costs for calcined solids were calculated, assuming cylindrical carriers of iron, lead, and uranium, with an inside diameter of 5 ft. The vessels containing the calcined solids are the 6-, 12-, and 24-in.-diam cylinders used for pot calcination. Carriers would contain thirty-six 6-in.-diam vessels, nine 12-in.-diam vessels, or four 24-in.-diam vessels.

A minimum age for each waste before shipping is necessary because the temperature of the waste must not be allowed to rise above the maximum calcination temperatures and because the temperature of the lead (for the case of lead carriers) must not approach its melting point. The carriers are air-filled and have no mechanical cooling equipment. Minimum ages for shipping in 6- and 24-in.-diam cylinders were 2.4 and 11 years for acid Purex, 1.0 and 3.0 years for reacidified Purex, 0.66 and 3.4 years for acid Thorex, 0.33 and 0.82 year for reacidified Thorex, and 0.33 year for acid Thorex glass in 6-in.-diam cylinders.

Weights and costs for carriers at minimum ages were about 100 tons and $50,000 for iron carriers, 80 tons and $120,000 for lead carriers, and 65 tons and $650,000 for uranium carriers. The shipping costs calculated for round-trip distances of 1000, 2000, and 3000 miles were the sums of carrier, rail freight, and handling charges. Shipping costs were lowest in all cases for lead carriers, but in some cases the use of lead carriers required higher minimum ages. At 1000 miles the use of iron carriers costs less than that of uranium

[16] R. L. Bradshaw *et al.*, *Evaluation of Ultimate Disposal Methods for Liquid and Solid Radioactive Wastes. I. Interim Liquid Storage*, ORNL-3128 (Aug. 7, 1961).

[17] J. J. Perona *et al.*, *Evaluation of Ultimate Disposal Methods for Liquid and Solid Radioactive Wastes. II. Conversion to Solid by Pot Calcination*, ORNL-3192 (Sept. 27, 1961).

Table 3.12. Pot Calcination Costs as Affected by Waste Types and Vessel Sizes

Waste Type	Total Processing Cost (mills/kwh$_e$)		
	6-in.-diam Vessels	12-in.-diam Vessels	24-in.-diam Vessels
Acid Purex–acid Thorex	1.6×10^{-2}	0.98×10^{-2}	0.87×10^{-2}
Acid Purex–acid Thorex glass	2.2		
Acid Purex–reacidified Thorex	3.8	1.9	1.5
Reacidified Purex–acid Thorex	2.8	1.5	1.2
Reacidified Purex–acid Thorex glass	3.4		
Reacidified Purex–reacidified Thorex	5.0	2.4	1.9

carriers, but at 3000 miles the cost of uranium carriers is less than that of iron carriers and approaches that of lead carriers (Figs. 3.23 and 3.24). Costs for lead carriers range from 0.70×10^{-3} mill/kwh$_e$ for acid Purex in four 24-in.-diam cylinders per carrier at 1000 miles to 32.3×10^{-3} mill/kwh$_e$ for reacidified Thorex in smaller cylinders at 3000 miles (Table 3.13).

Tentative costs were calculated for storage of cylinders of calcined waste buried in a vertical position in the floors of rooms in salt mines. The distance between the vertical axes of the cylinders is determined by the need for dissipating the heat of fission product decay without exceeding the calcination temperature in the cylinders or a temperature of 200°C in the salt. Acid Purex waste requires the largest spacing, ranging from 20 ft at 2.3 years to 11 ft at 30 years for 6-in.-diam cylinders; from 36 ft at 5.5 years to 23 ft at 30

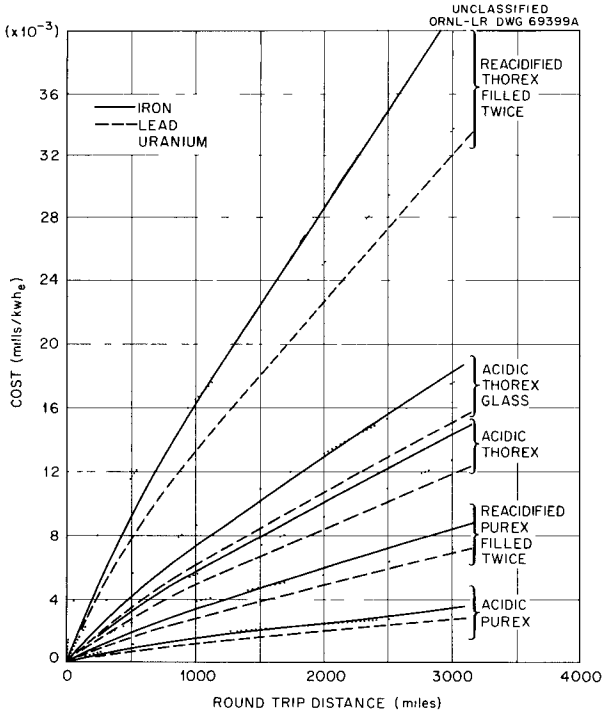

Fig. 3.23. Shipping Costs for Carriers Containing Thirty-six 6-in.-diam Cylinders or Nine 12-in.-diam Cylinders of Calcined Wastes.

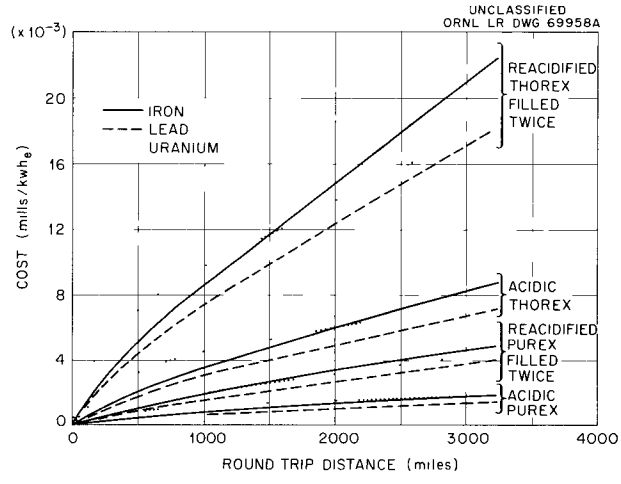

Fig. 3.24. Shipping Costs for Carriers Containing Four 24-in.-diam Cylinders of Calcined Wastes.

Table 3.13. Shipping Costs in 5-ft-ID Lead Carriers as a Function of Round-Trip-Distance Costs

Waste Type	Cost (mills/kwh$_e$)					
	Thirty-Six 6-in.-diam Cylinders per Carrier or Nine 12-in.-diam Cylinders per Carrier			Four 24-in.-diam Cylinders per Carrier		
	1000 Miles	2000 Miles	3000 Miles	1000 Miles	2000 Miles	3000 Miles
Acid Purex	1.23×10^{-3}	2.02×10^{-3}	2.80×10^{-3}	0.64×10^{-3}	1.00×10^{-3}	1.35×10^{-3}
Reacidified Purex filled twice	2.90	4.86	6.83	1.55	2.58	3.76
Acid Thorex	4.83	8.12	11.8	3.00	4.83	6.69
Reacidified Thorex filled twice	13.3	22.5	32.2	7.29	12.2	17.1
Acid Thorex glass (6-in. cylinders only)	6.09	10.7	15.0			

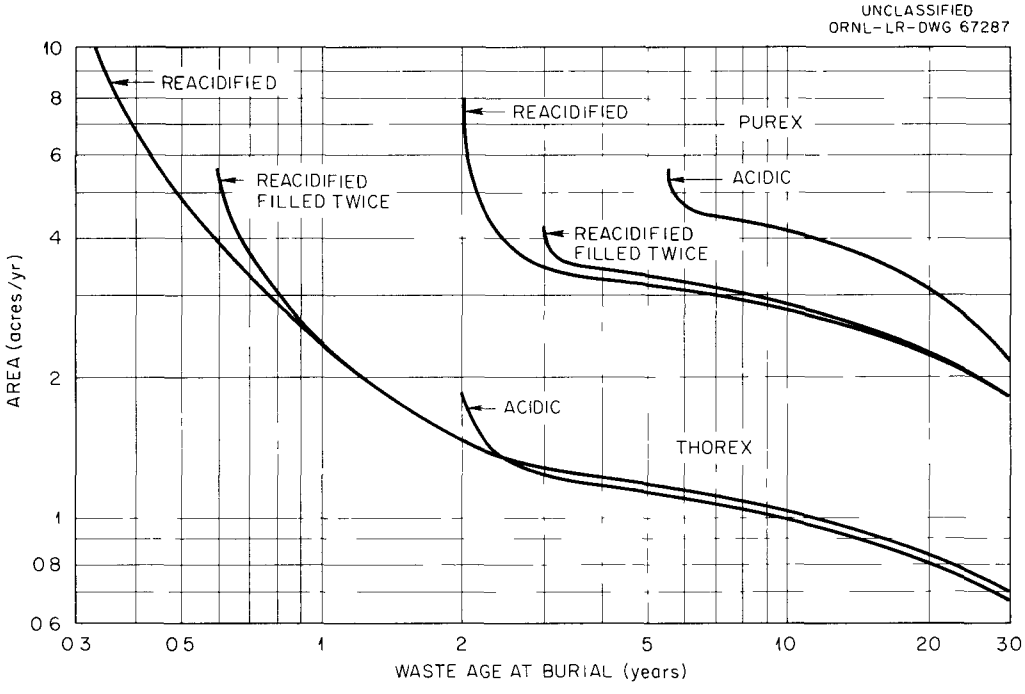

Fig. 3.25. Mined-Space Requirements in Salt Mines for Calcined Wastes in 12-in.-diam Cylinders Buried in Vertical Arrays.

years for 12-in.-diam cylinders; and 56 ft at 30 years for 24-in.-diam cylinders. Corresponding areas of mined space range from about 20 to 2 acres/year. As an example, mined-space requirements for the disposal of 12-in.-diam vessels are plotted in Fig. 3.25 as a function of waste age. Space requirements were also calculated for storage above the floor of rooms in a salt mine and were roughly the same as for burial in arrays in the floor. Space requirements for storage as

liquids were about 2.3 times as large, owing primarily to the lower limiting temperatures.

In the conceptual design of the disposal operation, the waste-container shipping cask is removed from a rail car and carried into a hot cell, which encloses the top of the waste shaft. The containers are then unloaded into a storage area from which they are removed for lowering down the shaft into a motorized carrier at the working level of the mine. The carrier moves out to the disposal area, lowers the container into a hole in the floor, and backfills the hole with fine crushed salt. Concurrently, salt is being mined in another corridor. A one-mile-square area is assumed to be served by a waste shaft. The operations will be conducted on one quadrant of the mine at a time, completely isolating the salt mining from the disposal operations. Disposal-operations personnel and equipment will use the mining shaft for entering and leaving, however.

Ventilating air will come down a compartment in the mining shaft, with a portion being split off into the disposal tunnel. The disposal-tunnel air will travel completely around the quadrant and exit up the waste shaft. The air will be drawn from the shaft, through the hot cell, through an absolute filter, and up a 200-ft-high stack. In order that ventilating air will never pass a filled storage area before it reaches the current working area, disposal operations will start at the most remote point and work back toward the shaft. The criteria for isolation and ventilation require that a double tunnel be driven completely around the quadrant and that the rooms on the outside of the peripheral tunnel be excavated before disposal operations start.

Cost figures were calculated for disposal at a depth of 1000 ft for two conditions of stability, one with very small structural flow and 2.5% dimensional closure due to thermal flow, and one with considerable structural flow and 100% thermal closure of the rooms. These figures for typical waste combinations are shown in Table 3.14 for waste ages at burial of 1, 3, 10, and 30 years. The costs of developing peripheral tunnels and storage space are based on an assumed cost of $2 per ton for salt removal. Shafts and life-of-shaft items were amortized over the time required to fill the entire square mile (8.5 years for 1-year cooling with 2.5% closure to 89 years for 30-year cooling with 100% closure).

Total costs ranged from 6×10^{-3} mill/kwh$_e$ for 100% room closure with 30-year-cooled wastes to 30×10^{-3} mill/kwh$_e$ for 1-year cooling and 2.5% closure. Sixty to eighty-five percent of the costs were for salt removal, indicating that it is important to have more accurate figures for this operation.

Table 3.14. Costs of Ultimate Storage of Calcined Wastes in Salt at a Depth of 1000 ft

Age of Waste (yr)	Type of Waste	Diameter of Cylinder (in.)	Cost (mills/kwh$_e$)	
			2.5% Closure	100% Closure
1	Reacidified Purex	6	3.06×10^{-2}	1.60×10^{-2}
	Acid Thorex	6		
3	Acid Purex	6	1.54	0.84
	Acid Thorex	12		
10	Reacidified Purex filled twice	12	1.25	0.70
	Acid Thorex	12		
30	Acid Purex	12	1.00	0.60
	Acid Thorex	24		

4. Solvent Extraction Technology

New solvent extraction agents are being developed for wider application of solvent extraction technology, particularly in radiochemical processing. A number of new extractants developed in the ORNL raw materials program are now commercially used for extracting uranium and other metals from acid ore leach liquors. Solvents that extract uranium by cation or anion exchange offer a new technology in which the principles of ion exchange are used on a liquid-liquid basis with the inherent engineering advantages of liquid-liquid systems. Extraction, by this and other mechanisms, of a large number of metals from a wide variety of different aqueous compositions is possible if extraction properties are controlled by the appropriate choice of reagent structure. A systematic experimental survey is in progress to explore their utility in fuel processing, waste treatment, fission product recovery, transuranium recoveries, and other heavy-metal separations.

Fundamental investigations, aimed at understanding the mechanisms of metal extraction by the various reagents, are in progress, and reagents intended for use with highly radioactive solutions are being examined for radiation stability and methods of removing deleterious degradation products.

Information already obtained about extractants containing different functional groups also suggests utility outside the field of liquid-liquid extraction. Some of the functional groups may be used profitably in ion exchange resins or in the "liquid gel" technique in which the solvents are held in beads of microporous plastics.

4.1 FINAL CYCLE PLUTONIUM RECOVERY BY AMINE EXTRACTION

The chemical flowsheet proposed,[1,2] for purification of plutonium by amine extraction after typical Purex extraction and separation from uranium, was tested with simulated feed in batch countercurrent runs and with actual Purex solutions in continuous countercurrent runs. Plutonium distributions were as predicted, with satisfactory recoveries and concentration factors, and physical performance was excellent, but decontamination factors from the actual Purex solutions were much lower than expected and lower than required for an acceptable plutonium product. Decontamination is being studied further.

Batch Countercurrent Tests

Plutonium distributions under various extraction, scrubbing, and stripping conditions (Table 4.1) and the physical performance of the system were checked at full plutonium concentration levels, in a bank of stirred separatory funnels, with Alamine 304 (trilaurylamine, TLA) in diethylbenzene as the extractant. The plutonium profiles agreed well with the predicted extraction isotherms (Fig. 4.1). Plutonium refluxing was negligible when 6 *M* HNO_3 was used for scrubbing and was measurable, but less than predicted from the distribution coefficients, when 0.5 *M* HNO_3 was used. This suggests somewhat slow reequilibration of plutonium in the scrubbing section. The raffinate loss with four extraction stages was about 0.3% of the plutonium in the feed, and about 0.01% remained in the stripped extractant.

Zirconium-95–niobium-95 tracer (~60% Nb–40% Zr γ activity) added to the feed solution at $\sim 10^6$ gamma counts min^{-1} ml^{-1}, the highest level

---

[1] *Chem. Technol. Div. Ann. Progr. Rept. May 31, 1961*, ORNL-3153, p 105.

[2] C. F. Coleman, *Final Cycle Plutonium Recovery by Amine Extraction*, ORNL CF-61-5-74 (May 24, 1961).

Table 4.1. Flowsheet Conditions in Batch Countercurrent Tests of Plutonium Purification Cycle

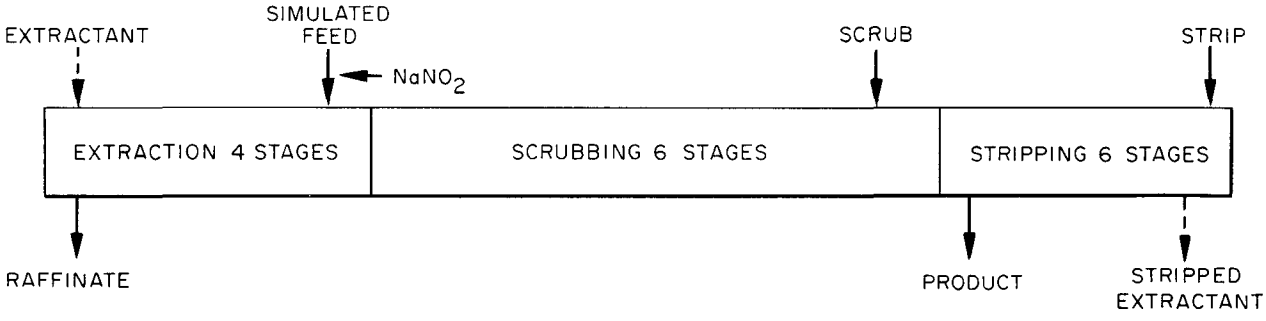

Stream	Relative Volume	Composition
Extractant	5, 15	0.1, 0.16, 0.3 *M* TLA in diethylbenzene
Feed	60	1 g Pu/liter, ~1.5 *M* HNO_3, 0.2 *M* $NaNO_2$ (initial)
Scrub	3, 6	0.25, 0.5, 6 *M* HNO_3
Strip	3, 4	2, 3, 4 *M* CH_3COOH

considered completely safe in the unshielded glove boxes used, could not be distinguished from background gamma in the product. This indicated a decontamination factor of 10^3, and radiochemical analyses indicated decontamination factors of the order of 10^4 each from zirconium and niobium.

Continuous Countercurrent Tests

In processing of Purex 1BP solution,[3] physical operation of KAPL Mini mixer-settlers was excellent. Run samples and the limited profile samples obtainable indicated consistency with the batch tests. The indicated efficiency of the extraction mixer-settlers was close to 50%, in agreement with experience in other extraction systems. Flowsheet conditions (Table 4.2) were varied within the ranges checked in the batch tests, with feed point varied to divide the 16-stage A-bank into either 5 extraction and 11 scrub or 9 extraction and 7 scrub stages.

Gamma decontamination factors were only 100–500 (Table 4.3), much lower than expected and than needed for plutonium purification. The number of scrub stages was the only variable of those tested that had an unquestionable affect on decontamination from zirconium-niobium. Decontamination was not improved by decreasing the amine concentration, which suggests that a small fraction, perhaps 0.5%, of the zirconium-niobium was in a form that was completely extracted by the 0.16 *M* amine (and might have been completely extracted at a still lower concentration). This fraction of amine-extractable species might have been present in the dissolver solution in small but persistent (metastable) amounts and concentrated into the 1BP, or it may have been formed either during Purex processing by complexing with organic degradation products of the TBP or diluent or slowly during the time (6 and 11 weeks) between withdrawal and use of the samples.

Decontamination from ruthenium was higher from feed TLA-3 than from feed TLA-2, presumably due to a difference in the ruthenium species or complexing agents present. This effect was larger than any that may have resulted from changing the extractant concentration or scrub acidity.

Cold Engineering Tests

In cold engineering tests in both pulsed columns and mixer-settlers, flooding was measured with feed containing 1.5 *M* nitric acid, scrub 0.5 *M* HNO_3, solvent 0.3 *M* Alamine 304, strip 2 *M* acetic acid, and solvent regeneration 1 *M* sodium carbonate at flow ratios of 100/10/25/5/7.5. Efficiency was measured with uranium as a stand-in

[3] Plant solution obtained through the cooperation of H. C. Rathvon, HAPO, and E. M. Shank, ORNL.

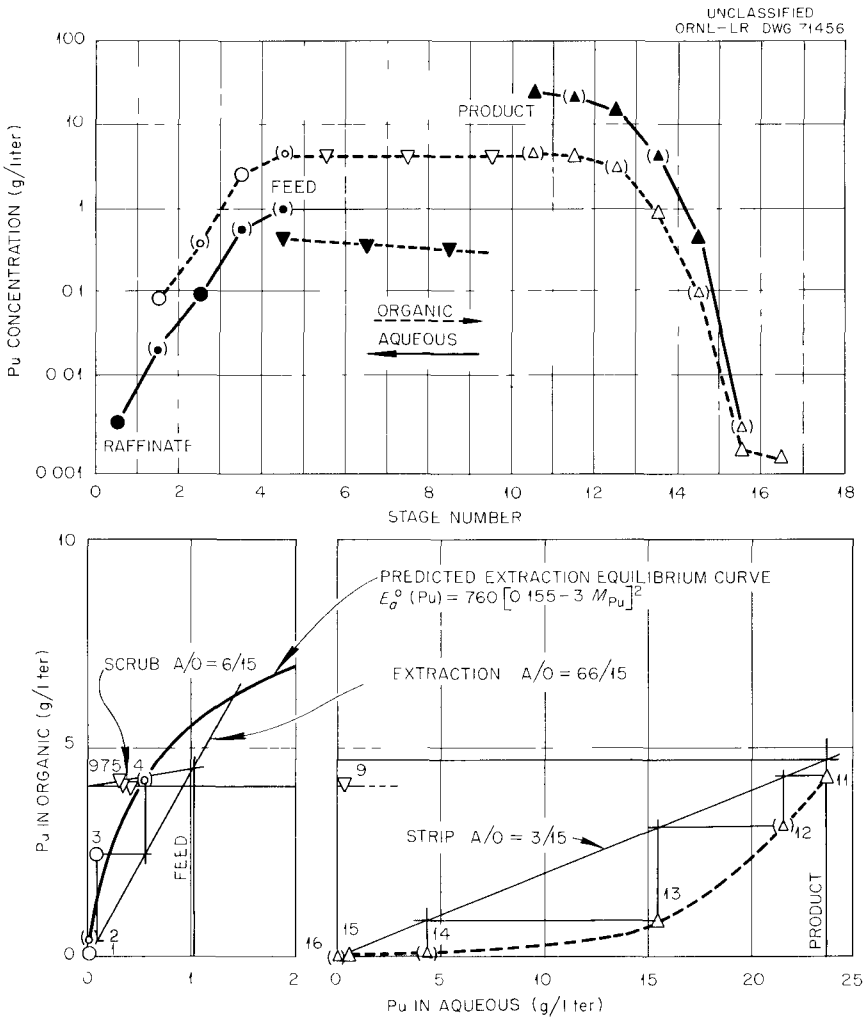

Fig. 4.1. Profile and McCabe-Thiele Diagram for Plutonium Purification Cycle. Batch countercurrent run 2C with simulated 1BP feed; 0.155 *M* TLA in diethylbenzene, 0.5 *M* HNO_3 scrub, and 3 *M* CH_3COOH strip; volume ratios, 60/15/6/3. Points in parentheses from material balance.

for plutonium, and the salting and stripping agents were adjusted to maintain the same flow ratio as the plutonium flowsheet. The solvent was treated for recycle by contacting with 1 *M* sodium carbonate.

The flow capacity of a 2-in.-diam-glass pulsed extraction-scrub column, containing sieve plates (0.125-in.-diam holes, 23% free area, 2-in. spacing) with the interface at the top of the column, ranged from 1200 to >2400 gal ft^{-2} hr^{-1} as the pulse frequency was decreased from 90 to 50 cpm at 1-in. amplitude (Fig. 4.2). A nozzle plate (0.125-in.-diam holes, 10% free area, 2-in. spacing) column, with the interface at the bottom, had flow capacities about half these values. The flow capacity for stripping and solvent treatment was nearly the same for each column and ranged from 130 to 560 gal ft^{-2} hr^{-1} as the pulse frequency was decreased from 70 to 25 cpm. Except for the sieve-plate extraction-scrub column, the flow capacity of equal-diameter columns at constant pulse frequency match the relative flow requirements for extraction, strip, and solvent treatment.

The stage efficiency of pulsed columns was measured with uranium as a stand-in for plutonium and the salting and stripping agents adjusted to maintain the same flow ratio as the plutonium flowsheet. The HETS for uranium extraction was

Table 4.2. Flowsheet Conditions in Continuous Countercurrent Tests of Plutonium Purification Cycle

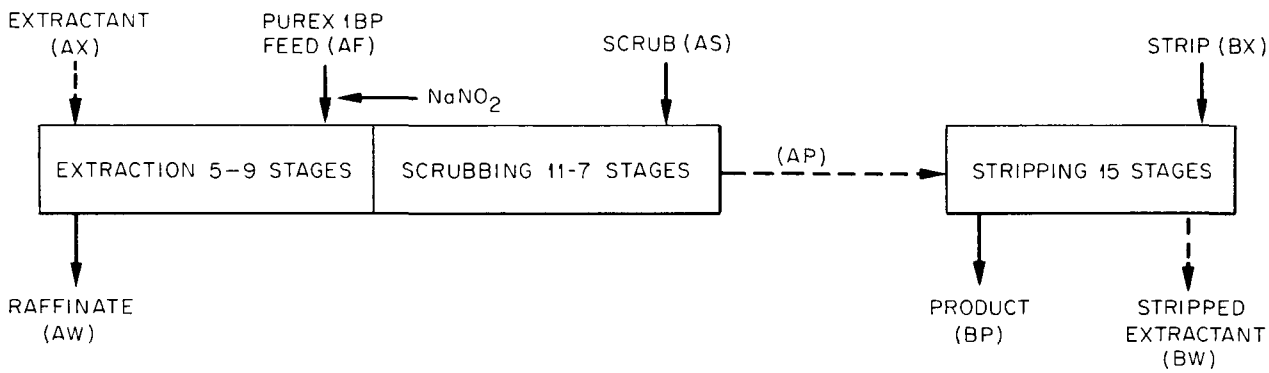

Stream	Nominal Flow (ml/min)	Composition
Extractant	0.74	0.16, 0.2 *M* TLA in diethylbenzene
Feed	2.96	Purex 1BP, ~3 *M* HNO_3, 0.1 *M* $NaNO_2$ (initial)
Scrub	0.29	0.5, 5 *M* HNO_3
Strip	0.29	3, 4 *M* CH_3COOH

Table 4.3. Decontamination Factors in Continuous Countercurrent Tests of Plutonium Purification Cycle

Run No.	Gross γ (counts min^{-1} ml^{-1})	TLA (*M*)	Scrub[a] HNO_3 (*M*)	Extraction Stages	Scrub Stages	Feed to Product D.F.		
						Gross γ	Zr-Nb γ	Ru γ
2a	1.91×10^7	0.198	0.5	5	11	500	500	160
2b		0.198	0.5	9	7	135	135	100
2c		0.16	0.5	9	7	135	135	135
3a	2.90×10^7	0.16	0.5	9	7	200	240	500
3b		0.16	5	5	11	470	440	750

[a]Plutonium stripped with 3 *M* CH_3COOH after 0.5 *M* HNO_3 scrub and with 4 *M* CH_3COOH after 5 *M* HNO_3 scrub.

4.2 ft at 70 cpm and 6.6 ft at 50 cpm in the sieve-plate column and 4.2 ft at 70 cpm in the nozzle-plate column. HETS values for uranium stripping decreased from 9.8 ft at 50 cpm to 3.2 ft at 90 cpm in the sieve-plate column and was 3.0 ft at 50 cpm in the nozzle-plate column.

The flow capacity of a pump-type mixer-settler for the amine-plutonium flowsheet was a function of mixer speed (Fig. 4.3). At low speeds flooding was caused by insufficient pumping of the aqueous interstage stream, and at high speeds the capacity was limited by flooding of the dispersion out of the settlers. The maximum flow capacity was 3.85 gal min^{-1} ft^{-2} at 1600 rpm for extraction, 1.71 gal min^{-1} ft^{-2} at 1200 rpm for stripping, and 1.85 gal min^{-1} ft^{-2} at 1400 rpm for solvent treatment. In

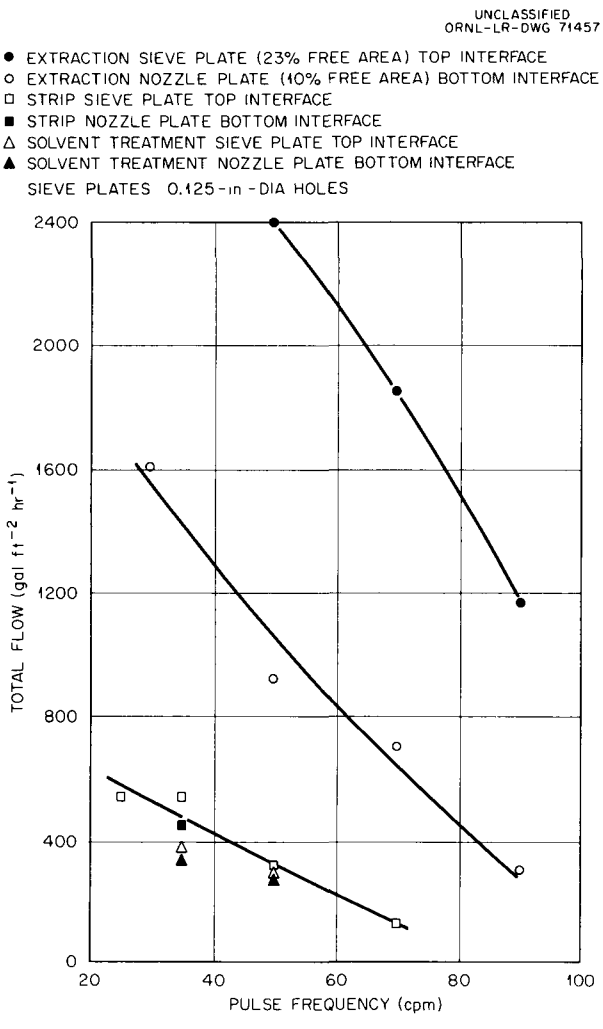

Fig. 4.2. Flow Capacity of 2-in.-diam Pulsed Columns with the Amine-Plutonium Flowsheet.

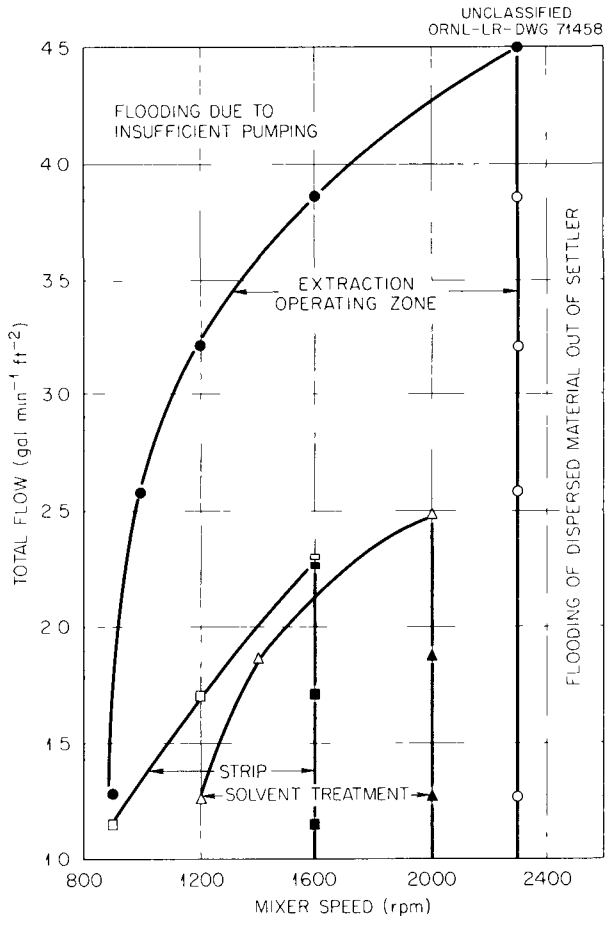

Fig. 4.3. Flow Capacity of Pump-type Mixer-Settler with Amine-Plutonium Flowsheet.

equal-size mixer-settler units the flow capacity of the extraction section limits the production capacity of the plant.

The stage efficiency of a pump-type mixer-settler for the amine plutonium flowsheet, using uranium as a stand-in for plutonium, was not very satisfactory. The overall efficiency for extraction was 50%, and for stripping, efficiency was only 30–40%. This difficulty was caused by not being able to balance the mixer speed required for adequate mixing and pumping. At the high speed required for good individual mixer efficiency, backmixing, due to either too much aqueous pumping or flooding of the settlers, lowered the overall efficiency. The low efficiency is not believed to be characteristic of the flowsheet, and other types of mixer-settlers would assuredly give better performance since satisfactory stage heights were obtained in pulsed columns and batch mixer-rate tests demonstrated rapid transfer.

Acetic Acid Stripping

The possibility of eliminating acetic acid from the plutonium product solution in the above flowsheet by distillation[2] is still being tested. Measurements of liquid-vapor equilibria in a modified Gilespie still confirmed the higher volatility of acetic acid than that of nitric over the range of aqueous solutions concerned, at least in the absence of metal ions. Figure 4.4 shows equilibrium acidities resulting from total initial

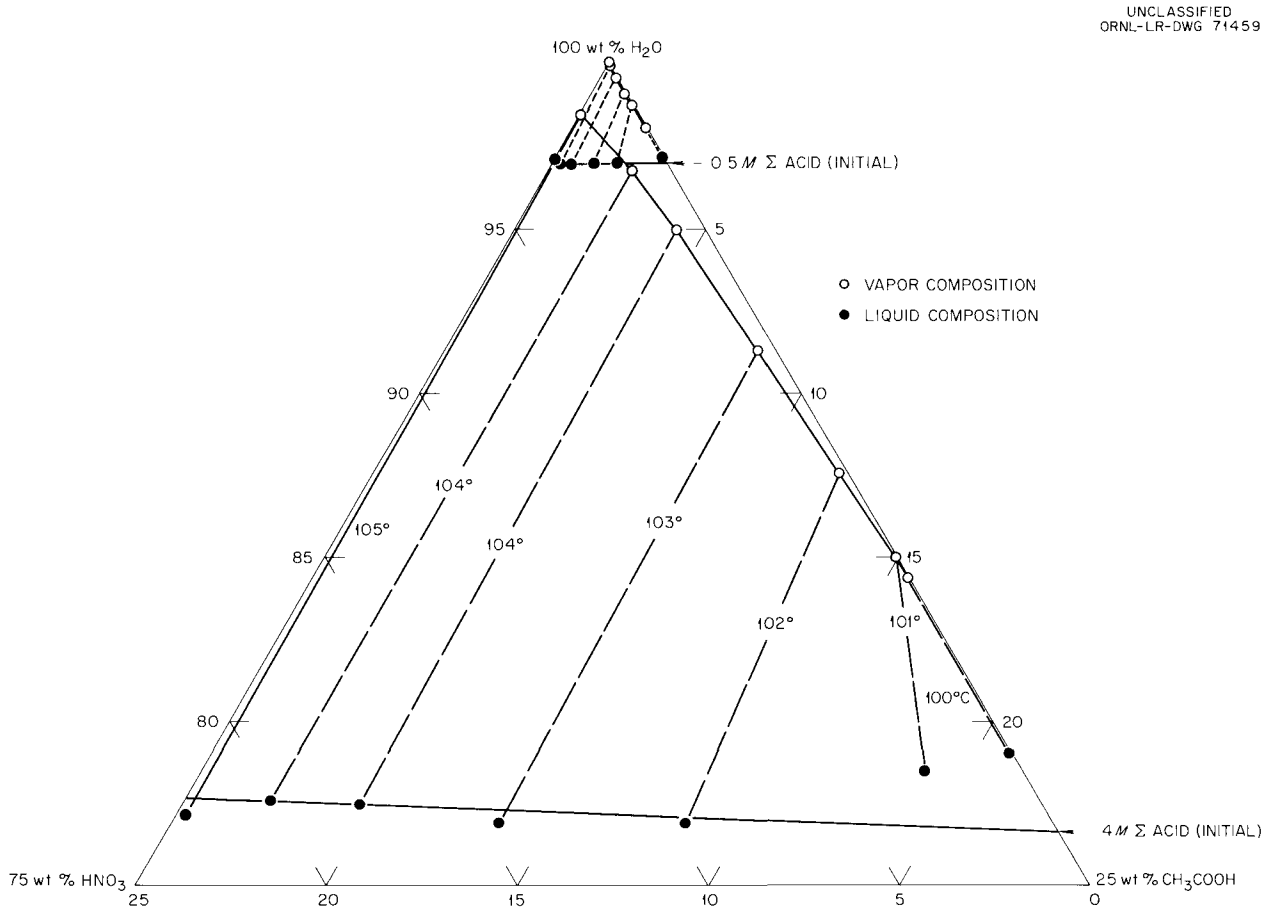

Fig. 4.4. Vapor-Liquid Phase Equilibria of Acetic Acid–Nitric Acid–Water Mixture.

acidities of 4 and 0.5 *M*; the curves at intermediate acidities are similar. Data from a modified Wiley-Harder still were in good agreement.

4.2 EXTRACTION OF RARE EARTHS BY TERTIARY AMINES FROM CHLORIDE SOLUTIONS

The proposed method for separating transplutoniums from lanthanides, by extraction with tertiary amines, from lithium chloride solutions[4] was studied with respect to separating lanthanides, yttrium, and scandium. Yttrium was less extractable than any of the lanthanides under all conditions tested, and separation of it from the lanthanides by a single-cycle multistage extraction process appears feasible. It is certain that yttrium will be separated even more completely than the lanthanides from the transplutonium elements.

The order of extractability of the lanthanides and their differences from yttrium varied with the composition of the amine, diluent, and aqueous solution (Fig. 4.5). In extractions from 11 *N* LiCl–0.01 *N* HCl, maximum extraction was near the middle of the lanthanide series. From 8 *N* LiCl–2 *N* $AlCl_3$, the heaviest elements were usually the most extractable. Extraction of yttrium and the lanthanides was proportional to approximately the square of the amine concentration in aromatic hydrocarbons, either pure or modified by tridecyl alcohol in constant ratio to the amine.

Extractions of americium had previously been found to be proportional to about the 18th power of

[4] R. D. Baybarz and B. Weaver, *Separation of Transplutoniums from Lanthanides by Tertiary Amine Extraction*, ORNL-3185 (Dec. 4, 1961).

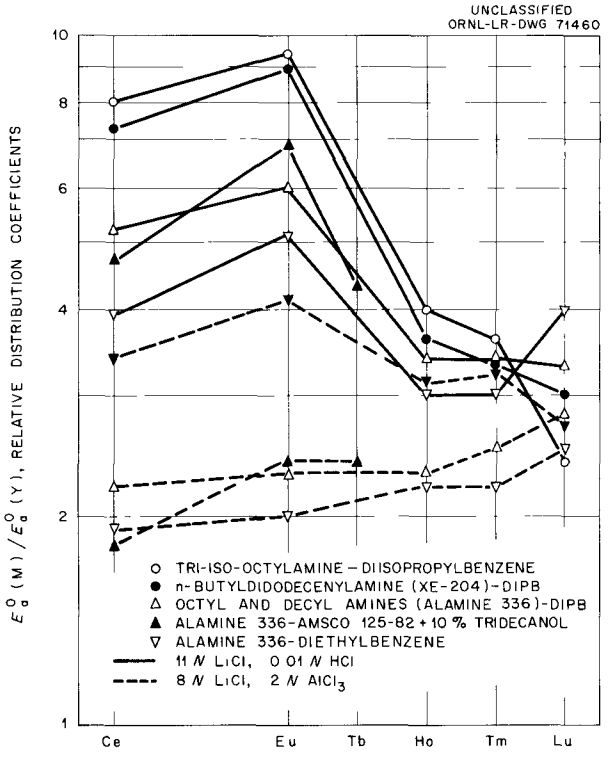

Fig. 4.5. Tertiary Amine Extraction of Lanthanides Compared with Yttrium.

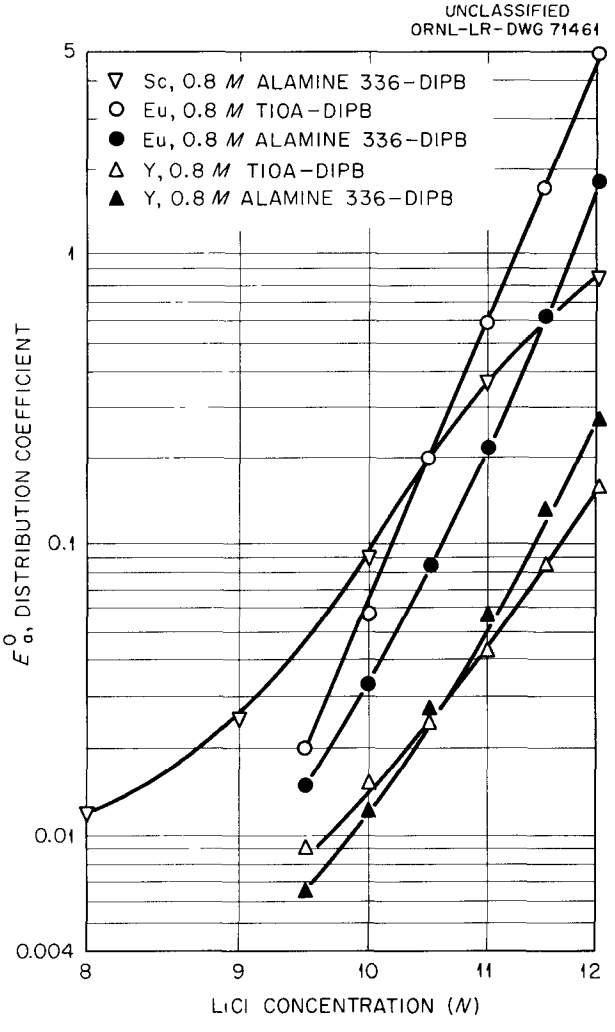

Fig. 4.6. Extraction Dependence on LiCl Concentration. Initial HCl, 0.01 *N*.

the chloride concentration under various conditions. In extractions by tri-iso-octylamine in diisopropylbenzene, extractability of europium was proportional to the 24th power of the lithium chloride concentration, compared with the 16th power for yttrium, thus permitting a higher separation between these elements at higher chloride concentrations (Fig. 4.6). Scandium was more extractable than europium at low chloride concentrations, but less extractable at high chloride concentrations. Scandium extraction varied greatly with amine composition and was higher from 8 *N* LiCl–2 *N* $AlCl_3$ than from LiCl–0.01 *N* HCl solutions, the reverse of the behavior of yttrium, the lanthanides, and the transplutoniums.

4.3 METAL NITRATE EXTRACTION BY AMINES[5]

The study of amine extraction characteristics of fission- and corrosion-product metals of interest in nitrate solutions was concentrated principally on extraction of the nitro and nitrato nitrosyl ruthenium complexes by trilaurylamine (TLA, Eastman No. 7727).[6] As anticipated from reported experience in other extraction systems, ruthenium extraction varied markedly both with the age of the aqueous solution, measured from time of dissolution of $RuNO(NO_3)_3 \cdot 2H_2O$ or $RuNO(NO_2)_2OH \cdot 2H_2O$, and with contact time in extraction (Figs. 4.7 and 4.8). Two-minute extractions of the nitrato complexes from < 1.5 *M* HNO_3 and of the nitro complexes at all acidities tested were lower from month-old

[5]Work done by the Department of Nuclear Engineering, MIT, under subcontract.

[6]E. A. Mason and R. E. Skavdahl, "Equilibrium Extraction Characteristics of Alkyl Amines and Nuclear Fuels Metals in Nitrate Systems," *Progr. Rept. X, July 1–Dec. 31, 1961*, Subcontract 1327, MITNE-14.

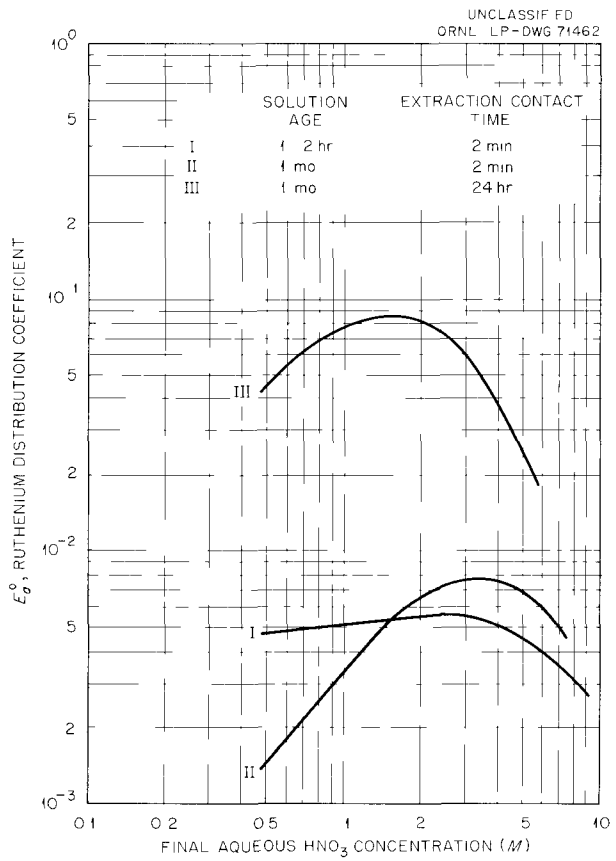

Fig. 4.7. Extraction of Nitrato Nitrosyl Ruthenium by 0.26 M TLA in Toluene. Initial aqueous ruthenium concentration ~6 g/liter.

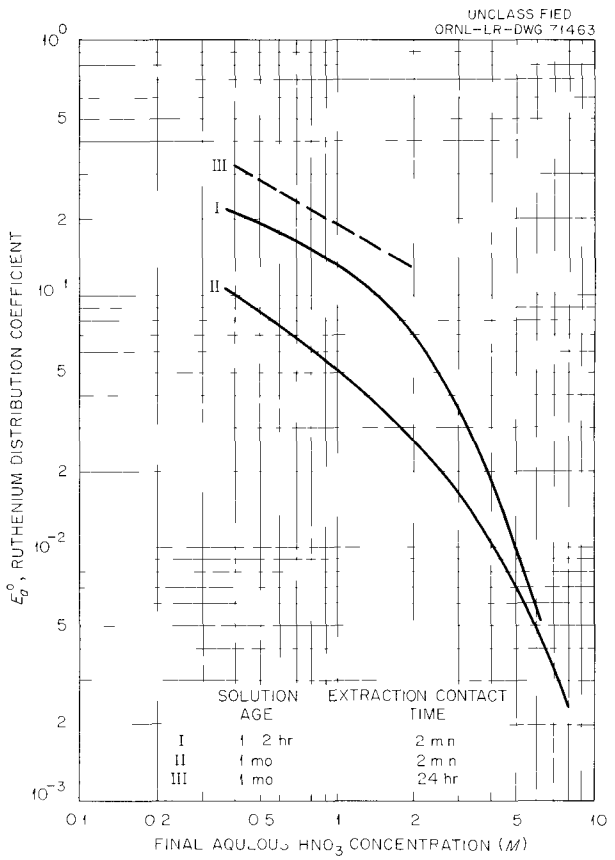

Fig. 4.8. Extraction of Nitro Nitrosyl Ruthenium by 0.26 M TLA in Toluene. Initial aqueous ruthenium concentration ~5 g/liter.

solutions than from fresh (1–2 hr) solutions, but 24-hr extractions from the month-old solutions were higher. Extraction coefficients varied with the 1 to 1.5 power of the amine concentration, and those of the nitro complexes with about the 1.2 power of the final aqueous ruthenium concentration.

In the presence of sodium nitrate, which was used to maintain the total aqueous nitrate concentration at ~6 M, extractions of the nitrato complexes were similar to those in Fig. 4.7 at high acidities but rose with decreasing acidity down to an acidity of <0.5 M HNO_3, instead of leveling off and dropping at <3 M HNO_3 as when no salt was present. The effect of sodium nitrate on extraction of the nitro complexes was less marked, giving curves approximately parallel to those without sodium nitrate (Fig. 4.8). With two-min extraction times, extractions were somewhat lower with than without sodium nitrate, but with 24-hr contact times, they were higher. Extractions with and without nitrate salt showed better correlation with excess nitric acid extracted by the amine nitrate solution (presumably a direct function of the aqueous nitric acid activity) than with the aqueous nitric acid concentration.

Work now reaching completion, with both spectrophotometric measurements and distribution measurements at various ruthenium loading levels, promises to give a complete differentiation of the nitrato complexes and evaluation of their separate extraction coefficients. The results indicate that the tetra- and penta-nitrato complexes are the most amine-extractable ones of this series, and suggest that they are extracted as un-ionized nitrato acids rather than as anions.

4.4 METAL CHLORIDE EXTRACTION BY AMINES

Extraction of iron(III) from hydrochloric acid and chloride salt solutions with typical primary, secondary, tertiary, and quaternary amines was studied preliminary to a larger program surveying extraction of many metals in these systems. In tests with a secondary amine, Amberlite LA-1, iron extraction coefficients were several times higher in diethylbenzene than in Amsco 125-82–alcohol diluent, and higher from LiCl solutions than from solutions of other chloride salts. With all amine types, extraction of iron increased with an increase in chloride concentration (Fig. 4.9).

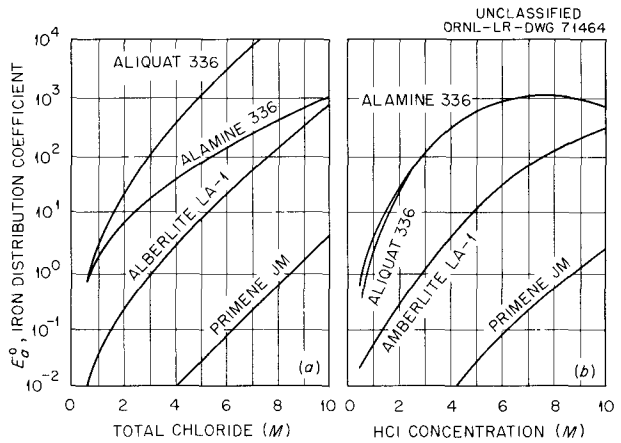

Fig. 4.9. Extraction of Fe(III) from Chloride Solutions. *Organic:* 0.1 *M amine chloride in diethylbenzene* (97% diethylbenzene–3% tridecanol diluent for Aliquat 336). Aqueous: 0.01 *M* Fe(III) in (*a*) LiCl–0.2 *M* HCl and (*b*) HCl. Contact: 10 min at 1/1 phase ratio.

The extraction power varied in the order Aliquat 336 (quaternary ammonium) > Alamine 336 (tertiary amine) > Amberlite LA-1 (secondary amine) >> Primene JM (primary amine).

4.5 ACID RECOVERY BY AMINE EXTRACTION

Preliminary tests indicate the applicability of sterically hindered tertiary amines for solvent extraction recovery of sulfuric acid from Sulfex process waste. Removal of the acid for recycle would significantly decrease the volume of waste from the Sulfex process.

The acid extraction ability of the long-chain alkyl amines has been known for many years, but their use as acid recovery agents has been discouraged by the difficulty of recovering the extracted acid from the solvent. It was found recently, however, that tertiary amines with alkyl branching close to the nitrogen are sufficiently weak bases that they can be stripped efficiently with water. Excessive branching cannot be tolerated since the amine is then too weak a base to give acceptable performance in the extraction cycle. Of the compounds tested, results were best with tri(2-ethylhexyl)amine, di(2-ethylhexyl)hexylamine, and N-benzyldi(2-ethylhexyl)amine, the last seeming to represent the best compromise between extraction ability and ease of stripping. Isotherms for extraction of acid from simulated Sulfex waste with the latter two compounds showed that >90% recovery of acid could be obtained in 3–4 ideal stages while loading the amine to ~1 mole H_2SO_4 per mole of amine (Fig. 4.10). Stripping isotherms indicated that ~1 *M* H_2SO_4 could be recovered from N-benzyldi(2-ethylhexyl)amine, but only ~0.5 *M* H_2SO_4 from di(2-ethylhexyl)hexylamine (Fig. 4.11).

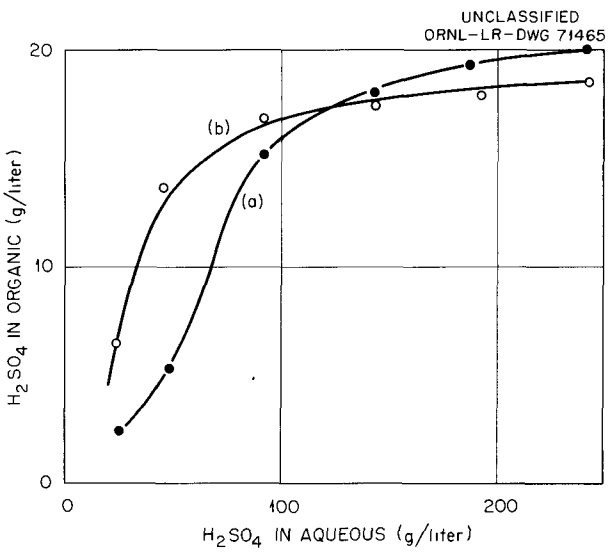

Fig. 4.10. Isotherms for Extraction of Sulfuric Acid from 1 *M* $FeSO_4$–2.5 *M* H_2SO_4 Solution with 0.2 *M* Amine in 16% Isodecanol–84% Amsco 125-82. (*a*) N-benzyldi(2-ethylhexyl)amine. (*b*) Di(2-ethylhexyl)hexylamine.

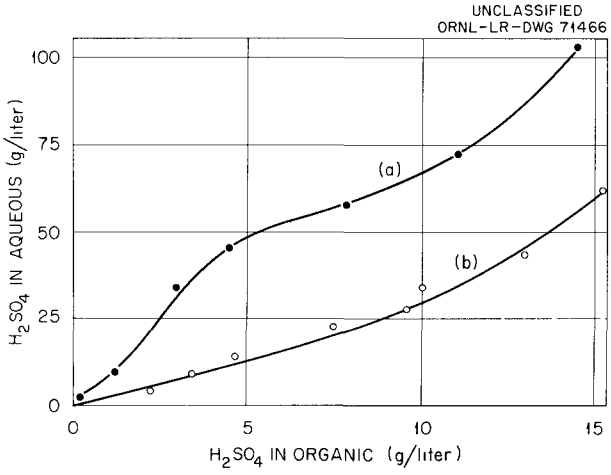

Fig. 4.11. Isotherms for Stripping Sulfuric Acid from Amines with Water. Organic: 0.2 *M* amine in 84% Amsco 125-82–16% isodecanol loaded to 18–19 g of H_2SO_4 per liter. (*a*) *N*-benzyldi(2-ethylhexyl)hexylamine. (*b*) Di(2-ethylhexyl)hexylamine.

4.6 EXTRACTION PERFORMANCE AND CLEANUP OF DEGRADED PROCESS EXTRACTANTS

Many of the difficulties encountered in the use of plant-degraded TBP–Amsco 125-82 solvent stem from degradation products of the Amsco 125-82 diluent. Nitroparaffins (RNO_2) give the same infrared spectrum as, and perform in, extraction tests similarly to a nitrogen-bearing component separated from nitric acid–degraded diluent.[7] Testing of solvent degradation (by both heating and irradiation), of solvent cleanup, and of new diluents was continued.

Solvent Degradation

Degradation of the Amsco 125-82 was shown[8] to be more severe when TBP was present than when it was not. Degradations by irradiation and by heating were essentially equivalent with respect to effects detected by Zr^{95}-Nb^{95} extraction, by total organic nitrogen determinations, and by spectrophotometric nitroparaffin determinations. The increased degradation is probably a consequence of nitrate and nitrite extraction by TBP, which increases the opportunity for nitration, and perhaps also of stabilization of the nitroparaffin compounds by complexing with TBP. The ultraviolet spectra of simple nitroparaffins give an intense band at around 200 mμ, as did a number of samples of Amsco or Amsco-TBP that had been exposed for various times to boiling nitric acid or to irradiation in the presence of nitric acid (Fig. 4.12). The absorbance, and therefore the concentration, of nitroparaffin increased linearly with exposure for both Amsco and TBP-Amsco. This was true whether the exposure was to irradiation or to boiling nitric acid. The irradiation dose scale at the top of Fig. 4.12*a* was arbitrarily adjusted to make the slope of the diluent radiation damage curve match that of the diluent chemical damage, and this resulted in good agreement of the single TBP-diluent chemical damage point with the TBP-diluent radiation damage. The slopes of the diluent and TBP-diluent damage curves indicate that nitration was at least twice as fast in the presence of TBP. Chemical analyses of the organic-phase nitrogen for a few of the degraded TBP-Amsco samples (Fig. 4.12*b*) indicated a fairly constant ratio of nitro groups (determined from ultraviolet measurements) to total nitrogen, regardless of the type of degradation. Not all nitrogen-containing degradation products are fission product extractants; e.g., nitro groups on tertiary carbon atoms or on aromatic rings cannot enolize to the extracting form.[9] Further, although the ultraviolet absorption data indicate that most of the nitrogen compounds are nitroparaffins and the chemical behavior of the solvent is consistent with nitroparaffin properties, other types of degradation products may have been formed.

Solvent Cleanup Tests

Efforts were continued to develop liquid-scrubbing methods for removing degradation products from used solvents, since these would be more convenient than the currently used solids-handling

[7] *Chem. Technol. Div. Ann. Progr. Rept. May 31, 1961*, ORNL-3153, p 109.

[8] *Chem. Technol. Div., Chem. Dev. Sec. C, Progr. Rept. Aug.–Sept. 1961*, ORNL TM-27, p 14.

[9] *Chem. Technol. Div. Ann. Progr. Rept. May 31, 1961*, ORNL-3153, p 111.

UNCLASSIFIED
ORNL-LR-DWG 71467

□, ■ EXPOSURE TO BOILING 2 *M* HNO_3 (EQUAL vol AQUEOUS AND ORGANIC PHASES UNDER TOTAL REFLUX)

○, ● EXPOSURE TO Co^{60} γ WHILE IN CONTACT WITH 2 *M* HNO_3 (EQUAL vol AQUEOUS AND ORGANIC PHASES MIXED DURING IRRADIATION)

□, ○ 1 *M* TBP AMSCO 125-82

■, ● AMSCO 125-82

SQUARES SHOW CHEMICAL TREATMENT AND CIRCLES RADIATION DOSAGE WITH CLOSED POINTS REPRESENTING TREATMENT OF DILUENT ABOVE AND OPEN POINTS TREATMENT IN THE PRESENCE OF TBP.

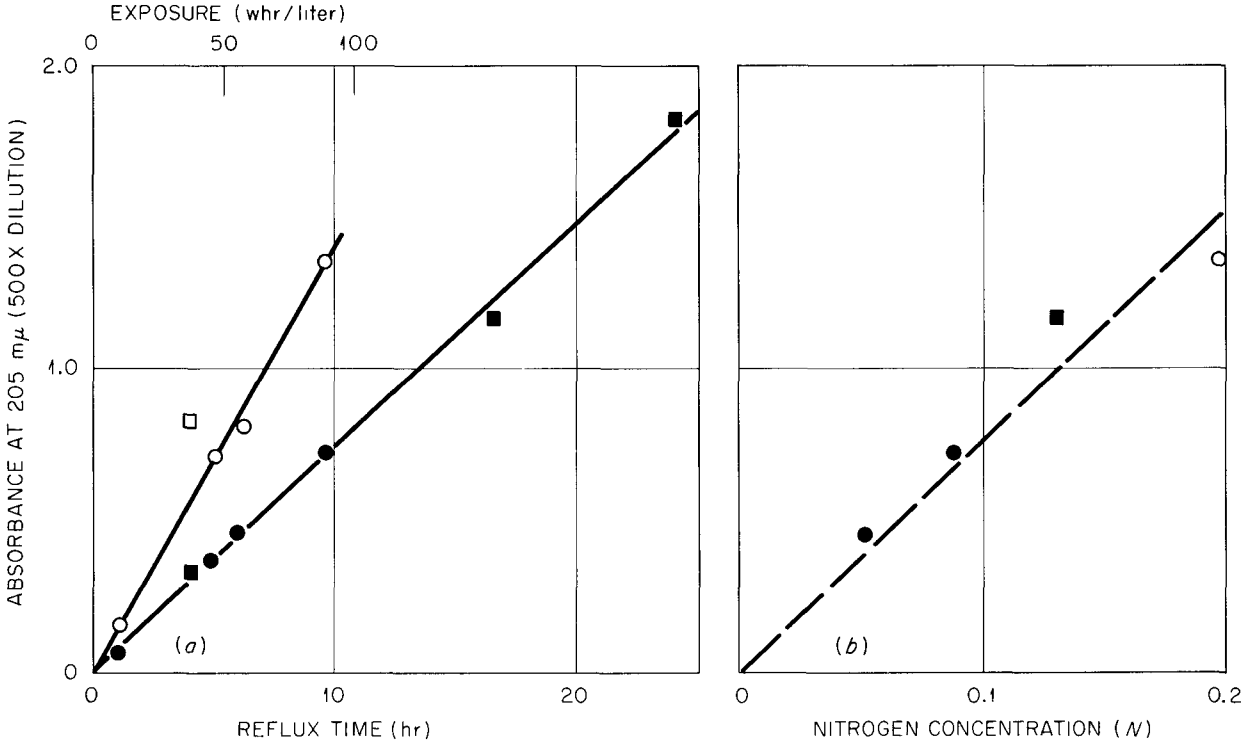

Fig. 4.12. Correlation with Absorbance of (*a*) Type of Degradation and (*b*) Organic Phase Nitrogen.

method.[10] Of nearly one hundred liquids or liquid-solid combinations tested, the most effective was ethanolamine (Table 4.4). After four stages of scrubbing with ethanolamine the extractant's zirconium-niobium extraction ability was indistinguishable from that of fresh TBP-Amsco, while after four caustic scrubbing stages the extraction was still several times that level. Apparently the amine salt of the nitroparaffin has appreciable solubility in the amine scrub solution. Unfortunately, there is a tendency for the TBP to distribute to the amine phase and the amine to the TBP phase. The amine, on a volume basis, costs slightly more than 1 *M* TBP, so that the economy of the process depends on the severity of reagent degradation and the phase ratios required for effective cleanup.

New Diluents

Aliphatic hydrocarbons with little or no chain branching have long been known to be relatively stable to attack by nitric acid and recently the

[10] G. L. Richardson, *Purex Solvent Washing with Basic Potassium Permanganate*, HW-50379 (May 29, 1957).

Table 4.4. Comparison of Sodium Hydroxide and Ethanolamine Cleanup of a Degraded Solvent[a]

In each test series a volume of the organic phase was scrubbed with successive equal-volume batches of fresh scrub solution; the organic phase thus treated was tested by extracting Zr^{95}-Nb^{95} from a 2 *M* tracer solution.

Scrub[b] Stage	Zr-Nb Extraction[c] by Organic Phase After Cleanup with	
	0.5 *N* Sodium Hydroxide	100% Ethanolamine
	As Scrubbed (counts sec^{-1} min^{-1})	As Scrubbed (counts sec^{-1} min^{-1})
1	800	400
2	325	200
3	300	150
4	300	70
Blank Extraction by Fresh 1 *M* TBP in Fresh Amsco 125-82		
	70	70

[a]Amsco 125-82 boiled 7 hr under total reflux with an equal volume of 8 *M* HNO_3. This was then diluted 10-fold with fresh Amsco and made to 1 *M* with fresh TBP. Nitrogen in final solvent $\approx$0.2 *M*.

[b]Equal volumes degraded solvent and scrub solution, 10 min, room temperature.

[c]Extraction from 2 *M* HNO_3, 10^4 counts sec^{-1} ml^{-1} Zr-Nb, equal phase ratio, 10 min contact, room temperature.

Savannah River Plant has been operating with *n*-dodecane. In laboratory degradation tests, all the simple aliphatic hydrocarbons tested were more stable than Amsco 125-82 (Table 4.5), which in turn is known to be more stable than diluents previously used in processing plants. Purification of such diluents by scrubbing with concentrated sulfuric acid has been common practice in the preparation of materials for physicochemical studies. This treatment of Amsco 125-82 improved its stability, in 1 *M* TBP solution, to degradation by boiling nitric acid.

The stability of the aromatic diluents tested varied widely with structure. Alkylbenzenes with two side chains were less stable than the corresponding monoalkylbenzene. Apparently one group directs and enhances the oxidation of the other. A similar effect was noted when a single side chain was cyclic (tetrahydronaphthalene and cyclohexylbenzene). There was indication in the monoalkylbenzenes that those with iso-branched side chains may be more stable than other corresponding isomers. *n*-Hexyl-, *n*-nonyl-, and dodecylbenzenes formed few zirconium-niobium-extracting species, and their flash points are acceptable for use in most plants. The good stability of the one test with triethylbenzene suggests that further testing of the polyalkylbenzenes is merited. Although nitration of the benzene ring does not form zirconium-niobium extractants, the factors influencing such nitration and the resulting effect on diluent properties, including safety, need further study.

4.7 SUPPRESSION OF ZIRCONIUM-NIOBIUM AND RUTHENIUM EXTRACTION BY TBP-AMSCO FROM AQUEOUS FEEDS PRETREATED WITH OXIMINOKETONES AND OXALIC ACID

Decontamination of uranium from zirconium-niobium and ruthenium was improved by treating the aqueous nitrate feeds with nitrous acid and acetone before solvent extraction with phosphates or phosphonates. A proposed[11] explanation for this is that the acetone reacts with nitrous acid to

[11]*Chem. Technol. Div. Ann. Progr. Rept. May 31, 1961*, ORNL-3153, p 112.

Table 4.5. Performance of Degraded Diluents

Extraction by 1 *M* TBP in diluent after chemical degradation with 2 *M* HNO_3 for 4 hr at ~100°C (total reflux) and removal of low-molecular-weight acids by carbonate scrubbing. Tracer solution initially 1×10^4 counts sec^{-1} ml^{-1} Zr^{95}-Nb^{95} γ, in 2 *M* HNO_3; extraction at equal phase ratios.

Diluent	Flash Point (°F)	Zr^{95}-Nb^{95} Extracted in Calcium Hydroxide Test[a] (counts sec^{-1} ml^{-1})
Amsco 125-82	128	4000
Amsco 125-82[b]	128	<100
n-Decane	115	1000
2,2,5-Trimethylhexane		80
n-Dodecane	165	125
n-Hexadecane		140
Solvesso-100	118	>6000
Solvesso-150	150	>6000
Benzene	12	160
Toluene	40	110
Xylene	63	100
Ethylbenzene	59	535
Diethylbenzene	138[c]	>6000
Triethylbenzene		140
Propylbenzene	86	80
Isopropylbenzene	102	30
Diisopropyl benzene	170[c]	>6000
n-Butylbenzene	160[c]	125
sec-Butylbenzene	126	130
tert-Butylbenzene	140[c]	120
Isobutylbenzene		45
Tetrahydronaphthalene		Decomposes
sec-Amylbenzene	~150[c]	1500
n-Hexylbenzene		120
Cyclohexylbenzene		>6000
n-Nonylbenzene		180
Dodecylbenzene (branched)		220
1,1-Diphenylethylene		Decomposes

[a]Modification of calcium hydroxide test described previously (*Chem. Technol. Div. Ann. Progr. Rept. May 31, 1961*, ORNL-3153, p 110). After carbonate scrubbing, organic phase was shaken for 1 hr with 50 g solid $Ca(OH)_2$ per liter of organic extract.

[b]Amsco 125-82 scrubbed with an equal volume of concentrated H_2SO_4 before making 1 *M* in fresh TBP and subjecting to HNO_3 degradation as above.

[c]Open cup, other entries closed cup.

form an oximinoketone, isonitrosoacetone, which is an aqueous complexing agent:

$$CH_3-\overset{\overset{O}{\|}}{C}-CH_3 + HONO \longrightarrow CH_3-\overset{\overset{O}{\|}}{C}-CH{=}NOH + H_2O.$$

Tests with the most readily available homolog, diacetylmonoxime, showed significant suppression of zirconium-niobium and ruthenium extraction from nitrate solutions by both fresh and degraded TBP–Amsco 125-82 solutions, with no depression of U(VI) and Pu(IV) extraction coefficients and slight depression of the thorium coefficient. However, further tests also established that oxalic acid, and, to a lesser extent, 2,3-butanedione, both formed during synthesis or decomposition of the diacetylmonoxime, accounted for a large part of the beneficial results. Other possible reaction products tested but found not to contribute significantly to suppression of zirconium-niobium and ruthenium extraction included simple ketones, simple oximes, and pyruvic, glycolic, and α-hydroxyisobutyric acids.

Oxalic acid was more effective than diacetylmonoxime or 3-oximino-2,4-pentanedione in suppressing zirconium-niobium and ruthenium extraction (Fig. 4.13). The difference is even greater than indicated by these overall curves, since a part of the apparent effect of the oximinoketones is presumably due to oxalic acid formed from them. In separate tests, 0.003 *M* oxalic acid was formed in 0.1 *M* diacetylmonoxime, and 0.007 *M* oxalic acid was formed in 0.1 *M* 3-oximino-2,4-pentanedione. These concentrations of oxalic acid

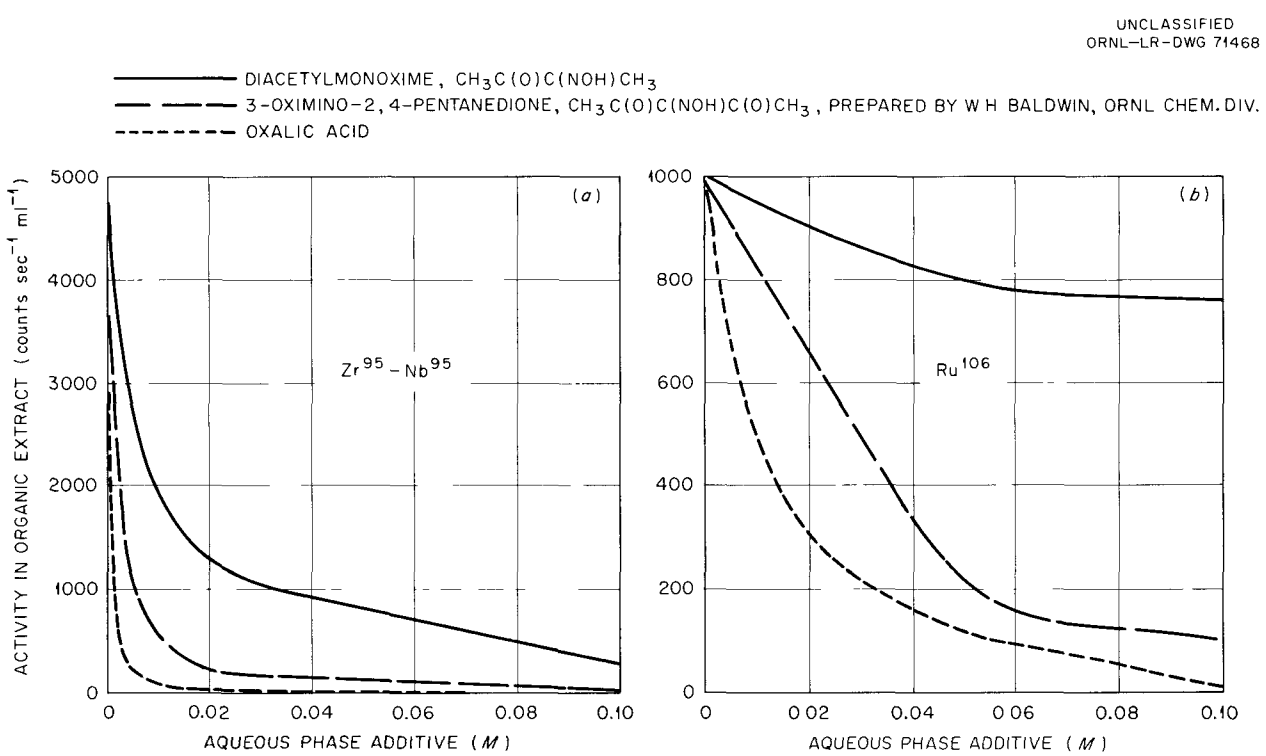

Fig. 4.13. Effect of Oximinoketone or Oxalic Acid Concentration in Aqueous Phase on Zr^{95}-Nb^{95} and Ru^{106} Extraction with 1 *M* TBP–Amsco. (*a*) Extraction by 1 *M* TBP in nitric acid–degraded Amsco 125-82 scrubbed with 0.2 *M* Na_2CO_3 and 50 g solid $Ca(OH)_2$ per liter of organic phase (Amsco was degraded by boiling under reflux with 8 *M* HNO_3 for 7 hr and then diluting 10X with fresh Amsco). (*b*) Extraction by fresh 1 *M* TBP in fresh Amsco 125-82 scrubbed with 0.2 *M* Na_2CO_3 and 2 *M* HNO_3. All extractions were made for 10 min at room temperature with equal volumes of aqueous and organic phases. Aqueous phase was initially 2 *M* HNO_3 with 10^4 *y* counts sec^{-1} ml^{-1} tracer ion. Treated ruthenium solution warmed at 80°C for 2 hr before extraction.

are sufficient to affect extraction significantly in the presence of the oximinoketones.

Oxalic acid itself is probably a feasible additive to improve decontamination under some conditions not yet specifiable. In preliminary batch extractions with 30% TBP–Amsco the U(VI) extraction coefficient was depressed 20%, thorium was completely precipitated, and the Pu(IV) coefficient was depressed by 65% with probably some precipitation when 0.02 *M* oxalic acid was added to 2 *M* HNO_3 containing the metal ions at 0.5–1 g/liter. In contrast, 0.05 *M* oxalic acid in a 2 *M* HNO_3 dissolver solution of irradiated fuel did not impair uranium and plutonium recovery by continuous countercurrent extraction with 30% TBP–Amsco. In this test, decontamination of uranium from gross β and γ fission product activity was improved 20–30 fold over corresponding runs without the oxalic acid. With 0.1 *M* diacetylmonoxime in a similar countercurrent test, uranium decontamination was improved 3–4 fold and, again, there was no adverse affect on uranium or plutonium recovery.

4.8 NEW EXTRACTANTS

The continuing examination of potential extractants supplied by reagent manufacturers includes consideration of new types of extractants, new structures of established types, improved quality of specific compounds, and new sources, especially for commercial quantities of reagents previously available only as specialties.

Commercial Supply of DSBPP

As a result of the demonstrated superiority of specially synthesized di-*sec*-butyl phenylphosphonate (DSBPP) in uranium-thorium separation,[12] a manufacturer[13] has prepared this reagent in commercial supply. The commercial reagent performed equally as well as the research batches and will be used at ORNL in a pilot demonstration of U^{233} purification. The experiments were made with 1 *M* DSBPP in xylene, U or Th at 1 g/liter in 2 *M* HNO_3, and A/O = 1/1 with 10 min contact at room temperature.

Batch	E_a^o(U)	E_a^o(Th)	SF_{Th}^{U}(calc)
OP 524, commercial	38	0.09	420
OP 521, research	42	0.12	350

New Amines and Acids

Some 30 new or modified amines, diamines, and quaternary ammoniums and four carboxylic acids, submitted by nine different manufacturers, were assayed and tested for performance in one or more standardized extraction tests. While none was outstandingly better than previously known compounds in the extractions tested, several (including some now commercially available) were commensurate in performance.

Amine Purification

An analytical procedure for separating amines from neutral impurities by column cation exchange in isopropanol medium[14] was adapted to separating tertiary amines from primary and secondary amines, utilizing their appreciable differences in base strength. Provisional procedures with either free-base amine or free base mixed with sulfate salt improved two trilaurylamine samples from 93 and 91 mole % to >98 mole % tertiary, principally by decreasing the secondary amine contents from ~6 and ~8 mole % to <1 mole %.

4.9 GEL-LIQUID EXTRACTION

Evaluations are being made of a newly proposed separations technique[15] in which organic extractants are absorbed in microporous plastic beads. The product has physical characteristics similar to those of ion exchange resins, but, since extraction of ions is due entirely to the organic liquid

---

[12] A. T. Gresky and R. G. Mansfield, *Uranium-Thorium Separation by Di-sec-butyl Phenylphosphonate Extraction*, ORNL CF-59-11-25 (Nov. 10, 1959).

[13] Victor Chemical Works, Div. of Stauffer Chemical Co., Chicago, Ill.

[14] J. P. Nelson, L. E. Peterson, and A. J. Milun, "Determination of Nonamines in High Molecular Weight Fatty Amines," *Anal. Chem.* 33, 1882–84 (1961).

[15] H. Small, "Gel-Liquid Extraction. The Extraction and Separation of Some Metal Salts Using Tri-*n*-butyl Phosphate Gels," *J. Inorg. Nucl. Chem.* 18, 232–44 (1961).

in the gel, properties such as separation factors are similar to those of the liquid extractant. In principle, it should be possible to use any solvent extraction reagent in a packed column.

In initial tests, gel columns were tested for application to the tertiary amine–lithium chloride extraction system in which transplutonium elements are separated from the lanthanides and other impurities.[16] In a typical test, about 7 wt % Alamine 336 was absorbed in polystyrene-divinylbenzene beads, provided by H. Small of Dow Chemical Co., the amine was converted to the chloride form with 2 *N* HCl, and a mixture of Am^{241} and Eu^{152} tracers was charged to the top of a 43-cm-high column. Slow elution by 13 *N* LiCl–0.005 *N* HCl gave complete separation of the mixture (Fig. 4.14). The Am^{241} was eluted more slowly than Eu^{152}.

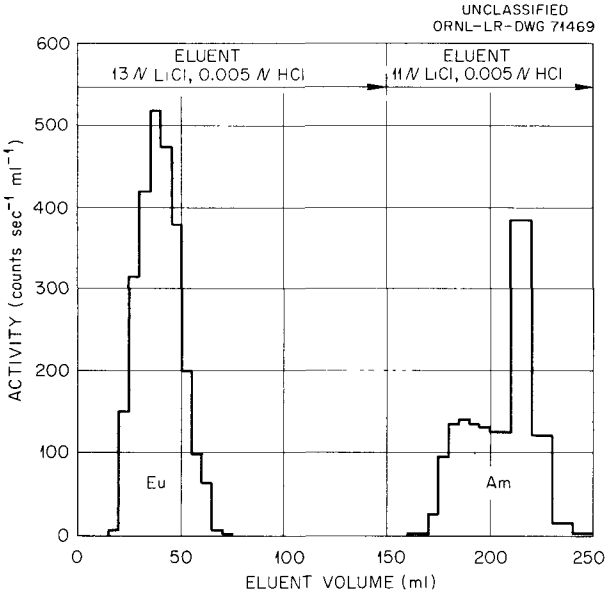

Fig. 4.14. Amine Gel Separation of Am^{241}-Eu^{152}.

In spite of the excellent separations, this technique was not a good choice for this particular application, since the polystyrene-divinylbenzene beads had a low capacity for the amine and throughput was limited by slow equilibration rates. Conventional liquid-liquid extraction, with its separation factor of 100, appears to be a better process.

There are other extraction systems, however, with low separation factors where the short column stage heights could be an advantage. Equally pertinent is that, in previous work, several potentially useful extractants have been prepared for which suitable liquid diluents have not been found. Also, other microporous plastics, of greater solvent capacity, are now being prepared by manufacturers. For example, Winsten Laboratories has produced microporous polyethylene granules which absorb extractants.

4.10 SOLVENT EXTRACTION EQUILIBRIA AND KINETICS

Alkaline Earth Extraction by Di(2-ethylhexyl)phosphate

Continued study of strontium extraction from 4 *M* sodium nitrate solutions by mixtures of sodium di(2-ethylhexyl)phosphate (NaD2EHP, NaX) plus di(2-ethylhexyl)phosphoric acid (D2EHPA, $[HX]_2$) in benzene was expedited by establishing that the measured glass-electrode pH is a linear function of log $[H^+]$ in those systems, within experimental error, for pH <4 and >7 (Fig. 4.15). The relation is pH + 0.6 = $-\log [H^+]$. Thus the slopes of E_a°(Sr) vs pH curves (Fig. 4.16) are meaningful in interpreting the hydrogen ion dependence of the strontium extraction. The slopes of the low-pH portions of the curves in Fig. 4.16 average ~ 1.7. These curves were obtained by pH titration of the two-phase system, with strontium distribution determined at each step by counting Sr^{85} in samples removed temporarily and returned without loss. In parallel tests with strontium nitrate replacing all sodium nitrate, the pH dependence was again close to two.

The maxima of the curves in Fig. 4.16 shift with pH in the same way that the NaX/ΣX mole ratio does, occurring in each curve near the point where the NaX/ΣX = 0.25. This is emphasized in a plot of E_a°(Sr) vs NaX/ΣX (Fig. 4.17). Extraction maxima were not found in strontium extractions from solutions in which strontium nitrate replaced all the sodium nitrate, or found in sodium extractions with or without strontium present. This indicates that the maxima in strontium extraction

[16] R. D. Baybarz and B. Weaver, *Separation of Transplutoniums from Lanthanides by Tertiary Amine Extraction*, ORNL-3185 (Dec. 4, 1961).

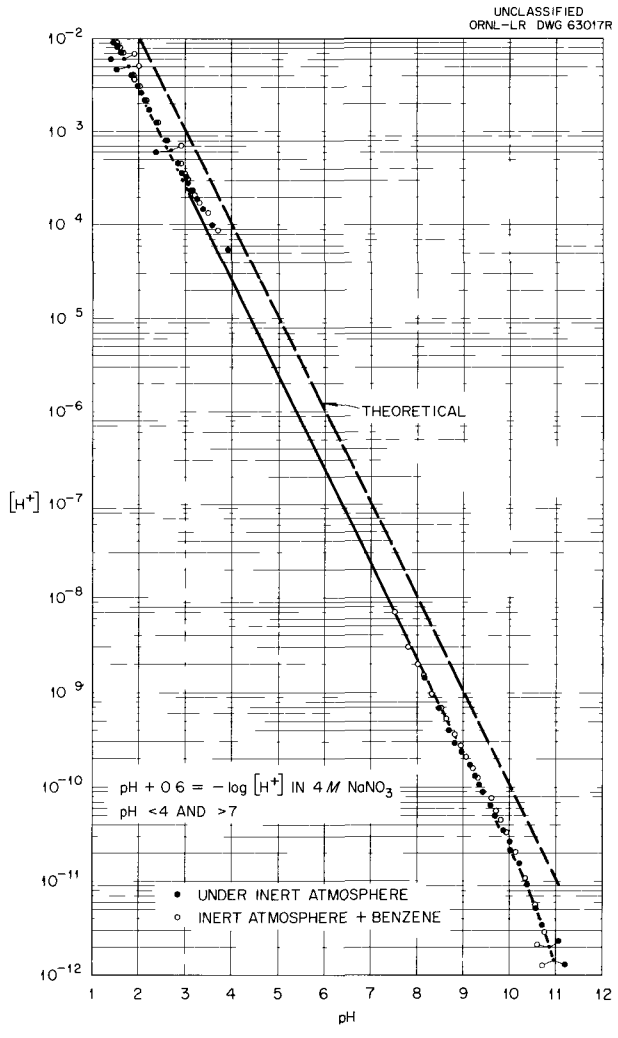

Fig. 4.15. $[H^+]$ vs Glass-Electrode pH for 4 M $NaNO_3$ Solutions.

from sodium nitrate solutions are associated with a particular organic phase composition containing gross sodium, perhaps a specific adduct of mole ratio $NaX/\Sigma X = 1/4$.

The dependence of strontium extraction on aqueous sodium nitrate activity, $a^{\pm}_{NaNO_3}$, has been established (under conditions where >10% of the organic reagent is in the sodium form) as $E_{Sr} \propto a^{\pm -2}_{NaNO_3}$ up to $a^{\pm}_{NaNO_3} = 1.5$ (~3.5 M $NaNO_3$). This dependence changes gradually to inverse first power at higher $[NaNO_3]$ (Fig. 4.18). These results taken with the hydrogen ion dependence mentioned above suggest the general equation, $Sr^{2+} + (n/y)(ZX)_y \rightarrow SrX_2 \cdot (ZX)_{n-2} + 2Z^+$ (where Z = H or Na). On the basis of this equation, reagent dependence for this system has been examined at several constant percent NaD2EHP values by plotting the log of $[H^+]^2_{aq} E_{Sr}$ vs the log of Σ[D2EHPA]. The slopes of the lines obtained (n/y in the above equation) varied from ~3 at 100% acid form to 0.95 at 100% NaD2EHP. This suggests an initial reaction

$$Sr^{2+} + 3(HR)_2 \rightarrow SrR_2 \cdot 4HR + 2H^+$$

since D2EHPA is a dimer. Diminishing values of n/y may reflect changes in n or y, or both, as more of the reagent is converted to the sodium salt.

Alkali Extraction by Di(2-ethylhexyl)phosphate

The relative affinities of the alkali metal ions for D2EHP in benzene were measured by equilibrating extractant solutions with aqueous solutions containing lithium, sodium, potassium, rubidium, and cesium simultaneously, each at 1 M, as mixtures of nitrate and hydroxide. The hydroxide contents were adjusted to give equilibrium organic phase mole ratios MX/ΣX of 0.1, 0.25, 0.5, 0.75, and 1. The extracts were stripped with hydrochloric acid for analysis by flame photometry.

With 0.5 M D2EHP the order of affinity, expressed as $M_{M,org}/M_{Cs,org} = E^{\circ}_a(M)/E^{\circ}_a(Cs)$ = separation factor, increased from cesium and rubidium (about the same within experimental scatter) through potassium and sodium to lithium (Fig. 4.19). Results with 0.1 and 0.05 M D2EHP were very similar. The separation factor for lithium over cesium increased considerably with the increase of hydrogen content in the extractant; for the other metals the spread was less and may have been within experimental scatter. Titration tests indicated that the affinity for hydrogen was greater than that for lithium by a factor of about 10^4.

While these results apply strictly only to the system measured, this same order of preference would be expected in D2EHPA extraction of the alkali ions from any system not shifted by specific aqueous phase complexing of the ions. Considering systems of reasonably similar aqueous ionic concentration and organic phase composition, the ratios shown in Fig. 4.17 can probably give a useful estimate of the exchange constant between pairs:

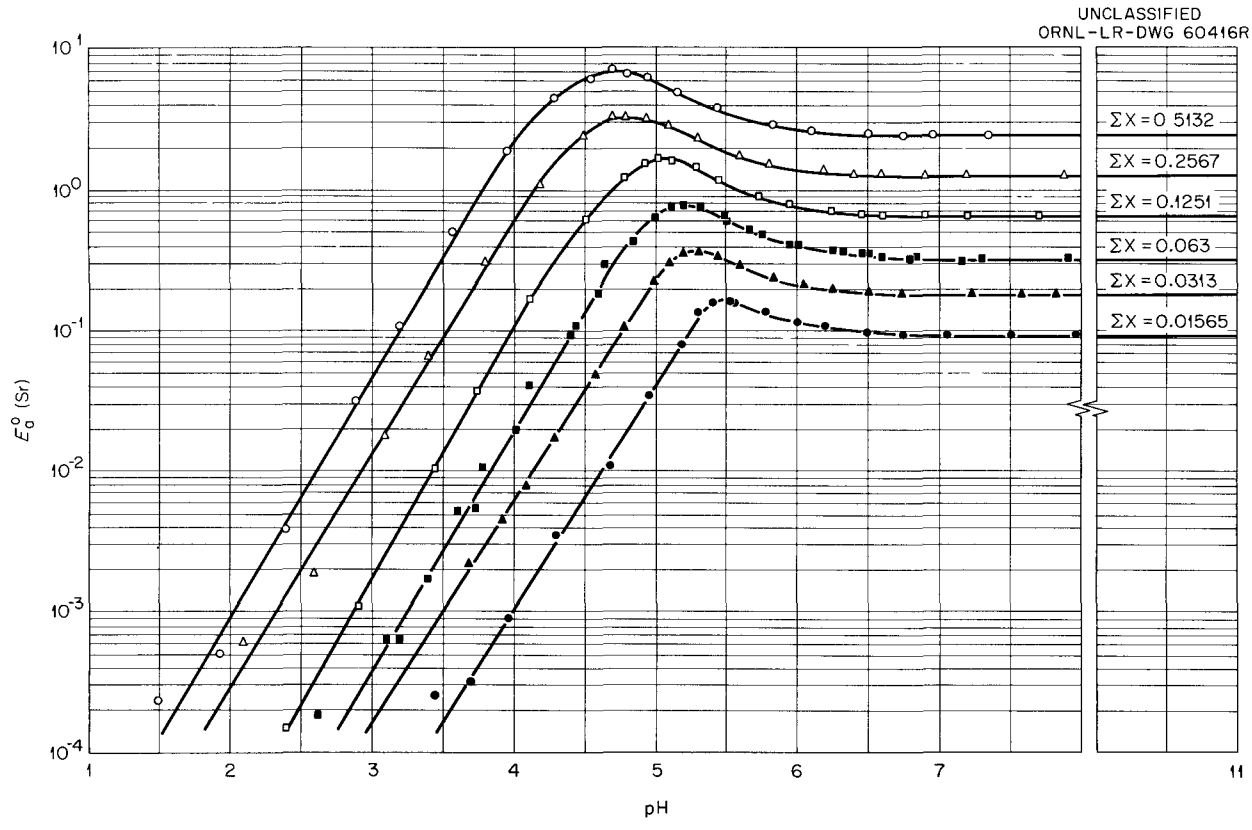

Fig. 4.16. Strontium Extraction by D2EHPA-NaD2EHP in Benzene as a Function of pH at Various Total Reagent Levels.

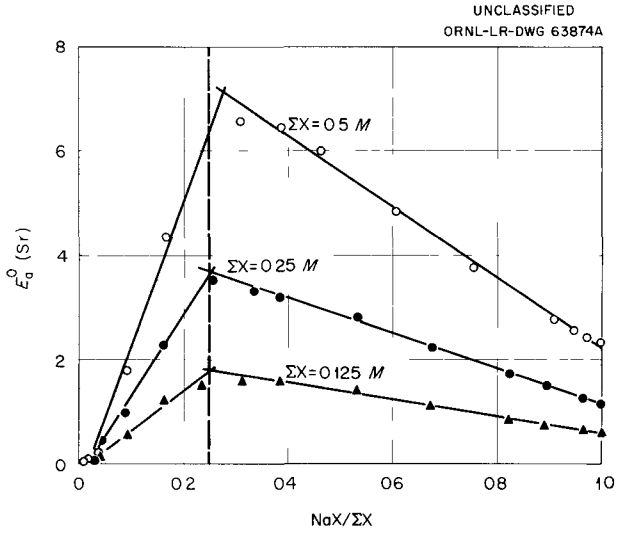

Fig. 4.17. E_a^o vs Fraction of D2EHPA in Sodium Form. Concentrations of 0.0625, 0.031, and 0.0156 M reagent gave the same result.

$$K = \frac{[M_1^+]_{aq}[M_2R]_{org}}{[M_2^+]_{aq}[M_1R]_{org}} = \frac{E_a^o(M_2)/E_a^o(Cs)}{E_a^o(M_1)/E_a^o(Cs)}.$$

The foregoing relations did not involve the spacing chosen for the ions along the abscissa of Fig. 4.19. The spacing used in this figure is according to the quotient (gaseous ionization potential)/(crystal radius)^3, plotted log-log for convenience. This parameter was tried, empirically, as reflecting some function of a charge density, and is of interest in that it shows far smoother correlation with the relative affinities (including hydrogen, Fig. 4.20) than do the parameters ordinarily used in ion exchange, such as hydrated ion radius or the Debye-Hückel $\mathring{a}$ term.

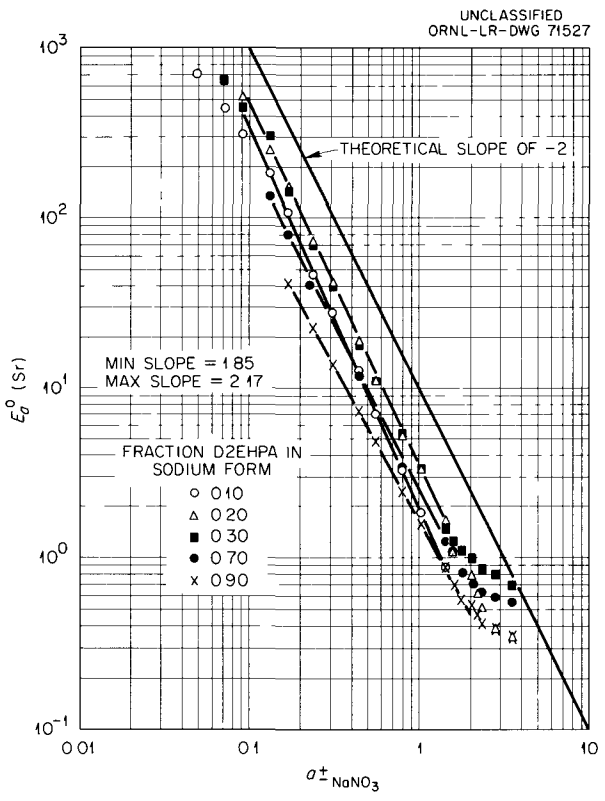

Fig. 4.18. Dependence of D2EHPA Strontium Extraction on Aqueous Sodium Nitrate Activity.

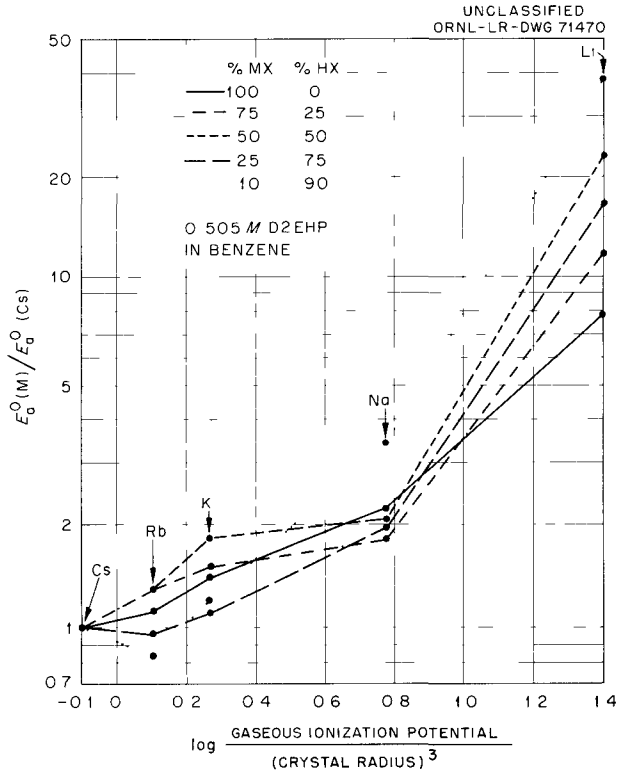

Fig. 4.19. Relative Extraction of Alkali Metal Ions by 0.505 *M* D2EHP in Benzene. Simultaneous extraction from nitrate hydroxide solutions containing each metal ion at 1 *M*.

Water Extraction by Sodium Di(2-ethylhexyl)phosphate

The previously reported[17] water extraction and volume increase on conversion of D2EHPA to its sodium salt was measured in more detail in the equilibration of D2EHPA in benzene with aqueous 4 *M* $NaNO_3$ plus NaOH.

Direct measurement of phase volume changes during incremental titrations showed that, at constant value of the mole ratio $NaX/\Sigma X$, the organic volume increase is a direct linear function of the NaX concentration reached (Fig. 4.21).

Direct determination of water in the equilibrium organic phases showed the mole ratio of water to sodium ions extracted to be independent of the total D2EHP concentration and to be a linear

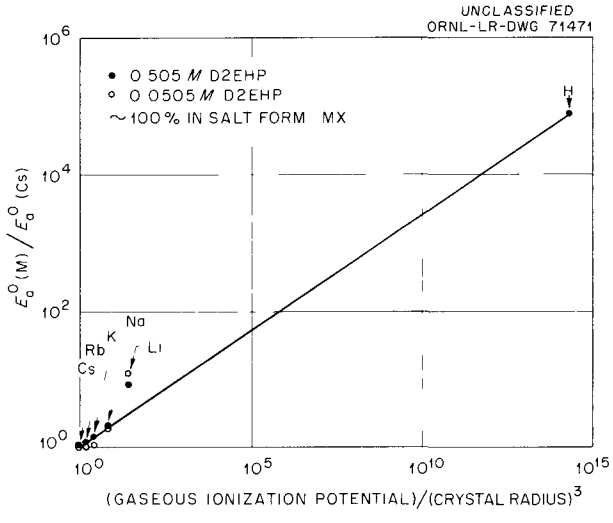

Fig. 4.20. Relative Extraction of Hydrogen and Alkali Metal Ions by D2EHP in Benzene. Simultaneous extraction from nitrate hydroxide solutions containing each metal ion at 1 *M*.

[17] C. A. Blake *et al.*, *Progress Report, Further Studies of the Dialkylphosphoric Acid Extraction (Dapex) Process for Uranium*, ORNL-2172, p 41 (Dec. 18, 1956).

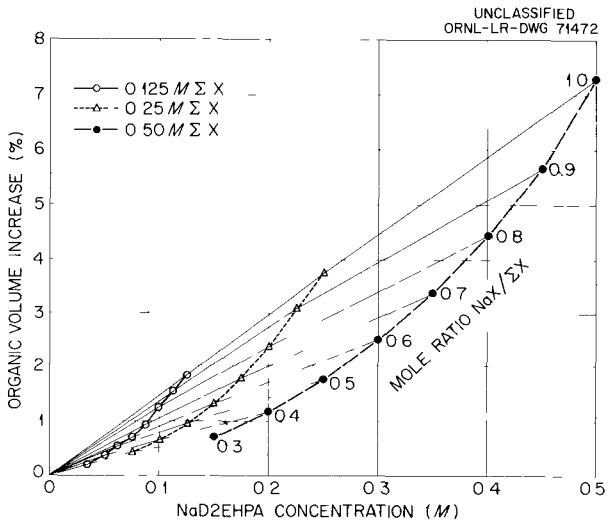

Fig. 4.21. Volume Increase on Extraction of Sodium Ion by D2EHPA in Benzene.

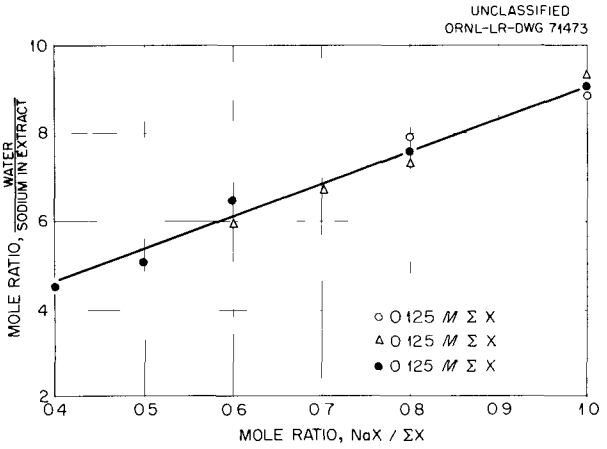

Fig. 4.22. Water Extraction Accompanying Sodium Extraction by D2EHPA in Benzene.

function of NaX/ΣX rather than of the NaX concentration (Fig. 4.22).

Kinetics of Sulfate Transfer During Amine Extraction of Uranium

The rate of tagged sulfate transfer from organic to aqueous solution during amine sulfate extraction of uranyl sulfate was measured to aid in distinguishing between two possible mechanisms of uranium transfer,

$$\underset{\cdots\cdots\cdots}{x(R_3NH)_2SO_4} + UO_2SO_4 \rightleftharpoons \underset{\cdots\cdots\cdots\cdots\cdots}{UO_2(R_3NH)_{2x}(SO_4)_{x+1}}, \quad (1)$$

$$\underset{\cdots\cdots\cdots}{x(R_3NH)_2SO_4} + UO_2(SO_4)_2^{2-} \rightleftharpoons \underset{\cdots\cdots\cdots\cdots\cdots}{UO_2(R_3NH)_{2x}(SO_4)_{x+1}} + SO_4^{2-}, \quad (2)$$

where the dots indicate the organic phase. The mechanisms cannot be distinguished by equilibrium measurements.

Di-*n*-decylamine sulfate (0.1 *N*) was used, with the total-system acidity adjusted to maintain the extractant essentially all in the normal sulfate form, thus avoiding any complication from displacement of bisulfate ion. Transfer of $S^{35}O_4^{2-}$ from organic to aqueous phase was measured during extraction of uranium from 0.0001 *M* H_2SO_4–0.012 *M* UO_2SO_4 and 0.5 *M* Na_2SO_4–0.0001 *M* H_2SO_4–0.012 *M* UO_2SO_4 solutions, and during equilibration with a series of *x M* Na_2SO_4–0.0001 *M* H_2SO_4 solutions matching the total sulfate in the solution at successive stages of the uranium extraction.

No increased S^{35} transfer from organic to aqueous phase during uranium extraction was observed. Such an increase would have been strong evidence for an important contribution by reaction (2). Its absence does not rule out this reaction but does support previous evidence[18] suggesting that the uranium is transferred as a neutral (or possibly cationic) rather than anionic species under the solution conditions examined.

Solvent Extraction System Activity Coefficients

In continued direct measurement of diluent vapor pressure differences, for use in determining organic-phase activity coefficients, the vapor pressure lowering of benzene was measured over wet solutions containing mixtures of di(2-ethylhexyl)phosphoric acid (HX) and its sodium salt (NaX). Results indicated considerable association at mole ratios NaX/ΣX = 0.25, 0.5, and 0.75 with ΣX = 0.4 *M*, corresponding to average aggregation numbers (calculated according to Raoult's law) of 3, 5, and 8, respectively.

[18] K. A. Allen, "The Relative Effects of the Uranyl Sulfate Complexes on the Rate of Extraction of Uranium from Acidic Aqueous Sulfate Solutions," *J. Phys. Chem.* 64, 667–70 (1960).

5. Fission Product Recovery

The objective of the fission product recovery program is the development of processes for recovering and purifying megacurie quantities of fission products from reactor-fuel processing wastes. Large quantities of certain of these elements are now being requested for industrial, space, and other applications, and there is evidence that the demand will increase. Since solvent extraction shows promise of great versatility, principle emphasis is being placed on this technique. Thus far, a solvent extraction process using di(2-ethylhexyl)phosphoric acid (D2EHPA) to recover strontium-90, for which there is a large demand, has been developed and further modified and operated successfully on a plant scale at Hanford. The same process can be used to recover rare earths, and the same solvent, under different conditions, can be used to recover zirconium-niobium. New solvents have been developed which are effective cesium extractants. In combination with the TBP process for promethium separation,[1] a versatile, integrated solvent extraction flowsheet can now be visualized for the recovery and purification of all fission products of principle importance from waste liquors.

5.1 SOLVENT EXTRACTION

Strontium and Rare Earths

The solvent extraction flowsheet[2] for recovering and separating strontium and mixed rare earths with D2EHPA was demonstrated successfully (Fig. 5.1) in continuous miniature mixer-settler equipment with Purex 1WW[3] waste solution from Hanford. Results, in general, confirmed the performance predicted on the basis of earlier batch and continuous tracer runs.

Iron and other cations were complexed with tartrate and the solution, after pH adjustment to 6, was fed to the first cycle, where strontium and rare earths were coextracted with 0.3 *M* D2EHPA (one-third in Na salt form)–0.15 *M* TBP–Amsco 125-82 and then costripped with 2 *M* HNO_3. Strontium recovery was 99.7% in extraction and >99.95% in stripping, for an overall first cycle recovery of 99.7%. Recovery of rare earths, based on total rare-earth activities, was less efficient. Approximately 94% of the total rare earths was extracted and ~86% of that extracted was stripped for an overall recovery of 80%. In subsequent batch extractions, rare-earth extraction from tartrate-complexed feed was slow (Fig. 5.2), and a longer mixer residence time might improve recoveries. In batch stripping tests, yttrium was stripped with more difficulty than the rare earths (Fig. 5.3), which may account for the apparent high rare-earth loss in the continuous run. The partial stripping might be an advantage, since it provides a means for separating yttrium from the rare earths of chief interest, Ce^{144} and Pm^{147}. Overall decontamination factors for strontium in the first cycle were 45 from Cs, 170 from Ru, 3000 from Zr-Nb, 2000 from Fe, 2000 from U, and 30 from Pu. Some emulsification occurred in the first extraction cycle owing to the formation of a small amount of solids in the feed but did not seriously interfere with extractor operation.

[1] B. Weaver and F. A. Kappelmann, *Purification of Promethium by Liquid-Liquid Extraction*, ORNL-2863 (Jan. 29, 1960).

[2] *Chem. Technol. Div. Ann. Progr. Rept. Aug. 31, 1960*, ORNL-2993, Fig. 14.1.

[3] Purex first-cycle extraction column raffinate, HAW, is evaporated 30-fold to give 1WW.

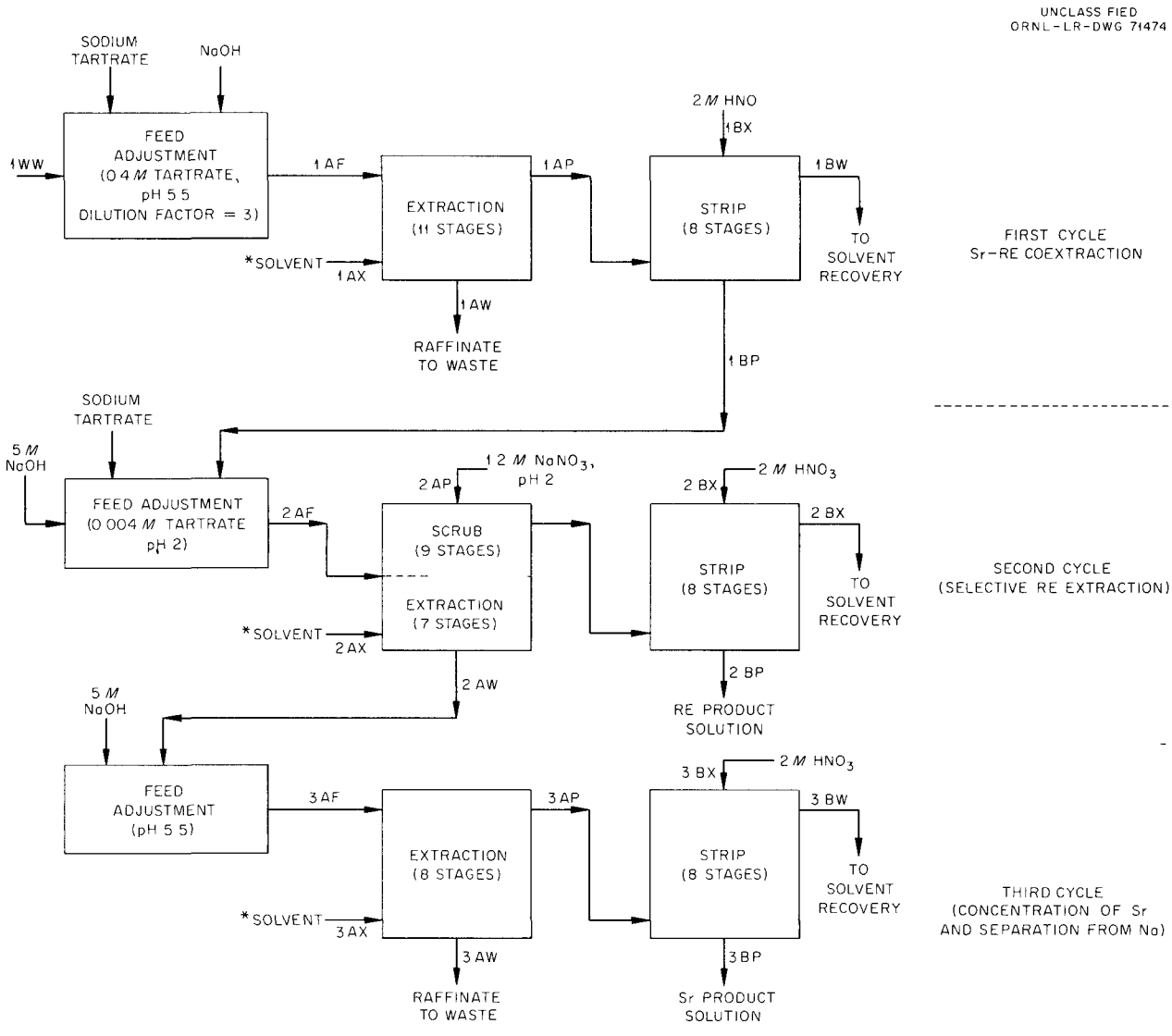

*SOLVENT 0.2 *M* D2EHPA–0.1 *M* D2EHP-Na SALT–0.15 *M* TBP IN AMSCO 125-82, SOLVENT USED ON A ONCE THROUGH BASIS IN THIS TEST

FLOW RATES, ml/min FIRST CYCLE 1AF 1, 1AX, 2 1BX, 0.4
SECOND CYCLE 2AF 3 2AX 0.5 2AS, 0.5, 2BX, 0.25
THIRD CYCLE 3AF, 3, 3AX, 0.5, 3BX, 0.25

Fig. 5.1. Flowsheet for Hot Cell Strontium–Rare Earth Recovery Run.

In the second cycle, rare earths were selectively extracted from the first-cycle strip product adjusted to pH 2. The extract was scrubbed with 1.2 *M* $NaNO_3$, to improve the separation from strontium, and stripped of its rare-earth content with 2 *M* HNO_3. Recovery of rare earths in the second cycle was >99%, with <1% of the strontium reporting to the rare-earth product solution. Decontamination factors were ~80 from Sr, 120 from Cs, 100 from Ru, 45 from Zr-Nb, and 170 from Na.

Third-cycle feed was prepared by adjusting the second-cycle raffinate to pH 6 with caustic. Strontium was 99% recovered in seven extraction and eight stripping stages with decontamination factors of 90 from Cs, 90 from Ru, and 170 from Zr-Nb. The product strip solution contained ~1.2 g of

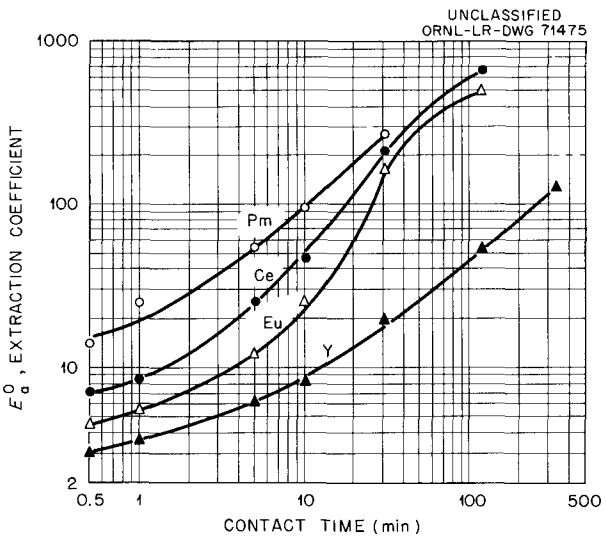

Fig. 5.2. Rate of Rare Earths and Yttrium Extraction from Tartrate Complexed Simulated Purex Waste Concentrate Solution at pH 6. Temperature, 23°C; organic, 0.3 *M* D2EHPA ($\frac{1}{3}$ sodium salt form)–0.15 *M* TBP–Amsco 125-82; organic/aqueous phase ratio, 2/1.

Sr, 1.4 g of Ni, and 20 g of Na per liter. Subsequent batch tests indicated that a nickel-free strontium product could be obtained by adding a small amount of ethylenediaminetetraacetic acid to the third-cycle feed to prevent extraction of nickel. Because of pump limitations, the organic/aqueous flow ratios used in the second- and third-cycle stripping were 2/1 rather than the 5/1 specified for the flowsheet and the rare-earth and strontium product solutions were correspondingly more dilute.

Further studies aimed at improving the efficiency of the strontium–rare-earth flowsheet included batch tests on acid scrubbing of the strontium extract, to improve separations from sodium, and a study of extraction and stripping of individual rare earths. These studies indicated that (1) a two-stage nitric acid scrub of the third-cycle extract would increase the Sr/Na separation factor for the third cycle by a factor of 10–100 over that obtained in the continuous demonstration run described above, and (2) the proposed organic to aqueous strip ratio for the third cycle can be increased by an order of magnitude to provide a much more concentrated strontium product solution. Strontium stripping was quantitative with 1.5 *M* HNO_3 in two stages at phase ratios as high as 75/1. Extraction of individual rare earths from tartrate-complexed simulated Purex waste concentrate at pH 6 was slow, with the extraction coefficients still increasing beyond 30 min contact time. However, in all cases the mass transfer in 1 min was 90–95% of that in 30 min. The order of extractability, at least up to 30 min contact

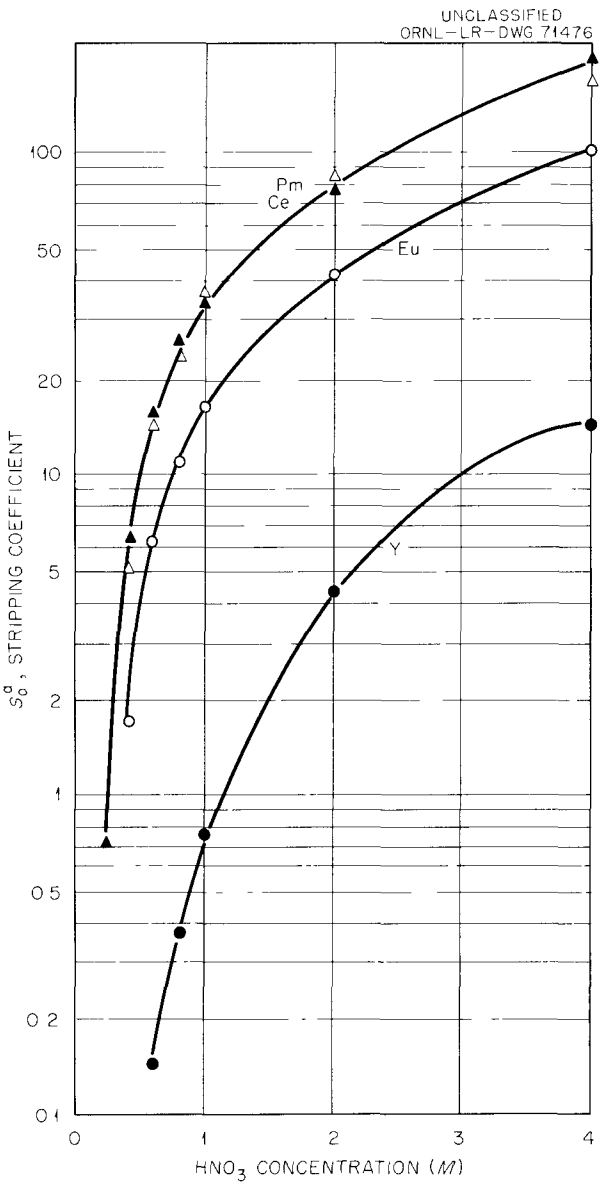

Fig. 5.3. Stripping of Rare Earths and Yttrium with HNO_3. Organic, 0.3 *M* D2EHPA ($\frac{1}{3}$ sodium salt form)–0.15 *M* TBP–Amsco 125-82 loaded from adjusted simulated Purex waste; phase ratio, 1/1; contact time, 5 min.

time, was Pm > Ce > Eu > Y. In contrast, equilibrium was reached in <5 min in extractions from sodium nitrate–nitric acid solution and the order of extractability over a wide pH range was Y > Eu > Ce, Pm (Fig. 5.4). In stripping rare earths from D2EHPA, with 0.2–4.0 *M* HNO_3, equilibrium was reached rapidly (<5 min) and the relative order of stripping was, as expected, inverse to that obtained in extractions from $NaNO_3$–HNO_3 solution, that is, stripping coefficients were Ce, Pm > Eu > Y.

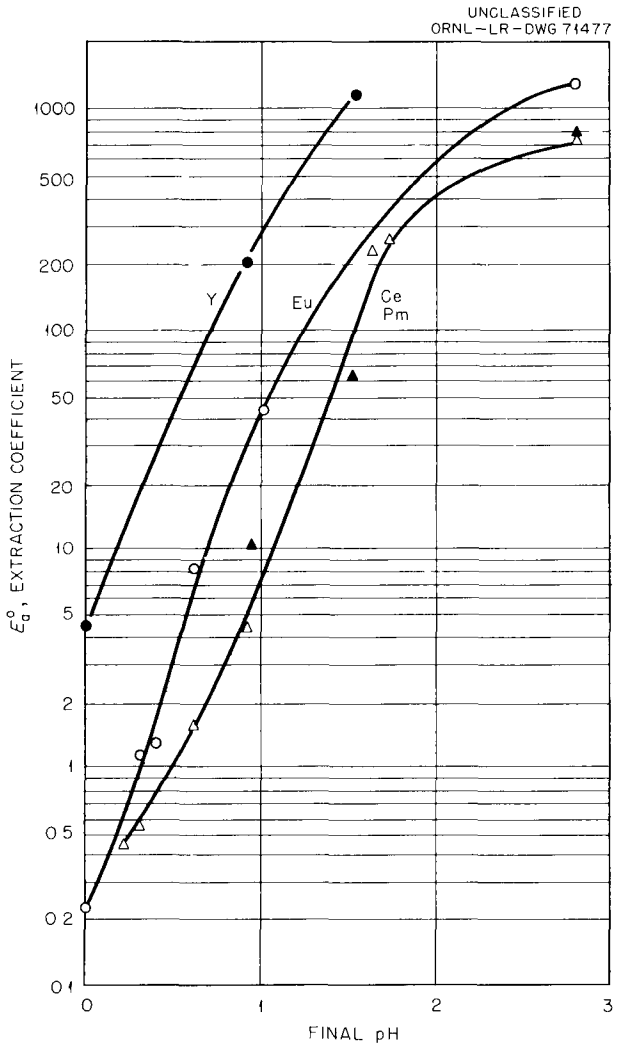

Fig. 5.4. Extraction of Rare Earths and Yttrium from $NaNO_3$-HNO_3 Solution (2 *M* Total Nitrate). Organic, 0.3 *M* D2EHPA ($\frac{1}{3}$ sodium salt form)–0.15 *M* TBP–Amsco 125-82; organic/aqueous phase ratio, 2/1; *contact time, 6 min.*

Strontium Extraction with Other Organophosphorus Acids

Comparison of strontium extractions from 0.5 *M* $NaNO_3$ solution with a number of organophosphorus acids (0.1 *M*), including mono- and dialkylphosphoric acids and phosphinic acids, showed large differences in extraction power (Fig. 5.5). Because of solubility limitations, different diluents were used for the various compounds, which may explain some of the performance variations noted. With the exception of dicyclohexylphosphinic acid, which gave strontium coefficients <0.1 over the pH range 3–11, all the compounds extracted strontium effectively, but only one, phenyl(1-hydroxy-2-ethylhexyl)phosphinic acid, showed extraction power greater than di(2-ethylhexyl)phosphoric acid (D2EHPA). The coefficient with phenyl(1-hydroxy-2-ethylhexyl)-phosphinic acid reached a maximum of 170 at pH

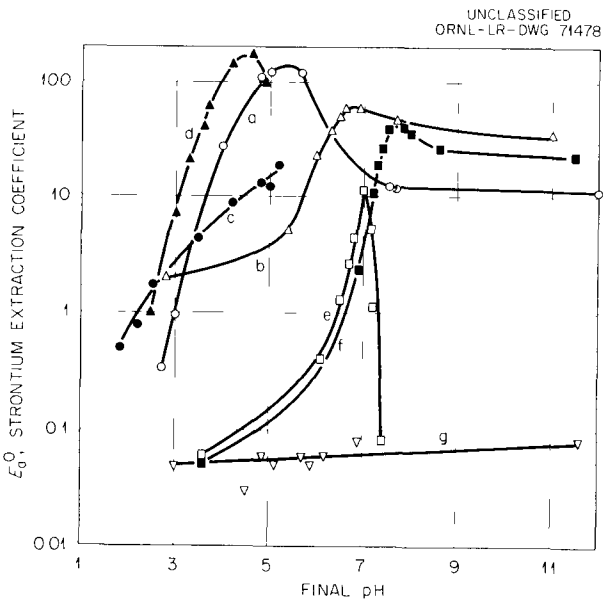

Fig. 5.5. Extraction of Strontium from 0.5 *M* $NaNO_3$ Solution with Various Organophosphorus Acids (0.1 *M*). (*a*) Di(2-ethylhexyl)phosphoric acid (D2EHPA) in Amsco 125-82 plus 3 vol % TBP, (*b*) bis(diisobutylmethyl)phosphoric acid in Amsco 125-82 plus 3 vol % TBP, (*c*) heptadecylphosphoric acid (HDPA) in kerosene, (*d*) phenyl(1-hydroxy-2-ethylhexyl)phosphinic acid in benzene, (*e*) di(*n*-hexyl)phosphinic acid in Amsco 125-82 plus 5 vol % TBP, (*f*) di(2-ethylhexyl)phosphinic acid in Amsco 125-82 plus 10 vol % TBP, (*g*) dicyclohexylphosphinic acid in benzene.

4.5 and then decreased to 95 at pH 4.9. In comparison, the coefficient with D2EHPA reached a maximum of ~130 at pH 5–6, whereas most of the other compounds reached maximum extraction in the pH range 6.5–7.5.

Cesium

A new process has been outlined for recovering cesium from Purex waste solutions at pH ~12 by extraction with substituted phenols (Fig. 5.6). Most of the studies on which this is based were made with tartrate-complexed simulated and tartrate-complexed formaldehyde-treated Purex waste concentrates, but the process is also applicable to treatment of Hanford tank farm supernatants. Of the compounds examined thus far, results were best with *p*-dodecylphenol (PDP) and especially *o*-phenylphenol (OPP) and 4-chloro-2-phenylphenol. These compounds have adequate extraction power for cesium recovery, give good decontamination from fission products and other components of the waste, and are easily stripped with nitric acid.

The phenol extractants are weakly acidic and not sufficiently ionized at pH values below 10 to give significant cesium extraction. In the pH range 11–12, however, coefficients for extraction of cesium from tartrate-complexed waste concentrate with 1 *M* solutions of OPP and 4-chloro-2-phenylphenol were 1–3, with the latter compound showing the higher extraction power (Table 5.1). The sodium salts of these two phenols have a high aqueous solubility, and, in the extraction contact, the fraction of the phenol converted to the sodium salt distributes almost quantitatively to the aqueous phase. With OPP, this reagent loss (organic/aqueous ratio of 3/1) increased from <1% to 15% with an increase in feed liquor pH from 10 to 13. The high distribution of the sodium salt to the aqueous allows attainment of high decontamination factors ($>10^3$) from sodium. The relatively high loss of phenol from the solvent phase causes lower than expected cesium extraction coefficients in batch tests, since the coefficient has a high (probably third) power dependence on phenol concentration. This effect was effectively counteracted in a countercurrent

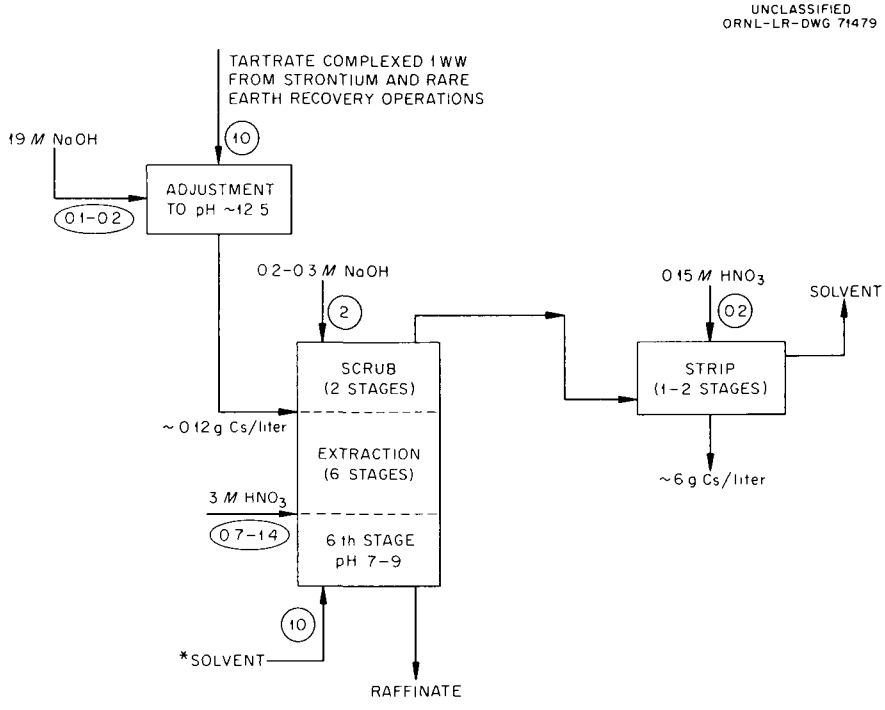

Fig. 5.6. Recovery of Cesium from Purex Waste by Extraction with Substituted Phenols. Circled numbers show relative volume flows.

Table 5.1. Extraction of Cesium from Adjusted Waste

Organic: 1 *M* OPP in xylene or 1 *M* 4-chloro-2-phenylphenol in diisopropylbenzene
Aqueous: simulated Purex 1WW,[a] tartrate-complexed (2 moles/mole Fe), diluted threefold with caustic to various excess NaOH concentrations
Contact: 2 min at organic/aqueous phase ratio of 3/1

Excess NaOH,[b] (*M*)	pH		Organic Na Concentration (g/liter)	Cesium Extraction Coefficient, E_a^o	Loss of Phenol to the Aqueous (%)
	Initial	*Final*			
			Extraction with OPP		
0.2	3.8	3.5	0.02	0.002	<1
0.5	10.0	9.9	0.02	0.16	<1
0.6	11.9	11.2	0.01	0.20	1
0.7	12.2	11.8	0.01	0.55	4
0.8	12.3	11.8	0.02	1.0	5
0.9	12.4	11.8	0.04	1.2	9
1.0	12.4	12.0	0.04	1.3	11
1.2	12.7	12.0	0.05	1.3	15
			Extraction with 4-chloro-2-phenylphenol		
0.4	6.9	6.9	<0.005	0.01	
0.6	12.1	11.1	0.02	1.3	
0.8	12.6	11.6	0.07	3.3	
1.0	12.9	11.7	0.08	3.2	
1.2	13.0	11.8	0.08	2.5	

[a]The simulated Purex waste contained (moles per liter): 4.0 H^+, 4.45 total NO_3, 1.0 SO_4, 0.6 Na, 0.5 Fe, 0.1 Al, 0.005 U, 0.01 Ni, 0.01 Cr, 0.01 PO_4, 0.0028 Cs, 0.0066 Zr, 0.0019 Sr, 0.0034 Ce(III), 0.0058 Sm, 0.0029 Ru.
[b]Caustic in excess of that required to neutralize the acid (1.33 *M*) in threefold diluted waste.

system (see below) by lowering the pH in the last extraction stage to 7–9, thereby converting the sodium phenate in the aqueous to phenol which distributed back to the solvent phase. This procedure prevented loss of extractant and maintained the phenol concentration in the solvent throughout the extraction system at the desired level (~1 *M* and higher), which ensured high extraction efficiency. PDP is a weaker acid than OPP or 4-chloro-2-phenylphenol and its sodium salt distributes less to the aqueous. Therefore it requires a higher pH feed for effective cesium extraction and gives less favorable separation from sodium.

Of the diluents used with the phenols, best results were obtained with substituted benzenes, for example, xylene and diisopropylbenzene, although favorable results but with somewhat lower cesium extraction coefficients were obtained with trichloroethylene, carbon tetrachloride, 80% Amsco 125-82–20% tridecanol, and 1,2-dichloroethane. Cesium extraction coefficients with nitrobenzene diluent were higher than with the substituted benzenes but phase separation was relatively poor.

The selectivity of the phenols for cesium over other fission products is excellent. Coefficients for extraction of Sr, Ru, Zr-Nb, and Eu from tartrate-complexed Purex waste concentrate with OPP and PDP were $< 10^{-3}$ under conditions where cesium coefficients ranged from 0.3 to 1.

The process flowsheet (Fig. 5.6) has been demonstrated successfully in batch countercurrent tests with adjusted simulated Purex waste concentrate. With 1 *M* 4-chloro-2-phenylphenol in diisopropylbenzene, 98.6% cesium recovery was obtained, from waste adjusted to pH 12.6, in six extraction stages at an organic/aqueous ratio of 1/1 (Table 5.2). The pH in the last extraction

Table 5.2. Batch Countercurrent Test with OPP

Organic: 1 *M* 4-chloro-2-phenylphenol in diisopropylbenzene
Aqueous: simulated Purex 1WW, tartrate-complexed (2 moles/mole Fe), diluted threefold with caustic to 0.6 *M* excess NaOH, contained 0.12 g Cs/liter and Cs^{134} tracer
Scrub solution: 0.3 *M* NaOH
Acid (to 6th extraction stage): 3 *M* HNO_3
Contact: batch countercurrent; 2 min contacts
Relative flows: organic/feed/scrub/acid = 1/1/0.2/0.08

Stage	pH	Cs γ-Activity (counts min^{-1} ml^{-1})		Cesium Extraction Coefficient, E_a°
		Organic	Aqueous	
Scrub-2	10.7	1.40×10^5	2.15×10^4	6.5
Scrub-1	11.1	1.44×10^5	1.94×10^4	7.4
Aqueous feed	12.6		1.39×10^5	
Extraction-1	11.5	1.44×10^5	5.66×10^4	2.5
Extraction-2	11.5	6.71×10^4	2.65×10^4	2.5
Extraction-3	11.5	3.08×10^4	1.23×10^4	2.5
Extraction-4	11.5	1.32×10^4	5.28×10^3	2.5
Extraction-5	11.5	4.25×10^3	1.87×10^3	2.3
Extraction-6	6.7	~10	1.89×10^3	<0.01

stage was controlled at ~7 by addition of nitric acid. The extract, after being scrubbed in two stages with 0.2 vol of 0.3 *M* NaOH, was stripped >99.8% by a single contact with 0.05 vol of 0.05 *M* HNO_3 to give a product solution containing 2.5 g of cesium and 0.21 g of sodium per liter. The overall Cs/Na decontamination factor for the experiment was ~6000. Under the same flowsheet conditions, but with feed adjusted to 0.8 *M* instead of 0.6 *M* excess NaOH, results were approximately equivalent with 1 *M* OPP in diisopropylbenzene.

Other Cesium Extractants

Other phenols of different structures are being evaluated for possible superior cesium extraction potential. Preliminary tests with a benzyl-substituted phenol, 4-*sec*-butyl-2-(α-methylbenzyl) in diisopropylbenzene showed a high Cs/Na separation factor, similar to OPP, a lower aqueous solubility of the sodium salt, and a much greater cesium extraction power (E_a° ~8 from modified simulated Purex waste concentrate compared to ~2.7 for OPP). From undiluted Hanford tank farm supernatants the cesium extraction coefficients were about 24 and 0.13, respectively.

Cesium extraction (E_a° = ~0.6) was moderate from tartrate-complexed simulated formaldehyde-treated Purex waste over the pH range 1.4–11.5 with 0.5 *M* dinonylnaphthalenesulfonic acid (DNNSA) in hexone. The selectivity of this reagent for cesium over iron(III), aluminum, zirconium-niobium, cerium(III), europium, and ruthenium was relatively poor in the pH range 1–3 but good above pH 5. Cesium was stripped effectively with 1–3 *M* HNO_3. Although DNNSA has shown some promise as a cesium extractant, it does not appear to be competitive with the phenols.

In extraction from 0.5 *M* $NaNO_3$ solution with 0.5 *M* monoheptadecylphosphoric acid (HDPA) in Amsco 125-82 the cesium extraction coefficient was ~2 and the Cs/Na separation factor ranged 20–40 over the pH range 1–11. Potential application of HDPA for cesium recovery appears limited

to treatment of relatively simple solutions, possibly in a secondary purification cycle, since results in tests with Purex 1WW waste solutions were not promising. Coefficients with 0.4 *M* HDPA in Amsco 125-82 from waste at pH ~0.5 were <0.05, and stable emulsions formed in equilibrations with tartrate-complexed waste ranging in pH from 2 to 8.

Zirconium-Niobium

Additional tests confirmed that zirconium and niobium are extracted slowly from acidic (4 *M* H^+) simulated Purex waste concentrate by 0.3 *M* D2EHPA–0.15 *M* TBP in Amsco 125-82, a hydrocarbon diluent. About 95% was extracted in 1 hr contact with an equal volume of solvent. Stripping with 1 *M* oxalic acid solution was effective. The presence of TBP in the solvent greatly improved the stripping but did not affect the extraction. Other, less sterically hindered, dialkylphosphoric acid extractants are being prepared in an attempt to increase the extraction rate. Other potential extractants, for example, amines and hydroxamic acids, are also being evaluated.

Extractions from Purex Waste Concentrate with Amines

In preliminary testing, amine extraction removed nitric acid, iron sulfate, and certain fission products from Purex waste. This treatment would greatly decrease the amounts of caustic and sodium tartrate needed to adjust the waste to conditions suitable for strontium and cesium extraction (see above), and the adjusted feed, owing to its lower salt content, would be more amenable to treatment by these processes.

In batch single-contact tests with 0.26 *M* Primene JM in Amsco 125-82, extraction of iron sulfate from simulated Purex waste concentrate (Table 5.1) was negligible until sufficient amine was supplied to extract most of the nitrate (Fig. 5.7). Iron extraction became significant at organic/aqueous phase ratios higher than 15/1, increasing to >96% at a phase ratio of 26/1. At this ratio, 96% of the nitrate and 43% of the sulfate were also extracted. Parallel extraction tests with fission product tracers added to the simulated waste showed 96, 82, and 18% extraction of Zr-Nb, Ru, and Ce(III), respectively, at an

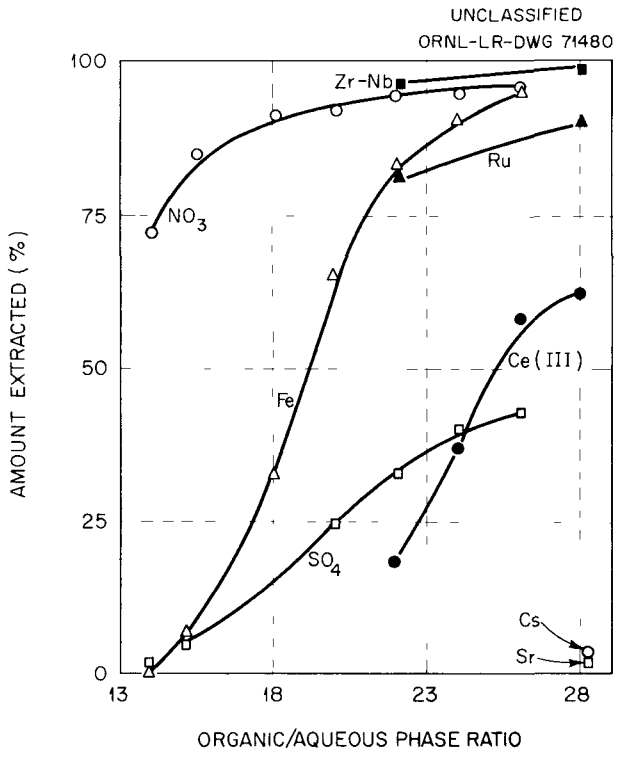

Fig. 5.7. Extraction of Nitric Acid, Iron Sulfate, and Fission Products from Purex Waste Solution with Primene JM (0.26 *M*) in Amsco 125-82. Mixture of amine and amine sulfate salt used in tests with phase ratios >16 to control final pH flow below 2.

organic/aqueous ratio of 22/1; these values increased to 99, 90, and 62% at a ratio of 28/1. At a ratio of 26/1, only ~3% of the cesium and 1.5% of the strontium were taken into the solvent phase, apparently mostly by aqueous entrainment. Scrubbing the extract with water or 0.3 *M* HNO_3 removed the rare earths but not the Zr-Nb or Ru.

These data suggest a single extraction contact to remove >95% of the nitric acid and iron, >98% of the Zr-Nb, and the bulk of the ruthenium and rare earths from Purex wastes without removing important amounts of strontium or cesium from the solution. Extraction of rare earths can be prevented, if desired, by accepting less efficient removal of iron, that is, by operating at a lower organic/aqueous ratio and/or by scrubbing the extract. Use of a multistage system would improve the efficiencies of the separation. The data also suggest methods for removing and isolating

certain fission products, for example, Zr-Nb and rare earths, and these possibilities are being examined.

5.2 ION EXCHANGE

Head-End Precipitation

A flowsheet (Fig. 5.8) was developed, on a laboratory scale, for recovering strontium from Purex 1WW[4] waste solution by a double precipitation as a head-end step prior to ion exchange. Sulfate ion is removed from the waste by addition of iron and nitric acid to 55–60% HNO_3, and strontium is recovered from an almost pure nitrate system, >85% HNO_3. The proposed procedure is:

1. Excess ferric (Fe^{3+}) ion is added to Purex 1WW as freshly precipitated $Fe_2O_3 \cdot xH_2O$ or partially dehydrated (boiling temperature of ~135°C) $Fe(NO_3)_3 \cdot 9H_2O$.
2. The solution is diluted with 90% HNO_3 to 55–60% HNO_3, which precipitates the sulfate as $Fe_2(SO_4)_3$.
3. The iron sulfate is filtered off and the filtrate concentrated by evaporation to a residue boiling temperature of 135°C.
4. This residue is made >85% HNO_3 with 90% HNO_3 to precipitate strontium; the mixture is kept at ~70°C for at least 12 hr[5] to minimize coprecipitation of iron and aluminum remaining in solution.
5. The mixture is filtered while warm and the strontium precipitate dissolved in 1 *M* HNO_3 for ion exchange processing.

In 100-ml batch experiments, 75–80% of the original strontium was recovered, contaminated with <1% each of Fe^{3+}, Al^{3+}, Na^+, and SO_4^{2-} (Table 5.3). The strontium yield could probably be increased 5–10% by minimizing the volume of liquid used to precipitate strontium at >85% HNO_3. Extrapolated solubility data[6] of the system $Sr(NO_3)_2$-HNO_3-H_2O indicated that >15% of the 20–25% strontium not recovered had dissolved in the large volume (1.7 liters) of >85% HNO_3 solution.

Ion Exchange

An inorganic ion exchanger, zirconium phosphate, adsorbed cesium strongly from simulated Purex waste solutions in the original acid state (4 *M* H^+) or after addition of tartrate and adjustment to pH 10 with caustic. However the maximum attainable loading is not more than 0.1 meq per g of solid. Since the capacity of the zirconium phosphate for cesium from pure solutions is >1 meq/g, prior removal of one or more interfering constituents may permit greater loadings.

---

[4]Purex first-cycle extraction column raffinate, HAW, is evaporated 30-fold to give 1WW.

[5]E. Glueckauf, *Improvements in or Relating to Method of Separating Strontium from Other Fission Products*, Brit. Patent 844,376 (Aug. 10, 1956).

[6]*Chem. Technol. Ann. Progr. Rept. May 31, 1961*, ORNL-3153, sec 14.3.

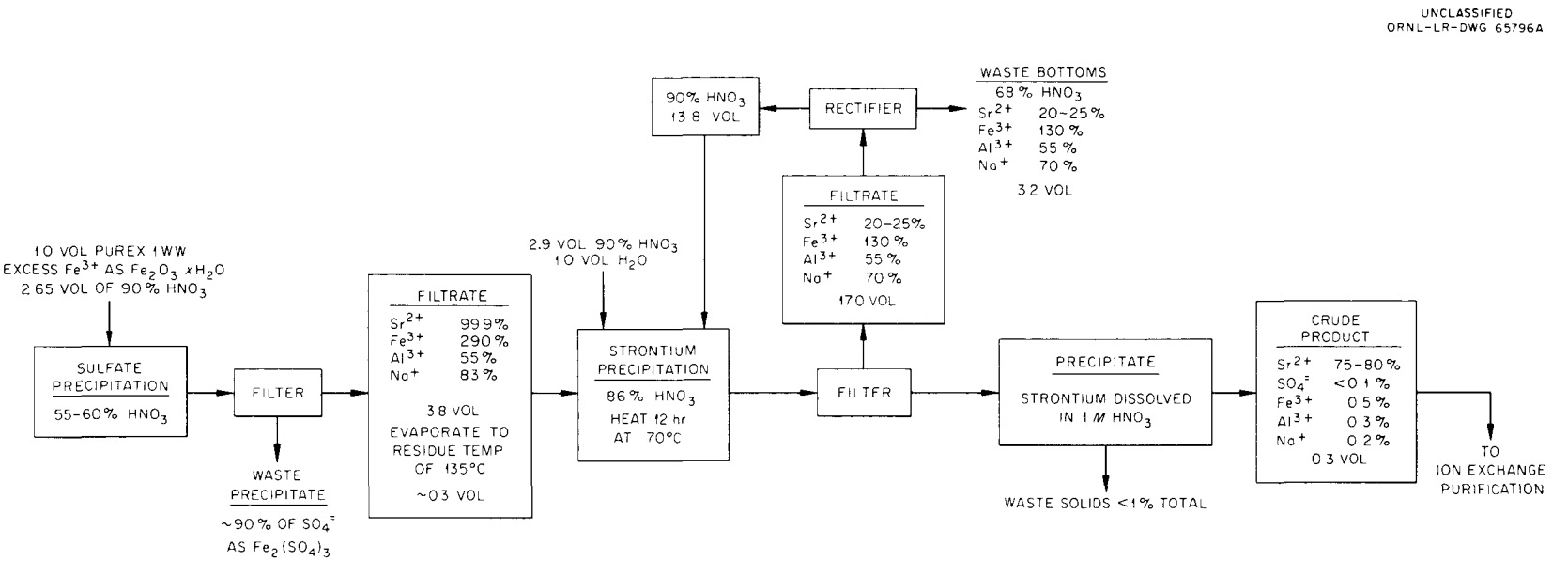

Fig. 5.8. Proposed Flow Diagram for Radioactive Strontium Recovery from Evaporated Purex Waste Solution. Percentages are based on total amount of iron in 100 ml of synthetic Purex concentrated waste; i.e., 5.6 M H^+, 6.1 M HNO_3^-, 1.0 M SO_4^{2-}, 0.5 M Fe^{3+}, 0.1 M Al^{3+}, 0.6 M Na^+, 0.002 M Sr^+, 0.01 M Ni^{2+}, 0.01 M Cr^{3+}, 0.01 M UO_2^{2+}, with stable elements equivalent to 3.75 g of gross fission products per liter.

Table 5.3. Strontium Recovery by a Head-End Double Precipitation from Purex Waste Concentrate-Nitric Acid Solutions

Feed solution: 100 ml of Purex 1WW (~30% HNO_3) containing 2.9×10^5 counts/min Sr^{85}, 9.49 g of SO_4^{2-}, 2.93 g of Fe^{3+}, 0.30 g of Al^{3+}, 1.43 g of Na^+

Material Analyzed	Amount Present (% of original)[a]				
	Sr^{85}	SO_4^{2-}	Fe^{3+}	Al^{3+}	Na^+
Filtrate[b] from SO_4^{2-} pptn, 383 ml of 59% HNO_3	99.9	7	290	55	83
Filtrate from SR pptn, 1720 ml of 86% HNO_3	20–25	7	130	55	70
Sr ppt[c]	75–80	0.1	0.5	0.3	0.2

[a] Sr^{85} determined by γ scintillation counting, other ions by standard wet chemical analyses.

[b] Sulfate precipitated by adding ~90 g of freshly prepared $Fe_2O_3 \cdot x H_2O$ to 100 ml of Purex 1WW, stirring 24 hr to ensure the presence of excess Fe^{3+}, diluting to 59% HNO_3 with 90% HNO_3, and stirring at least 48 hr to approach equilibrium conditions.

[c] Strontium precipitation performed by (1) reducing the filtrate volume of the sulfate precipitation step by evaporation to a residue temperature of 140°C, (2) adding water and 90% nitric acid to redissolve the residue, (3) diluting to 86% HNO_3 with 90% nitric acid, (4) heating the mixture and maintaining it at 70°C for 12 hr, (5) filtering while warm, and (6) dissolving the precipitate in ~30 ml 1 *N* HNO_3.

6. Transuranium Element Processing

A very high neutron-flux reactor, the High Flux Isotope Reactor, and a specialized chemical processing facility, the Transuranium Processing or TRU Facility are being built at Oak Ridge National Laboratory for the production of gram quantities of the transuranium elements. Their production in quantity will simplify research with these materials. With these larger quantities, it will be possible to greatly enlarge our knowledge of their general chemistry, solid state physics, and metallurgy.

Isotopes of Cm, Bk, Cf, Es, and Fm will result from the irradiation of 600 g of Pu^{242} and a 300-g mixture of Am^{243} with Cm^{244}. These feed materials are being produced by the long-term irradiation of 10-kg batches of Pu^{239} in a Savannah River Plant reactor. The irradiated Pu^{239} will be processed at Savannah River and the products shipped to Oak Ridge as PuO_2 and an Am-Cm solution containing the rare earth fission products. The rare earths will be removed and the actinide oxides fabricated into HFIR targets in the TRU Facility.

After irradiation in the HFIR, the targets will be returned to TRU for processing to recover Cm, Bk, Cf, and Es. The curium isotopes will then be refabricated into targets for production of heavier elements. This report summarizes the development of chemical separation processes, equipment development, and design of the TRU Facility.

6.1 CHEMICAL PROCESS DEVELOPMENT

The development of methods for the recovery of americium and curium from plutonium process

waste, and for the recovery of Am, Cm, Bk, Cf, Es, and Fm from irradiated HFIR targets has continued. The method proposed for americium-curium recovery from plutonium process waste (Fig. 6.1) consists in Am-Cm-RE concentration by anion exchange, conversion to a chloride system by amine extraction of HNO_3, and separation from rare earths by amine extraction from concentrated LiCl solution. The main-line HFIR target processing method (Fig. 6.2) consists in target dissolution in HCl; actinide separation from fission products and aluminum by tertiary amine extraction from concentrated LiCl solution; Bk, Cf, Es, and Fm separation from Am-Cm by phosphonate extraction from dilute HCl; Bk separation from Cf, Es, and Fm by dialkyl phosphate extraction of Bk(IV) from concentrated HNO_3; and Cf, Es, and Fm separation from each other by chromatographic elution from cation exchange resin. Development studies of these process steps were

UNCLASSIFIED
ORNL-LR-DWG 71481

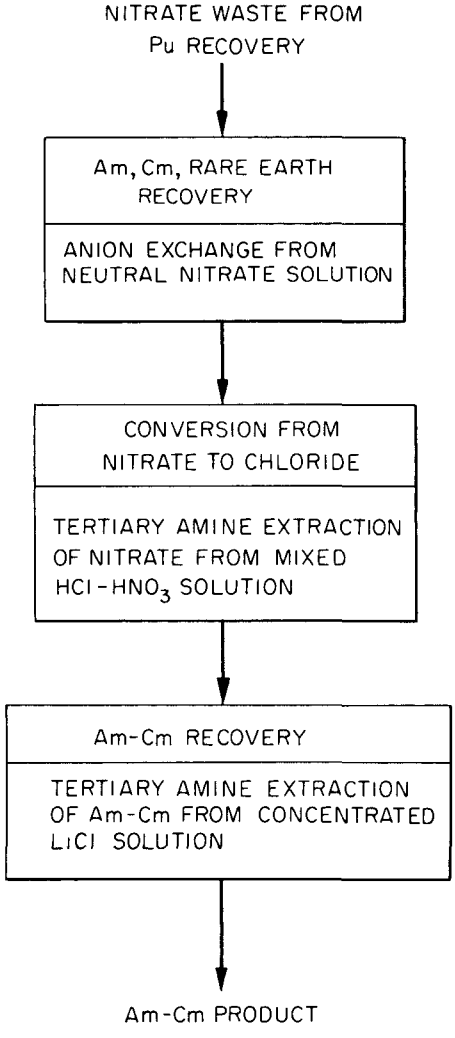

Fig. 6.1. Summary Flowsheet for Americium-Curium Recovery from Plutonium Process Waste.

UNCLASSIFIED
ORNL-LR-DWG 71482

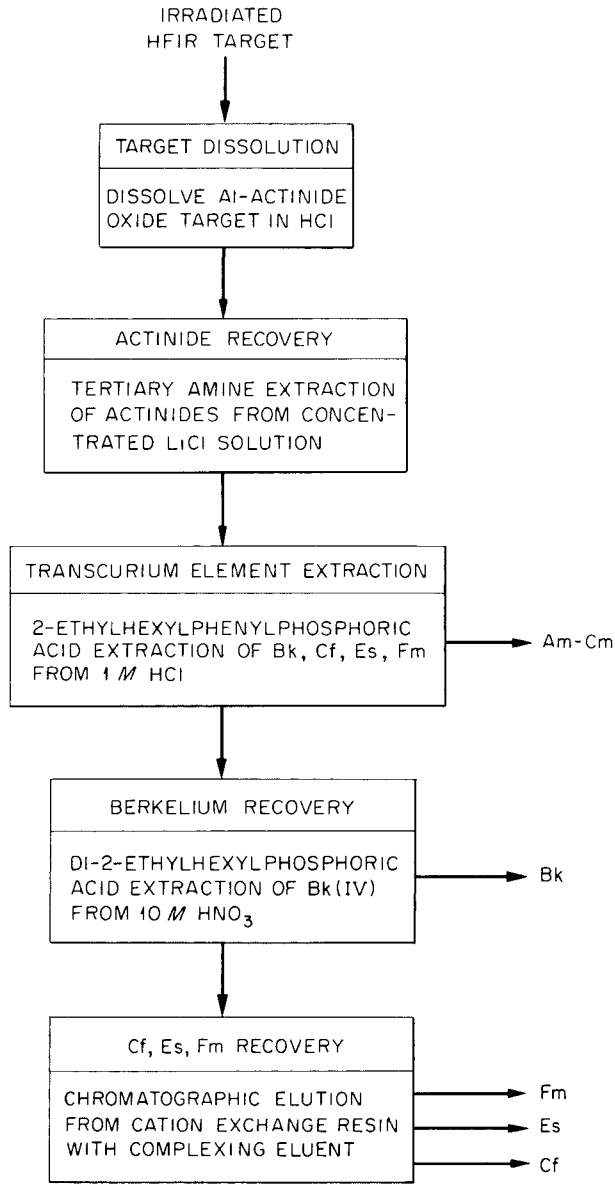

Fig. 6.2. Summary Flowsheet for HFIR Target Processing.

made in laboratory-scale experiments with synthetic solutions containing tracer amounts of the transuranium elements. Scouting work was also carried out to investigate the effect of high alpha activity levels on corrosion and to study the separation of Am and Cm by converting Am to higher oxidization states.

Aluminum-Silicon Alloy Dissolution in Hydrochloric Acid

When aluminum is irradiated in a nuclear reactor, some of it is transmuted to silicon, and, theoretically, approximately 3% of the aluminum in HFIR targets will be converted to silicon during an 18-month irradiation. Since the proposed process calls for target dissolution in hydrochloric acid, the effect of the silicon content on the dissolution rate is being studied. Preliminary investigation of hydrochloric acid dissolution of aluminum alloys containing various amounts of silicon were made with three alloys: X-8001 containing about 0.1% Si, an 1100 series alloy containing about 0.3% Si, and a specially prepared alloy containing 97% Al and 3% Si.

In the hydrochloric acid concentration range 1 to 6 *M*, the dissolution rate of all three alloys was proportional to the cube of the acid concentration (Fig. 6.3). For a given acidity, the dissolution rate was inversely proportional to the silicon content of the alloy. The dissolution rate of the 1100 series alloy, which contains about 0.3% Si, was approximately 10 times that of aluminum containing 3% Si, and the dissolution rate of X-8001 aluminum, which contains about 0.1% Si, was about 4 times that of the 1100 series aluminum. The dissolution rate of 97% Al–3% Si alloy in 6 *M* HCl in the temperature range 25 to 70°C doubled for every 8–9°C increase in temperature. Even the 3%-Si alloy can be dissolved at acceptable rates; for example, at 80°C, in 6 *N* HCl the rate was 10 mg min^{-1} cm^{-2}.

Tramex Process Development

The flowsheet for the Tramex process shown in Fig. 6.4 is essentially the same as that reported last year.[1] Trivalent actinides are extracted

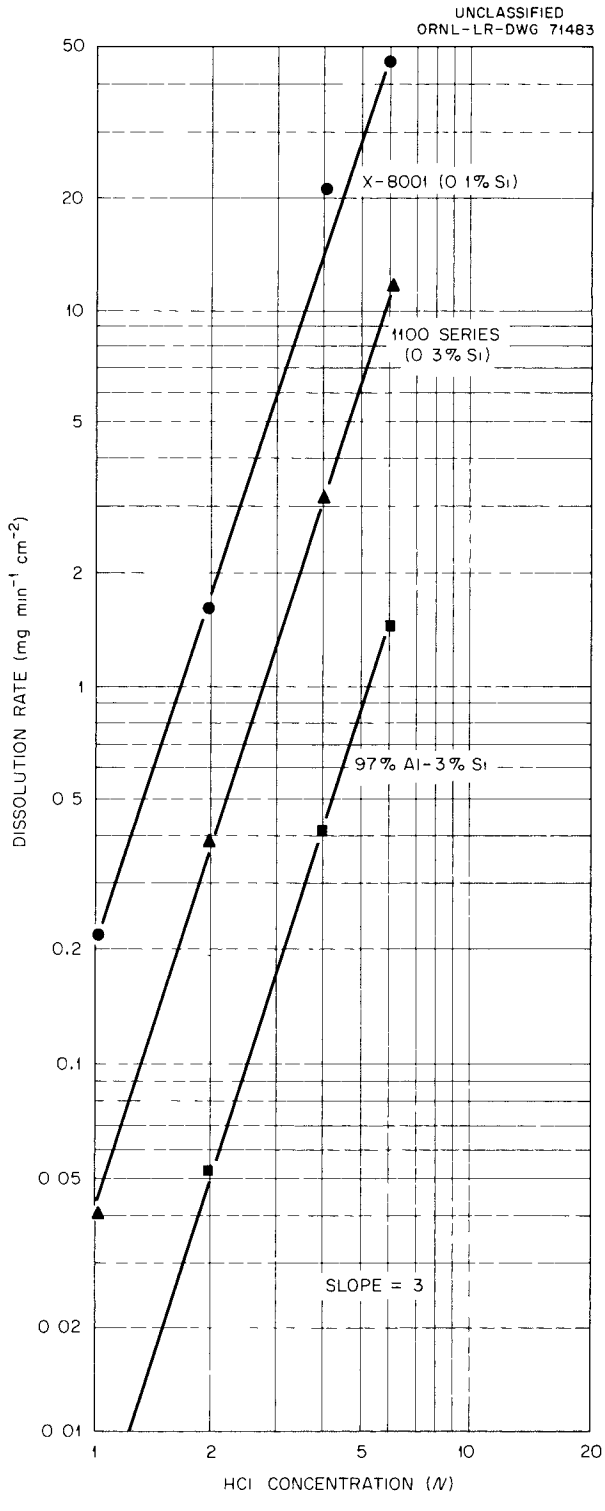

Fig. 6.3. Effect of Acid Concentration at 50°C on Rate of Dissolution of Aluminum Alloys in Hydrochloric Acid.

[1] *Chem. Technol. Div. Ann. Progr. Rept. May 31, 1961*, ORNL-3153.

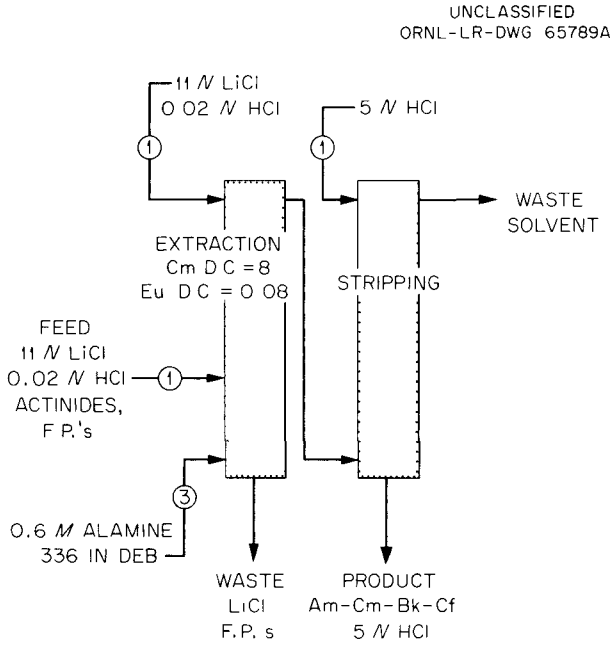

Fig. 6.4. Tramex Process for Separation of Actinides from Lanthanides by Tertiary Amine Extraction.

from 11 *M* LiCl containing 0.02 *M* HCl into 0.6 *M* Alamine 336 (a mixture of octyl and decyl tertiary amines) in diethylbenzene. The scrub solution is also 11 *M* LiCl containing 0.02 *M* HCl, and the stripping solution is 5 *M* HCl. The effects of variables such as LiCl concentration, acid concentration, and amine concentration were reconfirmed. Distribution coefficients of Am, Cm, Cf, Es, Fm, and rare earths were redetermined and agreed with those previously reported.[1] Some work was carried out to demonstrate feed preparation, and a number of laboratory-scale mixer-settler runs with synthetic feed solutions were made in order to demonstrate the flowsheet. Most of the recent development was directed at studying details of this system. The behavior of contaminant cations was determined, and the effects of various anions on americium and europium distribution coefficients were studied. The addition of surfactants and variations in temperature were investigated as means for improving phase separation. Most of this work has been reported elsewhere.[2,3]

Laboratory-scale mixer-settler runs were made with synthetic feeds containing tracer americium and nonradioactive rare earths to demonstrate separations that can be obtained with the flowsheet conditions given in Fig. 6.4. With 6 extraction, 6 scrub, and 6 stripping stages, total americium losses were about 0.01% and the decontamination factor from rare earths was greater than 10^4. Feed containing 11 *M* LiCl and low acid concentration can be prepared from hydrochloric acid solutions of actinides and lanthanides by adding LiCl, evaporating to a pot temperature of 135°C, and diluting with a small amount of water. The detailed procedures for this feed adjustment step are not yet complete.

From distribution coefficients determined for expected contaminants, it was concluded that the Tramex process will provide the desired separation from all except Ti^{4+} and Ni^{2+}, which will follow the trivalent actinides through the process. Those expected contaminants above Ru^{3+} in Table 6.1 will be extracted along with the actinides, but of those extracted, only Ti^{4+} and Ni^{2+} will be completely stripped with actinides, especially if a solvent scrub is used on the strip column. Ruthenium behavior is not completely predictable from these data since it exists as both tri- and tetravalent ions in these solutions.

By choosing the correct acidity for the strip column, it is possible to separate most of the extracted contaminants (Fig. 6.5). The distribution coefficient (o/a) for Am^{3+} was less than 0.001 over the acid range 0.5 to 10 *M* HCl. The distribution coefficients for Ti^{4+} and Ni^{2+} were less than 0.01 over this same range, and they will be stripped with the actinides. If the extracted Ru^{4+} is reduced to Ru^{3+} in the strip column, it will tend to follow the actinides.

The effects of anion contaminants on distribution coefficients were studied with Am^{3+}-representing actinides and Eu^{3+}-representing lanthanides. Trace amounts of fission product bromide and iodide and trace amounts of fluoride added during processing had little effect on americium and europium behavior. The effects became appreciable at concentrations greater than 0.1 *N*. Both americium and europium distribution coefficients increased rapidly with increasing

---

[2] R. D. Baybarz and Boyd Weaver, *Separation of Transplutoniums from Lanthanides by Tertiary Amine Extraction*, ORNL-3185 (Dec. 4, 1961).

[3] R. D. Baybarz and H. B. Kinser, *Separation of Transplutoniums and Lanthanides by Tertiary Amine Extraction. II. Contaminant Ions*, ORNL-3244 (Feb. 20, 1962).

Table 6.1. Distribution of Various Ions Between 0.6 *M* Alamine-336 in DEB and 10.85 *M* LiCl

Ion	Source	Distribution Coefficient (o/a)
Pd^{2+}	Fission product	530
Fe^{3+}	Target contaminant	410
Ti^{4+}	Corrosion product	150
Ru^{4+}	Fission product	54
TcO_4^-	Fission product	53
Zr^{4+}	Fission + corrosion product	15
Am^{3+}	Neutron capture of Pu^{242}	14
MoO_4^{2-}	Fission product	6.0
Ni^{2+}	Target contaminant	4.3
Ru^{3+}	Fission product	0.40
Eu^{3+}	Fission product	0.12
Ce^{3+}	Fission product	0.10
Y^{3+}	Fission product	0.020
Ba^{2+}	Fission product	0.008
Sr^{2+}	Fission product	0.006

nitrate concentration (Fig. 6.6). However, europium extraction increased more rapidly than americium extraction. As a result, the americium-europium separation factor decreased from more than 100 for 0.01 *N* NO_3^- to 1, or no separation, for about 0.7 *N* NO_3^-. Because of this adverse effect, it is important that all nitrate be removed when plutonium process wastes are converted to a chloride system for americium and curium recovery.

The time required for 0.6 *M* Alamine 336 in diethylbenzene and 11 *M* LiCl to separate after intimate mixing was about 3 min at 30°C. This is too long for efficient mixer-settler operation. Separation time was decreased by the addition of a surfactant and by increasing the temperature. Minnesota Mining and Manufacturing Co.'s FX-170 was one of the most effective surfactants tested. This is a nonionic fluorochemical with a solubilizing functional group. Addition of 100 to 1000 ppm of FX-170 to the aqueous phase decreased the phase separation time to about 30 sec. The surfactant had no effect on distribution coefficients or separation factors. Increasing the temperature from 30 to 50°C decreased the phase separation time from 3 min to 70 sec, and to 80°C, to 20 sec.

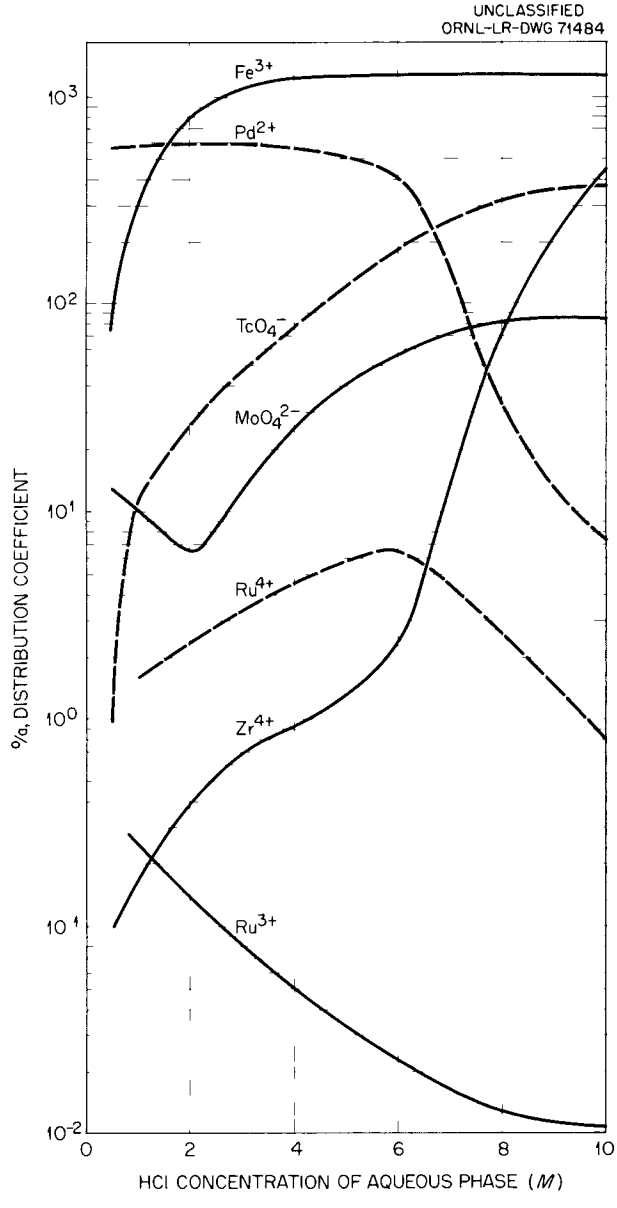

Fig. 6.5. Distribution Coefficients of Various Ions between 0.6 *M* Alamine 336 in Diethylbenzene and HCl Solutions as a Function of HCl Concentration.

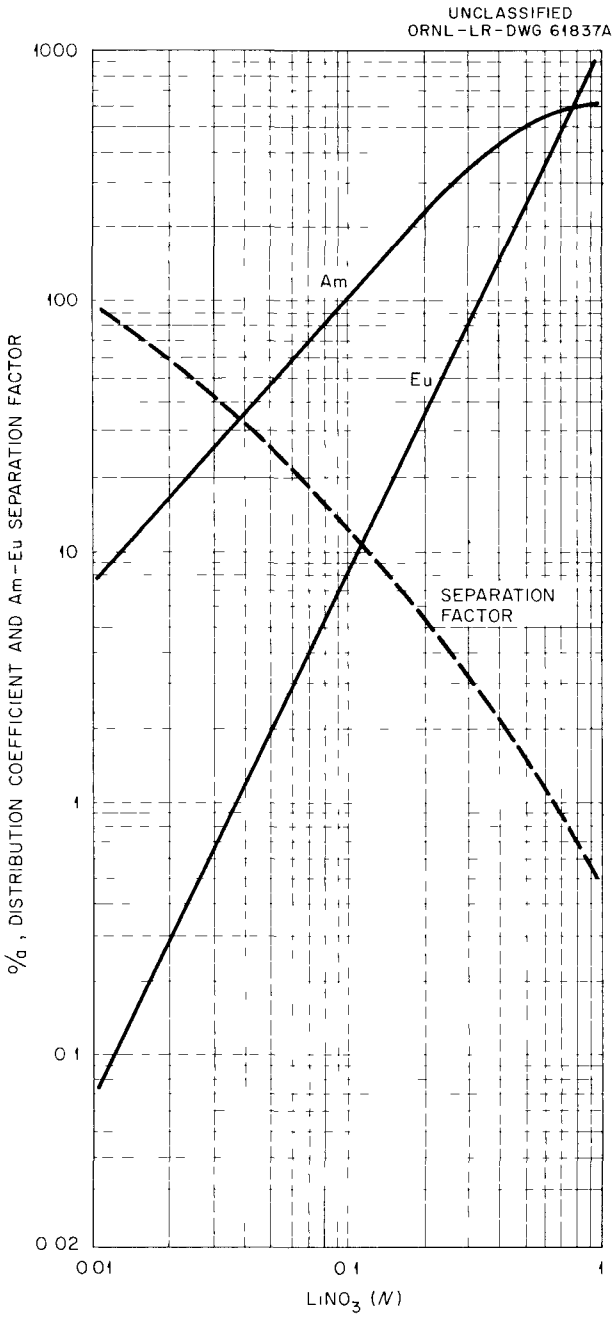

Fig. 6.6. Effect of Nitrate Concentration on Extraction of Americium and Europium into 0.6 *M* Alamine 336 in Xylene from 11 *M* LiCl.

Separation of Transcurium Elements from Americium and Curium by Phosphonate Extraction

The flowsheet in Fig. 6.7 is essentially the same as that presented last year. Trans-

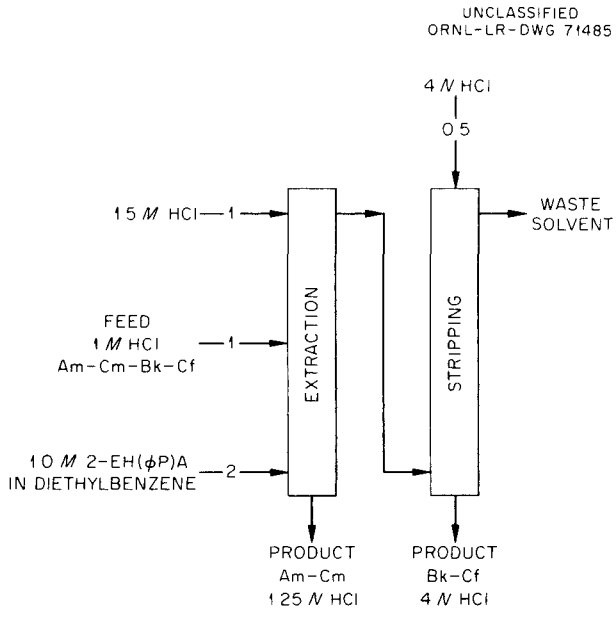

Fig. 6.7. Flowsheet of Process for Separating Transcurium Elements from Americium and Curium by Phosphonate Extraction.

curium elements are extracted from 1 *M* HCl feed into 1 *M* 2-ethylhexylphenylphosphonic acid [2-EH(ØP)A] in diethylbenzene (DEB). The scrub is 1.5 *M* HCl, and the strip is 4 *M* HCl. Batch countercurrent runs were made in order to demonstrate americium and californium separation. Distribution coefficients of the actinides were redetermined, and they agreed with those previously reported.[1] Distribution coefficients of the lanthanides were also determined. The effects of variables such as acid concentration, phosphonate concentration, and solvent diluent were studied. Behaviors of a number of contaminant ions were investigated. The results, summarized here, are reported in more detail elsewhere.[4]

Batch countercurrent runs were made with synthetic feeds containing tracer americium and californium to demonstrate separations obtainable with the process shown in Fig. 6.7. With 4 extraction, 3 scrub, and 3 strip stages, total californium losses were about 0.1%, and the americium decontamination factor was greater than 10^3. Other

[4] R. D. Baybarz, *Separation of Transplutonium Elements by Phosphonate Extraction*, ORNL-3273 (to be issued).

runs were made in a mixer-settler to test mechanical operation of this system. Because of a limited supply of californium and berkelium, synthetic feeds were used which contained europium tracer as a substitute for berkelium, and americium tracer. With 8 extraction and 8 scrub stages operating at about 50% efficiency, 99.9% of the europium was extracted, and the decontamination factor from americium was 2×10^3.

Distribution coefficients (o/a) found for trivalent actinides and trivalent lanthanides between 1.0 *M* 2-EH(ØP)A *in diethylbenzene and* 2 *M* HCl *are* given in Fig. 6.8. The major break in extractability between berkelium and curium, separation factor of 30, makes this an ideal system for separating the transcurium elements from americium and curium.

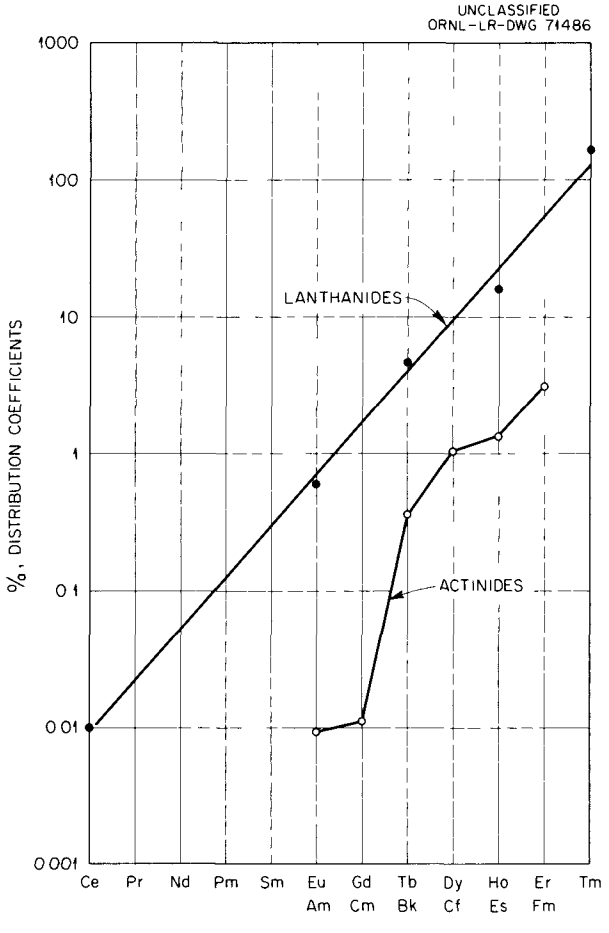

Fig. 6.8. Distribution of Actinides and Lanthanides between 1 *M* 2-EH(ϕP)A in DEB and 2 *M* HCl.

Separation factors for other adjacent actinides ranged from 1.3 to 3.3. For the lanthanide series there was a more uniform increase in distribution coefficient with atomic number. Separation factors between adjacent lanthanides were about 2.5. Distribution coefficients of both actinides and lanthanides were directly proportional to the cube of the 2-EH(ØP)A concentration, and inversely proportional to the cube of the acidity over the range 0.5 to 4 *M* HCl. Extraction decreased to a minimum at 5.5 to 7 *M* HCl and then increased *with increasing acidity. Selected examples of* actinide and lanthanide extraction as a function of acidity are given in Fig. 6.9. The diluent that carried the 2-EH(ØP)A also affected the distribution coefficients. Table 6.2 lists europium distribution coefficients between 1 *M* 2-EH(ØP)A in various diluents and 2 *M* HCl. Extraction was considerably greater with aliphatic diluents than with aromatic diluents.

Behaviors of contaminant ions that may be present in the feed for this separation were briefly

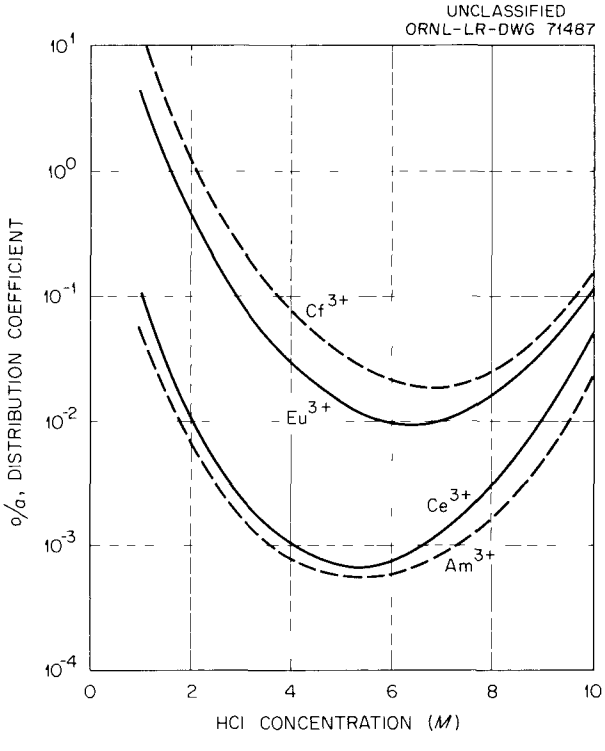

Fig. 6.9. Effect of Acid Concentration on Extraction of Actinides and Lanthanides into 1 *M* 2-EH(ϕP)A in DEB from HCl Solutions.

Table 6.2. Effect of Diluent on Europium Extraction

2 *M* HCl vs 1.0 *M* 2-EH(ØP)A

Diluent	Europium Distribution Coefficient (o/a)
n-heptane	4.8
Amsco 125-82	3.5
n-dodecane	3.4
Decalin	2.1
Cyclohexane	2.0
Triethylbenzene	0.89
Diethylbenzene	0.61
Carbon tetrachloride	0.52
Solvesso-100	0.42
Xylene	0.40
Toluene	0.37
Benzene	0.31

investigated. Results indicate that Zr^{4+}, Ti^{3+}, Fe^{3+}, MoO_4^{2-}, and Pu^{4+} will be quantitatively extracted with transcurium elements. When the transcurium elements are stripped from the organic phase with ¼ volume of 4 *M* HCl, most of these ions will remain in the organic phase. However, decontamination from Fe^{3+} and Ti^{3+} will be poor since both extraction factors (o/a) are only 2.4. The contaminants, Si^{2+}, Ru^{3+}, Al^{3+}, and Ni^{2+} will not be extracted but will remain in the aqueous phase with americium and curium.

Americium-Curium Recovery from Plutonium Process Waste by Anion Exchange

Studies on separation of americium and curium from rare earths by anion exchange were discontinued in view of the encouraging results obtained with amine extraction. However, the study of americium-curium behavior in concentrated nitrate solution was continued, and an anion exchange process for recovering americium and curium from plutonium-processing raffinates was developed and tested on a laboratory scale. The results summarized here are reported in more detail elsewhere.[5]

In this process (Fig. 6.10) americium, curium, and rare-earth fission products are sorbed from neutral concentrated aluminum nitrate solutions. While the process has general application, it was developed specifically to recover americium and curium present in highly irradiated plutonium-aluminum alloy, which is being processed here for plutonium recovery.

The feed is prepared by evaporating the plutonium raffinate to a solution temperature of 140°C and then diluting with water to an aluminum concentration of 2.6 *M*. The solution will be transferred by steam jet, which results in a minimum feed dilution of 10%. Fifteen column displacement volumes of feed are pumped through the column, which is packed with 50–100 mesh Dowex 1-10X resin at 70°C. Aluminum and iron are washed from the column with 5 displacement volumes of 8 *M* $LiNO_3$, and the product is eluted with 3 displacement volumes of 0.65 *M* HNO_3. In laboratory demonstrations, products containing 8.5 g of rare earths per liter and 0.05 *M* Al^{3+} were obtained from feeds containing 2.34 *M* Al^{3+}. No americium losses were detectable, and decontamination from iron was essentially complete.

The effects of resin particle size, feed flow rates, aluminum concentration, resin cross linkage, and temperature on sorption were investigated. Americium losses with 27 column volumes of feed and Dowex 1-10X resin were less than 1% for 50–100 mesh resin, 2.3% for 50–60 mesh, and 35% for 10–50 mesh (Fig. 6.11). Decreasing the resin cross linkage from 10 to 4% increased americium losses from 0.9 to 11% for 27 column volumes of feed. In experiments with europium tracer, losses increased from 0.1 to 23% for 15 column volumes of feed when the flow rate was increased from 2 to 4 ml min^{-1} cm^{-2}, and were of the order of 0.12, 0.27, 2.2, and 16% when aluminum feed concentrations were 2.7, 2.3, 2.0, and 1.8 *M*, respectively. Column temperature did not appear to be critical; results were satisfactory in the temperature range 60 to 85°C. Results with coarse Permutit SK resin were comparable to those with Dowex 1-10X.

[5] M. H. Lloyd, *Anion Exchange Recovery of Americium and Curium from Plutonium Process Waste*, ORNL-3291 (to be issued).

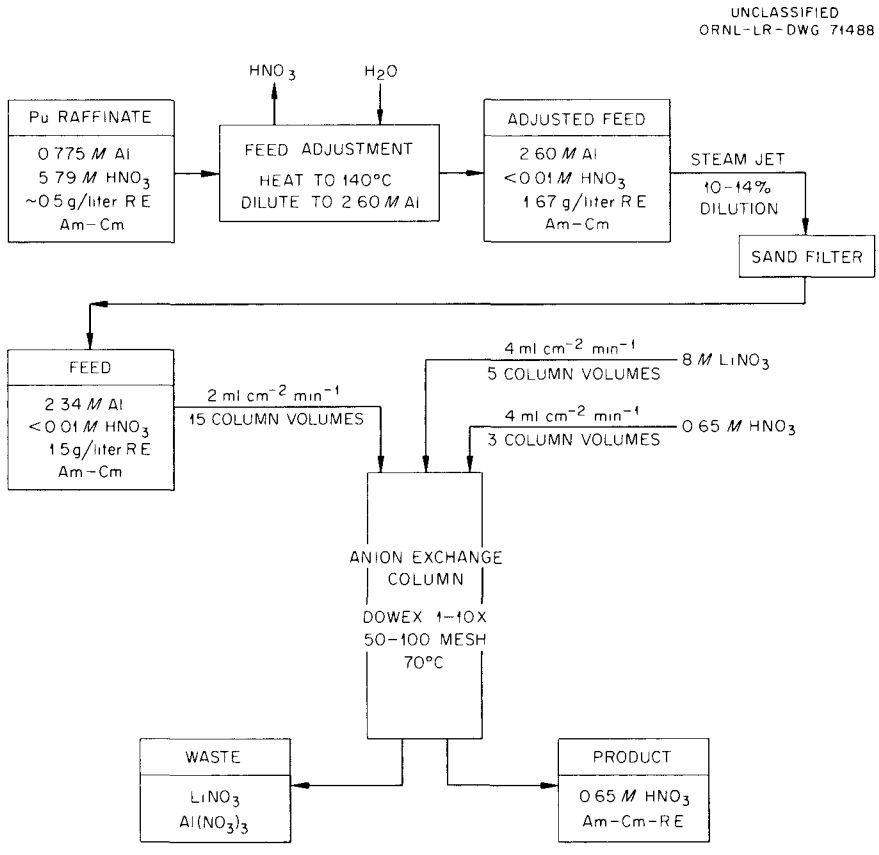

Fig. 6.10. Flowsheet of Anion Exchange Process for Recovery of Americium and Curium from Plutonium Process Waste.

Conversion from Nitrate to Chloride Solution by Amine Extraction

Conversion from a nitrate to a chloride system by extraction of HNO_3 into tertiary amine was demonstrated in laboratory-scale experiments with synthetic solutions. Feed containing 1 *M* HNO_3, 4 *M* HCl, 5 g/liter rare earths, 0.5 g/liter ruthenium, and tracer americium was contacted with 2.5 vol of 0.6 *M* Alamine 336 in diethylbenzene. Testing was carried out in a 16-stage mixer-settler operated as an extraction section only. The aqueous product contained 99.95% of the americium, less than 10% of the ruthenium, and less than 0.01 *M* HNO_3. This nitrate concentration is low enough that it will not interfere with subsequent separation of americium from rare earths by amine extraction from concentrated lithium chloride solution.

Dialkylphosphate Extraction of Bk^{4+}

In a brief investigation of Bk^{4+} extraction, both ozone and $KBrO_3$ were satisfactory oxidants for preparing Bk^{4+} in concentrated nitric acid solutions prior to extraction. Attempts to extract it from 8 *M* HNO_3 into 30% di-2-ethylhexylphosphoric acid (D2EHPA) in toluene, diethylbenzene, or Amsco 125-82 diluent were unsuccessful because of reduction by the diluent. Distribution coefficients (o/a) between 30% D2EHPA in decane or hexane diluent and 8 *M* HNO_3 were 10^3 for Bk^{4+} and 10^{-3} for Cm^{3+}; Zr^{4+} had almost the same extraction properties as Bk^{4+}.

Separation of Californium, Einsteinium, and Fermium by Cation Exchange

Separation of Cf, Es, and Fm by chromatographic elution with ammonium α-hydroxyisobutyrate from

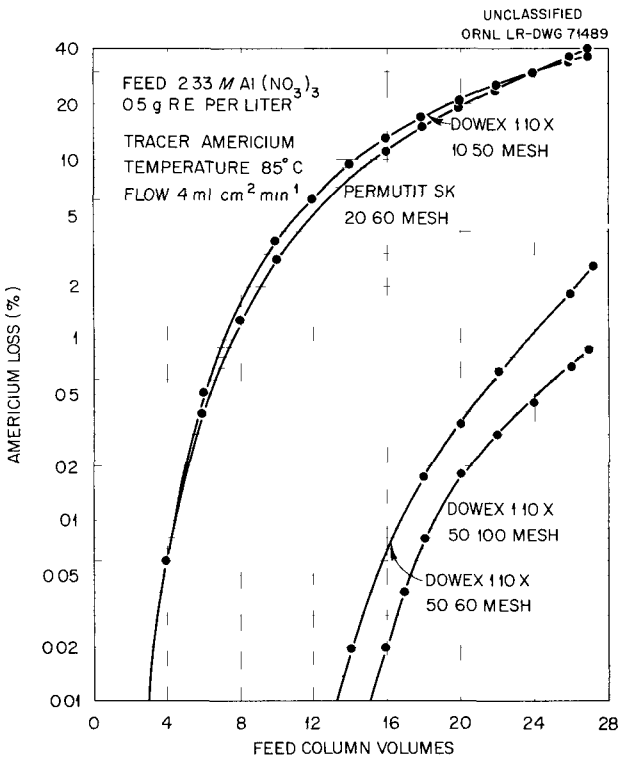

Fig. 6.11. Effect of Resin Type and Mesh Size on Americium Loading from 2.33 M $Al(NO_3)_3$.

cation exchange resin[6,7] was tested. Irradiation of 0.4 μg of Cf^{252} in the Oak Ridge Reactor for 28 days produced 0.26 nanogram of Es^{253} and about 0.3 picogram of Fm^{254}. After 1 day's decay, most of the fission products and target impurities were removed by anion exchange from concentrated HCl and LiCl solutions. The Cf, Es, and Fm were loaded on a column of Dowex 50-12X (200–400 mesh) resin, which had a cross sectional area of 0.03 cm^2 and a length of 20 cm. Elution with 0.4 M ammonium α-hydroxyisobutyrate at pH 4.1 was carried out at 80°C and at a flow rate of 0.6 ml min^{-1} cm^{-2}.

During elution fermium is removed first, followed by einsteinium and then californium. By the time 0.3% of the californium was eluted, 20% of the einsteinium and 60% of the fermium were recovered. When 10% of the californium was eluted, 80% of the einsteinium and 90% of the fermium were eluted.

The conditions needed for good separations are a perfect column with no channeling, very slow flow rates, and collection of small product fractions. During such a run a bubble developed near the bottom of the column and disturbance of the individual bands prevented separation. Considerable difficulty would probably be experienced in processing of large quantities of californium because of radiolytic gas bubbles.

The Use of Higher Americium Oxidization States to Separate Americium from Curium

In a brief investigation of methods of separating americium and curium based on oxidation of americium, Am^{4+} was readily produced by heating freshly precipitated $Am(OH)_3$ in 0.2 M NaOH–0.2 M NaOCl at 90°C for 30 min. The pink $Am(OH)_3$ changed to black $Am(OH)_4$, which was dissolved in 15 M NH_4F, with a solubility of about 5 g/liter. Curium remained trivalent, with a solubility of less than 1 mg per liter.

Treatment of freshly precipitated $Am(OH)_3$ with ozone in 0.05 M NaOH oxidized the americium to Am^{6+} and formed a soluble hydroxide complex with a solubility of more than 100 mg per liter. Again, curium remained trivalent and was insoluble.

When americium and curium hydroxides were dissolved in 3 M K_2CO_3 and treated with ozone, the americium was rapidly oxidized and formed an intense red-brown soluble Am^{6+} carbonate complex. Upon standing for 24 hr, the red-brown color disappeared and a precipitate of Am^{5+} carbonate formed, leaving the curium in solution. The precipitate contained 80% of the americium and less than 1% of the curium.

Separation by Inorganic Ion Exchangers

A systematic survey is being made of the possible utility of inorganic ion exchangers in radiochemical processing, especially in the recovery and separation of fission products and elements encountered in the production of transplutonium elements. The greater radiation stability of inorganic, compared with organic, exchangers offers a significant advantage.

[6] G. R. Choppin, B. G. Harvey, and S. G. Thompson, *J. Inorg. Nucl. Chem.* 2, 66 (1956).

[7] H. Louise Smith and Darleane C. Hoffman, *J. Inorg. Nucl. Chem.* 3, 243 (1956).

In preliminary tests, americium and europium were completely separated by elution of the europium from zirconium phosphate with a concentrated lithium chloride solution (Fig. 6.12); the americium was subsequently completely eluted with 1 *N* HCl. Separation of americium from cerium in similar experiments was small. Thus this technique does not provide a means of separating the transplutoniums from the fission product lanthanide group.

Zirconium phosphate, zirconium tungstate, and ammonium molybdophosphate differed considerably in the order of their adsorption of elements in the lanthanide series (Fig. 6.13). Single-stage separation factors between adjoining lanthanides were less than 1.4. A column elution from zirconium phosphate indicated no greater separation between americium and curium. Comparative adsorption and elution of other fission products and process-derived contaminants are being studied to determine the possibility of separating them from the transplutonium elements.

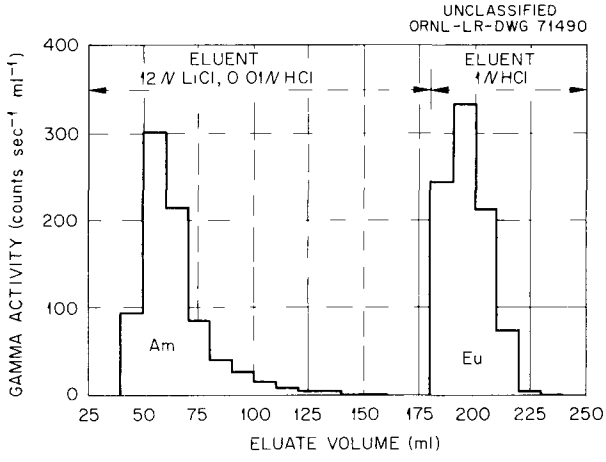

Fig. 6.12. Separation of Am^{241} from Eu^{152} by Zirconium Phosphate. Column 25 cm high, 20 ml volume.

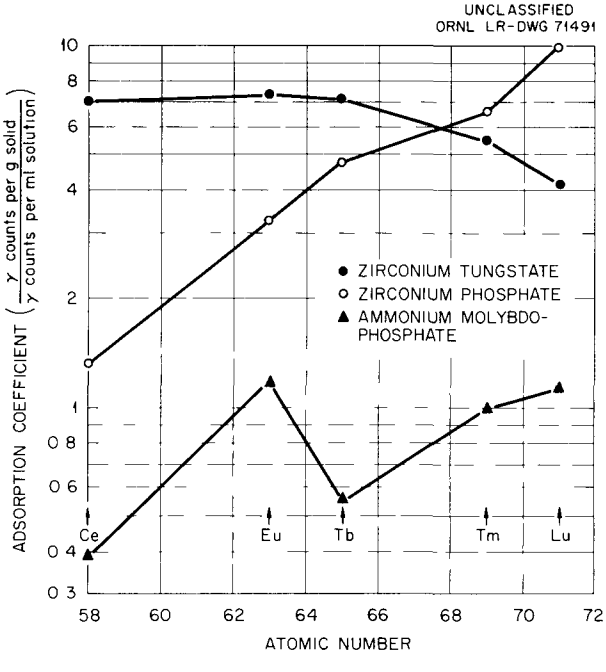

Fig. 6.13. Adsorption of Lanthanides from 10 N LiCl 0.01 N HCl.

Effect of Alpha Radiation on Corrosion

Scouting corrosion tests[8] were made on glass and welded specimens of tantalum, Hastelloys B and C, titanium 45A, and Zircaloy-2 exposed to chloride solutions containing Am^{241} (20 g/liter). This represents a power density of 2 w/liter. No direct effects of alpha radiation on corrosion were found. Secondary effects, which are attributed to the presence of H_2O_2 produced by radiolysis of water, were noted for Hastelloys B and C and for titanium 45A. Under conditions that allowed appreciable buildup of H_2O_2 concentration, the corrosion rates of Hastelloys B and C were increased, and the corrosion of titanium was drastically decreased. Corrosion rates of glass and tantalum were less than 1 mil/yr, and the corrosion of Zircaloy-2 was less than 10 mils/yr for all conditions tested.

The tests were made by immersing corrosion specimens (1 cm × 2 cm × $\frac{1}{32}$ to $\frac{1}{8}$ in. thick) in Pyrex glass test tubes containing 10 ml of solution. Other specimens were suspended in the vapor phase on a tantalum wire. Solutions used were 6 *M* HCl and 10 *M* LiCl–0.5 *M* HCl, each containing Am^{241} at a concentration of 20 g/liter. Control solutions were identical except that nonradioactive lanthanum was substituted for Am^{241}. Tests were made at 45°C and at near boiling for 7 days. Corrosion rates were determined by weighing the specimens both before and after exposure to the chloride solution.

[8] R. D. Baybarz, *The Effect of High Alpha Radiation on the Corrosion of Metals Exposed to Chloride Solutions*, ORNL-3265 (Mar. 27, 1962).

6.2 DESIGN OF EXPERIMENTAL FACILITIES

The TRU Processing Plant chemical flowsheets developed during the past few years were tested at radiation levels limited by the containment standards and shielding available in an alpha laboratory. Equipment in cells 3 and 4 of building 4507 will provide facilities for testing the processes discussed in Sec 6.1 at radiation levels to be encountered in the final processing plant. Americium-curium will be separated from rare-earth fission products and irradiated materials processed to isolate californium in these cells.

Figure 6.14 is the schematic equipment flowsheet for the final solvent extraction isolation of americium and curium from the plutonium processing raffinate. The bulk of the aluminum and fission products will be removed by ion exchange and the Am–Cm–rare-earth solution evaporated to 100 liters in cell 1, building 4507 in preparation for solvent extraction processing in cell 4.

Figure 6.15 is the schematic equipment flowsheet, including head-end equipment for the dissolution of a 6-month-irradiated HFIR target for carrying out actinide recovery and the separation of Am-Cm, Bk, Cf and higher-isotope fractions. This dissolution equipment and the equipment required for the separation of berkelium from californium and higher isotopes will be installed in cell 3.

Equipment Description and Arrangement

The equipment will be installed so that it may be removed by heavy-duty manipulators, an impact wrench, and a crane mounted in the large equipment-removal cubicle located on the top of the cell bank. The equipment will be in a modular arrangement to allow relocation or replacement of all cell tanks in a standard support frame (Fig. 6.16). The piping between tanks and racks will be joined with disconnects similar to those to be used in the TRU Facility, which will be operable with a manipulator. The solvent extraction equipment and other miscellaneous items will be located in racks supported on top of the tankage framework. These racks will also be removable through the roof hatch.

Figure 6.17 is an elevation view through the cell and service areas, and Fig. 6.18 illustrates a typical tank-piping arrangement.

Shielding

The highest neutron sources proposed for use in the cells will be in a 6-month-irradiated, 30-day-decayed HFIR target, whose properties are:

Cf^{252} content, μg	350
Cf^{254} content, % of Cf^{252}	0.52
Cf neutron source, neutrons/sec	3.5×10^9
1.7-Mev gamma source, Mev/sec	$\sim 2 \times 10^{13}$

The calculated dose rates from this target are:

Fission product gamma dose rate through window or wall, mr/hr	<0.01
Neutron dose rate through barytes wall, mrem/hr	0.026
Neutron dose rate through window, mrem/hr	3.3

These dose rates are expected to be accurate within a factor of 2, assuming that the neutron-source strengths are correct.

The fission product gamma attenuation through the wall and window, and the neutron attenuation through the wall, were calculated from measured attenuation coefficients and removal cross sections. The neutron attenuation through the window was determined with the Renupak neutron transport code on the IBM 7090 computer.

Schedule

The new Am–Cm–rare-earth storage tanks were installed in cell 4 pit in July. Process equipment installation and cell containment modification are scheduled to be essentially complete for initial cold checkout runs beginning in November 1962.

6.3 PROCESS DESIGN

When the TRU Facility is ready for full-scale operation in January 1966, the first HFIR loading of 31 rods will have been irradiated about 16 months, discharged from the reactor, and be awaiting processing. The chemical processing system is designed for a throughput rate of one target per day, which will permit processing 10

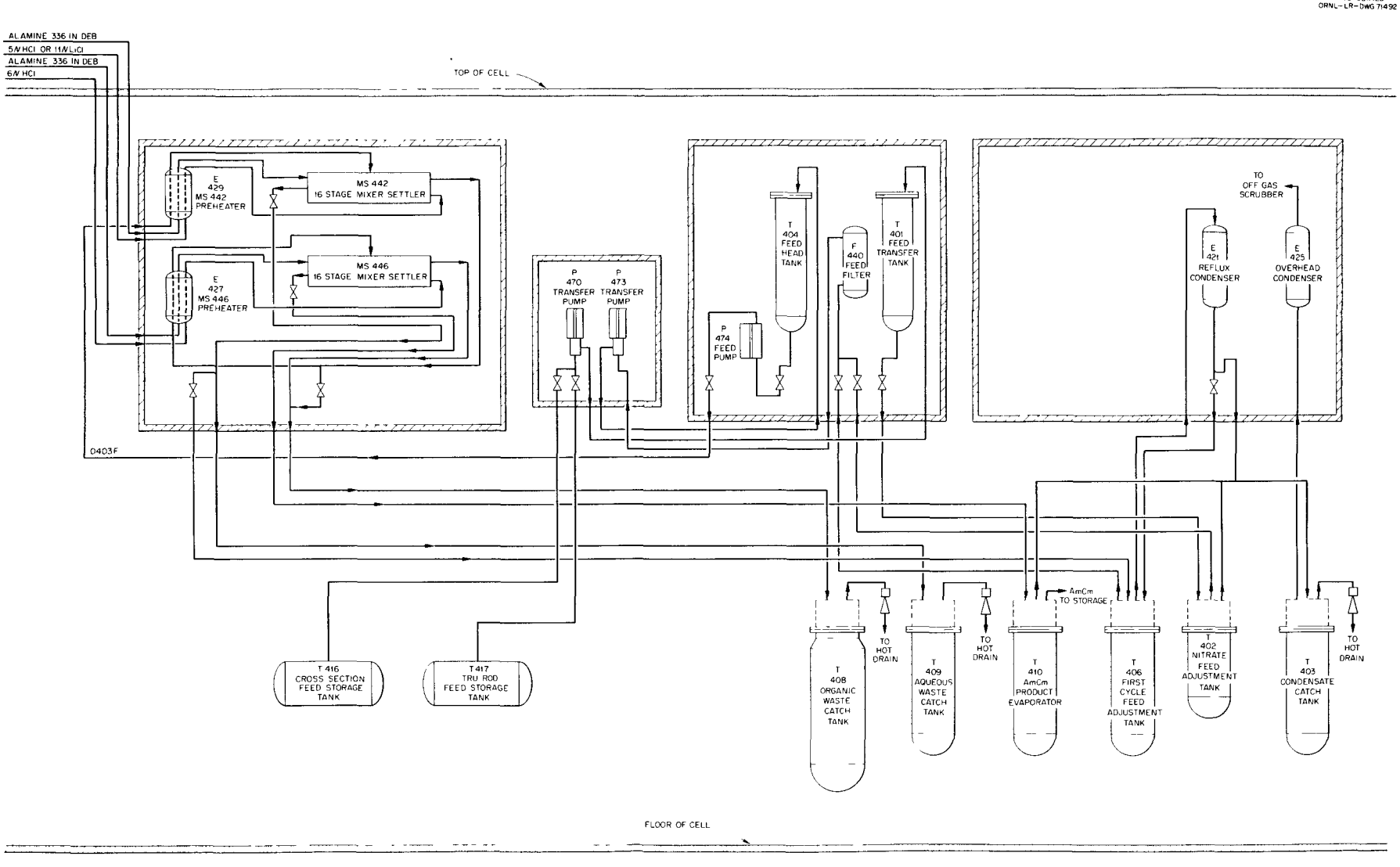

Fig. 6.14. Americium-Curium Recovery: Equipment Flowsheet.

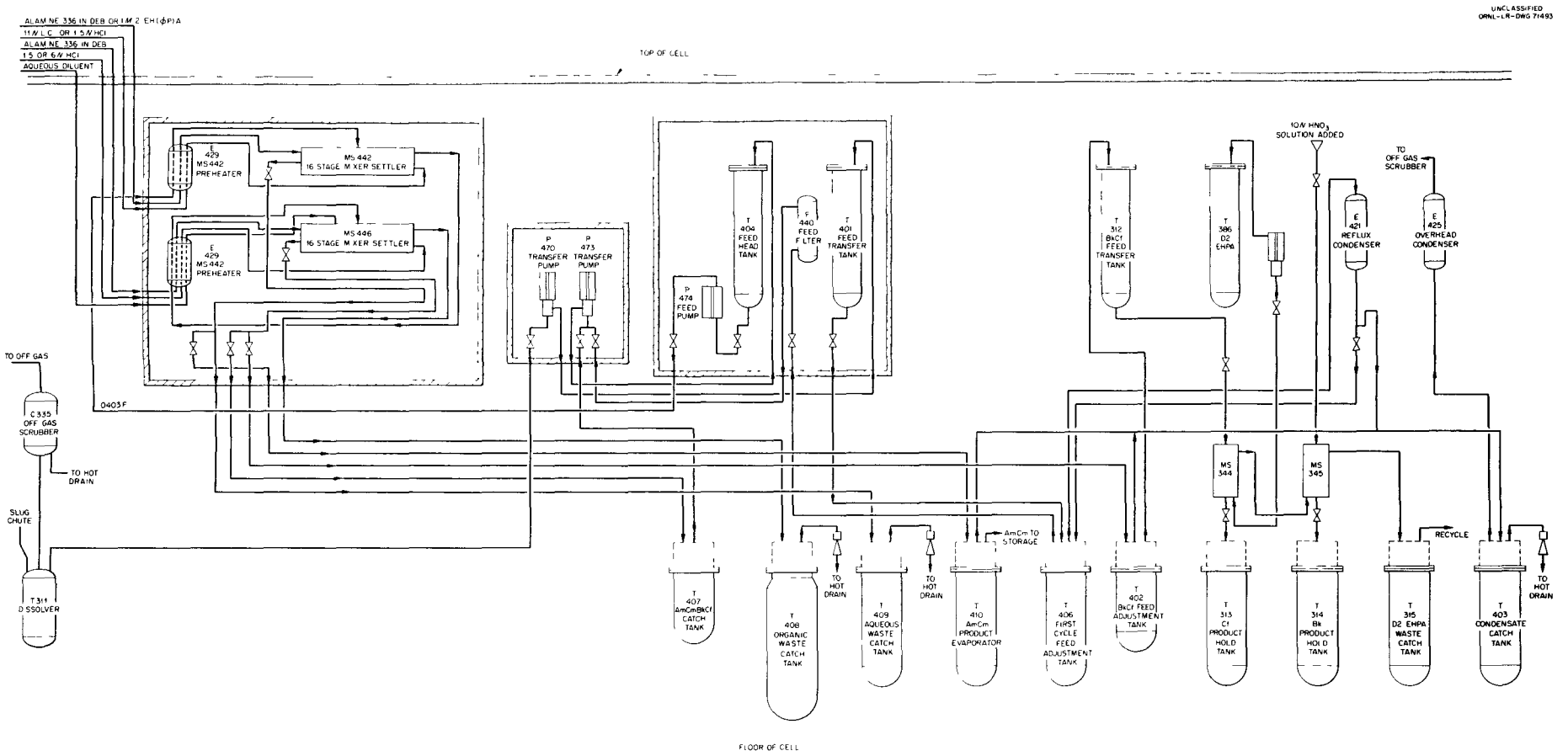

Fig. 6.15. Target Processing Equipment Flowsheet.

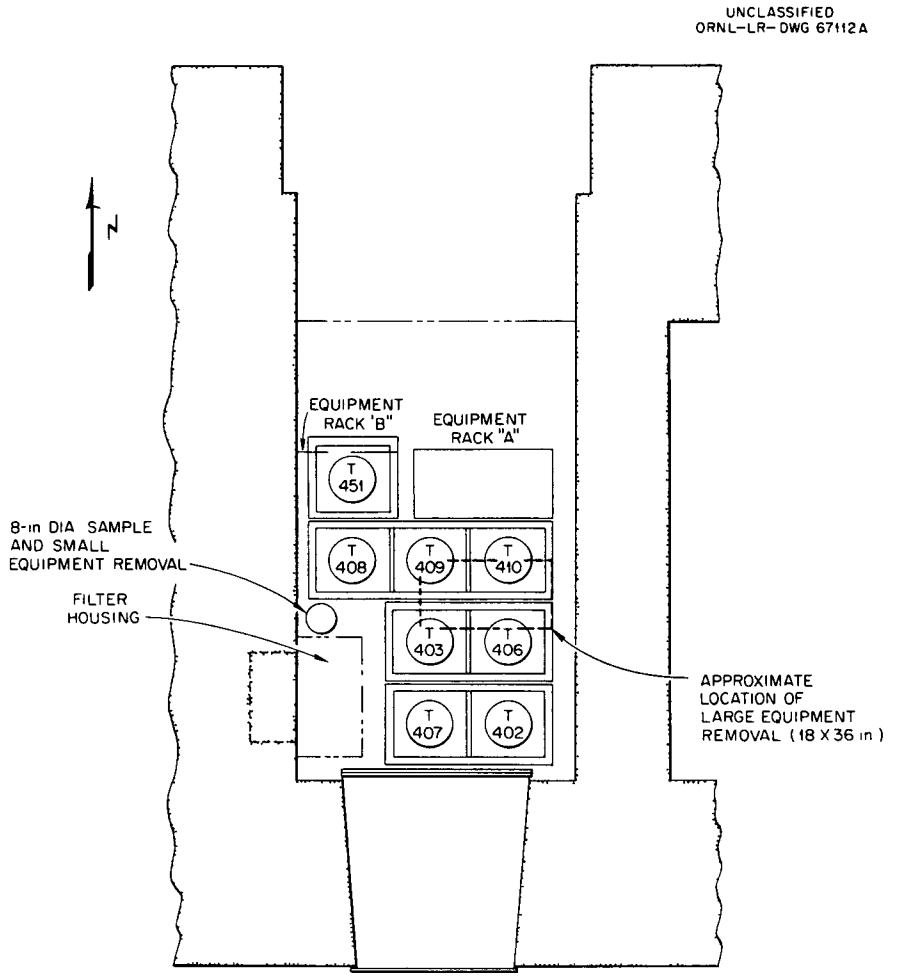

Fig. 6.16. Cell Equipment Plan.

first-cycle plutonium rods per month on a semi-continuous basis; thus, approximately three months will be required to process the first loading and fabricate the curium isotopes into recycle rods for further irradiation. At the design capacity, no more than 50% of the time will be required for main-line processing. The remainder is reserved for special separations, equipment modifications, and maintenance. On a long-term basis, about 40 target rods will be processed per year, half of which are first-cycle and the remainder recycle rods. One hundred milligrams of californium will be recovered from the initial HFIR loading, and two years after startup of the TRU Facility the californium inventory should reach 1 g.

Dissolution of Aluminum

The dissolution rate of the aluminum targets must be kept below 1 mg min^{-1} cm^{-2} in order to control the rate of evolution of hydrogen, the volume of which, plus purge gas to dilute it below the explosive level, could otherwise exceed the design capacity of the off-gas system. Calculations have shown that this can be done by temperature control of the dissolution rate because of the large heat transfer coefficient and the relatively modest temperature coefficient of the dissolution rate. Measurements of the heat transfer from dissolving aluminum showed effective heat transfer coefficients for a vertical rod

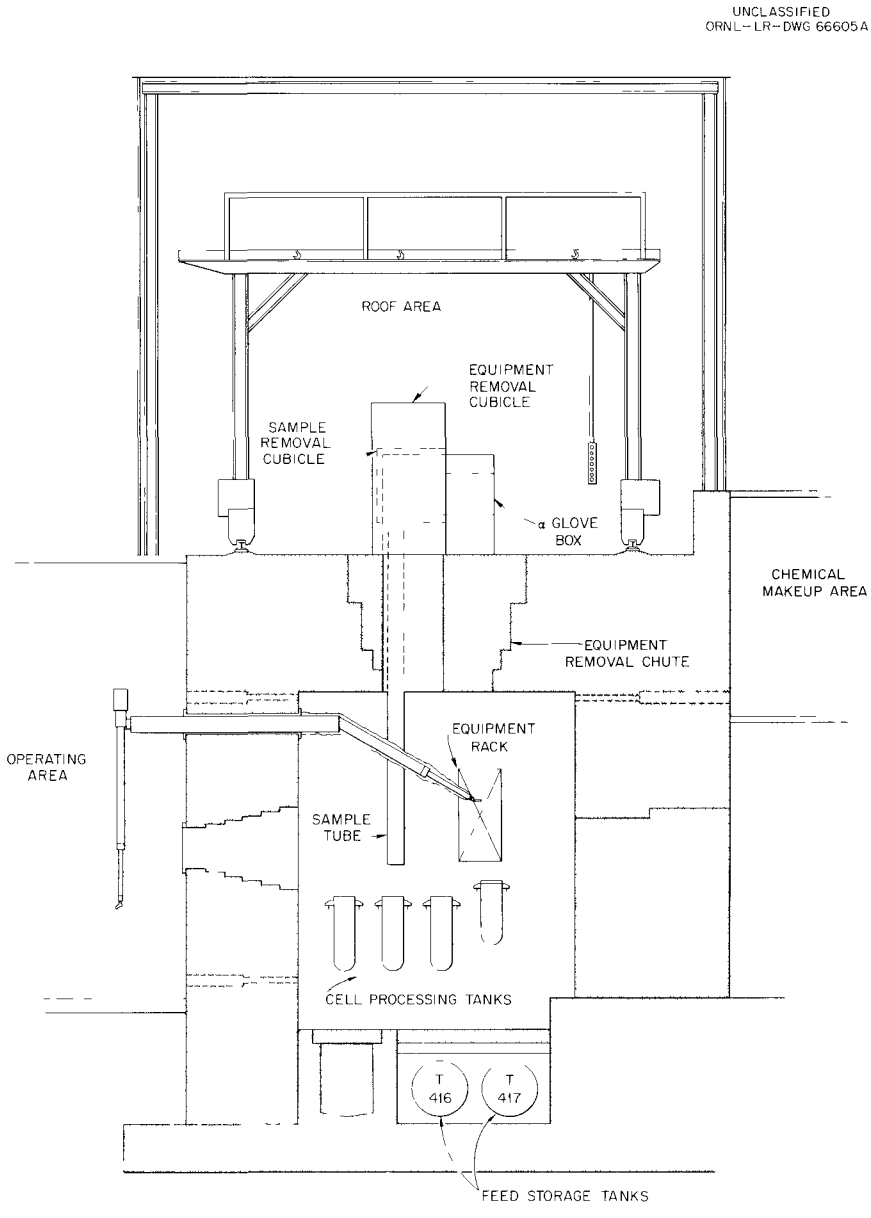

Fig. 6.17. Sectional View: Cell No. 4, Building 4507.

varying from 500 to 1300 Btu hr^{-1} ft^{-2} $(°F)^{-1}$, depending on the dissolution rate. Evidently the strong evolution of hydrogen from the aluminum surface creates as much circulation of the bulk liquid as a draft tube does. Heat transfer is probably further improved by the scouring action of the hydrogen bubbles as they agitate the stagnant surface film.

Solvent Extraction Calculations

An Oracle code, KREMSER-MURPHREE, was prepared and used to calculate the behavior of five actinide elements in the second solvent extraction cycle of TRU flowsheet and from distribution coefficient data. Results of four calculations (Fig. 6.19) showed that if the normalities of the feed

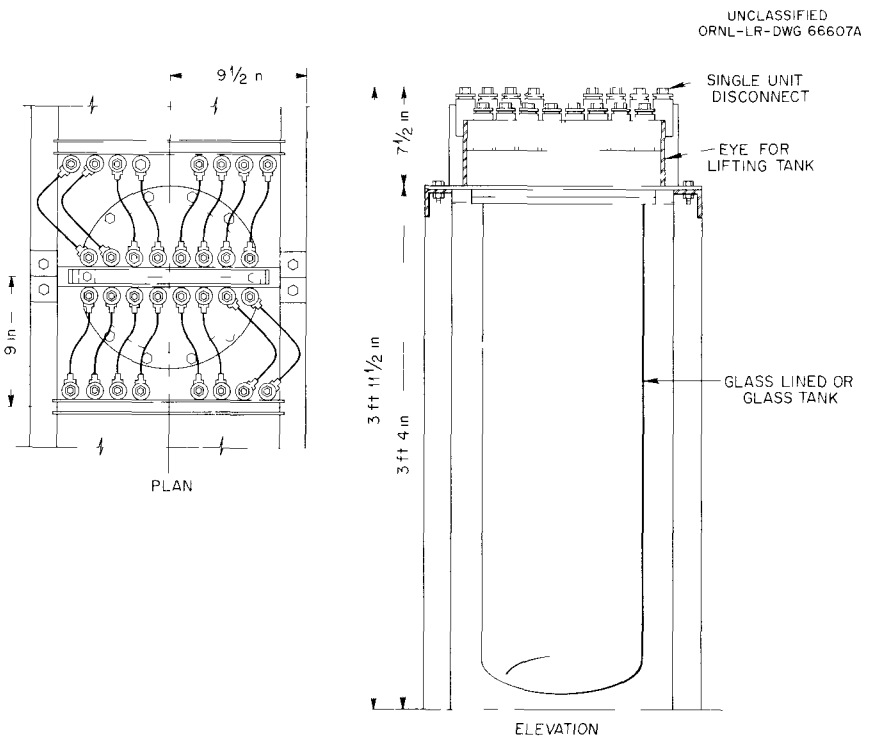

Fig. 6.18. Typical Cell Tank Piping Arrangement.

and scrub are less than 1.55, berkelium will be preferentially extracted and can be separated from curium. At an acid normality of 1.0, berkelium recovery would be greater than 99.9%, with curium contamination reduced by a factor of more than 10^5.

A further set of calculations was made for the same feed except that the feed acidity was constant at 0.5 *M* and the scrub acidity was varied. The results (Fig. 6.20) indicate an increase in over-all performance, with both an increase in berkelium recovery and a decrease in curium contamination of the berkelium product.

At higher acidities the berkelium will tend to remain in the raffinate and hence can be separated from californium, but the separation is probably not practical because of the smaller difference in distribution coefficients.

A partitioning solution with an acidity of 1.9 *N* and a feed of berkelium and californium in the organic phase were assumed. A berkelium recovery of 95% with the californium contamination decreased by a factor of 100 was specified. The scrub and extractant flow ratios were varied, and the number of stages required to achieve the specified separation were computed. The calculations (Fig. 6.21) showed that the separation of berkelium and californium by this system is very marginal.

A single calculation indicated that the separation of americium from curium is not practical. Conditions were probably not optimal, but 32 stages (70% efficiency) gave 99.6% curium recovery, with only half the americium removed.

HFIR Target Design

A preliminary HFIR target design has been developed in cooperation with groups in the Reactor Division and the Metals and Ceramics Division. The active portion of the target consists of a 20-in.-long column of 0.25-in.-diam × 0.50-in.-long pellets, which are fabricated by pressing about 18 vol % actinide oxide-82 vol % aluminum powder inside an aluminum can to a density (89 ± 3)% of theoretical. The 35-in.-long target is fabricated by

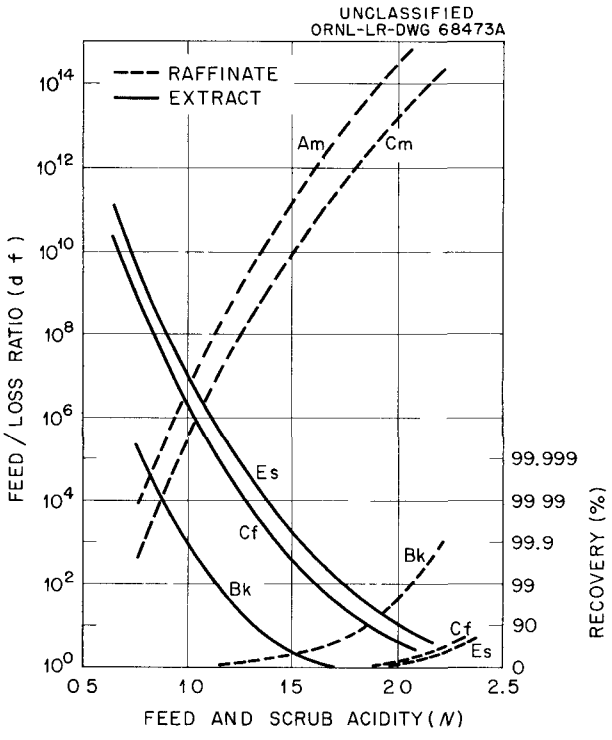

Fig. 6.19. Calculated Actinide Recovery and Decontamination in Phosphonate Extraction from HCl Solution by 1.0 M 2-EH(ϕP)A in DEB. Hydrochloric acid concentration in scrub same as that in feed. Extraction section: 8 stages, 70% Murphree efficiency. Scrubbing section: 8 stages, 70% Murphree efficiency. Scrub/feed flow ratio = 1; extraction/feed flow ratio = 2, Either ordinate can be used for all curves in Figs. 6.19 and 6.20. The one on the total expresses the results as a ratio of the amount of a component in the feed to the amount of that component lost. The other ordinate expresses the percentage recovery of that component.

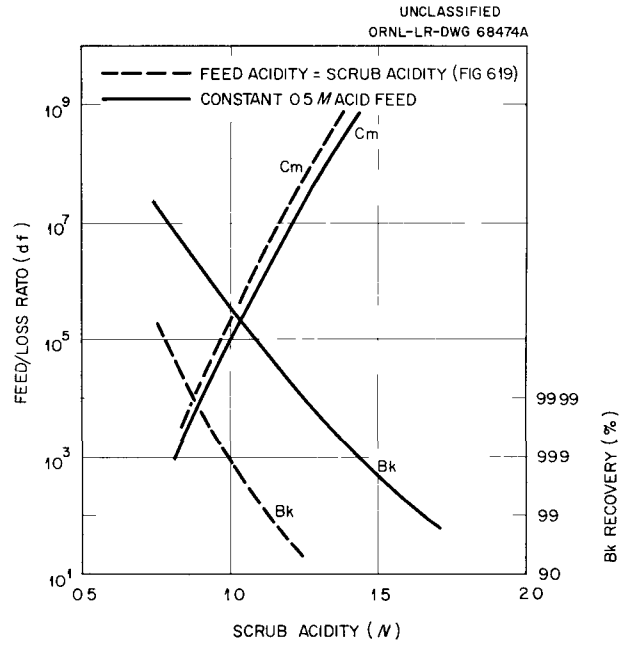

Fig. 6.20. Effect of Feed Acidity on Distribution of Berkelium and Curium between Raffinate and Extractant. (See Fig. 6.19.

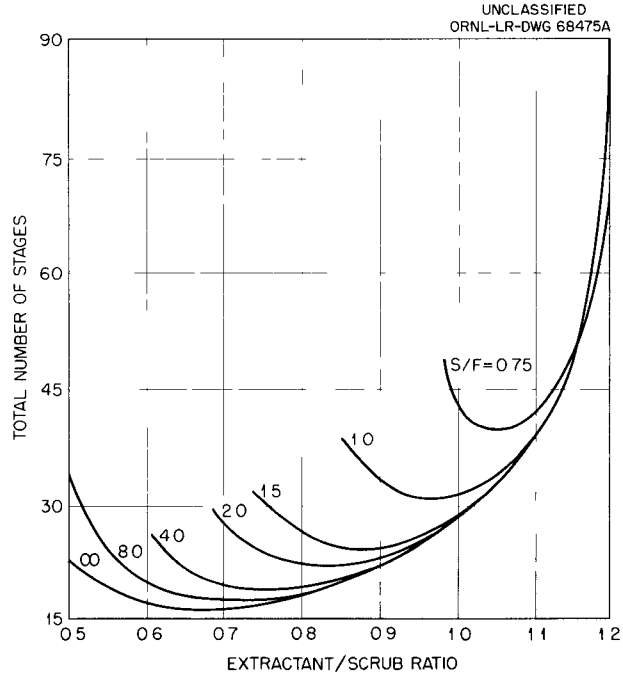

Fig. 6.21. Number of Stages Required to Partition Berkelium from Californium as a Function of Extractant/Scrub Ratio with Varying Scrub/Feed Ratio. Specifications: 95% berkelium recovery, californium decontamination factor of 100.

hydrostatically collapsing a finned, type X-8001 aluminum tube, sealed by welded end caps, onto the pellet column and tack-welding a hexagonal type X-8001 aluminum can to the fins.

The target is designed for irradiation to a total *nvt* of 1.5×10^{23} (1.5 yr at 3×10^{15} flux), with hot-spot heat fluxes of 10^6 Btu hr^{-1} ft^{-2}. Fission gas release in the target is to be accommodated by providing a reinforced void at each end of the pellet column.

The allowable transferable alpha contamination on the target surface was calculated to be approximately 10^4 dis/min per 100 cm^2 by considering the

allowable fission product and actinide concentration in the HFIR coolant and the possible effects of an accident during transfer of the target from TRU to HFIR.

6.4 PROCESS EQUIPMENT DEVELOPMENT

Solvent Extraction Contactors

The separation of transuranium elements from fission products and from each other requires several solvent extraction systems of widely divergent physical properties. A box type mixer-settler was modified to facilitate the testing of flowsheets and possible production application. The modifications were: a change in impeller design to improve mixing and installation of an interface control weir between stages to allow a wider range of mixer speed without causing excessive pumping and loss of interface, which results in loss of efficiency due to backmixing. The modified mixer-settler was demonstrated hydraulically with solvent-aqueous pairs having density differences ranging from 0.051 to 0.48 g/cc and viscosities from 0.81 to 6.0 centipoises (Table 6.3). The speed required for good dispersion and for loss of interface increased with density difference. The flow capacity decreased with increased viscosity of the organic (the continuous) phase but was nearly independent of the viscosity of the aqueous phase.

Stage efficiency was greater than 90% in the modified mixer-settler with a 30% TBP–1.5 *M* $Al(NO_3)_3$ system and with a 30% tertiary amine–11 *M* LiCl system, both of which have a relatively high viscosity aqueous phase and represent difficult extraction systems.

The development of small pulsed columns is also underway for the TRU facility because of their simplicity and better adaptability to remote

Table 6.3. Mixer-Settler Hydraulic Data

Test Solutions	Specific Gravity at 25°C	Specific Gravity Difference, Aqueous-Organic	Viscosity at 30°C (centipoises)	Mixer Speed Required for Good Dispersion (rpm)	Maximum[a] Flow Rate (ml/min)	Mixer Speed Required to Pump out Aqueous-Organic Interface at no Aqueous Flow (rpm)
1 wt % HNO_3,	1.00513		0.807		20	
85% TBP in Amsco	0.9547	0.0506	3.31	1000	20	> 1000
10 wt % HNO_3,	1.0335		0.826		20	
85% TBP in Amsco	0.9547	0.0788	3.31	1000	20	> 1000
1.5 *M* HCl,	1.0168		0.872		10	
30% Alamine-336 in DEB	0.8713	0.1455	6.05	1300	10	1400
1.5 *M* HCl,	1.0168		0.873		35	
Diethylbenzene	0.8603	0.1565	0.924	1300	35	1700
1 wt % HNO_3,	1.0053		0.807		20	
5% TBP in Amsco	0.7648	0.2405	1.26	1850	30	2150
11 *M* LiCl,	1.2420		5.96		8	
30% Alamine-336 in DEB	0.8713	0.3707	6.05	1600	8	> 2000
11 *M* LiCl,	1.2420		5.96		20	
5% TBP in Amsco	0.7648	0.4772	1.26	2770[b]	30	> 2770

[a] At mixer speed required to give good dispersion.

[b] Poor dispersion.

operation. Tests with the 30% amine–11 *M* LiCl system demonstrated 18 in. stage height in a sieve plate column with ¼-in. plate spacing and a pulse frequency of 100 to 190 cpm. The flow capacity was approximately 60 gal ft^{-2} hr^{-1} at 25°C and 120 gal ft^{-2} hr^{-1} at 50°C. Pulsed packed columns have a lower flow capacity and stage efficiency but are simpler in construction.

Disconnects

A test program to select a disconnect design for use in the TRU processing cells was completed. An area seal between a female half of 20° included angle and a male half of 18° angle appears superior to the line contact seal obtained with lower sealing forces. These seals leaked less than 10^{-8} cc of helium per second after ten makes and breaks. Leak-tight closures were also obtained for interchanged halves, for up to 0.5° misalignment, for 2–4 mil deep center punch marks to simulate mechanical damage, and for dimensional variations exceeding those necessary for economical manufacture. A continuous scratch across the sealing surface did cause leakage. In accelerated corrosion tests with aqua regia, the 1/16-in.-thick-wall tubing was completely penetrated by the acid without any leakage at the disconnect seal. A moment force of as much as 390-lb-in. from the connecting tubing will not prevent leak-tight closure.

The original design of the disconnect calls for welding the disconnect parts and the Hastelloy lines. Heat treatment of the disconnect, which increases the corrosive resistance of the weld, prevented a leak-tight closure. Other means of fastening the disconnect to the connecting tubing are being investigated.

Glovebox Fire Tests

Fire tests conducted in the proposed Transuranium glovebox demonstrated the necessity for promptly extinguishing the fire to prevent containment loss due to possible burn-through of the rubber gloves and to prevent heat buildup in the glovebox floor, which in each test produced an explosive mixture due to the increased evaporation rate of the solvent. Explosion tests demonstrated the necessity for preventing explosive concentrations in the glovebox; the ignition of an ortho-xylene air mixture just inside the explosive range produced pressure sufficient to rupture the window seals.

Tests of fire-extinguishing system components indicated that an optimal protection system would consist of a standard, commercial water-spray nozzle with a small reservoir containing 2 to 3 gal of water under a reliable pressure force such as a spring or dead weight.

6.5 TRU FACILITY DESIGN

The cell bank of the Transuranium Facility was decreased from twelve to nine cells (Fig. 6.22), and back access was provided for the two analytical cells. The pit area behind these cells is covered with 4-ft-thick shielding plugs.

A preliminary issue of the conceptual report was made on March 2, 1962. All Title I drawings were completed by the architect-engineer and reviewed by ORNL. A total of 105 drawings were required.

Title II engineering was initiated in May to be completed in mid-April 1963 (Fig. 6.23). About one year is allotted for process equipment installation and break-in, with initial hot operation scheduled for January 1, 1966.

Schematic flowsheets developed from chemical flowsheets for the main-line processing (Figs. 6.24 and 6.25) provide for dissolution, feed adjustment, and first-cycle solvent extraction in cell 7. Americium and curium will be separated from the higher actinides by solvent extraction, and Bk, Cf, Es, and Fm will be separated by ion exchange in cell 6. Flowsheets for product purification and special product separations (in cell 5) have not been developed.

In cell 4, curium will be purified and precipitated for subsequent calcination and fabrication into recycle rods. Tankage for the various processes is located, where possible, in tank pits of the respective cells where the solvent contactors or ion exchange columns are located. Tank-pit space in cells 1, 2, and 3 behind the target fabrication cubicles must be used for some product storage tanks and rework systems.

Conceptual Layouts

All vulnerable process equipment will be located on removable racks in the cubicles, with

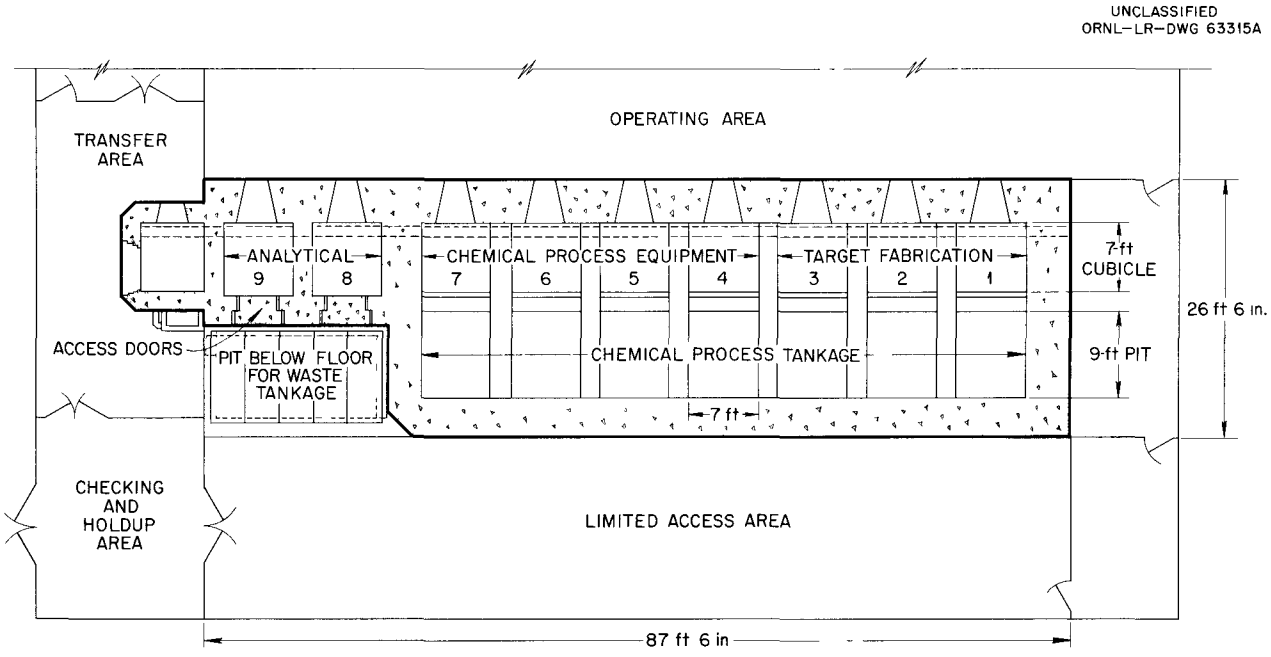

Fig. 6.22. Space Allocation in TRU Cell Bank.

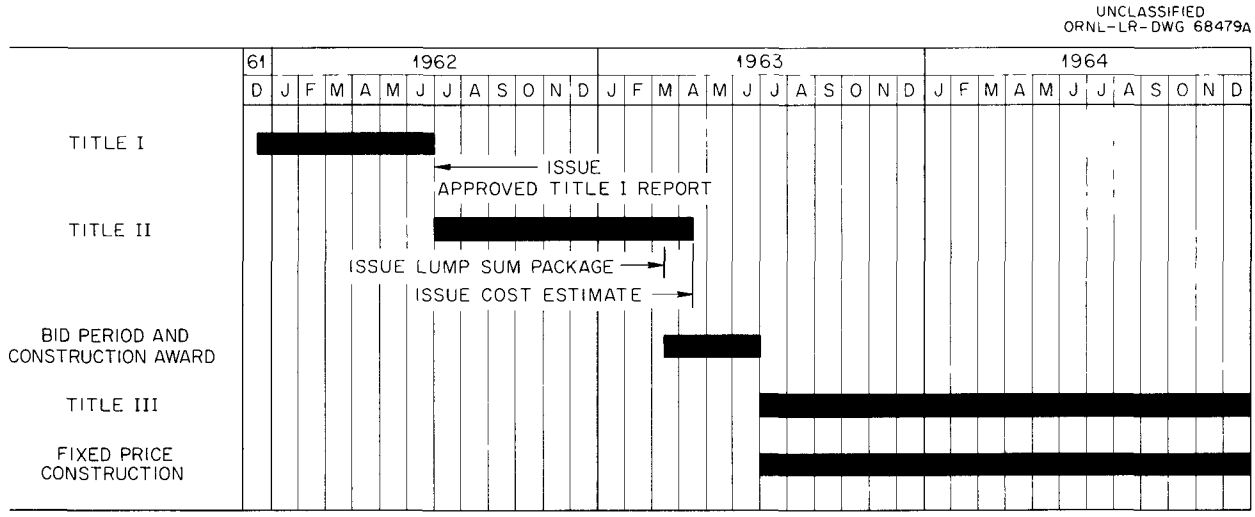

Fig. 6.23. TRU Engineering and Construction Schedule.

three racks about 36 in. long, 18 in. wide, and 6 ft high in each cubicle (see Fig. 6.26). Incorporated into the lower half of the back rack is a sampler system containing diaphragm pumps in order to pump solutions through the needle block assembly and the mechanisms for handling sample bottles. Service lines enter through the cubicle ceiling and are joined to the equipment at the rear of each rack with a standard TRU disconnect (Fig. 6.27). Process jumper lines, provided with similar disconnects, join the various equipment racks, samplers, and hot-disconnect wells through which solutions are routed to the tank pits behind the cubicles. Maintenance to be

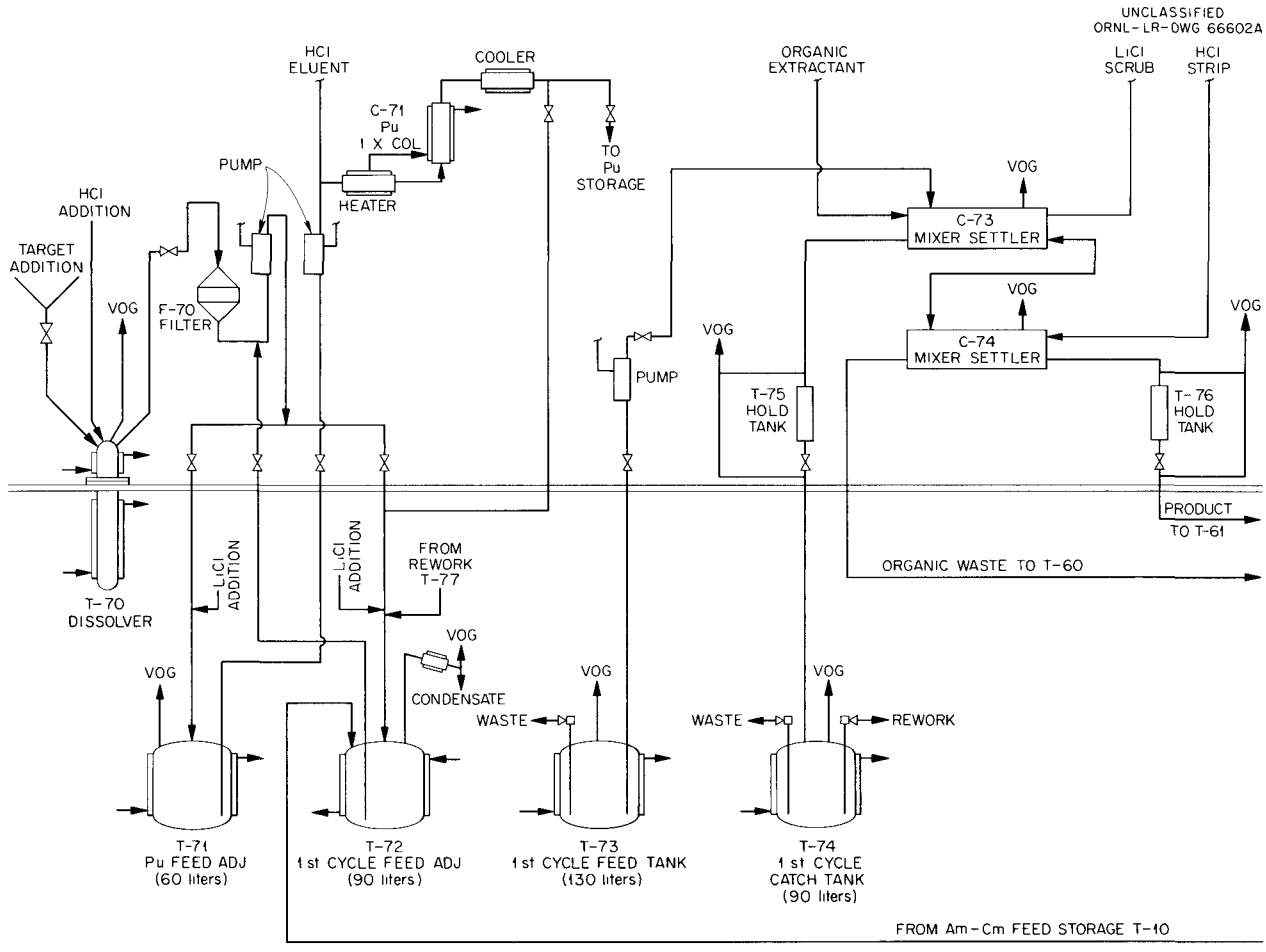

Fig. 6.24. Target Processing Equipment Flowsheet, Cell 7.

performed by the in-cell master-slave manipulators includes replacement of individual components such as pumps, valves, and sample needle blocks and installation of entirely new equipment racks. Conceptual layouts (e.g., Fig. 6.28) of all main-line process equipment were made to ensure that adequate space was available for all required operations.

All tanks (Figs. 6.29 and 6.30), which should require only infrequent maintenance, are located in the tank pits behind the cubicles. Because of the high probability of corrosion failures and the necessity for designing a flexible system that can be modified if desired, all tanks and piping in the tank pits are designed to be replaceable with the use of water-shielding and overhead-maintenance techniques. Service lines penetrate the rear wall and contain a disconnect at the inner cell wall. Process jumper lines, which connect the various tanks, waste and off-gas headers, and cubicle hot well, may be replaced or rerouted as required. Tank elevations are such that a minimum of 3 ft of water shielding covers all tanks when the pit is flooded to the maximum level. All disconnects are located above this water level so that the tanks will not fill when the cell is flooded.

Detailed Design Features

Hot Disconnect Well. – Spare lines will be incorporated into the two line bundles connecting cubicles and tank pits, but complete reliance on a permanent nonreplaceable installation does not

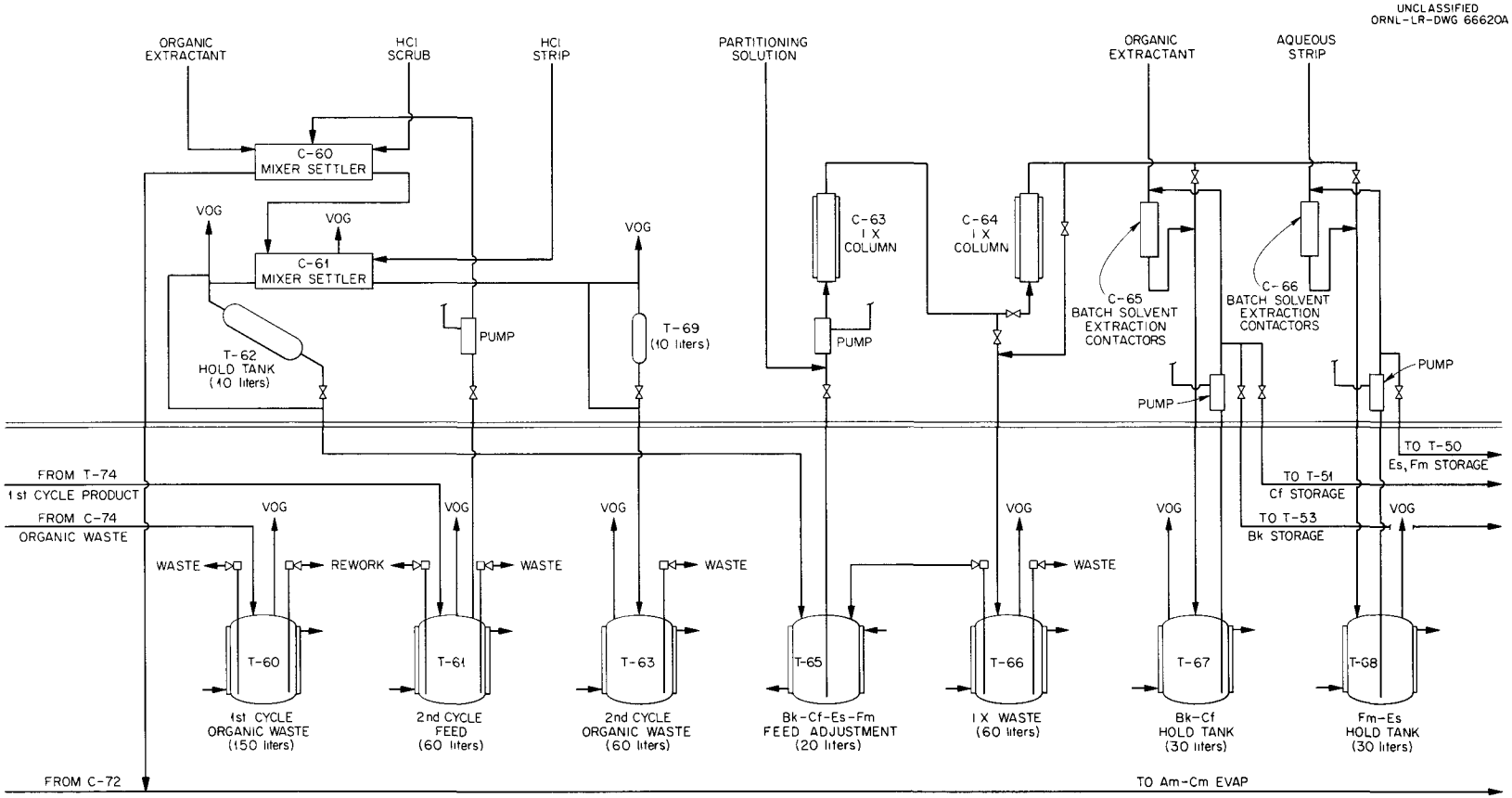

Fig. 6.25. TRU Equipment Flowsheet, Cell 6.

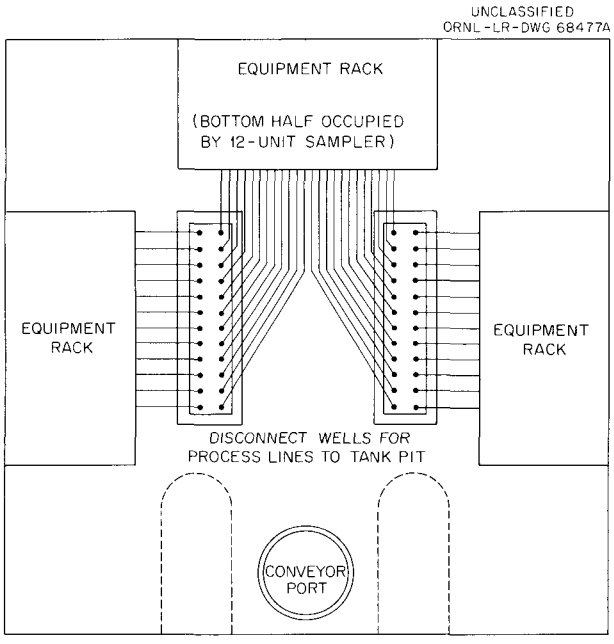

Fig. 6.26. Typical Cubicle Layout Plan.

appear logical. Therefore these line bundles with their hot-disconnect well in the cubicle floor and disconnect terminal block on the tank pit were designed for remote replacement (Fig. 6.31). After removal of all process jumper lines connected to both ends of this bundle, the well in the floor of the cubicle is unbolted from the cubicle and the assembly dropped onto tracks suspended from the cubicle floor. The entire unit is then withdrawn into the tank pit by a cable and pulley arrangement. A new bundle is installed by reversing these operations.

Tank-Pit Service Plug. – Service lines to the tank pits will be brought in through stepped concrete plugs (Fig. 6.32). All lines to any tank will be brought through the same plug. Present plans call for only one disconnect in each service line, to be located at the cell side of the plug. The female half of the disconnects on the tank end of the service lines will be mounted in a support bracket, which bolts to the face of the plug and at the same time aligns both halves of the disconnects. The 0.5-in.-diam lines are offset 1.5 in. in the plug to minimize streaming.

Vents on Steam Supply Lines to Process Jets. – A system designed to vent steam supply lines to process jets and thus prevent solution from being drawn back into the line by condensing steam functioned properly in engineering tests. A continuous air purge of 200 cc/min is discharged into the steam line from a 100-psi air header through a 500-cc accumulator. Following a jetting operation, residual steam is purged from the line before sufficient condensation occurs to suck solution more than a few inches up the steam line. Such a system is cheap, requires no elaborate instrumentation and thus should be essentially foolproof. The total purge rate through all jets (about 10 liters/min) will not tax the capacity of the off-gas system. Optimal purge rates and accumulator size were determined.

Plastic Materials of Construction

The decrease in the expected radiation levels in the TRU Facility, owing to the lower Cf^{254}

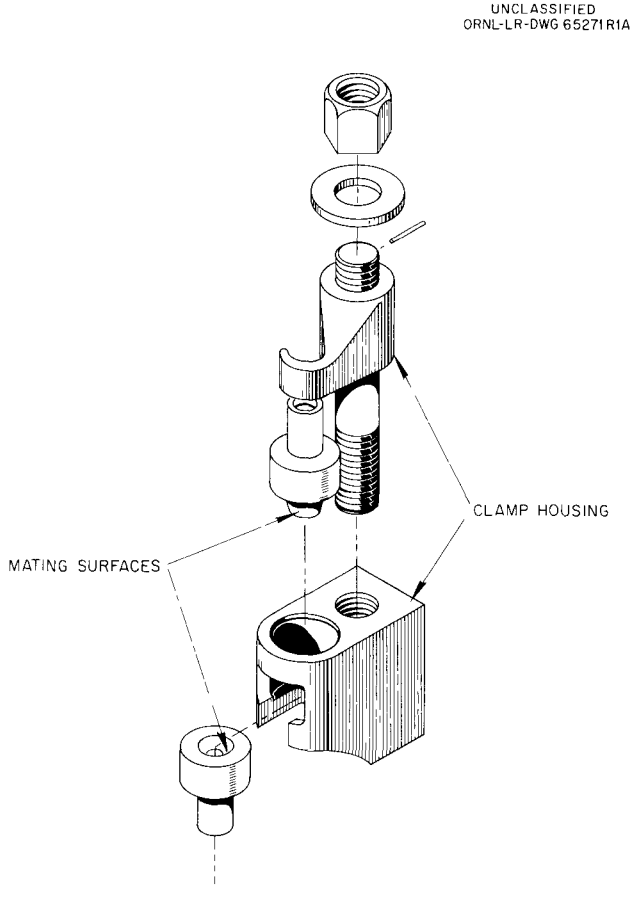

Fig. 6.27. TRU Process Disconnect.

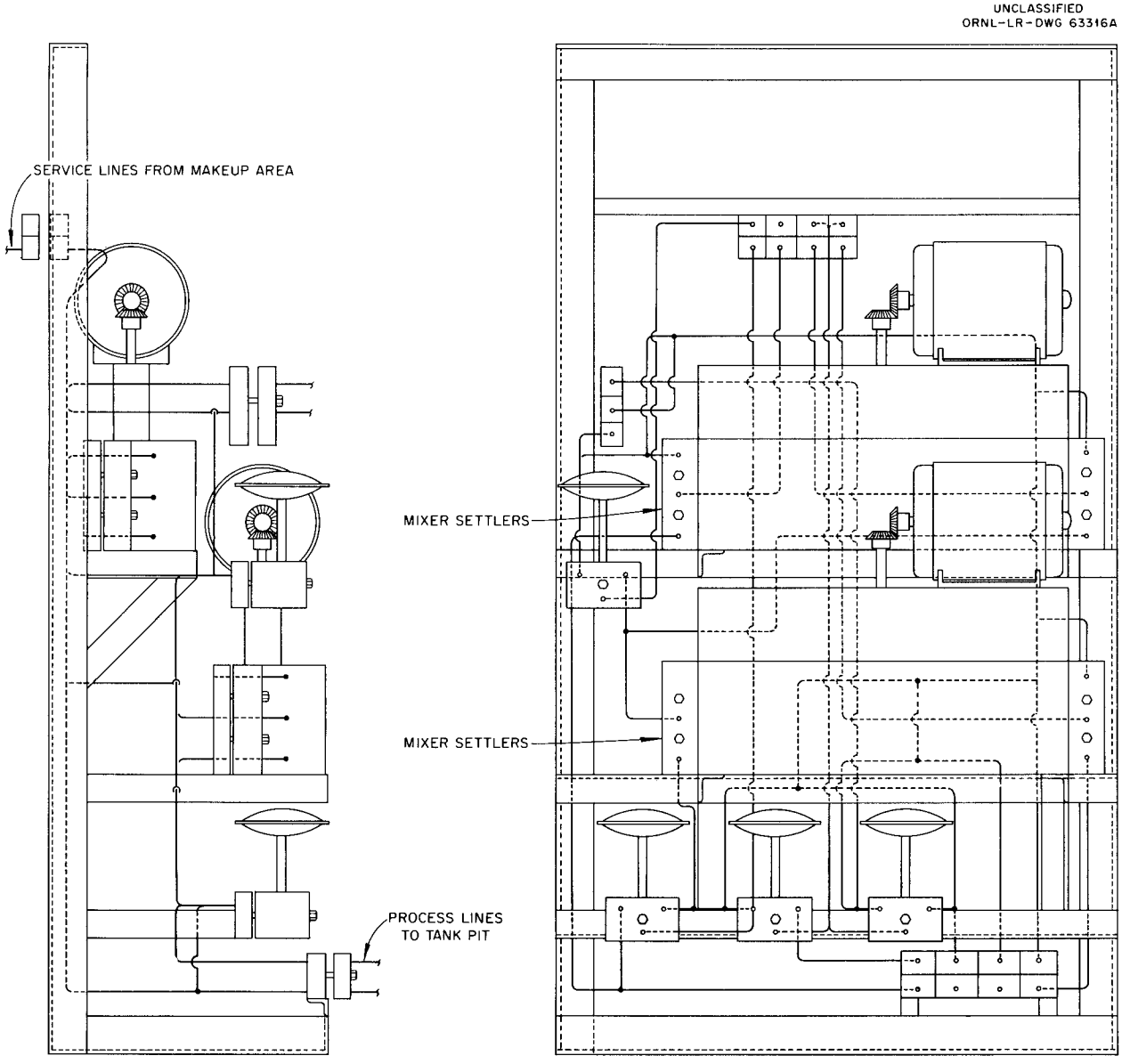

Fig. 6.28. TRU Process Cubicle Typical Equipment Rack.

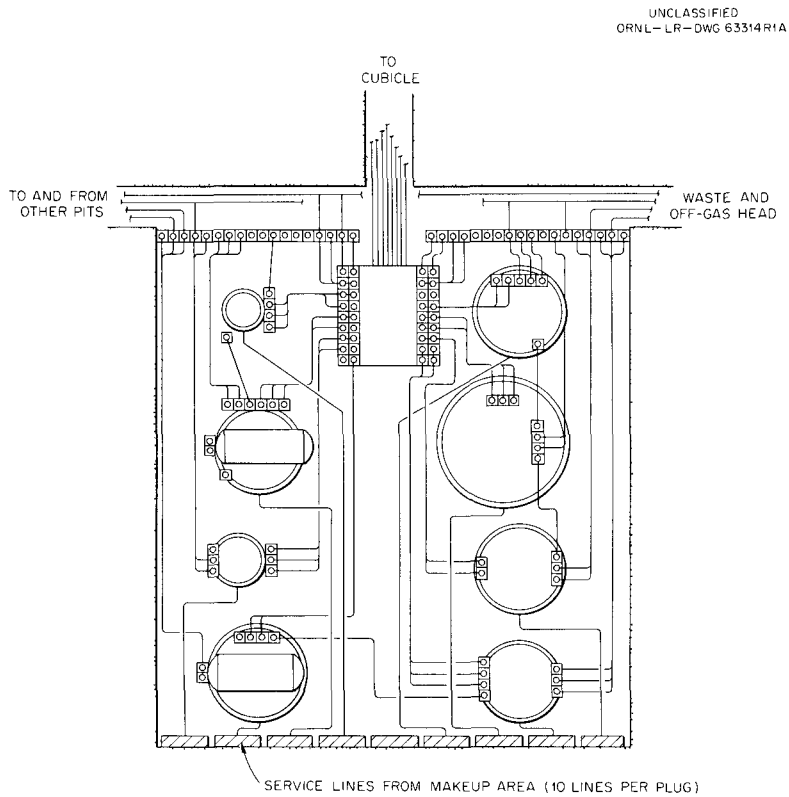

Fig. 6.29. Typical Tank Pit Piping Layout, Plan.

production rate now expected, permits consideration of organic compounds for certain applications in the cells and cubicles. A literature survey showed the following plastic materials to have the best probability of combining radiation resistance and resistance to chemicals used in the TRU chemical processing flowsheet:

	Exposure Resulting in Significant Damage, whr/g
Container and tubing materials	
Glass-fiber reinforced epoxy resins	20
Acrylic butadiene styrene	>0.25
Allyl diglycol carbonate (Homalite)	0.25
Polyethylene	0.25
Chlorinated polyether (Penton)	~0.1
Gasket and booting materials	
Acrylic nitriles	0.4
Hypalon	0.1
Neoprene	0.1

Shielding Studies

TRU shielding design is based on sources constituted by a solution containing 2×10^5 curies of Ce^{144}-Pr^{144} from burnup of 10 kg of Pu^{239} and by a fifth-cycle target, composed of residual actinides from successive High Flux Isotope Reactor irradiations, which contains 305 mg of californium and spontaneously emits 3×10^{12} fission neutrons per second. During the processing of these sources the radiation dose rate in normally occupied areas is to be no greater than 0.75 mrem/hr, with permissible hot spots around penetrations no greater than 2.5 mrem/hr.

With Renupak, a code for moments method solution of the neutron transport equation, and SDC, a gamma penetration code, it was determined that a cell shielding wall of 54 in. of magnetite concrete, of water content 12.2 lb/ft^3, density 210 lb/ft^3, satisfies the dose-rate criteria. The dose rate is controlled by fast neutrons from the fission source and is increased by factors of 5 and 50 if the water content is decreased to 6.1 and 3.0 lb/ft^3, respectively.

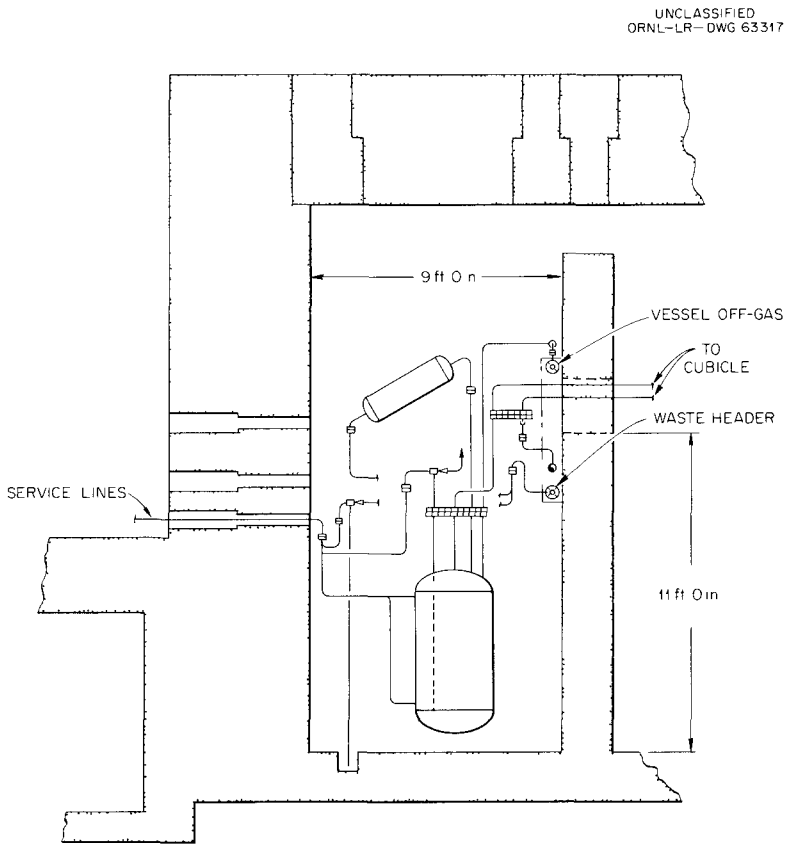

Fig. 6.30. Typical Tank Pit Piping Layout, Elevation.

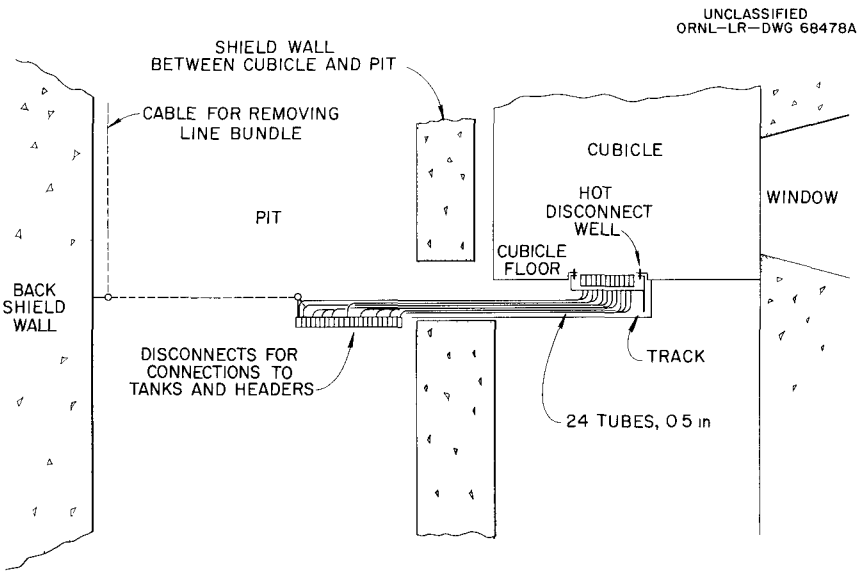

Fig. 6.31. Hot Disconnect Well Replacement Method.

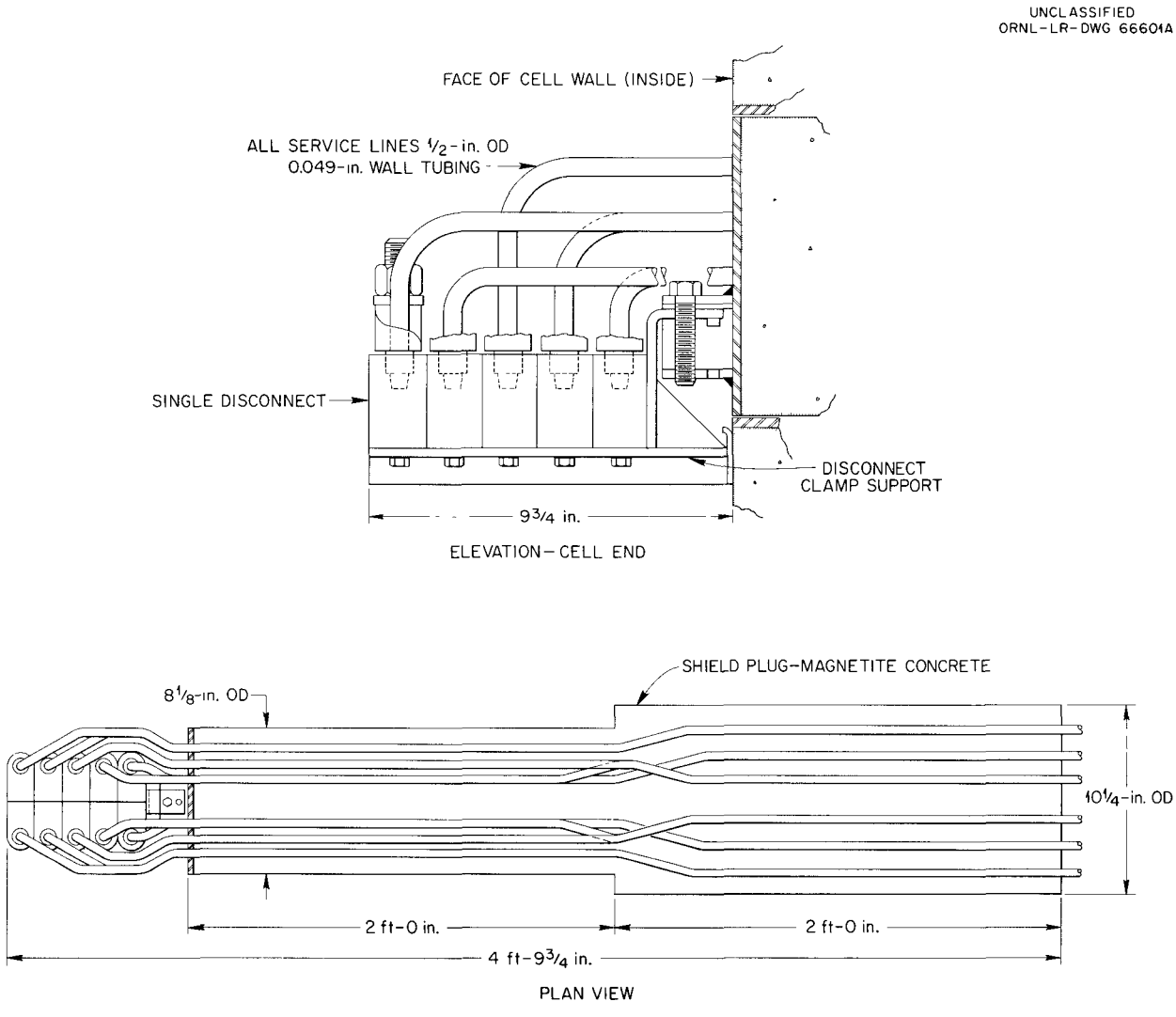

Fig. 6.32. Tank Pit Service Plug.

A 54-in.-thick cell shielding window, consisting of laminations of oil and 2.7-, 3.3-, and 6.2-g/cc glass, was tested at the ORNL Lid Tank Shielding Facility. Fission-neutron-removal cross sections of window components were determined to be 0.076, 0.080, and 0.095 ± 0.004 cm^{-1} for PPG 4966, Corning 8362, and Corning 8363 glasses, respectively. The effects of thickness and arrangements of laminations on neutron and gamma attenuation were studied. Dose rates measured through a full-length mockup of the window and calculated with Niobe, a code for numerical integration of the Boltzmann equation, indicate that the window is equivalent to magnetite concrete for fission source attenuation and has slightly less attenuation for pure hard-gamma sources.

Renupak and SDC were used to evaluate fission source carrier shields composed of concrete or combinations of lead or iron with borated paraffin.

Neutron Activation Calculations. – A computer program was prepared to determine the neutron activation of TRU components as a function of flux, exposure time, and decay time. Multigroup transport and diffusion codes were used to determine the neutron flux spectrum within cells. Concrete walls, windows, manipulators, and process vessels will survey less than 1 r/hr due

to neutron activation ten days after credible exposure to TRU fission sources.

Maximum Permissible Concentrations. – The relative hazards of the various nuclides produced by long-term irradiation of plutonium must be known for use in preparing hazards summary reports, evaluating waste treatment and disposal schemes, computing necessary decontamination of various components from each other, and finally, at the time of operation, for guides to allowable exposures and for judging whether operating practices are safe. The Health Physics Handbook does not list a number of important isotopes that will be encountered by the Transuranium Project, and the Health Physics Division is now evaluating hazards from these other isotopes. For use in the meantime, unofficial maximum permissible concentrations (Table 6.4) were calculated by the exact rules given in ICRP Publication 2.[9] The major differences in the method of obtaining these results from the method used to obtain those presented in Publication 2 are:

1. Latest information on half-lives and decay schemes were taken from Landolt-Bornstein, *Numerical Data and Functional Relationships in Science and Technology, New Series (Group 1, Nuclear Physics and Technology,* Vol. 1, *Energy Levels of Nucleii A = 5 = 257)* and recent ANL publications.
2. No account was taken of photon absorption.
3. The relative biological effectiveness (RBE) was assumed to be 20 for spontaneous fission fragments, and a weighting factor (n) equal to 5 was used for absorption in bone.
4. The total energy absorbed in the walls of the gastrointestinal tract from fission fragments is assumed to be 1% of the kinetic energy. This same assumption is usually made for alpha particles because experiments have shown that they do not penetrate the mucosa appreciably.

Hazards Evaluation

Hazards evaluation studies indicate that downwind personnel exposures and fallout levels arising from the maximum credible accidents in TRU will be acceptable. Since the secondary containment region, which surrounds the alpha laboratories and cells, is to be maintained at a vacuum of -0.3 in. (water gage) at all times, there is essentially no mechanism for the release of activity to the atmosphere except through filtered ventilation streams, even in the maximum credible rupture of a glovebox or cell cubicle. The filter removal efficiency and atmospheric dilution factors are adequate to protect the environment in these maximum credible accidents.

Although the hazard presented to the environment by TRU is small, the potential hazard to TRU operating personnel is large. Alpha-laboratory personnel could inhale a lethal quantity of actinides in a single breath in the event of the maximum credible glovebox rupture or a spill from a carrier rupture. This hazard will be minimized by limiting glovebox and transfer operations to those which have an adequately low probability for dispersing activity in the building.

During normal operation of the facility, rare gases, I^{131}, and alpha-emitting actinides will be released at average rates of less than 22, 0.07, and 10^{-5} curies/day, respectively. These releases will cause maximum downwind air concentrations equivalent to 0.25 mrem/hr and maximum beta and alpha ground deposits of 1000 and 4.5 dis/min per 100 cm^2, respectively.

---

[9] *Report of Committee II on Permissible Dose for Internal Radiation (1959),* ICRP Publication 2.

Table 6.4. Maximum Permissible Concentrations (Unofficial)

Nuclide	Water		Air		Body Burden		Specific Activity (curies/g)
	Critical Organ	$(MPC)_w$ ($\mu c/cm^3$)	Critical Organ	$(MPC)_a$ ($\mu c/cm^3$)	Critical Organ	Value (μc)	
Pu^{238}	Bone	1.53×10^{-4}	Bone	2.02×10^{-12}	Bone	0.046	17.4
Pu^{239}	Bone	1.35×10^{-4}	Bone	1.79×10^{-12}	Bone	0.045	0.061
Pu^{240}	Bone	1.35×10^{-4}	Bone	1.79×10^{-12}	Bone	0.045	0.227
Pu^{241}	Bone	7.14×10^{-3}	Bone	9.42×10^{-11}	Bone	0.990	112
Pu^{242}	Bone	1.42×10^{-4}	Bone	1.88×10^{-12}	Bone	0.048	3.90×10^{-3}
Pu^{243}	GI Tract	1.21×10^{-2}	GI Tract	2.14×10^{-6}	Bone	7.23	2.59×10^{6}
Pu^{244}	Bone	1.27×10^{-4}	Bone	1.68×10^{-12}	Bone	0.043	1.93×10^{-5}
Pu^{245}	GI Tract	1.35×10^{-3}	GI Tract	2.39×10^{-7}	Bone	3.04	1.21×10^{6}
Am^{241}	Bone	1.27×10^{-4}	Bone	5.57×10^{-12}	Bone	0.054	3.24
Am^{242m}	Bone	1.27×10^{-4}	Bone	5.57×10^{-12}	Bone	0.067	9.73
Am^{242}	GI Tract	2.73×10^{-3}	Liver	3.93×10^{-8}	Liver	0.064	8.10×10^{5}
Am^{243}	Bone	1.26×10^{-4}	Bone	5.56×10^{-12}	Bone	0.044	0.192
Am^{244m}	GI Tract	5.08×10^{-2}	Bone	3.99×10^{-6}	Bone	0.179	2.97×10^{7}
Am^{244}	GI Tract	9.10×10^{-3}	Bone	1.73×10^{-7}	Bone	0.180	1.27×10^{6}
Am^{245}	GI Tract	1.67×10^{-2}	GI Tract	2.96×10^{-6}	Liver	11.6	6.40×10^{6}
Cm^{242}	GI Tract	7.05×10^{-4}	Liver	1.19×10^{-10}	Liver	0.047	3.32×10^{3}
Cm^{243}	Bone	1.57×10^{-4}	Bone	6.88×10^{-12}	Bone	0.092	52.6
Cm^{244}	Bone	2.14×10^{-4}	Bone	9.40×10^{-12}	Bone	0.104	83.3
Cm^{245}	Bone	1.02×10^{-4}	Bone	4.50×10^{-12}	Bone	0.043	0.157
Cm^{246}	Bone	1.02×10^{-4}	Bone	4.49×10^{-12}	Bone	0.043	0.265
Cm^{247}	Bone	1.07×10^{-4}	Bone	4.71×10^{-12}	Bone	0.044	3.62×10^{-5}
Cm^{248}	Bone	1.32×10^{-5}	Bone	5.81×10^{-13}	Bone	0.0055	3.07×10^{-3}
Cm^{249}	GI Tract	8.25×10^{-2}	Liver	7.51×10^{-6}	Liver	0.827	1.18×10^{7}
Bk^{249}	GI Tract	0.140	Bone	7.76×10^{-10}	Bone	0.600	1.67×10^{3}
Bk^{250}	GI Tract	9.62×10^{-3}	Bone	1.37×10^{-7}	Bone	0.045	3.89×10^{6}
Cf^{249}	Bone	1.24×10^{-4}	Bone	1.64×10^{-12}	Bone	0.041	3.59
Cf^{250}	Bone	3.53×10^{-4}	Bone	4.66×10^{-12}	Bone	0.041	1.31×10^{2}
Cf^{251}	Bone	1.17×10^{-4}	Bone	1.55×10^{-12}	Bone	0.039	1.78
Cf^{252}	GI Tract	2.53×10^{-4}	Bone	6.83×10^{-12}	Bone	0.015	5.57×10^{2}
Cf^{253}	GI Tract	4.14×10^{-3}	Bone	8.24×10^{-10}	Bone	0.036	2.87×10^{4}
Cf^{254}	GI Tract	1.22×10^{-5}	Bone	5.42×10^{-12}	Bone	0.00075	9.19×10^{3}
Es^{253}	GI Tract	6.35×10^{-4}	Bone	7.44×10^{-10}	Bone	0.0368	2.58×10^{4}
Es^{254m}	GI Tract	5.40×10^{-4}	Bone	4.87×10^{-9}	Bone	0.0196	3.17×10^{5}
Es^{254}	GI Tract	6.70×10^{-4}	Bone	1.84×10^{-11}	Bone	0.0217	1.07×10^{3}
Es^{255}	GI Tract	6.91×10^{-4}	Bone	6.07×10^{-10}	Bone	0.0361	2.14×10^{4}
Fm^{254}	GI Tract	1.70×10^{-4}	Bone	6.03×10^{-8}	Bone	0.0202	3.81×10^{6}
Fm^{255}	GI Tract	7.72×10^{-4}	Bone	1.63×10^{-8}	Bone	0.0362	5.72×10^{5}
Fm^{256}	GI Tract	1.25×10^{-5}	GI Tract	2.21×10^{-9}	Bone	0.00076	4.59×10^{6}

7. Plutonium-Aluminum Alloy Fuel Processing

A program to recover the plutonium contained in 24 highly irradiated plutonium-aluminum fuel rods was carried out in cell 1, Building 4507. The objectives of the program were: to provide material for the determination of the nuclear properties of the higher isotopes of plutonium, the feed material for future transuranium flowsheet studies, and to demonstrate the recovery of highly burned plutonium by anion exchange methods.

The 5-ft-long by 0.94-in.-diam fuel rods were dissolved in boiling 6.0 *M* HNO_3 catalyzed with 0.05 *M* $Hg(NO_3)_2$ and 0.03 *M* fluoride, and plutonium was recovered from the solution by two cycles of anion exchange. Approximately 680 g of plutonium was processed, from which 675 g was isolated as specification grade material. Overall decontamination factors for the two anion exchange cycles with Permutit SK resin averaged 1×10^6. Losses from the operation totaled 0.9%, most of which occurred during scrubbing of the loaded resin beds.

7.1 DISSOLUTION

Fuel rods were dropped from the shielded carrier-charger into the dissolver vessel and then contacted with a solution containing 6 *M* HNO_3 and 0.05 *M* $Hg(NO_3)_2$ (Fig. 7.1). Enough fluoride ion (0.03 *M*) was added to the solution to prevent polymerization of plutonium.

In order to obtain information about the condition of the plutonium (isotopic content, burnup, polymerization) the first dissolution run was conducted with one fuel rod. An overall dissolution rate of 0.85 mg min^{-1} cm^{-2} was obtained over a 200-hr period at boiling temperature; two 65-liter portions of fresh dissolvent were used. Thereafter, the dissolution rate was increased by charging six fuel elements, dissolving the equivalent plutonium contained in one rod, and then periodically charging a fresh rod. The maximum plutonium dissolution rate was 1.6 g/hr. After the bulk of the plutonium metal heel had dissolved, two additional plutonium-aluminum alloy dissolution methods were attempted. The addition of 3 *M* HNO_3–2 *M* NaOH followed by neutralization and adjustment of the solution to 2–6 *M* with nitric acid gave a dissolution rate essentially twice that of the standard procedure. Amalgamation of the rod surface by treating with 1 *M* HNO_3–0.015 *M* Hg^{2+}–0.01 *M* NH_4F followed by rapid addition of nitric acid to raise the acidity to 6 *M* gave no noticeable increase in the dissolution rate (0.1 g/hr).

The dissolution rate was insensitive to changes in acid concentration over the range 4–6 *M*, fluoride concentration over the range 0–0.05 *M*, and solution temperature over the range 95 to 107°C.

7.2 FEED ADJUSTMENT

The valence of the plutonium was adjusted to the IV state in two steps: ferrous sulfamate was added to 0.03 *M* Fe^{2+} and then sodium nitrite to 0.05 *M* nitrite. The preferred method of acid adjustment after valence adjustment was batch addition of 13 *M* HNO_3 to a final acidity of 6–7 *M*. Continuous flowing stream acid adjustment was used early in the program, but degassing of the solution was insufficient prior to passage through the resin bed with the result that gas-filled voids appeared in the bed and channeling increased plutonium losses.

All feed solution was passed through a sand-bed filter before ion exchange to remove undissolved solids.

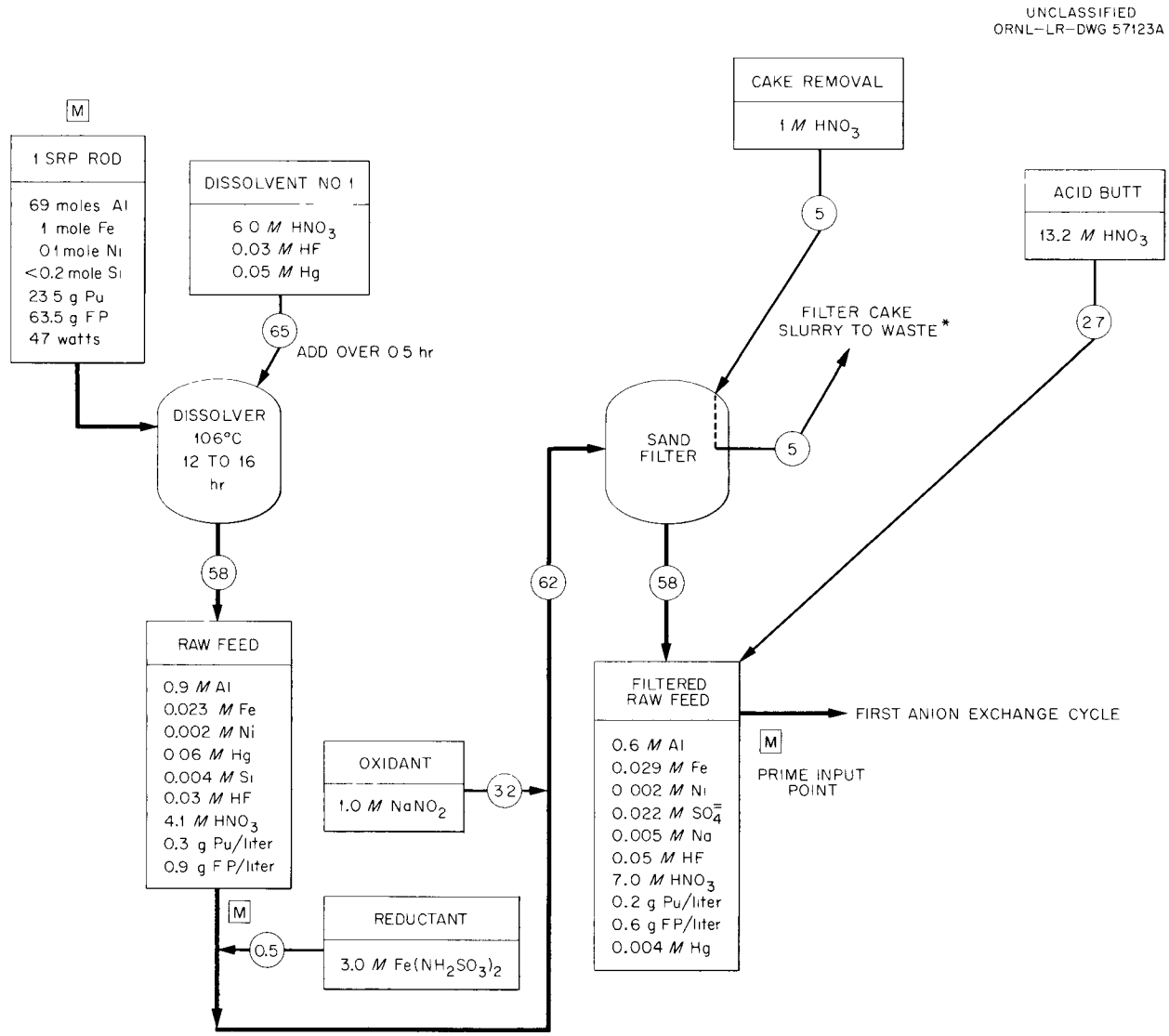

Fig. 7.1. Tentative Chemical Flowsheet for Feed Preparation in Processing of Plutonium-Aluminum Assemblies. Circled numbers are volumes in liters; "M" = measurement point. *Sampling impractical; cake will be washed to negligible plutonium content in washes before discharge.

7.3 ION EXCHANGE

Two essentially identical ion-exchange cycles were used, the only difference being 0.2 g of plutonium per liter and 0.5 *M* aluminum in the first cycle feed and 1.7 g of plutonium per liter and 0.01 *M* aluminum in the second (Figs. 7.2 and 7.3). The first-cycle product was batch adjusted to feed specifications prior to passage to the second-cycle columns. Decontamination factors averaged 1×10^4 and 100, respectively, across the first and second cycles. The second-cycle-product contaminants were principally Zr-Nb but the β and γ activities were essentially those of highly purified plutonium of the isotopic composition typical of this program.

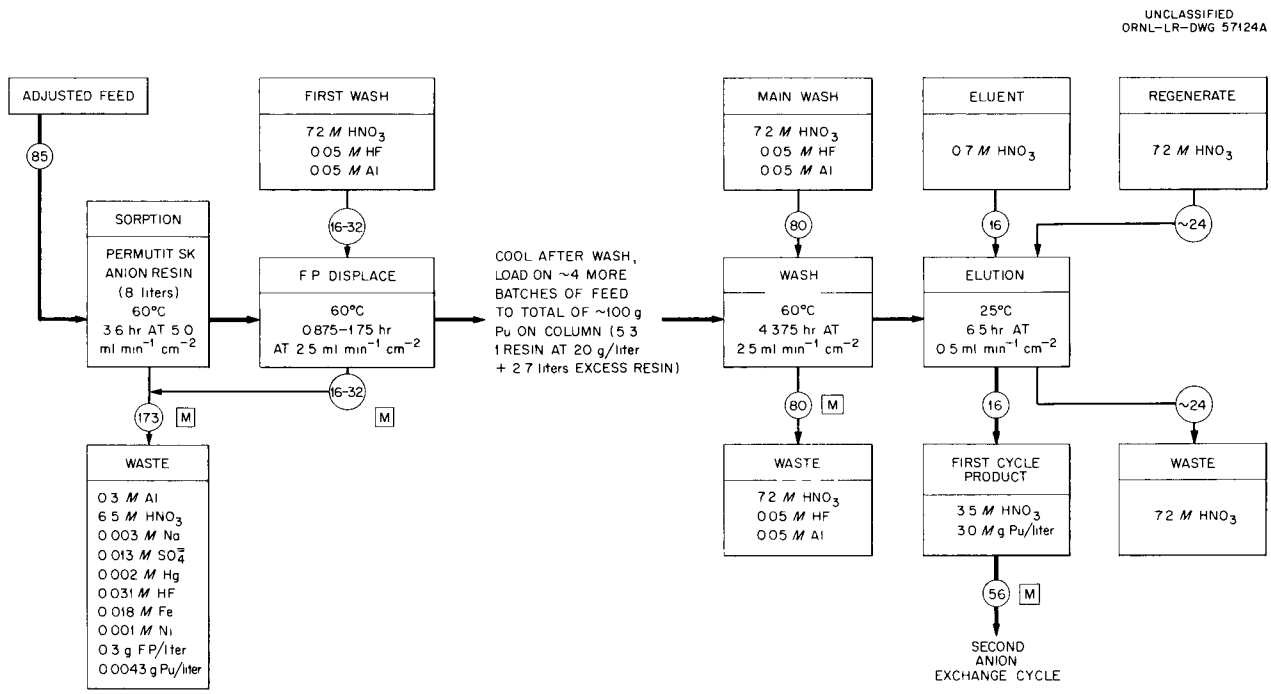

Fig. 7.2. Tentative Chemical Flowsheet for First Anion Exchange Cycle in Processing of Plutonium-Aluminum Assemblies. Second anion exchange cycle product is held in T-10 until material from about 8 rods has been eluted and then adjusted for second cycle feed. *Column held at low acidity and room temperature until regenerated with hot wash solution just prior to loading next batch.

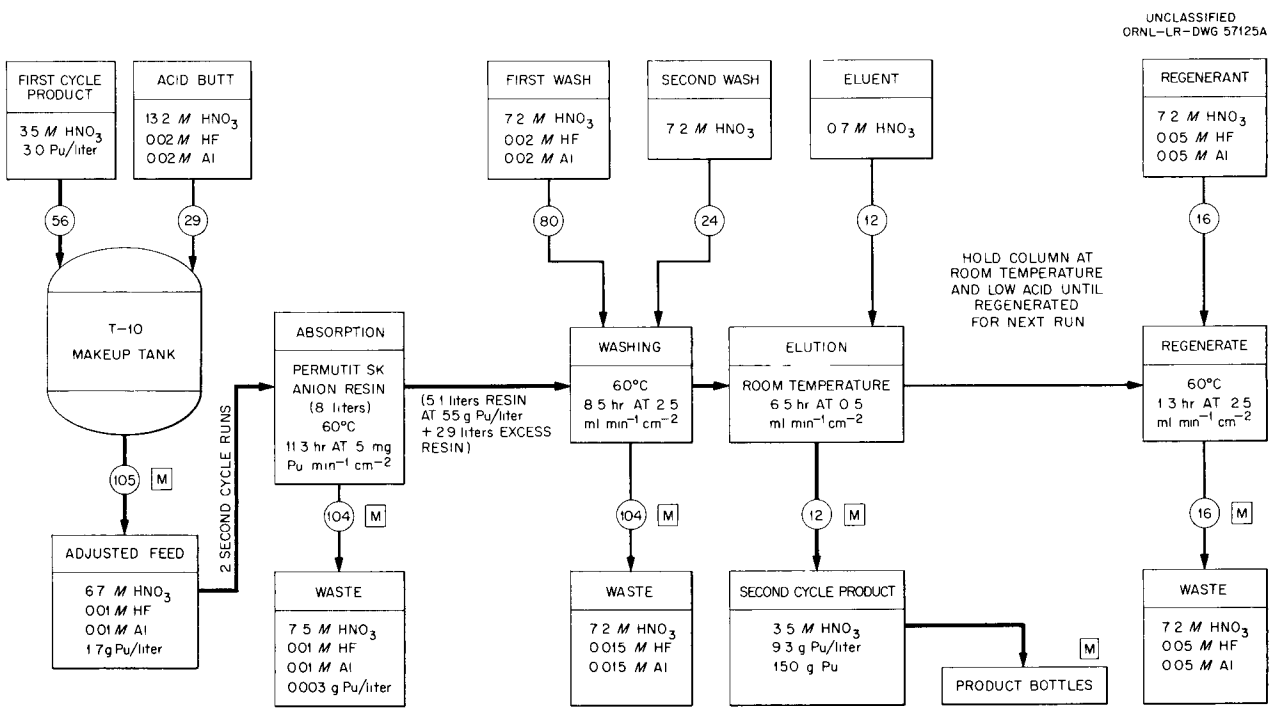

Fig. 7.3. Tentative Chemical Flowsheet for Second Anion Exchange Cycle in Processing of Plutonium-Aluminum Assemblies.

Sorption

Plutonium was sorbed on two 4-in.-diam by 42-in.-high beds of 20–50 mesh Permutit SK anion exchange resin held at 60°C. The flow rate was maintained at 1 to 2 ml min^{-1} cm^{-2} for minimum plutonium losses. Increasing the flow rate to 4–5 ml min^{-1} cm^{-2} increased the losses a factor of 3. Sorption losses across two cycles averaged 1%; 80% of the losses occurred during first-cycle scrubbing.

Scrubbing

Sorbed fission products and gross ionic contaminants were washed from the first-cycle loaded resin with 7 *M* HNO_3 containing 0.05 *M* fluoride and 0.05 *M* aluminum at 2 ml min^{-1} cm^{-2} and 60°C. Final washing of the second-cycle column was with 7 *M* HNO_3 to remove fluoride and aluminum.

Fluoride in the wash solution improved Zr-Nb decontamination by a factor of 5 to 10 at the expense of increased plutonium losses.

Elution

After loading and washing of the loaded resin bed, plutonium was eluted with 0.7 *M* HNO_3 at room temperature. The maximum plutonium concentration in the finished product was 14 g/liter and the final acid concentration was 2 *M*. The plutonium product from several resin-bed loadings was combined, mixed, and sampled, after which it was stored in geometrically safe shipping containers. All product met purity and radiation specifications.

Resin Degradation

Degradation from radiation exposure and/or chemical attack was observed by increased column pressure drop and losses about halfway through the program. The dose received by the resin, when the pressure drop across the bed became prohibitive (28 in. H_2O) and sorption losses were greater than 1%, was 4×10^8 rad, ~90% of which was α radiation. Solids in the final plutonium product proved to be degraded resin and corrosion products (iron). Silica was not present. The soluble degradation products extracted from the clear plutonium product consisted of a mixture of esters, ketones, amines, and pyridine characteristic of the resin; <5 ppm of nitro compounds was found. It was concluded that the plutonium product will be stable in storage, but caution should be exercised in evaporation of the solution until it can be examined completely.

---

8. Production of Uranium-232

A total of 32.9 mg of high-purity U^{232} was prepared for use in nuclear cross-section measurements. Its isotopic composition varied from 98.49 to 99.66% U^{232}, with 0.0127–0.0311% U^{233}, 0.032–0.0109% U^{235}, and 0.31–1.47% U^{238}. The principal product contained 21.58 mg of U^{232} with an isotopic composition of 98.9% U^{232}, 0.0127% U^{233}, 0.0095% U^{235}, and 1.075% U^{238}. The material was prepared from six Al-Pa_2O_5 cermet targets, which were fabricated with a total of 48.1 g of Pa^{231} and irradiated to ~4×10^{18} *nvt* in the ORR. The targets were processed by dissolution of the aluminum in 8 *M* HCl, dissolution of the irradiated Pa_2O_5 in 8 *M* HCl–6 *M* HF, selective sorption of the uranium on an anion exchange resin from 8 *M* HCl–0.6 *M* HF, elution by 0.5 *M* HCl, and purification by a second HCl-HF anion exchange cycle followed by tributyl phosphate extraction from 6 *M* HNO_3.

Another 1 g of U^{232} containing 1% U^{233} will be prepared by re-forming the Pa^{231} into targets, irradiating for the appropriate time, and processing

for uranium-protactinium separation. The protactinium will be stored for a year to allow the Pa^{233} formed during irradiation to decay and then purified, converted to the oxide, and returned to UKAEA, who loaned it for this program.

8.1 URANIUM CONTENT OF Pa_2O_5

Because of the large neutron cross section of U^{235}, appreciable amounts of this isotope in the U^{232} samples would interfere with some of the cross-section measurements to be made. The natural uranium content of the original Pa^{231} was determined to be 6.1 and 7.7 ppm by two independent determinations, both based on dilution methods. In the first, U^{233} was added to a solution sample of the Pa^{231}, and the uranium was separated from the Pa^{231} and mass analyzed. In the second, about 80 μg of U^{232} was produced in 244 mg of Pa_2O_5 by neutron irradiation, and the isolated uranium product was mass analyzed. This amount of natural uranium contamination would be equivalent to 85–105 ppm of U^{235} in the 30 mg of U^{232} produced from 50 g of Pa^{231} and was considered low enough for the intended use.

8.2 TARGET FABRICATION

The irradiation targets were welded aluminum cans, $\frac{5}{8}$ in. diam by $3\frac{1}{8}$ in. long, containing three or four Al-Pa_2O_5 pellets 0.45 in. in diam. The pellet column in each target was 2.15 to 2.50 in. long and contained 7.35 to 8.34 g of Pa^{231}.

Because of alpha and gamma activity associated with Pa^{231}, a semiremote fabrication method was developed for operation in glove boxes. Three boxes were required: one box was shielded with 2 in. of lead and equipped with both castle manipulators and gloves, a standard alpha glove box containing a small laboratory press, and another standard box for welding (Fig. 8.1).

A total of 56.6 g of Pa_2O_5 was mixed with 46.1 g of aluminum powder by tumbling in a polyethylene bottle in the lead-shielded box. The mixed powder was dispensed by volume measurement through double stopcocks into thin aluminum shells, the tops of which were crimped shut to prevent dusting and spilling. Castle manipulators were used in order to limit hand exposure during these operations. The loaded shells were transferred with unit shielding into the pressing box, where each pellet was pressed at 30 tons/in.^{2} in a die lubricated with stearic acid.

Pressed pellets were cleaned in acetone, dried at 250°C for 4 hr, and loaded into aluminum target cans for welding. By enclosing the cans so that only the inner surface was exposed to the alpha-contaminated pressing box, the cans were kept free of external contamination. Aluminum caps were welded to these cans in the welding box without contamination of either the outer surface of the cans or the inner surface of the glove box. All six targets prepared by this procedure passed both helium leak and dye penetrant tests.

8.3 PROTACTINIUM IRRADIATION

A single capsule containing 7.35 g of Pa^{231} was irradiated 10 hr in the ORR hydraulic tube No. 1 (core position F-8) at a calculated perturbed thermal neutron flux of 1.31×10^{14}. Approximately five weeks later, five capsules containing 40.6 g of Pa^{231} were irradiated simultaneously for 10 hr in the ORR hydraulic rabbit tubes Nos. 1, 2, and 3 at an average perturbed thermal neutron flux of 1.13×10^{14}. For these irradiations the resonance integral contribution to the effective Pa^{231} neutron cross section is less than 2 barns. With an effective Pa^{231} cross section of 212 barns, the quantity of U^{232} and corresponding U^{231} concentration from the two irradiations was calculated to be:

Perturbed Flux Time (nvt)	Decay (hr)	U^{232} (mg)	U^{233} (ppm)
4.7×10^{18}	0–43	4.81	223
	43–91	1.62	354
4.1×10^{18}	0–43	23.1	181
	43–77	6.17	290

The calculated values agreed well with the actual amount of U^{232} produced (Sec 8.5) but the calculated U^{233} contents were about 30% higher than actually observed.

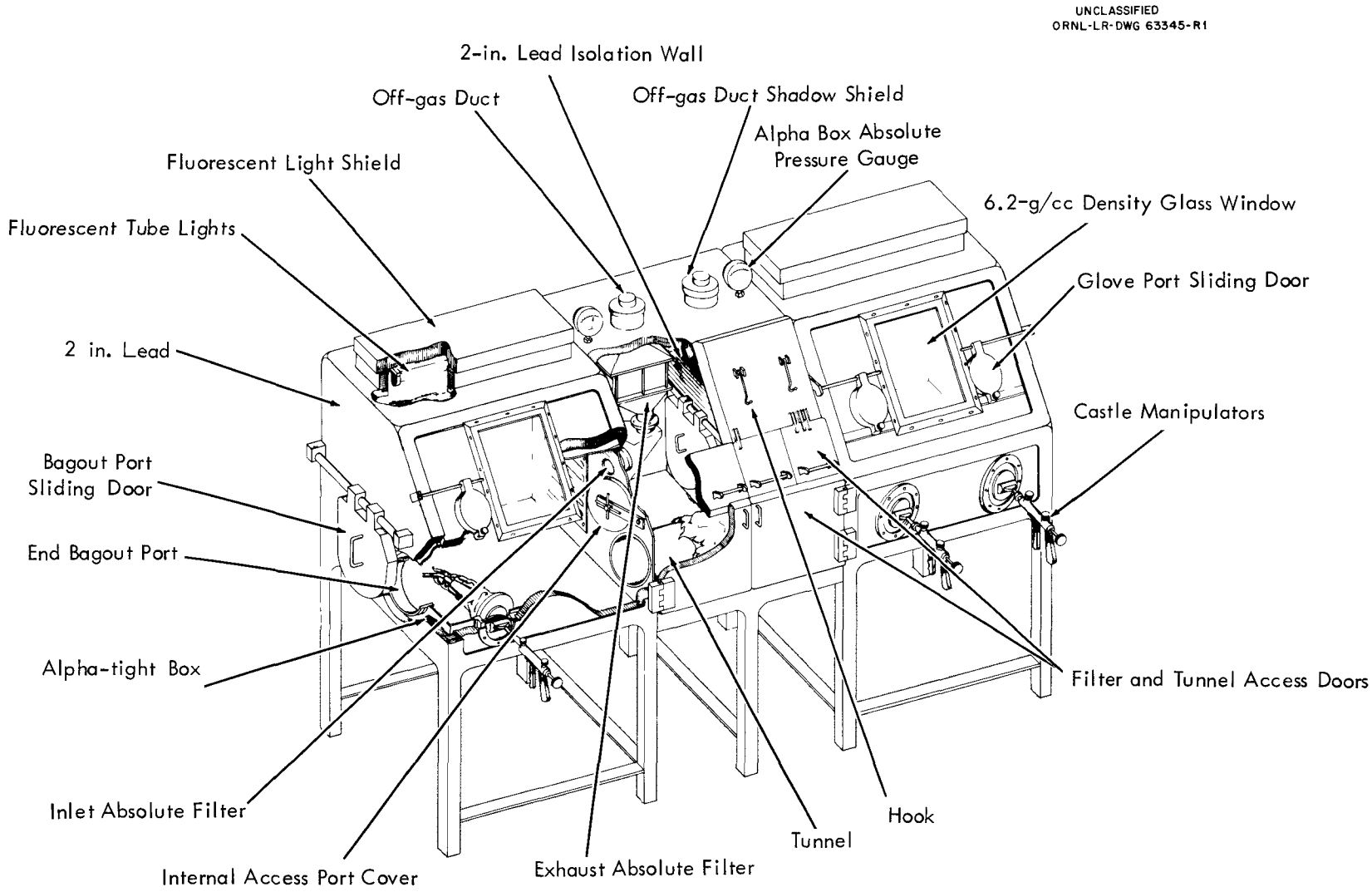

Fig. 8.1. Lead-Shielded Processing Box, Laboratory 1, Building 3508.

8.4 CHEMICAL PROCESSING OF URANIUM

Uranium-232 low in U^{233} was prepared in one run from a target containing 7.35 g of Pa^{231} about 43 hr and again about 91 hr after irradiation. In a second run, uranium was separated from five targets containing 40.7 g of Pa^{231} about 43 and 77 hr after irradiation (Table 8.1). The method was essentially the same as that reported earlier.[1,2] The aluminum cans and matrix were dissolved by slow addition of 7 *M* HCl, leaving most of the Pa_2O_5, uranium, and fission products. The final aluminum dissolver solution, about 1 *M* $AlCl_3$ and 4 *M* HCl, contained 0.14 mg of protactinium and 0.11 μg of uranium per milliliter. This solution was passed through a 400-ml column of Dowex 1-4X (50–100 mesh) resin at 0.8 ml min^{-1} cm^{-2} to sorb the traces of dissolved protactinium and uranium as chloride complexes. The dissolver and resin column were washed with 8 *M* HCl to remove residual aluminum. The solid residue, primarily Pa_2O_5, was dissolved by adding 7 *M* HCl–6 *M* HF and stirring at 70°C for 1 hr. The resulting solution, which contained 100 g of protactinium per liter, was diluted 1:10 with 7 *M* HCl. About 43 hr after the end of the irradiation, the primary protactinium-uranium separation was made by passing this solution through the same resin column previously used to sorb protactinium and uranium from aluminum dissolver solution. Under these conditions uranium is sorbed on the resin, and the protactinium fluoride complex passes through the column with the solution. The dissolver and resin were washed with 7 *M* HCl–0.6 *M* HF to remove residual protactinium. Crude U^{232} product was eluted from the column with 0.5 *M* HCl at a flow rate of 0.8 mg min^{-1} cm^{-2}. After additional U^{232} had grown into the protactinium solution by Pa^{232} decay, the ion exchange separation was repeated.

Typical curves showing protactinium and uranium content of column effluents are given in Fig. 8.2. All protactinium and uranium concentrations were determined by a combination of gross α and α-pulse analyses. Losses in the aluminum dissolver solution were low but could not be determined accurately because of the α-active Pa^{231} and U^{232} daughters in this stream and because of

[1] *Chem. Technol. Div. Ann. Progr. Rept. May 31, 1961* (ORNL-3153).

[2] J. M. Chilton and N. Jackson, *Preparation of U^{232} from Pa^{231}. Part I. Preliminary Work*, AERE-R 3727 (June 1961).

Table 8.1. Summary of U^{232} Production Runs

Solution	Run 1			Run 2		
	Volume (liters)	Total Pa (g)	Total U (mg)	Volume (liters)	Total Pu (g)	Total U (mg)
Al dissolver solution	0.4	0.060	0.046	6.2	*a*	*a*
Al waste	3.0	0.008[b]	~0[b]	9.0	0.021[b]	0.050[b]
Pa dissolver solution	1.4	6.4	3.30[c]	4.0	42.8	13.5[c]
Pa product	3.6	7.6	0.0011	5.8	42.7	6.7[d]
1st U product	0.9		5.0	0.9	0.06	20.2
1st U tailings	2.2	2×10^{-4}	0.004	2.7	5×10^{-4}	3×10^{-3}
2nd U product	0.9		1.9	0.9		5.9
2nd U tailings	2.2	2×10^{-4}	0.002	1.8	4×10^{-4}	0.03

[a] Not determined.

[b] Based on total counts in the energy range of U^{232} and Pa^{231}. However, no U^{232} or Pa^{231} peaks were observed as such.

[c] At the time of analysis, ~40-hr decay.

[d] Calculated value grown in from Pa^{232} decay after final processing = 6.9 mg.

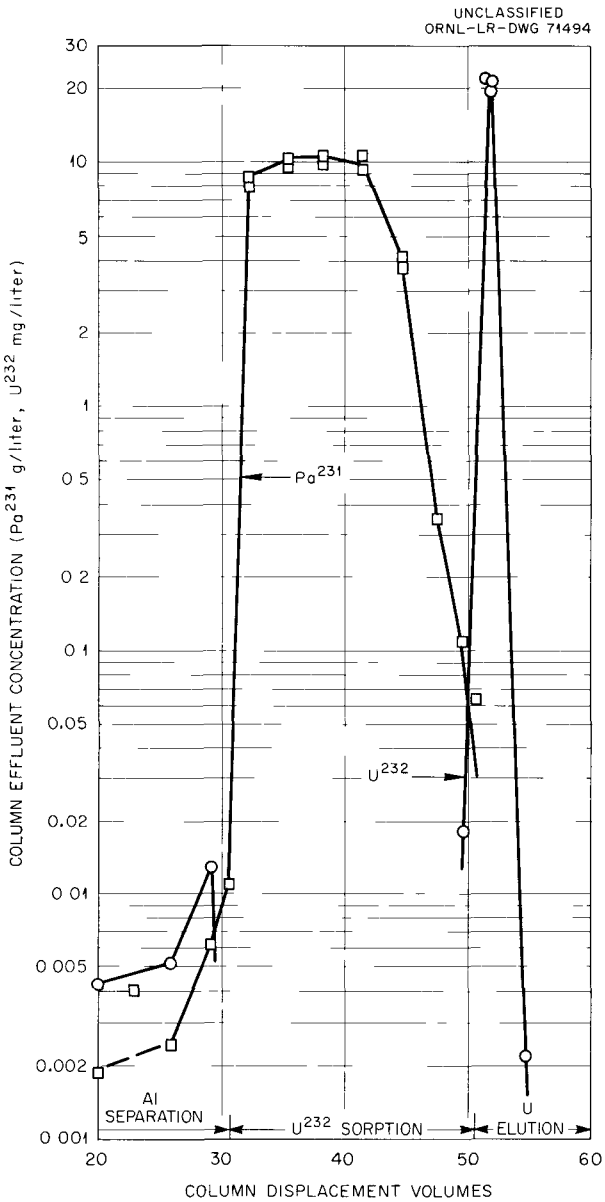

Fig. 8.2. Protactinium and Uranium Content of Column Effluent During First Uranium Product Separation of the 40.6 g Pa Run.

small amounts of U^{232} activity in the protactinium product and of protactinium activity in the U^{232} product.

The targets were processed in polyethylene equipment installed in a concrete-shielded cell equipped with AMF model 8 heavy-duty manipulators. The principal pieces of equipment used were (1) a jacketed dissolver, (2) Kel F filters in two solution transfer lines, (3) a small ion exchange column for uranium decontamination, (4) a modified model T8 finger pump with tygon tubing used for all solution transfer, (5) remotely operated micropipetter for making in-cell dilutions, (6) manipulator detonger, and (7) one-liter polyethylene bottles for solution storage.

The Čerenkov radiation from the decay of Pa^{232} was intense. In a photograph of the interior of the cell made during the primary protactinium-uranium separation (about 40 hr after irradiation) with only light from the radioactive solutions (Fig. 8.3), the dissolver, filter, ion exchange column, and product bottles are seen. After 5 days' decay, the hard radiation from 40 g of protactinium in solution was about 6000 r/hr at 1 ft. The nominal half life of Pa^{232} is 1.3 days.

Uranium Purification

The uranium was finally purified by a second anion exchange cycle to remove traces of protactinium and tributyl phosphate extraction from nitric acid to remove iron. A tertiary amine extraction method of separation of protactinium and uranium was developed (see Protactinium Chemistry, this report).

Uranium solutions in 1-liter polyethylene bottles were transferred from the shielded cell to the lead-shielded glove boxes (Fig. 8.1), where they were evaporated to reduce the volume and to increase the HCl concentration to 6 *M*. Concentrated HCl and HF solutions were added to adjust the solution to 8.0 *M* HCl–0.6 *M* HF. This solution was passed through a 35-ml column of Dowex 1-4X (50–100 mesh) resin to selectively sorb the uranium. The loaded resin was washed with 8.0 *M* HCl–0.6 *M* HF to remove all traces of protactinium, and the uranium was eluted with 0.5 *M* HCl. The uranium solution was converted from a hydrochloric acid solution to a 6 *M* HNO_3 solution by fuming to dryness with concentrated nitric acid several times, from which the uranium was quantitatively extracted by several passes of 20% tributyl phosphate. The organic solution was scrubbed with 6 *M* HNO_3 and stripped with water, and the uranium product solutions were evaporated to <25 ml. Gross α and α-pulse analyses of the final product solutions showed U^{232} as 96% of the total α radiation, with the remaining activity apparently U^{232} daughters. Isotopic purity (Table 8.2) was determined by mass analysis.

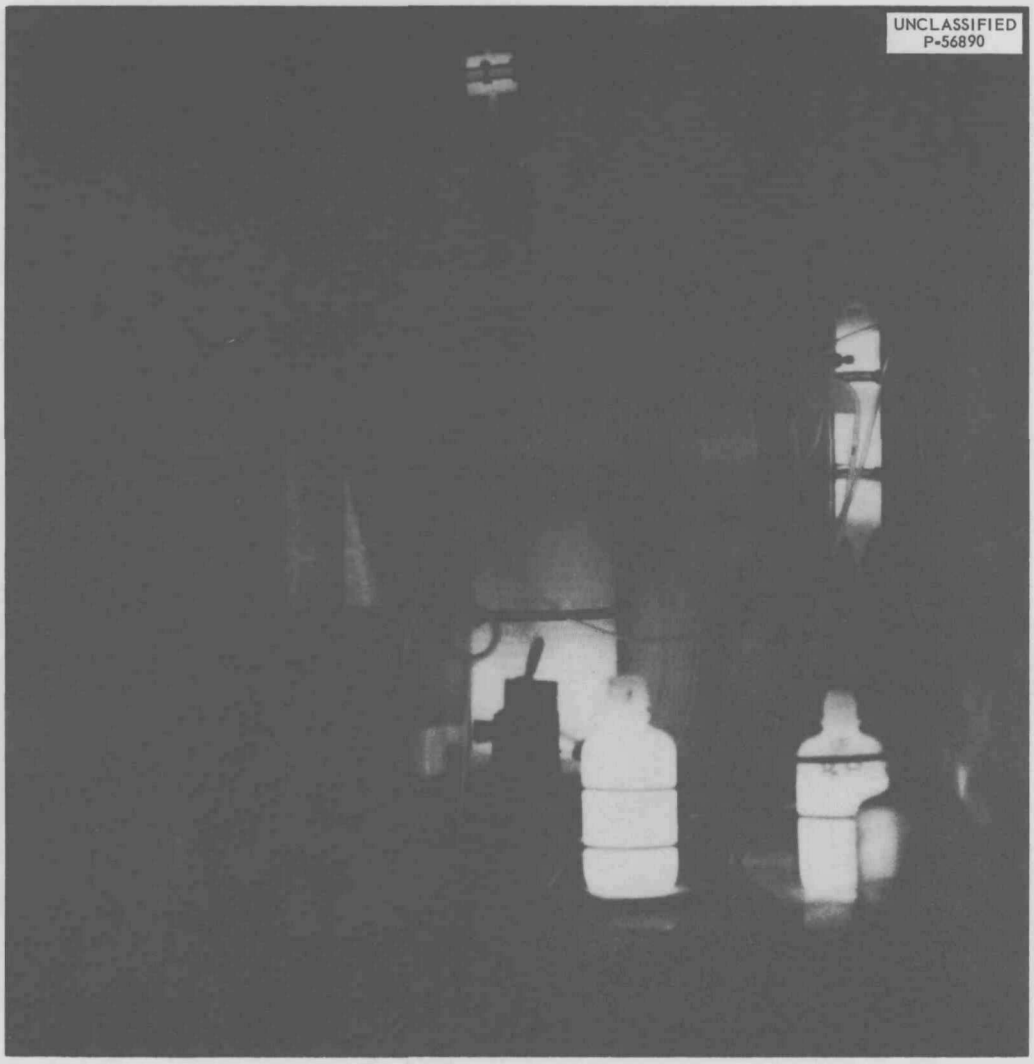

Fig. 8.3. Process Vessel Illuminated by Cerenkov Radiation During Processing of U^{232}. The radioactivity is primarily that of Pa^{232}. This picture was taken through the 4.5-ft-thick lead-glass window of the hot cell.

Table 8.2. Summary of U^{232} Product Solutions

Run No.	Irradiation Data			Uranium Products				
	Pa (g)	Flux	Decay Time (hr)	U^{232} (mg)	Isotopic Analysis (at. %)			
					U^{232}	U^{233}	U^{235}	U^{238}
1	7.35	3×10^{18}	0–43	4.29	98.90	0.0206	0.0090	1.068
			43–91	1.51	98.49	0.0311	0.0109	1.468
2	40.6	3×10^{18}	0–43	21.58	98.90	0.0127	0.0095	1.075
			43–77	5.49	99.66	0.0204	0.0032	0.312

9. Uranium Processing

9.1 RADIUM REMOVAL FROM URANIUM MILL WASTE STREAMS

Effluents from uranium mills normally contain certain radioisotopes (e.g., Ra^{226}, Ra^{223}, Th^{230}) at concentrations too high to legally permit their direct discharge to the environment, and considerable study has been devoted to eliminating this health hazard. With the exception of radium, all the isotopes can be removed adequately by lime neutralization of the acid waste, and the residual radium can be reduced to the specification limit by adsorption on barytes.[1] Recently, a study was initiated on some of the newer natural and synthetic zeolites to test possible advantages over barytes as radium adsorbers.

In preliminary batch tests, several materials, including clinoptilolite, Linde Molecular Sieves 13X9A and AW-500, Decalso, and barium phytate, removed radium effectively from simulated lime-neutralized acid waste solution (pH 7.8) which contained in grams per liter, 0.5 Ca, 0.08 Mg, 1 Na, 1 Cl, and 2.5 SO_4 along with Ra^{226} tracer. All the above adsorbents except the last were also tested in columns with favorable results, but the tests were not of sufficient duration to reach the radium breakthrough point. In the longest test, with a 6-in.-deep bed of 20–50 mesh clinoptilolite and a flow rate of 90 gal hr^{-1} ft^{-2}, the Ra^{226} activity in the first 500 column volumes of effluent was less than the specification limit, 10 picocuries/liter (1 picocurie = 10^{-12} curie). After passage of 2200 column volumes, the effluent activity was still less than 5% that of the head solution. The solution used for the column test was of the same composition as described above, spiked with 2300 picocuries of Ra^{226} per liter which is $\sim$20 times the concentration normally expected in lime-neutralized plant waste solution. The adsorbed radium was eluted efficiently with 1.8 *M* NH_4Cl–0.2 *M* HCl.

9.2 COATING UO_2 PARTICLES WITH BeO[2]

A slightly porous glass of beryllium oxide containing dispersed particles of UO_2 (< 10 μ) was produced by suspending the UO_2 in a syrupy solution of basic beryllium formate or oxalate, which was then dried and ignited to refractory BeO.

Small spherical beads of BeO containing the UO_2 particles were produced by dispersing the syrupy mixture in toluene containing a wetting agent (Aerosol OT) and partially drying them *in situ* by addition of acetone and then anhydrous ammonia. After acetone washing, vacuum desiccation, and oven drying, the beads can be ignited to BeO without sintering or distortion. However, the resulting refractory beads are porous and would require further densification to provide a continuous coating around the UO_2 particles.

---

[1] M. H. Feldman, *Summary Report 1959–1961*, WIN-125 (Sept. 30, 1961).

[2] W. J. McDowell, *Coating of UO_2 Particles with BeO by Solution Methods*, ORNL TM-220.

10. Protactinium Chemistry

The objective of the protactinium chemistry program has been to study the nature of the protactinium complexes in systems in which protactinium is reasonably soluble. Stable aqueous solutions of protactinium generally contain fluoride, sulfate, or organic complexing agents. For this work, sulfuric acid solutions were used, since the sulfate system is more amenable to available methods of investigation than fluorides and are more likely to have practical application than the organic complexing agents. Protactinium solubilities and distribution coefficients with some amines were measured, and spectrophotometric studies were made.

10.1 SOLUBILITY MEASUREMENTS

Solubility measurements confirmed that protactinium solubilities are low, 0.12–0.20 mg/ml, in 27 to 33 N sulfuric acid. In the 20 to 26 N range the results scattered badly, varying from 0.8 to 2 mg/ml. The results of each set of measurements were fairly constant through this acid range, but the sets were not consistent with one another. Below 20 N acid the solubility increased smoothly, with decreasing acid concentration, to about 6 mg/ml in 10 N acid. Below 9–10 N acid, reproducibility of results was much poorer, about an order of magnitude at 5 N acidity. However, in the range 10–20 N H_2SO_4, stable solutions with a protactinium concentration of 1 mg/ml were obtained, and these may well be of practical interest.

10.2 SOLVENT EXTRACTION

Scouting tests indicated that amines were good extractants for protactinium in sulfuric acid solutions, the order of extraction being tertiary < secondary < primary amines. The extractability increased approximately linearly with amine concentration at low concentrations, and increased quite rapidly with decreasing sulfuric acid concentration (Fig. 10.1). A plot of the distribution coefficient (o/a) as a function of the acid concentration (Fig. 10.2) shows a much steeper slope at acidities >9.4 N than at <7.6 N. Further study of this transition region is planned. In these tests the Pa^{231} concentration was 2–2.5 $\times$ 10^5 counts min^{-1} ml^{-1} in the organic phase (4–5 $\times$ 10^{-3} mg/ml).

The distribution coefficient data were reasonably reproducible even down to the range 3–4 N acid, although solubility data were not. The difference in behavior is probably due to the much lower protactinium concentration in the aqueous phase during D.C. measurements. At low acidities the D.C.'s are large, with the result that, if protactinium concentrations in the organic phase are in the range convenient for measurement by α counting (10^5–10^6 counts min^{-1} ml^{-1}), the concentration in the aqueous phase will be low ($\sim 10^{-5}$ mg/ml) compared to the concentrations observed in the solubility work. The decrease in the protactinium D.C. with 3.3 N acid and 0.3 N amine, compared to 0.1 N amine (Fig. 10.1) was duplicated and appeared to be a real effect.

A few measurements with Primene JM-T and Alamine 336 and 306 indicate a generally similar behavior. Extraction by Alamine is lower by an order of magnitude or more, and with Primene the D.C.'s are larger by at least an order of magnitude. Extraction with Primene JM-T in the lower sulfuric acid concentration range is so large that the D.C.'s could not be determined accurately, primarily because of the presence of α-active daughters of Pa^{231} which complicate the analysis.

10.3 SPECTROPHOTOMETRIC STUDIES

Protactinium in 15 to 34 N H_2SO_4 solution showed a single, rather broad absorption peak in the ultraviolet region, at about 2250 A. Absorption in the

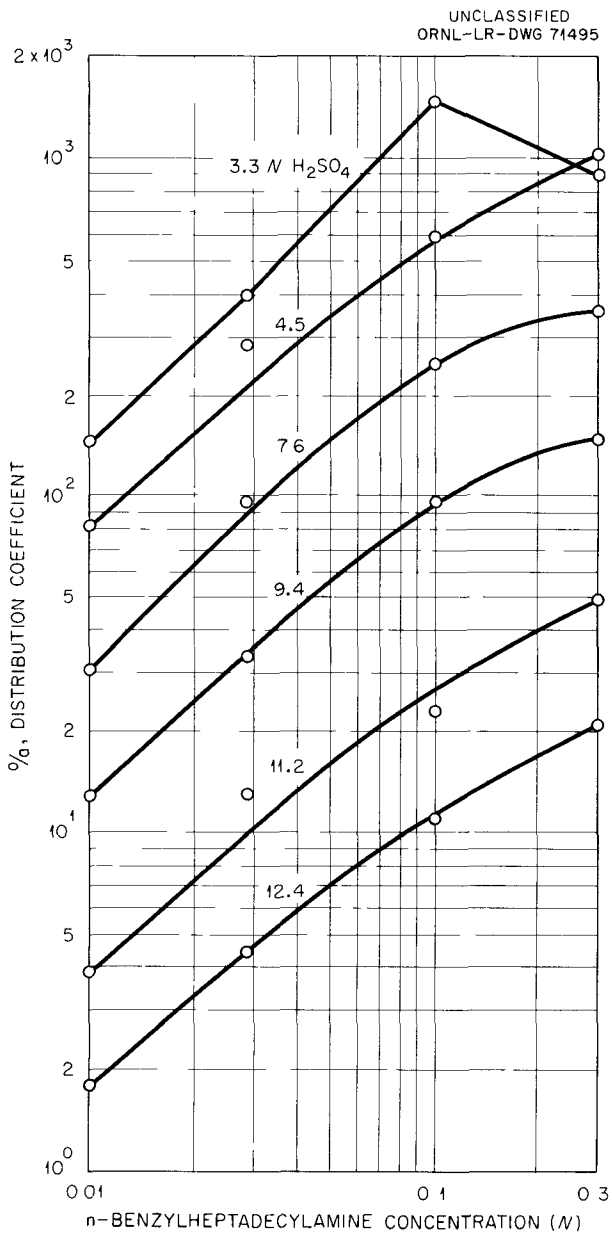

Fig. 10.1. Protactinium Distribution Coefficients, Sulfuric Acid vs *N*-Benzylheptadecyl Amine in DEB.

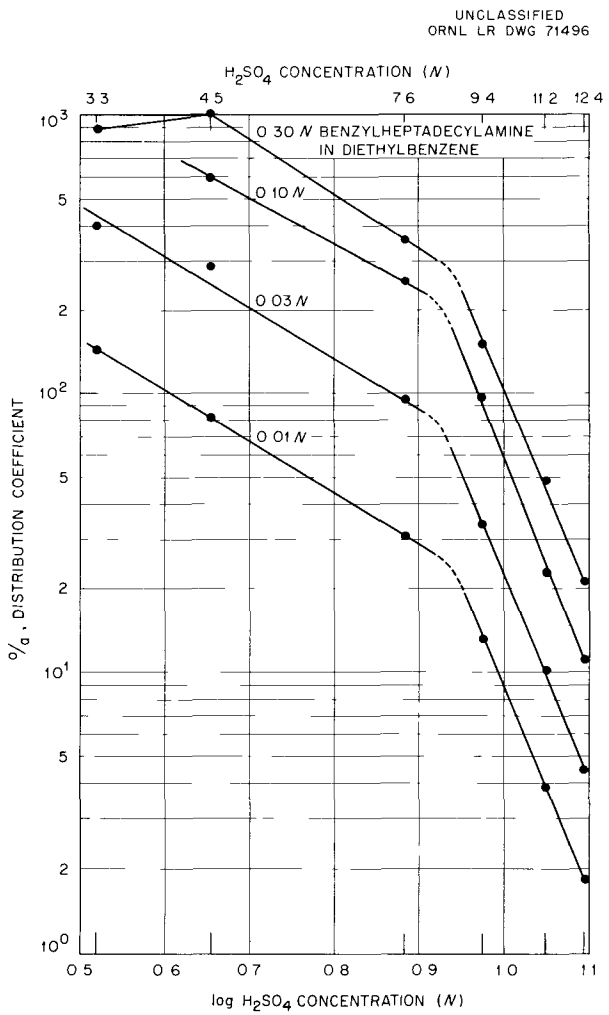

Fig. 10.2. Dependence of Protactinium Distribution Coefficient on H_2SO_4 Concentration.

sulfuric acid solvent precluded measurements below about 1950 A, at which point the absorption had decreased to 70% of the peak value. In 5 and 7.5 *N* acid the peak was shifted to shorter wave lengths, below the 1950 A cutoff, so it could not be well determined. Previously reported[1] results with HCl solutions indicated a peak at about 2120 A, but HCl absorption increases so rapidly in this region that the protactinium peak was not clearly defined. Further work in the 5 to 15 *N* H_2SO_4 concentration range is required to determine the change in the absorption peak that must occur in this region. It is hoped that these data will correlate with the solvent extraction data discussed above.

[1] A. T. Casey and A. G. Maddock, *J. Inorg. & Nucl. Chem.* 10, 58 (1959).

10.4 SEPARATION FROM HCl-HF SOLUTION

Tests on separation of uranium and protactinium from HCl-HF solutions with Alamine 306 in diethyl benzene indicated that separation factors greater than 10^4 could be obtained under a wide variety of conditions but were best from 8 *N* HCl–1 *N* HF (Fig. 10.3).

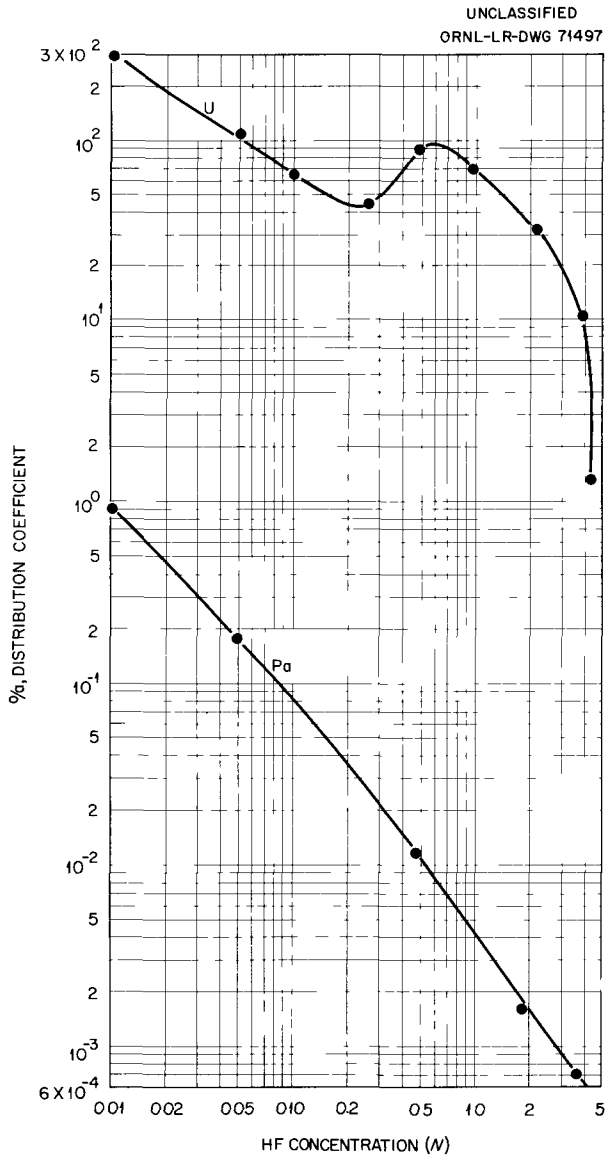

Fig. 10.3. Dependence of Uranium and Protactinium Distribution Coefficients on HF Concentration. Aqueous phase, 8 *N* (HCl + HF); organic phase, 0.1 *N* Alamine 306 in diethylbenzene.

11. Thorium Oxide Irradiations

The successful use of thorium oxide in a nuclear reactor requires that changes in its properties because of irradiation be predictable. The purpose of the thorium oxide irradiation studies is to determine the stability of thoria pellets and powders under reactor irradiation both dry and in water.

Because of its crystalline similarity to UO_2 (ref 1) which is particularly resistant to radiation damage, bulk ThO_2 should also resist radiation damage well. Experiments have already demonstrated that structural defects reach a maximum in UO_2 at exposures of $1–5 \times 10^{15}$ fissions/g. At this point the UO_2 contains about 1% interstitial atoms and shows a slight increase in lattice dimension. From this exposure up to 1×10^{20} fissions/g damage does not increase significantly, but above 1×10^{20} fissions/g, dimensional changes occur and the lattice breaks down because it can no longer hold the impurities introduced by the fission process.[2] Hence, no great change in the structural strength of ThO_2 during radiation exposures up to 1×10^{20} fissions/g is expected. However, material may spall off as a result of fission fragment recoils or the wear resistance may decrease.

11.1 THORIUM OXIDE PELLETS IRRADIATIONS

Code P-82 thorium oxide pellets (Fig. 11.1) prepared[3] from pressed powders with a final firing at 1650°C, which had shown the highest wear resistance of any pellet preparation,[4] were irradiated under D_2O at 250°C and dry in aluminum capsules under a helium atmosphere (estimated interior dry pellet temperature 150°C) for ~3 months (2×10^{20} *nvt*; 7×10^{16} fissions/g) with little damage.[5] The color of the wet irradiated pellets changed from a glossy tan to a dull gray black (Fig. 11.2). The dry-irradiated pellets from one capsule were black; those from another were partly covered by a metallic-like coating as yet unidentified (Fig. 11.3). Since the capsules were welded under helium with argon, the atmospheres may have been different, resulting in a different pellet temperature and hence a different postirradiation appearance. As received, the pellets showed a density of 9.16 g/cc. After 2 days' autoclaving under water at 250°C, the undried pellets had a density of 9.25 g/cc. The density of the irradiated pellets was 9.45 g/cc before drying and 9.34 g/cc after drying. Pellets from a control experiment had densities of 9.68 g/cc before drying and 9.40 g/cc after drying. Average weight loss as a result of the wet irradiation was 0.4%, and from the dry irradiation, <0.05%.

Pellets prepared by the technique used in preparing the P-82 pellets ordinarily have a wear-resistant, vitreous surface layer. In standard spouting bed tests,[6] this layer is worn away in the first hour or two and then the wear rate increases. Irradiation in water markedly enhanced the wear resistance of this layer (Table 11.1). Once the surface layer was removed, however, wear rates of the irradiated materials were comparable to those of the unirradiated materials.

---

[1] H. R. Hockstra, "Phase Relationships in the Uranium-Oxygen and Binary Oxide Systems," in *Uranium Dioxide: Properties and Nuclear Applications* (ed. by J. Belle), pp 230–31, Naval Reactors, Division of Reactor Development, USAEC, 1961.

[2] B. Lustman, "Irradiation Effects in Uranium Dioxide," *ibid.*, p 569.

[3] R. A. McNees *et al.*, *HRP Quart. Progr. Rept. Nov. 30, 1960*, ORNL-3061, p 101.

[4] S. A. Reed *et al.*, *ibid.*, pp 86–87.

[5] J. R. Parrott, Postirradiation Examination Group, Metals and Ceramics Division, ORNL.

[6] S. A. Reed, "Out-of-pile Evaluation of Thoria Pellets," to be published as an ORNL report.

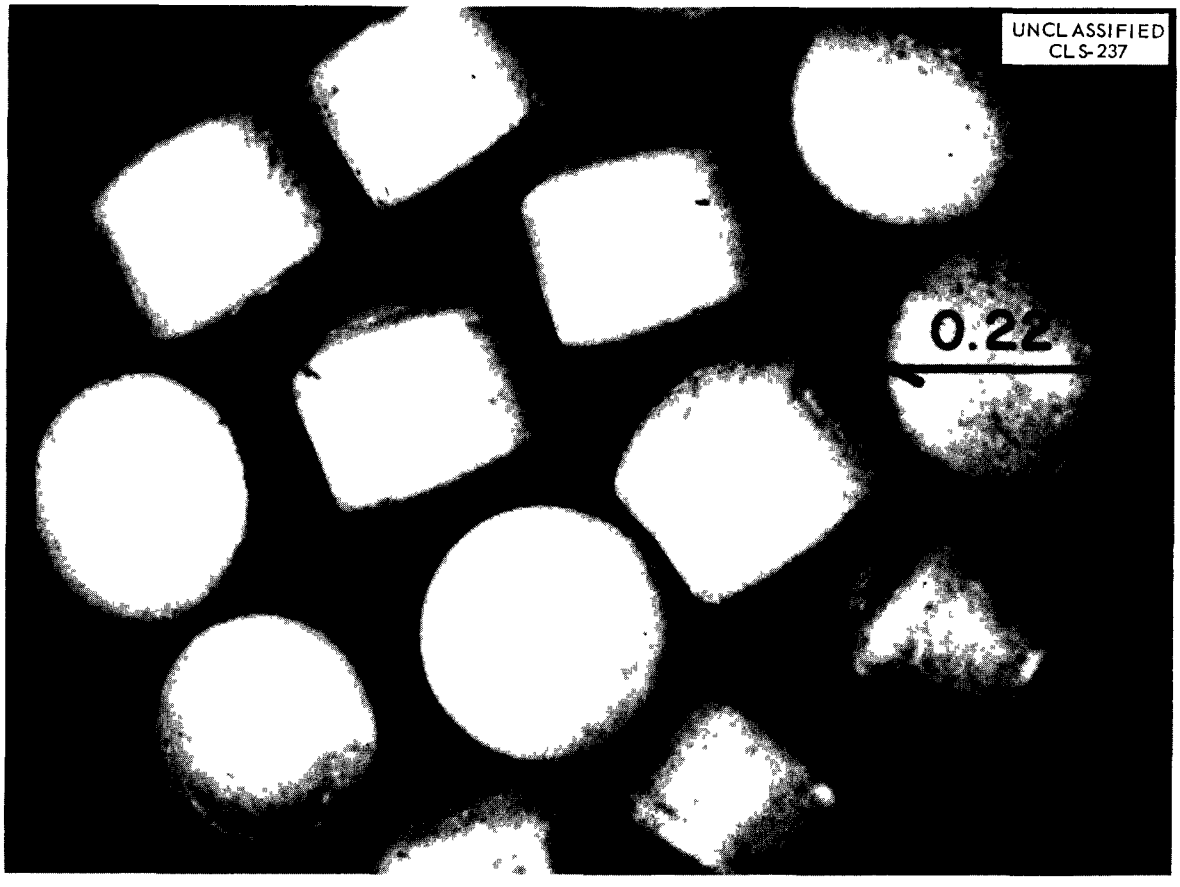

Fig. 11.1. Code P-82 Thoria Pellets.

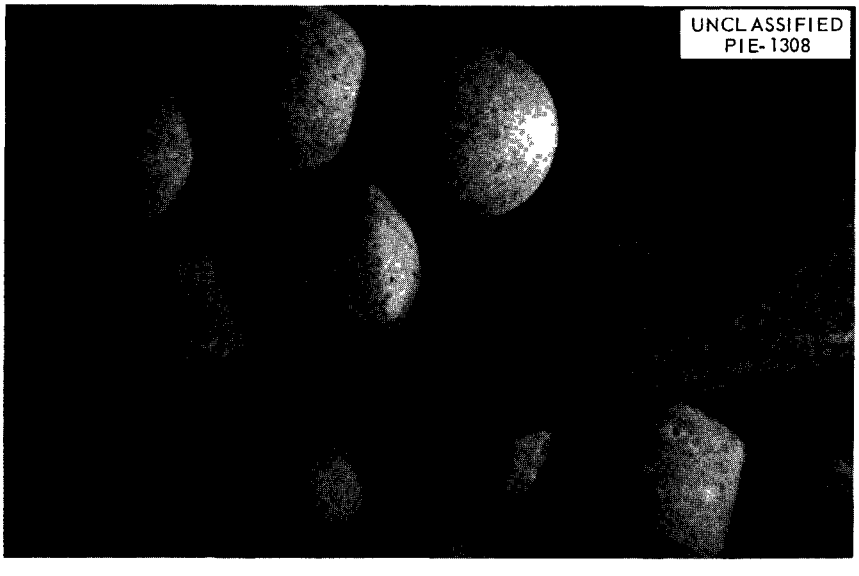

Fig. 11.2. Code P-82 Thorie Pellets Wet-Irradiated for 3 Months.

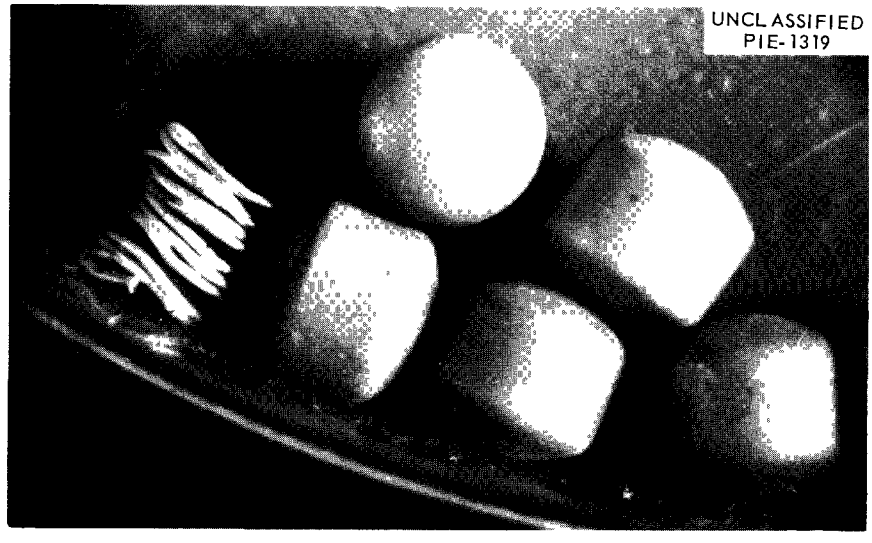

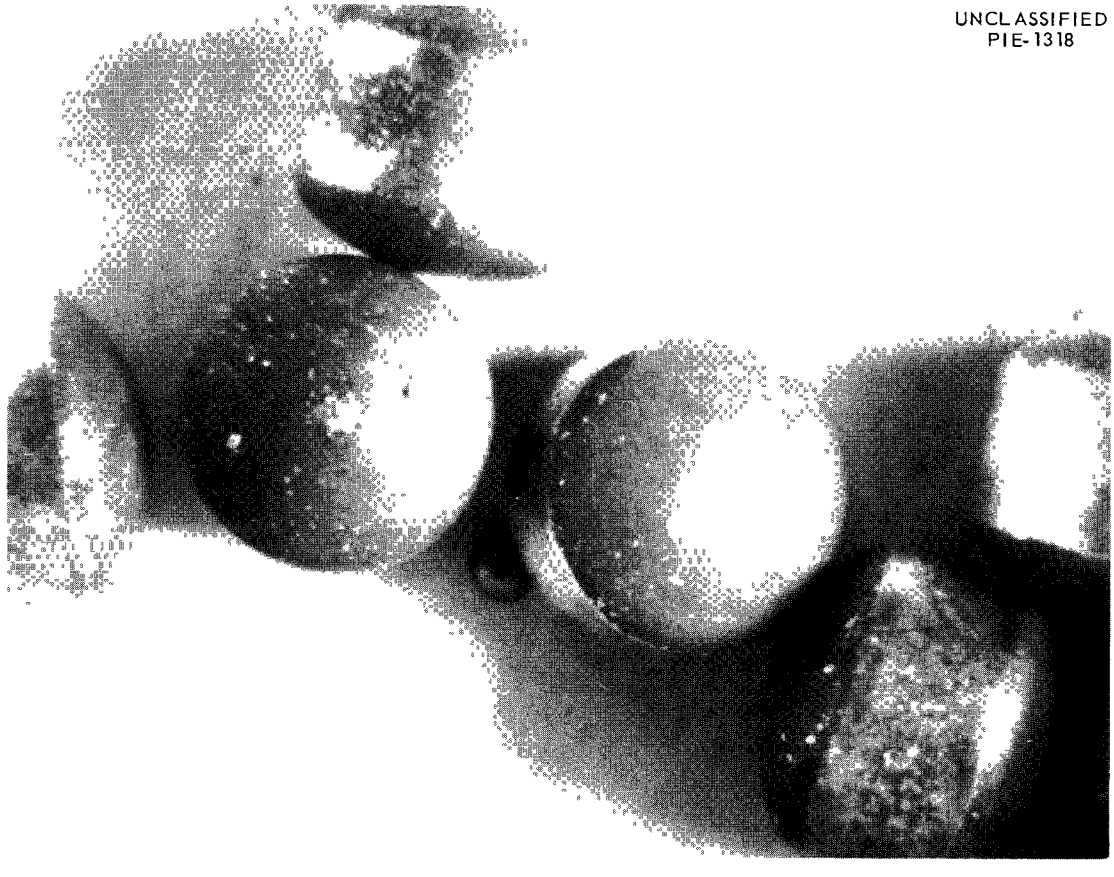

Fig. 11.3. Code P-82 Thoria Pellets Dry-Irradiated for 3 Months. (*a*) Homogeneous black color; (*b*) Metallic-like surface coating.

Table 11.1. Spouting Bed Wear Rates for Unirradiated and Irradiated P-82 Pellets

Exposure: 2×10^{20} *nvt*, 7×10^{16} fissions/g

Pellets	Weight Loss (%/hr)								
	1st	2d	3d	4th	5th	6th	7th	8th	9th–13th
Original pellets	0.06	0.08	0.07	0.17	0.15	0.43	0.20	0.30	0.32
Control pellets	0.11								
Dry-irradiated	0.03	0.22	0.22	0.32	0.37	0.22	0.37	0.27	0.33
Wet-irradiated	0.01	0.0	0.07	0.11	0.12	0.38	0.92	0.43	0.48

Nitrogen-adsorption pore size distribution data for the irradiated pellets and some treated for an extended time in 260°C water in a loop[7] indicated that irradiation in D_2O produced a small increase in void volume and a large number of small pores probably associated with individual fission events. Dry-irradiation did not increase the void volume significantly and produced a much smaller number of small pores. Porosity data on the material after the extended wear tests indicated the pores and enhanced void volume to be associated mainly with the surface shell rather than the bulk solid. Since both the irradiated and unirradiated material had densities less than 97% of theoretical, most of the void volume may be associated with pores of > 1100 A radius, which cannot be measured by the nitrogen-adsorption technique. Mercury porosimeter data for the original pellets showed pores as large as 2 μ.[8] The larger pores in the irradiated materials will be measured after a longer cooling or upon the development of the proper equipment.

Metallographs[9] of the original code P-82 thoria pellets and those irradiated in D_2O showed essentially no differences. Both the original and irradiated pellets were composed of heterogeneous structures with large dense and less dense regions, some 100 μ across, 1- to 2-μ pores, occasional pores 25–50 μ long and 10 μ wide (probably resulting from the manufacturing process), and some impurities. The interiors of the irradiated pellets showed a uniform, mottled gray-black coloration similar to that of the exterior surfaces.

11.2 IRRADIATION EXPERIMENT

Several different thoria powder and pellet preparations (50 g total) are being irradiated in D_2O in the LITR C-43 air-cooled facility at 250 to 300°C in an autoclave especially designed for multiple-sample irradiations. The purpose of the experiment is to determine whether or not any thorium oxide preparation is resistant enough to radiation damage in water to be considered for use in the blanket of a breeder-type reactor. The preparations include the code P-82 thoria pellets, sintered thoria powder compacts (prepared by a different method than the P-82 pellets),[10] shaped arc-fused thoria pellets, fired sol-gel thoria particles,[11] fired sol-gel thoria spheres (44–74 μ), arc-fused thoria fragments (44–74 μ), and 1600°C-fired thoria powder (DT-46). The preparations are separately contained in thin-walled annular stainless steel tubes designed to permit thermal convection of D_2O past the pellets. The slurry or smaller particle oxides are enclosed in single thin-walled tubes. Each sample is exposed to a common gas phase by means of sintered stainless steel closures with a 5-μ mean pore size. The experiment

[7] P. G. Dake, Special Analytical Services, Technical Division, ORGDP.

[8] S. A. Reed *et al.*, *HRP Quart. Progr. Rept. May 31, 1961*, ORNL-3167, p 84.

[9] R. J. Gray *et al.*, Metallography Group, Metals and Ceramics Division, ORNL.

[10] R. A. McNees *et al.*, *HRP Quart. Progr. Rept. May 31, 1961*, ORNL-3167, p 112.

[11] D. E. Ferguson *et al.*, "Preparation and Fabrication of ThO_2 Fuels," ORNL-3225, in press (see also chap. 13, this report).

has been operating since June 1961 and should continue until August 1962, at which time the thoria will have been exposed to a flux of $\sim 8 \times 10^{20}$ *nvt* and the U^{233} concentration will be ~ 0.5 wt %.

Samples of the multiple oxide preparations are also being irradiated dry in the LITR, the oxides are contained separately in welded aluminum capsules with helium atmospheres, and a wet out-of-pile control experiment is in progress.

11.3 RADIATION-INDUCED SINTERING OF THORIA POWDERS

The results of dry irradiation in the LITR of thoria powders fired at various temperatures were mentioned in part in a previous report[12] and are presented in detail in a topical report.[13] The following is a summary of the information contained in the topical report.

Thoria powders were prepared by refiring 650°C-fired D-16 thorium oxide[14] in platinum crucibles in air for 24 hr at 650, 800, 900, 1100, and 1500°C. Two series (C and D) were canned (air atmosphere) in aluminum capsules and irradiated in the LITR to an exposure of 1.5×10^{18} fissions/g.[15,16] Estimated maximum possible temperatures of the 650, 800, and 900°C-fired powders under irradiation were < 1000°C, of the 1100°C-fired powders, 600°C, and of the 1500°C-fired powders, 400°C. About 0.4% mass 233 isotopes was produced in each series with about 0.1% burnup of the original thorium atoms.

As a result of the irradiation, powders fired at ≤ 1100°C lost considerable surface area (Table 11.2), the 650, 800, and 900°C-fired oxides forming hard, red fragments, and the 1100°C-fired oxides chalky, off-white plugs. The 1500°C-fired materials lost little surface and were recovered as blue powders.

Crystallite size measurements by x-ray diffraction line broadening on the irradiated series D powders as recovered and after annealing 4 hr at 900°C (Table 11.2) showed no correlation with the specific surface areas. Lack of change in the x-ray-diffraction line broadening of the 1100 and 1500°C-fired materials as a result of the 900°C annealing indicates that the line broadening did not result from strain. The 900°C annealing removed the blue color of the centers of the 1500°C-fired oxide but did not change the color of the lower fired materials. The radiation-induced sintering in the lower fired materials probably resulted from recrystallization processes and material transport induced by fission fragment damage. Absence of sintering in the 1500°C-fired material, which had an original crystallite size of about 2000 A, shows that the effect was essentially confined to a volume of material of about 2000 A diam.

---

[12] J. P. McBride and O. O. Yarbro, *HRP Quart Progr Rept Apr 30, 1960*, ORNL-2947, p 82 (see also *Chem Technol Div Ann Progr Rept Aug 31, 1960*, ORNL-2993, p 124).

[13] J. P. McBride and S. D. Clinton, *Radiation Induced Sintering of Thoria Powders*, ORNL-3275.

[14] W. H. Carr, "Pilot Plant Preparation of Thorium Oxide," in *Reactor Handbook, Vol 1, Materials*, 2d ed., p 390, Interscience Publishers, N.Y., 1960.

[15] J. P. McBride and O. O. Yarbro, *HRP Quart Progr Rept Apr 30, 1960*, ORNL-2947, p 82.

[16] J. P. McBride, *HRP Quart Progr Rept July 31, 1960*, ORNL-3004, p 82.

Table 11.2. LITR Thoria Powder Irradiations

Temperature: $\leq$ 1000°C

Oxide Firing Temp (°C)	Thermal-Neutron Flux[a]		Average Particle Size (μ)			Specific Surface Area (m^2/g)			X-Ray Crystallite Size (A)		
										After 489 days' Irradiation	
	Series D	Series C	Before Irradiation	After 489 days, Series D	After 659 days, Series C	Before Irradiation	After 489 days, Series D	After 659 days, Series C	Before Irradiation	As Recovered	Annealed 4 hr at 900°C
	$\times 10^{-13}$										
650	2.6		2.4		1.3	28	1.0	<0.5	120	255[b]	390
800	1.6	1.1	2.7		3.5	15	<0.5	<0.5	220	400	446
900	1.7	1.0	2.4		1.7	8	<0.5	<0.5	500	560	440
1100	1.5	1.1	3.1	2.9	1.4	3.3	1.9	0.6	1140	540	570
1500	1.4	1.1	4.7	3.3	2.4	0.8	0.8	0.8	>2000	850[b]	820

[a] Fast flux, ~5.0 Mev, $Ti^{46}(n, p)Sc^{46}$, $\sim 1.5 \times 10^3$ nv, 489 days' irradiation = 1.5×10^{18} fissions/g.

[b] Probably low because of sample loading.

12. Gas Recombination Studies

12.1 CATALYST DEVELOPMENT

Detailed work on the development of a palladium-on-thoria catalyst for use in aqueous reactor slurries to recombine the radiolytic deuterium and oxygen is reported elsewhere.[1] The results indicate that under breeder blanket conditions at low deuterium partial pressures and under oxygen in excess of the stoichiometric ratio the specific catalytic activity is more than sufficient to recombine the radiolytic gases rapidly with very small concentrations of palladium. The experiments were made in gas-injection equipment[2] developed for the work.

Studies[3] of the effect of oxygen and deuterium pressures on the initial reaction rate showed that the reaction was first order with respect to the D_2 pressure and 0.5 order with respect to the O_2 pressure (Figs. 12.1 and 12.2):

$$\frac{dp}{dt} = kP_{D_2}P_{O_2}^{1/2}.$$

This relation appeared to be valid only when $P_{D_2}/P_{O_2} < 1$ and when the oxygen was injected first. At higher P_{D_2}/P_{O_2} ratios or when the order of injecting the gases into the system was reversed, the kinetic expression no longer held and the reaction rates were much faster than would be predicted by its use.

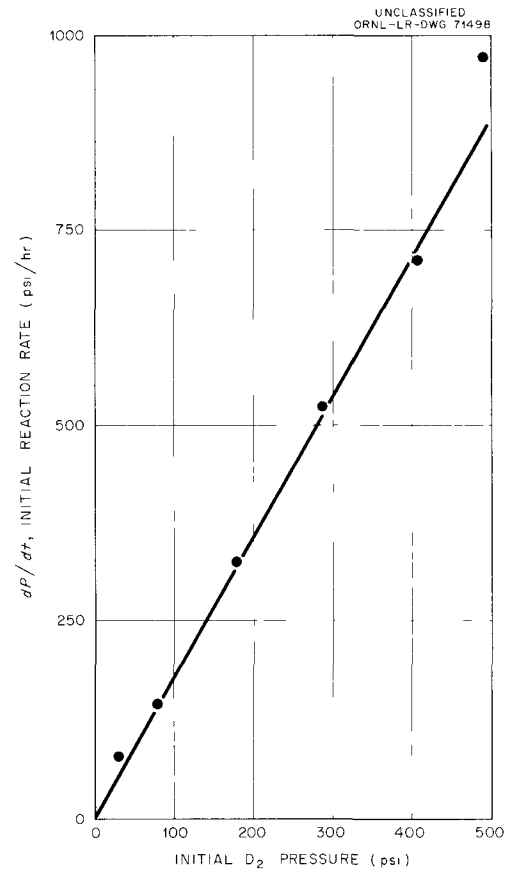

Fig. 12.1. Effect of Initial D_2 Pressure on the Reaction Rate of D_2-O_2 Mixtures in an Aqueous Thorium–0.3% Uranium Oxide Slurry. Slurry, 483 g Th per kg D_2O; catalyst, 640 ppm Pd (based on total Th); initial O_2 pressure, 320 psi; reaction temperature, 280°C.

The apparent activation energy of the reaction over the temperature range 250–280°C and with excess O_2 was 26 kcal/mole in a slurry containing 300 ppm Pd based on total thorium and 19 kcal/mole in a slurry containing 1000 ppm Pd (Fig. 12.3).

---

[1] L. E. Morse, *Initial Reaction Rates of Deuterium-Oxygen Mixtures in Aqueous Thorium Oxide Slurries Containing a Palladium on Thoria Catalyst*, ORNL-3295 (in preparation).

[2] J. P. McBride and L. E. Morse, HRP *Quart. Progr. Rept. Oct. 31, 1959*, ORNL-2879, p 175.

[3] J. P. McBride, L. E. Morse, and W. L. Pattison, *HRP Quart. Progr. Rept. May 31, 1961*, ORNL-3167, p 79.

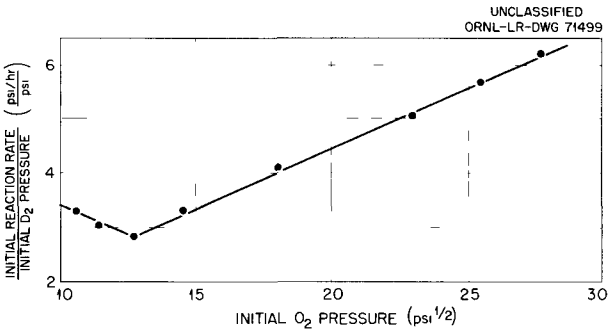

Fig. 12.2. Effect of Oxygen Partial Pressure on the Initial Reaction Rate of D_2-O_2 Mixtures in an Aqueous Thorium–0.5% Uranium Slurry. Slurry, 438 g Th per kg D_2O; catalyst, 640 ppm Pd (based on total Th); reaction temperature, 280°C.

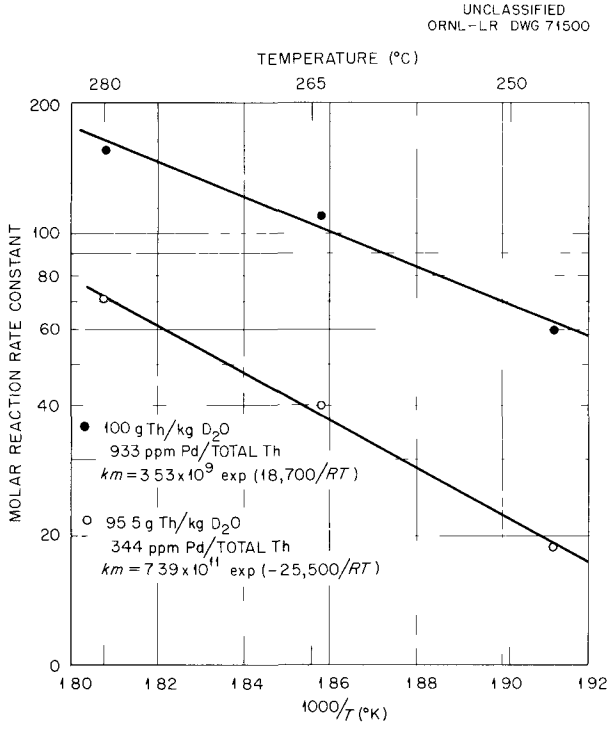

Fig. 12.3. Temperature Dependence of Molar Reaction Rate Constant.

The decrease in apparent activation energy with the higher palladium concentration may indicate that the reaction was in part diffusion controlled.

Fission product accumulation simulated by the addition of rare earth, cesium, and barium compounds in amounts equal to or greater than those expected to be present after about 1 year of irradiation (5×10^{13} thermal neutron flux) with continuous processing[4] did not affect the catalytic activity of a slurry containing 1000 ppm Pd based on total thorium and 100 g Th/kg D_2O. There was some enhancement of activity after the addition of iodine and tellurium compounds.

Definitive correlations between catalytic activities observed in laboratory autoclave experiments and those observed in pump loop experiments have not yet been obtained. In general, initial specific activities obtained in a pump loop appeared much lower than those observed in autoclave experiments and in addition catalytic activities in a pump loop appeared to decrease with time with a half life of several hundred hours.[5] Laboratory experiments with pumped slurries in one case[6] gave qualitative confirmation of a large decline of activity with time and in others[7] showed relatively little change.

Specific catalytic activities measured with slurries projected for use in in-pile autoclave corrosion experiments and slurries from mock-ups of such experiments were comparable to those obtained routinely with other slurry-catalyst systems.[3] Recombination rates obtained during in-pile tests in general did not correlate well with the laboratory data.[8,9] An experiment described below appears to indicate the lack of a deleterious radiation effect, but further studies are required for a definitive answer.

12.2 EFFECT OF IRRADIATION ON PALLADIUM-THORIA CATALYST[10]

The catalytic activity for the H_2-O_2 combination was determined for a slurry prepared from some of

[4] A. T. Gresky and E. D. Arnold, *Products Produced in the Continuous Neutron Irradiation of Thorium*, ORNL-1817, (Feb. 16, 1956).

[5] E. L. Compere *et al.*, *HRP Quart. Progr. Rept. Apr. 30, 1960*, ORNL-2947, p 107.

[6] J. P. McBride and L. E. Morse, *op. cit.*, p 88.

[7] J. P. McBride, L. E. Morse, and W. L. Pattison, *HRP Quart. Progr. Rept. Nov. 30, 1960*, ORNL-3061, p 78.

[8] E. L. Compere *et al.*, *HRP Quart. Progr. Rept. Apr. 30, 1960*, ORNL-2947, p 99.

[9] E. L. Compere *et al.*, *HRP Quart. Progr. Rept. July 31, 1960*, ORNL-3004, p 93.

[10] J. P. McBride and W. L. Pattison, *Gas Recombination Activity of Irradiated Slurry from Loop L-2-27S*, ORNL CF-62-2-88 (Feb. 12, 1962).

the dried, irradiated solids recovered from loop L-2-27S.[11] The material was a portion of that recovered from the loop dump tank. The specific activity at 280°C based on palladium concentration was at least as high as that obtained with other slurry-palladium catalyst systems that had not been irradiated[6] and more than sufficient to account for the low radiolytic gas pressures observed during in-pile operation of the loop if the postulated gamma-induced recombination should not be operative.

The experiments were carried out on the gas-injection equipment used in the catalyst development work.[2] The specific activity (normalized to 0.001 *m* Pd concentration) under a large excess of oxygen was equivalent to that obtained with unirradiated slurries [CPI (catalyst performance index) = 19 w/ml]. With H_2/O_2 ratios ≥ 0.7 activities were much higher (CPI = 25 to 96 w/ml). In an experiment that followed one in which a residual H_2 partial pressure remained at the completion of reaction, a CPI of ~4600 w/ml was observed. The very high activities at the higher H_2/O_2 ratios and after H_2 pretreatment are in accord with previous experience with unirradiated palladium catalyst-slurry systems.[7]

Hence one can conclude that the combination of simultaneous reactor irradiation and pumping under O_2 did not result in any deleterious effect on slurry catalytic activity, and drying of the irradiated slurry and subsequent resuspension in water of the dried solids had no apparent effect on catalytic behavior. Whether or not irradiation had induced a catalytic activity independent of the palladium is not known since no experiments have been made on irradiated slurry containing no catalyst. The conditions under which the above experiments were made and the excellent agreement in specific activity based on palladium concentration make it unlikely that irradiation effects alone are responsible for the catalytic activity.

[11] H. C. Savage *et al.*, *In-pile Loop Irradiation of Aqueous Thoria-Urania Slurry at Elevated Temperature. Design and In-pile Operation of Loop L-2-27S*, ORNL-3222.

13. Thorium Fuel Cycle Development

The sol-gel process[1] was developed to make dense UO_2-ThO_2 particles for the fabrication of fuel elements by vibratory compaction. Because of the radioactivity associated with thorium and U^{233} recycled from power reactors,[2] it is necessary to prepare the oxide and fabricate elements by remote operation behind shielding; hence process simplicity is highly desirable. The combination of the sol-gel process and vibratory compaction provides a simple economical system for processing and refabricating UO_2-ThO_2 fuels. This procedure is being developed in a joint effort by the Chemical Technology and Metals and Ceramics Divisions, with Chemical Technology primarily responsible for the fuel material preparation.

Emphasis in the oxide preparation program was primarily on sol-gel process development, engineering equipment development, and construction of a facility for preparation of 1000 fuel tubes for use in critical experiments at Brookhaven National Laboratory. The sol-gel process was also used to prepare uranium-thorium oxide particles containing up to 10 wt % uranium, thorium oxide spheroids of high attrition resistance for moving beds, 4 wt % plutonium thorium oxide dense fragments, and large, dense UO_2 particles.

[1] D. E. Ferguson *et al.*, *Preparation and Fabrication of ThO_2 Fuels*, ORNL-3225 (in press).

[2] D. E. Ferguson *et al.*, *Preparation and Fabrication of ThO_2 Fuels*, ORNL CF-61-6-114, p 2.

13.1 SOL-GEL PROCESS DEVELOPMENT

The process (Fig. 13.1) consists of four simple steps: preparation of ThO_2 from thorium nitrate by hydrothermal denitration, preparation of a sol by dispersion of the ThO_2 in dilute HNO_3 or uranyl nitrate solution, evaporation of the sol to a gel, and densification by low-temperature calcination.

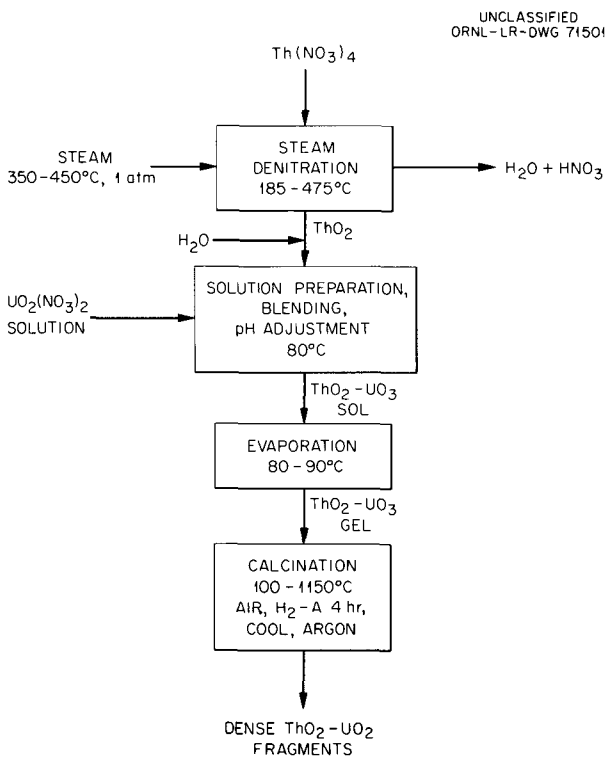

Fig. 13.1. Sol-Gel Process for ThO_2-UO_2.

Steam Denitration of Thorium Nitrate

In previous work,[1] a highly reactive ThO_2, crystallite size 70 A and surface area 80 m^2/g, was prepared by steam denitration of $Th(NO_3)_4$. For engineering scale tests, 30 kg of thorium nitrate was charged to a rotary steam kiln. As the kiln rotated, the wall temperature was raised to 185°C before steam was admitted at 350–450°C and 1 atm. Dehydration of thorium nitrate, and some denitration, began by the time 185°C was reached, but >90% of the nitrate was removed by the steam as the temperature increased to 475°C. The residual nitrate content of the product oxide depended on batch size and time at 475°C and was decreased to as low as 10 mmoles per mole of ThO_2 by air-drying after steam denitration. In the latest 13 runs, close control of specifications for the product was demonstrated, producing ThO_2 that was completely dispersible in dilute nitric acid or uranyl nitrate solution (Table 13.1).

Preparation of Sol

When properly prepared, the steam-denitration ThO_2 product was easily dispersed to a stable sol in dilute nitric acid and/or uranyl nitrate, by adding the powder to the liquid to make a 2 *M* ThO_2 suspension. The mixture was agitated at 80–90°C by recirculation through a centrifugal pump for ~2 hr. The total nitrate needed for optimum dispersion varied with the surface area of the ThO_2, and could be calculated from the crystallite size as determined by x-ray line broadening. It amounted to 0.0052 mmole of nitrate per square meter, corresponding to ~50% of the calculated ThO_2 surface-active sites[3] being occupied by nitrate. An inflection in the plot of pH vs nitric acid added occurred in sols at this nitrate concentration, at a pH of 3.1–3.3. Likewise, inflections in plots of conductivity vs NO_3^-/ThO_2 ratio occurred at this same nitrate/thoria surface ratio. At pH 3.2, ThO_2 or ThO_2-UO_3 sols behaved as though buffered, that is, the pH changed only very little with changes in concentration. The latter behavior is important in maintaining sorption of uranium on the ThO_2 surface during evaporation to a gel. If the pH is <3.1, uranium is dissolved from the solid ThO_2 surface as the sol is evaporated, which causes the gel to be nonuniform with respect to uranium content. At pH >3.3, the uranium segregated as an independent phase, which also produced nonuniformity. Knowledge of the total nitrate requirement and desired pH for a ThO_2 sol enables the operator to determine roughly the optimum concentration of the uranyl nitrate–HNO_3 solution to be used for dispersion of a given ThO_2 batch. The final pH adjustment can be made by addition of either nitric acid or ammonia.

---

[3] G. J. Spaepen, R. T. Wimber, and M. E. Wadsworth, *Adsorption of Silicia Acid on Thoria, Determined by Infra Red Spectroscopy*, Univ. of Utah Tech. Report V, Subcontract 1075 (June 30, 1959).

Evaporation

After the ThO_2-UO_3 sol has been adjusted to the optimum pH and NO_3/ThO_2 ratio, it is evaporated to a gel at atmospheric pressure, in stainless steel trays, at 80–90°C to avoid boiling. Boiling induced voidage into the gel, which was not removed by calcination. Use of temperatures below 80°C decreased particle densities and prolonged the step unnecessarily. The 3 wt % U–ThO_2 gel had a density of 6 to 7 g/cc and was easily sized by grinding. Five batches of sol-gel oxide sized at the gel stage were vibrated to a density of 8.7 g/cc in fuel tubes. Off-specification sizes at the gel stage were readily recycled by redispersing to sol by agitation in water.

Calcination

The dried gel was successfully densified by increasing the temperature at <300°C per hour to 1150°C and calcining 1 hr in air at this temperature, followed by calcining an additional 4 hr in argon containing 4% hydrogen (a noncombustible mixture) to reduce the uranium oxide to UO_2. The oxide was then cooled in argon to maintain the reduced uranium state and avoid absorption of H_2 and N_2. The density of oxide thus prepared was >99% of theoretical with an O/U ratio 2.02 ±0.01 (Table 13.2).

Table 13.1. Hydrothermal Denitration of Thorium Nitrate Crystals

Rotary calciner 12 in. diam × 48 in. long; walls preheated to 185°C; steam at 350°C, 1 atm, 20 lb/hr; calciner temperature increased to 475°C

No. of Runs	Steam		Air Calcination		Product	
	Total Time (hr)	Time at 475°C (hr)	Time (hr)	Temp (°C)	Wt (kg)	NO_3/ThO_2 mole ratio
5	6	2	0		15	0.027 ± 0.009
5	4	0.1	1	475	15	0.059 ± 0.005
3[a]	6.5	2.5	0		22.5	0.050 ± 0.006

[a] Initial steam 30 lb/hr for 2 hr at 405°C.

Table 13.2. Properties of Sol-Gel Uranium-Thorium Oxide

Batch	U^{235} Enrichment (%)	Batch Size (kg)	Method of U Addition[a]	Uranium Content (wt %)	O/U Ratio	Volatile Matter[b] (cc/g)	Compacted Density (g/cc)
Sol-gel D	93	1	ADU	2.4	2.01	0.012	8.7[c]
Sol-gel E	93	1	ADU	4.2	2.01	0.027	8.8[c]
U-3	93	4.5	ADU	5.0	2.01	0.055	8.8[d]
U-5	0.7	7	ADU	3.0	2.02	0.005	9.0[e]
U-6	0.7	7	$UO_2(NO_3)_2$	3.0	2.03	0.004	8.9[e]

[a] Ammonium diuranate and UO_3 added as slurry and $UO_2(NO_3)_2$ as solution.
[b] Volatile matter released in vacuum at 1200°C.
[c] Stainless steel tube $\frac{5}{16}$ in. diam by 11 in. long.
[d] Stainless steel tube $\frac{5}{16}$ in. diam by 48 in. long.
[e] Stainless steel tube $\frac{1}{2}$ in. diam by 48 in. long.

13.2 PROPERTIES OF SOL-GEL OXIDES

More than 50 kg of uranium-thorium oxides has been prepared by the sol-gel process, in which 2.4–5.0 wt % uranium was added as ammonium diuranate, uranium trioxide, or uranyl nitrate solution. The calcined, reduced oxide particles appear to be monolithic solid solutions in preparations containing up to 10 wt % uranium, showing only one phase in optical photomicrographs of etched and polished specimens. X-ray line-broadening data and electron micrographs indicate the material to be polycrystalline with crystal sizes > 2500 A.

Typical preparations (Table 13.2), some containing enriched uranium for irradiation testing, had properties favorable for use in reactors. Surface areas of all the oxides were <0.01 m^2/g, consistent with the high particle densities, > 9.9 g/cc. Excess oxygen was especially low in view of the low percentage of uranium. The residual volatile matter steadily decreased with improved calcination techniques.

13.3 SOL-GEL PRODUCT IRRADIATIONS

Eight fuel pins, 11 in. long and 5/16 in. OD containing sol-gel ThO_2 performed satisfactorily in the NRX reactor from April 1961 to May 1962. The peak cladding heat flux was 300,000 Btu hr^{-1} ft^{-2} at the start of the irradiation. At discharge the sol-gel fuel pins had accumulated between 10,000 and 17,000 Mwd per ton of thorium. They were replaced by six fuel pins 39 in. long containing sol-gel ThO_2-UO_2 (Table 13.2, U-3), and three fuel pins 11 in. long, each containing ThO_2-PuO_2 (4.0 wt % Pu^{239}) at a bulk density of 7.5 g/cc (not vibratorily compacted).

Seven 11-in.-long capsules were inserted in the MTR late in 1961. These specimens contained sol-gel E (Table 13.2) and arc-fused ThO_2-UO_2 (~4.0 wt % fully enriched uranium) vibrated to bulk densities between 8.6 and 8.7 g/cc. At the start of the irradiation the peak cladding heat flux was ~600,000 Btu hr^{-1} ft^{-2}. Two of these capsules were removed in April 1962 after 12,000 to 14,000 Mwd per ton of thorium for future post-irradiation examination. The irradiation of the remaining five is still in progress.

Two capsules, each containing sol-gel prepared ThO_2-UO_2 (Sol-Gel D, Table 13.2) with a central thermocouple have been irradiated in the ORR pool-side facility at an unperturbed thermal neutron flux of 3×10^{13} since January 1962. Each capsule was pneumatically vibrated to a bulk density of 8.6 g/cc and designed to operate at a linear heat output of 40,000 Btu hr^{-1} ft^{-1}. Average cladding temperatures are 1300 and 1000°F, respectively. During the three months of in-pile operation, the central temperature of the higher temperature capsule has decreased steadily from an initial 3600°F to ~2800°F. This decrease may be attributed to thermocouple drift, fuel sintering, or a combination of the two effects. The central thermocouple of the other capsule has remained essentially constant at 2700°F. Based on the design heat generation rate, the effective thermal conductivity of the ThO_2-UO_2 (center line to cladding surface) is 1.2 to 1.5 Btu hr^{-1} ft^{-1} $(°F)^{-1}$, which compares favorably with that of pellet fuels.

13.4 KILOROD FACILITY

The Chemical Technology and the Metals and Ceramics Divisions are designing and building an experimental facility, the Kilorod facility, to test and demonstrate the sol-gel-vibratory compaction procedure for manufacturing metal-clad oxide reactor fuel. Although designed primarily for experimental use, this facility will also be used to manufacture 1000 Zircaloy-clad ThO_2-$U^{233}O_2$ fuel tubes for a Brookhaven National Laboratory critical experiment. The Chemical Technology Division is responsible for removing U^{232} decay daughters from the U^{233} by solvent extraction and for preparing a mixed oxide, by the sol-gel process, suitable for sizing operations. The Metals and Ceramics Division will size the oxide particles, compact them in Zircaloy tubes by vibration, and weld the tubes closed.

The U^{233} from U^{232} decay daughters will be purified in the Thorex Pilot Plant solvent extraction equipment in cells 5, 6, and 7 of building 3019. The flowsheet used will be the thorium rejection type (Interim-23) with either tributyl phosphate or di-*sec*-butylphenyl phosphonate as solvent. The latter solvent is expected to provide improved separation of uranium from thorium, thus better removing Th^{228}, the first daughter product in the U^{232} decay chain. Criticality will be avoided by various combinations of batch size, geometry, fixed poisons, and concentration control.

Modifications to the Thorex Pilot Plant equipment are in progress.

Thorium oxide prepared in building 4501 in the rotary steam denitrator will be transferred to cell 4 of Building 3019, where the sol-gel and fuel refabrication equipment is being located. The ThO_2 and uranyl nitrate solution will be mixed in a blend tank located in a shielded cubicle on the third level inside the cell, and the sol will be pumped to a tray dryer. Four drying trays will be used per 15-kg batch, each tray being 27 in. square by 1 in. deep. The containment cubicles will be shielded with 4 in. of steel or 8 in. of 3.3-g/cc concrete. Because of the relatively low level of radiation inside the cubicle and the infrequency of operations in it, it is feasible to use the gloved hand with tongs for manipulation. However, all gloved ports will normally be shielded. The final oxide will be transferred through a chute to a lower level in cell 4 for sizing and fuel tube manufacture.

Design of all equipment is now completed, and fabrication and installation are in progress. Operation is scheduled to begin in September 1962.

13.5 THORIA PELLET PREPARATION BY SOL-GEL PROCESS

By rounding the particles while in the gel state it is possible to make spheres of ThO_2 by the basic sol-gel process. Such spheres are desirable as a blanket material for reactors with a static or fluidized thoria bed in direct contact with water. For such an application the thorium oxide spheres must be $\frac{1}{8}-\frac{1}{4}$ in. diam and be attrition resistant and stable in water at high temperatures.

Seven batches of rounded thoria particles in the 4–8 mesh range prepared by the sol-gel process had attrition losses of $<0.1\%$ per hour as tested in a hydraulic spouted bed. This test was based on an average weight loss from the fluidization of 10 g of pellets in three consecutive 1-hr tests. The pellets were made from three thoria sources: oxalate-precipitated 925°C-fired ThO_2 standard steam-denitrated thorium oxide, which was refired in air for 4 hr. Pellet preparation consisted of dispersion of thoria to sols with nitric acid slightly in excess of the quantity required for maximum dispersion, pH adjustment to the optimum with ammonia, evaporation to the gel, rounding the gel particles by tumbling in a high-fired thoria powder, and finally calcination to obtain densification and strength. For the steam-denitrated oxides the optimum pH was 3.1–3.3. For the high-fired oxalate-derived oxide it was about 2. The optimum calcination temperature to obtain maximum attrition resistance was 1400°C. One batch of rounded pellets made from the 925°C-fired oxalate had initial attrition rates of 0.04 wt % per hour; after they had been autoclaved in water at 265°C for 72 hr the attrition rate was 0.025 wt % per hour. Two pellet preparations containing 3 wt % uranium showed attrition rates of 0.051 and 0.054 wt % per hour. Therefore it appears that both pure thoria and thoria-urania pellets with high attrition resistance and good stability in water at high temperatures can be made by the sol-gel technique.

14. Thorium Recovery from Rocks

In the long-range future, nuclear fuel supplies for power production will inevitably depend on low-grade sources, since high-grade reserves of uranium and thorium are extremely limited. Information on the extent and probable treatment costs of low-grade thorium sources is being obtained. After tests of a large variety of granitic rocks from different locations,[1,2] current interest has centered principally on the Conway granite formations in New Hampshire which are higher-than-average in thorium content. Cursory tests have also been made with other granites and other types of thorium-bearing rocks.

14.1 GRANITE SAMPLE COLLECTION AND EXPLORATION

Additional analyses of granite samples collected from major granitic bodies throughout the United States and Canada continued to support earlier indications[1] that the Conway granite in New Hampshire is one of the more important reserves of thorium and uranium. The Conway formation was extensively surveyed in the summer of 1961 with a portable transistorized gamma-ray spectrometer.[3] From radiometric data (Fig. 14.1) obtained at several hundred outcroppings, the accessible surface of the main mass of the Conway granite was estimated to average 56 ± 6 ppm thorium. This compares with 12 ppm thorium in average grade granite. The main mass of the Conway granite includes an area of at least 300 sq miles, and, assuming that the thorium concentration persists with depth, the reserves of thorium in the Conway formations are estimated at tens of millions of tons. Drilling of the Conway formation during the summer of 1962 is planned to obtain information on the vertical distribution of thorium.

Several samples from less extensive granite formations in New Hampshire, Maine, Vermont, Massachusetts, and Rhode Island contained thorium in concentrations equivalent to the Conway formation. These areas will be explored further.

14.2 GRANITE MINERALOGY

Preliminary studies[3] of autoradiographs and photomicrographs suggest that a substantial fraction of the thorium and uranium in Conway granite

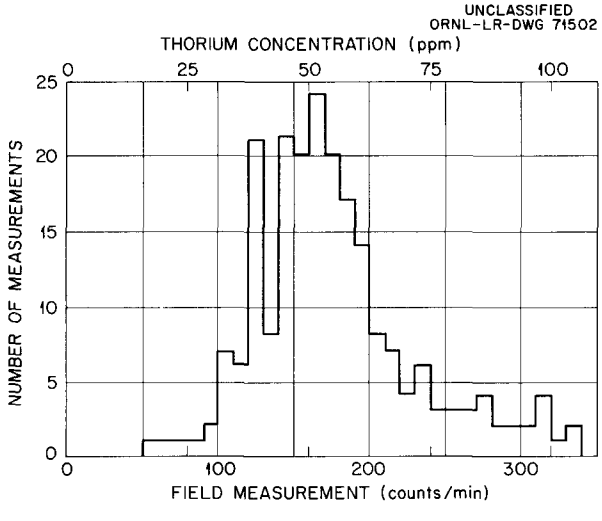

Fig. 14.1. Frequency Plot of Field Determinations on Conway Granite.

[1] *Chem. Technol. Ann. Progr. Rept. May 31, 1961*, ORNL-3153.

[2] H. Brown and L. T. Silver, "The Possibilities of Securing Long-Range Supplies of Uranium, Thorium, and other Substances from Igneous Rocks," *Proc. Intern. Conf. Peaceful Uses At. Energy, Geneva, 1955* 8, 129 (1956).

[3] By Rice University under subcontract to ORNL.

is contained in "hot grains" enclosed in biotite and that many of the "hot grains" are pyrochlore, conventionally $NaCaNb_2O_6F$, but commonly containing large amounts of other elements, including actinides and lanthanides. To the extent that these observations are true, physical beneficiation methods may be considered to concentrate the biotite fraction and thus the thorium. There should also be a positive correlation between the thorium and niobium content of these granites.

14.3 GRANITE PROCESSING AND COSTS

The Conway granite, in addition to having a relatively high thorium content, is generally more amenable to acid leaching than granite from most other formations studied. Recoveries in acid leaching of Conway granite from 13 widely scattered locations ranged from 52 to 85% for thorium and 26 to 75% for uranium (Table 14.1). The head samples contained 36–106 (av 58) ppm thorium and 6–19 (av 11) ppm uranium. The fineness of grinding in the range –20 to –200 mesh had no significant effect on recovery of thorium from Conway or from Pikes Peak granite samples.

Preliminary estimates of recovery costs for the 13 samples by a countercurrent sulfuric acid leach–amine extraction flowsheet ranged from $23 to $83 per pound of thorium plus uranium recovered (Table 14.1). These costs are considered acceptable for breeder reactor systems. If single-stage rather than countercurrent leaching must be used, costs would average about 10% higher due to the

Table 14.1. Estimated Costs for Recovering Thorium and Uranium from Conway Granite

Pulverized ore or –48 mesh, leached 6 hr at room temperature with 2 *N* H_2SO_4, 50% pulp density

Sample Location	Head Concentration (ppm)		Recovery in Leaching (%)		H_2SO_4 Consumption (lb per ton of ore)	Estimated Recovery Cost[a] ($ per lb Th + U)
	Th	U	Th	U		
North Conway quadrange, N. H.	50	13	60	26	93	70
Crawford Notch quad., N. H.	48	12	52	39	109	83
Plymouth quad., N. H.	54	12	84	73	80	42
North Conway quad., N. H.	56	7	53	51	66	64
Plymouth quad., N. H.	64	12	84	60	60	34
Franconia quad., N. H.	76	14	58	50	72	42
North Conway quad., N. H.	70[b]	14[b]	78[b]	60[b]	80[b]	34
North Conway quad., N. H.	45	6	67	49	93	70
Crawford Notch quad., N. H.	52	12	67	65	111	58
Ossipee Lake quad., N. H.	106[c]	13[c]	82[c]	75[c]	80[c]	23
Mt. Ascutney, Vt.	36	6	80[d]	49	55	64
North Conway quad., N. H.	46	10	85[d]	61	77	49
Mt. Chocorua quad., N. H.	51	8	81[d]	69	86	49
					Average	52

[a] Includes direct operating costs for mining (68¢/ton) and milling, overhead, contingency allowance, amortization (10 yr), and 14% annual return on capital investment.

[b] Average for five samples from Redstone Quarry.

[c] Average results obtained with two samples from Band Ledge Quarry.

[d] Leaching tests at 60% pulp density.

higher acid consumption. Bases for the estimates[4] were the same as described earlier.[1]

14.4 LATERIC SOILS AND VOLCANIC ROCKS

Preliminary analyses and tests of sublateritic soils from southeastern United States and volcanic rocks from Italy and Nevada indicated that these materials represent less promising sources of thorium than granites. The volcanic rocks contained 12–50 ppm thorium but were resistant to acid leaching. The sublateritic soil samples were uniformly low in thorium, that is, 5–16 ppm.

[4]Made in cooperation with A. H. Ross and Associates of Toronto, Canada.

15. Radiation Effects on Catalysts

15.1 CONVERSION OF CYCLOHEXANOL TO CYCLOHEXENE WITH $MgSO_4$ AND $MgSO_4$-Na_2SO_4 CATALYST

It has been reported that when small amounts of radioactive S^{35} are incorporated in $MgSO_4$ and $MgSO_4$-Na_2SO_4 catalysts, their catalytic activity for the dehydration of cyclohexanol is enhanced.[1,2] Initial experiments appeared to substantiate these results,[3] but difficulties were encountered in measuring the specific surface areas of the catalysts.[4] These difficulties were resolved by designing equipment so that atmospheric exposure of the catalyst was avoided. In subsequent experiments, in which comparisons were made on the basis of unit surface area, the radioactive catalysts were found to be less active catalytically than their nonradioactive counterparts.

Measurements of initial reaction rates with $MgSO_4$ catalysts showed the radioactive catalysts to be about half as active as the nonradioactive. After 7 to 12 hr use, the radioactive catalysts were one-half to one-third as active, depending on the temperature (Fig. 15.1*a*). Initially, both materials showed the same apparent energy of activation, but on aging the radioactive catalysts showed a greater increase in activation energy, with 6 kcal/mole difference at steady state.

Typical results with $MgSO_4$-Na_2SO_4 catalysts containing 2.5 wt % Na showed the radioactive catalysts to be less active than the nonradioactive, both before and after aging (Fig. 15.1*b*). With fresh catalyst the effect was greater than in the case of pure $MgSO_4$, even though the radioactivity was only about a third as much. After aging, the magnitude of the effect was the same. In general, the sodium-containing catalysts were less active per unit surface area than the $MgSO_4$ catalysts and showed higher apparent energies of activation except for fresh nonradioactive material. Results were similar with a sodium concentration of 0.98 wt %.

Aging curves for $MgSO_4$ catalysts showed a relatively sharp decrease in catalytic activity after about 5 hr use (Fig. 15.2), which is not explained. Curves for $MgSO_4$-Na_2SO_4 were similar. The effect appears to be irreversible and to require the presence of the reacting vapors. The surface area decrease of $< 10\%$ during aging cannot account for the loss of activity observed. Infrared, x-ray, and thermogravimetric studies of $MgSO_4$ surfaces showed that no phase change is involved and that even in the presence of water vapor no mono-

[1]A. A. Balandin *et al.*, *Dokl. Akad. Nauk SSSR* 121, 495 (1958).

[2]A. A. Balandin *et al.*, *Actes Congr. Intern. Catalyse, 2e, Paris, 1960* 2, 1415 (1961).

[3]*Chem. Technol. Div. Ann. Progr. Rept. Aug. 31, 1960*, ORNL-2993, chap. 17.

[4]*Chem. Technol. Div. Ann. Progr. Rept. May 31, 1961*, ORNL-3153, chap. 18.

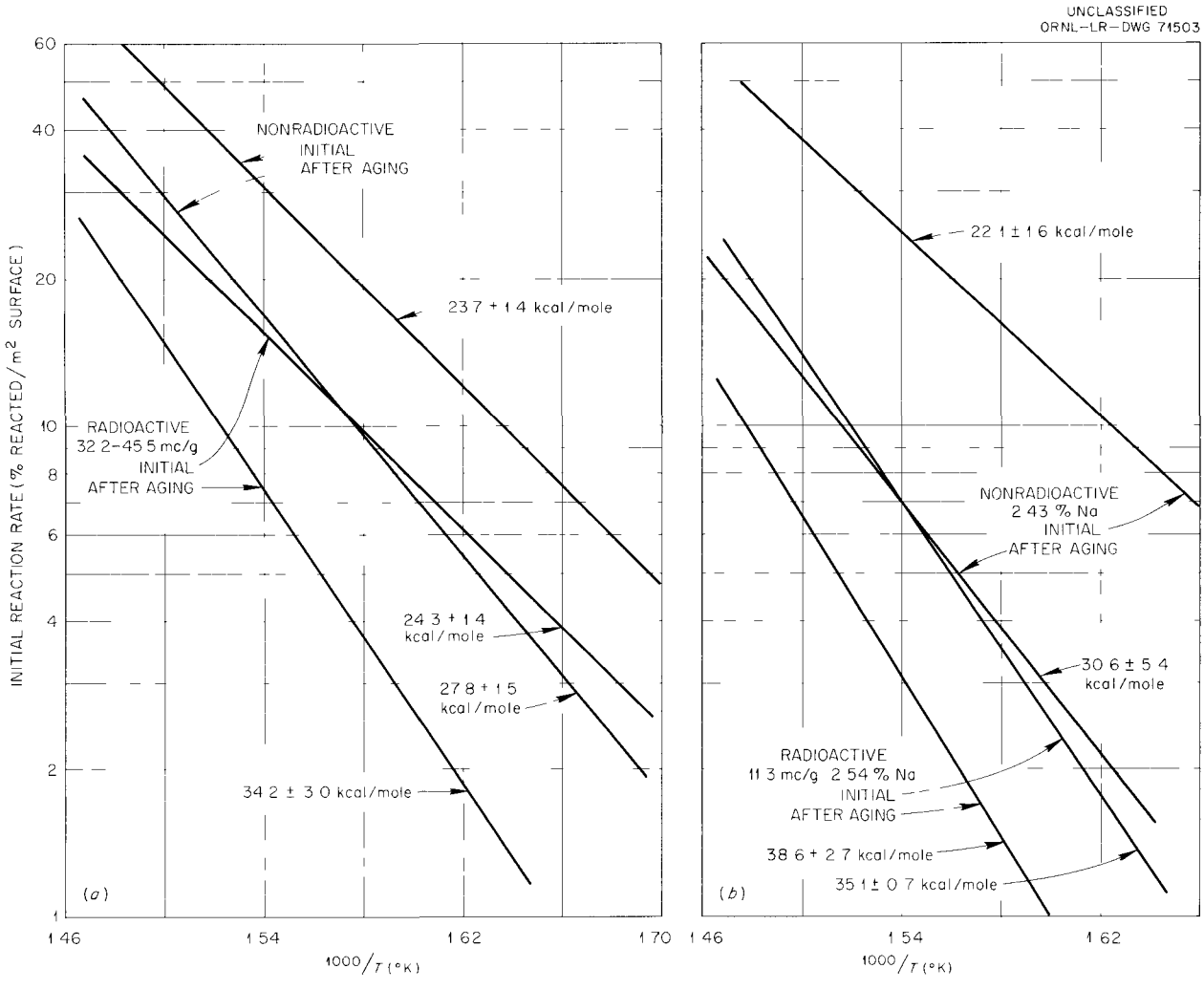

Fig. 15.1. Dehydration of Cyclohexanol on (*a*) $MgSO_4$ Catalysts and (*b*) $MgSO_4$-Na_2SO_4 Catalysts.

hydrate can exist at the temperatures used.[5] Dehydration of the monohydrate proceeded according to the equation

$$2\,MgSO_4 \cdot H_2O \rightleftharpoons Mg(HSO_4)_2 \cdot Mg(OH)_2 \rightleftharpoons 2\,MgSO_4 + 2H_2O\,.$$

The radioactive catalysts also lost catalytic activity with time in storage. This has been interpreted in the literature as unequivocal evidence that the level of radioactivity of the catalyst, which was decreasing with time, was the controlling factor.[2] However, it was found that nonradioactive catalysts also lose catalytic activity with time (Fig. 15.3), showing that the loss is not related to the radioactivity but is a property of the catalyst surface. For a given drying treatment, radioactive catalysts generally showed smaller crystallite sizes and larger specific surface areas than their nonradioactive counterparts. This phenomenon is believed to be responsible for the erroneous reports of enhanced catalytic activities on the addition of radioactive sulfur to these materials. All the evidence available indicates that any effect of the radioactivity is due only to its presence during the catalyst preparation stage and that its presence at the time of reaction is of no significance. This conclusion is supported by the

[5]Work done by University of Utah under subcontract.

previously reported observation that externally supplied radiations are without effect on the dehydration reaction.[2,4] Possibly the beta-particle tracks provide nucleation sites for crystallization, or perhaps small surface charges generated as a result of beta decay affect the growth and sintering properties of the crystallites.

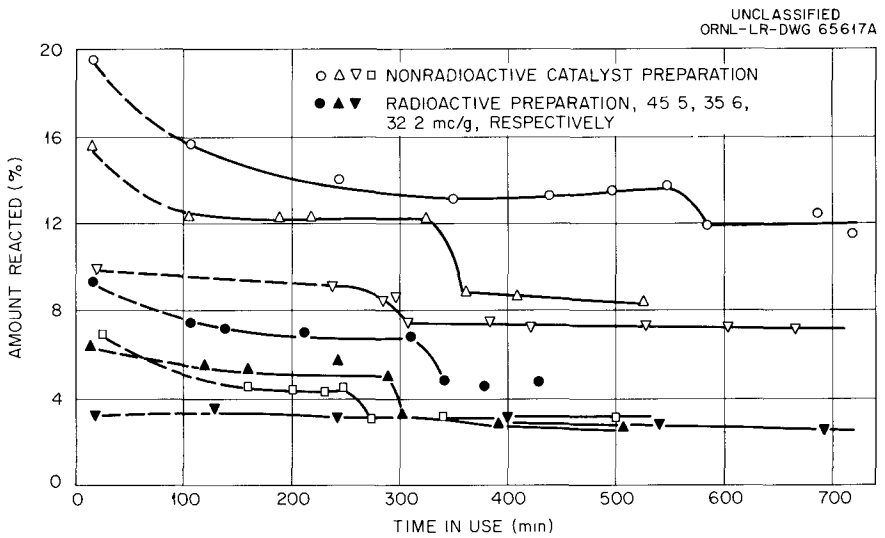

Fig. 15.2. Aging of Magnesium Sulfate Catalysts; 50 mg of Catalyst, 402–404°C.

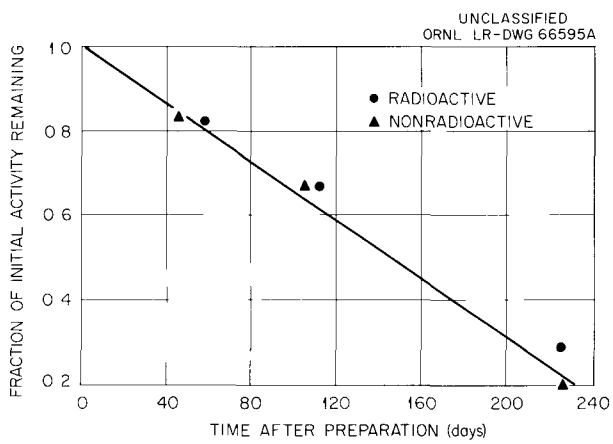

Fig. 15.3. Effect of Storage Time on Activity of Magnesium Sulfate–Sodium Sulfate Catalysts at 408°C.

16. High-Temperature Chemistry[1]

16.1 HIGH-TEMPERATURE HIGH-PRESSURE SPECTROPHOTOMETRIC SYSTEM

Detailed drawings for the spectrophotometer system[2] for operation at temperatures up to 330°C and at pressures up to 3000 psi were completed.[3] It is anticipated that with this system it will be possible to make measurements up to near the critical point (~372°C) in both water and deuterium oxide. The major parts of the system (Figs. 16.1 and 16.2) are: Cary model 14 PM spectrophotometer redesigned to provide a 20-cm optical path length and larger optical and cell components; optical bench; chopper and beam-alternator system and compartment; phototube and source compartment; high-pressure high-temperature cell compartment; cell assemblies; heating system; high-vacuum system; main spectrophotometer cart; and control console. Among the important features

[1]Joint program with the Analytical Chemistry Division. For additional details see *Anal. Chem. Div. Ann. Progr. Rept. Dec. 31, 1961*, ORNL-3243, p 20.

[2]*Chem. Technol. Div. Ann. Progr. Rept. May 31, 1961*, ORNL-3153, p 130.

[3]By Applied Physics Corporation, Monrovia, Calif., under subcontract.

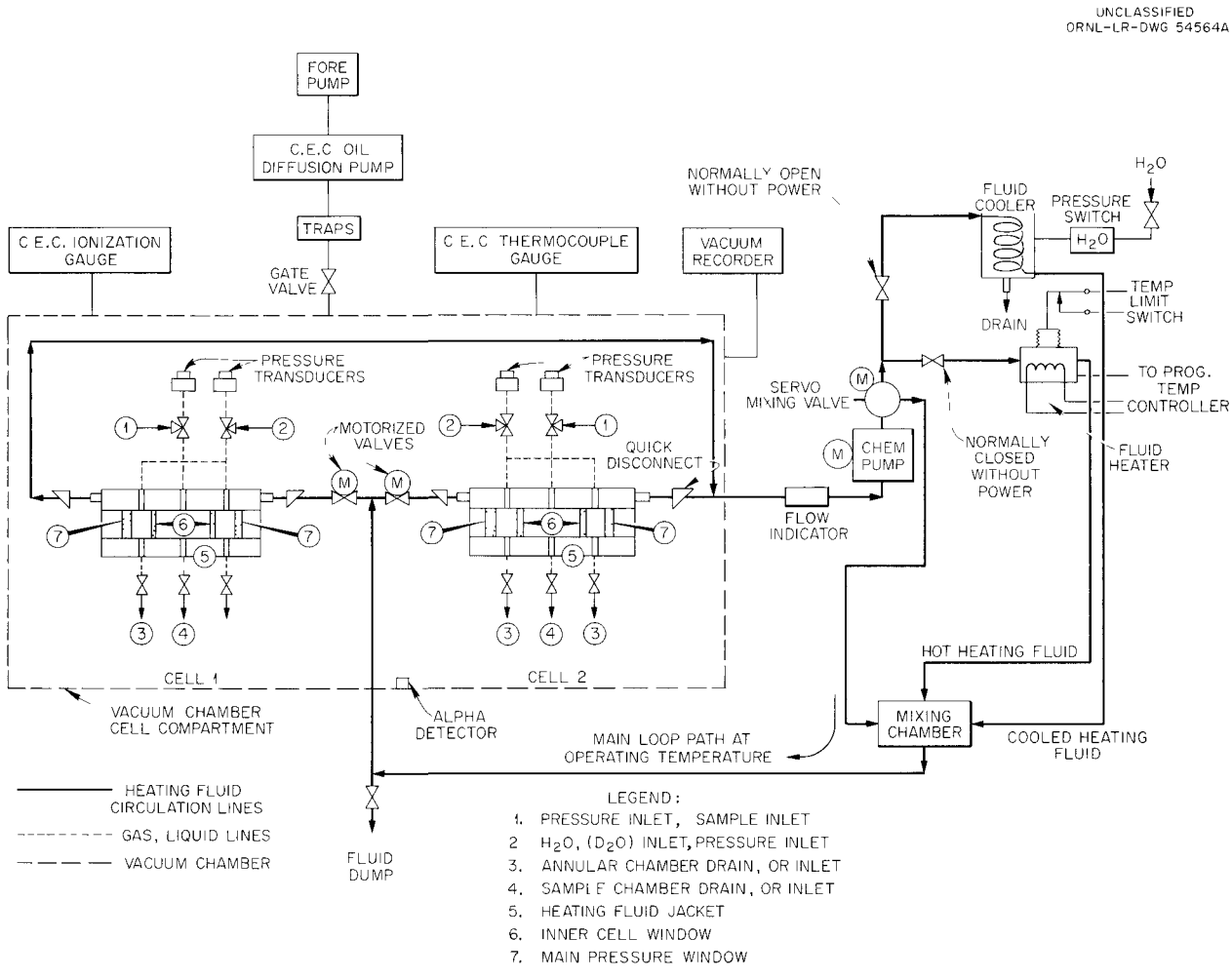

Fig. 16.1. Schematic Plan for High-Temperature High-Pressure Cells and Vacuum and Heating System.

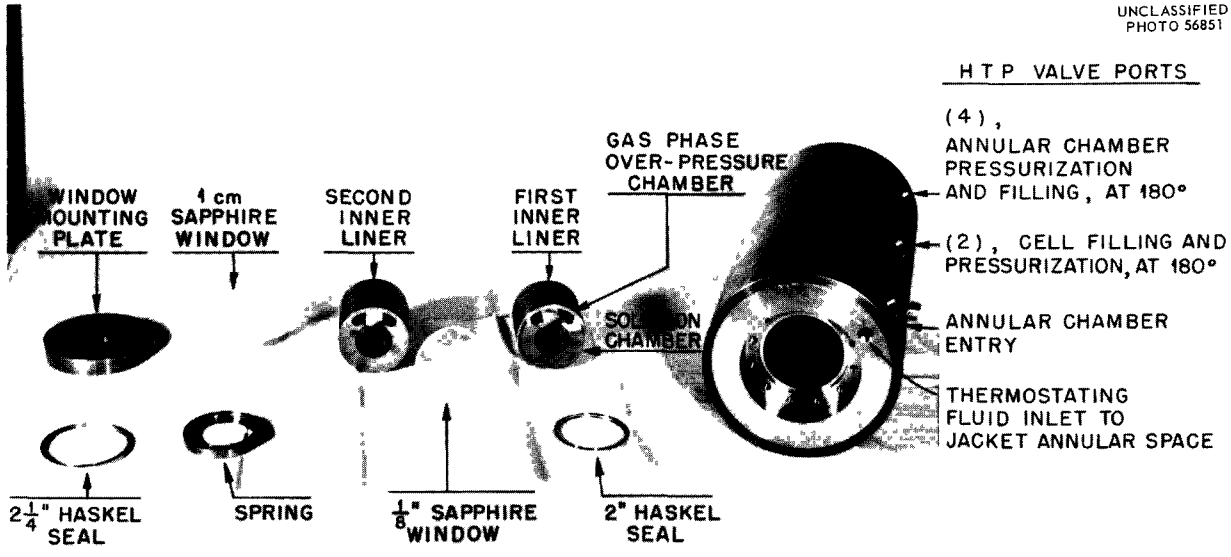

ORNL High-Temperature High Pressure Spectrophotometer Cell Assembly

(Components: approximately $\frac{1}{3}$ size)

Fig. 16.2. ORNL High-Temperature High-Pressure Spectrophotometer Cell Assembly.

of the system are an automatic digital data-readout system that reads out on IBM cards; a viewing port and mirror arrangement to permit visual observation of the test solution at all operating temperatures and pressures; and a variable, vertical, auxiliary slit system to permit spectral measurements on individual phases of two-phase systems. The absorption cells can be rocked while the system is operated at the maximum conditions of temperature and pressure in order to mix the solutions (or separate phases), to equilibrate the gas and liquid phases in the absorption cell, and to facilitate removal of bubbles that form on the windows.

16.2 MINIATURE CIRCULATING-LOOP SYSTEM FOR A CARY MODEL 14 PM SPECTROPHOTOMETER

A miniature loop system (Fig. 16.3) was designed and constructed for use with an unmodified Cary model 14 PM spectrophotometer for operation at moderate pressures (200 psi) and at temperatures up to about 150°C. The loop contains an in-line variable-porosity filter system and a sample container system that permits exposing corrosion specimens, ion exchange resins, and other solids to the circulating liquid.

16.3 MATHEMATICAL RESOLUTION OF SPECTRAL FINE STRUCTURE AND OVERLAPPING ABSORPTION SPECTRA BY MEANS OF HIGH-SPEED DIGITAL COMPUTING

Computer programs for the mathematical resolution of overlapping absorption spectra by the IBM 7090 computer are being written, and codes for the Oracle and IBM 704 are being converted for operation on the IBM 7090. The conversion includes the writing of curve-plotting programs for plotting IBM 7090 output on the curve-plotting facility of the Oracle. Use of a recently installed automatic, digital, data-output (on IBM cards) system for the Cary Model 14 PM spectrophotometer will implement the spectrophotometry program.

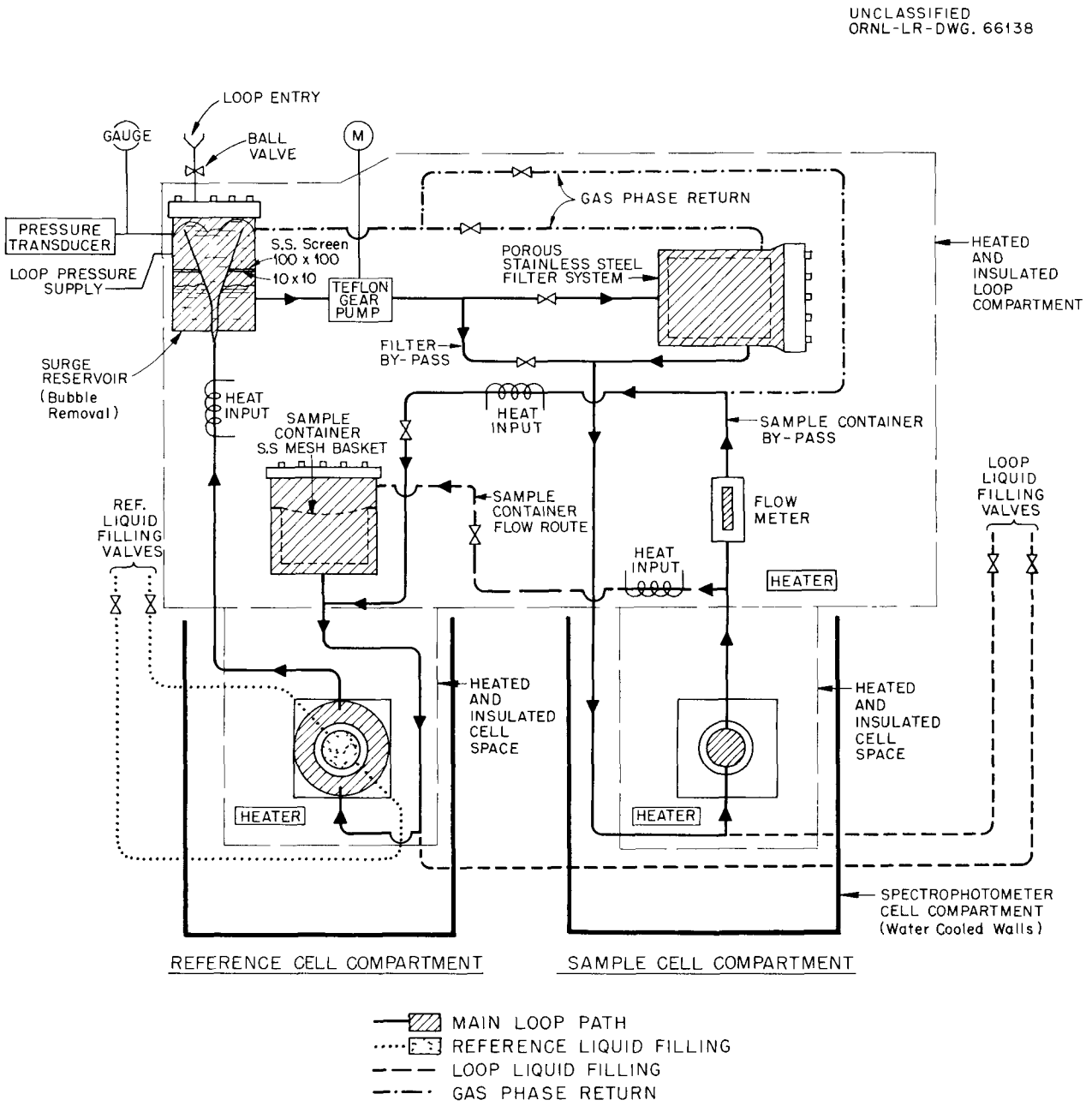

Fig. 16.3. Spectrophotometer Loop System for Operation at Elevated Temperatures and Pressures.

16.4 CALCULATED EFFECT OF CERENKOV RADIATION ON ABSORPTION SPECTROPHOTOMETRIC MEASUREMENTS ON INTENSELY RADIOACTIVE SOLUTIONS

Extraneous light from Cerenkov radiation is a potential source of interference in absorption spectrophotometric and other light-dependent measurements made on radioactive solutions, and the extent of the interference can be evaluated if the intensity of the Cerenkov radiation is known. A method based on graphical summation of photon contributions from electron energy distributions[4] was developed for calculating the intensity of Cerenkov radiation from specified beta- or gamma-emitting sources or from mixtures of such sources over the visible and near-ultraviolet spectral regions.

[4]R. G. Wymer and R. E. Biggers, *Cerenkov Radiation Intensity Calculations for Sr^{90} and Co^{60} in Water*, ORNL-3180 (Sept. 5, 1961).

17. Mechanisms of Separations Processes

17.1 DISTRIBUTION OF NITRIC ACID BETWEEN AQUEOUS AND TBP–HYDROCARBON DILUENT SOLUTIONS

Single-stage equilibrium data on the distribution of nitric acid between aqueous and TBP–Amsco 125-82 solutions, for all diluent/TBP ratios and for aqueous acidities of up to ~5 *M* were found[1-3] to be described by

$$\log \frac{(HNO_3)^c_{org}}{[HNO_3]^c_{aq}\{(TBP_s) - (HNO_3)^c_{org}\}} = \log\{B_1 + B_2(Y^\circ_{TBP} + Y^\circ_{H_2O})\} + B_3(Y^\circ_{TBP} + Y^\circ_{H_2O})^{1/2}\frac{(HNO_3)^c_{org}}{(TBP_s)}, \quad (1)$$

where brackets refer to activities; parentheses refer to concentrations; the superscript c designates molar concentrations; subscripts org and aq designate the organic and aqueous phases, respectively; B_1, B_2, and B_3 are constants; Y°_{TBP} and $Y^\circ_{H_2O}$ are the mole fractions of TBP and H_2O in the water-saturated, but acid-free, organic solution; and (TBP_s) is the stoichiometric molarity of TBP in the organic solution. The activity $[HNO_3]^c_{aq}$ was calculated as the product $(C_s y_s)^2$, where C_s and y_s are the stoichiometric molarity and activity coefficients of HNO_3 in aqueous solutions. The applicability of Eq. (1) to values of $(HNO_3)^c_{org}/(TBP_s)$ up to nearly 0.75 and the results of analyses for water in the organic phase[2] suggest that the extraction of nitric acid may be described by

$$[TBP + TBP\cdot H_2O]_{org} + (HNO_3)_{aq} \rightleftharpoons [TBP\cdot HNO_3 + TBP\cdot HNO_3\cdot H_2O]_{org}$$

the equilibrium constant for which is K^c_1 in molar units. This implies that neither TBP and the so-called complex $TBP\cdot H_2O$ nor $TBP\cdot HNO_3$ and $TBP\cdot HNO_3\cdot H_2O$ are distinguishable species. On this basis y_s may be defined as the mean molar activity coefficient of TBP and $TBP\cdot H_2O$, and similarly, y_{TN} as a mean molar activity coefficient of the species $TBP\cdot HNO_3$ and $TBP\cdot HNO_3\cdot H_2O$. From such a definition, the terms on the right-hand

[1]W. Davis, Jr., "Thermodynamics of Extraction of Nitric Acid by Tri-*n*-Butyl Phosphate–Hydrocarbon Diluent Solutions. Part I," to be published in *Nuclear Science and Engineering*.

[2]*Ibid.*, Part II.

[3]*Ibid.*, Part III.

side of the equality sign in Eq. (1) describe the quantities $K_1^c y_T$ and y_{TN}:

$$K_1^c y_T = B_1 + B_2(Y^o_{TBP} + Y^o_{H_2O}) \qquad (2)$$

and

$$\log y_{TN} = B_3(Y^o_{TBP} + Y^o_{H_2O})^{1/2} \frac{(HNO_3)^c_{org}}{(TBP_s)} . \qquad (3)$$

Many literature data[4-8] may be described by Eq. (1). Constants B_1, B_2, and B_3 (Table 17.1) determined for Amsco 125-82 in the present work[3] are also applicable to the odorless kerosene of refs 5 and 7, the corresponding constants for the diluent *n*-hexane, determined from the data of ref 6, are also applicable to ref 5 and are nearly the same as those determined for Amsco 125-82 (Table 17.1).

Equation (2) expresses the product $K_1^c y_T$. For diluent-free TBP its value is about 1 5, but neither K_1^c, nor y_T, the activity coefficient of TBP in H_2O-saturated TBP referred to unit activity coefficient for anhydrous TBP, can be calculated from the present work. The quantity y_T can be calculated from partial pressures of TBP over the anhydrous and water-saturated system. Preliminary values of these pressures, measured by the transpirational vapor pressure technique in conjunction with P^{32}-labeled TBP,[9] were ~0.8 μ Hg for TBP containing 0.2 wt % H_2O and 0.51 μ Hg for TBP saturated with H_2O, containing ~6.5 wt % H_2, or having a mole fraction of H_2O equal to 0.511 (ref 2). The 0.8 μ Hg pressure over nearly anhydrous TBP is lower by a factor of about 10 than the value for pure TBP calculated by extrapolation of the data of ref 10. A preliminary value of y_T for H_2O-saturated TBP is, therefore, 0.51/0.8 or ~0.64 if the sum of mole fractions (TBP + TBP·H_2O) is used, as suggested by the interpretation above that TBP and TBP·H_2O are not thermodynamically distinguishable species.

Previous calculations[1,3] of the distribution of HNO_3 between aqueous and TBP-diluent solutions were limited to aqueous acidities below ~5 *M* due to the discrepancy between the nitric acid activity coefficients given in the Landolt-Bornstein tables and those extrapolated from the data of Hartmann and Rosenfeld[11] for acidities above above ~3 *M*. Nitric acid vapor pressure data of Potier[12] and of Vandoni and Laudy[13] give further support to the existence of a discrepancy (Fig. 17.1) even though the lowest concentration of the vapor pressure measurements was ~8 *M*. To help establish the activity coefficients of HNO_3 more

[4] J. W. Codding, W. O. Haas, Jr., and F. K. Heumann, *Ind. Eng Chem* 50, 145 (1958).

[5] T. V. Healy and P. E. Brown, AERE C/R 1970 (June 6, 1956).

[6] D. R. Olander, L. Donadieu, and M. Benedict, *A I Ch E J* 7, 152 (1961).

[7] N. R. Geary, UKAEA-8142 (August 1955).

[8] A. T. Gresky *et al.*, ORNL-1367 (Dec. 17, 1952).

[9] A. Faure and W. Davis, Jr., ORNL-3236 (Nov. 29, 1961).

[10] D. P. Evans, W. C. Davies, and W. J. Jones, *J. Chem Soc.* 1930, 1310.

[11] F. Hartmann and P. Rosenfeld, *Z Physik Chem.* 164, 377 (1933).

[12] A. Potier, *Ann Fac Sci Univ. Toulouse Sci. Math. Sci Phys* 20, 1–98 (1956).

[13] M. R. Vandoni and M. Laudy, *J. Chim. Phys.* 49, 99 (1952).

Table 17.1. Values of Parameters of Eq. (1)

Diluent	B_1	σ_{B_1}	B_2	σ_{B_2}	(moles TBP/mole HNO_3) B_3	σ_{B_3}
Amsco 125-82	0.2295	0.0076	1.2470	0.0405	−1.6497	0.0370
n-Hexane[a]	0.2767	0.0125	1.4544	0.0550	−1.8788	0.0468

[a] The constants for *n*-hexane are based on the assumption that the molar volume of water in the organic phase is zero, this assumption was made because water concentrations in the organic phases were not measured (see ref 6). The resulting bias of the constants is small (see ref 3).

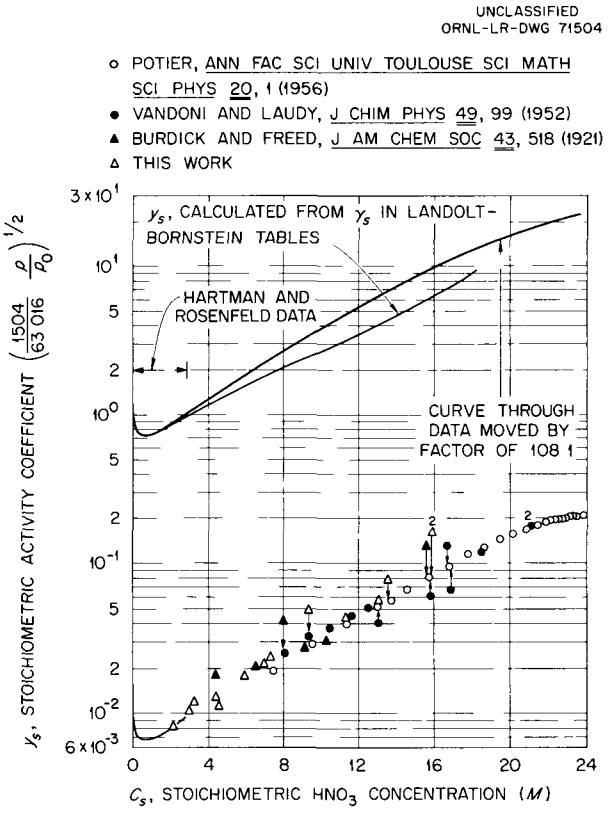

Fig. 17.1. Nitric Acid Activity Coefficients.

unambiguously, partial pressures of HNO_3 at 25.0°C over its aqueous solutions at concentrations down to ~2 *M* were measured by the transpiration technique. Although the precision of these measurements becomes poor below ~6 *M*, the data give further evidence that the Landolt-Bornstein table values of nitric acid activity coefficients are incorrectly low at concentrations above ~2 *M*. The combined vapor pressure data and the freezing point data of Hartmann and Rosenfeld are consistently correlated if the constant for the dissociation of nitric acid, given as $HNO_3 \rightleftharpoons H^+ + NO_3^-$, is, in molar units, and with the subscript u to emphasize reference to undissociated nitric acid,

$$K^c = \frac{[H^+][NO_3^-]}{[HNO_3]_u} = 1.169 \times 10^4 . \qquad (4)$$

The molar stoichiometric activity coefficient, y_s is related to the partial pressures p and p_o of HNO_3 over the solution and over pure (anhydrous) HNO_3 and to the stoichiometric concentration, C_s,

$$C_s = (HNO_3)_u + (H^+) = (HNO_3)_u + (NO_3^-)$$

by

$$y_s = \frac{(K^c)^{1/2}}{C_s} \sqrt{\frac{1504}{63.016}\frac{p}{p_o}} , \qquad (5)$$

where 1504 g is the mass of 1 liter of anhydrous nitric acid at 25°C and 63.016 is its molecular weight.

Activity coefficients of nitric acid, obtainable from Fig. 17.1, are being used at concentrations up to 16 *M* in studies of the distribution of nitric acid and uranyl nitrate between aqueous and TBP–Amsco 125-82 solutions.

17.2 FOAM SEPARATION

Physical Chemistry of Foams

Measured surface tensions of aqueous solutions containing the surfactant RWA-100, a sodium butylphenylphenolsulfonate, and varying quantities of one of the ions H^+ (10^{-4} to 1 *M*), Na^+ (5×10^{-2} to 1 *M*), Ca^{2+} (10^{-2} to 10^{-1} *M*), and Ce^{3+} (5×10^{-3} to 1.75×10^{-2} *M*) all can be described by the equation,[14]

$$\gamma = \gamma_0 - \Gamma_m RT \ln (1 + \alpha x) , \qquad (6)$$

where γ_0 and γ are the surface tensions, dynes/cm, of water and the solution, respectively; Γ_m is the saturated (monomolecular) surface concentration of surfactant-cation complex, moles/cm^2; R is the gas constant, 8.3144×10^7 ergs mole^{-1} (°K)$^{-1}$; T the absolute temperature, °K; x is the bulk phase concentration of the surfactant-cation complex, moles/cm^3; and α is a constant, cm^3/mole, that is descriptive of the tendency of the surfactant-cation complex to concentrate at the surface. Values of α were within ±10% of 1.4×10^6 cm^3/mole for all cations, indicating that for a constant bulk phase concentration of the undissociated surfactant-cation complex, the surface

[14] *Chem. Technol. Div. Ann. Progr. Rept. May 31, 1961*, ORNL-3153.

activity is independent of the nature of the cation. However, because the surfactant-cation complex dissociates to varying degrees in the solution, the concentration of the undissociated surfactant-cation complex is strongly dependent on the total cation concentration, cation valence, and pH. Changes in these variables therefore result in separation of cations from each other with the same surfactant.

The quantity Γ_m was determined for sodium dodecylbenzene sulfonate by both surface tension measurements and by single-stage total-recycle foam-column separation measurements. The agreement between the values, 3.2×10^{-10} moles/cm^2 in both cases, adds strong support to the previously proposed use[14] of the Gibbs-Langmuir equations in correlating foam separation results.

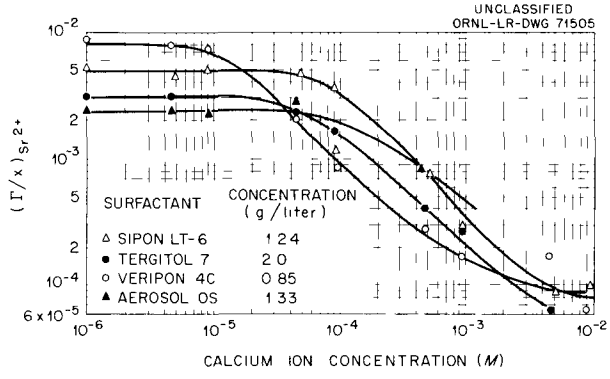

Fig. 17.2. Effect of Calcium Concentration on Separation of Strontium in the Presence of Various Surfactants.

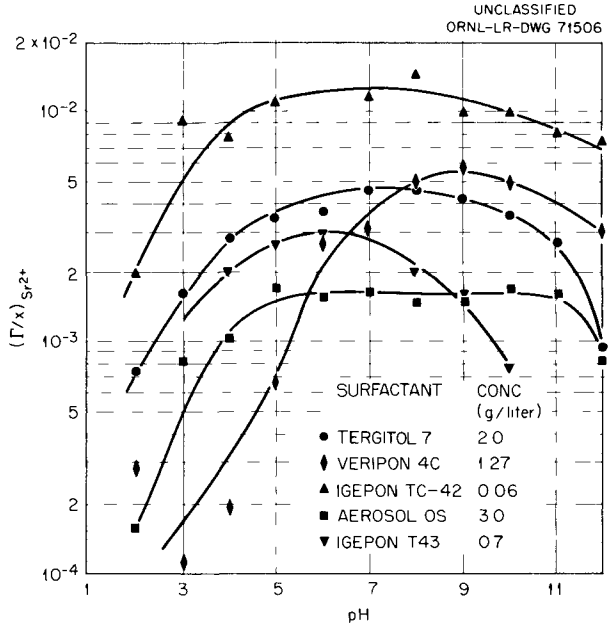

Fig. 17.3. Effect of pH on Separation of Strontium in the Presence of Various Surfactants.

Surfactant Screening Tests

The program[14,15] to screen a representative sample, 107 in number, of commercially available surfactants was essentially completed. From these tests the following materials were selected for more intensive study for application to specific problems, such as low-activity waste decontamination: Aerosol OS, sodium dodecylbenzene sulfonate, Igepon T43, Igepon TC-42, RWA-100, Sipon LT-6, Tergitol 7, and Veripon 4C. Sodium dodecylbenzene sulfonate gave the highest distribution coefficient, $\Gamma/x = 5 \times 10^{-2}$ (moles/cm^2)/(moles/cm^3), for strontium of any observed to date. In terms of a 50 A bubble film thickness, τ, the quantity $\Gamma/(\tau x)$, which is similar in meaning to the distribution coefficient of solvent extraction, is 10^5.

Various chemical factors, such as Na^+ and Ca^{2+} concentrations and pH, changed the efficiency of separating Cs^+ or Sr^{2+} from solutions. Calcium interference (Fig. 17.2) is important in the foam decontamination of low-activity wastes from strontium since the strontium distribution coefficient starts to decrease when the Ca^{2+} concentration exceeds $\sim 10^{-4}$ M, even with the better surfactants. Generally, the pH effect is not too important since the strontium distribution coefficient remains high with one or more of the surfactants in the range pH = 2–12 (Fig. 17.3).

Countercurrent Foam Column Parameters

The decontamination factor, volume reduction, volumetric throughput rate, and distribution coefficient are some of the more important variables of countercurrent foam column operation. To establish some of the relations between these parameters, a series of experiments was performed in which foam density and linear foam velocity

[15] J. J. Weinstock *et al.*, Radiation Applications, Inc., "Foam Separation," RAI-100 (Oct. 1, 1961).

were varied. It was found that the height of a theoretical transfer unit for removal of strontium tracer in 2- or 6-in.-diam columns was only 1–2 cm when the feed consisted of ORNL tap water (simulated low-activity-level waste) that had been made basic to pH = 11.8 by the addition of 10^{-2} *M* NaOH and whose calcium concentration had thereby been reduced from ~27 to 3.3 ppm. With such a low theoretical transfer unit value, the foam height needed to obtain good decontamination was only about 1 ft. No efforts have yet been made to maximize solution throughput rates; however, values of 1.65 gal min^{-1} ft^{-3} of foam were obtained.

Applications

Two of the potential applications of foam separation studied during the past year were removal of cesium from 6 *M* $NaNO_3$ solutions (such as evaporated neutralized Purex waste solution, IWW) and decontamination of ORNL low-activity-level waste. In the first application copper ferrocyanide was added to 6 *M* $NaNO_3$ solution to form the insoluble cesium copper ferrocyanide, which was removed, with gelatin as the surfactant, by a combination of foaming and flotation. In a nonoptimum batch experiment, 96% of the tracer cesium was recovered with a volume reduction >300 and a cesium radioactivity distribution coefficient of 3×10^5 (counts per g of solid)/(counts per ml of solution).

Studies of the decontamination of ORNL low-activity waste were directed primarily toward removal of strontium since Sr^{90} is the most deleterious component of this waste. Further, since calcium interferes with strontium removal (Fig. 17.3), a head-end precipitator was built to remove this cation as $CaCO_3$ and magnesium as $Mg(OH)_2$ (Fig. 17.4). By adding 5×10^{-3} *M* each of NaOH and Na_2CO_3 to simulated ORNL low-activity waste, an equilibrium strontium decontamination factor of 10^2 and 97.5% calcium removal were achieved. The distribution coefficient, K_D, for strontium between solid and solution was 1.4×10^6 (counts per g of solid)/(counts per ml of solution). Operation of a continuous precipitator without filtration and with upflow agitation of the sludge produced a clear solution having only ~2 ppm total hardness as $CaCO_3$, with a strontium DF of ~150. Cesium decontamination factors of 10–40 were achieved by adding grundite clay to the precipitator in quantities of ~0.5 lb per 1000 gal. With sodium dodecylbenzene sulfonate as the surfactant, a solution similar to that produced from the precipitator (Fig. 17.3) was decontaminated from strontium by factors up to 5000 in a 6-in.-diam countercurrent foam column. Volume reductions, which were not optimized, ranged from 25 to 1000. Further tests showed that the resulting foam condensate can be evaporated to dryness (volume reduction $>10^3$) by the addition of a few ppm of silicone antifoaming agent.

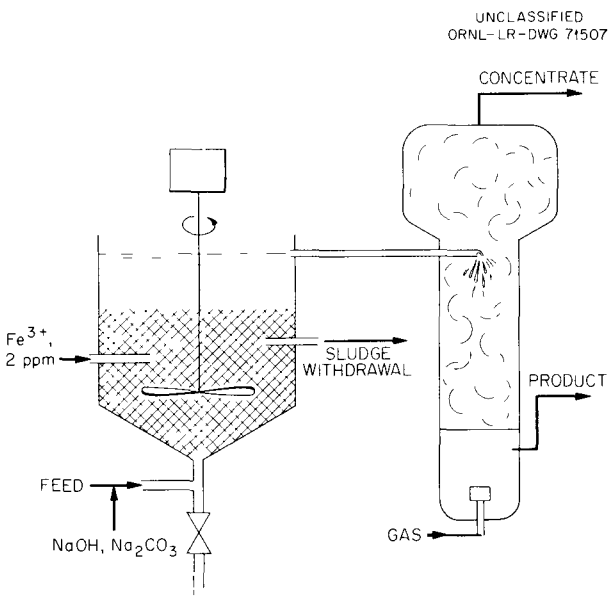

Fig. 17.4. Proposed Flowsheet for ORNL Low-Activity-Level Waste Decontamination.

18. Equipment Decontamination

Details of decontamination research are given in the Gas Cooled Reactor quarterly reports.[1] A topical report is in press.[2]

18.1 DECONTAMINATION OF GAS LOOP PIPING[3]

Thirteen stainless steel samples of helium-and-air gas loop piping from Brookhaven were decontaminated by spraying them with 0.4 *M* ammonium oxalate–0.1 *M* ammonium citrate–0.35 *M* hydrogen peroxide at pH 4.0. In 2 hr at 95°C, the gross γ decontamination factor from irradiated UO_2, Sr^{89}, Y^{91}, Zr^{95}-Nb^{95}, Ru^{106}, Ba^{140}-La^{140}, and Ce^{144} averaged about 210.

18.2 SIMULATION OF EGCR CONTAMINATION, I^{131} AND Cs^{137}[4]

Carrier-free I^{131} was volatilized in 750°C helium from iodide residues after first drying the iodide mixed with H_2O_2. In a second method, I^{131} was liberated by heating neutron-irradiated tellurium. The helium was then passed over steels and aluminum at lower temperatures. The best decontaminant for the steels was boiling 29% NaOH (D.F. $\sim 10^3$ in 20 min). Oxalate-peroxide at 95°C decontaminated the aluminum to background level in 1 hr, but was not as effective as NaOH on the steels.

Carrier-free Cs^{137} was similarly volatilized in helium by melting calcium metal with Cs^{137} chloride. Decontamination of metals contaminated in the gas phase was about 1×10^3 in 20 min at 95°C with oxalate-peroxide solution.

18.3 HYDROGEN PEROXIDE AS CORROSION INHIBITOR[5,6]

Corrosion of carbon steel by 0.4 *M* ammonium oxalate solutions at pH 4.0 and 95°C was increased by hydrogen peroxide in concentrations up to about 0.1 *M*, but the steel was passivated at higher peroxide concentrations. Studies of the passivation phenomenon resulted in the development of mildly acidic and highly effective decontaminating solutions containing oxalate, sulfate, phosphate, citrate, and fluoride ions, which corroded carbon steel at 0.01 mil/hr or less at 95°C. The gradual oxidation of oxalate when mixed with hydrogen peroxide, catalyzed by ferric ions in solution, raised the pH continuously, keeping the solutions in the range of passivity. A typical decontaminating solution of this type, with a useful lifetime of at least 12 hr at 95°C in contact with carbon steel, was 0.40 *M* ammonium oxalate–0.16 *M* ammonium citrate–0.34 *M* hydrogen peroxide at a pH of 4.0. At lower temperatures, carbon steel remained passive at lower pH's, but decontamination was less effective. Another application of the passivity phenomenon was the use of solutions which when rubbed at room temperature onto mild

---

[1] *GCR Quart. Progr. Rept. Dec. 31, 1961*, ORNL-3254.

[2] A. B. Meservey, *Decontamination Studies for Application to the Experimental Gas-Cooled Reactor: A Status Report*, ORNL-3308 (in press).

[3] M. F. Osborne, J. A. Conlin, and A. B. Meservey, *Fission Product Deposition and Decontamination of of BNL Gas-Cooled Loop*, CF-61-7-49 (July 20, 1961).

[4] P. S. Lawson, *Decontamination Studies*, ORNL TM-6 (Sept. 20, 1961).

[5] A. B. Meservey, *Corrosion Inhibition by Hydrogen Peroxide in Decontamination Solutions*, ORNL TM-120 (Jan. 23, 1962). Also presented at the American Chemical Society, 141st National Meeting, Washington, D.C., Mar. 27, 1962.

[6] A. B. Meservey, chap. 5-1 in *Progress in Nuclear Energy*, ser IV, vol 4, Pergamon, New York, 1961.

steel with a sponge were slightly corrosive, but to which the steel became passive when rubbing ceased. A solution of this type was 0.4 *M* ammonium oxalate–0.2 *M* ammonium acetate–0.7 *M* H_2O_2 at pH 2.0.

Acetate vapors corroded carbon steel in the gas phase when acetate was used as a buffer in oxalate-peroxide solutions, but when the steel was wet intermittently by the solution, such as by spraying, the metal surface was not corroded.

Neither stress corrosion cracking nor crevice corrosion was observed on mild steel coupons after as much as 36 hr at 95°C in an oxalate-peroxide-citrate formula. Fluoride complexed with aluminum was permissible in acidic formulas for carbon steel when the peroxide concentration was above 0.4 *M* to provide passivity. Fluoride in oxalate-peroxide solutions was corrosive to aluminum, but the corrosivity was decreased through the addition of aluminum nitrate to complex the fluoride.

18.4 DECONTAMINATION FROM PLUTONIUM AND AMERICIUM

When type 347 stainless steel samples, from a Thorex process cell contaminated with tenacious plutonium, were treated 30 min at 90°C in acidic fluorides, corrosion-inhibited with hydrogen peroxide, decontamination factors were 1000 to 3000. Solutions were 0.1 *M* NaF in 1 *M* HNO_3, 0.4 *M* oxalic acid, or 0.3 *M* H_2SO_4, all containing 1 *M* H_2O_2. Other stainless steel coupons contaminated with nonsmearable americium were decontaminated in 20 min at 95°C by factors of 23 to 635 by various acidic reagents. Fluoride aided the decontamination from americium also.

---

19. Radiation Damage to Ion Exchange Resin

Individual samples of tapped 8, 12, 16, and 20% cross-linked Dowex 50W cation exchange resin decreased in volume 8.7, 6.0, 0.7, and 0.7%, respectively, after an irradiation of 0.75×10^9 r (~2 whr per g of dry resin) in a flowing stream of water. Analyses (Table 19.1) of the exposed samples indicated an average specific volume (ml of wet resin per g of oven-dried resin) increase of (14.15 ±2.44)%, which partially compensated for the 10–20% weight loss (oven-dried basis) caused by decomposition and dissolution in the water. The radiation-induced swelling of resin particles did not cause any apparent fissuring or fragmentation. Structually, a 2–4% polymer decross-linking was indicated by a 10–15% increase in moisture content.

The samples lost 40–50% of their strong acid capacity but gained 5% in weak acid capacity (Table 19.1). These results differ from those of static experiments, where, after a dose of the same order of magnitude, 12% cross-linked Dowex 50W maintained its total capacity by a compensating effect, i.e., replacement of lost strong-acid groups by weak-acid groups.[1] Analysis of Dowex 50W X-12 resin used by the Isotopes Division for promethium-147 recovery in an essentially static system indicated also that the total capacity was retained after a calculated beta-energy dose of $4.4–4.8 \times 10^9$ r (12-13 whr per g of dry resin).[2]

The concentration of sulfur in the exposed resin, as determined by titration of strong acid capacity, was only 75–80% of that found by actual resin analysis. This suggests that only 75–80% of the total sulfur remaining in the exposed resin was present as the active sulfonate (HSO_3^-) group.

Analyses of the collected effluents from each exposed resin bed indicate that degradation products included sulfate, sulfonate, and oxalate ions in

---

[1] L. L. Smith and H. J. Groh, *The Effect of Gamma Ratiation on Ion Exchange Resins*, DP-549 (February 1961).

[2] *Chem. Technol. Div. Ann. Progr. Rept. Aug. 31, 1960*, ORNL-2993, sec 18.1.

Table 19.1. Properties of Irradiated Dowex 50W Resin

Irradiation field: 0.012 w per g of dry resin.
Prior to use, resin samples treated with 1 M NaOH, C_2H_5OH, and 1.4 M HNO_3, with water rinses between each two reagents.

Cross Linkage	Material	Specific Wet Volume $\left(\frac{\text{ml wet resin}}{\text{g dry resin}}\right)$	Wt Loss (%)	Vol Ratio, Exposed/Original	Moisture Content (wt %)	Capacity[a]			Sulfur Content		$G(-S)^c$
						Total Loss (%)	Specific Total[b] (meq/g)	Specific, Strong Acid[b] (meq/g)	Specific, Strong Acid Equiv. (wt %)	Analysis (wt %)	
X-8 (20–50 mesh)	Original	2.506			50.3		4.80	4.80	15.4	15.4	
	Exposed 0.76×10^{-9} r	2.865	20.1	0.913	54.7	45.2	3.42	3.18	10.2	13.7	1.0
X-12 (20–50 mesh)	Original	2.208			44.5		4.85	4.85	15.5	14.9	
	Exposed 0.77×10^{-9} r	2.538	18.2	0.940	49.2	43.3	3.53	3.38	10.8	13.5	1.1
X-16 (20–50 mesh)	Original	2.119			42.7		4.81	4.81	15.4	15.5	
	Exposed 0.75×10^{-9} r	2.347	10.3	0.993	46.0	35.1	3.69	3.47	11.1	14.5	1.2
X-20 (20–100 mesh)	Original	1.786			35.6		4.59	4.59	14.7	14.2	
	Exposed 0.77×10^{-9} r	2.083	14.9	0.993	41.8	36.7	3.41	3.27	10.5	12.9	1.6

[a] Determined by titration.
[b] Dry basis.
[c] Sulfur atoms lost per 100 w of energy absorbed.

the acid form. Sulfur determinations on the exposed resin samples gave a $G(-S)$ value of 1.0-1.2 atoms S per 100 ev of energy absorbed. A $G(-S)$ of about 0.5 was calculated from analyses of degradation products sorbed on the anion exchange resin columns. Expressed in terms of H_2SO_4 specific conductance,[3] these $G(-S)$ values, which are measures of the loss of active sulfonate groups from the resin matrix, correspond to 50–100 μmho/cm. This is only 10–25% of the maximum specific conductance to be accounted for in the resin column effluent (Fig. 19.1). Thus organic radiation degradation products of the resin polymer appear to contribute the major amount of acidity.

In other experiments, 80 wt % of a sample of 8% cross-linked Dowex 50W dissolved in the water stream, and it lost 95% of its total capacity after an exposure of 3.9×10^9 r (13.8 whr per g of dry resin). Amberlite 200, a porous resin considered to be >20% cross-linked, after a dose of 0.97×10^9 r (2.6 whr per g of dry resin) showed an 8% increase in moisture, 20% in surface area, and 25% in median pore diameter. The 15% mass loss and 44% total capacity loss showed by this resin may be compared with the 18.2% mass loss and 43% total capacity loss of the nonporous Dowex 50W, 12% cross-linked, resin (Table 19.1).

The experiments were made by circulating demineralized water (<1 μmho/cm) through fixed beds of the resin exposed to a 10,000-curie cobalt-60 source.[4] The resin column effluent solution was passed through a series of cells that continuously monitored the solution pH and electrical conductivity and a strong base anion exchange resin column that concentrated the sorbable products from cation resin degradation.

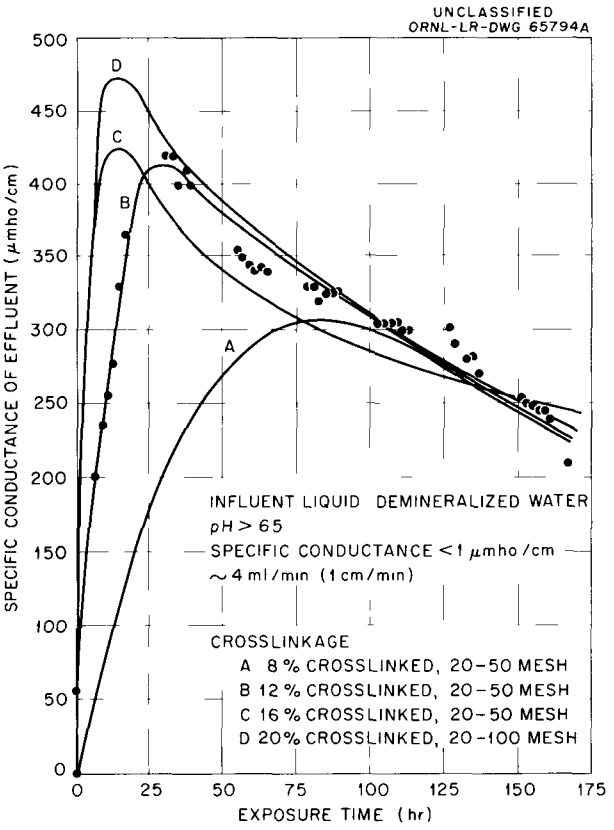

Fig. 19.1. Variation of Specific Conductance of Aqueous Solution Effluent from Dowex 50W Resins, H^+ Form. Crosslinkage as indicated. Data points are plotted for 12%-crosslinked resin to indicate experimental uncertainty.

[3] M. Hlasko and A. Salitowna, "Measurement of the Electrolytic Conductivity of Extremely Dilute Solutions," *Bull. intern. acad. polan. sci., Classe sci. math. nat., 1935A*, 189 (1935).

[4] *Chem. Technol. Div. Ann. Progr. Rept. May 31, 1961*, ORNL-3153, sec 19.1.

20. Fuel Shipping Studies

The AEC is attempting to develop practical criteria to govern the shipment of highly radioactive materials, such as spent fuel elements. As part of the ORNL Reactor Evaluation Program, studies were made on damage (to protype casks) resulting from impact loading and on the dissipation of self-generated heat from fuel in casks.

20.1 FUEL CARRIER DROP TESTS

In order to provide some guarantee that reactor fuel casks have a high degree of integrity to high-impact loading that could result in a transportation accident, the AEC specifies (in proposed fuel shipping regulation CFR Title 10, Part 72) that a cask must maintain its shielding integrity after a 15-ft free fall onto a solid unyielding object. Since most fuel shipping casks are composite structures and data on possible cask damage cannot be calculated with any degree of certainty, data are being obtained experimentally on inexpensive scale models which should permit scaleup to actual cask sizes.

Eight model casks of three designs have been built and are being drop tested. All have an inner and outer steel shell and a lead-filled annulus. Five casks are 36 in. long, 18 in. OD, 10 in. ID, and weigh 2725 lb; two are 60 in. long, 30 in. OD, 18 in. ID, and weigh ~11,760 lb; and one is 35 in. long, 31 in. OD, 27 in. ID, and weighs ~3750 lb.

In preliminary tests[1] two of the smallest casks were coated with a brittle lacquer (Stresscote) and dropped in a horizontal attitude from heights of from 6 in. to 4 ft. Cracks in the lacquer appeared where the strain in the steel shells exceeded 0.012 in./in. (Fig. 20.1). The maximum strain lines were perpendicular to the observed cracks.

In subsequent tests[1] of the first series the casks were instrumented (Fig. 20.2). Compressometers indicated the maximum deflection in the cavity at impact, and accelerometers measured the deceleration of the point on the cask to which they were attached. Inertia switches were preset to function under a certain shock load and were used to check the information obtained from the accelerometers. The strain gages were positioned to measure the strain at a point of interest.

The second series of tests[2] was made by dropping the casks in a horizontal attitude from heights of from 6 to 16 ft (Table 20.1). Strain gages and compressometers (Fig. 20.3) were located similarly to those in the first series.

The casks have also been dropped with the axes vertical and at an angle, but the data have not yet been analyzed. After the largest casks have been dropped, the data will be correlated with the data obtained from dropping the smallest casks to indicate whether the data from model testing can be satisfactorily scaled up and help is setting some of the important parameters in cask design.

20.2 HEAT TRANSFER STUDIES

Data on the probable temperature rise due to fission product decay heat in spent fuel elements during shipping was obtained with electrically heated fuel rods. The simulated fuel bundles studied contained from 4 to 64 tubes and were heated in air-filled casks 24 in. long and either 12 or 16 in. ID. By assuming that the bulk of the heat is transferred by radiation, it was generally possible to predict the temperatures of the center pins within 20°C (at temperatures between 200 and 300°C). In order to be able to predict the temperature distribution within the bundle accurate values were obtained of the configuration (or shape) factors for radiant heat transfer between various tubes in square arrays, but a semiempirical method was used to obtain the overall gray-body radiation factors from these configurations. The calculation of the predicted temperature distribution in the array was coded for use on an IBM 7090 computer.

[1] Made at the University of Tennessee under a subcontract.

[2] Made at ORNL.

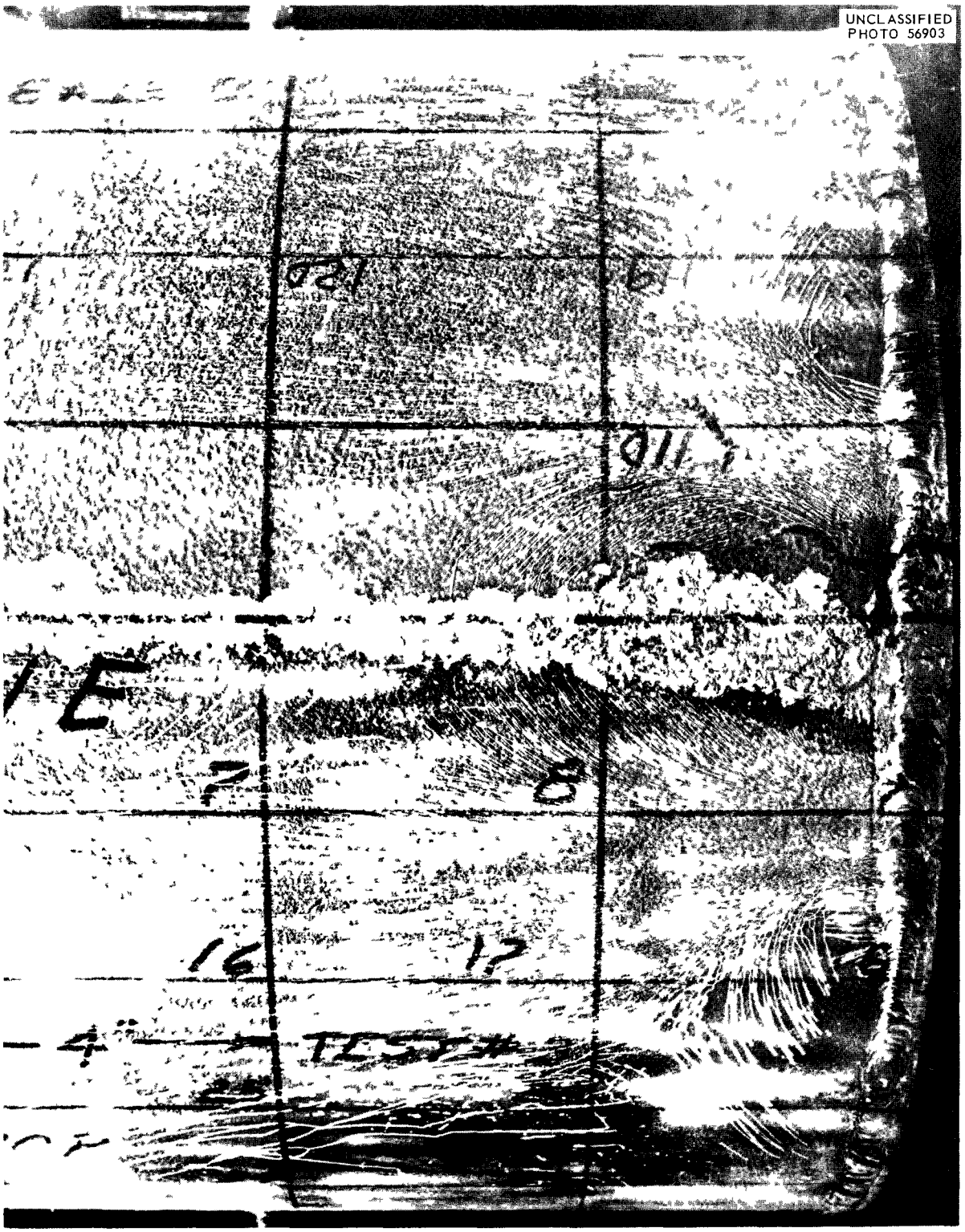

Fig. 20.1. Crack Pattern, on the Line of Impact, in Lacquer Coating on 2725-lb Cask Dropped from a Height of 4 ft.

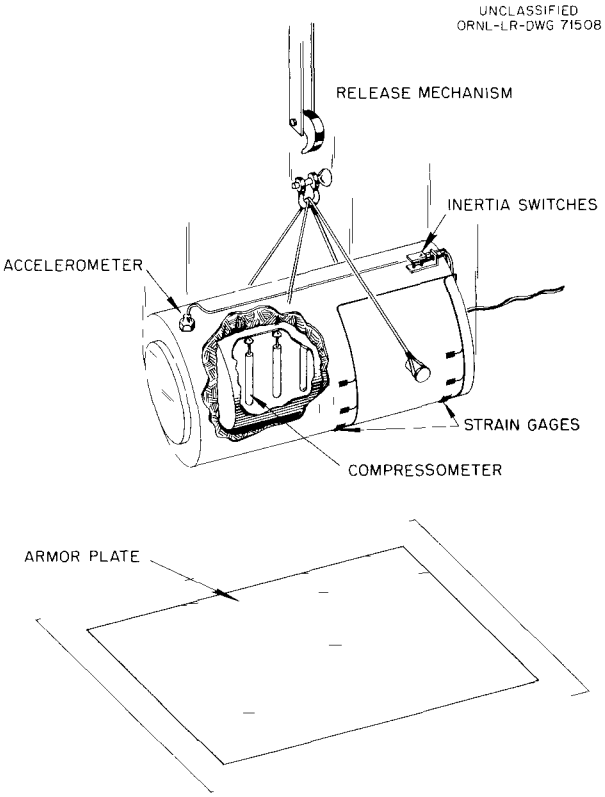

Fig. 20.2. Schematic Arrangement of Cask Drop Test Equipment and Instrumentation.

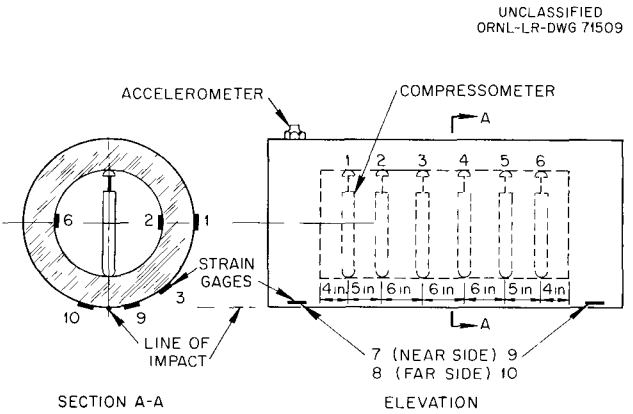

Fig. 20.3. Location of Strain Gages and Compressometer Used in 6- and 8-ft Drop Tests of 2725-lb Cask.

Table 20.1. Strain and Deflection at Various Positions on the 2725-lb Cask Dropped from 6 and 8 ft

Drop		Strain Measured by Gages Nos. 1–10 (μin./in.)								Deflection Measured by Compressometers Nos. 1–6 (in.)					
No.	Height (ft)	1	2	3	6	7	8	9	10	1	2	3	4	5	6
							Maximum								
1	6	140	2050	370	760	940		800	1600	0.161	0.126	0.132	0.118	0.105	0.047
2	6	280	2075	330	2280	490		640	1090						
3	7.85	600	3000	1040	2900	2350	1040	940	660	0.130	0.158	0.173	0.160	0.123	0.104
							Permanent								
1	6	50	720	370	760	565		490	1350	0.050	0.061	0.099	0.073	0.062	0.011
2	6		410	200	560	280		320	820						
3	7.85	140	1040	780	840	2020	440	520	90	0.053	0.058	0.059	0.059	0.047	0.029

Note: Accelerometer readings in tests 1, 2, and 3 were 1100, 470, and 1475g, respectively. It is interesting to note the consistency of strain gages 2 and 6 which were placed opposite each other in the cask cavity.

21. Gas-Cooled Reactor Coolant Purification

Anticipated contaminants of the helium coolant in gas-cooled reactors are nonradioactive gases such as H_2, CO, CO_2, H_2O, and hydrocarbons; radioactive gases such as Xe and Kr; and particulates. These contaminants are to be maintained at low levels by continuous purification of at least a portion of the coolant.

21.1 REMOVAL OF NONRADIOACTIVE CONTAMINANTS

The proposed method of removing nonradioactive gaseous contaminants is oxidation of all oxidizable contaminants (H_2, CO, and hydrocarbons) to H_2O and CO_2 and removal of the H_2O and CO_2 by sorption. Oxidation of the contaminants by oxygen in a fixed-bed catalyst and by a fixed bed of CuO and cosorption of H_2O and CO_2 by fixed beds of molecular sieves were investigated.

Kinetics of the Catalyzed Oxidation of H_2, CO, and CH_4

A kinetic study was made of the catalyzed oxidation of H_2, CO, and CH_4 by O_2 in a flowing stream of helium passing through a fixed bed of American Metals Products Ni-Cr-Pd ribbon catalyst. The catalyst, which is the type to be used by the EGCR,[1] was evaluated for a range of operating parameters which should cover EGCR operation.

Empirical correlations suitable for design purposes were determined for the effects of temperatures of 400–600°C, of total gas mass flow rates of 0.083 to 1.0 g-moles cm^{-2} min^{-1}, and contamination levels of ~0.5 to 2.0 vol %. The design equations developed were:

for hydrogen,

$$V_H = \frac{5.12 \times 10^{-7} F\, e^{(2200/RT)}}{G^{0.37}(y_{H_0} - 2y_{O_0})} \ln \frac{y_{H_f} y_{O_0}}{y_{H_0} y_{O_f}}, \quad (1)$$

for carbon monoxide,

$$V_C = \frac{5.77 \times 10^{-7} F\, e^{(2400/RT)}}{G^{0.34}(y_{C_0} - 2y_{O_0})} \ln \frac{y_{C_f} y_{O_0}}{y_{C_0} y_{O_f}}, \quad (2)$$

for methane,

$$V_{CH} = \frac{2.45 \times 10^{-6} F\, e^{(3950/RT)}}{G^{0.51}(2y_{CH_0} - y_{O_0})} \ln \frac{y_{CH_f} y_{O_0}}{y_{CH_0} y_{O_f}}, \quad (3)$$

where

V_H, V_C, V_{CH} = volume, cc, of catalyst in reactor necessary for reaction of H_2, CO, and CH_4,

F = gas feed rate, cc/min,

$y_{H_0}, y_{C_0}, y_{CH_0}, y_{O_0}$ = inlet mole fraction of H_2, CO, CH_4, and O_2,

$y_{H_f}, y_{C_f}, y_{CH_f}, y_{O_f}$ = effluent mole fraction of H_2, CO, CH_4, and O_2,

G = mass flow rate, g-moles cm^{-2} min^{-1},

T = temperature, °K,

R = gas constant, 1.99 cal $(°K)^{-1}$ $g\text{-mole}^{-1}$.

The oxidation preference in the catalytic bed was hydrogen first, carbon monoxide second, and methane last. When simultaneous oxidation of two or more contaminants is contemplated, necessary reactor volumes are additive for the contaminants,

[1] C. D. Scott, *Evaluation of the EGCR Catalytic Oxidizer for Oxidation of Hydrogen, Carbon Monoxide, and Methane*, ORNL TM-61 (1961).

and the oxygen mole fraction to be used is the total unused oxygen in the gas stream.

Oxidation of H_2, CO, and CH_4 by Fixed Beds of CuO Pellets

A kinetic study on the oxidation of H_2, CO, and CH_4 from a flowing stream of He by fixed beds of nominal $\frac{1}{8}$-in.-diam right-circular cylinders of CuO was made with the following ranges of operating conditions:

Temperature	400–600°C
Pressure	10.2–30.0 atm
Gas mass flow rate	0.0058–0.050 g cm^{-2} sec^{-1}
Contaminant concentration	0.0008–1.21 vol %

The reaction mechanisms of each reaction were determined, and differential equations were developed to describe the gas-phase contaminant concentration in the fixed bed as a function of time and bed height. Mass transfer of the H_2 or CO from the bulk gas stream to the CuO reaction site is the rate-controlling mechanism for the H_2 and CO oxidation. The rate of CH_4 reaction was controlled by the amount of available Cu-CuO reaction surface in the individual CuO particles.

The mathematical model for each type of reaction may be described by differential equations, which must be solved simultaneously for a solution of the contaminant concentration as a function of time and bed position. For the H_2 and CO reactions:[2]

$$\left(\frac{\partial C}{\partial t}\right)_z + u\left(\frac{\partial C}{\partial z}\right)_t = -\frac{1}{\epsilon}\left(\frac{\partial n}{\partial t}\right)_z , \tag{4}$$

$$\left(\frac{\partial n}{\partial t}\right)_z = kaC\left[1 - \frac{ka(r_e - r_i)}{4\pi\alpha\tau D r_e r_i + ka(r_e - r_i)}\right] , \tag{5}$$

$$\left(\frac{\partial r_i}{\partial t}\right)_z = -\frac{1}{4\pi b r_i^2 \tau}\left(\frac{\partial n}{\partial t}\right)_z . \tag{6}$$

For the CH_4 reaction:[3]

$$\left(\frac{\partial C}{\partial t}\right)_z + u\left(\frac{\partial C}{\partial z}\right)_t = -\frac{1}{4\epsilon}\left(\frac{\partial n}{\partial t}\right)_z , \tag{7}$$

$$\left(\frac{\partial n}{\partial t}\right)_z = -k' K C_{(n)}^{2/3} , \tag{8}$$

where

C = gas-phase contaminant concentration, g-moles/cc,

t = reaction time, sec,

z = bed height measured from gas inlet point, cm,

u = interstitial gas velocity, cm/sec,

ϵ = external bed porosity, void volume per total volume,

n = molecular density of Cu in pellet per unit vol of bed, g-moles/cc,

k = mass transfer coefficient across external gas film, cm/sec,

a = effective mass transfer area between fluid and CuO pellets, cm^2/cm^3,

r_e = radius of equivalent CuO pellet sphere, cm,

r_i = radius of Cu-CuO reaction interface in the pellet, cm,

α = effective internal pellet porosity, ratio of effective internal void volume to total pellet volume, dimensionless,

D = molecular diffusivity of H_2 or CO in gas phase, cm^2/sec,

τ = specific average CuO pellet density, pellets/cm^3,

b = initial CuO density in pellet, g-moles/cc,

k' = reaction rate constant for CH_4 reaction,

K = constant dependent on physical properties of CuO pellets.

The above sets of equations were solved by finite difference methods on a high-speed digital computer. From the solutions the gas-phase concentration, of any contaminant in the effluent of

[2]C. D. Scott, *The Rate of Reaction of Hydrogen from Hydrogen-Helium Streams with Fixed Beds of Copper Oxide*, ORNL-3292 (1962).

[3]M. E. Whatley, *et al.*, *Unit Operations Section Monthly Progress Report, October 1961*, ORNL TM-121 (1962).

a fixed bed of CuO through which contaminated He was flowing, could be predicted.

Cosorption of H_2O and CO_2 from Flowing Streams of Helium by Fixed Beds of Molecular Sieves

A series of kinetic tests was made on the sorption of H_2O and CO_2, individually and together, from flowing streams of helium by fixed beds of Linde type 5-A molecular sieves. Operating conditions were 25–30°C, 10.2–30.0 atm, gas mass flow rates of 0.0058–0.017 g cm^{-2} sec^{-1}, and contaminant concentration $\sim$0.01 to 0.2 vol %.

Results have not been fully evaluated; however, molecular sieves can remove H_2O and CO_2 down to a level <10 ppm and, in cosorption, the H_2O tends to displace sorbed CO_2.

21.2 MEASUREMENT OF PARTICULATE SIZE DISTRIBUTION AND CONCENTRATION BY LIGHT SCATTERING

An experimental investigation was started on the measurement of particulate size distribution and concentration in gas streams by a light-scattering technique, that is, measurement of the frequency and intensity of light reflected from a 90° source by the individual particles in a gas stream. An experimental device consisting of a light source, necessary optics, and light detector was designed and built, and instrumentation is in progress. The initial phase of the experimental program will be directed toward generation of a gas stream contaminated with known particulate concentration and size distribution to be used as a standard for the light-scattering device.

22. Chemical Engineering Research

22.1 THERMAL DIFFUSION IN AQUEOUS SALT SOLUTIONS[1]

Work on thermal diffusion in aqueous salt solutions was completed with runs on a folded 50-ft-long Jury column. The column is assembled like a sandwich consisting of an upper and lower copper plate to conduct heat to and from the solutions, an upper and lower gasket about $\frac{1}{8}$ in. thick through which the folded channel is cut, and a central cellophane membrane which separates the hot- and cold-side liquids (Fig. 22.1). It was necessary to bond a 0.004-in.-thick Teflon coating to the solution sides of the copper plates to eliminate the electrical path between the inlet and outlet. The concentration cell between inlet and outlet produced anomalous diffusion results.

Data from the most recent 50-ft-column run (Fig. 22.2), although the column was not yet at steady state, show good concentration ratios at the rela-

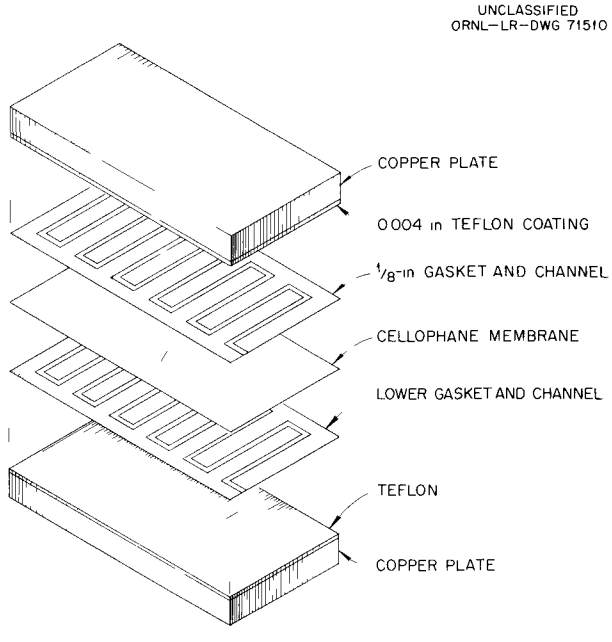

Fig. 22.1. Components of the 50-ft-long Thermal Diffusion Column Used for Studying Separation of Ions in Aqueous Salt Solutions.

[1]Work done by University of Tennessee under subcontract.

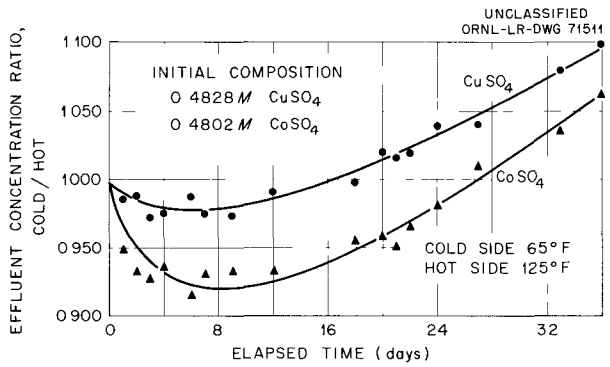

Fig. 22.2. Thermal-Diffusion Column Operation at Total Reflux, 24.3 ml/hr. Cold side 65°F, hot side 125°F. Initial solution composition 0.4828 *M* $CuSO_4$, 0.4802 *M* $CoSO_4$.

tively high (for this type of device) flow rate of 24.3 ml/hr. The reason for the initial dip in concentration ratio is not known, but these minima occurred several weeks after startup in runs made before the plates had been Teflon coated. Extrapolation of the data from 1-ft-long column runs (Fig. 22.3) indicates that a 50-ft-long column will have about 16 stages with this flow rate. The theoretical HTU's for a flow rate of 6 ml/hr are based on the slug-flow model. HTU's calculated from the laminar-flow mathematical model are about twice as large. The reason for the disagreement between the theoretical HTU's and those observed experimentally in the 1-ft-long column is not yet known, but could be due in some way to the distortion of the flow profile by the viscosity gradient produced by the temperature distribution. The very large error in the point for copper sulfate (2 ml/hr) is a reflection of the error in estimating the point of intersection of two very nearly parallel lines in the graphical computation of the point.

22.2 HIGH-SPEED CONTACTOR

The Mark II stacked clone contactor was reported[2] to give a very high throughput but generally low efficiencies with the system 0.08 *M* HNO_3–benzoic acid–Amsco. It was surmised at the time that backmixing of one or both phases was responsible for the poor efficiencies. In subsequent studies with the 1 *M* $NaNO_3$–uranyl nitrate–18.3% TBP-Amsco, efficiencies were even lower. Calculations on the IBM 7090 computer in conjunction with tracer injection tests on the contactor with LiCl showed that the degree of backmixing could not account for the low efficiencies. The contactor produced a definitely demarcated cylindrical vortex consisting of a very fine aqueous-continuous dispersion surrounded by a relatively clear aqueous region. This suggested that although liquid shear was adequate to form extremely fine organic droplets, gross mixing was inadequate to give good approach to equilibrium; that is, aqueous bypassing was occurring.

A hydroclone stage was designed incorporating a 0.5-in.-diam cylindrical section (Fig. 22.4). Four distinct variations of this general type with differing underflow geometries and differing transition sections between the 0.5-in.-diam cylinder and the 1.5-in.-diam spin section were built and tested for extraction efficiency in conjunction with five variations of vortex finder arrangements. The best two operated at stage efficiencies of 40–75% and throughputs of 1200–2000 cc/min of both phases. The system was 1 *M* $NaNO_3$–uranyl nitrate–18.3% TBP-Amsco.

[2] *Chem. Technol. Div. Ann. Progr. Rept. May 31, 1961*, ORNL-3153, p 125.

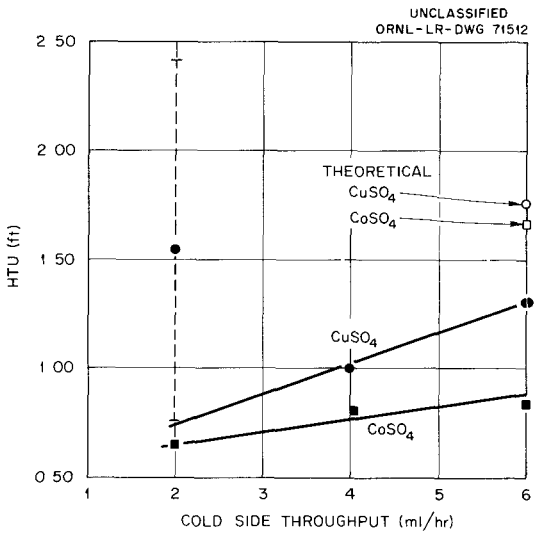

Fig. 22.3. HTU's Developed in a 1-ft-long Thermal Diffusion Column with Aqueous Solutions of Cobalt and Copper Sulfates. The dotted line on the left shows the error in the copper sulfate value at a throughput of 2 ml/hr.

Fig. 22.4. Mark IV Stacked Clone Contactor.

23. CANE Program

The Chemical Applications of Nuclear Explosives (CANE) Program at ORNL included the following areas of investigation: (1) participation in the Lawrence Radiation Laboratory radioisotope recovery experiment in the Project Gnome nuclear event at Carlsbad, New Mexico, on December 10, 1961, by the inclusion of five ORNL-designed experiments; (2) a study of hypervelocity jet formation for target-materials and shock-chemistry tests in support work at Frankford Arsenal; and (3) laboratory chemical studies on tritium-hydrogen exchange reactions.

23.1 PROJECT GNOME PARTICIPATION

ORNL participation in the Lawrence Radiation Laboratory radioisotope recovery experiment of Project Gnome consisted of experiments on sequenced gas sampling, hypervelocity jet, shock chemistry, and study of samples from the detonation zone and samples of gas from the power measuring experiment. The purpose of these experiments was to obtain chemical data on radioisotope production in contained nuclear detonations and on means for sampling and recovering radioisotope products.

In the prompt sampling experiment, an LRL-designed filter sampler for particulate matter and an integral gas sampler and the ORNL sequenced-gas-sampling equipment were located at the earth's surface directly above the nuclear device and connected to the detonation chamber with a 12-in. pipe evacuated to 50 μ Hg absolute pressure. The seven chambers of the ORNL sampler were designed to take samples over the following post-shot times: 0 to 50 msec, 40 to 75 msec, 60 to 90 msec, 75 to 150 msec, 150 msec to 1 sec, 1 to 10 sec, and 0 to 10 sec. Small quantities of radioisotopes – H^3, Tl^{204}, Po^{210}, Th^{230}, U^{233}, Pu^{238}, Am^{244}, and Cm^{242} – were placed in the nuclear detonation chamber. Six of the seven sample chambers operated successfully; however, the sampling pipe was broken approximately midway between the detonation chamber and the earth's surface before any significant quantity of detonation products could pass through to the LRL and ORNL sampling equipment. The sequenced sampler is undamaged and uncontaminated and can be used for a radioisotope recovery experiment being considered for the next Plowshare experiment.

In the relatively crude hypervelocity jet experiment of Project Gnome, a lining of zinc amalgam was applied as a tracer inside the lower end of the vertical pipe at the detonation chamber. No evidence was found that material was jetted to the filter sampler before the pipe parted. The sampling pipe was not prepared to produce a jet, but probably a jet of some type forms in the pipe where the pipe leaves the detonation chamber.

Specimens from ORNL were included in the LRL experiment and were installed in the salt medium near the detonation chamber to determine the effect of nuclear shock on chemical reactions and metallurgical properties. The specimens include mixtures of $N_2 + H_2$, $N_2 + O_2$, and $N_2 + C$ at several thousand psi pressure and the metals aluminum and thorium. These specimens will be recovered in the near future by mining. Samples for study of the detonation zone debris were obtained by core drilling and mining into the detonation zone and by sampling the steam withdrawn from the detonation zone in the power measuring experiment. They will be delivered to ORNL for further testing.

23.2 HYPERVELOCITY JET EXPERIMENTS[1,2]

Uranium and uranium-coated copper cones, made at Y-12, were tested successfully with high explosives. The uranium jets formed were jetted at speeds of 10 to 100 km/sec. At 100 ft the diameter of the jet was less than 1 in. Therefore it appears feasible to produce satisfactory jets and control them without cumbersome and expensive electrical focusing devices.

In a chemical shock experiment with high explosives, sodium chloride specimens underwent about 0.1% decomposition when shocked to about 2 megabars.

23.3 TRITIUM-HYDROGEN EXCHANGE

Chemical studies were made on tritium exchange in the reaction $H_2 + HTO \rightarrow HT + H_2O$ and on the kinetics and stoichiometry of the hydrogen reduction of calcium sulfate and of magnesium sulfate. Tritium exchange was catalyzed at 600°C by a number of oxygenated salts that occur in natural salt formations. Calcium sulfate, which is the most abundant impurity, was the best catalyst. Sodium chloride did not catalyze the exchange. Exchange was not necessarily optimized but values as high as 53 and 93% of statistical exchange were achieved with pure $CaSO_4$ and Drierite in deep bed tests. Even under diffusion-controlled conditions, where reactant gases were passed over layers of fine $CaSO_4$ powder, exchange percentages were 28% of statistical exchange. In high-temperature studies of the exchange in a plasma jet at 10,000–12,000°K, with D_2 as a stand-in for T_2, exchange was very rapid. For 40-msec residence time and a D_2/H_2O ratio of 10/1, 82% of the water-hydrogen exchanged with deuterium. The results of all exchange experiments suggest that tritium produced by a contained nuclear explosion will be lost to environmental water.

The reductions of calcium sulfate and of magnesium sulfate were found to involve the following reactions:

$$MeSO_4 + H_2 \longrightarrow MeSO_3 + H_2O\,, \qquad (1)$$

$$MeSO_3 \longrightarrow MeO + SO_2\,, \qquad (2)$$

$$7H_2 + 3SO_2 \longrightarrow 6H_2O + H_2S + S_2\,, \qquad (3)$$

$$4MeO + 2S_2 \longrightarrow 3MeS + MeSO_4\,, \qquad (4)$$

$$4MeO + 4SO_2 \longrightarrow MeS + 3MeSO_4\,, \qquad (5)$$

$$MeS + 2SO_2 \longrightarrow MeSO_4 + S_2\,, \qquad (6)$$

$$MeS + H_2O \longrightarrow MeO + H_2S\,, \qquad (7)$$

where Me = Ca or Mg.

The reductions were studied over temperature ranges where the rates were easily measurable. Magnesium sulfate was studied at temperatures of 734 and 784°C, and calcium sulfate was studied at 885 and 915°C. The final products for $MgSO_4$ reductions were MgO, SO_2, H_2S, H_2O, and S_2. MgS was detected in the solid residue to the extent of 11 ppm, which is negligible. At 734°C, the mole percentages of the original sulfate converted to H_2S, SO_2, and S were 43.4, 31.4, and 25.2, respectively, whereas at 784°C the values were 14.7, 44.4, and 40.4. The consumption of H_2 per mole of $MgSO_4$ was 2.8 moles at 734°C and 2.3 moles at 784°C. The final products of $CaSO_4$ reductions are CaS, CaO, SO_2, H_2S, H_2O, and S. The products CaO, SO_2, H_2S, and S are formed only in small amounts at 885°C; the mole percentages of the original sulfate converted to CaO, SO_2, H_2S, and S were 6, 1.9, 2.0, and 1.0, respectively. Measured hydrogen consumption per mole of $CaSO_4$ was 3.9–4.0 at 885 and 915°C.

The reductions of fixed beds of $MgSO_4$ and of $CaSO_4$ with hydrogen were autocatalytic. The reduction rate was maximum when approximately half of the original sulfate was reduced. An apparent activation energy of 18 kcal/mole was calculated for the reduction of $MgSO_4$ when the variation in the maximum observed reduction rate with temperature was used for the calculations.

---

[1] Made at Frankford Arsenal, Philadelphia.

[2] *Chem. Technol. Div. Ann. Progr. Rept. May 31, 1961*, ORNL-3153, p 131.

24. Assistance Programs

24.1 AHBR AND MSCR PROCESSING PLANT STUDIES

At the request of the Reactor Division, several conceptual plant studies and estimates were made for on-site fuel processing and reconstitution facilities for the AHBR (Aqueous Homogeneous Breeder Reactor) and the MSCR (Molten Salt Converter Reactor), both of which are based on a Th-U^{233} fuel cycle. The proposed power output of each reactor is 1000 Mw_e. Conceptual designs and cost estimates for both reactors were prepared by the Reactor Division and Sargent and Lundy. The Chemical Technology Division provided sufficient supplementary data to obtain total fuel cycle costs for both reactors. For each reactor two irradiation time cycles were evaluated, and, for each of the four fuel processing situations, flowsheets, equipment lists, building layouts, and operating requirements were prepared. Only the initial capital investment was estimated for a remote-maintenance facility located at the reactor site. It was assumed that certain facilities, services, and utilities provided for the reactor would be shared by the processing plant. AHBR fuel processing was based on the Thorex-sol-gel process and MSCR fuel recovery on the fluoride volatility process.

AHBR Fuel Processing Study

The AHBR fuel processing flowsheet is based on the daily removal and processing of a fraction of the UO_2SO_4-D_2O core solution and the ThO_2 blanket pellets. The core solution is continuously run through a hydroclone in the reactor fuel circuit. A small part of the overflow is continuously bled off, evaporated to 75 g of uranium per liter, and decayed 7 days. The uranium is then precipitated as UO_4, which is filtered off, and the precipitate is redissolved in D_2SO_4 and returned to the reactor core. The filtrate is evaporated to a concentrated slurry for D_2O recovery and then diluted to 4 *M* sulfate. The slurry underflow from the hydroclone is evaporated for D_2O recovery, the resulting solids are dissolved, in a two-step procedure, in 10.8 *M* H_2SO_4, and then combined with the filtrate from the UO_4 filtration for 90 days' decay before solvent extraction. The blanket thoria pellets decay 10 days and are then dissolved in 13 *M* HNO_3–0.04 *M* HF–0.1 *M* $Al(NO_3)_3$. This solution, the 90-day-decayed dissolved clone bottoms, and the UO_4 filtrate solution are combined and solvent-extracted to effect Th-U-Pa separation. The recovered thorium nitrate is converted to ThO_2 by the sol-gel process, repelleted, and returned to the reactor blanket. The uranium nitrate from solvent extraction is converted to UO_2SO_4 in D_2O by UO_4 precipitation and cake dissolution in D_2SO_4 and returned to the reactor core. The protactinium stream from solvent extraction is stored for 200 days and then processed through the mainline extraction equipment for U^{233} recovery. A hot cell facility is provided to process breeding gain for sale.

In the reactor that has a core-to-blanket thermal power ratio of 60:40, the processing plant blanket capacity is 266 kg of thorium per day containing 2.84 kg of uranium. The core hydroclone overflow (2400 liters/day) contains 3.6 kg of uranium, and the underflow (173 liters/day) contains 0.26 kg of uranium in 2.6 kg of total solids. In the alternative case, where the core-to-blanket thermal power ratio is 90.10, 1117 kg of ThO_2 containing 3.00 kg of uranium is processed daily. The core hydroclone overflow (2400 liters/day) contains 3.6 kg of uranium, the same as the previous case, and the underflow (213 liters/day) contains 320 g of uranium in 2.6 kg of solids.

All process equipment items for the smaller processing plant are located in a remotely maintained canyon 257 ft long by 29 ft wide. The

canyon contains six processing cells, three maintenance service cells, and a crane maintenance area. The maximum shielding required, through first-cycle extraction, is 6.5 ft. An air lock to hold a rail car is located at right angles to one end of the canyon. Samples for control analysis are taken in three sampling caves, serviced by remote manipulators, and located in a regulated corridor that runs the length of the canyon.

A single-story auxiliary area, 190 by 70 ft, houses the cold chemical makeup, warehouse, shop, process control room, hot and cold analytical laboratories, offices, and change facilities. A second story, 72 by 60 ft, houses building services and laboratory fans and filters.

The larger plant is the same as the smaller except that the canyon area is 277 by 31 ft and the maximum shielding is 7 ft.

The total capital investment for the smaller processing plant was estimated to be $13,918,000. The estimated investment for the larger plant was $15,718,000.

MSCR Fuel Processing Study

Preliminary process designs of two fluoride volatility plants, capable of recovering decontaminated uranium from spent molten fluoride salt fuel, were completed in sufficient detail to develop supplementary capital cost data for two MSCR conceptual design estimates. The smaller plant processes 1.2 ft^3/day of fuel containing 35 kg Th, 2.83 kg U, and 61 g of Pa^{233}. The capacity of the larger plant is 12 ft^3/day of fuel containing 350 kg of Th, 28.3 kg U, and 65 g of Pa.

The reactor for which the chemical plants were designed is fueled with 1780 ft^3 of 68-23-9 mole % LiF-BeF_2-ThF_4 containing sufficient UF_4, about 0.66 mole %, to maintain criticality and has a power production rate of 2500 Mw_{th} (1000 Mw_e). The total uranium inventory, which includes all isotopes from U^{233} to U^{238}, is about 4200 kg, of this total, the fissionable components, U^{233} plus U^{235}, are in the range 2627 to 2815 kg, depending on the processing rate. In addition, the system contains 52,000 kg of Th and 90.7–96 kg of Pa^{233} A nominal conversion ratio of 0.8 was assumed for the system, the remainder of the fuel being supplied by purchase of fully enriched U^{235}.

Design bases for the chemical processing plant included on-site processing, the use of existing technology except when extrapolation was absolutely necessary, and recovery of uranium only, with the Th and LiF-BeF_2 carrier salt discarded as waste. Storage of the spent fuel for 4.5 days and 27.5 days prior to fluorination for the 1.2- and 12-ft^3/day plants, respectively, is included. The UF_6 is removed from the salt by fluorination and is further purified by NaF sorption-desorption, collected in cold traps, liquefied and drained to product receivers, converted to UF_4 in a reduction tower of conventional design, added to fresh carrier salt containing thorium and additional fissile material, and returned to the reactor. The waste salt from the fluorination is held for protactinium decay until the undecayed protactinium amounts to only 0.1% of the bred U^{233}. For the 1.2-ft^3/day plant, the time is 130 days, and for the 12-ft^3/day plant, 175 days. After protactinium decay, the salt is again fluorinated and the recovered UF_6 is added to the main stream without the NaF sorption-desorption cycle. Following the second fluorination, the waste salt is stored for 1000 days, until the heat evolution rate is low enough to allow it to be transferred to permanent waste storage.

The two plant layouts are similar in both size and arrangement to the AHBR processing plants. The cell area of the smaller plant is 5700 ft^2 and the auxiliary area 33,400 ft^2. The cell and auxiliary areas for the larger plant are 13,400 and 38,800 ft^2, respectively. The large difference in the two cell areas results from the large area required for protactinium decay storage and the 1000-day final-waste storage equipment.

One of the most troublesome features of the MSCR fuel processing plant designs was that of making suitable provision for removing the fission product decay heat. In Table 24.1 are summarized the heat evolution rates for both plants during prefluorination, Pa^{233} decay, and interim waste storage. In the 1.2-ft^3/day plant, heat is removed from the two 4-ft^3 prefluorination salt-storage tanks by a design similar to that planned for the MSRE drain-and-fill tank. This system involves the use of triple-walled bayonets submerged in the salt. Water is introduced into the center of each bayonet, is vaporized, and is ejected into a stream dome through the center annulus. An air gap is provided in the outer annulus to control thermal stresses. In the 12-ft^3/day plant, a similar but slightly more elaborate design is used for the first two 30-ft^3-capacity tanks. Each of approximately 300 1.5-in. NPS sched 40 bayonets will be positioned in a 2.5-in. NPS sched 10 pipe located

Table 24.1. Average Total Heat Release

Type of Storage	Processing Rate 1.2 ft^3/day, Irradiation 1483 days		Processing Rate 12 ft^3/day, Irradiation 148.3 days	
	Decay[a] (days)	Heat Release (Mw)	Decay[a] (days)	Heat Release (Mw)
Prefluorination	6	0.097	25	0.985
Pa^{233} decay	132	0.678	175	1.568
Interim waste	1006	1.025	1002	1.037
Total	1144	1.800	1202	3.590

[a]Days in each type of storage.

in tube sheets. Hence, the storage volume available will be only the annuli between these two pipes and the volume of the lower head of the vessel not occupied by bayonets. The other four prefluorination storage tanks in the 12-ft^3/day plant and all of the Pa^{233} decay storage tanks in both plants will be located in water-jacketed thimbles. Interim-waste storage vessels in both plants will be located in thimbles submerged in a water-filled canal.

The total capital investment of the smaller plant was estimated to be $12,556,000. The estimated cost of the larger plant is $25,750,000.

24.2 HIGH-RADIATION-LEVEL ANALYTICAL LABORATORY

At the request of the ORNL Analytical Chemistry Division, coordination of the design of the High-Radiation-Level Analytical Laboratory (HRLAL) was continued. Final design of the HRLAL by the Vitro Engineering Company was completed in December 1961. The facility consists of one unloading cell, one storage cell, six work cells, three laboratories, an operating area, cell access area, decontamination area, service equipment area, change room, and offices. The entire facility is housed in a two-floor structure with a gross floor area of 18,100 ft^2 (ref 1).

The Title I design, completed June 10, 1961, consumed 120 man-weeks in the preparation of 17 drawings and 103 pages of specifications. The Title II effort, completed Dec. 8, 1961, required an effort of 550 man-weeks to produce 63 drawings and 595 pages of specifications.

The design was submitted to nine construction contractors for bid in January 1961, and bids were opened Mar. 1, 1962. The low bid, $1,739,000, was a $375,000 overrun of the project at the final design 5% contingency level. About 70% of the overrun was attributed to conventional construction items and 30% to the special Hastelloy C and type 304L stainless steel liquid and gaseous waste disposal systems. In March 1962 approval was obtained to increase the project cost from $2,000,000 to $2,500,000 to cover the overrun and slightly increase the contingency. The construction contract has not yet been awarded.

24.3 PLANT WASTE IMPROVEMENTS

Approval and funds for the design and construction of the ORNL Plant Waste Modifications[2] Project, at a cost of $1,700,000, were received, and design of the facility from criteria supplied by the Chemical Technology Division was begun by the UCNC-ORNL and Paducah Engineering Departments. The project includes (1) a separate Melton Valley

[1]*Chem. Technol. Div. Ann. Progr. Rept. May 31, 1961*, ORNL-3153, p 135.

[2]Frank Browder, *A Study of Proposed Modifications to the ORNL Process Waste System*, ORNL-3332 (in press).

low- and intermediate-activity-level waste collection and transfer system to the waste facilities in the main plant area, (2) an intermediate- and high-activity-level waste evaporator, and (3) a pair of 50,000-gal high-activity-level water-cooled stainless steel acid-waste storage tanks. The latter two facilities are to be located at the site formerly designated for building 2527. During the past year the term "Melton Valley waste system" was officially substituted for the "Low Level Treatment Facility." The new facilities have been described previously.[3]

Consulation on design of the project was provided, and all drawings and specifications are being reviewed in considerable detail as an assistance effort to the ORNL Operations Division. The Melton Valley collection and transfer system is scheduled to be completed in February 1963, and the waste evaporator and storage tanks in April 1964.

24.4 THORIUM FUEL CYCLE DEVELOPMENT FACILITY

ORNL has proposed that a Thorium Fuel Cycle Development Facility be built in Melton Valley, starting in FY 1964, for joint development use by the Chemical Technology and Metals and Ceramics Divisions. The first preliminary design and cost estimate, prepared by Vitro Corporation in 1961,[4] indicated a facility cost of $4,000,000. Design of the facility, which was called the U^{233} Metallurgical Development Facility,[1] was based on the premise that thorium and uranium would be supplied to the facility as a nitrate solution or in some other appropriate form and that its fission product radioactivity would be small relative to the radioactivity contributed by the decay of U^{232} and its daughters. The facility was to consist of three major cells with a total inside area of ~1250 ft^2 plus supporting structures with ~20,000 ft^2 floor area.

Subsequently, the AEC decided that the scope of the project should be expanded to provide a facility in which the entire thorium fuel cycle, including fuel processing and reconstitution and assembly fabrication, could be studied on an engineering scale. The new facility, which has been named the Thorium Fuel Cycle Development Facility (TFCDF), is to be fully flexible, with sufficient shielding to permit development of processes that produce little decontamination from fission products, and is to be designed so that an inert atmosphere may be provided for certain cells at a later date. A new architect-engineer, Giffels and Rossetti, Inc., of Detroit, Mich., is completing a conceptual design and cost estimate for the expanded facility. Early scoping studies indicate a cost of $6,000,000. The new layout shows five major cells with a combined inside area of ~2500 ft^2 plus a contaminated equipment storage cell with an area of ~500 ft^2. The floor space in the associated building is ~24,000 ft^2. The shielding walls are 5.5 ft of normal concrete, which is sufficient to reduce the radiation dose rate to one-tenth of tolerance for a fully irradiated (23,000 Mwd/ton) quarter section of a Consolidated Edison Thorium Reactor fuel assembly 90 days after removal from the reactor.

Equipment to fabricate stainless-steel-clad ThO_2-UO_2 fuel elements by the sol-gel–vibratory compaction process will be installed initially as part of the project, however, the facility is designed in modular fashion to accommodate a wide variety of processes. In four of the five cells, remote means will be provided to install, maintain, and remove process equipment. Only the cell that is to house equipment for operations on the closed and cleaned fuel tubes will use contact maintenance exclusively.

24.5 METAL RECOVERY CANAL CLEANOUT

The removal, canning, and shipment of 25 tons of Brookhaven Reactor fuel began in January 1962 and was completed July 1. This fuel, which had been stored in the Metal Recovery Building canal for 1 to 2 years, consists of 1.05-in.-OD by 4-in.-long irradiated natural uranium pieces that had been assembled in 10-ft aluminum cans fitted with 0.125-in. fins. After irradiation in the reactor and 1–2 years' decay at the reactor site, the fins on the cans were collapsed and the cans sheared into 4-in. lengths and shipped to ORNL for storage and recovery. Storage was in 2- by 2- by 2-ft stainless steel bins stacked three deep over half the canal length. During storage the exposed fuel was

[3] *Chem. Technol. Div. Ann. Progr Rept. May 31, 1961*, ORNL-3153, p 137.

[4] *Conceptual Design Report on U^{233}*, Metallurgical Laboratory, KLX-1835.

attacked by the canal water, resulting in finely divided, easily dispersed particles of uranium oxide, and marine growth in the canal water produced undesirable collections of silt, which aggravated handling the fuel pieces. The activity burden of the canal water, which initially was ~1 μc/ml with Cs^{137} accounting for >95% of the total, was decreased to 0.2 μc/ml by intermittent purging with process water.

The fuel pieces were transferred with tongs under 7 ft of water from the storage bins to 11- by 12- by 39-in.-long all-aluminum containers called "bundles," which held ~350 pieces. After the bundles had been filled, aluminum covers were bolted on with aluminum bolts, and the bundles were leak-tested. The loaded bundles were then transferred, under water, to 15-ton shipping casks (each holding two bundles), and the loaded cask was raised from the canal and purged with process water. The cavity water level was adjusted and the exterior of the cask was decontaminated for shipment, to a processing site, on a trailer equipped with a heated enclosure to prevent freezing in cold weather.

Personnel exposures during the operation averaged ~6 mrem per man-hr of work. Air activity remained below the level requiring respiratory protection during loading operations but rose above this level for unidentified alpha and beta-gamma activity when normally wet walls were exposed and allowed to dry during canal purging. Intermittent purging was necessary to maintain the average activity burden of the canal water at 0.2–0.3 μc/ml and the radiation levels in the working areas in the range 25–35 mr/hr.

After the storage bins were emptied, they were raised near the surface and the bulk of the silt was dredged out, leaving the larger fuel fragments. These were discharged to the canal floor and the bin was raised to a stainless steel drain pan where the remaining silt and fragments were rinsed away. The bins were then transported to the burial ground for permanent disposal.

The use of Cu^{2+} for marine life control was successful but was later abandoned when it appeared that metals such as iron and perhaps uranium were reacting with copper, thereby reducing visibility and increasing the activity burden of the canal water. Thereafter, visibility in the canal water was controlled by continuously filtering the water through a 40-μ sintered stainless steel filter (Fig. 24.1). Material on the filter was removed from the unit by frequent backwashing with water and intermittently soaking with 13 *M* HNO_3. All backwash water and canal water purged from the system were sent to intermediate-activity-level waste disposal tanks.

A loading rate of ~2000 fuel pieces per week could be maintained after installation of the filter improved visibility, compared with ~1000 when visibility was poor.

Under the canal abandonment program, the canal area was fenced off from the rest of the Metal Recovery Facility grounds, a new jet and line were installed to permit emptying of the canal to waste tank W-5, and a closed-circuit pump and filter system was installed on the canal to permit removal of particulate matter from the water to reduce contamination and improve visibility. The filter originally used a 10-μ pore size filter unit; the initial flow rate of >100 gpm was slowed to ~10 gpm in 20 min by the filter cake. Substitution of 40-μ pore size filter media resulted in a final rate of ~30 gpm after 8 hr.

The shipment of BNL fuel to SRP was completed the end of May 1962, and decontamination of the canal is expected to be finished by July 31, 1962.

24.6 SAFETY AND CONTAINMENT

Assistance work on plant safety and containment included (1) completion of the containment changes and additions to buildings 4507 and 3508; (2) shipment of all BNL fuel in the building 3505 canal to SRP and subsequent cleanup and abandonment of the canal; (3) installation of an improved off-gas ventilation system for the HRLAF cells; (4) design and cost estimation of a contaminated off-gas filter carrier for general plant use; (5) completion of the new alpha laboratory in room 211 of building 3019; (6) completion of the relocated U^{233} solution storage facility in cell 3 of building 3019; (7) an independent hazards evaluation of the HRLEL for the Metals and Ceramics Division; (8) a 16-hr course on "Radiochemical Facility Hazard Evaluation" prepared for and presented to the Office of Radiation Safety and Control.

Modifications were made to building 3508 to ensure conformance with Laboratory standards for containment and hazard control. These modifications included expansion and modification of the laboratory ventilation supply and exhaust systems, provision for emergency power and instrumentation

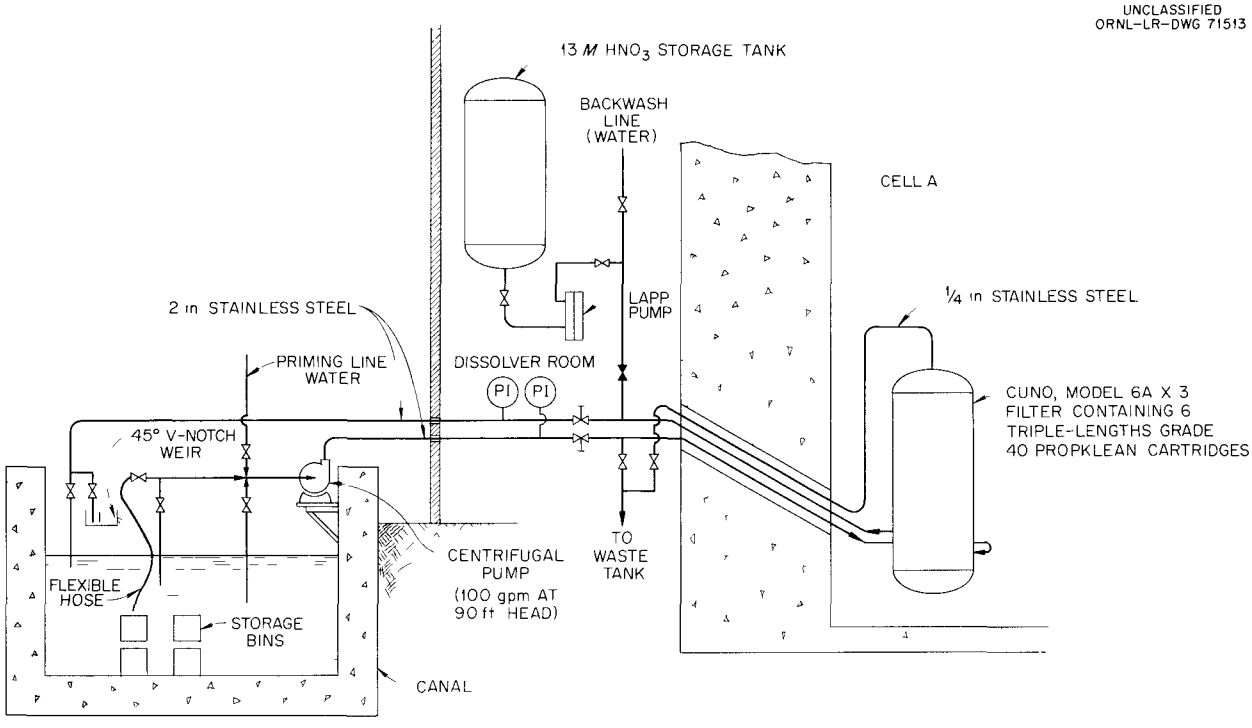

Fig. 24.1. Metal Recovery Building Canal Filter System.

to ensure hazard control of the building attic, and other changes to ensure proper distribution and flow of building air. The changes to building 4507 described previously[1] were completed in September 1961.

An exit air filtration system with a capacity of 18,000 cfm for cleaning the exhaust air from the HRLAF cells in building 3019 was installed in the ducting to the 3020 stack and placed in operation. This facility consists of a bank of roughing filters (American Air Filter deep-bed pocket type filters using two beds of filterdown, FG-25 and FG-50) and a bank of final filters (standard fire-resistant AEC-type absolute filters) in series. The filter housing consists of 1-ft-thick concrete for shielding. Minor modifications to existing ductwork and the purchase of a new exhaust fan were required to complete the installation.

A preliminary design cost and estimate of a shielded carrier for general plant use in removing radioactive filters from the several ORNL shielded off-gas filter facilities was prepared. It may be used with the Radiochemical Processing Pilot Plant and HRLAF filter facilities at building 3019 and the cell ventilation filters for buildings 4501, 4505, and 4507. Two 3-in.-thick steel plate shields with removable top and bottom are proposed, one for removing the prefilters and a larger one for removing the absolute filters. Each shield contains a disposable alpha-tight sheet metal can. The prefilter shield is estimated to weigh 5 tons and the absolute filter shield 8 tons. The fabrication cost of both shields is estimated to be $12,000 \pm 25\%$.

The conversion of room 211 of building 3019 from a U^{233} isolation laboratory to an alpha research laboratory was completed. The room was first stripped and decontaminated and then refurbished as an alpha laboratory for chemical development use. Changes included addition of a stainless steel floor, an air lock entryway, a smooth hung ceiling with recessed lighting, glove boxes, a glove box ventilation system, and ventilation of the room to the pilot plant cell off-gas system to ensure that reduced pressure is always maintained in the room. Radiation monitors and other devices were added to comply with containment standards.

Relocation of the U^{233} solution storage system from the pipe tunnel to cell 3 in building 3019 was completed. A new critically safe storage tank was

fabricated and installed and is now in service. The storage tank is a unit-shielded, 3-ft-diam, 225-gal tank completely packed with 1.5-in. Pyrex Raschig rings to a glass volume of ~23%. The glass rings contain 11.6 wt % B_2O_3. The tank was designed to hold up to 60 kg of U^{233} aqueous solution at a concentration of 100–200 g/liter.

Assistance was given to the Metals and Ceramics Division in the preparation of a hazards evaluation report for the High-Radiation-Level Examination Laboratory (HRLEL), now nearing completion. Quantities of radioactive and hazardous materials to be handled in the facility and properties of the HRLEL containment and ventilation systems were summarized. HRLEL shields were evaluated with the PHOEBE code for determination of fission product sources, SDC for determination of gamma attenuation, and RENUPAK for determination of neutron penetration. An Oracle program was written for calculation of the pressure and temperature transients that would result from a fire in a cell. The analyses indicate that the facility is well equipped to withstand credible fires and explosions without serious damage to the cell, intolerable personnel exposures from escaping gases or aerosols, or hazardous levels of downwind ground contamination.

A quantitative hazard evaluation course consisting of 16 hr of instruction was presented to members of the Office of Radiation Safety and Control. The topics covered were meteorology; effects of fires and chemical, mechanical, and nuclear explosions; and evaluation of personnel dose and fallout following a credible accident. Two reports, ORNL TM-16, "Radiochemical Facility Hazard Evaluation," and ORNL TM-19, "The Evaluation of Radioactive Releases from Chemical Plants," were prepared to aid in hazard evaluation studies.

24.7 CRITICALITY STUDIES

Assistance efforts on criticality problems included (1) neutron multiplication measurements on the U^{233} storage tank in building 3019; (2) an exhaustive study on the feasibility and safety of using soluble nuclear poisons as a primary criticality control; (3) design and installation of a stainless-steel-clad borax-filled poison network for the Volatility Pilot Plant caustic filter; and (4) drop-testing of a model of the Pyrex-filled HRT fuel solution carrier.

Neutron multiplication measurements made on the Pyrex-Raschig-ring-filled U^{233} storage tank as it was slowly filled with 11 kg of aqueous $U^{233}O_2(NO_3)_2$ solution at a concentration of 100 g of uranium per liter indicated that the tank was critically safe for >150 liters of aqueous solution with a U^{233} concentration of 115 g/liter. However, until more U^{233} is available for storage in the tank, the effectiveness of the rings as a fixed poison for U^{233} solutions cannot be realistically assessed.

Studies of the feasibility of using soluble neutron poisons as a primary criticality control in shielded radiochemical facilities included multigroup machine calculations of the required content and concentration of poisons in solutions of fissile and fertile material; a compilation of data on the detection, stability, decontamination, and costs of soluble neutron poisons; and an assessment of the possible effects of a nuclear excursion. It was concluded that the use of soluble poisons is a feasible method of control in view of the many advantages and the tolerable effects of a possible accident in a heavily shielded area. It is believed that soluble poison control may be made as reliable as any other method of control through adequate process development work and provision of multiple independent safeguards.

A fixed nuclear poison lattice for the Fluoride Volatility Pilot Plant caustic filter, which is 16 in. diam by 36 in. high, was designed, evaluated, and installed. The lattice consists of parallel plates of stainless-steel-clad borax, which extend to within 1 in. of the vessel wall and are spaced such that the maximum borax-to-borax separation is $2\frac{1}{8}$ in. The borax thickness in the individual plates varies from $\frac{1}{8}$ to $\frac{7}{8}$ in. A mathematical analogy with ORNL Pyrex pipe criticality experiments indicates that the poisoned vessel may safely contain at least 3.5 kg of U^{235} at any concentration.

Drop tests were made with a steel container filled with water and 1.5-in.-OD by 1.75-in.-long by 0.125-in.-wall borosilicate glass Raschig rings to obtain qualitative information on the effects of accidental dropping of the HRT fuel transfer carrier, which is a lead-shielded, 120-liter vessel containing approximately 24 vol % 19% B_2O_3-borosilicate glass as Raschig rings. The test container was chosen such that a drop from an equivalent height would result in more shock in the test container than in the fuel transfer carrier. A

single drop from a height of 3 ft onto a steel surface resulted in breakage of ~20% of the rings into two or more pieces and ~5% decrease in packed height. Five successive drops from a height of 5 ft resulted in breakage of ~50% of the rings and a 20% decrease in the packed height.

The carrier subsequently was used to transfer HRT fuel solution containing 11 kg of U^{235} at a concentration of approximately 200 g/liter from the HRT to the Fission Product Development Laboratory for uranium recovery.

24.8 CARRIERS AND CHARGERS

Carriers and chargers that were designed and built included the 1WW carrier for shipment of 4.5 gal of waste solution from Hanford and Idaho to ORNL, a carrier for transporting the declad SRE fuel to SRP, a carrier for shipping 14-in.-long irradiated fuel samples from the MTR, ETR, and NRX reactors to ORNL for hot cell experiments, and an analytical transfer cask for use at the HRLAF. A 40-in.-long irradiated fuel sample carrier and an analytical transfer cask for use at the HRLAF, to avoid continued contamination of the building 4507 analytical carrier, were designed but have not yet been built . The analytical and the SRE fuel carriers used lead for shielding, all the others used depleted uranium. The carrier for transporting plutonium-aluminum fuel from SRP to ORNL, which was designed over a year ago, was completed and is now in use.

The 1WW carrier design was intensively evaluated for safety with the proposed AEC regulation CFR, Title 10, Part 72 as a basis of review. This carrier, which weighs three tons, is designed to contain ~100,000 curies of fission product activity in aqueous solution. The solution is contained in a stainless steel tank 12 in. diam by 14 in. high and is shielded with 5 in. of depleted uranium. The shield has an outer and inner stainless steel liner, the inner liner is separated from the tank by a mercury film. Appropriate filling, emptying, and vent lines penetrate the top of the cask and are shielded with a second shielded dome cover.

Review of the design indicated that the carrier has full double containment. The method of fastening the carrier to the gondola car is sufficient to withstand 60 g deceleration. A fire shield provides complete protection in case the cask should be involved in a gasoline or oil fire for 1 hr. The cask can adequately dissipate 1000 Btu/hr of fission product heat at an ambient temperature of 100°F without the solution temperature exceeding 175°F. Experimental data indicate that there will be no pressure buildup from radiolytic dissociation of the solution, however, the cask is designed to withstand 20 psig internal pressure. The carrier shielding is more than adequate to meet the ICC regulation of 200 mr/hr at the surface and 10 mr/hr at 1 meter. In its proposed use criticality is of no concern.

24.9 EUROCHEMIC ASSISTANCE

ORNL's contribution to the Eurochemic Assistance Program consisted in coordination of the program and review and exchange of pertinent technical information on radiochemical processing of irradiated fuels. About 280 USAEC-originated documents and 55 miscellaneous items were sent to Eurochemic. The 25 Eurochemic documents previously received were edited and reproduced, and limited distribution was made pending resolution of the US-Eurochemic document exchange agreement. Forty-four Eurochemic documents were reproduced and distributed without editing, and 14 were translated and distributed.

The US technical advisor who was at Eurochemic left on May 10, 1962. The replacement advisor is E. M. Shank, ORNL.

The preproject study (scope) for the various Eurochemic facilities at Mol, Belgium, has been completed, and detailed design is in progress. Construction has started on several of the main buildings. Foundation work is in progress for the main processing building, the research laboratory structure is well above grade level, and the general services structure is nearing completion. The overall project is about 40% designed and 10% constructed. Current official costs are $24,000,000 for construction, with a $30,700,000 total investment.

Processing conditions for the final plutonium purification step have been frozen. This step will use a 10% TLA extraction followed by direct precipitation from the organic product. Engineering flowsheets and equipment layouts have not yet been started.

The final preproject study has been prepared for the modifications and the additional facilities required to permit enriched uranium processing. This study will be submitted to the board of directors in June 1962. A final decision is not expected until November, pending the results of negotiations with the USAEC and Euratom. A preliminary cost estimate indicates that an additional $1,500,000 in capital investment will be required.

25. Publications and Speeches

POWER REACTOR FUEL PROCESSING

Blanco, R. E., and C. D. Waston, "Head-End Processes for Solid Fuels," *Reactor Handbook, Vol II, Fuel Processing*, chap. 3, Interscience, New York, 1961.

Blanco, R. E., and E. L. Anderson, *Trip Report-Survey of Research and Development in Nuclear Fuel Reprocessing at Harwell, Dounreay, Windscale-United Kingdom, Fontenay aux Roses-France, and Mol-Belgium*, WASH-1035 (1961).

Blanco, R. E., L. M. Ferris, and C. D. Watson, "Preparation of Stainless Steel, Zirconium, and Graphite Clad and Base Reactor Fuels for Solvent Extraction," ORNL TM-131 (Jan. 29, 1962), presented at Nuclear Congress, June 4–7, 1962, New York.

Blanco, R. E., and C. D. Watson, "Recent Advances in Aqueous Processing," presented at American Nuclear Society Meeting, Nov. 7–9, 1961, Chicago.

Blanco, R. E., L. M. Ferris, and D. E. Ferguson, *Aqueous Processing of Thorium Fuels*, ORNL-3219 (Feb. 28, 1962).

Ferris, L. M., and L. A. Kambach, *Uranium Recovery from KIWI Fuel Elements: Laboratory Development*, ORNL-3196 (Dec. 4, 1961).

Ferris, L. M., A. H. Kibbey, and M. J. Bradley, *Processes for Recovery of Uranium and Thorium from Graphite-Base Fuel Elements. Part II*, ORNL-3186 (Nov. 16, 1961).

Bradley, M. J., and L. M. Ferris, "Recovering Uranium from Graphite Fuel Elements," *Ind. Eng. Chem.* 53, 279 (1961).

Bradley, M. J., and L. M. Ferris, *Processing of Uranium Carbide Reactor Fuels. I. Reaction with Water and HCl*, ORNL-3101 (Aug. 1, 1961).

Bradley, M. J., and L. M. Ferris, "Hydrolysis of Uranium Carbides Between 25 and 100°C. I. Uranium Monocarbide," presented at American Chemical Society Meeting, Washington, D.C., March 1962.

Warren, K. S., L. M. Ferris, and A. H. Kibbey, *Dissolution of BeO- and Al_2O_3-Base Reactor Fuel Elements. Part 1*, ORNL-3220 (Jan. 30, 1962).

Ferris, L. M., *Aqueous Processes for Dissolution of Uranium-Molybdenum Alloy Reactor Fuel Elements*, ORNL-3068 (June 30, 1961).

Ferris, L. M., "Solubility of Molybdic Oxide and Its Hydrates in Nitric Acid, Nitric Acid–Ferric Nitrate, and Nitric Acid–Uranyl Nitrate Solutions," *J. Chem. Eng. Data* 6, 600 (1961).

Ferris, L. M., and A. H. Kibbey, *Miscellaneous Experiments Relating to the Processing of CETR Fuel by Sulfex-Thorex and Darex-Thorex Processes*, ORNL-3143 (Aug. 16, 1961).

Clark, W. E., and T. A. Gens, *Corrosion of Titanium in Solutions Used for Dissolution of Zirconium Alloys*, ORNL-3118 (October 1961).

Gens, T. A., "New Developments in Uranium-Zirconium Alloy Fuel Reprocessing," *Nucl. Sci. Eng.* 9, 488–94 (1961).

Kitts, F. G., and W. E. Clark, *The Darex Process. Treatment of Stainless Steel Reactor Fuels with Dilute Aqua-Regia*, ORNL-2712 (May 23, 1962).

Gens, T. A., *Zircex and Modified Zirflex Processes for Dissolution of 8% U–91% Zr–1% H TRIGA Reactor Fuel*, ORNL-3065 (November 1961).

Gens, T. A., and R. E. Blanco, "Modified Zirflex Process for Dissolution of 1 to 10% U–Zr Alloy Fuels in Aqueous NH_4F-NH_4NO_3-H_2O_2," *Nucl. Sci. Eng.* **11**, 267–73 (1961).

Gens, T. A., "Chloride Volatility Processing of Nuclear Fuels," presented at 54th Annual AIChE Meeting, New York, Dec. 2–7, 1961 (ORNL CF-61-3-43).

Gens, T. A., *The Chemistry of Niobium in Processing of Nuclear Fuels*, ORNL-3241 (January 1962).

Moore, J. G., and R. H. Rainey, *Extraction of Niobium-95 from Nitric Acid Solutions with Tri-n-butyl Phosphoric Acid*, ORNL-3295 (in press).

Baybarz, R. D., *The Effect of High Alpha Radiation on the Corrosion of Metals Exposed to Chloride Solutions*, ORNL-3265 (Mar. 27, 1962).

Moore, J. G., "The Removal of Niobium-95 from Zirconium Solutions with Vycor Glass," *J. Inorg. Nucl. Chem.* **20**, 166–67 (1961).

Moore, J. G., and R. H. Rainey, "The Chemical Feasibility of Nuclear Poisons in the U-Th Fuel Processing Systems," *Nucl. Sci. Eng.* **11**, 278–85 (1961).

Rainey, R. H., and J. G. Moore, *Laboratory Development of the Acid Thorex Process for Recovery of Consolidated Edison Thorium Reactor Fuel*, ORNL-3155 (Apr. 27, 1962).

Rainey, R. H., and J. G. Moore, "Laboratory Development of the Acid Thorex Process for Recovery of Thorium Reactor Fuels," *Nucl. Sci. Eng.* **10**, 367–71 (1961).

Adams, J. B., A. M. Bemis, and C. D. Watson, *Comparative Cost Study of Processing Stainless Steel-Jacketed UO_2: Mechanical Shear-Leach vs Sulfex-Core Dissolution*, ORNL-3227 (Apr. 6, 1962).

Watson, C. D., B. C. Finney, and S. Sinichak, *Mechanical Dejacketing of SRE Core I Fuel*, 12 min, 16 mm color movie, in sound, September 1961.

Watson, C. D., B. C. Finney, and S. Sinichak, *Shearing of Power Reactor Fuels*," 4 min, 16 mm color movie, silent, September 1961.

Adams, J. B., *A Survey of the Hazards Involved in Processing Liquid Metal Bonded Fuels*, ORNL-3147 (July 31, 1961).

FLUORIDE VOLATILITY PROCESSING

Carr, W. H., S. Mann, and E. C. Moncrief, "Uranium-Zirconium Alloy Fuel Processing in the ORNL Volatility Pilot Plant," presented at the 54th Annual AIChE Meeting, New York, Dec. 2–7, 1961 (ORNL CF-61-7-13, AIChE preprint 150).

Cathers, G. I., M. R. Bennett, and R. L. Jolley, "The Application of Fused Salt Fluoride Volatility Processing to Various Reactor Fuels," presented at 54th Annual AIChE Meeting, New York, Dec. 2–7, 1961 (AIChE preprint 148).

Litman, A. P., and R. P. Milford, "Corrosion Associated with the Oak Ridge National Laboratory Fused Salt–Fluoride Volatility Process," presented at Symposium on Fused Salt Corrosion, Fall Meeting of the Electrochemical Society, Detroit, Michigan, Oct. 1–5, 1961.

Milford, R. P., Sydney Mann, J. B. Ruch, and W. H. Carr, Jr., "Recovering Uranium Submarine Fuels," *Ind. Eng. Chem.* **53**, 357 (1961).

Guthrie, C. E., "Recent Developments in the ORNL Volatility Process," presented at the Nuclear Fuels Symposium, Fall Meeting of AIME, Detroit, Michigan, Oct. 24, 1961.

Horton, R. W., S. H. Stainker, and M. E. Whatley, "Correlation of Fused Salt Dissolution Data," presented at the 54th Annual AIChE Meeting, New York, Dec. 2–7, 1961 (ORNL CF-61-4-14, AIChE preprint 149).

Cathers, G. I., "Dissociation Pressure of MoF_6-NaF Complex and the Interaction of Other Hexafluorides with NaF," presented at American Chemical Society Meeting, Chicago, Sept. 3–10, 1961.

Cathers, G. I., "Fluoride Volatility Processing of Highly Enriched Uranium Fuels," presented at American Nuclear Society Meeting, Chicago, Nov. 7–9, 1961.

Cathers, G. I., and R. L. Jolley, *Recovery of PuF_6 by Fluorination of Fused Fluoride Salts*," ORNL-3298 (in press).

Cathers, G. I., R. L. Jolley, and H. F. Soard, *Use of Fused Salt–Fluoride Volatility Process with Irradiated Urania Decayed 15–30 Days*, ORNL-3280 (July 2, 1962).

Cathers, G. I., R. L. Jolley, and E. C. Moncrief, *Laboratory-Scale Demonstration of the Fused Salt Volatility Process*, ORNL TM-80, Dec. 6, 1961; *Nuclear Science and Engineering* (in press).

WASTE TREATMENT AND DISPOSAL

Hancher, C. W., and J. C. Suddath, "Pot Calcination of Simulated Radioactive Waste with Continuous Evaporation," ORNL TM-117, December 1961, presented at AIChE Meeting, Los Angeles, February 1962.

Perona, J. J., *The Effects of Internal Heat Generation on Pot Calcination Rates for Radioactive Wastes*, ORNL-3163 (Oct. 9, 1961).

Godbee, H. W., and W. E. Clark, *The Use of Phosphite and Hypophosphite to Fix Ruthenium from High-Activity Wastes in Solid Media*, ORNL TM-125 (Jan. 30, 1962).

Clark, W. E., "Fixation of High Level Wastes in Glass," presented at meeting of 3252nd U.S. Army Research and Development Unit, Oct. 4, 1961.

Perona, J. J., R. L. Bradshaw, J. T. Roberts, and J. O. Blomeke, "Evaluation of Ultimate Disposal Methods for Liquid and Solid Radioactive Wastes: Status Report," presented at Second AEC Working Meeting on Ground Disposal of Radioactive Wastes, Chalk River, Ontario, Sept. 26–29, 1961 (ORNL TM-86).

Godbee, H. W., and J. T. Roberts, *Laboratory Development of a Pot Calcination Process for Converting Liquid Wastes to Solids*, ORNL-2986 (Aug. 30, 1961).

Perona, J. J., "The Effects of Internal Heat Generation on Pot Calcination Rates for Radioactive Wastes," presented at First Inter-American Congress of Chemical Engineers, San Juan, Puerto Rico, Oct. 23–28, 1961 (ORNL-3163).

Bradshaw, R. L., J. J. Perona, J. T. Roberts, and J. O. Blomeke, *Evaluation of Ultimate Disposal Methods for Liquid and Solid Radioactive Wastes. I. Interim Liquid Storage*, ORNL-3128 (Aug. 7, 1961).

Perona, J. J., R. L. Bradshaw, J. T. Roberts, and J. O. Blomeke, *Evaluation of Ultimate Disposal Methods for Liquid and Solid Radioactive Wastes. II. Conversion to Solid by Pot Calcination*, ORNL-3192 (Sept. 27, 1961).

SOLVENT EXTRACTION RESEARCH

Coleman, C. F., C. A. Blake, Jr., and K. B. Brown, "Separations by Liquid Ion Exchange," presented at the American Chemical Society, Division of Analytical Chemistry, Summer Symposium, Cleveland, Ohio, June 22, 1961.

Coleman, C. F., C. A. Blake, Jr., and K. B. Brown, "Analytical Potential of Separations by Liquid Ion Exchange," *Talanta* 9, 297–323 (1962).

Davis, W., Jr., *Purification of Degraded Tributyl Phosphate–Hydrocarbon Diluent Solutions by Distillation: Status Summary*, ORNL-3203 (Nov. 29, 1961).

Faure, A., and W. Davis, Jr., *Measurement of the Vapor Pressure of TBP*, ORNL-3236 (Nov. 29, 1961).

Davis, W., Jr., "Thermodynamics of Extraction of Nitric Acid by Tri-*n*-Butyl Phosphate–Hydrocarbon Diluent Solutions. I. Distribution Studies with TBP in Amsco 125-82 at Intermediate and Low Acidities," *Nucl. Sci. Eng.* (in press).

Davis, W., Jr., *ibid.*, Part II. "Densities, Molar Volumes, and Water Solubilities of TBP-Amsco 125-82-HNO_3-H_2O Solutions," *Nucl. Sci. Eng.* (in press).

Davis, W., Jr., *ibid.*, Part III. "Comparison of Literature Data," *Nucl. Sci. Eng.* (in press).

Weaver, Boyd, *Extraction of Neptunium from Acidic Solutions by Organic Nitrogen and Phosphorus Compounds*, ORNL-3194 (Oct. 5, 1961).

Wischow, R. P., and D. E. Horner, *Recovery of Strontium and Rare Earths from Purex Wastes by Solvent Extraction*," ORNL-3204 (Jan. 15, 1962).

Seeley, F. G., F. J. Hurst, and D. J. Crouse, *Solvent Extraction of Uranium from Carbonate Solutions*," ORNL-3106 (Aug. 16, 1961).

McDowell, W. J., and K. A. Allen, "Thorium Extraction by Di-*n*-Decylamine Sulfate in Benzene," *J. Phys. Chem.* 65, 1358 (1961).

TRANSURANIUM ELEMENT PROCESSING

Klima, B. B., "Transuranium Development Facility," *Trans. Am. Nucl. Soc.* 4(2) (1961), presented at American Nuclear Society Meeting, Chicago, Nov. 7–9, 1961.

Lloyd, M. H., and R. E. Leuze, "Anion Exchange Separation of Trivalent Actinides and Lanthanides," *Nucl. Sci. Eng.* 11, 274–77 (1961).

Baybarz, R. D., and R. E. Leuze, "Separation of Transplutonium and Rare Earth Elements by Liquid-Liquid Extraction," *Nucl. Sci. Eng.* 11, 90–94 (1961).

Baybarz, R. D., and Boyd Weaver, *Separation of Transplutoniums from Lanthanides by Tertiary Amine Extraction*, ORNL-3185 (Dec. 4, 1961).

Baybarz, R. D., and H. B. Kinser, *Separation of Transplutoniums and Lanthanides by Tertiary Amine Extraction. II. Contaminant Ions*, ORNL-3244 (Feb. 20, 1962).

Baybarz, R. D., *Separation of Transplutonium Elements by Phosphonate Extraction*, ORNL-3273 (July 20, 1962).

Ferguson, D. E., *Transuranium Quarterly Progress Report for Period Ending Feb. 28, 1962*, ORNL-3290.

PRODUCTION OF U^{232}

Chilton, J. M., and N. Jackson, *Preparation of U^{232} from Pa^{231}. I. Preliminary Work*, AERE-R3727 (June 1961).

THORIUM OXIDE IRRADIATION

McBride, J. P., and S. D. Clinton, *Radiation-Induced Sintering of Thoria Powders*, ORNL-3275 (in press).

GAS RECOMBINATION STUDIES

McBride, J. P., *Radiation Stability of Aqueous Thoria and Thoria-Urania Slurries*, ORNL-3274 (in press).

McBride, J. P., *Method of Combining Hydrogen and Oxygen*, U.S. Patent 3,023,085.

THORIUM FUEL CYCLE

Ferguson, D. E., O. C. Dean, and P. A. Haas, "Preparation of Oxide Fuels for Vibratory Compaction by the Sol-Gel Process," presented at the AEC-Sponsored Symposium on Powder-Packed Uranium Dioxide Fuel Elements, Hartford, Conn., Nov. 29–Dec. 1, 1961 (ORNL TM-53).

Ferguson, D. E., E. D. Arnold, W. S. Ernst, Jr., and O. C. Dean, "Preparation and Fabrication of ThO_2 Fuels," presented at the CNEN Symposium on Thorium Fuel Cycle, Sixth Nuclear Congress, Rome, Italy, June 13–15, 1961 (ORNL-3225, June 1962). Printed originally as ORNL CF-61-6-114.

Ullmann, J. W., "Some Major Fuel-Cycle Problems," presented at Small and Medium Power Reactors Meeting, IAEA, Vienna, 1961.

Carter, W. L., L. G. Alexander, R. H. Chapman, B. W. Kinyon, J. W. Miller, and R. Van Winkle, "Thorium Reactor Evaluation: Fuel Yield and Fuel Costs in Five Thermal Breeders," *Trans. Am. Nucl. Soc.* 4(2) (1961), presented at American Nuclear Society Meeting, Chicago, Nov. 7–9, 1961.

Ferguson, D. E., O. C. Dean, and P. A. Haas, "Preparation of Oxide Fuels for Vibratory Compaction by Sol-Gel Process," presented at AEC-Sponsored Symposium on Powder-Packed Uranium Dioxide Fuel Elements, Hartford, Conn., Nov. 29–Dec 1, 1961 (ORNL TM-53).

RADIATION EFFECTS ON CATALYSTS

Krohn, N. A., and H. A. Smith (University of Tennessee), "The Influence of X-Rays on Catalytic Activity as Related to Incorporated Radioactivity," *J. Phys. Chem.* 65, 1919 (1961).

HIGH TEMPERATURE CHEMISTRY

Krohn, N. A., and R. G. Wymer, "X-Ray Method for Determining Liquid Densities at High Temperatures and Pressures," *Anal. Chem.* 34, 121 (1962).

Krohn, N. A., and R. G. Wymer, "Measuring Liquid Densities at High Temperatures and Pressures," contribution to the *Encyclopedia of X- and Gamma Rays*, in preparation, Rheinhold, G. L. Clark, ed.

Wymer, R. G., and R. E. Biggers, *Cerenkov Radiation Intensity Calculations for Sr^{90} and Co^{60} in Water*, ORNL-3180 (Sept. 5, 1961).

EQUIPMENT DECONTAMINATION

Meservey, A. B., "Procedures and Practices for the Decontamination of Plant and Equipment," in *Progress in Nuclear Energy*, series 4, vol 4, Pergamon, London (1961).

Meservey, A. B., "Corrosion Inhibition by Hydrogen Peroxide in Decontamination Solutions," presented at the 141st Meeting, American Chemical Society, March 1962.

FUEL SHIPPING STUDIES

Shappert, L. B., "Shipping Container Drop Test Program at ORNL," presented at Evaluation and Planning Meeting at U.S. Atomic Energy Commission, Germantown, Maryland (Mar. 26, 1962).

Shappert, L. B., *ibid.*, at Working Meeting on AEC Shipping Container Testing Programs at Johns Hopkins University, Baltimore, sponsored by Johns Hopkins University and U.S. Atomic Energy Commission, May 3, 1962.

CHEMICAL ENGINEERING RESEARCH

Watson, J. S., *A Study of the Kinetics of Uranyl Sulfate Exchange with a Strong Base Anion Resin*, ORNL-3296 (June 1962).

GCR COOLANT PURIFICATION

Scott, C. D., "Removal of Hydrogen, Carbon Monoxide, and Methane from Gas-Cooled Reactor Helium Coolants," presented at 7th AEC Air Cleaning Conference at Brookhaven National Laboratory, Oct. 10–12, 1961 (ORNL TM-20, Oct. 6, 1961).

Scott, C. D., *The Rate of Reaction of Hydrogen from Hydrogen-Helium Streams with Fixed Beds of Copper*, ORNL-3292 (May 1962).

CHEMICAL APPLICATIONS OF NUCLEAR EXPLOSIONS

Landry, J. W., "Project Plowshare – Peaceful Uses of Nuclear Explosives," presented to: Civitan Club, Clinton, Tenn., Nov. 1, 1961; Rotary Club, Clinton, Tenn., September 1961; U.S. Navy Nuclear Science Seminar, Oak Ridge, Tenn., November 1961; and U.S. Army Nuclear Science Seminar, Oak Ridge, Tenn., June 1961.

Landry, J. W., "Excavation with Nuclear Explosives," presented to U.S. Navy Reserve, Oak Ridge, Tenn., June 1961.

Landry, J. W., "Project Gnome," presented to U.S. Army Reserve, Oak Ridge, Tenn., January 1962.

Landry, J. W., "Peaceful Uses of Nuclear Explosives," presented to ORNL Electronuclear Division, May 8, 1962.

MISCELLANEOUS

Perona, J. J., W. E. Dunn, and H. F. Johnson, *Calculated Transient Pressures Due to Impulse and Ramp Perturbations to Ventilating Systems in Buildings 3019, 3026, 3508, and 4507*, ORNL-3086 (Aug. 1, 1961).

Bresee, J. C., and J. T. Long, "Design Philosophy for Direct-Maintenance Radiochemical Processing Plants," presented at Nuclear Congress, New York, June 4–7, 1962 (ORNL TM-153).

Nichols, J. P., "The Seventh AEC Air Cleaning Conference," report given at ORNL Nuclear Safety Seminar (Dec. 15, 1961).

Nichols, J. P., E. D. Arnold, and A. T. Gresky, "The Evaluation of Radioactive Releases from Chemical Plants," presented at the Seventh AEC Air Cleaning Seminar, Brookhaven National Laboratory, Oct. 10–12, 1961.

Nichols, J. P., "Idaho Chemical Processing Plant Criticality Incident of January 25, 1961, *Nucl. Safety* 3(2) (December 1961).

Nichols, J. P., and E. D. Arnold, "Hazards Analysis of Chemical Processing Facilities, *Nucl. Safety* 3(1) (September 1961).

Nichols, J. P., "Radiochemical Facility Hazard Evaluation Course," given at ORNL Office of Radiation Safety and Control (8 sessions), June 15–July 15, 1961.

Holmes, J. M., "Removal of Contaminants from Gas Streams," *Nucl. Safety* 2(4) (June 1961).

Burch, W. D., and L. B. Shappert, "Behavior of Iodine and Xenon in the Homogeneous Reactor Test," *Trans. Am. Nucl. Soc.* 4(2) (November 1961), presented at American Nuclear Society Meeting, Chicago, Nov. 7–9, 1961.

Landry, J. W., "Inline Instrumentation: Gamma Monitor, Uranium Colorimeter," presented at Instrument Society of America, Fall Instrument-Automation Conference and Exhibit, Los Angeles, Sept. 11–15, 1961 (Preprint No. 3-LA-61).

Moncrief, E. C., and M. C. Hill, "Digital Computer Processing of Pilot Plant Data," presented at Nuclear Congress, New York, June 4–7, 1962 (ORNL TM-95).

Scott, C. D., "Direct Reduction of Uranium Hexafluoride to Uranium Metal by Use of Sodium," presented at American Chemical Society Meeting, Washington, D.C., Mar. 20–29, 1962 (ORNL TM-92, Dec. 30, 1961); to be published in *Industrial and Engineering Chemistry Process Development Quarterly.*

Blanco, R. E., and J. T. Roberts, "Separation of Lithium Isotopes by Batch or Continuous Ion Exchange with Decalso or Dowex-50 Media," *Progress in Nuclear Energy*, series IV, vol 4, Pergamon, 1961.

Kelly, M. J., J. W. Landry, T. S. Mackey, and R. W. Stelzner, "Inline Applications of Gamma Monitoring and Uranium Colorimetry," presented at ISA-AIEE-IRE Joint Nuclear Instrumentation Symposium, Raleigh, N.C., Sept. 26, 1961, IRE, *Trans. Nucl. Sci.* **NS-8**, 89 (1961) (issued originally as ORNL-2978).

Mackey, T. S., *Inline Densimeter for Pulsed Column Liquid Density, Pulse Amplitude, and Pulse Frequency Measurements*, ORNL-3129 (July 7, 1961).

Klima, B. B., "Lead Ring Gives Tight Seal in Packed Columns," *Chem. Eng.* 68(16), 146 (1961).

Wymer, R. G., *Advanced Technologies Seminar No. 9, March 8, 1961, Status of Direct Conversion Technology*, ORNL CF-61-6-18 (June 5, 1961).

PROGRESS REPORTS

Chemical Development Section B

For February 1961, ORNL CF-61-3-50

For March 1961, ORNL CF-61-4-108

For April–June 1961, ORNL TM-1

For July–September 1961, ORNL TM-81

For October–December 1961, ORNL TM-177

Chemical Development Section C

For April–July 1961, ORNL CF-61-7-76

For August–September 1961, ORNL TM-27

For October–December 1961, ORNL TM-107

For January–March 1962, ORNL TM-181

Chemical Technology and Health Physics Divisions

Waste Treatment and Disposal Progress Report for April and May 1961, ORNL CF-61-7-3

Waste Treatment and Disposal Progress Report for June and July 1961, ORNL TM-15

Waste Treatment and Disposal Progress Report for August and September 1961, ORNL TM-49

Waste Treatment and Disposal Progress Report for October and November 1961, ORNL TM-133

Waste Treatment and Disposal Progress Report for December 1961 and January 1962, ORNL TM-169

SEMINARS

1961		
June 6	A Study of Proposed Modifications to the ORNL Low-Level Waste System	F. N. Browder F. C. McCullough
June 13	Beryllium Oxide Coating of Submicron UO_2 Particles	K. A. Allen W. J. McDowell
June 20	Present Development of Volatility Processing	G. I. Cathers
	Processing of Stainless Steel and Oxide Fuels	M. R. Bennett
	Fluorination of Plutonium from Fused Salts	R. L. Jolley
July 11	A Review of Microorganism Research and Technology	A. T. Gresky
July 18	Thorium Oxide Irradiations	J. P. McBride
	Design of In-Pile Experiments	S. D. Clinton
July 25	Processing of Uranium Carbide Fuel	M. J. Bradley
	Dissolution of Beryllium Oxide Reactor Fuel Elements	K. S. Warren
Aug. 1	Conversion of High-Level Wastes to Solids by Pot Calcination	C. W. Hancher J. M. Holmes
Aug. 8	Processing of Graphite Fuels	L. M. Ferris B. A. Hannaford
Aug. 22	Extraction of Nitric Acid by TBP Solutions	W. Davis, Jr.
Aug. 29	Chemical Technology Division Program	F. L. Culler, Jr.
Sept. 5	European Waste Disposal Program	J. T. Roberts J. O. Blomeke
Sept. 19	Zircex Process Studies	T. A. Gens
Oct. 10	Chemistry of U^{232}-Pa^{231} Separation	J. M. Chilton
Oct. 17	Design of Experiments	D. A. Gardiner, Math Panel
Oct. 27	Status of Eurochemic and Plutonium Purification	R. Rometsch, Eurochemic
Oct. 31	Extraction of Strontium by D2EHPA and Its Sodium Salt	W. J. McDowell
Nov. 7	Some Aspects of Beryllium Chemistry at AEC Research Establishment, Sydney	H. J. de Bruin
Nov. 14	GCR Coolant Clean-Up Decontamination Studies	C. D. Scott A. B. Meservey
Nov. 21	Process Equipment Design Status of the Transuranium Facility	W. E. Unger O. O. Yarbro T. S. Mackey
Nov. 28	Dissemination of Engineering Information by DTIE and Educational Materials Program for Students and Teachers	R. E. C. Duthie, AEC
Dec. 5	Three Years Behind the Paper Curtain	J. E. Bigelow
Dec. 12	Materials of Construction for Possible Multipurpose Chemical Reprocessing Schemes	W. E. Clark
1962		
Jan. 16	Fission Product Recovery	D. E. Horner
Jan. 23	Transuranium Radiation, Shielding, and Hazards Calculations	E. D. Arnold J. P. Nichols

Jan. 30	Design of PaU Facility Australia from the Inside	B. B. Klima Malcolm Baillie
Feb. 6	Project Gnome	J. W. Landry
Feb. 27	Ion Exchange Research Foam Separation	W. C. Yee Ernesto Schonfeld
Mar. 6	Low-Level Waste Treatment Pilot Plant Design and Operation	W. R. Whitson R. E. Brooksbank
Mar. 13	Phoebe – A U^{235} Fission Product Activity Code	E. D. Arnold
Mar. 20	Contribution of Diluent Nitration to the Extraction Performance of Degraded Process Extractants and Utilization of Feed Pretreatment to Improve Zr-Nb and Ru Decontamination	C. A. Blake
Mar. 27	Radiation Safety and Control	T. A. Arehart, Director's Dept.
Apr. 3	Japan TOKAI Research Establishment and Scenic Japan	Tetsuo Aochi
Apr. 10	Neuflex Process	C. F. Coleman F. G. Kitts
Apr. 24	Recent Developments in Solvent Extraction Processes Extraction and Adsorption Studies of Niobium and Protactinium	R. H. Rainey J. G. Moore
May 1	Thorium-U^{233} Oxide Fuel Rod Facility	J. T. Lamartine, Metals and Ceramics B. B. Klima
May 8	Some Infrared Studies on Magnesium Sulfate Dehydration	F. A. Olson, University of Utah
May 15	Design Study of a Uranium Recovery Plant for a 2500 Mwt	W. L. Carter
	Molten-Salt Converter Reactor	R. P. Milford
May 22	Recovery of Thorium (and Uranium) from Granite	F. J. Hurst
May 29	Fuel Heat Transfer Studies	J. S. Watson
	Model Cask Drop Tests	L. B. Shappert
June 5	Production of Transuranium Elements Chemical Processing Requirements for Transuranium Elements	W. D. Burch R. E. Leuze
June 12	Americium-Curium Recovery from Plutonium Process Waste	M. H. Lloyd
	Separation of Transuranium Elements from Rare Earth by Tertiary Amine Extraction and Separation of Transuranium Elements by Phosphonate Extraction	R. D. Baybarz
June 19	Extraction and Purification of Plutonium by Amines	C. F. Coleman
June 26	Fixation of High-Level Radioactive Wastes in Solid Form	W. E. Clark H. W. Godbee

ORNL-3314
UC-10 – Chemical Separations Processes for Plutonium and Uranium
TID-4500 (17th ed., Rev.)

INTERNAL DISTRIBUTION

1. Biology Library
2-4. Central Research Library
5. Reactor Division Library
6-175. Laboratory Records Department
176. Laboratory Records, ORNL, R.C.
177. Laboratory Shift Supervisor
178-179. ORNL – Y-12 Technical Library Document Reference Section
180. C. A. Blake
181. R. E. Blanco
182. J. O. Blomeke
183. R. E. Brooksbank
184. G. E. Boyd
185. J. C. Bresee
186. R. B. Briggs
187. K. B. Brown
188. F. R. Bruce
189. W. H. Carr
190. G. T. Cathers
191. W. E. Clark
192. C. F. Coleman
193. D. J. Crouse
194-221. F. L. Culler
222. W. Davis
223. O. C. Dean
224. D. E. Ferguson
225. L. M. Ferris
226. J. R. Flanary
227. H. E. Goeller
228. A. T. Gresky
229. W. R. Grimes
230. P. A. Haas
231. C. S. Harrill
232. A. Hollaender
233. R. W. Horton
234. A. R. Irvine
235. R. G. Jordon (Y-12)
236. W. H. Jordon
237. M. T. Kelley
238. J. A. Lane
239. C. E. Larson
240. R. E. Leuze
241. H. G. MacPherson
242. R. P. Milford
243. K. Z. Morgan
244. J. P. Murray (K-25)
245. E. L. Nicholson
246. R. H. Rainey
247. A. D. Ryon
248. H. E. Seagren
249. M. J. Skinner
250. A. H. Snell
251. J. C. Suddath
252. J. A. Swartout
253. E. H. Taylor
254. W. E. Unger
255. C. D. Watson
256. B. S. Weaver
257. A. M. Weinberg
258. M. E. Whatley
259. R. G. Wymer
260. J. J. Katz (consultant)
261. T. H. Pigford (consultant)
262. H. Worthington (consultant)
263. C. E. Winters (consultant)

EXTERNAL DISTRIBUTION

264. R. W. McNamee, Union Carbide Corporation, New York
265. Sylvania Electric Products, Inc.
266. Division of Research and Development, AEC, ORO
267-774. Given distribution as shown in TID-4500 (17th ed., Rev.) under Chemical Separations Processes for Plutonium and Uranium Category (75 copies – OTS)